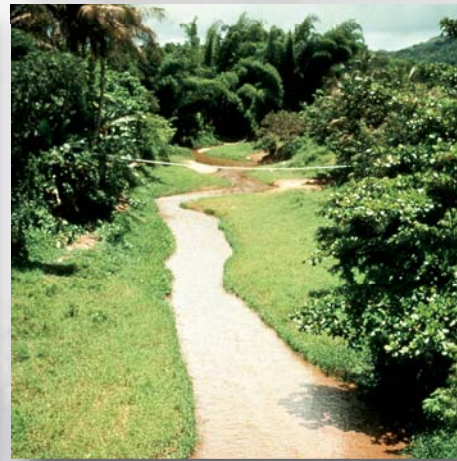
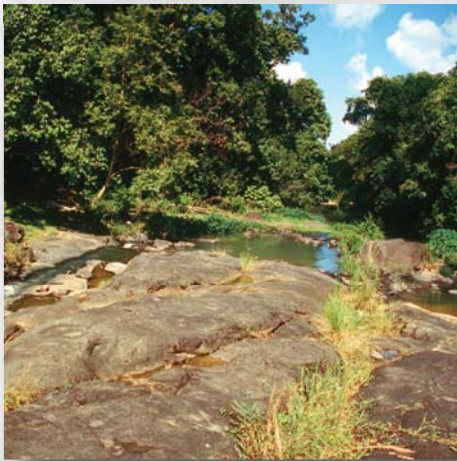
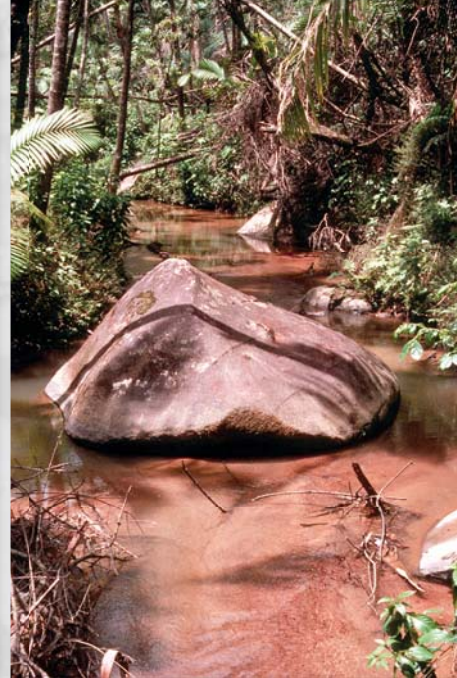


Water Quality and Landscape Processes of Four Watersheds in Eastern Puerto Rico



Professional Paper 1789

Cover: Main channels of four study rivers in eastern Puerto Rico. The top row shows the rivers with naturally forested watersheds (left, Río Mameyes; right, Río Icacos), and the bottom row shows the rivers with agriculturally developed watersheds (left, Río Canóvanas; right, Río Cayaguás). Rivers that drain volcanic and volcanioclastic bedrock with little to no quartz are on the left, and rivers that drain quartz-rich granitic bedrock are on the right. Whether natural or developed, channels of rivers draining bedrock with little to no quartz contain mostly cobbles and boulders, and channels of rivers draining quartz-rich bedrock contain quartz-rich sand.

Water Quality and Landscape Processes of Four Watersheds in Eastern Puerto Rico

Edited by Sheila F. Murphy and Robert F. Stallard

Contributions by Heather L. Buss, William A. Gould,¹ Matthew C. Larsen,
Zhigang Liu,² Sebastián Martinuzzi,³ Sheila F. Murphy, Robert F. Stallard,
Isabel K. Parés-Ramos,⁴ Arthur F. White, and Xiaoming Zou^{2,5}

¹ U.S. Department of Agriculture Forest Service, International Institute of Tropical Forestry

² Institute for Tropical Ecosystem Studies, University of Puerto Rico

³ Department of Forest and Wildlife Ecology, University of Wisconsin

⁴ Department of Biology, University of Puerto Rico

⁵ XishuangbannaTropical Botanical Garden, Chinese Academy of Sciences

Volume comprises Chapters A, B, C, D, E, F, G, H, and I

Professional Paper 1789

**U.S. Department of the Interior
U.S. Geological Survey**

U.S. Department of the Interior
KEN SALAZAR, Secretary

U.S. Geological Survey
Marcia K. McNutt, Director

U.S. Geological Survey, Reston, Virginia: 2012

For more information on the USGS—the Federal source for science about the Earth, its natural and living resources, natural hazards, and the environment, visit <http://www.usgs.gov> or call 1–888–ASK–USGS.

For an overview of USGS information products, including maps, imagery, and publications, visit <http://www.usgs.gov/pubprod>

To order this and other USGS information products, visit <http://store.usgs.gov>

Any use of trade, firm, or product names is for descriptive purposes only and does not imply endorsement by the U.S. Government.

Although this information product, for the most part, is in the public domain, it also may contain copyrighted materials as noted in the text. Permission to reproduce copyrighted items must be secured from the copyright owner.

Suggested citation:
Murphy, S.F., and Stallard, R.F., eds., 2012, Water quality and landscape processes of four watersheds in eastern Puerto Rico: U.S. Geological Survey Professional Paper 1789, 292 p.

Volume Contents

Foreword	iv
By Matthew C. Larsen	
Executive Summary	v
By Sheila F. Murphy and Robert F. Stallard	
A. Physiography, Geology, and Land Cover of Four Watersheds in Eastern Puerto Rico	1
By Sheila F. Murphy, Robert F. Stallard, Matthew C. Larsen, and William A. Gould	
B. Land Use, Population Dynamics, and Land-Cover Change in Eastern Puerto Rico	25
By William A. Gould, Sebastián Martinuzzi, and Isabel K. Parés-Ramos	
C. Hydrology and Climate of Four Watersheds in Eastern Puerto Rico.....	43
By Sheila F. Murphy and Robert F. Stallard	
D. Atmospheric Inputs to Watersheds of the Luquillo Mountains in Eastern Puerto Rico	85
By Robert F. Stallard	
E. Water Quality and Mass Transport in Four Watersheds in Eastern Puerto Rico	113
By Robert F. Stallard and Sheila F. Murphy	
F. Landslides and Sediment Budgets in Four Watersheds in Eastern Puerto Rico	153
By Matthew C. Larsen	
G. Effects of Earthworms on Slopewash, Surface Runoff, and Fine-Litter Transport on a Humid-Tropical Forested Hillslope in Eastern Puerto Rico.....	179
By Matthew C. Larsen, Zhigang Liu, and Xiaoming Zou	
H. Weathering, Landscape Equilibrium, and Carbon in Four Watersheds in Eastern Puerto Rico	199
By Robert F. Stallard	
I. Weathering Processes in the Icacos and Mameyes Watersheds in Eastern Puerto Rico	249
By Heather L. Buss and Arthur F. White	
Appendix 1. Data Processing and Computation to Characterize Hydrology and Compare Water Quality of Four Watersheds in Eastern Puerto Rico.....	263
Appendix 2. Methods Used to Analyze Water Quality of Four Watersheds in Eastern Puerto Rico	289

Foreword

By Matthew C. Larsen

Humans face a future limited by the increasing effects of environmental problems and resource scarcity. The world's population is now consuming water and energy, and using agricultural and other land resources, at per capita rates that will be challenging to sustain. Environmental degradation is intensifying conflict over resources. Local consequences are exacerbated by climate change, manifested as changes in the timing and distribution of rainfall and runoff. As our influence on Earth's lands and waters grows more substantial, we need to understand and quantify these effects to preserve our well-being. Earth sciences are central to meeting this need because they guide the monitoring, assessment, and modeling of natural processes that help us to understand our interaction with the environment. The U.S. Geological Survey has a long history of providing authoritative earth science to inform local and national decision makers as they confront difficult choices in a changing world.

The low-latitude regions of Earth, in particular, are undergoing profound, rapid landscape change. Humid-tropical watersheds of eastern Puerto Rico, at 18° North latitude, provide a natural laboratory that allows researchers to quantify and better understand this change and how it impinges on the human world. In recognition of this opportunity, the National Science Foundation's Long-Term Ecological Research program and the U.S. Geological Survey's Water, Energy, and Biogeochemical Budgets (WEBB) program have operated in eastern Puerto Rico for several decades. WEBB program scientists have studied hydrologic, geologic, geomorphic, and anthropogenic processes in eastern Puerto Rico in an effort to generalize their results to the broader tropical world. Long time-series of streamflow, water-quality, suspended-sediment, meteorological, and land-use data, collected by Federal and by Commonwealth of Puerto Rico agencies, record the effects of landscape changes that are characteristic of environmental challenges that we all face. This publication summarizes research based on these data, and it provides insights into how landscape change may increase soil erosion, reservoir sedimentation, and landslide hazards while decreasing soil-nutrient content and surface-water quality.

In the 1990s the Puerto Rico Tourism Company invited travelers to "discover the continent of Puerto Rico." In a very different sense, Puerto Rico's landscape and the results of our studies there provide a microcosm of the challenges faced by societies on islands and continental landmasses. What choices will we make as we confront future limitations of land and resources? What scientific information will we need to guide these choices? The science presented in this volume improves our understanding of the ramifications of landscape changes by using analysis of watershed-scale geologic, hydrologic, and geomorphic processes, and it can help guide policymakers and resource managers as they confront difficult choices.

Executive Summary

By Sheila F. Murphy and Robert F. Stallard

Puerto Rico is in a state of rapid, ongoing change. Locally, agricultural lands are undergoing reforestation, while coastal areas are becoming heavily urbanized. The area is also changing because of the introduction of nonnative species, water supply projects, and the construction of roads and other infrastructure. Superimposed on these local phenomena are slower, larger scale changes, such as the deposition of airborne pollutants and natural and human-induced climate change. Owing to the island's steep topography, low water-storage capacity, and dependence on trade-wind precipitation, Puerto Rico's people, ecosystems, and water supply are vulnerable to extreme weather such as hurricanes, floods, and droughts. Eastern Puerto Rico offers a natural laboratory for separating geologic and land-cover influences from regional- and global-scale influences because of its various bedrock types and the changing land cover surrounding intact, mature forest of the Luquillo Experimental Forest (which is contiguous with El Yunque National Forest). Accordingly, a multiyear assessment of hydrological and biogeochemical processes was designed to develop an understanding of the effects of these differences on local climate, streamflow, water quality, and ecosystems, and to form the basis for a long-term and event-based program of climate and hydrologic monitoring.

Focusing on small watersheds allows for integrated studies of hydrologic and chemical processes, owing to minimal spatial variability of geology, land use, and climate. For two decades, the U.S. Geological Survey has been evaluating the processes controlling fluxes of water, energy, and elements throughout a range of temporal and spatial scales in small watersheds at five sites in different parts of the nation. The Water, Energy, and Biogeochemical Budgets Project in eastern Puerto Rico represents a montane, humid-tropical environment, in which lie four watersheds of differing geology and land use. Two watersheds are located on coarse-grained granitic rocks (Icacos and Cayaguás), and two are located on fine-grained volcanic rocks and volcaniclastic sedimentary rocks (Mameyes and Canóvanas). For each bedrock type, one watershed is covered with mature rainforest (Icacos and Mameyes); the other is undergoing reforestation after being used as agricultural land (Cayaguás and Canóvanas). These watersheds, like most of the rest of Puerto Rico, were subjected to intensive agriculture in the 19th and early 20th century, but they have been undergoing reforestation as a result of a shift from an agricultural economy to an industrial one and subsequent human migration to urban areas (discussed in chapters A and B in this volume).

Puerto Rico lies directly in the path of the easterly trade winds, which deliver steady rainfall to the mountains and steer weather systems called tropical waves toward the island. Hurricanes and tropical storms derived from these systems typically deliver the majority of yearly rainfall and occur from May to December (chapter C). Northern cold fronts can also deliver heavy rainfall for several days at a time, typically from December through February. These storms vary greatly in frequency and intensity, contributing to substantial interannual variation in precipitation and stream discharge. The largest storms can have profound geomorphic consequences, such as landslides, debris flows, deep gullying on deforested lands, excavation and suspension of sediment in stream channels, and delivery of a substantial fraction of annual stream sediment load (chapters F and G). Past deforestation and agricultural activities in the Cayaguás and Canóvanas watersheds led to profoundly accelerated erosion and soil loss, and this material continues to be remobilized during large storms.

Rainfall varies greatly over small distances in eastern Puerto Rico owing to differences in elevation, topographic position, aspect, and proximity to the ocean. The Icacos and Mameyes watersheds, located on the eastern side of the Luquillo Mountains, are the wettest of the four watersheds studied, and their highest elevations receive more than 4,000 millimeters of rain annually (chapter C). Precipitation increases with elevation in these watersheds. The Canóvanas and Cayaguás watersheds, located on the western side of the Luquillo Mountains, are considerably drier, and precipitation and elevation are not correlated. Precipitation and runoff in all watersheds show large interannual variation and are highest in years when major storms—such as Hurricanes Hortense (1996) and Georges (1998)—strike eastern Puerto Rico. These large storms typically produce similar runoff in all of the study watersheds, suggesting that higher annual runoff in the eastern, windward side of the Luquillo Mountains (which includes the Mameyes and Icacos watersheds) is caused by smaller, more-routine rain events. When one considers watershed-wide water budgets, the windward or leeward aspect of a watershed is more important than differing geology and land cover.

Regional weather patterns and consequent sources of air masses influence the type and timing of atmospheric contributions to eastern Puerto Rico. Nitrogen loads in precipitation at a National Atmospheric Deposition Project site in eastern Puerto Rico have roughly doubled since measurements began in 1985 (chapter D). Eastern Puerto Rico also receives marine salts and Saharan Desert dust in rainfall. The proportion of material delivered by these sources varies seasonally; deposition of marine salts is greatest in January, whereas material from North America is deposited primarily in January, April, and May, and Saharan Desert dust peaks in June and July. Saharan dust typically contributes enough alkalinity in June and July to neutralize acidity in precipitation. During large storms, entrainment of ocean spray and foam can lead to highly elevated concentrations of chloride in stream waters (chapter E).

Because infrequent, large storms play a major role in erosion of landscapes and can lead to a change in hydrologic flow paths, the Water, Energy and Biogeochemical Budgets Project focused on high-runoff events; we sampled 263 storms, including all major hurricanes that occurred between 1991 and 2005 (chapter C, appendix 1). Nearly 5,000 routine and event samples were analyzed for parameters that allow determination of denudation rates based on suspended and dissolved loads; 860 of these samples were analyzed for a comprehensive suite of chemical constituents. Of samples analyzed for comprehensive chemistry and for sediment, 543 were collected at runoff rates greater than 1 millimeter per hour, 256 at rates exceeding 10 millimeters per hour, and 3 at rates exceeding 90 millimeters per hour. Streams have rarely been sampled during events with such high runoff rates.

The rivers studied are generally similar in water-quality characteristics. Most chemical constituents show similar trends in the four watersheds, which imply considerable similarity in runoff generation and flow-path structuring despite differences in geology, soils, land cover, and weathering styles (chapter E). The rivers with lowest mean-annual runoff rates and highest ratios of evapotranspiration to runoff (Cayaguás and Canóvanas) tend to have higher concentrations of nonbioactive constituents. These developed watersheds typically have higher concentrations of nutrients (potassium, nitrate, ammonium ion, phosphate), perhaps indicating additional agricultural or wastewater sources. Projecting watershed yields to a common, intermediate mean-annual runoff (1,860 millimeters per year) generally decreased or did not change the range of yields of constituents that are the primary indicators of chemical weathering, biological activity on the landscape, or atmospheric contributions (dissolved bedrock, sodium, silica, chloride, dissolved organic carbon, and calcium), further indicating no dominant influence of either

geology or land cover (chapter H). Magnesium and inorganic carbon showed a dependence on geology, possibly due to the presence of carbonates or mafic rocks. Projected yields of nutrients and particulate constituents (suspended solids and particulate organic carbon), however, were far in excess of equilibrium yields, and they were much greater for developed landscapes as compared with forested watersheds, consistent with the known effects of land clearing, agricultural activities, and domestic wastewater inputs.

Physical and chemical weathering rates of the four watersheds studied are high. Bedrock in the Icacos (granitic rock) and Mameyes (volcaniclastic rock) watersheds have some of the highest documented rates of chemical weathering of silicate rocks in the world (chapter I). Physical denudation rates based on mass balances are higher than expected for a steady-state system; this excess is substantial in all watersheds except the Mameyes (forested watershed on volcaniclastic bedrock; chapter H). Deforestation and agriculture can explain the accelerated physical erosion in the two developed watersheds (Canóvanas and Cayaguás). Physical erosion rates of the granitic watersheds are seven-fold as great as those for the volcaniclastic watersheds, owing to greater permeability and thus higher rates of water filtration and greater susceptibility to landsliding (chapters C and F). The reason for such high rates of physical erosion in the Icacos watershed (forested watershed on granitic bedrock) is unclear but may be related to changes in forest quality or to the history of road construction. The elevated physical erosion drives an increased particulate organic carbon flux, one that is large and is important to the carbon cycle. This increased flux is also sustainable because soil-carbon replacement is rapid.

It is crucial to understand long-term geomorphological, hydrological, and biogeochemical processes in tropical regions, because these regions occupy about a quarter of Earth's land surface, yet they contribute a substantially higher fraction of the water, solutes, and sediment discharged to the world's oceans. Nearly half of Earth's population lives in the tropics, and therefore development stresses are intense and can potentially harm soil resources, water quality, and water supply and in addition increase landslide and flood hazards. Small watersheds in eastern Puerto Rico provide an excellent opportunity to examine these processes and their connection to climate, geology, and land cover. The 15-year Water, Energy, and Biogeochemical Budget dataset, which includes discharge, field parameters, suspended sediment, major cations and anions, and nutrients, is available from the U.S. Geological Survey's National Water Information System (<http://waterdata.usgs.gov/nwis>). The dataset provides a baseline for characterizing future environmental change and will improve our understanding of the interdependencies of land, water, and biological resources and their responses to changes in climate and land use. Because eastern Puerto Rico resembles many tropical regions in terms of geology and patterns of development, implications from this study are transferable to other tropical regions facing deforestation, rapid land-use change, and climate change.

Acknowledgments

The work in Puerto Rico could not have been done without the assistance of numerous people. In alphabetical order, an incomplete list includes the following: George Aiken, Ellen Axtmann, Sean Baran, Susan Brantley, Mary-Margaret Coates, Paul Collar, Iris Concepción, Russ Curtis, Pedro Díaz, Marcelle Fabregas, Robert Hirsch, Laura Hubbard, Ariel Lugo, Deborah Martin, Joel Martinez, Erik Oerter, Jennifer Riggs, Manuel Rosario, Cathy Rubin, Abdul Wahab Sadeqi, F.N. Scatena, Jamie Shanley, Angel Torres-Sánchez, Heriberto Torres, Joe Troester, Ank Webbers, and

Allen Zack. Helpful reviews of individual chapters and appendices were provided by Alex Blum, W. Troy Baisden, Brian Ebel, Allen Gellis, Jonathan Godt, G. González, Cliff R. Hupp, Andy Kurtz, Ariel Lugo, William McDowell, John Moody, Jake Peters, Fred Quiñones, Deborah Report, Susan Riggins, F.N. Scatena, Martha Scholl, Jamie Shanley, Jonathan Stock, Gordon Tribble, Frank Wadsworth, John Walker, and Richard Webb. Two individuals deserve special acknowledgment: Ellen Axtmann helped implement and ran chemical analyses for the first half of the program, and Angel Torres-Sánchez, who was the first technician, was crucial in field-testing procedures and in helping adapt to the complexities of event sampling in a challenging environment.

Physiography, Geology, and Land Cover of Four Watersheds in Eastern Puerto Rico

By Sheila F. Murphy, Robert F. Stallard, Matthew C. Larsen, and William A. Gould

Chapter A of
**Water Quality and Landscape Processes of Four Watersheds in
Eastern Puerto Rico**

Edited by Sheila F. Murphy and Robert F. Stallard

Professional Paper 1789–A

**U.S. Department of the Interior
U.S. Geological Survey**

Contents

Abstract.....	5
Introduction.....	5
Site Description.....	5
Physiography.....	7
Geology.....	10
Geology in Watersheds Dominated by Volcaniclastic Rock	10
Geology in Watersheds Dominated by Granitic Rock.....	12
Soil and Saprolite.....	13
Soils in Watersheds Dominated by Volcaniclastic Rock	13
Soils in Watersheds Dominated by Granitic Rock.....	14
Vegetation and Land Use.....	15
Land Cover of Forested Watersheds	16
Land Cover of Developed Watersheds.....	18
Summary.....	18
Acknowledgments.....	20
References.....	20

Figures

1. Maps of Puerto Rico and study watersheds.....	6
2. Digital elevation model of elevation and relief of Puerto Rico, showing major mountain ranges and study watersheds	7
3. Digital elevation model of relief of eastern Puerto Rico showing study watersheds, and elevation profiles along three lines of cross section.....	8
4. Diagrams of percentage of watershed area with each aspect, for the Canóvanas, Cayaguás, Icacos, and Mameyes watersheds.....	9
5–9. Maps of the following:	
5. Generalized geology of Puerto Rico	10
6. Detailed geology of study watersheds, Puerto Rico	11
7. Ecological life zones of Puerto Rico.....	15
8. Generalized land cover of Puerto Rico in 2003.....	16
9. Detailed land cover of study watersheds in 2003	17
10. Diagram of population density in a barrio in Canóvanas watershed and a barrio in Cayaguás watershed	20

Tables

1. Geomorphic and geographic characteristics of study watersheds	9
2. Geology of study watersheds, eastern Puerto Rico	12
3. Mineral content of granitic intrusions, eastern Puerto Rico.....	13
4. Land cover and land-cover dynamics in study watersheds, eastern Puerto Rico.....	19

Abbreviations Used in This Report

cm	centimeter
km	kilometer
km ²	square kilometer
m	meter
mm	millimeter
Ma	mega-annum, 1 million years old
USDA	U.S. Department of Agriculture
USGS	U.S. Geological Survey
WEBB	Water, Energy, and Biogeochemical Budgets

Conversion Factors

Multiply	By	To obtain
Length		
centimeter (cm)	0.3937	inch (in.)
millimeter (mm)	0.03937	inch (in.)
meter (m)	3.281	foot (ft)
kilometer (km)	0.6214	mile (mi)
Area		
square kilometer (km ²)	0.3861	square mile (mi ²)

Physiography, Geology, and Land Cover of Four Watersheds in Eastern Puerto Rico

By Sheila F. Murphy,¹ Robert F. Stallard,¹ Matthew C. Larsen,² and William A. Gould³

Abstract

Four watersheds with differing geology and land cover in eastern Puerto Rico have been studied on a long-term basis by the U.S. Geological Survey to evaluate water, energy, and biogeochemical budgets. These watersheds are typical of tropical, island-arc settings found in many parts of the world. Two watersheds are located on coarse-grained granitic rocks that weather to quartz- and clay-rich, sandy soils, and two are located on fine-grained volcanic rocks and volcaniclastic sedimentary rocks that weather to quartz-poor, fine-grained soils. For each bedrock type, one watershed is covered with mature forest, and the other watershed, like most of Puerto Rico, has transformed from relatively undisturbed pre-European forest to intensive agriculture in the 19th and early 20th centuries, and further to ongoing reforestation that began in the middle of the 20th century. The comparison of water chemistry and hydrology in these watersheds allows an evaluation of the effects of land-use history and geology on hydrologic regimes and erosion rates. This chapter describes the physiography, geology, and land cover of the four watersheds and provides background information for the remaining chapters in this volume.

Introduction

Five field sites across the nation are being monitored long-term as part of the U.S. Geological Survey's (USGS) Water, Energy, and Biogeochemical Budgets (WEBB) program (Baedecker and Friedman, 2000). The Puerto Rico WEBB site, located in eastern Puerto Rico, represents a montane, humid-tropical environment. Its geology and land cover are typical of large regions of the humid tropics, particularly

montane regions that are affected by hurricanes (Larsen and Stallard, 2000). The Puerto Rico WEBB project has been evaluating hydrological, chemical, and sediment budgets and processes in four watersheds of differing geology and land use in eastern Puerto Rico since 1991 (Larsen and others, 1993). Two watersheds are located on coarse-grained granitic rocks, and two are located primarily on a combination of fine-grained volcanic and volcaniclastic sedimentary rocks. For each bedrock type, one watershed is covered with mature forest, and the other watershed has been affected by agricultural land use typical of eastern Puerto Rico. The comparison of water chemistry and hydrology in these watersheds allows an evaluation of the effects of land-use history and geology on hydrologic regimes and erosion rates.

This chapter describes and compares the physiography, geology, soils, vegetation, and land cover of the watersheds. Climate and hydrology are described in Murphy and Stallard (2012), land-cover change is discussed in Gould and others (2012), and erosional processes are described in Larsen (2012). These comparisons provide context for data presented in the remaining chapters.

Site Description

Puerto Rico is a 9,000-square kilometer (km^2) island within the Greater Antilles, located about 1,700 km southeast of Miami, Fla., at about latitude 18°N., longitude 66°W. (fig. 1). The WEBB study watersheds discussed here and in other chapters of this professional paper are gaged subwatersheds of larger watersheds having the same name. The Mameyes (17.8 km^2) and Icacos (3.26 km^2) watersheds are located inside El Yunque National Forest, a 113- km^2 forest preserve administered by the U.S. Department of Agriculture (USDA) Forest Service. El Yunque National Forest is conterminous with the Luquillo Experimental Forest (fig. 1), which has been the site of a National Science Foundation Long-Term Ecological Research project since 1985, and it is designated an International Biosphere Reserve by the United Nations Educational, Scientific, and Cultural Organization. The Cayaguás (26.4 km^2) and Canóvanas (25.5 km^2) watersheds are located within the partially urbanized, agriculturally developed yet reforesting, Río Grande de Loíza watershed (fig. 1).

¹U.S. Geological Survey, 3215 Marine St. Suite E127, Boulder, Colo. 80303, USA

²U.S. Geological Survey, 436 National Center, Reston, Va. 20192, USA

³U.S. Department of Agriculture Forest Service, International Institute of Tropical Forestry, Jardín Botánico Sur, 1201 Calle Ceiba, Río Piedras, Puerto Rico 00926

6 Water Quality and Landscape Processes of Four Watersheds in Eastern Puerto Rico

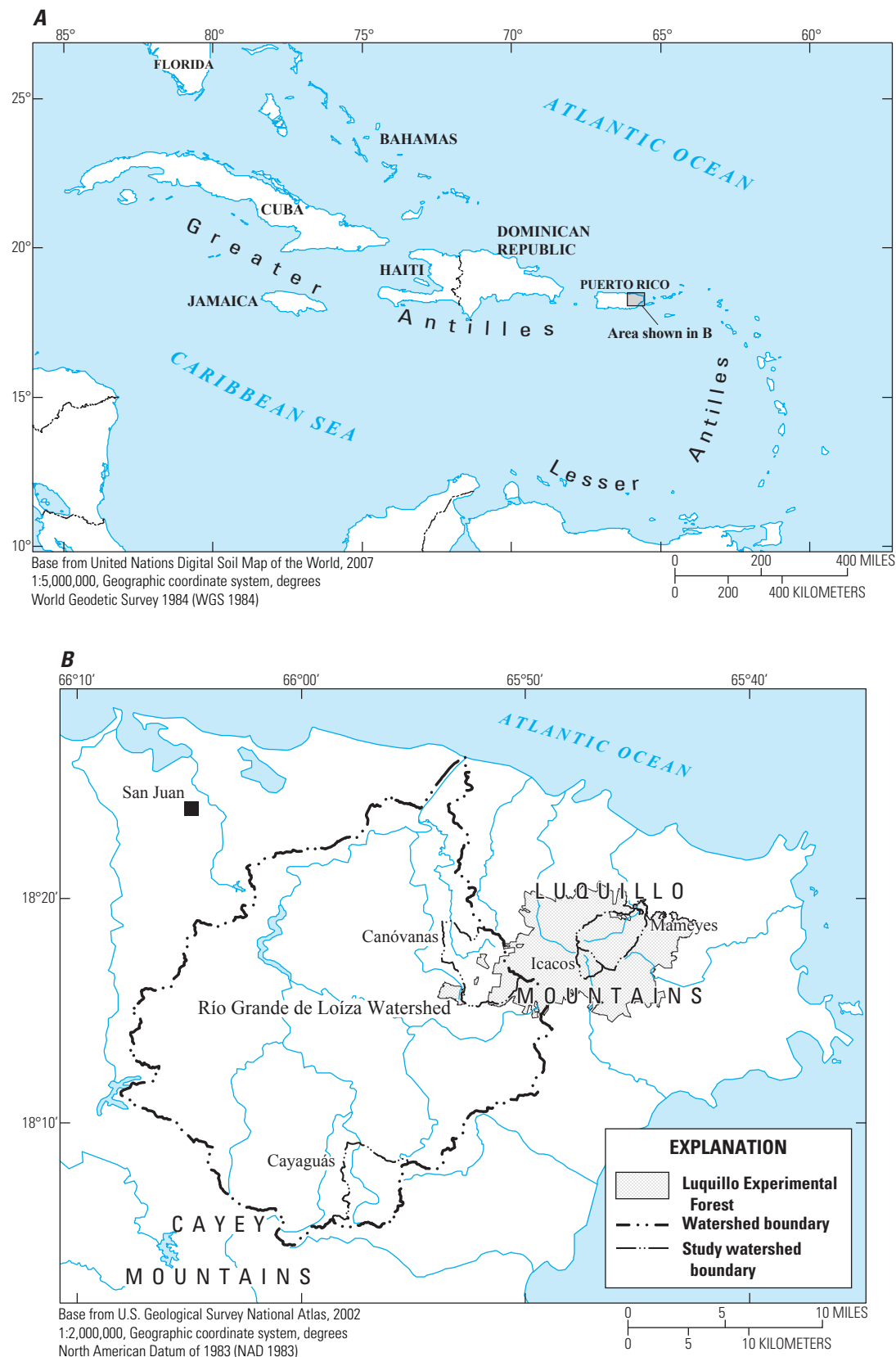


Figure 1. Location of Puerto Rico and study watersheds, eastern Puerto Rico.

Physiography

Puerto Rico is mountainous with central highlands surrounded by flat-lying coastal plains and alluvial valleys (fig. 2). Mountain ranges generally are oriented east-west and dominate the southern two-thirds of the island. Stream channels are steep, and most river valleys are deeply incised. Accelerated weathering in the north-facing watersheds, compared with the slower weathering on the drier southern slopes, has shifted the divide south such that streams are longer and their slopes are gentler on the north side of the island than on the south (Ramos-Ginés, 1999).

The Mameyes, Icacos, and Canóvanas watersheds drain the rugged Luquillo Mountains (fig. 2). The Mameyes watershed is located on the eastern side of the Luquillo Mountains (fig. 3). Slopes in this watershed mostly face north, northeast, and east (fig. 4), directly into the dominant east and northeast wind directions (Calvesbert, 1970). The Canóvanas watershed

is on the western side of the Luquillo Mountains, with southwest to northwest aspects, facing away from prevailing winds. Relief in the Mameyes and Canóvanas watersheds is almost 1,000 meters (m) (table 1). The smaller Icacos watershed is located at elevations between about 620 and 832 m, and slopes typically face east, southeast, and southwest (fig. 4). A ridge approaching 800 m elevation separates the Icacos and Mameyes watersheds. Five peaks are higher than 1,000 m in the Luquillo Mountains (U.S. Geological Survey, 1967); the highest, El Toro (1,075 m), is located between the Icacos and Canóvanas watersheds (fig. 3). The Cayaguás watershed, located southwest of the Luquillo Mountains, consists of low hills and alluvial valleys; the Cayey Mountains are located to the west (fig. 2). Slopes in the Cayaguás watershed show no predominant orientation (fig. 4). Hillslopes and channels are steep in all of the WEBB watersheds, and mean hillslopes range from 0.189 (10.7°) in the Cayaguás watershed to 0.365 (20.0°) in the Mameyes watershed (table 1).

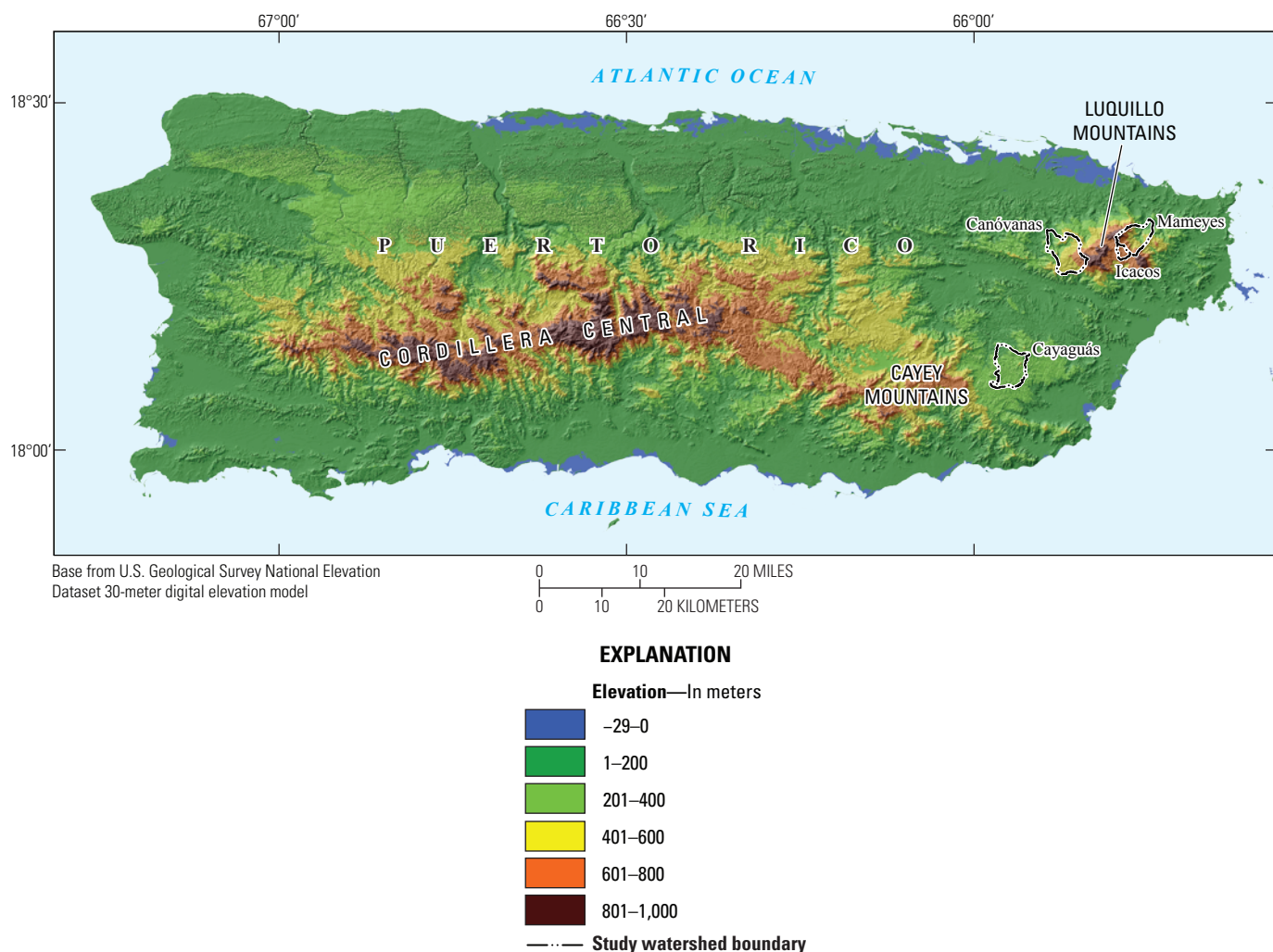


Figure 2. Elevation and relief of Puerto Rico, showing major mountain ranges and study watersheds (outlined).

8 Water Quality and Landscape Processes of Four Watersheds in Eastern Puerto Rico

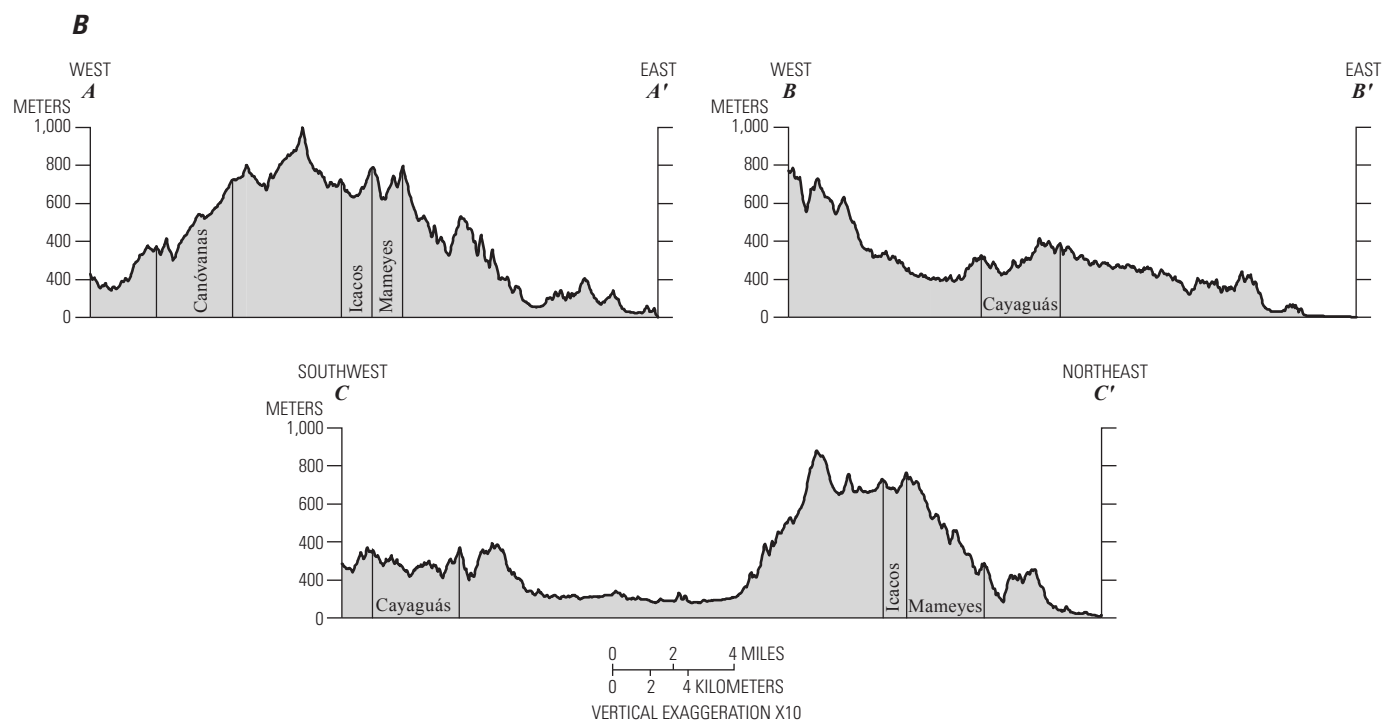
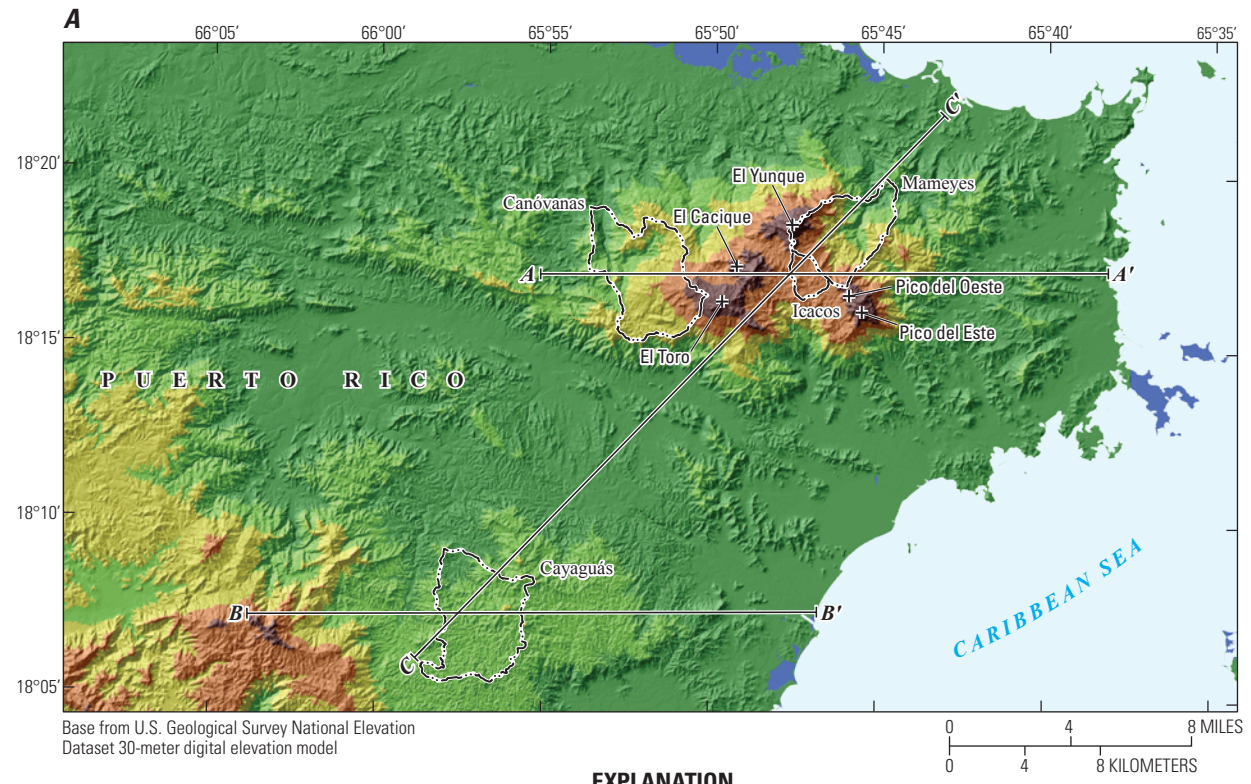


Figure 3. A, Elevation and relief of eastern Puerto Rico, showing study watersheds (outlined), and three lines of cross section; B, elevation profiles along lines of cross section.

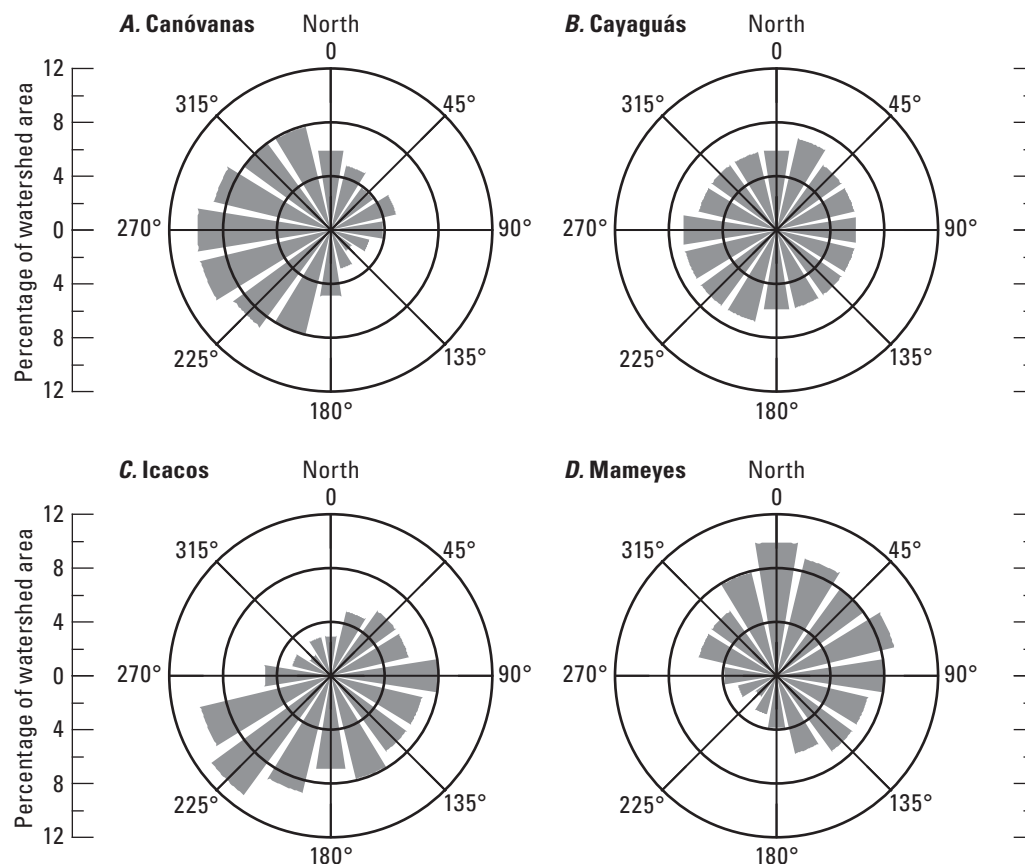


Figure 4. Percentage of watershed area with each aspect, Canóvanas, Cayaguás, Icacos, and Mameyes watersheds (determined from elevation data from U.S. Geological Survey).

Table 1. Geomorphic and geographic characteristics of study watersheds.

[Values calculated from geographic information system data unless otherwise noted. Slope values are dimensionless]

Characteristic	Icacos	Mameyes	Canóvanas	Cayaguás
Area, square kilometers ¹	3.26	17.8	25.5	26.4
Minimum elevation, meters	620	83	70	156
Maximum elevation, meters	832	1,050	956	445
Mean elevation, meters	686	508	464	287
Mean hillslope of watershed ²	0.222	0.365	0.255	0.189
Mean channel slope ²	0.073	0.21	0.151	0.12
Main channel length, kilometers ²	2.01	13.6	21.33	23.5
Total channel length, kilometers ²	2.91	24.02	34.37	49.46
Dominant bedrock type	Granitic Forest	Volcaniclastic Forest	Volcaniclastic Agricultural	Granitic Agricultural
Dominant land use history				

¹Díaz and others (2004).

²Larsen (1997).

Geology

Puerto Rico is a volcanic island-arc terrain with a geologic record spanning about 150 million years (Bawiec, 1998). It was formed by volcanism and sedimentation characteristic of tectonically active plate boundaries, and it consists of a core of volcanic and plutonic rocks surrounded by younger sedimentary rocks. The WEBB watersheds overlie igneous rocks typical of island-arc terrains. The Luquillo Mountains and the Loíza watershed are underlain largely by marine-deposited volcaniclastic rock with intrusions of granitic rock (figs. 5 and 6; Broedel, 1961; Seiders, 1971a,b,c; M'Gonigle, 1978, 1979; Rogers and others, 1979; Bawiec, 1998). Folding and large-scale strike-slip faulting have deformed strata, resulting in westerly dips such that strata grow progressively younger toward the northwest (Jolly and others, 1998).

Geology in Watersheds Dominated by Volcaniclastic Rock

The Mameyes and Canóvanas watersheds are underlain primarily by Cretaceous, marine-deposited, quartz-poor volcaniclastic rocks. The bedrock of the Mameyes watershed is primarily Fajardo, Tabonuco, and Hato Puerco Formations (41, 38, and 3 percent of the watershed, respectively; another 18 percent of the watershed is underlain by the Río Blanco quartz diorite intrusion, discussed in the next section). The Canóvanas watershed is almost entirely underlain by the Hato Puerco and Lomas Formations (87 and 12 percent, respectively; fig. 6, table 2). The oldest of these formations, the Fajardo Formation, is about 105 to 100 million years old (Ma) (Jolly and others, 1998). Its lithology varies substantially and it has been divided into several members (Briggs, 1973; Briggs and Aguilar-Cortés, 1980).

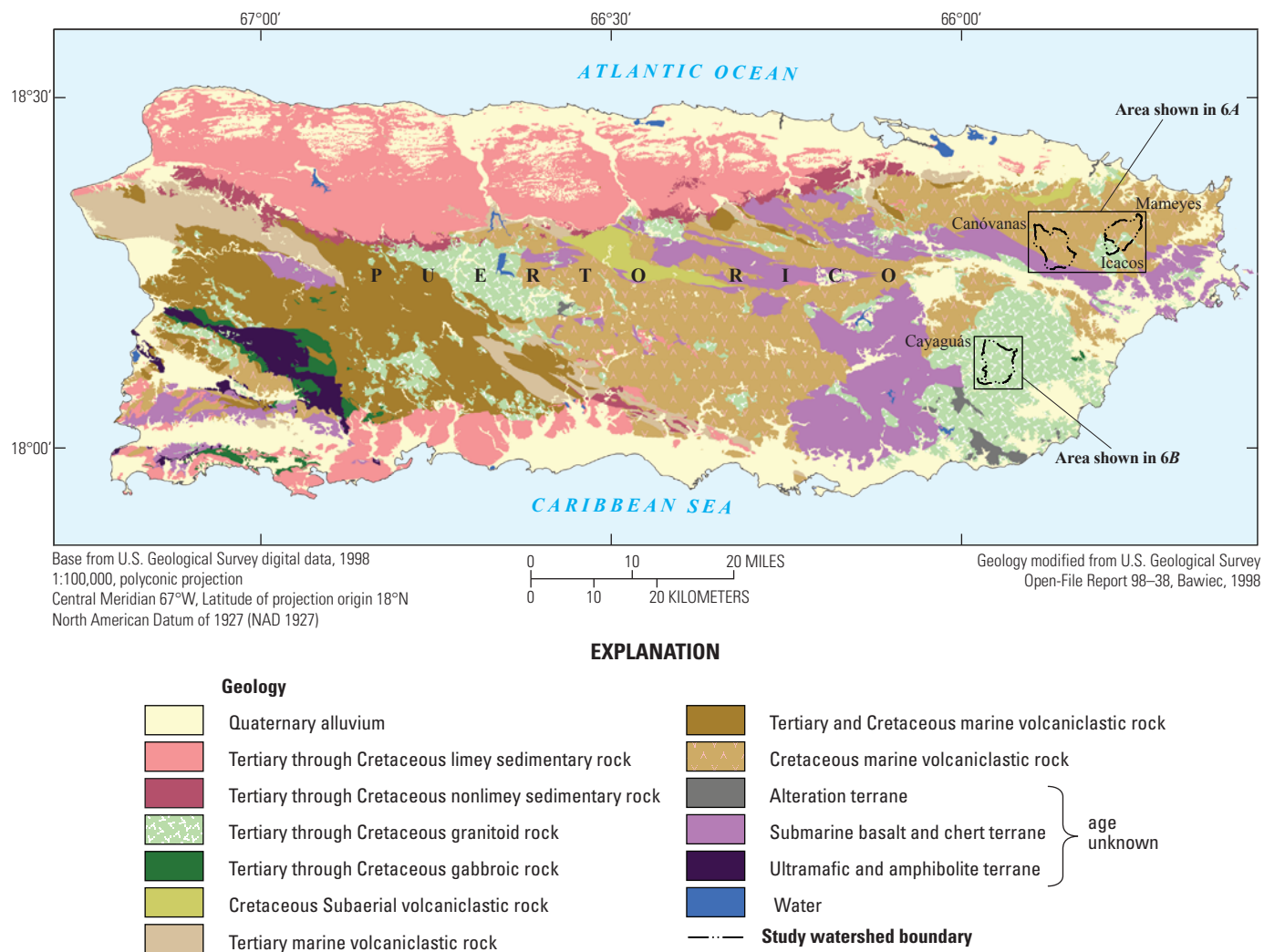


Figure 5. Generalized geology of Puerto Rico (from Bawiec, 1998); study watersheds outlined.

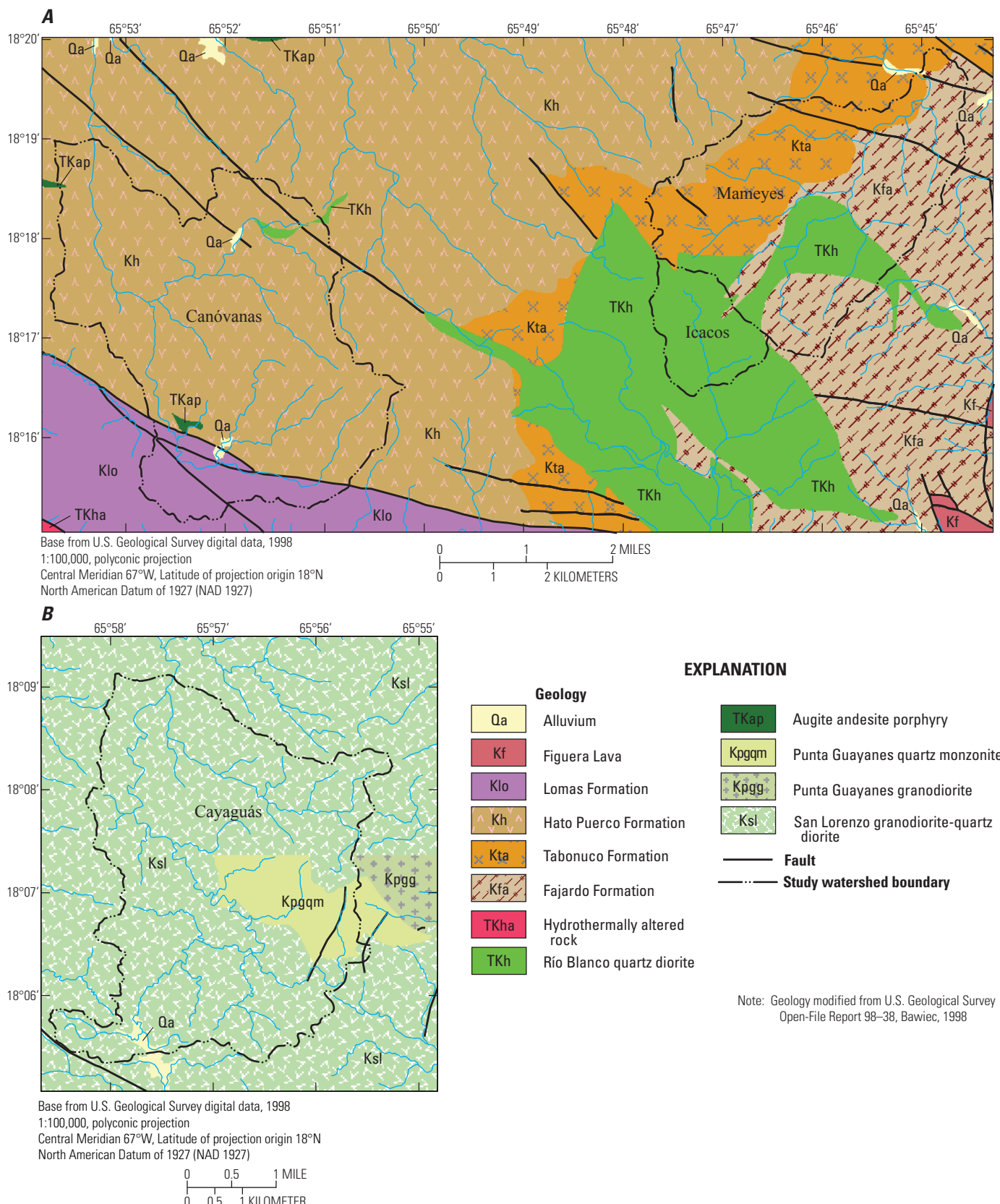


Figure 6. Detailed geology of study watersheds, eastern Puerto Rico (from Bawiec, 1998).

Table 2. Geology of study watersheds, eastern Puerto Rico.¹

Watershed and formation	Symbol	Rock type	Percent
Canóvanas			
Hato Puerco Formation	Kh	Volcaniclastic	87.2
Lomas Formation	Klo	Volcaniclastic	11.5
Río Blanco quartz diorite	TKh	Intrusive	0.5
Alluvium	Qa	Alluvium	0.4
Augite andesite porphyry	Tkap	Intrusive	0.3
Cayaguás			
San Lorenzo granodiorite-quartz diorite	Ksl	Intrusive	88.0
Punta Guayanes quartz monzonite	Kpgqm	Intrusive	11.3
Alluvium	Qa	Alluvium	0.6
Punta Guayanes granodiorite	Kpgg	Intrusive	0.02
Icacos			
Río Blanco quartz diorite	TKh	Intrusive	98.5
Fajardo Formation	Kfa	Volcaniclastic	1.2
Tabonuco Formation	Kta	Volcaniclastic	0.4
Mameyes			
Fajardo Formation	Kfa	Volcaniclastic	40.9
Tabonuco Formation	Kta	Volcaniclastic	37.9
Río Blanco quartz diorite	TKh	Intrusive	17.8
Hato Puerco Formation	Kh	Volcaniclastic	3.3
Alluvium	Qa	Alluvium	0.04

¹Adapted from Bawiec (1998).

Thick-bedded tuff breccias, with large clasts of andesite, dominate. They are interbedded with coarse-grained tuff, tuffaceous sandstone, and black cherty siltstone. The Fajardo Formation is largely noncalcareous, except for sporadic calcareous sandstone and siltstone beds and calcareous tuffs (Briggs, 1973).

The Fajardo Formation grades into the overlying Tabonuco Formation, which is about 100 Ma (Jolly and others, 1998). It contains more mudstone and less very thick bedded sandstone and breccia than the Fajardo Formation (Seiders, 1971b). About 60 percent of the Tabonuco Formation consists of volcanic sandstones, which are usually light gray, calcareous, moderately sorted, and fine to very coarse grained, and which are composed primarily of angular volcanic rock fragments and subordinate plagioclase, clinopyroxene, and rare quartz grains (Seiders, 1971b). About 30 percent of the Tabonuco Formation consists of dark gray, thin-bedded to rarely thick-bedded, laminated mudstones, which can be slightly to highly calcareous. About 10 percent of the Tabonuco Formation consists of volcanic breccia and conglomerate.

The Hato Puerco Formation overlies the Tabonuco Formation and is about 97 to 90 Ma (fig. 6; Jolly and others, 1998). More than half of the formation is composed of andesitic to basaltic volcanic sandstone, which contains volcanic lithic clasts, grains of plagioclase, clinopyroxene, and hornblende, and sparse grains and boulders of limestone (Seiders, 1971a). About 30 to 40 percent of the formation consists of volcanic breccias that contain angular to subrounded pieces of andesite or basalt, with fragments of limestone that can make up as much as 30 percent of the breccia. Calcareous mudstone and andesitic to basaltic porphyritic lava are present in minor amounts. The Hato Puerco contains more carbonate material than the Fajardo or Tabonuco Formations, particularly

in the vicinity of the Río Canóvanas stream channel, where outcrops of calcareous shales and tuffaceous limestone are common (Meyerhoff, 1931; Seiders, 1971a). Calcareous rocks require relatively small outcrop areas to have a marked effect on stream chemistry (Stallard, 1995), and the larger amount of carbonate rocks in the Canóvanas watershed compared with the Mameyes watershed is reflected in stream chemistry (Stallard and Murphy, 2012).

The Lomas Formation, found in the southern part of the Canóvanas watershed, consists of gray-green, thick-bedded, poorly sorted andesitic to basaltic volcanic breccia and sandstone, with minor pillow lava locally (Seiders, 1971c). Strata commonly contain pumice, vesicular lava fragments, and grains of plagioclase and clinopyroxene, and calcite is locally abundant in the matrix (Seiders, 1971c). This formation is seen at the surface only in fault blocks and is not observed in depositional contact with other formations; on the basis of its similarities with other formations in the region, it has been estimated to be between 90 and 85 Ma (Jolly and others, 1998).

The intrusion of the Río Blanco quartz diorite (discussed in the next section) metamorphosed the Fajardo, Tabonuco, and Hato Puerco Formations within a 2–4 km contact zone (Bawiec, 1998), resulting in rocks that are typically harder; the divide between the Mameyes and Icacos watersheds was formed on the slightly hardened rocks of the metamorphic aureole. In the metamorphosed rocks, hornblende, garnet, epidote, chlorite, iron sulfide minerals, gold, copper, and quartz, and aplite veins have been identified (Seiders, 1971a,c; Bawiec, 1998). Gold-, silver-, and copper-bearing deposits were first worked by the Spanish in the early 1600s; production was limited to several small adits within the contact zone (Wadsworth, 1970; Cardona, 1984; Bawiec, 1998). Placer gold from weathered metamorphosed rocks was mined intermittently in the Mameyes and Loíza watersheds beginning in the 1500s.

Geology in Watersheds Dominated by Granitic Rock

The Icacos and Cayaguás watersheds are primarily underlain by Upper Cretaceous and Tertiary granitic rocks. Almost all (99 percent) of the Icacos watershed is underlain by the Río Blanco quartz diorite (fig. 6, table 2), which intruded the surrounding volcaniclastic rocks about 49 to 42 Ma (Smith and others, 1998). The Río Blanco quartz diorite is light-gray, medium- to coarse-grained, and commonly contains plagioclase, quartz, amphibole, and minor biotite in a fine- to medium-crystalline groundmass of quartz, amphibole, orthoclase, and plagioclase, and with accessory zircon, tourmaline, sphene, and epidote (Seiders, 1971a,b; table 3). Plagioclase ranges from fresh to sericitized. Hornblende is commonly altered to chlorite, calcite, and epidote (Seiders, 1971a). Biotite is commonly fresh, but it is also altered to chlorite (Murphy and others, 1998). In some areas the Río Blanco quartz diorite contains pyrite, molybdenite, or disseminated chalcopyrite (Bawiec, 1998).

About 88 percent of the Cayaguás watershed is underlain by the San Lorenzo granodiorite–quartz diorite intrusion (fig. 6, table 2), which has been dated to be about 73 Ma (Rogers and others, 1979; Bawiec, 1998). This intrusion occupies a 500-km² area in southeastern Puerto Rico. It is a medium- to dark-gray, granitic-textured, medium-crystalline, generally massive granodiorite which grades into quartz diorite and locally into quartz monzonite. It is composed generally of plagioclase, potassium feldspar, quartz, hornblende, and minor biotite and accessory magnetite, sphene, apatite, and zircon (Rogers and others, 1979) (table 3). Many plagioclase grains are partly sericitized and argillized. Hornblende is commonly altered to chlorite and epidote, and biotite is commonly altered to chlorite.

About 11 percent of the Cayaguás watershed has been mapped as Punta Guayanés quartz monzonite, which has been dated at about 66 Ma (Rogers and others, 1979). This rock type ranges in composition from quartz monzonite to granodiorite, but in general it is granitic-textured, medium crystalline, and composed of abundant plagioclase, potassium feldspar, and quartz, with subordinate hornblende, minor biotite, and accessory magnetite, sphene, apatite, and zircon (table 3). Most plagioclase grains are sericitized to various degrees, and hornblende is commonly altered to chlorite and epidote (Rogers and others, 1979). The southern part of the watershed was mapped to greater detail by Rogers and others (1979) than the northern part (Broedel, 1961); Broedel classified all rocks simply as granodiorite. The greater amount of quartz and lesser amount of plagioclase in the quartz monzonite may make the monzonite more resistant to weathering than the granodiorite, and they may explain why hillslopes underlain by monzonite in the watershed have higher elevation and greater relief than elsewhere in the basin (Larsen, 1997). The quartz monzonite may actually underlie a larger

portion of the Cayaguás basin than the reported 11 percent, because this accentuated topography is expressed elsewhere in areas mapped as granodiorite.

The effect of geology on channel morphology in the WEBB watersheds is evident in the bed material and particle size (see cover photograph). Stream channels in the Icacos and Cayaguás watersheds typically have sand-bed channels and floodplains that are dominantly sandy alluvium with occasional boulders. Median grain size (D_{50}) is 0.6 millimeters (mm) and 0.5 mm, respectively, in the two channels (Larsen, 1997). Channels in the Mameyes and Canóvanas watersheds are generally characterized by little to no floodplain and channels lined with bedrock, boulders, or cobbles, with little bed sediment. Median grain size in these two channels is 70 mm and 110 mm, respectively (Larsen, 1997).

Soil and Saprolite

Intense, continuous weathering in the warm, humid-tropical climate of the Luquillo Mountains and the Loíza watershed has produced a mantle of soil overlying both granitic and volcaniclastic bedrock that is as much as 24 m thick (Simon and others, 1990; White and others, 1998). Below the surface-soil horizons, which show strong bioturbation (Brown and others, 1983; Brown and others, 1995; González and others, 1996) and subsoil movement (Lewis, 1974; Larsen and others, 1999), is commonly a layer of saprolite. Saprolite is soil that is derived from bedrock that has been thoroughly decomposed through isovolumetric chemical weathering; it remains in place and retains the appearance of the bedrock structure (American Geological Institute, 1976). The composition of the underlying bedrock, particularly the quartz content, determines the chemical and physical properties of the saprolite (Meyerhoff, 1931; Schellekens and others, 2004; Buss and White, 2012; Stallard, 2012).

Soils in Watersheds Dominated by Volcaniclastic Rock

The volcaniclastic rocks underlying the Mameyes and Canóvanas watersheds are generally quartz poor, and they are composed predominantly of basic feldspars and ferromagnesian minerals (Seiders, 1971a,b,c; Briggs, 1973). In the saprolite, these minerals weather to kaolinite and other clay minerals of the 1:1 lattice type, iron and aluminum oxides, and small amounts of quartz (Huffaker, 2002). Relic grains of plagioclase and mafic minerals are recognizable in some hand specimens of the saprolite (Scatena, 1989). Geoelectric soundings indicate a gradual change from unweathered bedrock to less-weathered saprolite to highly weathered saprolite; active weathering occurs in the less-weathered saprolite (Schellekens and others, 2004). Clay-lined faults and joints, which are common in the saprolite, make primary sedimentary structures difficult to distinguish.

Table 3. Mineral content of granitic intrusions, eastern Puerto Rico.

[--, not available]

Mineral	Average mineral content of bedrock (weight percent)		
	Río Blanco ¹	San Lorenzo ²	Quartz monzonite of Punta Guayanés ²
Plagioclase	55.8	51	35
Quartz	26.0	20.5	33
Amphibole	7.3	11	1.5
K-feldspar	5.0	11	28
Biotite	3.6	4.5	2
Accessory ³	1.4	--	--
Apatite	0.2	--	--
Iron oxide	0.7	1.5	0.5
Total	100	99.5	100

¹Seiders (1971b).

²Rogers and others (1979).

³Accessory minerals: Río Blanco—epidote, sphene, tourmaline, zircon; San Lorenzo—apatite, sphene, zircon, and minor augite, myrmekite; Punta Guayanés—apatite, sphene, zircon.

The volcaniclastic saprolite is overlain by clay-rich, quartz-poor soils that are typically 0.8 to 1.0 m deep (Huffaker, 2002). Soils developed on the volcaniclastic rocks are finer grained than those developed on the granitic rocks, and they have lower permeability and infiltration rates than granitic soils (Simon and others, 1990; Murphy and Stallard, 2012). Dense clays in the volcaniclastic soils retard deep infiltration, causing water to follow a shallow trajectory and reach streams quickly (McDowell and others, 1992). Because of the generally high soil moisture content in the Luquillo Mountains, soils are quickly saturated during storms, leading to saturation overflow (Larsen and others, 1999). As such, during periods of intense rainfall, water is commonly observed flowing over the surface in rills and ephemeral gullies.

At the highest elevations in the Mameyes watershed, corresponding with palo colorado forest (see Vegetation and Land Use section), soils overlying the volcaniclastic rock consist primarily of the Yunque clay loam and Moteado clay soils, which are Oxisols, and the Guayabota clay loam and Palm clay soils, which are Inceptisols (Huffaker, 2002). These soils range from poorly drained (on concave slopes) to moderately well drained (on convex slopes). The Inceptisols presumably reflect the greater rainfall in the highest elevations and wetter areas near rivers. At lower elevations, corresponding with tabonuco forest, soils overlying the volcaniclastic rocks consist primarily of Zarzal clay and Cristal clay loam soils, which are Oxisols, and range from somewhat poorly drained (concave slopes) to well drained (convex slopes) (Huffaker, 2002).

The Canóvanas watershed contains a variety of soil types, including Oxisols (Yunque, Moteado, Zarzal, and Cristal clay or clay loams, discussed in the previous paragraph, and the deep, moderately well drained Los Guineos clay), Inceptisols (Mucara silty clay loam and Caguabo clay loam, which are shallow to moderately deep and well drained), Ultisols (Humatas clay and Naranjito silty clay loam, which are deep to moderately deep and well drained), and minor Mollisols (Reilly silty clay loam, found in the floodplain) (Boccheciamamp, 1977; Huffaker, 2002). As a result of past agricultural cultivation, much of the original surface layers of several of the soils in the lower part of the Canóvanas watershed, including the Los Guineos, Humatas, Mucara, and Naranjito soils, have been removed by erosion (Boccheciamamp, 1977).

Soils in Watersheds Dominated by Granitic Rock

The quartz-rich granitic rocks underlying the Iacos and Cayaguás watersheds weather to a saprolite composed of quartz, weathered biotite, and kaolinite, and other clays and sesquioxides (Boccheciamamp, 1978; Murphy and others, 1998; White and others, 1998). Huffaker (2002) contends that the granitic rocks weather more rapidly than the volcanic rocks, and that if other conditions are equal, the regolith overlying the granitic rocks is thicker than that in volcanic areas. The Río Blanco quartz diorite, which underlies the Iacos watershed, has been the subject of extensive studies on chemical weathering rates (including White and Blum, 1995; Dong and others,

1998; Murphy and others, 1998; White and others, 1998; Schulz and White, 1999; Turner and others, 2003; Buss and others, 2005, 2008, 2009; Fletcher and others, 2006; Pett-Ridge and others, 2009; Minyard and others, 2011; Buss and White, 2012). The relatively young age of the Río Blanco quartz diorite, combined with high rainfall and temperature, results in the Iacos watershed having one of the highest documented chemical weathering rates of granitic rocks in the world (White and Blum, 1995; White and others, 1998). The weathering front has been estimated to proceed about 1 centimeter (cm) per 100 years on the basis of cosmogenic evidence (Brown and others, 1995). Stallard (1995) argues that minerals such as intergranular calcite and volatiles in fluid inclusions derived from the late-stage cooling of magma greatly enhance the susceptibility of younger plutons, such as the Río Blanco quartz diorite, to weathering, compared with identical rock types of Precambrian age, where volatiles have migrated out and late-stage minerals have recrystallized. The transition between the quartz-diorite bedrock and saprolite consists of a 20- to 60-cm-thick zone characterized by fracture-bound concentric shells, termed rindlets (Turner and others, 2003; Fletcher and others, 2006; Buss and others, 2008; Buss and White, 2012). The majority of weathering in the watershed occurs in this transition zone, as individual rindlets become progressively more altered away from joint planes. The San Lorenzo granodiorite-quartz diorite, which underlies the Cayaguás watershed, has not been well studied, but because of its similar composition and age it presumably weathers in a comparable manner.

On hillslopes, saprolite is overlain by 0.5–2 m of soil, which is typically sandy and loamy, with a thin, organic-rich A horizon and a layer of translocated clays concentrated in the B horizon (Simon and others, 1990; Huffaker, 2002). Soil thickness on ridges in the Iacos watershed has been observed to be more than ten-fold greater (Simon and others, 1990). Soils on the granitic rocks have higher permeability and infiltration rates than those on the volcaniclastic rocks, allowing greater water infiltration (Simon and others, 1990). The coarse soil is easily eroded and is highly susceptible to landslides when subjected to intensive agricultural activity or other disturbance (Larsen, 2012).

Soils overlying the Río Blanco quartz diorite in the Iacos watershed primarily consist of Picacho and Utuado loamy soils. These Inceptisols are very deep (greater than 150 cm) and somewhat poorly drained (Huffaker, 2002). The Iacos flood plain and low terraces at middle elevations are overlain by the Iacos loam, an Inceptisol which is very deep (greater than 150 cm) and somewhat poorly drained. Quartz persists through the entire profile, becoming more fine grained nearer the surface (Brown and others, 1995).

Soils at the highest elevations in the Cayaguás watershed consist primarily of the Lirios silty clay loam, which is a well-drained Ultisol (Boccheciamamp, 1978). Soils at lower elevations primarily consist of the Pandura sandy loam, an Inceptisol. Owing to past agricultural cultivation, both of these soils have lost much of their original surface layers through erosion. By using geomorphic evidence, Larsen

and Santiago-Román (2001) estimate that the surface of the Cayaguás basin has been lowered an average of 660 mm since about 1820, comparable to the 500 mm of surface-lowering estimated by using cosmogenic Be¹⁰ (Brown and others, 1998).

Vegetation and Land Use

All of the natural ecological life zones of Puerto Rico (as developed by Ewel and Whitmore, 1973) are forest (fig. 7). Three life zones dominate the island: subtropical moist forest (58 percent of the main island), subtropical wet forest (23 percent), and subtropical dry forest (18 percent) (Birdsey and Weaver, 1982). Subtropical rain forest, lower montane wet forest, and lower montane rain forest occupy a little more than 1 percent of the island at high elevations, including most of the Mameyes and Icacos watersheds. Historical accounts suggest that, like many other Caribbean islands, Puerto Rico was heavily forested (about 95 percent) prior to European

settlement (Wadsworth, 1950; Birdsey and Weaver, 1982). The island's diverse physiography and tropical location result in diverse flora and fauna and a high level of endemism (Gould and others, 2008); however, plant diversity is lower than that at mainland tropical sites (Ashton and others, 2004).

In the 16th century, European settlers began clearing forests for pasture, cropland, timber, and fuel. By 1828, forest covered about 66 percent of Puerto Rico (Wadsworth, 1950). Pressure on land resources increased in the 19th and 20th centuries owing to population growth, expanding production of sugar cane and coffee, economic depression, and the effects of several severe hurricanes. By the late 1940s, forest cover of Puerto Rico had declined to 6 percent; cropland and pasture each accounted for about 42 percent of land cover; the remaining 10 percent contained urban areas and wasteland (Koenig, 1953; Birdsey and Weaver, 1982). During this period, Puerto Rico was one of the most severely deforested regions in the world. Soil erosion related to this deforestation released high loads of sediment from hillslopes to footslopes, valley floors,

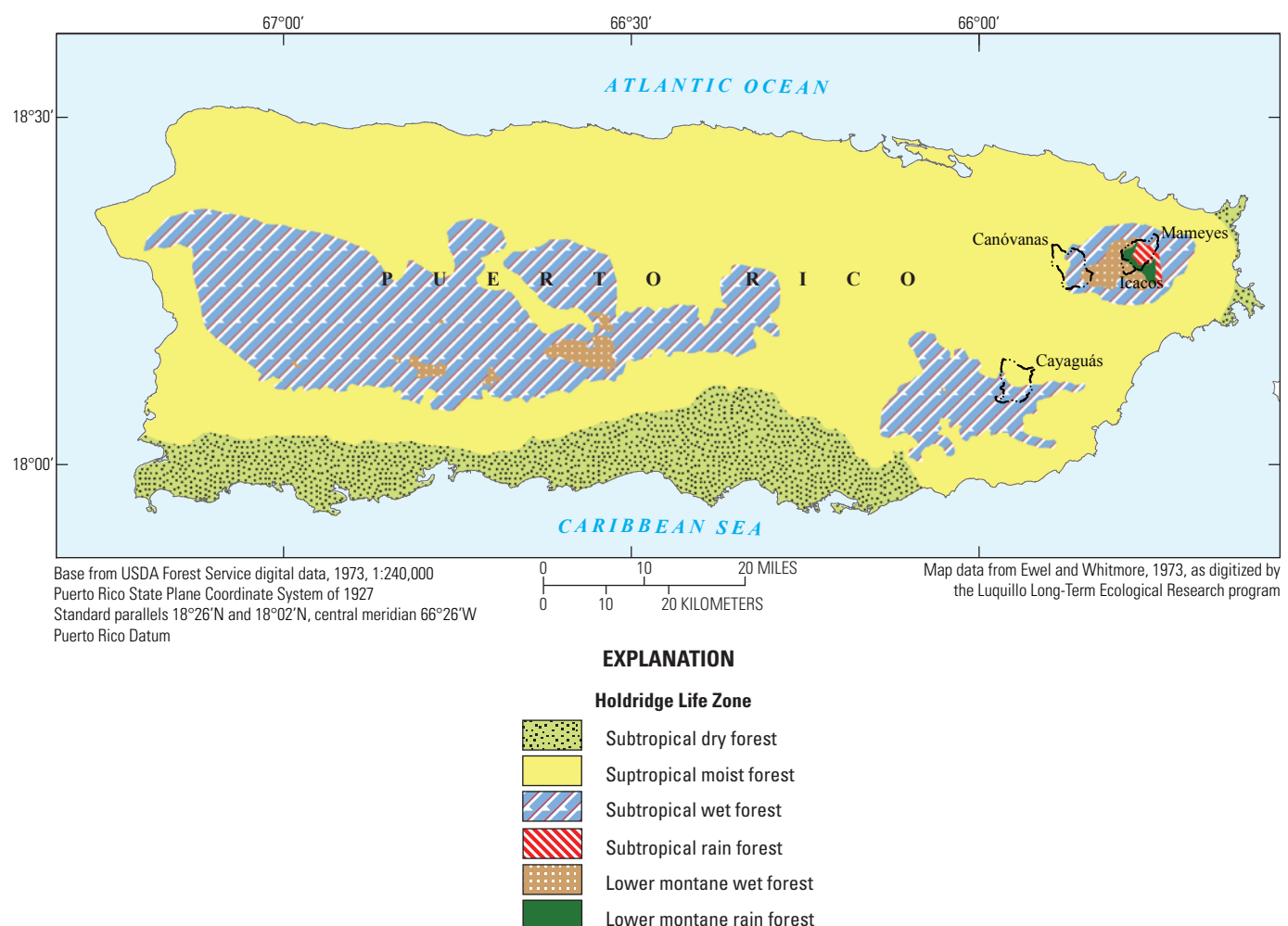


Figure 7. Ecological life zones of Puerto Rico (from Luquillo Long-Term Ecological Research program; digitized from Ewel and Whitmore, 1973).

and streams channels (Larsen, 2012). Much of the remaining forest was in the Luquillo Mountains, because access to this area was limited by steep slopes, high annual rainfall, and its designation as a reserve by the Spanish crown in 1876 and later by the U.S. Government (Zimmerman and others, 1995).

A shift in Puerto Rico's economic base that began in the late 1940s, partly as a result of the U.S. Government's "Operation Bootstrap," led to reforestation (Rudel and others, 2000). In 1934, about 43 percent of the island's gross national product came from agriculture but only 7 percent from industry; by 1996, agriculture and industry contributed 1 percent and 41 percent respectively to the gross national product (López and others, 2001). As Puerto Ricans moved from rural areas to cities on the island or migrated to the United States, agricultural land cover in Puerto Rico declined by 95 percent from 1951 to 2000 (Kennaway and Helmer, 2007). Much of this abandoned land reverted to forest. By 1980, forest cover of Puerto Rico had increased to 31 percent (Franco and others, 1997). In 2003, forest, woodland, and shrubland represented about 44 percent of land area (Gould and others, 2012) (figs. 8 and 9).

Meanwhile, population density of Puerto Rico has increased more than threefold during the last century,

resulting in one of the highest densities in the world: more than 400 people/km² (López and others, 2001). Puerto Rico now has the highest road density of any Caribbean island, 2.5 km of paved roads per square kilometer (Lugo, 1996). On the basis of population density and remote sensing of developed areas, about 16 percent of the island is considered urban land use, 50 percent is suburban, and 34 percent is rural (Martinuzzi and others, 2007). Eleven percent of the island has developed surface, and about 60 percent of this surface corresponds with high-density development (Martinuzzi and others, 2007). In the San Juan metropolitan area, filling of the mangroves and mudflats has restricted circulation and impaired water quality (Webb and Gómez-Gómez, 1998). Land has been converted to urban uses mostly in lowland regions and on lesser slopes.

Land Cover of Forested Watersheds

The four study watersheds were selected, in part, for differing land cover. The Icacos watershed is almost entirely covered by mature montane wet evergreen forest, which

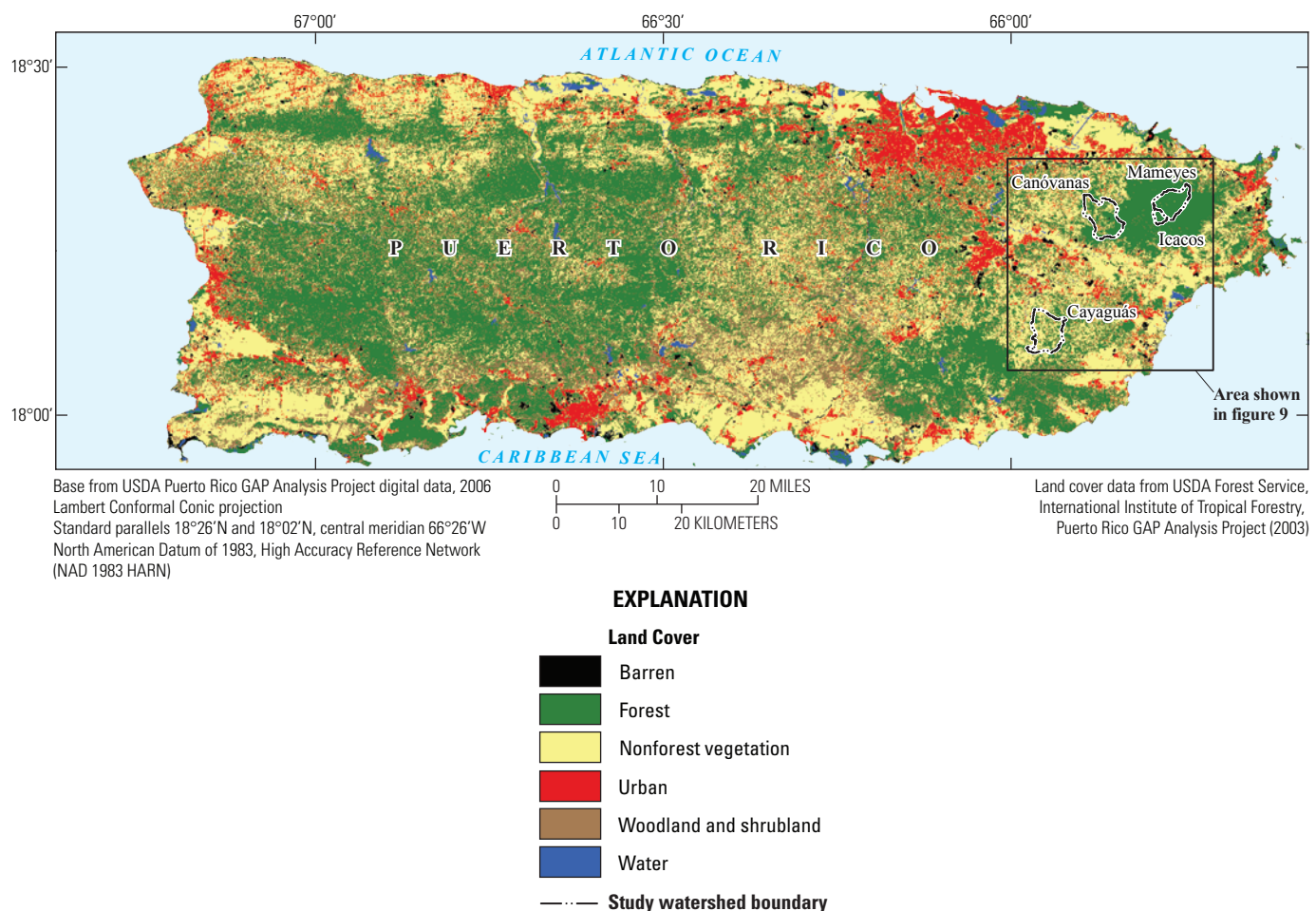


Figure 8. Generalized land cover of Puerto Rico in 2003 (from Gould and others, 2008).

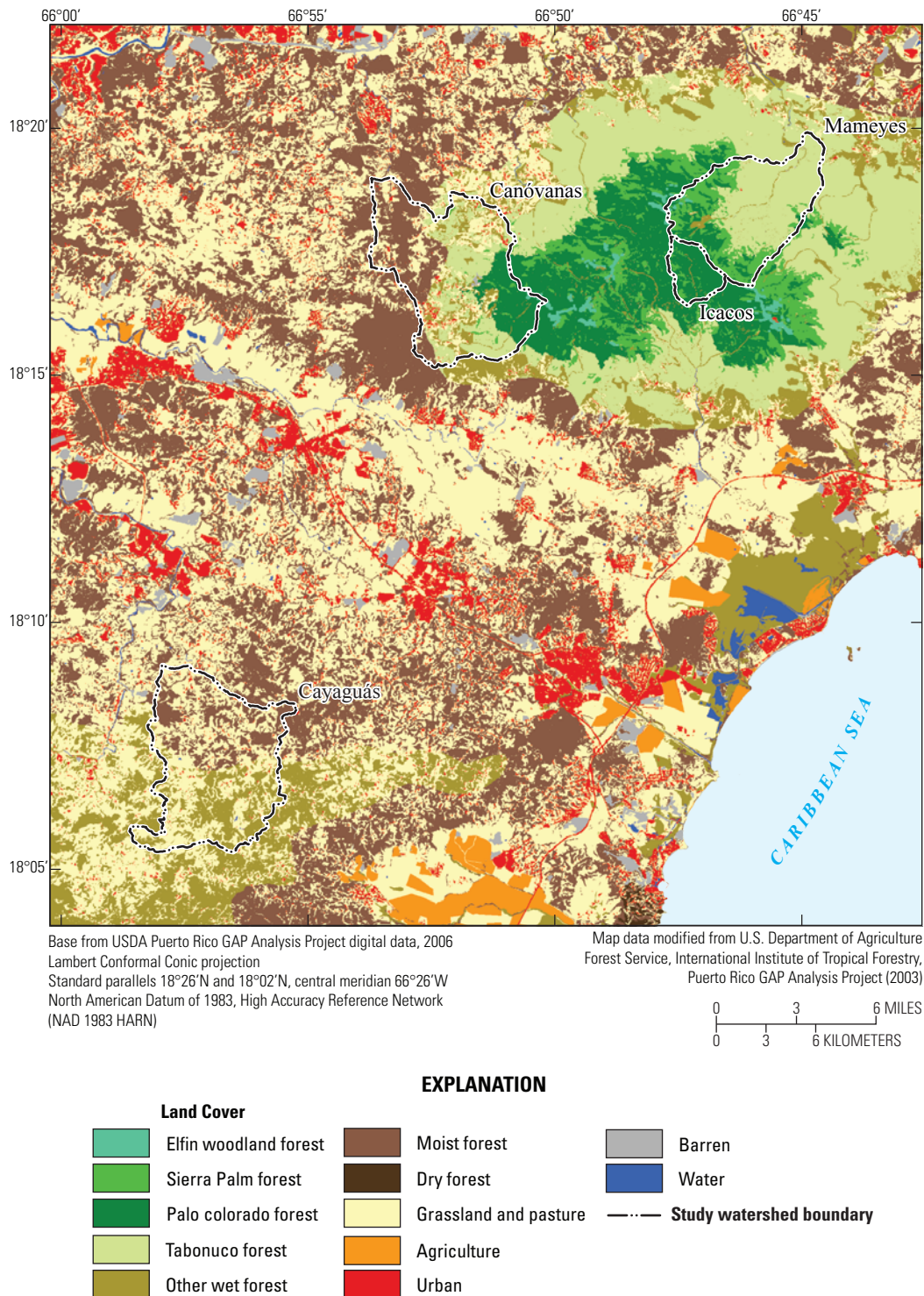


Figure 9. Detailed land cover of study watersheds in 2003 (from Gould and others, 2008).

includes about 85 percent palo colorado forest, 13 percent sierra palm forest, and 2 percent other montane wet forest (Gould and others, 2008) (fig. 9; table 4). Prominent trees are palo colorado (*Cyrilla racemiflora*), caititillo (*Micromelis garciniaefolia*, *M. chrysophylloides*), and laurel sabino (*Magnolia splendens*) (Foster and others, 1999). The Mameyes watershed also consists primarily of mature montane wet evergreen forest, but it is larger and has a much greater variation in elevation than the Icacos watershed, and thus it has more varied forest. Land cover is about 57 percent tabonuco forest, 25 percent sierra palm forest, 14 percent palo colorado forest, 1 percent elfin woodland, and 2 percent other montane wet forest (Gould and others, 2008, 2012) (table 4). Above 600 m, vegetation in the Mameyes watershed is primarily palo colorado and sierra palm forest. Elfin woodland, characterized by short, slow-growing vegetation, develops on ridges above 900 m elevation (Weaver, 1986, 1989, 1990). Elevations below 600 m are primarily tabonuco forest. This forest is dominated by the tabonuco tree (*Dacryodes excelsa*), but 170 tree species have been described for this forest type (Foster and others, 1999).

Forest cover in much of the Icacos and Mameyes watersheds persisted during the nadir of forest cover in Puerto Rico in the 1940s, and those watersheds have maintained a continuous forest canopy since that time (table 4). As discussed above, steep topography, harsh conditions, and governmental protection limited access for development or forest conversion. Although the Luquillo Mountains were less affected by development than other areas of Puerto Rico, they are not pristine; cattle production, shade coffee, timber extraction, subsistence farming, and charcoal production were practiced in the late 1800s and in the 1900s, primarily below 600 m elevation. The USDA Forest Service purchased much of the lower-elevation land in the Luquillo Mountains in the 1930s (Zimmerman and others, 1995). Nonnative bamboo was introduced from Asia in the 1930s and 1940s along roads to stabilize slopes; however, during major disturbances such as hurricanes, extensive bamboo root systems can actually help cause catastrophic slope failures (O'Connor and others, 2000). Bamboo is expanding downstream in streams within the Mameyes watershed at a rate of 8 meters per year (O'Connor and others, 2000). Large stands of bamboo are observed in the Mameyes and Icacos watersheds, especially near roads.

Land Cover of Developed Watersheds

In the Canóvanas watershed, land cover is currently about 71 percent forest, 26 percent grassland or pasture, and 3 percent urban (Gould and others, 2008) (table 4). Above 600 m elevation, land cover is primarily palo colorado forest, similar to the Icacos and Mameyes watersheds (fig. 9, table 4). Between 400 and 600 m, land cover is primarily tabonuco forest and grassland or pasture. Below 400 m, land cover is primarily secondary lowland moist forest and grassland or pasture. The Canóvanas watershed has a mixed land-use history. Elevations above 600 m were forested in

the middle 20th century, but most of the lower watershed was used for pasture, coffee, and fruit crops, and to a lesser degree, bananas and sugar cane (Kennaway and Helmer, 2007). Between the 1950s and the 1970s, the predominant land cover shifted from agriculture and pasture to forest, and forest cover in the watershed increased by 44 percent (table 4). These decades correspond with a low point in population density of the Cubuy barrio, which is entirely within the Canóvanas watershed and represents the majority of the land area in the watershed (fig. 10). Current population density has returned to that of the 1950s, but land use is predominantly residential as opposed to agricultural (Martinuzzi and others, 2007; Parés-Ramos and others, 2008).

Current land cover in the Cayaguás watershed is 57 percent pasture, 41 percent forest or shrubland (primarily lowland moist forest and montane wet forest) and 2 percent urban (fig. 9, table 4). Fifty years ago, the Cayaguás watershed was almost entirely devoted to agricultural activities, such as pasture, fruit crops, and tobacco (Kennaway and Helmer, 2007). Forest cover has increased about 20 percent since the late 1970s, primarily at the expense of pasture and grasslands (table 4). Population densities in the Quebrada Arenas barrio, which is entirely within the Cayaguás watershed and represents most of the land area in the watershed, reached a low point in the 1980 census (fig. 10). Population has since been rising owing to increased residential land use (Martinuzzi and others, 2007; Parés-Ramos and others, 2008).

Summary

Four watersheds in eastern Puerto Rico have been studied since 1991 as part of the U.S. Geological Survey's Water, Energy, and Biogeochemical Budget program. These watersheds differ in geology, soils, and land cover. The Icacos watershed is underlain by granitic rock, which weathers to quartz- and clay-rich, sandy soils. Land cover is primarily old-growth wet forest, and human disturbance has been minimal. The Mameyes watershed is primarily underlain by volcaniclastic rock, which weathers to quartz-poor, fine-grained soils. This watershed also contains largely old-growth wet forest. The Canóvanas watershed is underlain by volcaniclastic rocks and soils that are similar to those in the Mameyes, but historical agricultural practices at lower elevations have led to substantial erosion of soils. This watershed has largely reforested since the 1950s. The Cayaguás watershed is underlain by granitic rock; this watershed was also historically used for agriculture and has been deeply eroded. It has undergone some reforestation since the 1970s. Past soil erosion in the Canóvanas and Cayaguás watersheds released high loads of sediment from hillslopes to footslopes, valley floors, and stream channels. The reforestation of these watersheds, and of Puerto Rico, may serve as a prototype for the hydrological and chemical response of other tropical areas that are shifting from an agricultural to an industrial economy.

Table 4. Land cover and land-cover dynamics in study watersheds, eastern Puerto Rico.

[Land-cover dynamics are indicated as percentage increase or decrease from 1936, 1950 (Lugo and others, 2004), and 1977 (Ramos and Lugo, 1994) for woody (forest, shrubland, and woodland), herbaceous (grassland, pastures, agriculture), and developed areas. In 1936 and 1950, the Cayaguás watershed was primarily agricultural and nonforested. --, not analyzed]

Land cover type	Icacos			Maneves			Canóvanas			Cayaguás			
	2003		Percent change since 1936	2003		Percent change since 1936	2003		Percent change since 1936	2003		Percent change since 1936	
	land cover ¹	percent	1950	1977	land cover	1950	1977	land cover	1950	1977	land cover	1950	
Woody	99.9	0	0	99.6	1	0	71.3	47	44	2	41.7	--	
Palo Colorado forest	85.4	--	--	13.9	--	--	14.2	--	--	--	0.00	--	
Sierra palm forest	12.7	--	--	25.3	--	--	1.60	--	--	--	0.00	--	
Elfin woodland	0.00	--	--	1.07	--	--	0.38	--	--	--	0.00	--	
Tabonuco forest	0.00	--	--	57.0	--	--	24.5	--	--	--	0.00	--	
Other montane wet forest, shrubland, woodland	1.84	--	--	2.36	--	--	10.4	--	--	--	21.5	--	
Lowland moist forest, shrubland, woodland	0.00	--	--	0.00	--	--	20.2	--	--	--	19.8	--	
Abandoned and active coffee plantations	0.00	--	--	0.00	--	--	0.00	--	--	--	0.37	--	
Herbaceous	0.15	0	0	0.32	-1	0	0	25.68	-41	-48	3	56.7	--
Moist grasslands and pastures	0.15	--	--	0.32	--	--	25.68	--	--	--	56.7	--	
Developed	0.00	0	0	0.02	0	0	2.79	3	3	-4	1.55	--	
Low-density urban development	0.00	--	--	0.02	--	--	2.79	--	--	--	1.55	--	
Other	0.00	0	0	0.05	0	0	0.25	0	0	0	0.08	--	
Baren	0.00	--	--	0.04	--	--	0.25	--	--	--	0.00	--	
Freshwater	0.00	--	--	0.004	--	--	0.00	--	--	--	0.08	--	
Total	100			100			100			100		100	

¹From Gould and others, 2008.

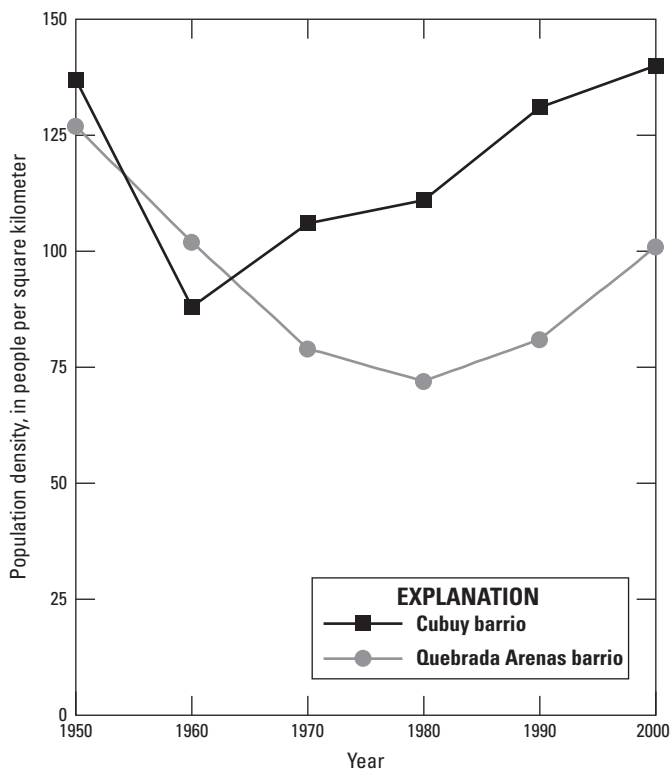


Figure 10. Population density in the Cubuy barrio (in Canóvanas watershed) and the Quebrada Arenas barrio (in Cayaguás watershed) (from U.S. Census, 2000).

Acknowledgments

This chapter was greatly improved by reviews by John F. Walker and Richard M.T. Webb of the U.S. Geological Survey and F.N. Scatena of the University of Pennsylvania.

References

- American Geological Institute, 1976, Dictionary of geological terms: Garden City, N.Y., Anchor Press. 472 p.
- Ashton, P.S., and CTFS Working Group, 2004, Floristics and vegetation of the forest dynamics plots, in Losos, E.C., and Leigh, E.G. Jr., eds., Tropical forest diversity and dynamism—Findings from a large-scale plot network: Chicago, Ill., The University of Chicago Press, p. 90–102.
- Baedecker, M.J., and Friedman, L.C., 2000, Water, energy, and biogeochemical budgets—A watershed research program: U.S. Geological Survey Fact Sheet 165–99, 4 p.
- Bawiec, W. J., 1998, Geology, geochemistry, geophysics, mineral occurrences, and mineral resource assessment for the commonwealth of Puerto Rico: U.S. Geological Survey Open-File Report 98–38, CD-ROM.
- Birdsey, R.A., and Weaver, P.L., 1982, The forest resources of Puerto Rico: U.S. Department of Agriculture Forest Service, Southern Forest Experiment Station, Resources Bulletin SO–85, 65 p.
- Boccheciampi, R.A., 1977, Soil survey of the Humacao area of eastern Puerto Rico: U.S. Department of Agriculture Soil Conservation Service, 103 p.
- Boccheciampi, R.A., 1978, Soil survey of San Juan area of Puerto Rico: U.S. Department of Agriculture Soil Conservation Service, 141 p.
- Briggs, R.P., 1973, The Lower Cretaceous Figuera Lava and Fajardo Formation in the stratigraphy of northeastern Puerto Rico: U.S. Geological Survey Bulletin 1372–G, 10 p.
- Briggs, R.P., and Aguilar-Cortés, E., 1980, Geologic map of the Fajardo and Cayo Icacos quadrangles, Puerto Rico: U.S. Geological Survey Miscellaneous Geologic Investigations Map I–1153, scale 1:20,000, 1 sheet.
- Broedel, C.H., 1961, Preliminary geologic map showing iron and copper prospects in the Juncos quadrangle, Puerto Rico: U.S. Geological Survey Miscellaneous Geologic Investigations Map I–326.
- Brown, E.T., Stallard, R.F., Larsen, M.C., Bour, D.L., Raisbeck, G.M., and Yiou, F., 1998, Pre-anthropogenic denudation rates of a perturbed watershed (Cayaguás River, Puerto Rico) estimated from in-situ-produced ^{10}Be in river-borne quartz: Earth and Planetary Science Letters, v. 160, p. 723–728.
- Brown, E.T., Stallard, R.F., Larsen, M.C., Raisbeck, G.M., and Yiou, F., 1995, Denudation rates based on accumulation of in-situ-produced ^{10}Be compared with watershed mass balance results in the Luquillo Experimental Forest, Puerto Rico: Earth and Planetary Science Letters, v. 129, p. 193–202.
- Brown, Sandra, Lugo, A.E., Silander, Susan, and Liegel, Leon, 1983, Research history and opportunities in Luquillo Experimental Forest: U.S. Department of Agriculture Forest Service, Southern Forest Experimental Station, New Orleans, LA, General Technical Report SO–44, 128 p.
- Buss, H.L., Bruns, M.A., Schultz, M.J., Moore, J., Mathur, C.F., and Brantley, S.L., 2005, The coupling of biological iron cycling and mineral weathering during saprolite formation, Luquillo Mountains, Puerto Rico: Geobiology, v. 3, p. 247–260.
- Buss, H.L., Mathur, R., White, A.F., and Brantley, S.L., 2009, Phosphorous and iron cycling in deep saprolite, Luquillo Mountains, Puerto Rico: Chemical Geology, v. 269, p. 52–61.

- Buss, H.L., Sak, P.B., Webb, S.M., and Brantley, S.L., 2008, Weathering of the Rio Blanco quartz diorite, Luquillo Mountains, Puerto Rico—Coupling oxidation, dissolution, and fracturing: *Geochimica et Cosmochimica Acta*, v. 72, p. 4488–4507.
- Buss, H.L., and White, A.F., 2012, Weathering processes in the Río Icacos and Río Mameyes watersheds in eastern Puerto Rico, ch. I in Murphy, S.F., and Stallard, R.F., eds., Water quality and landscape processes of four watersheds in eastern Puerto Rico: U.S. Geological Survey Professional Paper 1789, p. 249–262.
- Calvesbert, R.J., 1970, Climate of Puerto Rico and the U.S. Virgin Islands: U.S. Department of Commerce, Climatology of the United States 60–52, 29 p.
- Cardona, W.A., 1984, El Yunque mineral prospects, eastern Puerto Rico: Caribbean Journal of Science, v. 20, p. 79–87.
- Díaz, P.L., Aquino, Zaida, Figueroa-Alamo, Carlos, García, René, and Sánchez, A.V., 2004, Water resources data for Puerto Rico and the U.S. Virgin Islands, water year 2002: U.S. Geological Survey Water-Data Report PR-02-1, 652 p.
- Dong, Hailiang, Peacor, D.R., and Murphy, S.F., 1998, TEM study of progressive alteration of igneous biotite to kaolinite throughout a weathered soil profile: *Geochimica et Cosmochimica Acta*, v. 62, p. 1881–1887.
- Ewel, J.J., and Whitmore, J.L., 1973, The ecological life zones of Puerto Rico and the Virgin Islands: U.S. Department of Agriculture Forest Service, Institute of Tropical Forestry, Research Paper ITF-18, Río Piedras, Puerto Rico, 72 p.
- Fletcher, R.C., Buss, H.L., and Brantley, S.L., 2006, A spheroidal weathering model coupling porewater chemistry to soil thickness during steady-state denudation: *Earth and Planetary Science Letters*, v. 244, p. 444–457.
- Foster, D.R., Fluet, M., and Boose, E.R., 1999, Human or natural disturbance—Landscape-scale dynamics of the tropical forests of Puerto Rico: *Ecological Applications*, v. 9, p. 555–572.
- Franco, P.A., Weaver, P.L., and Eggen-McIntosh, S., 1997, Forest resources of Puerto Rico, 1990: U.S. Department of Agriculture Forest Service, Southern Research Station, Ashville, NC, Resource Bulletin SRS-22, 45 p.
- González, Grizelle, Zou, Xiaoming, and Borges, Sonia, 1996, Earthworm abundance and species composition in abandoned tropical croplands—Comparisons of tree plantations and secondary forests: *Pedobiologia*, v. 40, p. 385–391.
- Gould, W.A., Alarcón, C., Fevold, B., Jiménez, M.E., Martinuzzi, Sebastian, Potts, G., Quiñones M., Solórzano, M., and Ventosa, E., 2008, The Puerto Rico Gap Analysis Project, vol. 1, Land cover, vertebrate species distributions, and land stewardship: U.S. Department of Agriculture Forest Service, International Institute of Tropical Forestry, Río Piedras, Puerto Rico, General Technical Report IITF-GTR-39, 165 p.
- Gould, W.A., Martinuzzi, Sebastian, and Parés-Ramos, I.K., 2012, Land use, population dynamics, and land-cover change in eastern Puerto Rico, ch. B in Murphy, S.F., and Stallard, R.F., eds., Water quality and landscape processes of four watersheds in eastern Puerto Rico: U.S. Geological Survey Professional Paper 1789, p. 25–42.
- Huffaker, Loren, 2002, Soil survey of Caribbean National Forest and Luquillo Experimental Forest, Commonwealth of Puerto Rico: U.S. Department of Agriculture Natural Resources Conservation Service, Washington, D.C., 181 p.
- Jolly, W.T., Lidiak, E.G., Schellekens, J.H., and Santos, J., 1998, Volcanism, tectonic and stratigraphic correlations in Puerto Rico, in Lidiak, E.G., and Larue, D.K., eds., Tectonics and geochemistry of the northeastern Caribbean: Geological Society of America Special Paper 322, p. 1–34.
- Kennaway, T., and Helmer, E.H., 2007, The forest types and ages cleared for land development in Puerto Rico: *GIScience and Remote Sensing*, v. 44, p. 356–382.
- Koenig, Nathan, 1953, A comprehensive agricultural program for Puerto Rico: Washington, D.C., U.S. Department of Agriculture and Commonwealth of Puerto Rico, 290 p.
- Larsen, M.C., 1997, Tropical geomorphology and geomorphic work—A study of geomorphic processes and sediment and water budgets in montane humid-tropical forested and developed watersheds, Puerto Rico: Boulder, University of Colorado Geography Department, Ph.D. dissertation, 341 p.
- Larsen, M.C., 2012, Landslides and sediment budgets in four watersheds in eastern Puerto Rico, ch. F in Murphy, S.F., and Stallard, R.F., eds., Water quality and landscape processes of four watersheds in eastern Puerto Rico: U.S. Geological Survey Professional Paper 1789, p. 153–178.
- Larsen, M.C., Collar, P.D., and Stallard, R.F., 1993, Research plan for the investigation of water, energy, and biogeochemical budgets in the Luquillo mountains, Puerto Rico: U.S. Geological Survey Open-File Report 92-150, 19 p.
- Larsen, M.C., and Santiago-Román, A., 2001, Mass wasting and sediment storage in a small montane watershed—An extreme case of anthropogenic disturbance in the humid tropics, in Dorava, J.M., Palcsak, B.B., Fitzpatrick, F., and Montgomery, D., eds., *Geomorphic processes and riverine habitat*: American Geophysical Union Monographs, Water Science & Application Series, v. 4, p. 119–138.
- Larsen, M.C., and Stallard, R.F., 2000, Water, energy, and biogeochemical budgets, Luquillo Mountains, Puerto Rico: U.S. Geological Survey Fact Sheet 163-99, 4 p.

22 Water Quality and Landscape Processes of Four Watersheds in Eastern Puerto Rico

- Larsen, M.C., Torres-Sánchez, A.J., and Concepción, I.M., 1999, Slopewash, surface runoff, and fine-litter transport in forest and landslide scars in humid-tropical steeplands, Luquillo Experimental Forest, Puerto Rico: Earth Surface Processes and Landforms, v. 24, p. 481–502.
- Lewis, L.A., 1974, Slow movement of earth under tropical rain forest conditions: *Geology*, v. 2, p. 9–10.
- López, T.M., Aide, T.M., and Thomlinson, J.R., 2001, Urban expansion and the loss of prime agricultural lands in Puerto Rico: *Ambio*, v. 30, p. 49–54.
- Lugo, A.E., 1996, Caribbean island landscapes—Indicators of the effects of economic growth on the region: *Environment and Development Economics*, v. 1, p. 128–136.
- Lugo, A.E., López, T.M., Ramos González, O.M., and Velez, L.L., and others, 2004, *Urbanización de los terrenos en la periferia de El Yunque*: U.S. Department of Agriculture Forest Service Report WO–66, 29 p.
- Martinuzzi, Sebastian, Gould, W.A., and Ramos González, O.M., 2007, Land development, land use, and urban sprawl in Puerto Rico—Integrating remote sensing and population census data: *Landscape and Urban Planning*, v. 79, p. 288–297.
- McDowell, W.H., Bowden, W.B., and Asbury, C.E., 1992, Riparian nitrogen dynamics in two geomorphologically distinct tropical rain forest watersheds—Subsurface solute patterns: *Biogeochemistry*, v. 18, p. 53–75.
- Meyerhoff, H.A., 1931, The geology of the Fajardo district, Porto Rico: New York Academy of Sciences, Scientific survey of Porto Rico and the Virgin Islands, v. II, pt. 3, p. 201–360.
- M'Gonigle, J.W., 1978, Geologic map of the Humacao quadrangle, Puerto Rico: U.S. Geological Survey Miscellaneous Investigations Series Map I–1070, scale 1:20,000.
- M'Gonigle, J.W., 1979, Geologic map of the Naguabo and part of the Punta Puerca quadrangles, Puerto Rico: U.S. Geological Survey Miscellaneous Investigations Series Map I–1099, scale 1:20,000.
- Minyard, M.L., Bruns, M.A., Martinez, C.E., Liemann, L.J., Buss, H.L., and Brantley, S.L., 2011, Halloysite nanotubes and bacteria at the saprolite-bedrock interface, Rio Icacos watershed, Puerto Rico: *Soil Science Society of America Journal*, v. 75, p. 348–356.
- Murphy, S.F., Brantley, S.L., Blum, A.E., White, A.F., and Dong, H., 1998, Chemical weathering in a tropical watershed, Luquillo Mountains, Puerto Rico II—Rate and mechanism of biotite weathering: *Geochimica et Cosmochimica Acta*, v. 62, p. 227–243.
- Murphy, S.F., and Stallard, R.F., 2012, Hydrology and climate of four watersheds in eastern Puerto Rico, ch. C in Murphy, S.F., and Stallard, R.F., eds., *Water quality and landscape processes of four watersheds in eastern Puerto Rico: U.S. Geological Survey Professional Paper 1789*, p. 43–84.
- O'Connor, P.J., Covich, A.P., Scatena, F.N., and Loope, L.L., 2000, Nonindigenous bamboo along headwater streams of the Luquillo Mountains, Puerto Rico—Leaf fall, aquatic leaf decay and patterns of invasion: *Journal of Tropical Ecology*, v. 16, p. 499–516.
- Parés-Ramos, I.K., Gould, W.A., and Aide, T.M., 2008, Agricultural abandonment, suburban growth, and forest expansion in Puerto Rico between 1991 and 2000: *Ecology and Society*, v. 13, no. 2; p. 1. Last accessed on September 18, 2008 at <http://www.ecologyandsociety.org/vol13/iss2/art1/>
- Pett-Ridge, J.C., Derry, L.A., and Kurtz, A.C., 2009, Sr isotopes as a tracer of weathering processes and dust inputs in a tropical granitoid watershed, Luquillo Mountains, Puerto Rico: *Geochimica et Cosmochimica Acta*, v. 73, p. 25–43.
- Ramos, O.M., and Lugo, A.E., 1994, Mapa de la vegetación de Puerto Rico: *Acta Científica*, v. 8, p. 63–66.
- Ramos-Ginés, Orlando, 1999, Estimation of magnitude and frequency of floods for streams in Puerto Rico—New empirical models: U.S. Geological Survey Water-Resources Investigations Report 99–4142, 41 p.
- Rogers, C.L., Cram, C.M., Pease, M.H., and Tischler, M.S., 1979, Geologic map of the Yabucoa and Punta Tuna quadrangles, Puerto Rico: U.S. Geological Survey Miscellaneous Investigations Map I–1086, scale 1:20,000.
- Rudel, T.K., Perez-Lugo, M., and Zichal, H., 2000, When fields revert to forest—Development and spontaneous reforestation in postwar Puerto Rico: *Professional Geographer*, v. 52, p. 386–397.
- Scatena, F.N., 1989, An introduction to the physiography and history of the Bisley experimental watersheds in the Luquillo Mountains of Puerto Rico: U.S. Department of Agriculture General Technical Report SO–72, 22 p.
- Schellekens, Jaap, Scatena, F.N., Bruijnzeel, L.A., van Dijk, A.I.J.M., Groen, M.M.A., and van Hogenzand, R.J.P., 2004, Stormflow generation in a small rainforest catchment in the Luquillo Experimental Forest, Puerto Rico: *Hydrological Processes*, v. 18, p. 505–530.
- Schulz, M.S., and White, A.F., 1999, Chemical weathering in a tropical watershed, Luquillo Mountains, Puerto Rico III—Quartz dissolution rates: *Geochimica et Cosmochimica Acta*, v. 63, p. 337–350.
- Seiders, V.M., 1971a, Cretaceous and lower Tertiary stratigraphy of the Gurabo and El Yunque quadrangles, Puerto Rico: U.S. Geological Survey Bulletin 1294–F, 58 p., 1 pl.

- Seiders, V.M., 1971b, Geologic map of the El Yunque Quadrangle, Puerto Rico. U.S. Geological Survey Miscellaneous Geological Investigations Map I-658, scale 1:20,000.
- Seiders, V.M., 1971c, Geologic map of the Gurabo quadrangle, Puerto Rico: U.S. Geological Survey Miscellaneous Geological Investigations Map I-657, scale 1: 20,000.
- Simon, Andrew, Larsen, M.C., and Hupp, C.R., 1990, The role of soil processes in determining mechanisms of slope failure and hillslope development in a humid-tropical forest, eastern Puerto Rico, in Kneuper, P.L.K., and McFadden, L.D., eds., Soils and landscape evolution: Geomorphology, v. 3, p. 263–286.
- Smith, A.L., Schellekens, J.H., and Muriel Díaz, A.-L., 1998, Batholiths as markers of tectonic change in the northeastern Caribbean: Geological Society of America Special Paper, v. 322, p. 99–122.
- Stallard, R.F., 1995, Relating chemical and physical erosion, in White, A.F., and Brantley, S.L., eds., Chemical weathering rates of silicate minerals: Washington, D.C., Mineralogical Society of America Reviews in Mineralogy, v. 31, p. 543–564.
- Stallard, R.F., 2012, Weathering, landscape equilibrium, and carbon in four watersheds in eastern Puerto Rico, ch. H in Murphy, S.F., and Stallard, R.F., eds., Water quality and landscape processes of four watersheds in eastern Puerto Rico: U.S. Geological Survey Professional Paper 1789, p. 199–248.
- Stallard, R.F., and Murphy, S.F., 2012, Water quality and mass transport in four watersheds in eastern Puerto Rico, ch. E in Murphy, S.F., and Stallard, R.F., eds., Water quality and landscape processes of four watersheds in eastern Puerto Rico: U.S. Geological Survey Professional Paper 1789, p. 113–152.
- Turner, B.F., Stallard, R.F., and Brantley, S.L., 2003, Investigation of in situ weathering of quartz diorite bedrock in the Río Icacos Basin, Luquillo Experimental Forest, Puerto Rico: Chemical Geology, v. 202, p. 313–341.
- U.S. Census Bureau, 2000, United States Census 2000: last accessed on April 2, 2011 at <http://www.census.gov/main/www/cen2000.html>
- U.S. Geological Survey, 1967, El Yunque quadrangle, Puerto Rico: U.S. Geological Survey topographic map, 7.5 minute series, 1 sheet.
- Wadsworth, F.H., 1950, Notes on the climax forests of Puerto Rico and their destruction and conservation prior to 1990: Caribbean Forester, v. 11, p. 38–56.
- Wadsworth, F.H., 1970, Review of past research in the Luquillo Mountains of Puerto Rico, in Odum, H.T., and Pigeon, R.F., eds., A tropical rain forest: Springfield, Va., National Technical Information Service, p. B33–B46.
- Weaver, P.L., 1986, Growth and age of *Cyrilla racemiflora* L. in montane forests of Puerto Rico: Interciencia, v. 11, p. 221–227.
- Weaver, P.L., 1989, Rare trees in the Colorado Forest of Puerto Rico's Luquillo Mountains: Natural Areas Journal, v. 9, p. 169–173.
- Weaver, P.L., 1990, Succession in the elfin woodland of the Luquillo Mountains of Puerto Rico: Biotropica, v. 22, p. 83–89.
- Webb, R.M.T., and Gómez-Gómez, F., 1998, Synoptic survey of water quality and bottom sediments, San Juan Bay estuary system, Puerto Rico, December 1994 –July 1995: U.S. Geological Survey Water-Resources Investigations Report 97-4144, 48 p. + appendix.
- White, A.F., and Blum, A.E., 1995, Effects of climate on chemical weathering rates in watersheds: Geochimica et Cosmochimica Acta, v. 59, p. 1729–1747.
- White, A.F., Blum, A.E., Schulz, M.S., Vivit, D.V., Stonestrom, D.A., Larsen, M.C., Murphy, S.F., and Eberl, D.D., 1998, Chemical weathering in a tropical watershed, Luquillo Mountains, Puerto Rico I—Long-term versus short-term weathering fluxes: Geochimica et Cosmochimica Acta, v. 62, p. 209–226.
- Zimmerman, J.K., Aide, T.M., Rosario, M., Serrano, M., and Herrera, L., 1995, Effects of land management and a recent hurricane on forest structure and composition in the Luquillo Experimental Forest, Puerto Rico: Forest Ecology and Management, v. 77, p. 65–76.

Land Use, Population Dynamics, and Land-Cover Change in Eastern Puerto Rico

By William A. Gould, Sebastián Martinuzzi, and Isabel K. Parés-Ramos

Chapter B of
**Water Quality and Landscape Processes of Four Watersheds in
Eastern Puerto Rico**

Edited by Sheila F. Murphy and Robert F. Stallard

Professional Paper 1789–B

**U.S. Department of the Interior
U.S. Geological Survey**

Contents

Abstract.....	29
Introduction.....	29
Land Cover	32
Land Use.....	32
Population Dynamics.....	38
Land-Cover Change.....	38
Conclusion.....	40
Acknowledgments.....	41
References.....	41

Figures

1–4. Maps showing the following:

1. Location of Puerto Rico and study area	30
2. Simplified land cover of eastern Puerto Rico	35
3. Urban, suburban, and rural land-use classes and protected conservation areas in eastern Puerto Rico	36
4. Neighborhood population dynamics in eastern Puerto Rico, 1990 to 2000.....	37
5. Diagram of population trends in land-use categories, 1950 to 2000	35
6. Map of trends in forest, pasture and agriculture, urban, and mangrove extent, 1936–2003, eastern Puerto Rico	39
7. Diagram of trends in forest, pasture and agriculture, urban, and mangrove extent, 1936–2003, eastern Puerto Rico	40

Tables

1. Percentage of land area occupied by watershed, municipality, and national forest areas in eastern Puerto Rico	31
2. Area of land-cover types in eastern Puerto Rico.....	33
3. Area of simplified land cover in eastern Puerto Rico.....	34
4. Urban, suburban (densely populated rural), and rural (sparsely populated rural) land-use classes and protected conservation areas for eastern Puerto Rico	34
5. Land-cover transition matrix of eastern Puerto Rico between 1991 and 2003.....	40

Abbreviations Used in This Report

km	kilometer
km ²	square kilometer
m ²	square meter
mm	millimeter
WEBB	Water, Energy, and Biogeochemical Budgets

Conversion Factors

Multiply	By	To obtain
Length		
millimeter (mm)	0.03937	inch (in.)
kilometer (km)	0.6214	mile (mi)
Area		
square meter (m ²)	10.76	square foot (ft ²)
square kilometer (km ²)	0.3861	square mile (mi ²)

Land Use, Population Dynamics, and Land-Cover Change in Eastern Puerto Rico

By William A. Gould,¹ Sebastián Martinuzzi,² and Isabel K. Parés-Ramos³

Abstract

We assessed current and historic land use and land cover in the Luquillo Mountains and surrounding area in eastern Puerto Rico, including four small subwatersheds that are study watersheds of the U.S. Geological Survey's Water, Energy, and Biogeochemical Budgets (WEBB) program. This region occupies an area of 1,616 square kilometers, about 18 percent of the total land in Puerto Rico. Closed forests occupy about 37 percent of the area, woodlands and shrublands 7 percent, nonforest vegetation 43 percent, urban development 10 percent, and water and natural barrens total less than 2 percent. The area has been classified into three main land-use categories by integrating recent census information (population density per barrio in the year 2000) with satellite image analyses (degree of developed area versus natural land cover). Urban land use (in this analysis, land with more than 20 percent developed cover within a 1-square-kilometer area and population density greater than 500 people per square kilometer) covered 16 percent of eastern Puerto Rico. Suburban land use (more than 80 percent natural land cover, more than 500 people per square kilometer, and primarily residential) covers 50 percent of the area. Rural land use (more than 80 percent natural land cover, less than 500 people per square kilometer, and primarily active or abandoned agricultural, wetland, steep slope, or protected conservation areas) covered 34 percent of the area. Our analysis of land-cover change indicates that in the 1990s, forest cover increased at the expense of woodlands and grasslands. Urban development increased by 16 percent during that time. The most pronounced change in the last seven decades has been the shift from a nonforested to a forested landscape and the intensification of the ring of urbanization that surrounds the long-protected Luquillo Experimental Forest.

Introduction

The island of Puerto Rico is at a geographic and cultural crossroads where human activities are influencing changes in the environment, climate, and land use and land cover. Puerto Rico, which is bordered by the Atlantic Ocean on the north and the Caribbean Sea on the south, lies at the juncture of the Greater and Lesser Antilles (fig. 1). It is in the path of hurricanes and tropical storms approaching the western hemisphere (Salvia, 1972; Weaver, 1986; Scatena and Larsen, 1991, Murphy and Stallard, 2012), atmospheric dust from the African continent (Reid and others, 2003, Stallard, 2012), and distinct air masses arriving from across the Atlantic or from the eastern seaboard of the United States (Malmgren and others, 1998). At a broad scale, these climatic events are controlled by cyclic global climate patterns as well as by human-induced carbon emissions that are changing climate (Huber and Knutti, 2012). At a more local scale, ecosystems respond to a range of environmental conditions and are influenced by historical patterns of changing land use in eastern Puerto Rico.

Eastern Puerto Rico is a good region in which to assess changes in land use and land cover for a number of ecological and social reasons. All six of the Holdridge life zones in Puerto Rico can be found along a transect of less than 15 kilometers (km) between the coast and the upper Luquillo Mountains (Holdridge, 1967; Ewel and Whitmore, 1973). Ecological diversity is affected by natural and human factors and by the strong climatic gradients caused by moisture-laden trade winds rising to pass over the Luquillo Mountains (García-Martinó and others, 1996; Murphy and Stallard, 2012). Mean annual rainfall increases with elevation from about 1,400 millimeters (mm) to about 5,000 mm per year, and mean annual temperature decreases with elevation from about 27.5°C to about 19.5°C along this gradient (Gould and others, 2006). The coastal hills and plains, along with the Luquillo Mountains, form a matrix of ridge, slope, valley, and depression that influences soil moisture, soil development, and vegetation (Weaver, 1991; Basnet, 1992). Long-term climatic trends, aeolian inputs (Reid and others, 2003, Stallard, 2012), storm events (Salvia, 1972; Weaver, 1986; Scatena and Larsen, 1991), climatic gradients, and topographic patterns all help to shape the landscape and control potential vegetation and land cover.

¹U.S. Department of Agriculture Forest Service, International Institute of Tropical Forestry, 1201 Calle Ceiba, Río Piedras, Puerto Rico

²Department of Forest and Wildlife Ecology, University of Wisconsin, 1630 Linden Drive, Madison, Wisconsin 53706

³Department of Biology, University of Puerto Rico, Río Piedras, Puerto Rico 00931–3360.

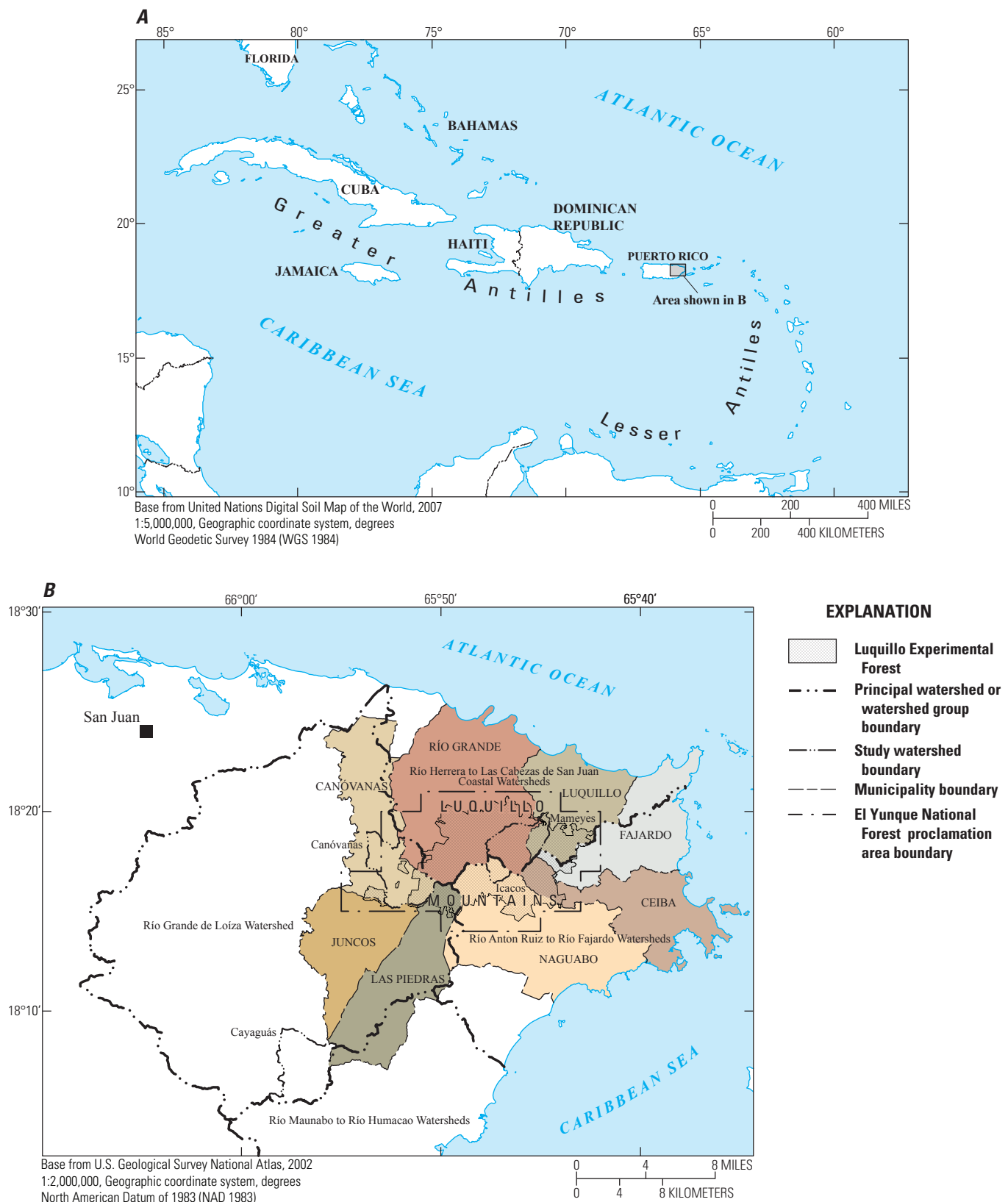


Figure 1. Location of Puerto Rico and study area, eastern Puerto Rico (see also table 1).

In addition to these complex environmental gradients and dynamics, eastern Puerto Rico has a long history of human activity, and the intensity of land use has differed with time. Pre-Columbian, low-intensity subsistence fishing, farming, hunting, and gathering lasted several thousand years. European colonization and exploitation of forest resources for timber and subsistence agriculture began about 500 years ago and increased slowly for the next three centuries. Intensive farming of sugarcane, tobacco, and coffee for export began more than 200 years ago (Dietz, 1986). The decline in agricultural production and growth of industry during the last six decades shifted much former agricultural land to cattle pasture or to completely abandoned land. Forest is now regenerating on those abandoned lands (Thomlinson and others, 1996; Aide and others, 2000; Chinea, 2002). Recent improvements in infrastructure and transportation systems, increasing population, and the virtual absence of land-use planning strategies have led to the conversion of many former agricultural lands to residential and commercial uses, suburban sprawl (Thomlinson and Rivera, 2000; López and others, 2001; Grau and others, 2003; Martinuzzi and others, 2007), depopulation of urban centers, and urban to suburban migration (Parés-Ramos and others, 2008). Finally, the region has a complex matrix of protected and unprotected areas (Helmer, 2004; Gould and others, 2008) and diverse zoning regulations (Lugo and others, 2000, 2004), which have led to differences in human use and in the responses of the landscape to the history of human activities (Zimmerman and others, 1995; Aide and others, 2000; Thompson, 2002). All of these human activities have had considerable

effect on the land-cover and land-use history of eastern Puerto Rico. The resulting land-use dynamics span a gradient from stable (areas that have maintained relatively consistent land-use intensities (older urban centers, current agricultural areas, mangrove forests, and forested peaks) to dynamic (areas that have fluctuated substantially during the previous 100 years between high- and low-intensity agriculture and agricultural abandonment and, more recently, shifted to urbanization).

Analyses of changes in land use and land cover in eastern Puerto Rico have focused mainly on land cover and change in four areas: (1) within the boundaries of the Luquillo Experimental Forest (whose boundaries match those of El Yunque National Forest) (Crow, 1980; Brown and others, 1983; Scatena, 1989; Weaver, 1990; Foster and others, 1999; Thompson and others, 2002), (2) within the proclamation area (a zone outside the national forest boundary in which the U.S. Congress authorized the U.S. Forest Service to purchase lands for conservation purposes) (Lugo and others, 2000), (3) within the eight municipalities that have jurisdiction of land outside the periphery of the Luquillo Experimental Forest (Thomlinson and others, 1996; Ramos González, 2001; Lugo and others, 2004), and (4) within the four principal watersheds or watershed groups that have all or part of their source in the Luquillo mountains (Ortíz-Zayas and Scatena, 2004) (fig. 1).

In this chapter we assess land use and land cover of the area encompassed by four principal watersheds or watershed groups in eastern Puerto Rico (table 1): Río Grande de Loíza, Río Anton Ruiz to Río Fajardo, Río Herrera to Las Cabezas de San Juan, and Río Maunabo to Río Humacao. These watersheds include four small subwatersheds that are study

Table 1. Watershed, municipality, and national forest areas of eastern Puerto Rico and their percentage of land area in Puerto Rico.

[<, less than]

Region	Area	
	(hectares)	(percent)
Principal watershed or watershed group	161,650	18.1
Río Grande de Loíza watershed	75,098	
Río Anton Ruiz to Río Fajardo watersheds	31,336	
Río Herrera to Las Cabezas de San Juan Coastal watersheds	26,865	
Río Maunabo to Río Humacao watersheds	28,351	
Municipalities surrounding Luquillo Experimental Forest	75,234	8.4
Río Grande	15,747	
Canóvanas	8,552	
Luquillo	6,710	
Fajardo	7,709	
Ceiba	7,429	
Naguabo	13,404	
Las Piedras	8,790	
Juncos	6,893	
Study watersheds	7,346	<1
Cayaguás	2,605	
Canóvanas	2,655	
Iacacos	325	
Mameyes	1,761	
El Yunque National Forest proclamation area	22,417	2.5
El Yunque National Forest/Luquillo Experimental Forest	11,429	1.3

watersheds of the U.S. Geological Survey's Water, Energy, and Biogeochemical Budgets (WEBB) program (fig. 1, table 1): Cayaguás, Canóvanas, Icacos, and Mameyes (Murphy and others, 2012). This region occupies an area of 1,616 square kilometers (km^2), about 18 percent of the total land in Puerto Rico (table 1). In addition, we describe population dynamics and analyze land-cover changes within the eight municipalities that surround the Luquillo Experimental Forest. This region has been an important area for research and land management because of the regulatory control that the surrounding municipal governments have on development in its periphery. However, a historic lack of enforcement of these regulations has resulted in subsequent building violations (Lugo and others, 2004). Nevertheless, the residents of these municipalities retain a strong interest in and reliance on the ecosystem services of the Luquillo Mountains, particularly as a source of fresh water and recreational opportunities.

Land Cover

A recent land-cover assessment developed by the Puerto Rico Gap Analysis Project identified 70 land-cover types on the island (Gould and others, 2008). Fifty-one of these land-cover types occur within the four principal watersheds of eastern Puerto Rico (table 2). Forest, woodland, and shrubland were the most common land-use types, covering 44 percent of the land area. Thirty-three forest, woodland, or shrubland classes were identified; these classes are based on forest age, degree of canopy cover, underlying substrate, and whether the vegetation is dry, moist, wet, or flooded. Eight dry forest or woodland classes cover about 1 percent of the total area, and they include important eastern dry forests near the coast. Twelve moist-forest types, which cover 25 percent of the area, are primarily composed of the lowland moist forests and woodlands on the lower slopes of the Luquillo Mountains and in the southeastern part of the Río Grande de Loíza watershed. Eleven wet-forest classes, which cover 16 percent of the region, are found on the upper slopes of the Luquillo Mountains (including most of the protected forests within the Luquillo Experimental Forest) and in mountains to the southeast of the Forest. Flooded coastal forests, which cover 1.4 percent of the total land area, include saline mangrove forests and freshwater *Pterocarpus* swamps. Structurally developed forests (in this classification, those forests more than 25 years old) were identified on 1977 imagery (Ramos and Lugo, 1994) in 20 percent of the area.

Six grassland or herbaceous classes, covering 41 percent of the land area of eastern Puerto Rico, include dry and moist pasture and grassland, and seasonally flooded and emergent saline and nonsaline wetlands (table 2). Three developed classes, covering 12 percent of the area, are high-density urban

development (more than 50 percent impervious surface within a 9-hectare area), low-density urban development (more than 50 percent impervious, primarily vegetated, surface within a 9-hectare area), and artificial barrens, which are typically bulldozed areas (table 2; Martinuzzi and others, 2007). The remaining 3 percent of land area consists of natural barrens, agricultural lands other than pasture, and open water.

This detailed classification can be simplified into a set of six classes: forests (closed forest, greater than 60 percent tree cover), woodlands (open forests, 25 to 60 percent tree cover) and shrublands, nonforest vegetation (grasslands and wetlands), natural barrens, urban and artificial barrens (bulldozed areas), and water (fig. 2). Forests occupy about 37 percent of the total land area, woodlands and shrublands 7 percent, nonforest vegetation 43 percent, urban and artificial barrens 12 percent, and water and natural barrens total less than 2 percent (table 3).

Land Use

Eastern Puerto Rico consists of 175 barrios, or neighborhoods, a geographic unit used in the census of population in the U.S. Census every 10 years (U.S. Census Bureau, 2001). This area has been classified into three main land-use categories by integrating recent census information (population density per barrio in the year 2000) with satellite image analyses (relative amount of developed area and natural land cover (Martinuzzi and others, 2007, 2008; Gould and others, 2008). In this analysis, the urban land-use class has greater than 20 percent developed cover within a 1- km^2 area and population density greater than 500 people per square kilometer. Two rural classes, both with more than 80 percent natural land cover, were identified: a densely populated rural ("suburban") class, which is primarily residential and has more than 500 people per square kilometer, and a sparsely populated rural ("rural") class, which has less than 500 people per square kilometer and is primarily active or abandoned agricultural, wetland, steep slope, or protected conservation areas (Martinuzzi and others, 2007). The urban, suburban, and rural classes cover 16 percent, 50 percent, and 34 percent, respectively, of eastern Puerto Rico (fig. 3, table 4). This is a higher suburban-to-rural ratio when compared with the island as a whole (Martinuzzi and others, 2007). These patterns of population growth and distribution have been controlled by the topography of the island (flat areas are more easily developed), as well as by socioeconomic factors such as sugarcane farming, housing, road networks, and conservation efforts (Grau and others, 2003; Helmer, 2004; Parés-Ramos and others, 2008). Ten percent of eastern Puerto Rico is protected for conservation, compared with an 8 percent average of protected area in the island as a whole (Gould and others, 2008) (fig. 3, table 4).

Table 2. Area of land-cover types in eastern Puerto Rico, from derived analysis of 1999–2003 Landsat ETM+ imagery.

[Gould and others (2008). Land-cover types organized by dominant physiography and climate. <, less than; *, most abundant land-cover types]

Land-cover type	Area	
	(hectares)	(percent)
Total area	161,700	100
Forest, woodland, and shrubland	71,112	44.0
Dry		
Mature secondary lowland dry alluvial semideciduous forest	1,775	1.1
Young secondary lowland dry alluvial semideciduous forest	135	0.1
Lowland dry alluvial shrubland and woodland	277	0.2
Mature secondary lowland dry noncalcareous semideciduous forest	104	0.1
Young secondary lowland dry noncalcareous semideciduous forest	329	0.2
Lowland dry noncalcareous shrubland and woodland	666	0.4
Lowland dry riparian forest	246	0.2
Lowland dry riparian shrubland and woodland	14	<0.1
Moist	40,908	25.3
Mature secondary lowland moist alluvial evergreen forest	4	<0.1
Young secondary lowland moist alluvial evergreen forest	362	0.2
Lowland moist alluvial shrubland and woodland	1,804	1.12
Mature secondary moist limestone evergreen and semideciduous forest	1,235	0.8
Young secondary moist limestone evergreen and semideciduous forest	119	0.1
Moist limestone shrubland and woodland	28	<0.1
Mature secondary moist noncalcareous evergreen forest	27	<0.1
*Young secondary lowland moist noncalcareous evergreen forest	10,352	6.4
Lowland moist noncalcareous shrubland and woodland	18,881	11.7
Lowland moist abandoned and active coffee plantations	7,625	4.7
Lowland moist riparian forest	41	<0.1
Lowland moist riparian shrubland and woodland	241	0.2
Wet	26,126	16.2
Mature secondary montane wet alluvial evergreen forest	193	0.1
Young secondary montane wet alluvial evergreen forest	180	0.1
Montane wet alluvial shrubland and woodland	164	0.1
Mature secondary montane wet noncalcareous evergreen forest	60	<0.1
Mature primary tabonuco and secondary montane wet noncalcareous evergreen forest	3,315	2.1
Mature primary palo colorado and secondary montane wet noncalcareous evergreen forest	8,715	5.4
Mature primary sierra palm and secondary montane wet noncalcareous evergreen forest	3,712	2.3
Mature primary elfin woodland and secondary montane wet noncalcareous evergreen cloud forest	2,633	1.6
Young secondary montane wet noncalcareous evergreen forest	257	0.2
Montane wet noncalcareous evergreen shrubland and woodland	5,315	3.3
Montane wet evergreen abandoned and active coffee plantation	1,698	1.1
Flooded	77	0.1
Mangrove forest and shrubland	2,304	1.4
Freshwater <i>Pterocarpus</i> swamp	2,129	1.3
Grasslands and herbaceous vegetation	175	0.1
Dry grasslands and pastures	66,063	40.9
*Moist grasslands and pastures	487	0.3
Seasonally flooded herbaceous nonsaline wetlands	58,444	36.1
Seasonally flooded herbaceous saline wetlands	5,620	3.5
Emergent herbaceous nonsaline wetlands	1,210	0.7
Emergent herbaceous saline wetlands	248	0.2
Agriculture	53	<0.1
Hay and row crops	3,223	2.0
Woody agriculture and plantations	2,895	1.8
	328	0.2

Table 2. Area of land-cover types in eastern Puerto Rico, from derived analysis of 1999–2003 Landsat ETM+ imagery.—Continued

[Gould and others (2008). Land-cover types organized by dominant physiography and climate. <, less than; *, most abundant land-cover types]

Land-cover type	Area	
	(hectares)	(percent)
Natural barrens	444	0.3
Rocky cliffs and shelves	29	<0.1
Gravel beaches and stony shoreline	14	<0.1
Fine to coarse sandy beaches, mixed sand and gravel beaches	214	0.1
Riparian and other natural barrens	45	<0.1
Salt and mudflats	142	0.1
Developed areas	19,542	12.1
*High-density urban development	9,224	5.7
Low-density urban development	7,474	4.6
Artificial barrens	2,844	1.8
Water	1,317	0.8
Freshwater	823	0.5
Salt water	494	0.3

Table 3. Area of simplified land cover in eastern Puerto Rico from derived analysis of recent (1999–2003) Landsat ETM+ imagery.

[From Gould and others (2008); <, less than]

Land-cover type	Area	
	(hectares)	(percent)
Forest	60,157	37
Woodland and shrubland	11,183	7
Nonforest vegetation	68,883	43
Natural barrens	324	<1
Urban and artificial barrens	19,494	12
Water	1,309	1
Total	161,351	100

Table 4. Urban, suburban (densely populated rural), and rural (sparsely populated rural) land-use classes and protected conservation areas in eastern Puerto Rico.

[From Martinuzzi and others (2007); <, less than]

Land-use class	Protected area (hectares)	Unprotected area (hectares)	Total area (hectares)	Percent protected	Percent of 161,401 hectares
Urban	155	25,644	25,809	<1	16
Suburban	2,884	77,283	80,167	4	50
Rural	13,125	42,300	55,425	24	34
Total	16,173	145,228	161,401	10	100

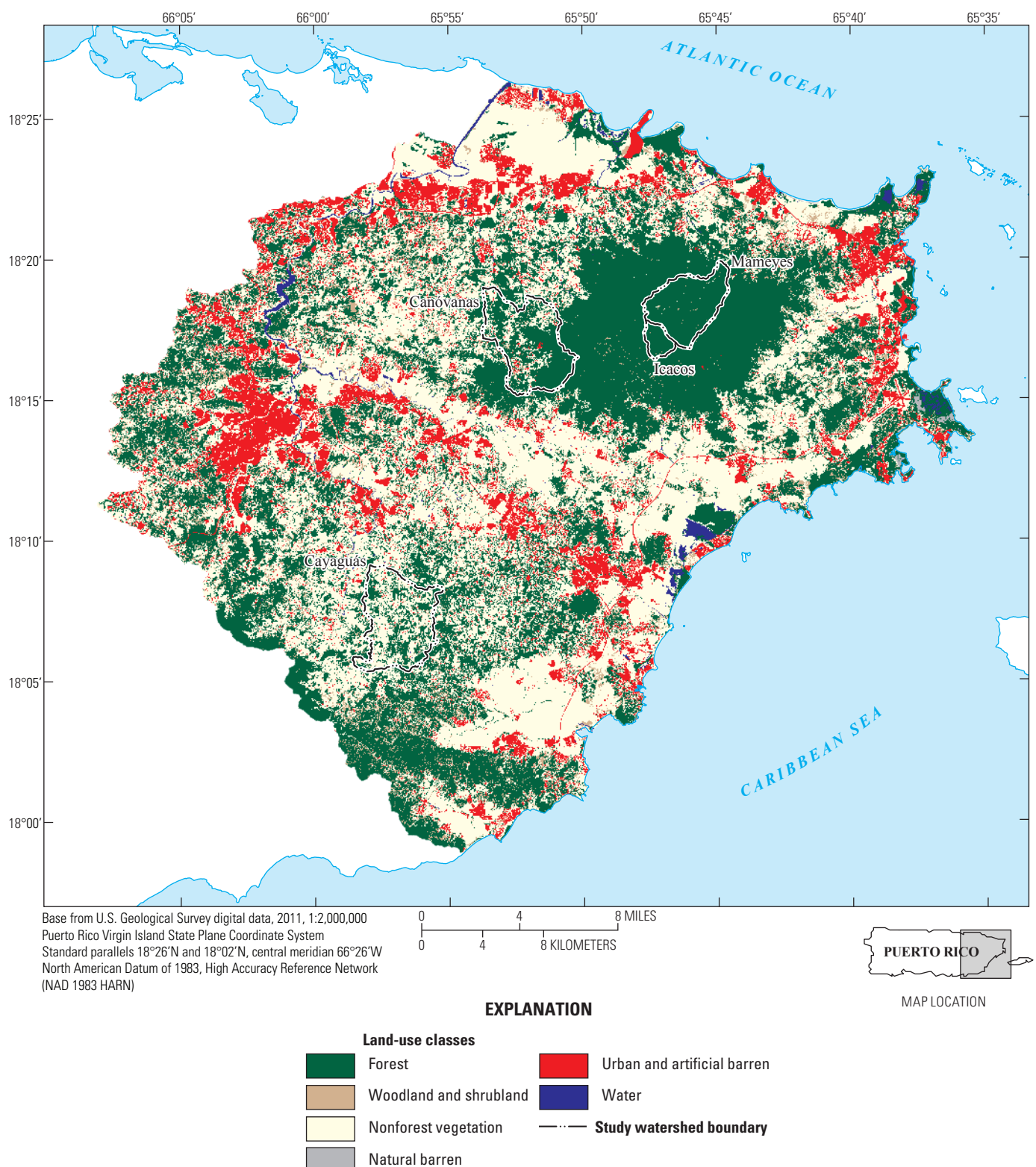


Figure 2. Simplified land cover of eastern Puerto Rico (modified from Gould and others, 2008).

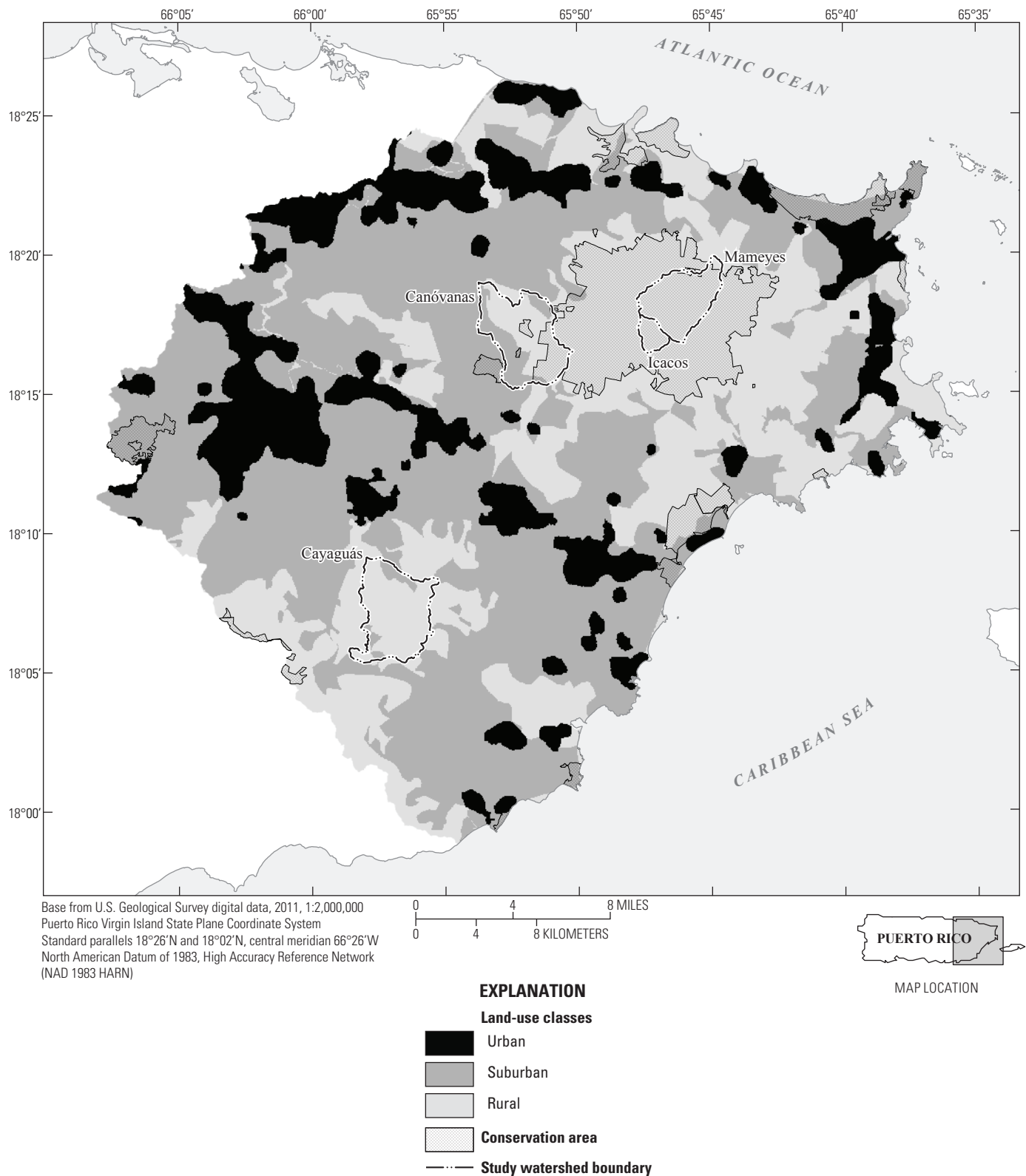


Figure 3. Urban, suburban, and rural land-use classes and protected conservation areas in eastern Puerto Rico (following Martinuzzi and others, 2007).

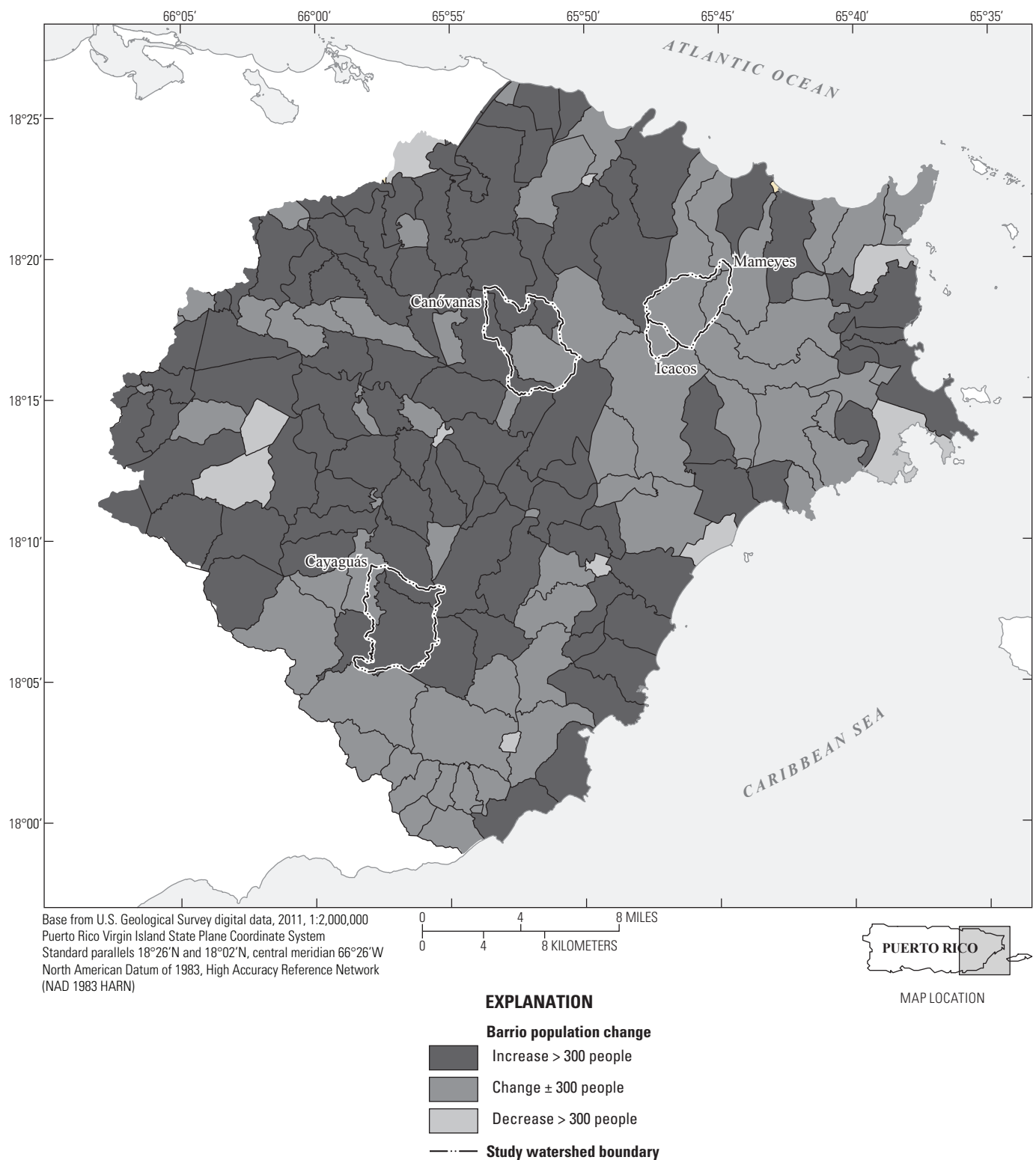


Figure 4. Barrio (neighborhood) population dynamics in eastern Puerto Rico, 1990–2000 (from Parés-Ramos and others, 2008).

Population Dynamics

From 1990 to 2000, overall population trends in Puerto Rico were characterized by an increase in suburban population and housing density, by suburbanization of the rural landscape, and by population decline in several urban centers (Parés-Ramos and others, 2008). In eastern Puerto Rico, only 10 of 175 barrios (6 percent) lost population from 1990 to 2000 (fig. 4), and nine of these barrios were urban. Seventy-three barrios (42 percent) showed little population change (± 300 people) and of these, 42 percent were classified as rural, 40 percent as suburban, and 12 percent as urban barrios. In 92 barrios, population increased markedly (300–6,800 new inhabitants), and of these barrios 9 percent were classified as urban, 77 percent as suburban, and 14 percent as rural. This trend follows the island-wide trend of population increasing in the suburban areas and decreasing in older urban centers outside of the island's main metropolitan area (San Juan), which has occurred mostly at the expense of grasslands (Parés-Ramos and others, 2008). In the past, suburban and urban areas in eastern Puerto Rico were characterized by relatively similar rates of population growth, but recently (1990–2000) there has been a more rapid increase in suburban population density and housing units (fig. 5), influencing land-use patterns in this area.

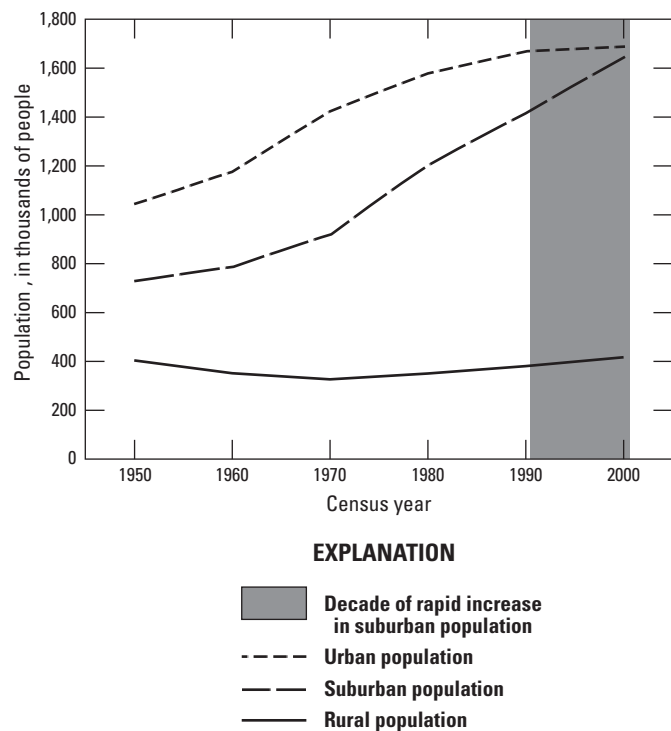


Figure 5. Population trends in land-use categories, 1950–2000, in eastern Puerto Rico.

Land-Cover Change

We compared two recent classifications of land cover to assess land-cover change in eastern Puerto Rico between 1991 (Helmer and others, 2002) and 2003 (Gould and others, 2008). Both assessments are based on the classification of Landsat satellite imagery but differ in methods and classification criteria. The 1991 assessment used a 30-square meter (m^2) pixel resolution, whereas the 2003 assessment used a 15- m^2 pixel resolution. The classification of 1991 imagery has 28 classes for eastern Puerto Rico, whereas the classification of 2003 imagery has 51 classes. The finer resolution of the 2003 classification resulted in areas of residential development (such as houses surrounded by vegetation) to be more precisely delineated, reducing the mapped amount of developed area. Therefore, the 1991 classification overestimates urban areas relative to the 2003 classification. Additionally, geographic representation of mountainous areas in two dimensions always results in distortion of the spatial relationship between land-surface features, and lack of coregistration of pixels between the two classifications may lead to errors. In order to minimize differences in classification schemes, both classifications were reduced to six general classes (see fig. 2) and resampled to 15- m^2 -pixel resolution. Although these differences in methods affect the accuracy of the land-cover change assessment, some inferences about the direction of change in land cover can be drawn from an analysis of a transition matrix of the two classifications.

Our analysis showed that forest cover increased at the expense of woodlands and grasslands, as the trend toward forest regeneration on abandoned land continued (table 5). Urban development (urban and artificial barrens) increased by 16 percent during the period 1991 to 2003. We also assessed long-term land cover by comparing the degree of forest, pasture and agriculture, urban, and mangrove cover in the eight municipalities surrounding the Luquillo Experimental Forest in the years 1936, 1950, 1977, 1995, and 2003 (fig. 6) (Lugo and others, 2004; Gould and others, 2008). We modified the original estimates of urban cover of Lugo and others (2004) for the 1936–1995 classification because of the finer resolution of the 2003 estimate of urban cover. We made the assumption (generally true, but with some exceptions) that once areas were urbanized, they would not revert to natural cover. Therefore, any areas classified as urban in early years, but as natural vegetation in 2003, were changed to that natural cover for all years. The most pronounced change in the last 7 decades has been the shift from pasture and agriculture to a forested landscape and the intensification of the ring of urbanization that surrounds the long-protected Luquillo Experimental Forest (figs. 6, 7).

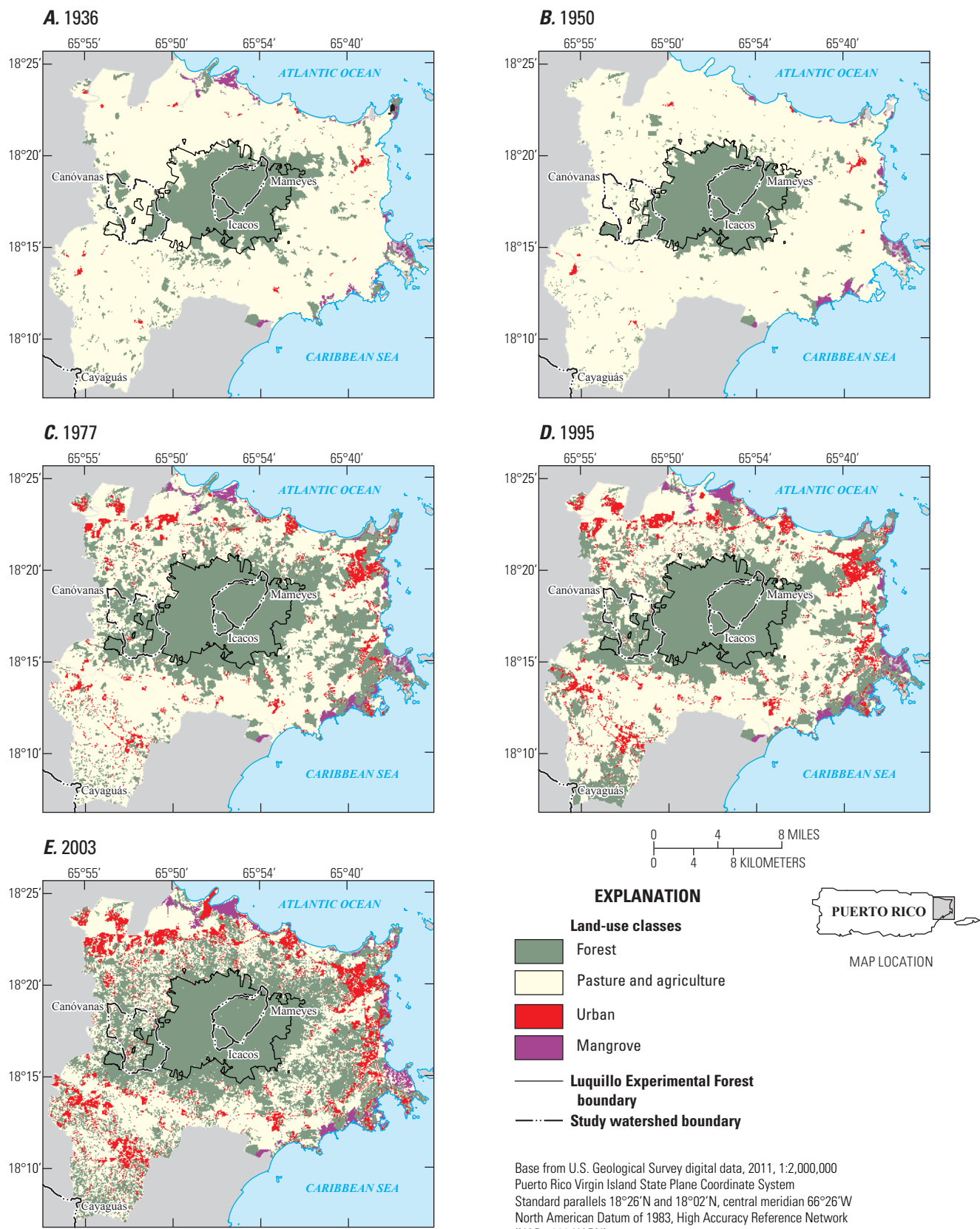


Figure 6. Trends in forest, pasture and agriculture, urban, and mangrove extent, 1936–2003, in eastern Puerto Rico. (Information for years 1936–1995 modified from Lugo and others, 2004.)

Table 5. Land-cover transition matrix of eastern Puerto Rico, 1991 and 2003, based on Landsat satellite imagery analyses for those two years.

[The 1991 classification modified from Helmer and others (2002); 2003 classification modified from Gould and others (2008). Example of how to read matrix: cell in row 1, column 2 states that 1,902 hectares were classified as Forest in 1991 and as Woodland and shrubland in 2003; <, less than]

Land-cover categories, 1991 imagery (hectares)	Land-cover categories, 2003 imagery (hectares)					Total 1991 (hectares)	1991 Percent	Change 1991 to 2003	
	Forest and shrubland	Pasture and agriculture	Natural barrens	Urban and artificial barrens	Water			(hectares)	(percent)
Forest	29,011	1,902	5,063	103	1,045	237	37,361	23	22,647 61
Woodland and shrubland	15,086	3,052	8,800	9	1,469	42	28,458	18	-17,335 -60
Pasture and agriculture	14,342	5,407	48,675	80	7,939	458	76,901	48	-8,282 -11
Natural barrens	106	15	165	166	40	20	512	<1	-103 -20
Urban and artificial barrens (developed areas)	1,367	721	5,703	43	8,752	73	16,659	10	2,620 16
Water	96	26	213	7	34	451	827	1	453 55
Total 2003	60,008	11,123	68,619	408	19,279	1,281	160,716	100	
Percent 2003	37	7	43	<1	12	1	100		

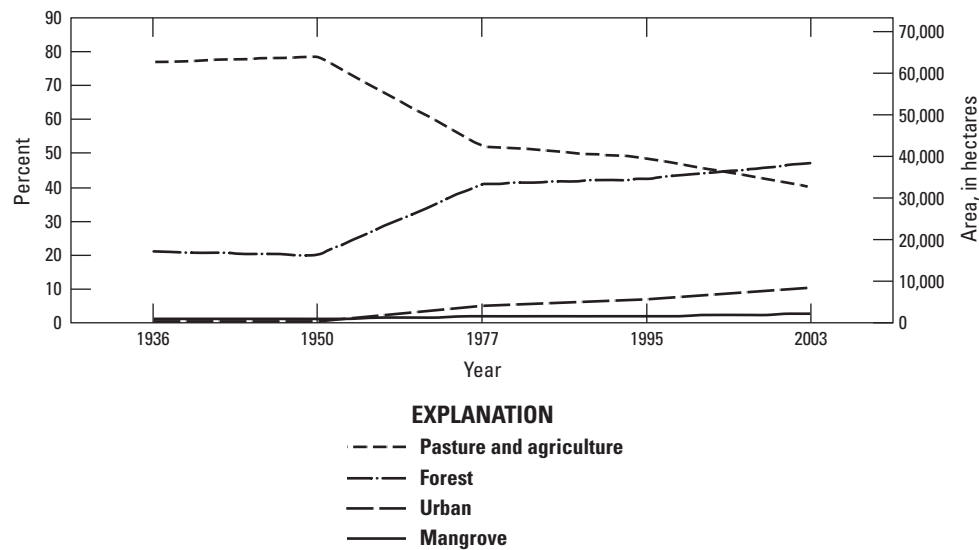


Figure 7. Diagram of trends in forest, pasture and agriculture, urban, and mangrove extent, 1936–2003, eastern Puerto Rico.

Conclusion

This analysis provides a comprehensive view of land cover, land use, population dynamics, and land-cover change in eastern Puerto Rico. Principal trends in land use and land-cover patterns during the last several decades include a sharp decline in agriculture; the conversion of grassland, woodland, and shrubland to closed forest; and urbanization of the landscape. Land-cover changes differ in their degree of permanence and in their effects on ecosystem services. However, the shift from vegetated natural surfaces to impermeable developed surfaces has stronger and more long-term effects. Not only are impermeable surfaces difficult to restore from an ecological standpoint, they are a result of human investments of time

and capital that represent an inertia difficult to counteract in restoring natural systems. Therefore, the trend towards increasing urbanization in the limited land area of eastern Puerto Rico needs to be assessed in the context of those limitations—that is, which portions of this diverse landscape are being urbanized, what degree of urbanization is desirable, and what ecosystem services are now being lost or may be lost owing to current and future levels of urbanization. An important observation from this analysis is the loss of natural land cover in the coastal areas, highlighting the need to protect the coastal hills and plains and the matrix of habitats that include the mangrove forests and river systems of the coastal area. Additionally, although areas of new forest cover are increasing, little research describes their ecosystem structure or the function of these secondary forests in eastern Puerto Rico.

Acknowledgments

Thanks to reviewers G. González, F. Wadsworth, and A.E. Lugo. This research was supported by the U.S. Geological Survey Biological Resources Division Gap Analysis Project: Puerto Rico Gap Analysis Project (agreement 01HQPG0031) and the International Institute of Tropical Forestry (IITF) GIS and Remote Sensing Laboratory. All research at IITF is done in collaboration with the University of Puerto Rico.

References

- Aide, T.M., Zimmerman, J.K., Pascarella, J.B., Rivera, L., and Marcano-Vega, H., 2000, Forest regeneration in a chronosequence of tropical abandoned pastures—Implications for restoration ecology: *Restoration Ecology*, v. 8, p. 328–338.
- Basnet, Khagda, 1992, Effects of topography on the pattern of trees in tabonuco (*Dacryodes excelsa*) dominated rain forest of Puerto Rico: *Biotropica*, v. 24, p. 31–42.
- Brown, Sandra, Lugo, A.E., Silander, S., and Liegel, L., 1983, Research history and opportunities in the Luquillo Experimental Forest, in New Orleans, La., U.S. Department of Agriculture Forest Service, Southern Forest Experimental Station General Technical Report SO-44, 128 pages.
- Chinea, J.D., 2002, Tropical forest succession on abandoned farms in the Humacao Municipality of eastern Puerto Rico: *Forest Ecology and Management*, v. 167, p. 195–207.
- Crow, G.T., 1980, A rain forest chronicle—A thirty year record of change in structure and composition at El Verde, Puerto Rico: *Biotropica*, v. 12, p. 42–45.
- Dietz, J.L., 1986, Economic history of Puerto Rico: Princeton, New Jersey, Princeton University Press, 337 p.
- Ewel, J.J., and Whitmore, J.L., 1973, The ecological life zones of Puerto Rico and the Virgin Islands: Río Piedras, Puerto Rico, U.S. Department of Agriculture Forest Service International Institute of Tropical Forestry, Río Piedras, Puerto Rico, Forest Service Research Paper ITF-18, 72 p.
- Foster, D.R., Fluet, M., and Boose, E.R., 1999, Human or natural disturbance—Landscape-scale dynamics of the tropical forests of Puerto Rico: *Ecological Applications*, v. 9, p. 555–572.
- García-Martinó, A.R., Scatena, F.N., Warner, G.S., and Civco, D.L., 1996, Rainfall, runoff, and elevation relationships in the Luquillo Mountains of Puerto Rico: *Caribbean Journal of Science*, v. 12, p. 413–424.
- Gould, W.A., Alarcón, C., Fevold, B., Jiménez, M.E., Martinuzzi, S., Potts, G., Quiñones, M., Solórzano, M., and Ventosa, E., 2008, The Puerto Rico Gap Analysis Project, v. 1, Landcover, vertebrate species distributions, and land stewardship: U.S. Department of Agriculture Forest Service, International Institute of Tropical Forestry, Río Piedras, Puerto Rico, General Technical Report IITF-GTR-39, 165 pp.
- Gould, W.A., González, G., and Carrero Rivera, G., 2006, Structure and composition of vegetation along an elevational gradient in Puerto Rico: *Journal of Vegetation Science*, v. 17, p. 653–664.
- Grau, H.R., Aide, T.M., Zimmerman, J.K., Thomlinson, J.R., Helmer, E., and Zou, X., 2003, The ecological consequences of socioeconomic and land-use changes in postagriculture Puerto Rico: *BioScience*, v. 53, p. 1159–1168.
- Helmer, E.H., 2004, Forest conservation and land development in Puerto Rico: *Landscape Ecology*, v. 19, p. 29–40.
- Helmer, E.H., Ramos, O., López, T.M., Quiñones, M., and Díaz, W., 2002, Mapping the forest type and land cover of Puerto Rico—A component of the Caribbean biodiversity hotspot: *Caribbean Journal of Science*, v. 38, p. 165–183.
- Holdridge, L.R., 1967, Life zone ecology: San Jose, Costa Rica, Tropical Science Center, 206 p.
- Huber, Markus, and Knutti, Reto, 2012, Anthropogenic and natural warming inferred from changes in Earth's energy balance: *Nature Geoscience*, v. 5, p. 31–36.
- López, T.M., Aide, T.M., and Thomlinson, J.R., 2001, Urban expansion and the loss of prime agricultural lands in Puerto Rico: *Ambio*, v. 30, p. 49–54.
- Lugo, A.E., López, T.M., and Ramos, O.M., 2000, Zonificación de terrenos en la periferia de El Yunque: U.S. Department of Agriculture Forest Service International Institute of Tropical Forestry, Río Piedras, Puerto Rico, General Technical Report IITF-16, 12 p.
- Lugo, A.E., López, T.M., Ramos González, O.M., and Velez, L.L., 2004, Urbanización de los terrenos en la periferia de El Yunque: U.S. Department of Agriculture Forest Service General Technical Report WO-66, 29 p.
- Malmgren, B.A., Winter, A., and Chen, D., 1998, El Niño–Southern Oscillation and North Atlantic Oscillation control of climate in Puerto Rico: *Journal of Climate*, v. 15, p. 2713–2717.
- Martinuzzi, Sebastián, Gould, W.A., and Ramos González, O.M., 2007, Land development, land use, and urban sprawl in Puerto Rico integrating remote sensing and population census data: *Landscape and Urban Planning*, v. 79, p. 288–297.

- Martinuzzi, Sebastián, Gould, W.A., Ramos González, O.M., and Jiménez, M.E., 2008, Urban and rural land use in Puerto Rico, Research map IITF-RMAP-01, Río Piedras, Puerto Rico: U.S. Department of Agriculture Forest Service International Institute of Tropical Forestry, scale 1: 260,000.
- Murphy, S.F., and Stallard, R.F., 2012, Hydrology and climate of four watersheds in eastern Puerto Rico, ch. C in Murphy, S.F., and Stallard, R.F., eds., Water quality and landscape processes of four watersheds in eastern Puerto Rico: U.S. Geological Survey Professional Paper 1789, 43–84 p.
- Murphy, S.F., Stallard, R.F., Larsen, M.C., and Gould, W.A., 2012, Physiography, geology, and land cover of four watersheds in eastern Puerto Rico, ch. A in Murphy, S.F., and Stallard, R.F., eds., Water quality and landscape processes of four watersheds in eastern Puerto Rico: U.S. Geological Survey Professional Paper 1789, 1–24 p.
- Ortiz-Zayas, J.R., and Scatena, F.N., 2004, Integrated water resources management in the Luquillo Mountains, Puerto Rico—An evolving process: *International Journal of Water Resources Development*, v. 20, p. 387–398.
- Parés-Ramos, I.K., Gould, W.A., and Aide, T.M., 2008, Agricultural abandonment, suburban growth, and forest expansion in Puerto Rico between 1991 and 2000: *Ecology and Society*, v. 13, no. 2, article number 1.
- Ramos, O.M., and Lugo, A.E., 1994, Mapa de la vegetación de Puerto Rico: *Acta Científica*, v. 8, p. 63–66.
- Ramos González, O.M., 2001, Assessing vegetation and land cover changes in northeastern Puerto Rico, 1978–1995: *Caribbean Journal of Science*, v. 37, p. 95–106.
- Reid, E.A., Reid, J.S., Meier, M.M., Dunlap, M.R., Cliff, S.S., Broumas, A., Perry, K., and Maring, H., 2003, Characterization of African dust transported to Puerto Rico by individual particle and size segregated bulk analysis: *Journal of Geophysical Research*, v. 108, no. D19, 8591, p. 1–22.
- Salivia, L.A., 1972, Historia de los temporales de Puerto Rico y las Antillas, 1492 a 1970: Río Piedras, Puerto Rico, P.R. Editorial Edil, Inc., University of Puerto Rico, 385 pp.
- Scatena, F.N., 1989, An introduction to the physiography and history of the Bisley Experimental Watersheds in the Luquillo Mountains of Puerto Rico: U.S. Department of Agriculture Forest Service, Southern Experimental Station General Technical Report SO-72, 22 p.
- Scatena, F.N., and Larsen, M., 1991, Physical aspects of Hurricane Hugo in Puerto Rico: *Biotropica*, v. 23, p. 317–23.
- Stallard, R.F., 2012, Atmospheric inputs to watersheds in the Luquillo Mountains of eastern Puerto Rico, ch. D in Murphy, S.F., and Stallard, R.F., eds., Water quality and landscape processes of four watersheds in eastern Puerto Rico: U.S. Geological Survey Professional Paper 1789, p. 85–112.
- Thomlinson, J.R., and Rivera, L., 2000, Suburban growth in Luquillo, Puerto Rico—Some consequences of development on natural and seminatural systems: *Landscape Urban Plan*, v. 49, p. 15–23.
- Thomlinson, J.R., Serrano, M.I., López, T.M., Aide, T.M., and Zimmerman, J.K., 1996, Land-use dynamics in a post-agricultural Puerto Rican landscape (1936–1988): *Biotropica*, v. 28, p. 525–536.
- Thompson, Jill, Brokaw, N., Zimmerman, J.K., Waide, R.B., Everham, E.M., III, Lodge, D.J., Taylor, C.M., García-Montiel, D., and Fluet, M., 2002, Land use history, environment, and tree composition in a tropical forest: *Ecological Applications*, v. 12, p. 1344–1363.
- U.S. Census Bureau, 2001, Population change and distribution 1990 to 2000: *Census 2000 Brief*, <http://www.census.gov/prod/2001pubs/c2kbr01-2.pdf>.
- Weaver, P.L., 1986, Hurricane damage and recovery in the montane forests of the Luquillo Mountains of Puerto Rico: *Caribbean Journal of Science*, v. 22, p. 53–70.
- Weaver, P.L., 1990, Succession in the elfin woodland of the Luquillo Mountains of Puerto Rico: *Biotropica*, v. 22, p. 83–89.
- Weaver, P.L., 1991, Environmental gradients affect forest composition in the Luquillo mountains of Puerto Rico: *Interciencia*, v. 16, p. 1442–151.
- Zimmerman, J.K., Aide, T.M., Rosario, M., Serrano, M., and Herrera, L., 1995, Effects of land management and a recent hurricane on forest structure and composition in the Luquillo Experimental Forest, Puerto Rico: *Forest Ecology and Management*, v. 77, p. 65–76.

Hydrology and Climate of Four Watersheds in Eastern Puerto Rico

By Sheila F. Murphy and Robert F. Stallard

Chapter C of
**Water Quality and Landscape Processes of Four Watersheds in
Eastern Puerto Rico**

Edited by Sheila F. Murphy and Robert F. Stallard

Professional Paper 1789-C

**U.S. Department of the Interior
U.S. Geological Survey**

Contents

Abstract.....	47
Introduction.....	47
Climate and Hydrology of Eastern Puerto Rico.....	49
Climate Variability and Change.....	53
Relation of Land Cover to Climate and Hydrology	54
Cloud Forest.....	54
Interpretive Approach.....	56
Precipitation.....	56
Regression Model of Precipitation Based on Elevation.....	57
Spatially Based Precipitation Model.....	57
Precipitation Based on Land Cover	57
Cloud Drip.....	57
Runoff.....	59
Groundwater and Storage.....	60
Water-Supply Inputs and Outputs.....	60
Evapotranspiration.....	60
Error Estimation for Water Budgets.....	61
Precipitation and Runoff in Eastern Puerto Rico.....	62
Water Budgets for Study Watersheds	75
Summary.....	77
Acknowledgments.....	78
References.....	78

Figures

1. Maps of Caribbean showing Puerto Rico and study watersheds	48
2. Map of hurricane tracks over or near Puerto Rico since 1850	50
3. Digital elevation model of elevation and relief of Puerto Rico.....	51
4. Map of mean annual precipitation of Puerto Rico	51
5. Map of eastern Puerto Rico showing location of sites, Luquillo Experimental Forest, and El Toro Wilderness	52
6–15. Diagrams of the following:	
6. Indices of oscillations that affected Puerto Rico, 1950–2010.....	55
7. Elevation versus mean annual precipitation (1991–2005) at stations in or near study watersheds, eastern Puerto Rico	62
8. Mean daily precipitation by year at stations in or near study watersheds, eastern Puerto Rico	64
9. Mean daily runoff by year at U.S. Geological Survey stream-gaging stations, eastern Puerto Rico	66
10. Distribution of log of mean annual runoff from study watersheds and Río Fajardo for periods of record.....	69
11. Mean daily precipitation by month at stations in or near study watersheds.....	70

12. Mean daily runoff per month at U.S. Geological Survey stream-gaging stations, eastern Puerto Rico	71
13. Percent occurrence of hourly precipitation intensity at U.S. Geological Survey stream-gaging stations (1991–2005), eastern Puerto Rico.....	72
14. Percent occurrence of hourly runoff intensity at U.S. Geological Survey stream-gaging stations (1991–2005), eastern Puerto Rico	73
15. Runoff and precipitation at U.S. Geological Survey stream-gaging stations during and after Tropical Storm Dean, August 2001	74

Tables

1. Temperature statistics for 1991–2005 at meteorological stations in or near study watersheds, eastern Puerto Rico	50
2. Stream-gaging and precipitation stations, eastern Puerto Rico	53
3. Precipitation and evapotranspiration rates reported in literature, eastern Puerto Rico	58
4. Total annual precipitation at stations in or near study watersheds, 1991–2005	63
5. Annual runoff, stream statistics, and stream characteristics study of watersheds	65
6. Statistical properties of annual runoff of study watersheds and Río Fajardo, 1991–2005	67
7. Summaries of successive regressions of annual runoff and precipitation in eastern Puerto Rico	68
8. Rainfall intensity at U.S. Geological Survey stations during major storms in eastern Puerto Rico, 1991–2005	72
9. Runoff rates from study watersheds and percentage of time that hourly runoff is below those rates, at percentiles of annual runoff volume.....	73
10. Modeled recessions of study watersheds after storm events	76
11. Annual precipitation estimated by various methods	77
12. Annual water budgets of study watersheds	77

Abbreviations Used in This Report

km	kilometer
km ²	square kilometer
m	meter
mm	millimeter
mm day ⁻¹	millimeters per day
mm h ⁻¹	millimeters per hour
mm yr ⁻¹	millimeters per year
m s ⁻¹	meters per second
m ³ s ⁻¹	cubic meters per second
yr	year

AR	autoregressive
BP	before present
ENSO	El Niño–Southern Oscillation
ET	evapotranspiration
IMA	integrated-moving-average
LTER	Long-Term Ecological Research
NOAA	National Oceanographic and Atmospheric Administration
PRISM	parameter-elevation regressions independent slopes model
USGS	U.S. Geological Survey
WEBB	Water, Energy, and Biogeochemical Budgets

Conversion Factors

Multiply	By	To obtain
Length		
millimeter (mm)	0.03937	inch (in.)
meter (m)	3.281	foot (ft)
kilometer (km)	0.6214	mile (mi)
Area		
square kilometer (km^2)	0.3861	square mile (mi^2)
Flow rate		
meter per second (m s^{-1})	3.281	feet per second (ft s^{-1})
cubic meters per second ($\text{m}^3 \text{s}^{-1}$)	35.31	cubic feet per second ($\text{ft}^3 \text{s}^{-1}$)
millimeters per hour (mm h^{-1})	0.03937	inches per hour (in. h^{-1})
millimeters per day (mm h^{-1})	0.03937	inches per day (in. h^{-1})
millimeters per year (mm yr^{-1})	0.03937	inches per year (in. yr^{-1})

Hydrology and Climate of Four Watersheds in Eastern Puerto Rico

By Sheila F. Murphy and Robert F. Stallard

Abstract

Puerto Rico lies directly in the path of the easterly trade winds, which deliver steady rainfall to the mountains and steer tropical wave systems toward the island. Hurricanes and tropical storms derived from these tropical waves differ in frequency and intensity, contributing to substantial interannual variation in precipitation and stream discharge. Puerto Rico's steep topography and small water-storage capacity leave the island's water supply and developed flood plains vulnerable to extreme weather events, such as hurricanes, floods, and droughts. This vulnerability may increase in the future owing to ongoing change, both local (such as land-cover shifts, water-supply projects, and construction of roads and other infrastructure) and regional (climate variability and change). Climate change, which could lead to more intense and prolonged droughts as well as an increase in the magnitude and frequency of destructive storms in the Caribbean, may alter temperature and affect the availability of water for human and ecosystem needs. Accurate assessment of hydrologic regimes and water budgets is therefore crucial for effective management of water resources.

As part of the U.S. Geological Survey's Water, Energy, and Biogeochemical Budgets program, hydrologic and geomorphologic processes and stream chemistry of four small watersheds in eastern Puerto Rico, which differ in geology and land cover, have been studied since 1991. Spatial and temporal characteristics of precipitation and stream discharge, along with water budgets, were determined for the watersheds for the period 1991 to 2005. The locations of the watersheds relative to the Luquillo Mountains and the range's associated rain shadow dominate hydrological processes, dwarfing influences of land cover. The influence of geology is reflected in recession characteristics of the rivers (recession is faster in soils overlying volcaniclastic bedrock) and in hillslope geomorphic processes (sediment is delivered at higher rates from soils overlying granitic bedrock).

Introduction

Five field sites throughout the United States have been monitored since 1991 as part of the U.S. Geological Survey's (USGS) Water, Energy, and Biogeochemical Budgets (WEBB) program (Baedecker and Friedman, 2000). The WEBB site located in eastern Puerto Rico represents a montane, humid-tropical environment. The site consists of four small watersheds that are part of two important water-supply sources for the island: the Luquillo Mountains and the Río Grande de Loíza watershed (fig. 1). River segments within the Icacos and Mameyes watersheds are designated as wild and scenic rivers, which requires that they remain in an essentially primitive condition and free of impoundments (Ortiz-Zayas and Scatena, 2004; Interagency Wild and Scenic Rivers Council, 2008). The four watersheds have different geology and land cover. Two watersheds (Icacos and Cayaguás) are located on coarse-grained granitic rocks, and two (Mameyes and Canóvanas) are located on fine-grained volcanic and volcaniclastic rocks. For each bedrock type, one watershed is dominated by mature wet tropical forest (Icacos and Mameyes), and one watershed has been affected by agricultural land use (Canóvanas and Cayaguás). The four watersheds have been closely monitored since 1991 to evaluate the effects of geology, land cover, geomorphic processes, atmospheric deposition, and other factors on stream water quality and quantity. Geology and land cover are discussed in Murphy and others (2012), geomorphic processes in Larsen (2012), and water quality in Stallard and Murphy (2012). This chapter describes the climate and hydrology of these watersheds, assesses spatial and temporal characteristics of precipitation inputs and stream-discharge outputs, and assesses water budgets by using several methods. This analysis considers stream-discharge, precipitation, and evapotranspiration data, mainly from the USGS, the National Atmospheric and Oceanic Administration (NOAA), and the National Science Foundation-funded Long-Term Ecological Research Program (LTER) Program.

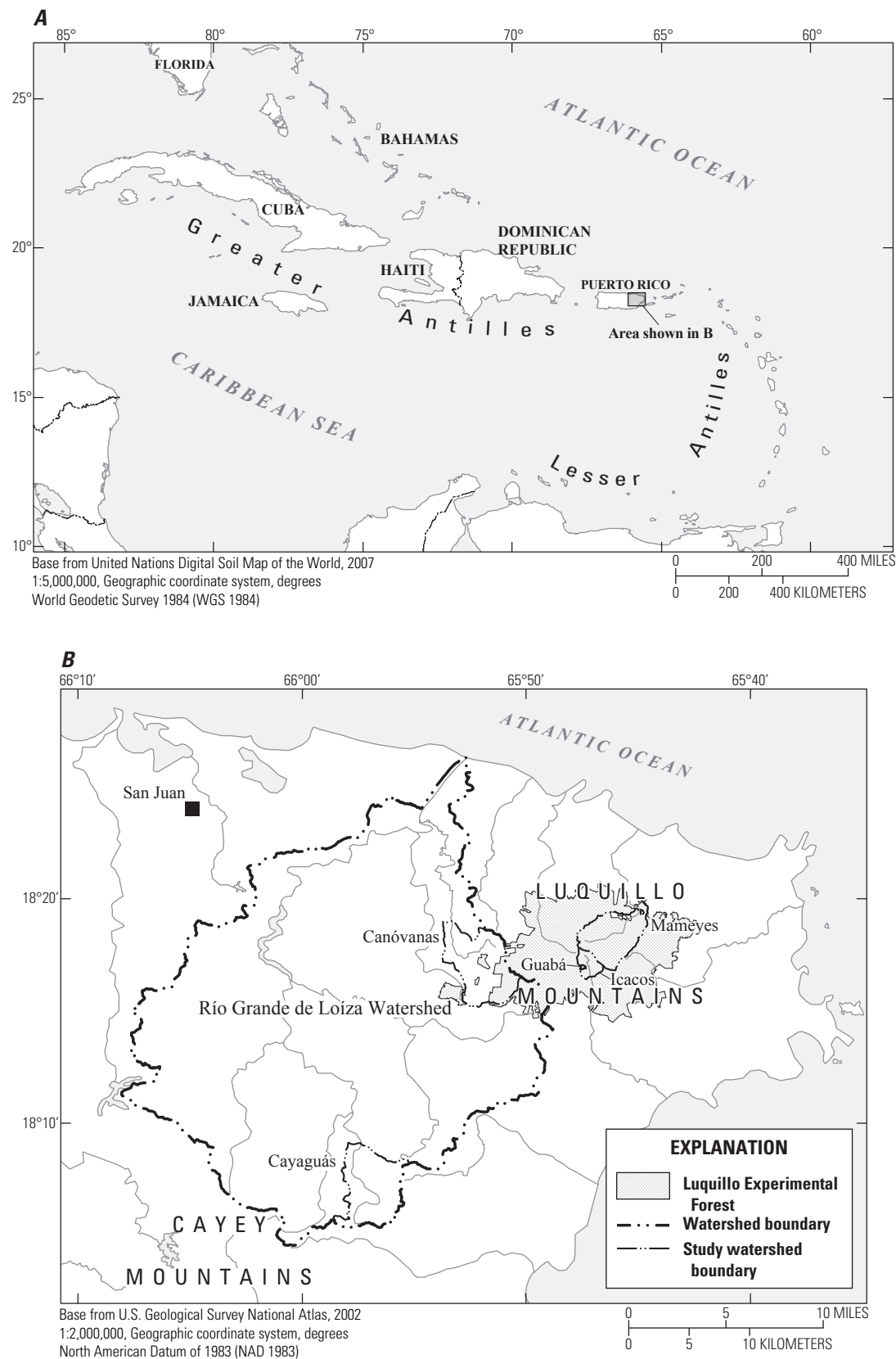


Figure 1. Location of Puerto Rico and study watersheds, eastern Puerto Rico.

Climate and Hydrology of Eastern Puerto Rico

The island of Puerto Rico has a humid tropical climate with a narrow range of daily temperature because of its location in the tropics and the buffering effect of the ocean (table 1). Weather is dominated by the easterly trade winds, which are predominantly from the east-northeast (Calvesbert, 1970). Hurricanes and other large storms embedded in the trade winds deliver about 70 percent of yearly rainfall; such storms affect the Caribbean about nine times a year on average (Calvesbert, 1970; Musk, 1988). Since 1851, 10 hurricanes have passed within 50 kilometers (km) of the Luquillo Mountains (fig. 2). During this study (in 1998), Hurricane Georges, the most destructive hurricane to strike Puerto Rico since San Ciprian in 1932, delivered more than 630 mm of rainfall in the central mountains and triggered extensive flooding and debris flows (Bennett and Mojica, 1998; Smith and others, 2005; Larsen and Webb, 2009). Cold fronts moving from North America into the Caribbean during winter months (December through April) can also cause major rainstorms that last for days; the amount of precipitation caused by these storms depends on the intensity and rate of progression of the cold front (Calvesbert, 1970). Such massive storms can mobilize sediment and debris into stream channels, cause sedimentation of reservoirs, and degrade coral reefs (Zack and Larsen, 1993; Webb and Soler-López, 1997; Warne and others, 2005; Larsen and Webb, 2009).

The path of trade winds over Puerto Rico's substantial topography (fig. 3) causes rainfall to vary greatly throughout the island (fig. 4). Pico del Este, on the southeastern side of the Luquillo Mountains (fig. 5) is the first summit crossed by the trade winds; orographic lifting produces frequent rain showers and the highest annual precipitation recorded in Puerto Rico. About 29 percent of precipitation at higher altitude in the mountains is from trade-wind-associated rainfall (Scholl and others, 2009). Precipitation on the eastern side of the Luquillo Mountains (and thus in the Mameyes and Icacos watersheds) is closely related to elevation: it ranges from 1,500 mm annually on the north coastal plain to almost 5,000 mm at high elevations (Brown and others, 1983). Precipitation on the western side of the Luquillo Mountains, including the Canóvanas watershed, is less well characterized; few data have been

collected (table 2) and little work has been done there, except to note the existence of a rain shadow and that forests characteristic of drier conditions are found there (Ewel and Whitmore, 1973; Brown and others, 1983).

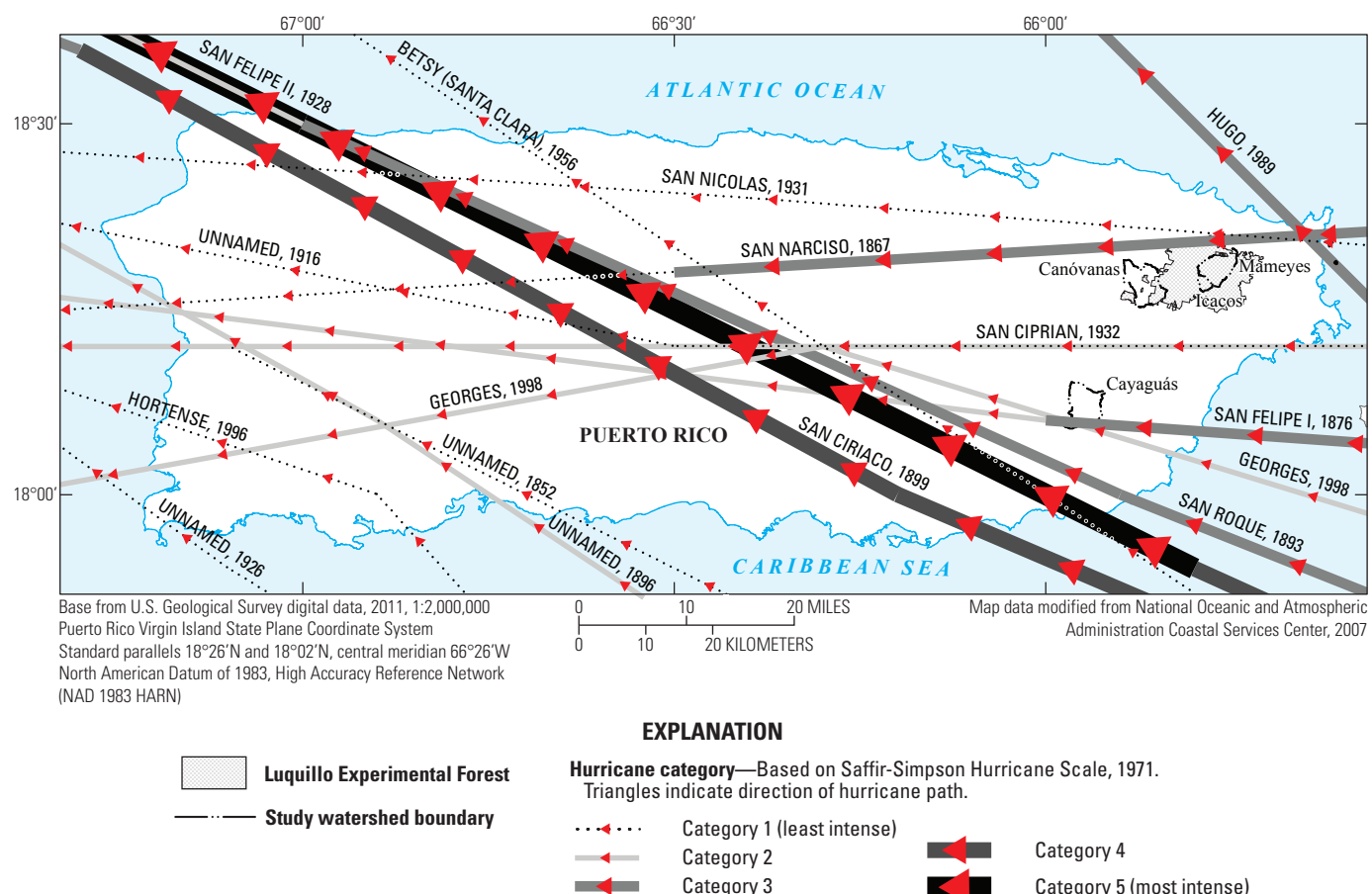
Stream valleys in Puerto Rico are narrow, short, and steep owing to the island's east-west-trending mountain chain (Cordillera Central) that divides a relatively narrow north-south dimension (fig. 3). Streams therefore respond rapidly to precipitation; Puerto Rico has the greatest threat of flash flooding of any state or territory under the jurisdiction of the U.S. National Weather Service (Carter, 1997). In order to mitigate flood peaks and to store this water for year-round use, several reservoirs have been constructed. The Loíza Reservoir, which receives water from the Cayaguás and Canóvanas watersheds (fig. 1), supplies about one third of the 11.9 cubic meters per second ($\text{m}^3 \text{ s}^{-1}$) of water delivered to San Juan (population 421,958 in 2000) (U.S. Census Bureau, 2000; Quiñones, 2010). Water withdrawals in and around the Luquillo Experimental Forest provide about $2.2 \text{ m}^3 \text{ s}^{-1}$ of potable water to Puerto Rico (Scatena and Johnson, 2001), which is about 7 percent of the 2010 island consumption of $31.8 \text{ m}^3 \text{ s}^{-1}$ (Quiñones, 2010). In 1999, water extracted from the streams that drain the Luquillo Mountains was estimated to be worth about US\$25 million per year in terms of the cost paid by consumers (Larsen and Stallard, 2000). Water shortages are a chronic problem in Puerto Rico. Reservoir storage is lost because of high sedimentation associated with storms (Webb and Soler-López, 1997). In the 20th century, major droughts affected the island in 1966–1968, 1971–1974, 1976–1977, and 1993–1995 (Larsen, 2000). During this study, the 1993–1995 drought led to severe water rationing for the city of San Juan; in response, residents collected water in open containers, which lead to outbreaks of dengue fever (Rigau-Pérez and others, 2001). Droughts may also contribute (through dryness or warming), along with atmospheric chemical changes, to Puerto Rico's ongoing amphibian die-off (Stallard, 2001; Burrowes and others, 2004; Longo and others, 2010). Because of strong orographic controls on the distribution of rainfall and the characteristic patchiness of convective rainfall in the tropics, the intensity of droughts in Puerto Rico can differ markedly in short distances (Larsen, 2000).

Table 1. Temperature statistics for 1991–2005 at meteorological stations in or near study watersheds, eastern Puerto Rico.

[From National Oceanic and Atmospheric Administration (2008), and U.S. Geological Survey Automated Data Processing System internal data, written commun. (2008). ID, identification number; Met, meteorological station; USGS, U.S. Geological Survey; NOAA, National Oceanic and Atmospheric Administration]

Station	Operator	Operator Station ID	Elevation (meters)	Mean daily temperature (degrees Celsius)	Mean minimum daily temperature (degrees Celsius)	Mean maximum daily temperature (degrees Celsius)	Dates excluded ¹
Bisley Met	USGS	50065549	482	22.8	21.2	25.5	1/1991–5/1991, 5/1998–2/2000
Icacos Met	USGS	50075001	600	21.4	19.1	25.3	1/1991–3/1992, 2/1997–2/1999, 3/2002–12/2005
Juncos 1SE	NOAA	665064	65	25.7	20.6	30.6	None
Pico Del Este	NOAA	666992	1,051	18.6	16.4	20.4	7/2005–12/2005

¹Some dates excluded due to missing data or obvious errors; shorter time periods may also be excluded.

**Figure 2.** Hurricanes that have passed over or near Puerto Rico since 1850 (from National Oceanic and Atmospheric Administration Coastal Service Center, 2007).

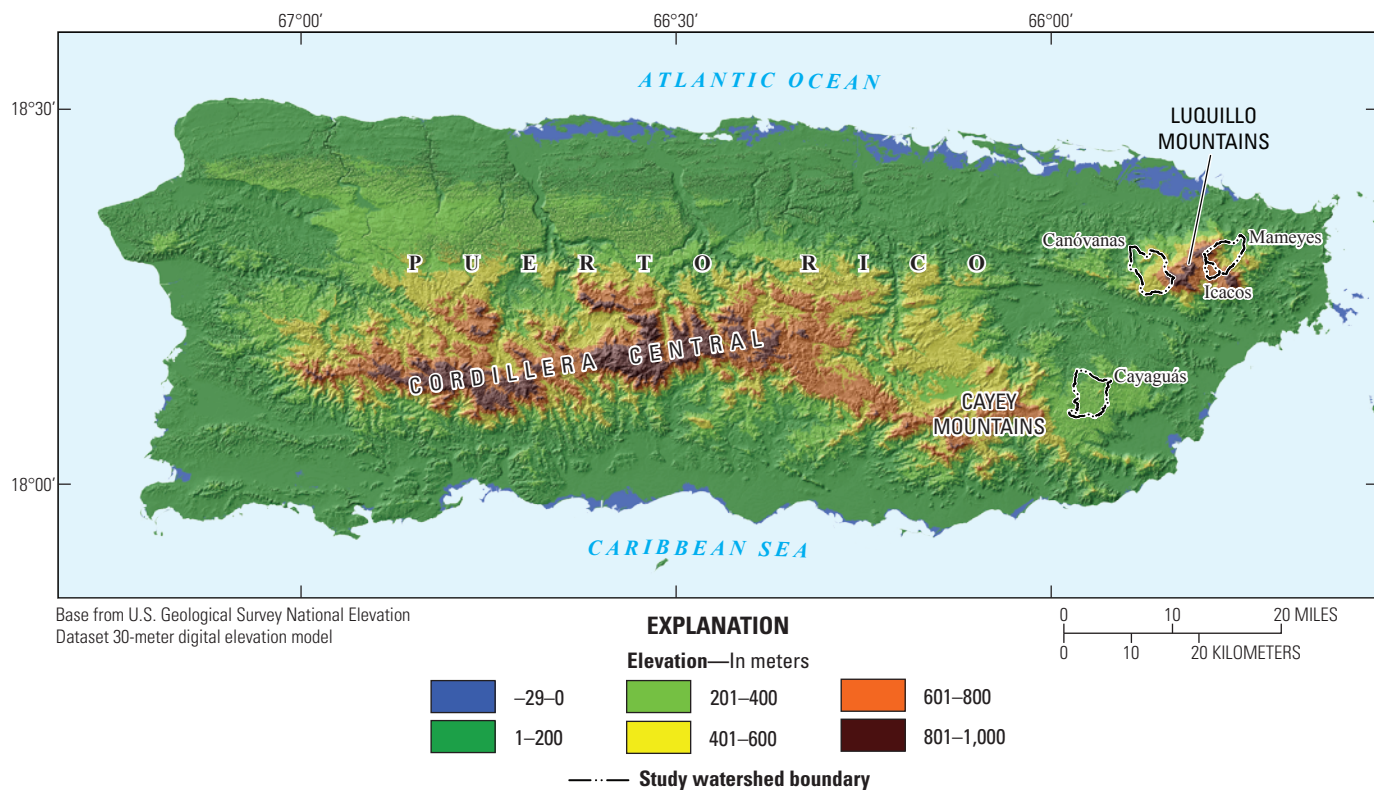


Figure 3. Elevation and relief of Puerto Rico.

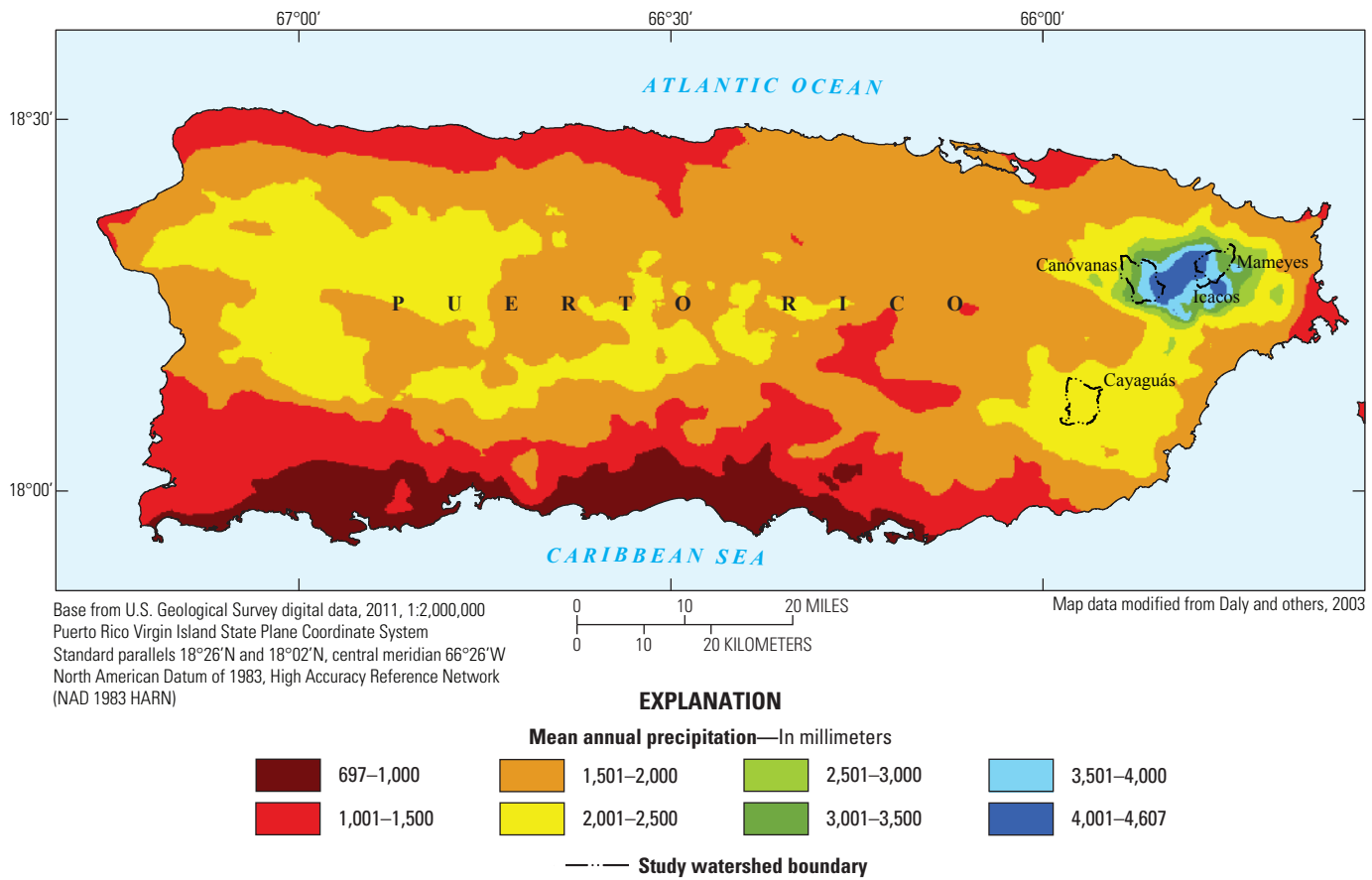


Figure 4. Mean annual precipitation of Puerto Rico, based on PRISM model for 1963 to 1995 (from Daly and others, 2003).

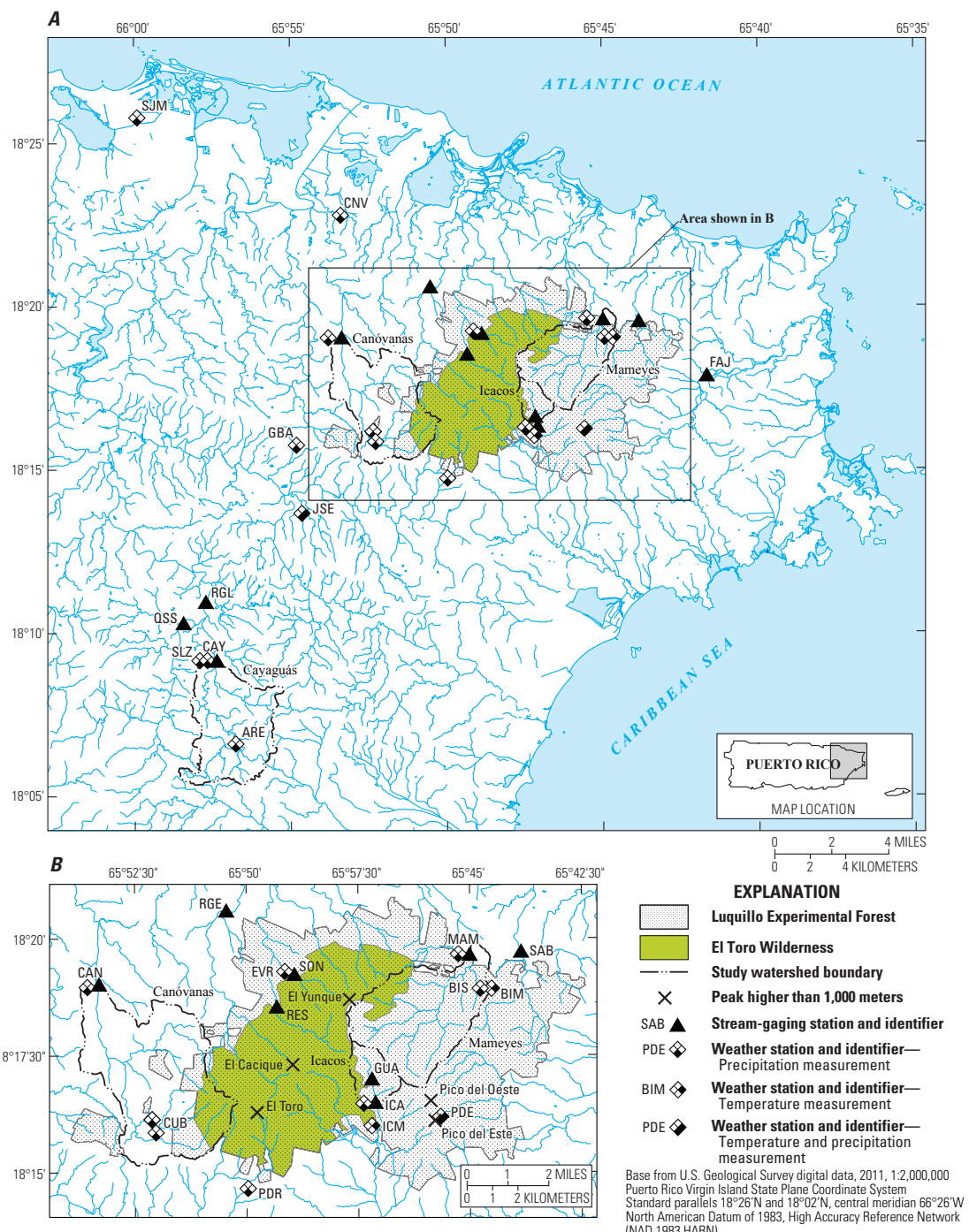


Figure 5. Location of stations, Luquillo Experimental Forest, and El Toro Wilderness (refer to table 2 for names of stations represented here by three initials; “CUB” was located at the southern site from 1986 to 1996 and at the northern site from 1996 to present).

Table 2. Stream-gaging and precipitation stations, eastern Puerto Rico.

[--, not available; m, meters; ID, identification code; USGS, U.S. Geological Survey; LTER, Long-Term Ecological Research; NOAA, National Oceanic and Atmospheric Administration; P, precipitation station; T, air temperature station; S, stream-gaging station]

ID	Station	Operator	Operator station ID	Elevation (m)	Type	Land cover ¹
ARE	Quebrada Arenas	USGS	50999960	270	P	Pasture, lowland wet forest
BIM	Bisley Meteorological Station	USGS	50065549	482	T	Tabonuco forest
BIS	Bisley Tower	LTER	--	360	P	Tabonuco forest
CAN	Río Canóvanas near Campo Rico	USGS	50061800	68	P, S	Pasture
CAY	Río Cayaguás at Cerro Gordo	USGS	50051310	150	P, S	Pasture, urban, moist forest
CNV	Canóvanas (NOAA)	NOAA	661590	9	P	Urban, wetlands
CUB	Cubuy	NOAA	663113	600 ²	P	Pasture, montane wet forest
EVR	El Verde	LTER	--	350	P	Tabonuco forest
FAJ	Río Fajardo near Fajardo	USGS	50071000	42	S	Lowland moist forest, pasture
GBA	Gurabo Abajo	USGS	50999959	285	P	Pasture, moist forest
GUA	Quebrada Guabá near Naguabo	USGS	50074950	640 ³	S	Colorado forest, palm forest
ICA	Río Icacos near Naguabo	USGS	50075000	616 ⁴	P, S	Colorado forest, palm forest
ICM	Icacos Meteorological Station	USGS	50075001	600	T	Tabonuco forest
JSE	Juncos 1SE	NOAA	665064	65	P, T	Urban, pasture
MAM	Rio Mameyes near Sabana	USGS	50065500	84	P, S	Tabonuco forest
PDE	Pico del Este	NOAA	666992	1,051	P, T	Palm forest, colorado forest
PDR	Pueblito del Río	USGS	50999958	341	P	Pasture, moist forest
QSS	Quebrada Salvatierra near San Lorenzo	USGS	50051180	100	S	Pasture, moist forest
RES	Río Espíritu Santo near Río Grande	USGS	50063800	12	S	Tabonuco forest
RGE	Río Grande near El Verde	USGS	50064200	40	S	Moist forest, pasture
RGL	Río Grande de Loíza at Highway 183 near San Lorenzo	USGS	50051800	80	S	Pasture, urban, moist forest
RSS	Río Sabana at Sabana	USGS	50067000	80	S	Montane wet forest
SJM	San Juan LM Marin Airport	NOAA	668812	3	P	Urban
SLZ	San Lorenzo 3S	NOAA	668815	155	P	Pasture, urban
SON	Quebrada Sonadora near El Verde ⁵	USGS	50063435	375	S	Tabonuco forest

¹Gould and others, 2008.

²Located at 600 m from 1996 to 2005 (northern site, fig. 5), and at 500 m from 1991 to 1996 (southern site, fig. 5).

³Rain gage located at 648 m, but not included owing to potential underestimates (see Interpretive Approach section).

⁴Rain gage located at 643 m.

⁵Owing to large number of missing years during this study, precipitation data not used.

Climate Variability and Change

The climate of Puerto Rico is influenced by several global-scale climate patterns. The El Niño–Southern Oscillation (ENSO), which involves both ocean and atmospheric interactions, has an average recurrence interval of 3.8 years for El Niño episodes of moderate and greater intensity (Quinn and others, 1987). A negative Southern Oscillation Index, which corresponds with an El Niño episode, tends to be associated with warmer years and fewer tropical storms in Puerto Rico (Gray, 1984; Malmgren and others, 1998). The North Atlantic Oscillation, which is strictly atmospheric, is a slower and more irregular (8–10 years) climate fluctuation (Hurrell and others, 2003). A low North Atlantic Oscillation appears to force storms south towards the Caribbean (Elsner and others, 2000) and results in higher mean annual precipitation in Puerto Rico (Malmgren and others, 1998). The Atlantic Multidecadal Oscillation involves both the ocean and the atmosphere and is manifested as a 0.4°C fluctuation of North Atlantic sea-surface temperatures that

lasts several decades (Kerr, 2000, 2005; Knight and others, 2006). Long-term records of tree rings (Gray and others, 2004) and African lake sediments (Shanahan and others, 2009) indicate that this oscillation has persisted for at least 3,000 years as strong, well-coupled oscillations in 30- to 50-year cycles. A high Atlantic Multidecadal Oscillation corresponds to a wet Sahel and to more frequent and intense hurricanes in the Atlantic Ocean (Landsea and Gray, 1992; Kerr, 2005; Knight and others, 2006). The effects of warming on hurricanes may be strictly physical (Knight and others, 2006); however, Sahel rainfall is best modeled with vegetative feedbacks acting on oscillation-induced temperature fluctuations, which produce both lags and amplifications (Zeng and others, 1999). Saharan dust appears to suppress hurricane formation (Dunion and Veldon, 2004), offering an alternative physical explanation of why wetter times in the Sahel (which generate less dust) might increase the formation or intensity of hurricanes. During the 15 years of this study, the Southern Oscillation Index, North Atlantic Oscillation, and Atlantic Multidecadal Oscillation indices varied

widely (fig. 6). The Atlantic Multidecadal Oscillation, after several decades of predominantly negative values, reversed to positive values in 1995 and remained so for most of this study. The close relations between these indices and precipitation complicate the interpretation of long-term hydrologic trends, and they suggest that rigorous characterizations of precipitation or streamflow in the region will require many decades, particularly if the effects of climate change are being evaluated.

Assessing long-term climate change in Puerto Rico is difficult owing to the lack of robust climate proxies, such as tree rings or natural lakes, which would provide pollen records to assess past vegetation and hence climate. However, pollen from lake sediments in nearby Haiti provides clues to the climate of the region (Hodell and others, 1991; Higuera-Gundy and others, 1999). Pollen at the base of a lake core (estimated to be 10,000 years old) indicates cool, dry conditions. Xeric vegetation persisted until a forest expansion at about 7,000 years before present (BP). During the mid-Holocene (7,000 years to 3,500 years BP), lake levels were high and moist-forest vegetation was at its most abundant. Since 3,500 years BP, vegetation reflected ongoing drying conditions; many of the land mammals went extinct in this interval. Other circum-Caribbean sites show parallel trends (Higuera-Gundy and others, 1999). Historical data in Puerto Rico, such as the loss of water from springs and wells that had historically been used for water supply, corroborate ongoing drying for the last 500 years (Zack and Larsen, 1993; Scatena, 1998; Larsen, 2000); however, for these indicators of drying it would be difficult to entirely separate climate shifts from locally driven land-use changes, such as deforestation and soil compaction by grazing and agriculture.

Climate models produced by the Intergovernmental Panel on Climate Change (Christensen and others, 2007) have forecast that the trend of increasing dryness in Puerto Rico will continue. An increase in the frequency and severity of droughts, and changes in the temperature and humidity of the lower atmosphere, could lead to an increase in the altitude of the typical cloud base and the concomitant upward shift of ecological zones on mountains (Still and others, 1999; Lawton and others, 2001; van der Molen and others, 2006). This higher elevation of cloud base could help to decrease orographic precipitation, which provides about 30 percent of annual precipitation in the Luquillo Mountains (Scholl and others, 2009), and could reduce part of Puerto Rico's water supply. The intensity and number of large hurricanes in the Atlantic are predicted to increase this century (Emanuel, 2005), which could lead to greater loss of human life, infrastructure, and habitat as a result of mass wasting, flooding, and defoliation. Hurricane Hugo nearly decimated the population of the endangered Puerto Rican parrot (*Amazona vittata*), which had already been made vulnerable through decades of deforestation and the encroachment of nest-site competitors (Beissinger and others, 2008).

Relation of Land Cover to Climate and Hydrology

In less than 500 years, Puerto Rico was transformed from an island covered by about 95 percent forest (before European settlement) to about 6 percent forest in the 1950s (Wadsworth, 1950; Birdsey and Weaver, 1982; Kennaway and Helmer, 2007). A shift from an agricultural to an industrial economy, and a subsequent population migration from rural to urban areas, has led to a regrowth of forests; today, about half of the island is mature or secondary forest (Kennaway and Helmer, 2007; Gould and others, 2012). The reforestation of Puerto Rico, including two of the watersheds in this study (Canóvanas and Cayaguás), may affect local climate and hydrologic processes. Nonforested landscapes tend to have lower rates of evapotranspiration owing to the reduction of canopy interception and transpiration compared to forests (Lawton and others, 2001, and references therein), leading to an increase in annual runoff of typically 300 to 500 mm (Bruijnzeel, 2004; Jackson and others, 2005). Deforestation may also modify flood peaks (Bruijnzeel, 2004; Center for International Forestry Research, 2005; Bradshaw and others, 2007; Alila and others, 2009; van Dijk and others, 2009). Where soil and drainage patterns are not highly disturbed, increased runoff from deforestation infiltrates soil and may be manifested as increased base flow. When soil is compacted or additional drainage networks such as trails and roads are created, much of the increase is in near-surface or surface flow; storm peaks increase and streams rise and fall more quickly in response to storms. These changes may have a pronounced downstream effect only in watersheds less than 100 km² in area (Center for International Forestry Research, 2005).

Cloud Forest

One of the primary factors controlling vegetation type in the Luquillo Mountains is cloud-base elevation (Wadsworth, 1951; Ewel and Whitmore, 1973; Brown and others, 1983). The highest peaks in the Luquillo Mountains are often shrouded in clouds, which typically form when trade winds force air upslope (Roe, 2005). The elevation of the cloud base is related to the trade-wind boundary layer, a zone of turbulently mixed air below the base of trade-wind cumulus clouds. Over the oceans, complex feedbacks associated with moisture transport (cloud growth and rain) driven by shallow-cumulus convection, control the elevation of the trade-wind boundary layer and the rate of sea-surface evaporation (Rauber and others, 2007). Accordingly, the elevation of the cloud base is largely controlled by sea-surface conditions, but its altitude is susceptible to changes in regional climate, sea-surface temperature, and land cover. The cloud base over the ocean region to the east of Puerto Rico is typically around 600 meters (m), but it can be as low as 400 m (Snodgrass and others, 2009, and references therein). In the Luquillo Mountains, the cloud condensation level is typically between 600 and 800 m (Eugster and others, 2006), and the cloud base moves up during the day and down at night. We do not have a precise description of this

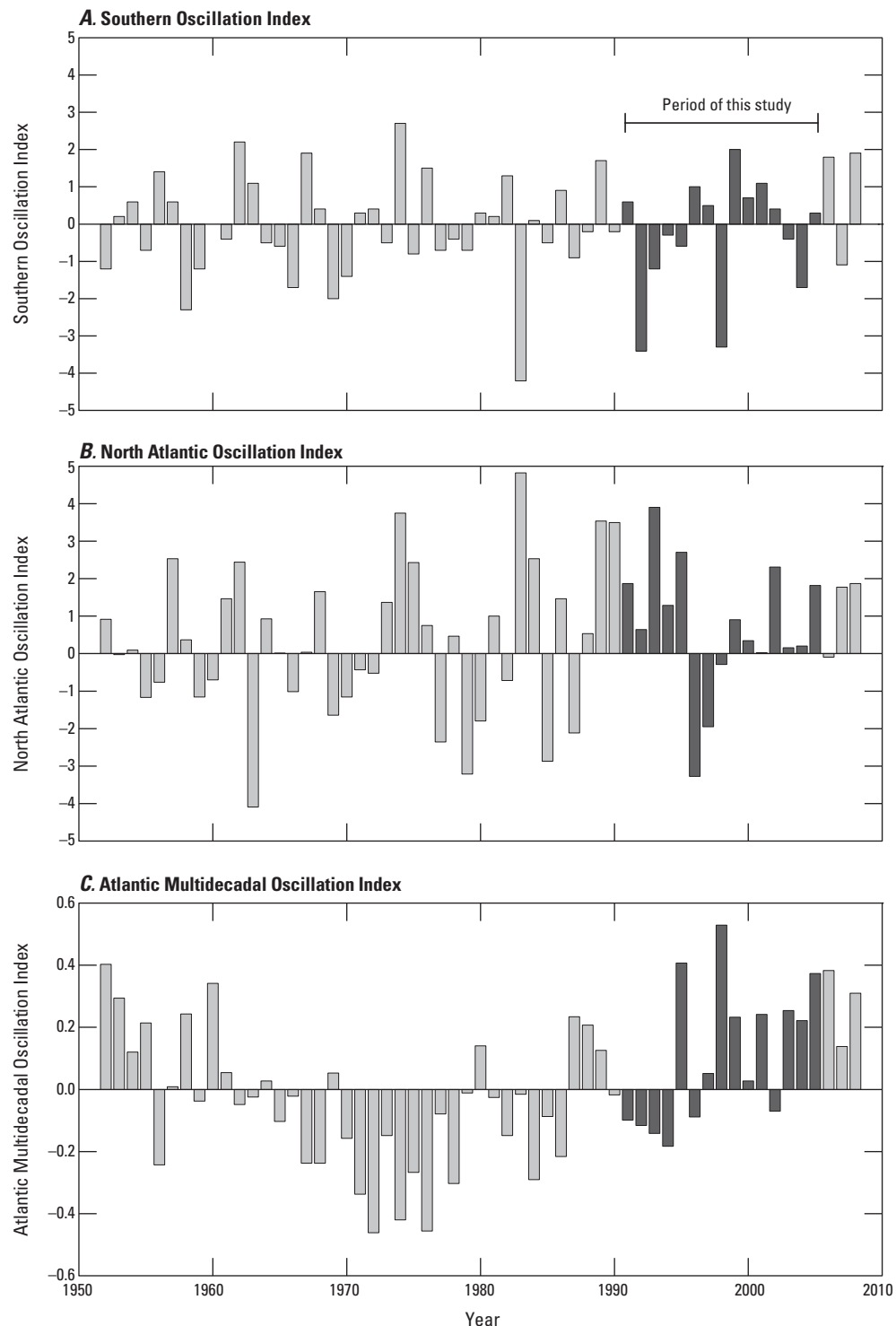


Figure 6. Indices of oscillations that affected Puerto Rico, 1950–2010 (National Oceanic and Atmospheric Administration, 2010).

cycle, but we have observed that as the day progresses, cloud base rises tens of meters above the low divide between the Mameyes and Icacos watersheds (at about 750-m elevation). Cloud forest vegetation (colorado forest, mixed palm forest, elfin cloud forest, and montane shrublands) grows above about 600 m and is adapted to high humidity, droplet deposition, reduced transpiration, and low-light conditions (Murphy and others, 2012).

Conversely, land cover can influence the altitude of the cloud base, and even the presence or absence of trade-wind cumuli, in eastern Puerto Rico. Trade wind velocities in the region are typically 1 to 5 meters per second ($m\ s^{-1}$) (Lawton and others, 2001), and the Luquillo Mountains are less than 20 km from the coast, so air from the ocean has about 1 to 5 hours to interact with land before reaching the mountain summits. At these time scales, terrestrial heating and evapotranspiration may decrease or increase precipitation, depending on land cover. For example, the defoliation of much of the east flank of the Luquillo Mountains by Hurricane Hugo in 1989 was associated with an observable increase in the altitude of the cloud base (Scatena and Larsen, 1991).

Interpretive Approach

Hydrology in the Luquillo Experimental Forest, which contains the Mameyes and Icacos watersheds, has been studied by many researchers (including Lugo, 1986; McDowell and others, 1992; Scatena, 1995, 2001; García-Martinó and others, 1996; Larsen and Concepción, 1998; Pringle, 2000; Schellekens and others, 2000, 2004; Scatena and Johnson, 2001; Rivera-Ramírez and others, 2002; Ortiz-Zayas and Scatena, 2004; Peters and others, 2006; Crook and others, 2007; and many others). Much less work has been done on the hydrology of the Cayaguás and Canóvanas watersheds (Larsen and Concepción, 1998; Larsen and Simon, 1993). Our analysis of precipitation, discharge, and evapotranspiration data in eastern Puerto Rico for the period 1991 to 2005 had three objectives: (1) comparison of the spatial and temporal characteristics of precipitation inputs and stream-discharge outputs for the four WEBB watersheds, (2) determination of water budgets, and (3) hydrologic interpretation to allow accurate assessments of weathering rates and fluxes of dissolved constituents and sediment (Larsen, 2012; Stallard, 2012; Stallard and Murphy, 2012).

Precipitation

Precipitation in eastern Puerto Rico shows wide spatial variation related to elevation, topographic position, and proximity to the ocean (fig. 4). Therefore, the density of precipitation stations in the region (fig. 5) is not ideal for estimating precipitation at the local scale. The Canóvanas watershed is particularly challenging, owing to its wide range in elevation (70 to 960 m) and the sparsity of precipitation stations in and

near the watershed. Three methods were used to estimate mean annual precipitation in the study watersheds: (1) the relation between elevation and precipitation; (2) a spatially based model of precipitation in Puerto Rico (Daly and others, 2003; and (3) reported evapotranspiration and precipitation data for land-cover types within each watershed. Land-cover-based estimates of water budgets have numerous methodological difficulties, but because of earlier deforestation and recent afforestation, they are used here as a guide to the potential effects of the ongoing afforestation in the Canóvanas and Cayaguás watersheds.

Daily precipitation data from NOAA (National Oceanic and Atmospheric Administration, 2008), the USGS (Automated Data Processing System internal data, written commun., 2008), and the Luquillo LTER program (Long Term Ecological Research Network, 2008) for stations in and near the watersheds were summed to obtain annual precipitation during the study period (1991–2005). Hourly data from the NOAA cooperator station Cubuy, within the Canóvanas watershed (CUB, fig. 5), were summed to obtain daily and annual precipitation in order to improve spatial coverage (data for this station are reported only on days when precipitation is recorded). Annual precipitation data for the LTER Bisley Tower station (BIS, fig. 5) were obtained from Heartsill-Scaley and others (2007) and from F.N. Scatena, University of Pennsylvania (written commun., 2009). Mean annual precipitation during the study period was then calculated for each station.

In or near the Icacos and Mameyes watersheds, precipitation stations included in this analysis are located at the stream-gaging stations at the mouth of each watershed (ICA and MAM), within the Mameyes watershed at the LTER Bisley Tower (BIS), and at two stations located within 4 km of the watershed boundaries (EVR and PDE) (table 2, fig. 5). Precipitation data from the USGS Guabá stream-gaging station and the USGS Bisley and Icacos meteorological stations were not included because we believe that these stations under-report precipitation. Mean annual precipitation values were anomalously low for their elevations, and precipitation at the USGS Bisley station was much lower than at the nearby LTER Bisley Tower station. The USGS Bisley station is located at the top of a ridge that is exposed to high winds; precipitation has been observed to fall at 45 degree angles and not enter the gage (Angel Torres-Sánchez, USGS, oral commun., 2008). The Guabá station is located along a narrow road and is overshadowed by forest canopy, which probably prevents some precipitation from reaching the station.

In or near the Canóvanas watershed, precipitation stations included in this analysis are located at the stream-gaging station at the mouth of the watershed (CAN), within the watershed (CUB), and at three stations located between 2 and 5 km from the watershed boundary (GBA, JSE, and PDR) (table 2, fig. 5). Precipitation stations located within or near the Cayaguás watershed included in this analysis are located within the watershed (ARE), and at or near the mouth of the watershed (CAY and SLZ).

We also evaluated variable-time-step precipitation data from USGS stations at the mouth of each of the four studied watersheds to evaluate storm duration and maximum precipitation events. These data were obtained internally from the USGS (on file at the Caribbean Water Science Center, Guaynabo, Puerto Rico) and converted to 15-minute and 1-hour intervals. Missing data were interpolated.

In order to evaluate the effect of climate variability on precipitation and runoff in eastern Puerto Rico, the relations of three climate indices (El Niño–Southern Oscillation, North Atlantic Oscillation, and Atlantic Multidecadal Oscillation) with precipitation and runoff were evaluated with a least-squares linear regression. The NOAA precipitation stations Pico del Este (PDE) and Canóvanas (CNV, which is in a different location than the USGS stream-gaging station of the same name; table 2, fig. 5) have the longest records in eastern Puerto Rico and were thus used in this assessment. Only one stream-gaging station in eastern Puerto Rico, on the Río Fajardo (station 50071000, Río Fajardo near Fajardo; FAJ on fig. 5), has a discharge record adequately long to compare with multidecade climate indices. In order to assess how much variance in annual precipitation in eastern Puerto Rico can be accounted for by regional-scale climate events, a simple linear regression was performed to determine how well precipitation at each station can be predicted by precipitation at nearby stations.

Regression Model of Precipitation Based on Elevation

Elevation and precipitation have been found to be closely related in the Luquillo Experimental Forest, on the basis of stations located on the northern and eastern side of the Luquillo Mountains (Brown and others, 1983; García-Martino and others, 1996). Following García-Martino and others' (1996) evaluation of 18 stations, a simple polynomial regression of elevation (in meters) and mean annual precipitation (in millimeters) was developed by using the Pico del Este, Icacos, Mameyes, LTER Bisley Tower, and El Verde stations for the study period. The equation

$$\text{Mean annual precipitation} = 2,177.7 + 4.498 \cdot \text{elevation} - 0.0023 \cdot (\text{elevation})^2 \quad (1)$$

is very similar to that of García-Martino and others (1996) ($2,301.21 + 3.8 \cdot \text{elevation} - 0.0016 \cdot (\text{elevation})^2$). For the WEBB watersheds on the eastern side of the Luquillo Mountains (Icacos and Mameyes), we used equation 1 to estimate precipitation at the midpoint elevation of 50-m contour intervals (determined for each watershed by using a geographic information system, <http://www.esri.com/>), multiplied precipitation at each interval by the fraction of watershed within that interval, and summed to obtain total precipitation. Owing to the lack of precipitation data on the western side of the Luquillo Mountains, the extent of the

rain shadow they cause is not well known; stations west of the Luquillo Experimental Forest (fig. 5) do not have the close relation of elevation and precipitation. To accommodate for rain-shadow effects in the Canóvanas and Cayaguás watersheds, we corrected equation 1 as follows. For each watershed (the two watersheds were handled separately, because we assumed different rain-shadow effects), we calculated the rainfall that would be expected for each nearby precipitation station on the basis of equation 1. Observed and predicted precipitation at nearby stations were each averaged, and the ratio of observed to predicted was used to calculate a “rain shadow correction”—one for the Canóvanas watershed (0.560), and one for the Cayaguás (0.721). We multiplied the precipitation estimated by equation 1 at 50-m contour elevation midpoints by the correction factor for each watershed, and then we estimated total precipitation in each watershed by weighting for elevation.

Spatially Based Precipitation Model

A spatially based model of precipitation was also used to estimate precipitation in the watersheds. The PRISM (parameter-elevation regressions independent slopes model) mean annual precipitation dataset (Daly and others, 2003) incorporates point data, a digital elevation model, and other geographic data sets to generate gridded estimates of precipitation (fig. 4) and other climatic parameters. These data were overlain with the four watershed boundaries using geographic information systems to estimate mean precipitation in the watersheds.

Precipitation Based on Land Cover

Published mean annual precipitation values for land-cover types present in the four studied watersheds were averaged to obtain mean annual precipitation for each land-cover type (table 3). The mean annual precipitation for each land cover was then multiplied by the percentage of land cover in each watershed (see Murphy and others, 2012, their table 4), and these values were summed to obtain the mean annual precipitation for each watershed. Precipitation data have not been reported for secondary montane wet forest and montane wet shrubland or woodland, so these land-cover types were assigned mean annual precipitation of the most similar land-cover type, tabonuco forest. Because urban land, barren land, and water totaled less than 7 percent of the area in each watershed and they were typically located next to pasture (Murphy and others, 2012, their fig. 9), mean annual precipitation for pasture was used for these land-cover types.

Cloud Drip

Direct deposition of water from clouds onto vegetation is an important, but difficult to quantify, ecological and hydrological phenomenon in higher tropical mountains. Researchers have estimated that cloud drip contributes an additional

Table 3. Precipitation and evapotranspiration rates reported in literature, eastern Puerto Rico.

[Mean values rounded to three significant figures. km, kilometers; m, meters; mm yr⁻¹, millimeters per year; P, precipitation; ET, evapotranspiration; --, used value from previous study (see P method); LEF, Luquillo Experimental Forest]

Study	Region	Land cover	Elevation (m)	Annual P (mm yr ⁻¹)	Annual ET (mm yr ⁻¹)	P method	ET method
Pasture							
Van der Molen, 2002	15 km west of San Juan	Pasture (<i>Paspalum</i>)	2	1,700	1,383	Climate station data	Penman-Monteith method
Van der Molen, 2002	Fajardo airport	Grassland	30	1,625	1,011	Climate station data	Penman-Monteith method
Mean				1,660	1,200		
Lowland moist forest							
Ewel and Whitmore, 1973	San Juan airport	Subtropical moist forest	4	1,632	1,341	Climate station data	Tosi method (Ewel and others, 1968)
Van der Molen, 2002	15 km west of San Juan	Lowland wetland forest ¹	2	1,700	1,219	Climate station data	Penman-Monteith method
Mean				1,670	1,280		
Tabonuco							
Odum, Moore, and Burns, 1970	Espíritu Santo watershed (within LEF)	Tabonuco	424	3,869	1,558 ²	Measured	Field experiments (throughfall, stemflow, transpiration)
García-Martino and others, 1996	LEF	Tabonuco	402 ³	3,537	1,707	Precipitation-elevation regression	Water budget
Schellekens and others, 2000	Bisley (within Mameyes)	Tabonuco	265–456	3,584 ²	1,093 ²	Measured	Penman-Monteith and temperature fluctuation methods
Van der Molen, 2002	LEF	Tabonuco	356	--	1,066	García-Martino and others (1996)	Penman-Monteith method
Wu and others, 2006	LEF	Tabonuco	<600	--	1,252	García-Martino and others (1996)	Satellite imagery and model ⁴
Mean				3,660	1,340		
Colorado							
García-Martino and others, 1996	LEF	Colorado	720 ³	4,191	994	Precipitation-elevation regression	Water budget
Van der Molen, 2002	LEF	Colorado	780	--	1,044	García-Martino and others (1996)	Penman-Monteith method
Wu and others, 2006	LEF	Colorado	600–900	--	1,069	García-Martino and others (1996)	Satellite imagery and model ⁴
Mean				4,190	1,040		
Palm							
Frangi and Lugo, 1985	Espíritu Santo watershed (within LEF)	Palm	750	3,725	831	Measured	Field experiment (throughfall, stemflow, transpiration)
García-Martino and others, 1996	LEF	Palm	711 ³	4,167	1,009	Precipitation-elevation regression	Water budget
Van der Molen, 2002	LEF	Palm	900	--	694	García-Martino and others (1996)	Penman-Monteith method
Wu and others, 2006	LEF	Palm	600–900	--	1,051	García-Martino and others (1996)	Satellite imagery and model ⁴
Mean				4,020	900		
Elfin							
García-Martino and others, 1996	LEF	Elfin	897 ³	4,408 ⁵	1,144	Precipitation-elevation regression	Water budget
Van der Molen, 2002	LEF	Short cloud forest	>900	--	704	García-Martino and others (1996)	Penman-Monteith method
Wu and others, 2006	LEF	Elfin	>900	--	591	García-Martino and others (1996)	Satellite imagery and model ⁴
Mean				4,410	810		

¹*Pterocarpus officinalis*.

²Average of two values.

³Weighted average elevation of forest type in Luquillo Experimental Forest.

⁴Granger and Gray (1989).

⁵Does not include 10 percent addition for cloud moisture reported in García-Martino and others (1996).

6.6 to 18 percent to measured rainfall in the eastern Luquillo Mountains (Baynton, 1969; Weaver, 1972; Schellekens and others, 1998; Holwerda and others, 2006). Holwerda and others (2006) estimated annual cloud drip at 1,010-m elevation on Pico del Este to be 770 millimeters per year (mm yr^{-1}) by using a water budget method and 785 mm yr^{-1} by using the eddy-covariance method (which was corrected by using the water budget method). We estimated cloud drip at different elevations in the Icacos and Mameyes watersheds by interpolation, assigning a rate of zero mm yr^{-1} at 600 m, and Holwerda's water budget rate of 770 mm yr^{-1} at 1,000 m. To simplify the calculation we assigned interpolated values to 50-m elevation zones: 600 to 650 m, 650 to 700 m, and so on. We then calculated the percentage of each watershed in the 50-m elevation zones, estimated the total cloud drip from each elevation zone, and summed to estimate total cloud drip contribution for the Icacos and Mameyes watersheds.

It is uncertain to what degree cloud drip in a watershed is affected by the rain shadow west of the Luquillo Mountains. Leeward sites on Pico del Este receive about 60 percent less cloud drip than windward sites (Weaver, 1972), similar to the ratio of observed to predicted rainfall (0.560) that was used to calculate a correction for rainfall in the Canóvanas watershed. We therefore calculated the amount of cloud drip in the Canóvanas watershed by the same method as we used for the Icacos and Mameyes watersheds, then multiplied that amount by 0.560 to correct for this watershed's leeward location. The maximum elevation of the Cayaguás watershed is 445 m (Murphy and others, 2012, their table 1), below the cloud condensation level in eastern Puerto Rico, and therefore this watershed is assumed to not receive any cloud drip.

Runoff

Instantaneous discharge data were obtained internally for the five USGS WEBB stream-gaging stations: four located at the mouths of the studied watersheds (CAN, CAY, ICA, and MAM), plus one station within the Icacos watershed that is near the mouth of the Quebrada Guabá watershed (GUA) (table 2, fig. 5) (U.S. Geological Survey, 2010). The Icacos, Guabá, Cayaguás, and Canóvanas stations typically record discharge every 15 minutes; discharge at the Mameyes station is typically recorded every 5 minutes. All stream gages had gaps in discharge data during the study period, ranging from 30 minutes to more than a year. The longest data gaps were generally associated with the time needed to rebuild a gage lost in a large storm. For data gaps of less than 1 day, real-time discharge values were linearly interpolated from adjacent data. For all longer data gaps, discharge data were interpolated from daily-mean-discharge data using cubic splines on cumulative daily discharge (appendix 1). The Canóvanas and Guabá stream-gaging stations had especially long data gaps in 1991 and 1992. Discharge data from the Guabá stream-gaging station (activated in June 1992) are considered dubious after April 2003, when a large storm severely altered the Guabá stream channel.

Available daily mean-discharge values for the Canóvanas and Guabá stream-gaging stations correlate well with discharge at the Cayaguás and Icacos stream-gaging stations, respectively, so linear regressions (Helsel and Hirsch, 2002) were used to estimate discharge for the missing data. Corrections to discharge data for the Icacos stream-gaging station caused by a gradual datum shift from 1973 to 1993 (recognized in 2003) were also included in this analysis (appendix 1).

Discharge from each watershed was converted to runoff by dividing by drainage area. The drainage area of the Guabá stream-gaging station has been previously reported as 0.13 or 0.31 km^2 , and reported runoff was based on those drainage areas (U.S. Geological Survey, 1994–2006). We estimate a drainage area of 0.115 km^2 , on the basis of walking the drainage divide, recording the route with a global positioning system, and confirming the route by using satellite imagery. Calendar-year annual runoff values are reported for the study period (1991–2005) and were used to calculate mean annual runoff for that period.

Annual runoff values for the periods of record for the WEBB stream-gaging stations, along with those from the nearby Río Fajardo stream-gaging station (which has the longest runoff record in eastern Puerto Rico; fig. 5) were evaluated for statistical properties and variability. Annual runoff for every year was normalized to the geometric mean of annual runoff (normalized runoff=raw runoff/geometric mean) for the period of record for each river (based on the assumption that the processes that drive the variance around the geometric means of annual runoff behave similarly in the watersheds). The resulting normalized mean for each river was thus zero; this mean, along with the standard deviation of the log-runoff data, was used to calculate the lowest 1 percent of annual runoff (a one-in-one-hundred-years dry year) and the highest 1 percent (a one-in-one-hundred-years wet year). Annual runoff for all watersheds was aggregated into one dataset, and the variance of the aggregated data was evaluated. Also, a simple linear regression was used to test how well annual runoff for each WEBB river can be predicted by annual runoff in nearby rivers (Helsel and Hirsch, 2002).

Flow duration, maximum runoff events, and recession characteristics were evaluated from corrected 15-minute and hourly runoff data at the five USGS WEBB stream-gaging stations (CAN, CAY, GUA, ICA, and MAM, table 2). Runoff-rate percentile classes, which are based on the amount of time a river is within a given runoff range, were developed using an approach similar to that used by USGS WaterWatch (U.S. Geological Survey, 2009). The runoff rates in each percentile class for each river were calculated using all real-time runoff measurements during the 15-year study period.

Base-flow recession curves were assessed for the five USGS WEBB stream-gaging stations. Periods with monotonically decreasing runoff were identified from smoothed 5- or 15-minute measurements recorded at stream-gaging stations and from daily average data (appendix 1) and confirmed by a lack of precipitation at nearby rain gages. A rise in discharge indicated a new storm and signaled the end of

each recession. Following standard practice, the first 2 days of each recession were excluded to eliminate the influence of shallow-soil flow paths. We used observed discharge at 24-hour intervals rather than mean daily discharge and started data tabulation from the end of the recession and worked backward to minimize the lag period.

Mathematical formulations of base-flow recession curves can be empirical or based on reservoir models. The simplest recession model, and the only valid model for recessions of less than 10 days, is a linear (short for log-linear) recession (Chapman, 1999):

$$Q_t = Q_0 \cdot e^{-t/\tau} = Q_0 \cdot k^t, \quad (2)$$

where Q is discharge (in our calculations, we used runoff, $R=Q/\text{area}$, to compare watersheds of different drainage areas), Q_0 is discharge at the beginning of the recession, t is time ($t=0$ at the start of recession), τ is the turnover time, and k is the recession constant. A large k value indicates slow drainage (and greater storage), whereas a smaller k value indicates rapid drainage (and little storage). If many distinct groundwater reservoirs exist, a nonlinear model may be required (Chapman, 1999).

Assuming a simple aquifer with linear response, storage, S , is given by

$$S_t = Q_t \cdot \tau = Q_t / \ln(k). \quad (3)$$

Rivera-Ramírez and others (2002) examined recessions in the Río Fajardo and Río Espíritu Santo, in eastern Puerto Rico, using a variety of graphical and statistical approaches, and concluded that two regression approaches developed by Vogel and Kroll (1996) for interpreting the linear recession were the most robust. These approaches treat consecutive pairs of discharge measurements as either an integrated-moving-average (IMA) process or as a simple autoregressive (AR(1)) process, both of which have straightforward least-squares solutions for k . We evaluated recessions using these two approaches. We divided the predicted runoff rate at the end of recessions by the observed rate and calculated a margin of error at 95 percent confidence for this ratio for all modeled recessions. We also calculated the length of time needed to recede from the 10-percent runoff-rate percentile to the 1-percent runoff-rate percentile, and from the 1-percent runoff-rate percentile to the minimum runoff recorded at each river during the study period.

Groundwater and Storage

The four studied watersheds are underlain primarily by granitic, volcanic, and densely cemented volcaniclastic rocks (Murphy and others, 2012) that are typically not noted for being highly permeable. Springs are not common in the watersheds. Limestones are rare, and karst topography is nonexistent. Eastern Puerto Rico streams respond quickly to precipitation; recession curves suggest that

little water remains in storage (Rivera-Ramírez and others, 2002). Groundwater in storage in these upland watersheds is not well characterized but is sufficient to maintain flow in rivers that drain the studied watersheds, even during the driest periods. In general, base flow represents groundwater storage, and we posit our assessment of groundwater storage on this assumption. Hall (1968) presents numerous mathematical formulations of base-flow recession curves; some are based on reservoir models and others are empirical. The recession curves discussed in the previous section were used to estimate base flow, and hence groundwater storage (as an average depth throughout the area of the watershed, or linear storage) for the 1-percent runoff-rate percentile, S_1 (subscript 1 refers to the IMA recession model), and for the minimum observed runoff rate, S_A (subscript A refers to the AR(1) recession model). We used the effective water column needed to support the 1-percent runoff-rate to estimate and compare groundwater storage in the watersheds and for estimating errors in this intercomparison.

Water-Supply Inputs and Outputs

Comprehensive reviews of water intakes in the Luquillo Experimental Forest are available from Larsen and Concepción (1998) and Crook and others (2007, 2009). Thirty-one water intakes withdraw water from rivers draining this forest, including six that were added between 1994 and 2004. Few of these intakes are upstream of the USGS stream-gaging station evaluated here. There are no intakes in the Icacos watershed. U.S. Department of Agriculture Forest Service facilities withdraw less than 4 mm annually from the Mameyes watershed, and much of this water remains within the watershed (Larsen and Concepción, 1998). Documented public supply withdrawals are few in the Canóvanas and Cayaguás watersheds and total about 46 and 3 mm annually, respectively (Larsen and Concepción, 1998; Crook and others, 2007). Not only are these withdrawals small, but in order to be used to correct a water budget, the water must cross a drainage divide and bypass the watershed outlet, which is unlikely for these watersheds. Larsen and Concepción (1998) estimate that 78 percent and 89 percent of households in the Canóvanas and Cayaguás watersheds, respectively, have septic systems; using U.S. Census data and mean water consumption rates, they estimated that septic systems contribute about 10 and 5 mm to these watersheds.

Evapotranspiration

Evapotranspiration (ET) consists of several distinct sources: evaporation from the soil surface (E_s), evaporation from wet canopy (E_c), and transpiration (T), which is the transfer of water through plant stomata during photosynthesis:

$$ET = E_s + E_c + T. \quad (4)$$

All of these sources can be difficult to quantify. Some workers have calculated potential ET, or maximum ET under conditions of unlimited moisture supply, in the Luquillo Experimental Forest (Schellekens and others, 2000; Van der Molen, 2002; Wang and others, 2003) (table 3). This equation can be used to estimate wind-caused evaporation (which is essentially zero with either no wind or 100 percent humidity) and solar-radiation-driven evaporation (which is zero in darkness and reduced under low light) (Monteith, 1965; Howell and Evett, 2004). Other workers have also estimated ET in this forest with field experiments (Odum, Moore, and Burns, 1970; Frangi and Lugo, 1985), water budgets (García-Martino and others, 1996; Larsen and Concepción, 1998; Crook and others, 2007), and hydrologic models combined with satellite imagery (Wu and others, 2006) (table 3). These studies describe ET rates that generally decrease with increasing elevation in the forest. Reported ET rates are highest in the tabonuco forest (elevations below 600 m; table 3); ET in lowland rainforest, such as the tabonuco forest, is driven predominantly by solar radiation (Dietrich and others, 1982). ET is lowest in the elfin forest (elevations over 900 m), where frequent clouds and humidity near 100 percent for much of the time reduce ET substantially.

Few studies of ET have been undertaken in eastern Puerto Rico in the two major land covers in the Cayaguás and Canóvanas watersheds, pasture and lowland moist forest (Lugo, 1986; van der Molen, 2002). These studies typically suggest higher rates of ET in pasture and lowland moist forest than in the other forest types, with the exception of tabonuco forest. Nonforested landscapes tend to have lower rates of ET than forested watersheds, owing to the reduction of canopy interception (Lawton and others, 2001, and references therein). One study in Puerto Rico, however, had opposite results: van der Molen and others (2006) found grasslands to be cooler and more humid than nearby forest. However, this study compared an unusually wet grassland to a coastal monodominant forest type, a *Pterocarpus* swamp forest (Ewel and Whitmore, 1973). Water in the *Pterocarpus* swamp is brackish and soils are presumably anoxic; both characteristics would reduce ET, leading to both less cooling and drier conditions.

Evapotranspiration estimates for different land-cover types (table 3) were averaged to obtain mean ET values for each land-cover type in each watershed. The mean ET for each land cover was multiplied by the percentage of land cover in each watershed; these values were summed to obtain the mean ET for each watershed.

Evapotranspiration was also estimated from water budgets by subtracting watershed outputs from inputs:

$$ET = P + D + S - R - W - G, \quad (5)$$

where P is precipitation, D is cloud drip, S is septic sources, R is runoff, W is withdrawals, and G is groundwater recharge. If we assume that errors and uncertainty are

small, the differences between outputs and inputs for each watershed should approximate ET estimated by use of land cover estimations.

Error Estimation for Water Budgets

Many potential errors exist in measuring rainfall, both systematic (related to gage height and design, evaporation losses, splash in and out, and wind speed over the gage) and nonsystematic (related to site-specific factors, instrument malfunction, and observer error) (Barry, 2008). The overall systematic error for rain gages has been estimated to be about 5 to 15 percent for rainfall (Barry, 2008). The high level of spatial variability in precipitation in eastern Puerto Rico adds potential error when one estimates watershed-wide precipitation. Daly and others (2003) estimated error in the PRISM model for Puerto Rico with cross-validation and found that errors were greatest where spatial precipitation gradients are greatest and there is the most station-to-station variability in precipitation; in eastern Puerto Rico, error ranged from 0 to 35 percent (Daly and others, 2003, their fig. 12). A simple linear regression between one precipitation station and another in eastern Puerto Rico accounts for between 61 and 84 percent of variance; estimating precipitation at one station from three other stations accounts for between 75 and 94 percent of variance. It is unlikely that measurement error would exceed variance; therefore we estimate a maximum error in precipitation for the 15-year period of this study to be 15 percent, on the basis of the higher end of the error range of Barry (2008).

For error in cloud drip, we estimated an error of 45 percent, based on the error reported by Holwerda and others (2006) for hourly cloud-drip measurements.

The accuracy of discharge measurements can be affected by several factors, such as cross-section uniformity, velocity uniformity, and streambed conditions (Sauer and Meyer, 1992). The accuracy of the USGS stream-gaging stations is described in water-data reports as “excellent” (about 95 percent of the daily discharges is within 5 percent); “good” (within 10 percent); “fair” (within 15 percent) and “poor” (less than “fair” accuracy). Records for WEBB stream-gaging stations were considered fair during the study period with the exception of the Cayaguás, which was poor owing to shifting waves of sand (Díaz and others, 2004). A simple linear regression between runoff for any WEBB river and another eastern Puerto Rico river accounts for 78 to 86 percent of variance; estimating runoff for a WEBB river using runoff for three nearby rivers accounted for between 94 and 99 percent of variance. It is unlikely that measurement error would exceed variance; therefore we estimate a maximum error in discharge for the 15-year period of this study to be 15 percent for the Icacos, Mameyes, and Canóvanas rivers, and 20 percent for the Cayaguás rivers, on the basis of USGS estimates of accuracy for these stream-gaging stations.

The net water input or output for a watershed is zero if water is withdrawn from within a watershed and then recycled within the watershed. It is impractical to determine the cycle for all withdrawals and septic systems in the watersheds. In addition, the accuracy of reported values is probably low; 63 percent of the total water deliveries in Puerto Rico are unaccounted for, owing to leaks in the distribution system (half of the total deliveries), illegal connections, or accounting errors (Quiñones, 2010). Therefore, we have estimated an error of 100 percent for water withdrawals and septic system inputs.

Groundwater storage was estimated from recession curves and converted to an average depth throughout the area of each watershed. The 95-percent confidence interval of the logarithms (Helsel and Hirsch, 2002) of predicted base flow to the observed base flow was used to estimate error in effective groundwater storage.

Errors in estimating evapotranspiration from water budgets were calculated as the square root of the sum of squares for errors (Helsel and Hirsch, 2002) of each budget component.

Precipitation and Runoff in Eastern Puerto Rico

Mean annual precipitation at stations on the eastern side of the Luquillo Mountains (and hence the Mameyes and Icacos watersheds) ranged from about 2,500 mm to more than 4,000 mm (about 6.8 to 11 mm per day (mm day^{-1})) during the study period, and it was closely correlated with elevation (table 4; figs. 7, 8). Precipitation at stations in and near the Canóvanas and Cayaguás watersheds, on the western and southwestern side of the mountains, was substantially lower and not well correlated with elevation. Differences in precipitation at stations of similar elevations there may be due to differing rain-shadow effects, local topography, or recording errors.

As with precipitation, runoff was higher from the Icacos and Mameyes watersheds than from the Canóvanas and Cayaguás watersheds (table 5, fig. 9). While all four watersheds had substantial interannual variation in precipitation and runoff, mean annual runoff during the 1991–2005 study period was similar to the mean annual runoff for the periods of record (tables 5 and 6). A simple linear regression between runoff from any of the four watersheds and another eastern Puerto Rico river accounts for between 78 and 86 percent of variance (table 7), indicating that regional-scale weather patterns account for most of the interannual variability of runoff. Some of these regional weather patterns are related to climate oscillations (fig. 6); three climate indices (El Niño–Southern Oscillation, North Atlantic Oscillation, and Atlantic Multidecadal Oscillation) accounted for 46 percent of annual variance in precipitation at Pico del Este. The period of the longest climate cycle that affects the region, the Atlantic Multidecadal Oscillation (60 to 80 years; Kerr, 2000, 2005), is substantially

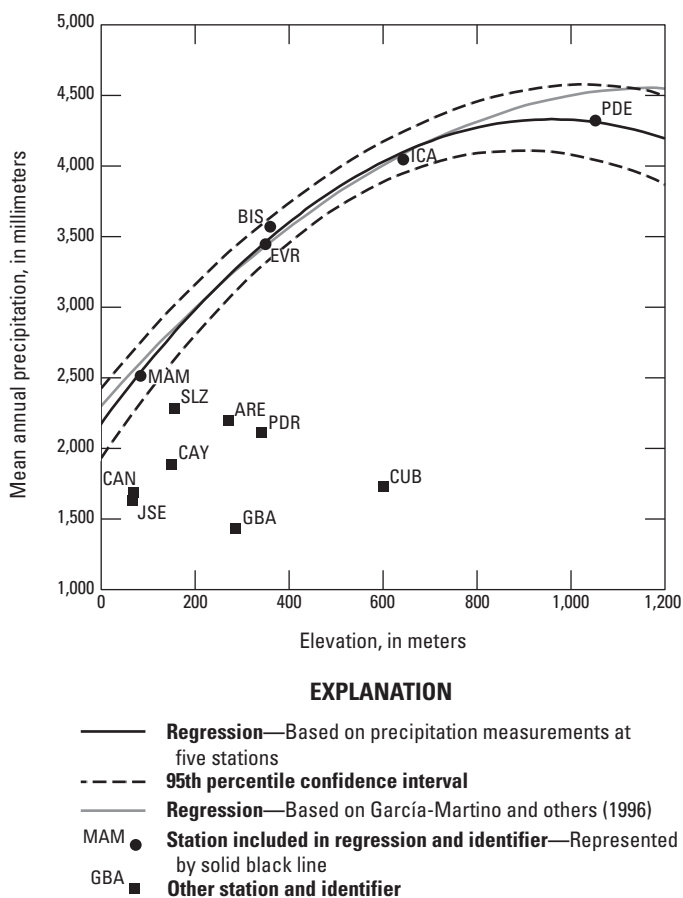


Figure 7. Elevation compared with mean annual precipitation (1991–2005) at stations in or near the study watersheds (Refer to table 2 for names of stations represented here by three initials).

longer than the longest period of record for any river in the region (47 years; table 6). Therefore, continued long-term streamflow monitoring will be needed to determine the effects of secular climate change, as compared to natural cycles, in these watersheds.

For WEBB rivers with the longest periods of record (Canóvanas, Cayaguás, and Mameyes), and the nearby Río Fajardo (FAJ in fig. 5), distributions of mean annual runoff are nearly log normal (fig. 10). When all the data are normalized to their geometric means and aggregated into a single data set, the distribution is even closer to normal (table 6). Because most of the interannual variability of the rivers appears to be caused by regional weather patterns (table 7), it is probable that rivers with shorter periods of records (Icacos and Guabá) are also log normal. Therefore we can calculate the lowest and highest 1 percent of annual runoff (that is, the one-in-one-hundred-years driest year, and the one-in-one-hundred-years wettest year, respectively) for all rivers; these percentiles are about a factor of 1.5 to 2.6 greater or less than the geometric mean (table 6). The rivers with the lowest mean-annual runoff (Canóvanas, Cayaguás, and Fajardo; table 6) have the highest fractions, indicating deeper droughts

Table 4. Total annual precipitation at stations in or near study watersheds, 1991–2005.[For information on sources and locations, see table 2. --, not available; mm d⁻¹, millimeters per day; mm yr⁻¹, millimeters per year; P, precipitation]

Year	Quebrada Bisley Arenas	Río tower	Río Canóvanas	Cubuy	El Verde	Gurabo Abajo	Río Icacos	Juncos 1SE	Río Mameyes	Pico del Este ¹	Puebloito del Río	San Lorenzo 3S
Annual precipitation (mm yr ⁻¹)												
1991	1,890	2,880	--	1,490	1,550	2,650	990	--	1,140	--	3,860	1,060
1992	2,870	3,860	--	1,810	1,950	1,880	1,620	--	1,600	2,220	4,930	2,110
1993	2,210	3,340	--	1,670	1,770	2,610	1,130	2,890	1,630	--	4,010	1,920
1994	1,860	2,680	1,000	1,280	1,420	1,320	800	3,240	1,180	1,980	3,460	1,940
1995	2,050	3,290	1,840	1,360	1,730	3,530	1,490	3,310	1,490	2,550	3,650	1,990
1996	2,050	3,750	2,200	2,280	1,950	4,580	--	4,880	1,950	3,040	5,380	2,880
1997	2,050	3,490	1,230	1,770	1,490	3,320	970	3,680	1,440	2,080	4,240	2,010
1998	2,590	4,010	1,630	2,710	2,220	5,290	2,110	4,970	2,430	2,890	5,120	3,190
1999	2,290	3,840	2,140	2,020	1,880	3,990	1,490	4,290	1,670	1,990	4,900	2,440
2000	1,640	2,690	1,270	1,770	1,380	2,830	1,280	3,600	1,310	1,760	3,840	1,720
2001	2,040	3,240	1,720	1,830	1,810	3,400	1,390	4,220	1,620	2,270	4,140	2,150
2002	1,780	2,650	1,310	1,500	1,640	3,130	1,240	3,670	1,100	1,970	3,870	1,720
2003	2,740	5,060	1,670	2,600	1,720	4,150	2,040	4,740	2,520	3,660	4,960	3,020
2004	2,300	4,500	2,080	2,110	1,690	5,210	1,400	5,000	1,440	3,410	4,020	3,130
2005	2,570	4,300	2,150	2,070	--	3,810	2,100	4,120	1,980	2,900	4,470	2,230
Mean ²	2,200	3,570 ³	1,690	1,880	1,730 ⁴	3,450	1,430	4,050	1,630	2,520	4,320	2,110
Years of missing data	None	None	1991–1993	None	2005	None	1996	1991–1992	None	1990–1991, 1993	None ¹	None
Maximum daily P, mm d ⁻¹	240	--	310	504	246	243	427	458	313	343	318	315
Date of maximum daily P, mm d ⁻¹	8/22/2001	--	9/10/1996	9/10/1996	9/21/1998	11/8/2001	9/22/1998	9/10/1996	9/10/1996	4/17/2003	11/12/03 ⁵	9/10/1996

¹Several dates were missing for this station; a regression based on the relation between precipitation at the Pico del Este station and the Icacos and El Verde stations was used to estimate daily precipitation on missing dates (Precipitation at Pico del Este = 0.649 • Precipitation at El Verde + 0.599 • Precipitation at Icacos).²Calculated from daily totals of hourly precipitation.³Calculated from annual totals from Hearlisl-Seale and others (2007) and F.N. Sealea, University of Pennsylvania.⁴Obtained from daily totals of hourly precipitation.⁵A higher value of 550 mm was recorded on 9/11/96, but because no value was recorded on 9/10/96, the value was divided over the 2-day period.

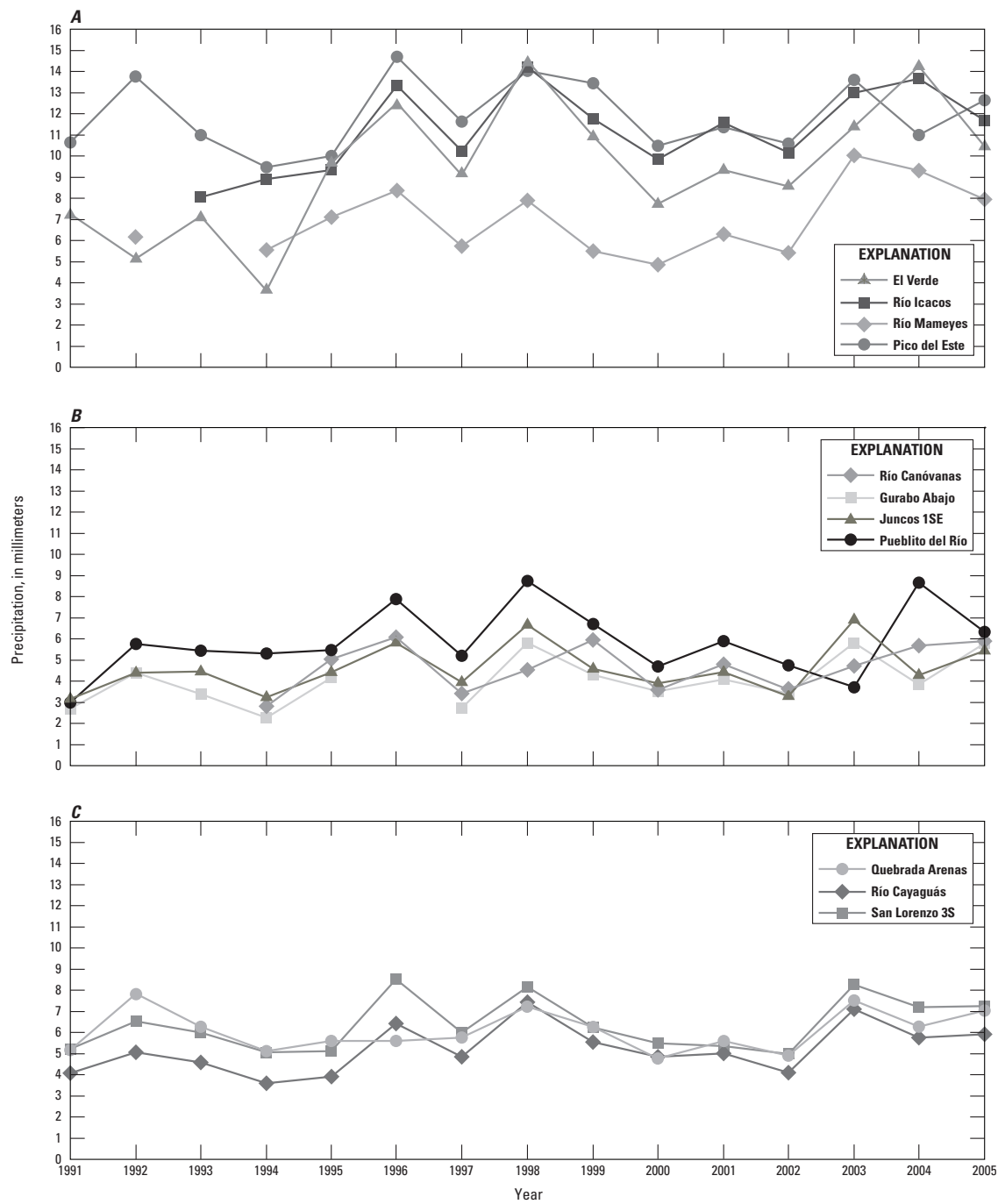


Figure 8. Mean daily precipitation by year at stations in or near study watersheds, eastern Puerto Rico. *A*, Mameyes and Icacos watersheds, *B*, Canóvanas watershed, and *C*, Cayaguás watershed (from Long Term Ecological Research Network, 2008; National Oceanic and Atmospheric Administration, 2008; U.S. Geological Survey Automated Data Processing System internal data, written commun., 2008). Missing data for Pico del Este estimated by regression with El Verde and Icacos stations.

Table 5. Annual runoff, stream statistics, and stream characteristics of study watersheds.[km, kilometers; km², square kilometers; m, meters; m³ s⁻¹, cubic meters per second; mm d⁻¹, millimeters per day; mm yr⁻¹, millimeters per year; -- not determined]

Parameter	Canóvanas ¹	Cayaguás	Guabá ²	Icacos	Mameyes
	Annual runoff ³ (mm yr ⁻¹)				
1991	470	650	2,700	3,090	2,330
1992	910	1,550	4,210	3,550	2,900
1993	670	1,600	2,960	2,940	2,690
1994	370	850	2,510	2,380	1,680
1995	810	940	2,760	3,510	2,320
1996	1,450	2,240	4,110	4,990	2,930
1997	700	1,760	3,480	3,930	2,430
1998	1,550	3,300	4,250	4,960	3,650
1999	1,310	2,120	4,120	4,190	3,250
2000	600	1,340	3,490	3,330	2,220
2001	710	1,060	3,520	3,400	2,630
2002	680	900	2,960	3,100	2,400
2003	1,420	1,910	4,450	4,170	3,400
2004	1,540	1,770	4,590	4,610	3,550
2005	1,450	2,240	4,260	4,290	2,930
Mean, 1991–2005	970	1,620	3,630	3,760	2,750
Mean daily runoff, mm d ⁻¹	2.7	4.4	9.9	10	7.5
Highest daily runoff, mm d ⁻¹	410	480	490 ⁴	430	257
Date of maximum daily runoff, mm d ⁻¹	9/10/1996	9/10/1996	9/10/1996	9/10/1996	9/10/1996
Period of record statistics					
Period of record ⁵	1967–2006	1977–2006	1992–2002	1945–1953, 1979–2006	1967–1973, 1983–2006
Mean annual discharge ⁶ , m ³ s ⁻¹	0.80	1.3	0.012	0.41	1.6
Mean annual runoff ⁶ , mm yr ⁻¹	990	1,580	3,450 ⁴	3,940	2,860
Highest daily mean discharge, m ³ s ⁻¹	120.0	140.0	0.65	20.0	80.0
Highest daily mean runoff, mm d ⁻¹	410	480	490 ⁴	430	380
Date of highest daily mean runoff	9/10/1996	9/10/1996	9/10/1996	9/10/1996	9/18/1989
Lowest daily mean discharge, m ³ s ⁻¹	0.023	0.20	0.002	0.042	0.20
Lowest daily mean runoff, mm d ⁻¹	0.077	0.66	1.3	1.1	0.95
Date of lowest daily mean runoff	7/24/1977	2/4/1981	5/31/1999	3/22/1946	4/20/1970
Maximum peak flow, m ³ s ⁻¹	489.9	402.1	3.3	--	580.6
Date of maximum peak flow	9/21/1998	8/22/2001	5/30/2002	4/17/2003	9/18/1989
Instantaneous low flow, m ³ s ⁻¹	0.023	0.20	0.001	--	0.14
Date of instantaneous low flow	7/24/1977	2/4/1981	5/1/1997	--	4/8/1970
Stream characteristics					
Elevation of gage, m	68	150	640	616	84
Mean elevation of watershed, m	464	287	702	686	508
Maximum elevation of watershed, m	956	445	767	832	1,050
Drainage area, km ²	25.5	26.4	0.114 ⁴	3.26	17.8
Stream order ⁷	4	4	--	2	3
Mean channel slope ⁷	0.15	0.12	--	0.073	0.21
Main channel length ⁷ , km	21.3	23.5	--	2.0	13.6
Total channel length ⁷ , km	34.4	49.5	--	2.9	24.0

¹Runoff in parts of 1991 and 1992 estimated from regression with Cayaguás stream-gaging station.²Runoff in 1991, 2004, 2005 and parts of 1992 and 2003 estimated from regression with Icacos stream-gaging station.³Based on corrected daily values for calendar year, as described in text.⁴Based on area determined as described in text (which is different from that reported in U.S. Geological Survey, 2006).⁵From U.S. Geological Survey (2006), except for Guabá (Díaz and others, 2004). A large storm on April 17, 2003, severely damaged the Guabá gage; data reported after that date are not used in this report.⁶Water year (October 1–September 30).⁷From Larsen (1997).

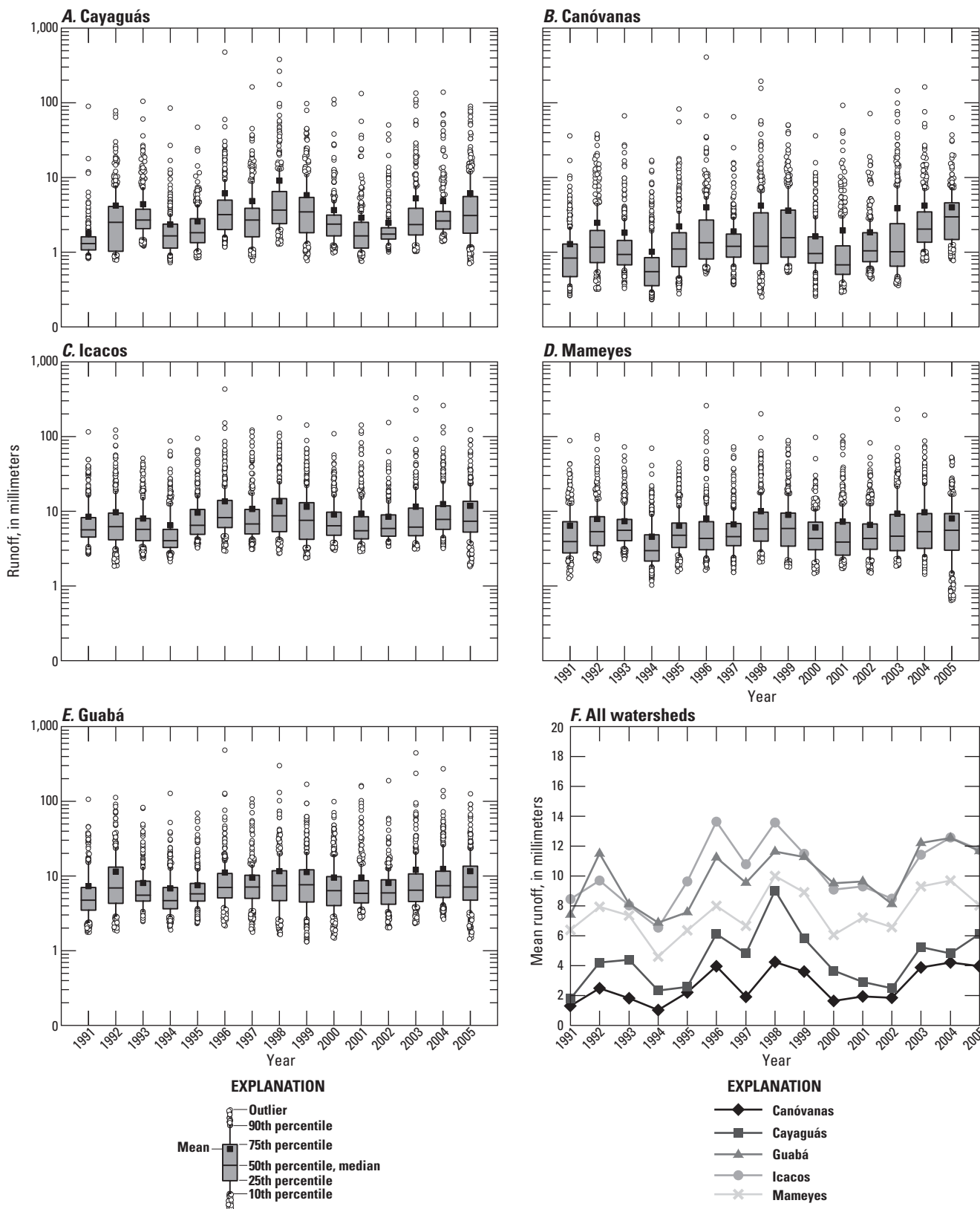


Figure 9. Mean daily runoff by year at U.S. Geological Survey stream-gaging stations (estimated from 5- or 15-minute discharge data from U.S. Geological Survey, 2010), eastern Puerto Rico. *A–E*, Standard box plots (Helsel and Hirsch, 2008) showing interquartile range in five watersheds; *F*, mean annual precipitation of same five watersheds. Runoff for Guabá in years 1991, 2004, and 2005 and portions of 1992 and 2003 estimated by regression with Icacos station; runoff for Canóvanas for portions of years 1991 and 1992 estimated by regression with Cayaguás station.

Table 6. Statistical properties of annual runoff of study watersheds and Río Fajardo (stream-gaging station 50071000, Río Fajardo near Fajardo) for years of record.[mm yr⁻¹, millimeters per year; --, not applicable]

Property	Watershed						All rivers, combined and normalized
	Fajardo	Canóvanas	Cayaguás	Mameyes	Icacos	Guabá	
Years of record	47	41	31	31	14	10	174
Annual runoff (mm yr ⁻¹)							
Mean	1,540	990	1,550	2,830	3,810	3,420	--
Geometric mean	1,460	910	1,440	2,760	3,730	3,370	--
Median	1,460	840	1,550	2,750	3,770	3,490	--
Standard deviation	520	420	590	620	740	580	--
Skewness	1.08	1.08	0.73	1.21	-0.08	0.03	--
Kurtosis	2.15	1.14	0.66	3.23	-0.57	-1.35	--
Log of runoff							
Mean	3.16	2.96	3.16	3.44	3.57	3.53	0.00
Median	3.16	2.93	3.19	3.44	3.58	3.54	-0.01
Standard deviation	0.14	0.18	0.17	0.09	0.09	0.07	0.14
Skewness	0.08	0.10	-0.22	0.25	-0.53	-0.19	0.00
Kurtosis	-0.19	-0.23	-0.41	1.19	0.06	-1.20	0.26
Highest and lowest 1 percent of mean annual runoff							
Lowest 1 percent (fraction of geometric mean)	0.47	0.39	0.41	0.61	0.62	0.67	0.47
Highest 1 percent (fraction of geometric mean)	2.1	2.6	2.5	1.6	1.6	1.5	2.1
1-in-100-year dry year, mm yr ⁻¹	680	350	580	1,690	2,330	2,260	--
1-in-100-year wet year, mm yr ⁻¹	3,130	2,340	3,540	4,510	5,970	5,030	--

and relatively greater wet conditions for the wettest years. During the periods of records, annual runoff values greater than the one-in-one-hundred-years wet year occurred in the Mameyes in 1970 and in the Fajardo in 1979 (U.S. Geological Survey, 2010). Annual runoff values less than the one-in-one hundred-years dry year occurred in the Mameyes in 1994; runoff from the Canóvanas that year was very close to the driest year (U.S. Geological Survey, 2010). Runoff from the Canóvanas watershed (2,340 mm yr⁻¹) during the wettest 1 percent of years is only slightly greater than the driest 1 percent of years for the Icacos watershed (2,330 mm yr⁻¹).

The driest time of the year in eastern Puerto Rico is typically January through April, and March is the driest month (fig. 11). According to the criterion used by tropical forest biologists to indicate a markedly dry season—at least 3 consecutive months of precipitation averaging less than 100 mm per month (Ashton and others, 2004)—none of the studied watersheds have a markedly dry season. Precipitation is typically greatest September through November; stations on the north and east sides of the Luquillo Mountains commonly also record high precipitation in May. Monthly runoff generally follows the same trend as monthly rainfall, and runoff typically is least during February through April and greatest during September through December (fig. 12).

On average, rain fell between 11 percent (Canóvanas and Cayaguás) and 21 percent (Icacos) of the time (on an hourly basis) in the study watersheds during the study period (fig. 13). Rainfall intensities greater than 10 mm h⁻¹ occurred 0.8 percent of the time that rain fell; when rainless time is included, this percentage is about 0.008 percent (about 42 minutes) of a year.

Peak hourly rainfall ranged from 64 mm (at the Canóvanas stream-gaging station) to 93 mm (at the Icacos stream-gaging station), and peak 15-minute rainfall ranged from 27 mm (at the Canóvanas stream-gaging station) to 34 mm (at the Mameyes stream-gaging station) (table 8).

For 84 percent of the time or more, on an hourly basis, runoff from the studied watersheds was in the lowest 50th percentile (table 9). At these lower runoff rates, the hourly runoff from the WEBB rivers were arrayed in the same sequence as annual runoff; at the 50th percentile, runoff from the Canóvanas was 0.25 mm h⁻¹, and runoff from the Icacos was 0.57 mm h⁻¹. Runoff from the WEBB watersheds was in the top 10th percentile only between 0.06 and 0.33 percent of the time; at this runoff percentile, runoff rates for the watersheds ranged from 5 to 11 mm h⁻¹ and were not proportional to annual runoff (fig. 14). Maximum runoff rates for the largest storms were commonly similar among all four study watersheds (table 9), suggesting that higher annual runoff in the Icacos and Mameyes watersheds is probably controlled by frequent, smaller rain events related to orographic precipitation.

The flow duration curves for all studied watersheds are generally steep (fig. 14), consistent with streams that have highly variable flows and are dominated by direct runoff (Searcy, 1959). The steep slope at the ends of the curves suggests a negligible amount of storage.

Greatest precipitation and runoff (both totals and rates) during the study period are associated with major storms that struck eastern Puerto Rico, such as Hurricane Hortense in 1996, Hurricane Georges in 1998, an upper level trough and a tropical wave in 2003, and Tropical Storm Jeanne in 2004

Table 7. Summaries of successive regressions of annual runoff and precipitation in eastern Puerto Rico.[For river and stream-gage abbreviations, see table 2. mm yr⁻¹, millimeters per year; r, correlation coefficient]

Stream gage	River A		River B		River C		r	Variance (percent)
	Constant (mm yr ⁻¹)	Slope	Runoff (mm yr ⁻¹)	Slope	Runoff (mm yr ⁻¹)	Slope	Runoff (mm yr ⁻¹)	
Canóvanas								
CAN	= -105	+	0.723	x	FAJ	--	--	0.93
CAN	= -337	+	0.546	x	FAJ	+ 0.212	x	0.96
CAN	= -425	+	0.362	x	FAJ	+ 0.176	x	0.98
CAY	= -193	+	0.775	x	RES	--	--	0.88
CAY	= -387	+	0.432	x	RES	+ 1.075	x	0.93
CAY	= -87	+	0.570	x	RES	+ 1.198	x	0.95
ICA	= 1,684	+	0.891	x	RES	--	--	0.93
ICA	= 1,387	+	0.654	x	RES	+ 0.480	x	0.96
ICA	= 1,533	+	0.475	x	RES	+ 0.337	x	0.97
MAM	= 1,614	+	1.169	x	CAN	--	--	0.90
MAM	= 1,465	+	0.668	x	CAN	+ 0.351	x	0.93
MAM	= 1,390	+	0.313	x	CAN	+ 0.425	x	0.94
Cayaguás								
CAN	= 179	+	1.033	x	SIM	--	--	0.78
CAN	= 180	+	1.380	x	SIM	+ -0.293	x	0.83
CAN	= -11	+	1.167	x	SIM	+ -0.511	x	0.88
CAY	= -191	+	0.940	x	SLZ	--	--	0.956
CAY	= -802	+	0.655	x	SIM	+ 0.295	x	0.979
CAY	= -649	+	0.837	x	SIM	+ 0.222	x	0.981
CUB	= 629	+	0.784	x	SIM	--	--	0.91
CUB	= 674	+	1.001	x	SIM	+ -0.139	x	0.95
CUB	= 719	+	1.254	x	SIM	+ -0.149	x	0.97
Icacos								
CBA	= -173	+	1.168	x	SIM	--	--	0.81
CBA	= -174	+	0.522	x	SIM	+ 0.546	x	0.94
CBA	= -164	+	1.024	x	SIM	+ 0.390	x	0.95
ICA	= 1,414	+	1.494	x	CNR	--	--	0.92
ICA	= 2,546	+	2.271	x	CNR	+ -1.481	x	0.96
ICA	= 1,993	+	2.067	x	CNR	+ -1.731	x	0.97
Mameyes								
MAM	= -109	+	0.724	x	BIS	--	--	0.89
MAM	= 930	+	0.942	x	BIS	+ -0.430	x	0.93
MAM	= 1,536	+	0.827	x	BIS	+ -0.734	x	0.97

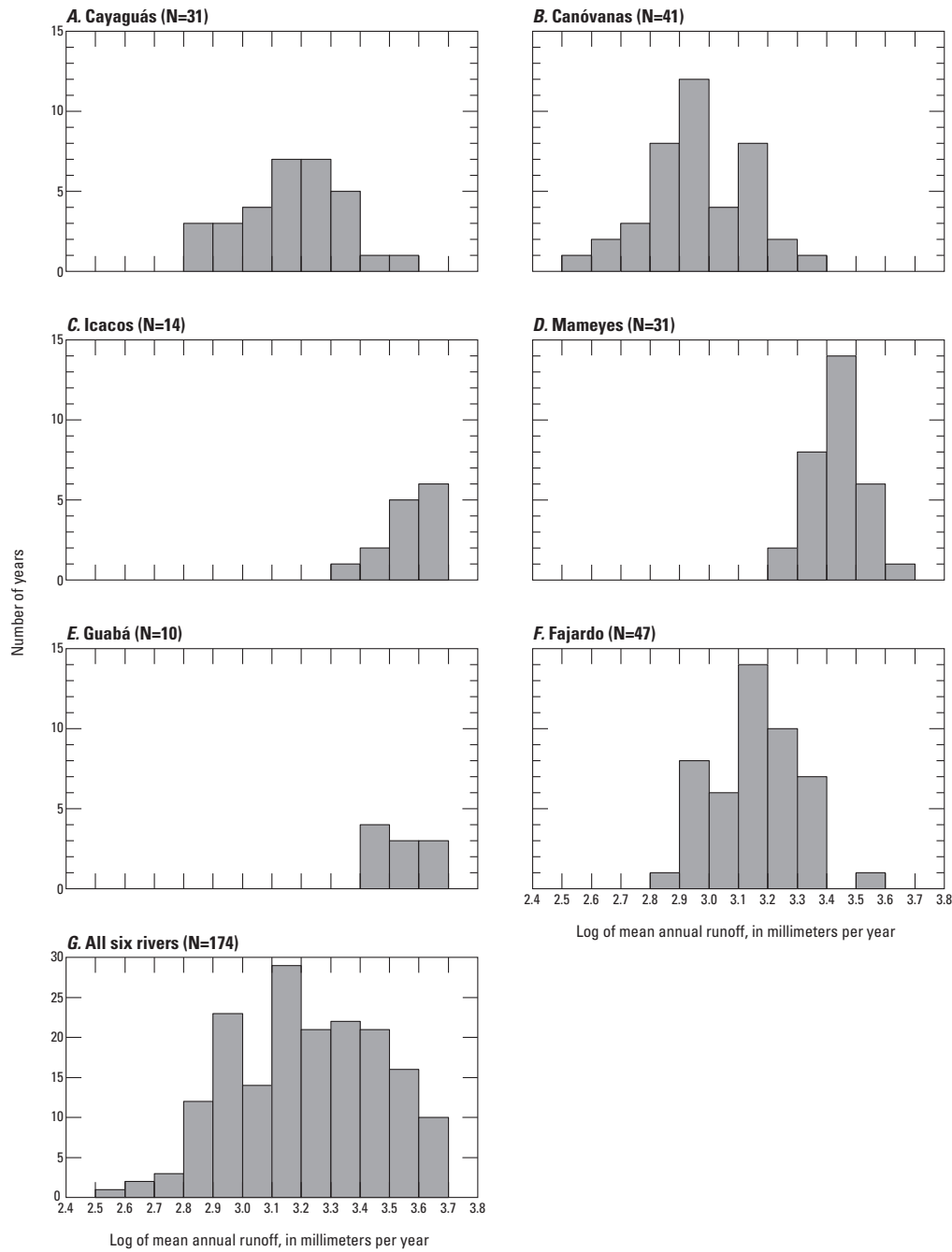


Figure 10. Distribution of log of mean annual runoff from study watersheds and Río Fajardo (stream-gaging station 50071000, Río Fajardo near Fajardo) for periods of record.

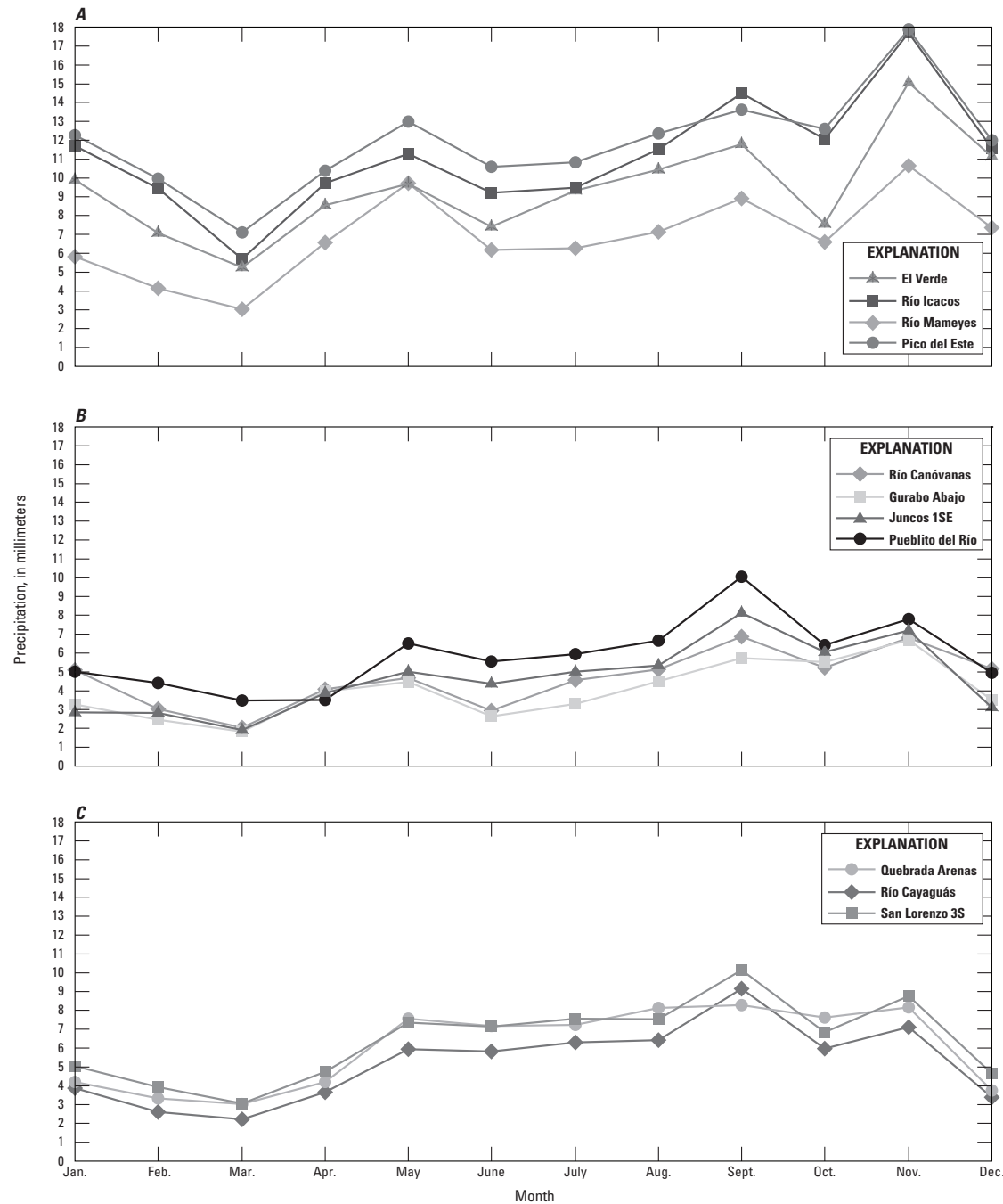


Figure 11. Mean daily precipitation by month at stations in or near study watersheds. *A*, Mameyes and Icacos watersheds, *B*, Canóvanas watershed, and *C*, Cayaguás watershed (from Long Term Ecological Research Network, 2008; National Oceanic and Atmospheric Administration, 2008; U.S. Geological Survey Automated Data Processing System internal data, written commun., 2008). Missing data for Pico del Este estimated by regression with El Verde and Icacos stations.

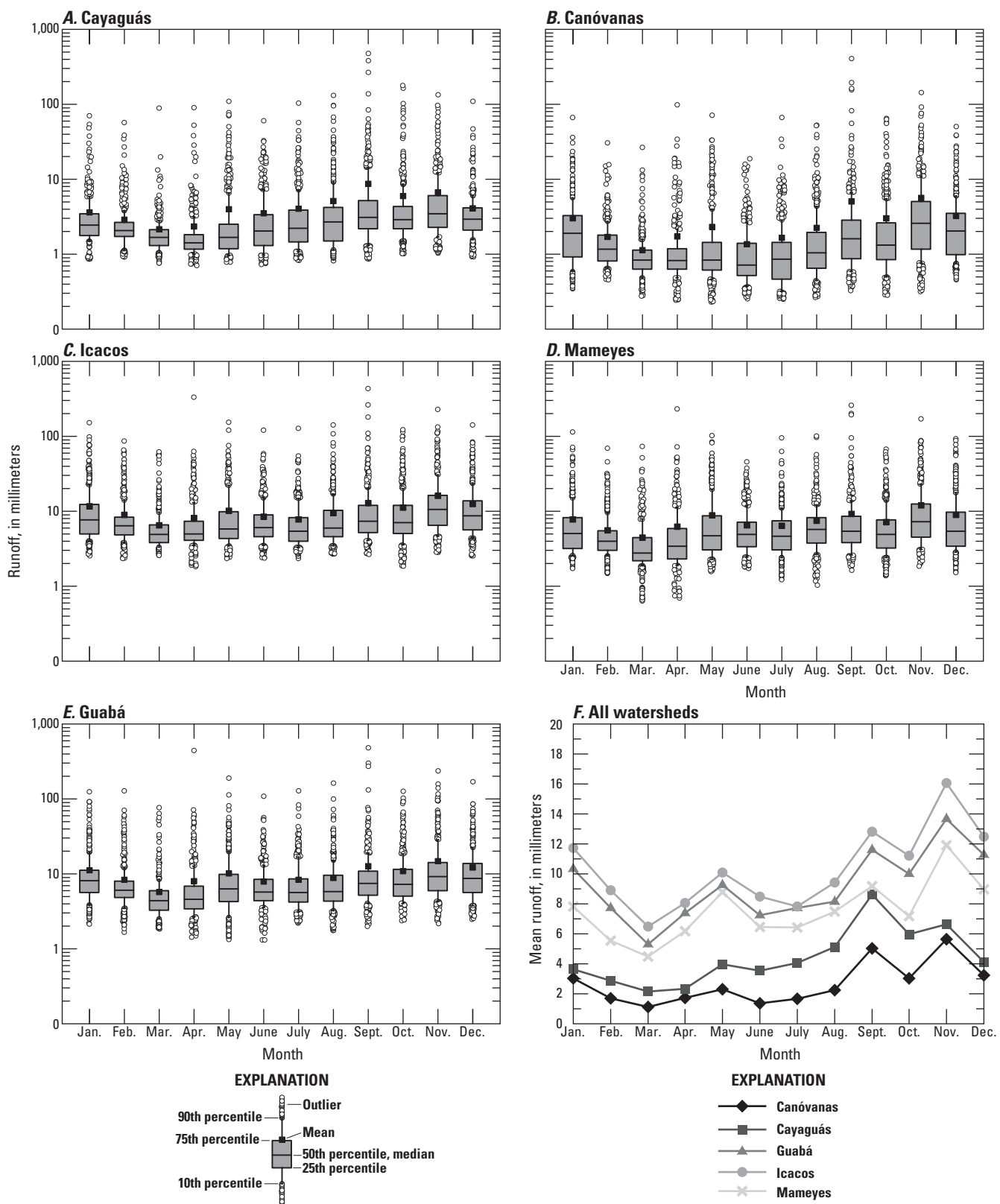


Figure 12. Mean daily runoff by month at U.S. Geological Survey stream-gaging stations (estimated from 5- or 15-minute discharge data from U.S. Geological Survey, 2010). A–E, Standard box plots (Helsel and Hirsch, 2008) showing interquartile range in five watersheds; F, mean annual precipitation of same five watersheds. Runoff for Guabá in years 1991, 2004, and 2005 and portions of 1992 and 2003 estimated by regression with Icacos station; runoff for Canóvanas for portions of years 1991 and 1992 estimated by regression with Cayaguás station.

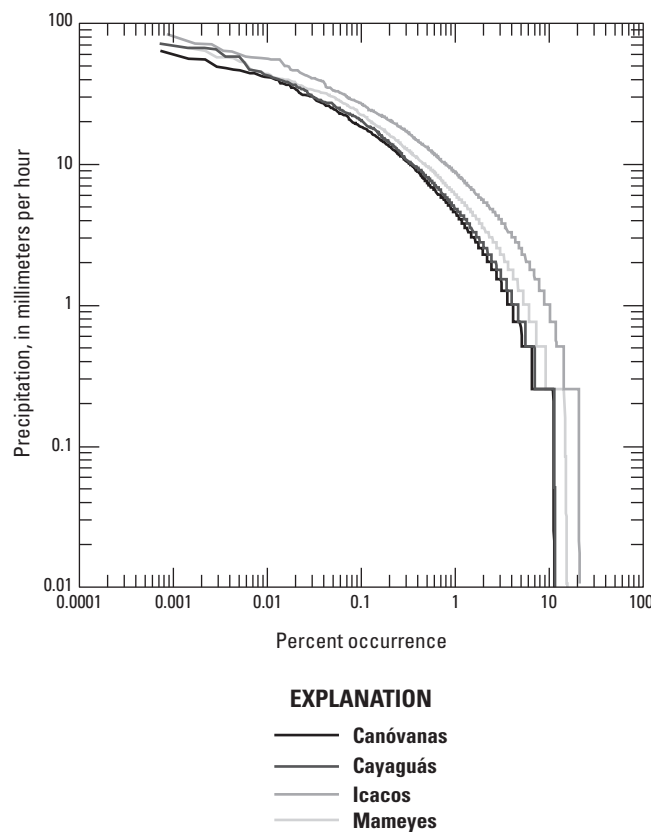


Figure 13. Percent occurrence of hourly precipitation intensity at U.S. Geological Survey stream-gaging stations (1991–2005).

Table 8. Rainfall intensity at U.S. Geological Survey stations during major storms in eastern Puerto Rico, 1991–2005.

[From U.S. Geological Survey Automated Data Processing System internal data, written commun., 2008. --, not available; h, hour; mm h⁻¹, millimeters per hour]

Date	Event	Canóvanas			Cayaguás			Guabá			Icacos			Mameyes		
		0.25	1	24	0.25	1	24	0.25	1	24	0.25	1	24	0.25	1	24
25-Feb-1995	Unknown	28	17	2	12	4	0	64	29	3	125	83	6	44	18	3
13-May-1996	Unknown	12	3	0	4	1	0	52	28	3	60	28	4	136	64	9
10-Sep-1996	Hurricane Hortense	76	37	13 ¹	76	72	21	96	48	17	108	47	19	36	29	12
21-Sep-1998	Hurricane Georges	96	64	5	84	67	9	72	51	9	96	72	12	36	34	5
22-Oct-1998	Unknown	84	28	4	88	45	8	40	32	5	72	38	6	44	20	3
22-Aug-2001	Tropical Storm Dean	108	46	4	132	76	9	88	58	10	76	57	11	109	71	7
17-Apr-2003	Upper-level trough	40	19	5	56	40	5	120	92	15	124	93	18	88	71	14
12-Nov-2003	Tropical wave	--	--	--	44	18	6	64	53	12	68	55	14	72	58	11
15-Sep-2004	Tropical Storm Jeanne	88	55	9	52	27	6	80	57	9	96	60	14	76	57	13
11-Apr-2005	Unknown	4	1	0	125	40	4	52	29	2	48	32	2	36	30	2
Maximum		108	64	13	132	76	21	120	92	17	125	93	19	136	71	14

¹The hurricane destroyed the gage during storm, so precipitation may actually have been higher.

Table 9. Runoff rates (1991–2005) from study watersheds and percentage of time that hourly runoff was below those rates, at percentiles of annual runoff volume.

[mm h⁻¹, millimeters per hour]

Watershed	Minimum runoff	Percentile of annual runoff volume								Maximum runoff	
		1	5	10	25	50	75	90	95		
Runoff rate (mm h ⁻¹)											
Canóvanas	0.009	0.019	0.030	0.041	0.083	0.25	1.4	8.1	20	43	66
Cayaguás	0.020	0.042	0.057	0.073	0.11	0.27	1.8	7.8	18	41	54
Guabá	0.036	0.11	0.16	0.20	0.29	0.48	1.8	11	25	64	98
Icacos	0.059	0.13	0.17	0.20	0.29	0.57	2.1	7.5	14	36	85
Mameyes	0.024	0.084	0.12	0.14	0.22	0.46	1.5	4.9	11	43	86
Time spent below given runoff (percent)											
Canóvanas	0	7	26	42	72	93	99.3	99.94	99.981	99.998	100
Cayaguás	0	5	19	33	63	91	99.0	99.89	99.967	99.996	100
Guabá	0	5	17	29	55	84	98	99.82	99.951	99.995	100
Icacos	0	4	16	28	57	86	98	99.67	99.901	99.991	100
Mameyes	0	5	18	31	59	86	98	99.68	99.921	99.994	100

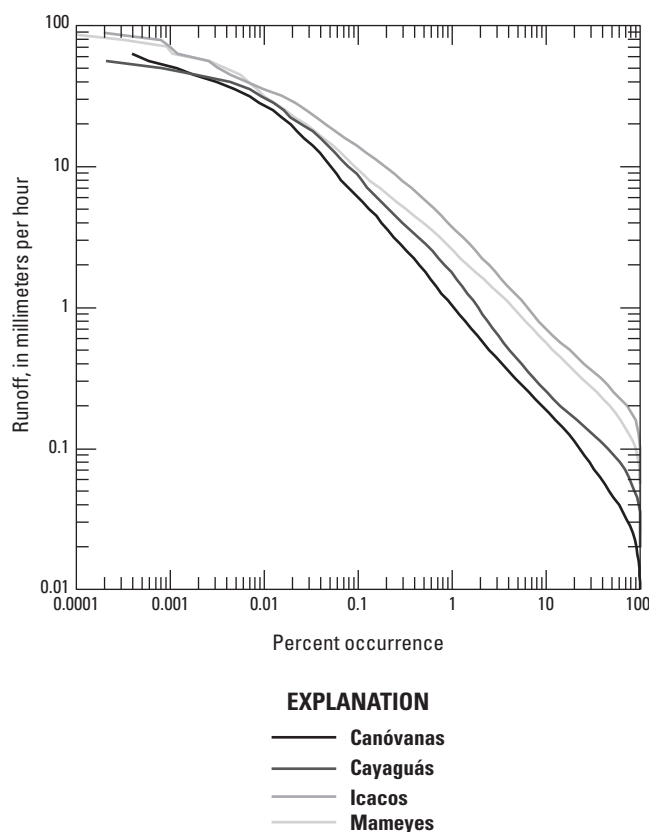


Figure 14. Percent occurrence of hourly runoff intensity at U.S. Geological Survey stream-gaging stations (1991–2005).

(table 8). Discharge caused by such storms can be several hundred times greater than average discharge and can deliver a substantial fraction of annual discharge. For example, Hurricane Hortense delivered more than 500 mm of rain in eastern Puerto Rico in less than 3 days, which produced the highest daily runoff (about 260–490 mm day⁻¹) of all studied watersheds during the study period (table 5); this 1 day of runoff accounted for about 28 percent of total annual discharge from the Canóvanas watershed in 1996. An upper-level trough in April 2003 produced more than 400 mm rain in 3 days. This storm was particularly intense in the Icacos watershed, where it delivered more than 90 mm in 1 hour (table 8) and altered the Guabá's stream channel so severely that discharge data at the Guabá stream-gaging station after that date are not useable.

At the high runoff rates that result from these large storms, hydrologic flow paths shift from moving into ground-water to shallower, lateral flow paths or overland flow (Schellekens and others, 2004), and water is rapidly transported to streams. Runoff can increase from base flow to peak discharge in minutes; high flows typically last only a few hours, and rivers typically return to base-flow conditions a few hours later. For example, when Tropical Storm Dean passed through eastern Puerto Rico in August 2001, the rise to peak discharge in the studied watersheds occurred in minutes to a few hours, and the recession typically lasted less than a day (fig. 15). This storm was selected because it was large enough to affect all of the studied watersheds but did not destroy any stream or rain gages, and it was preceded and followed by relatively rainless periods.

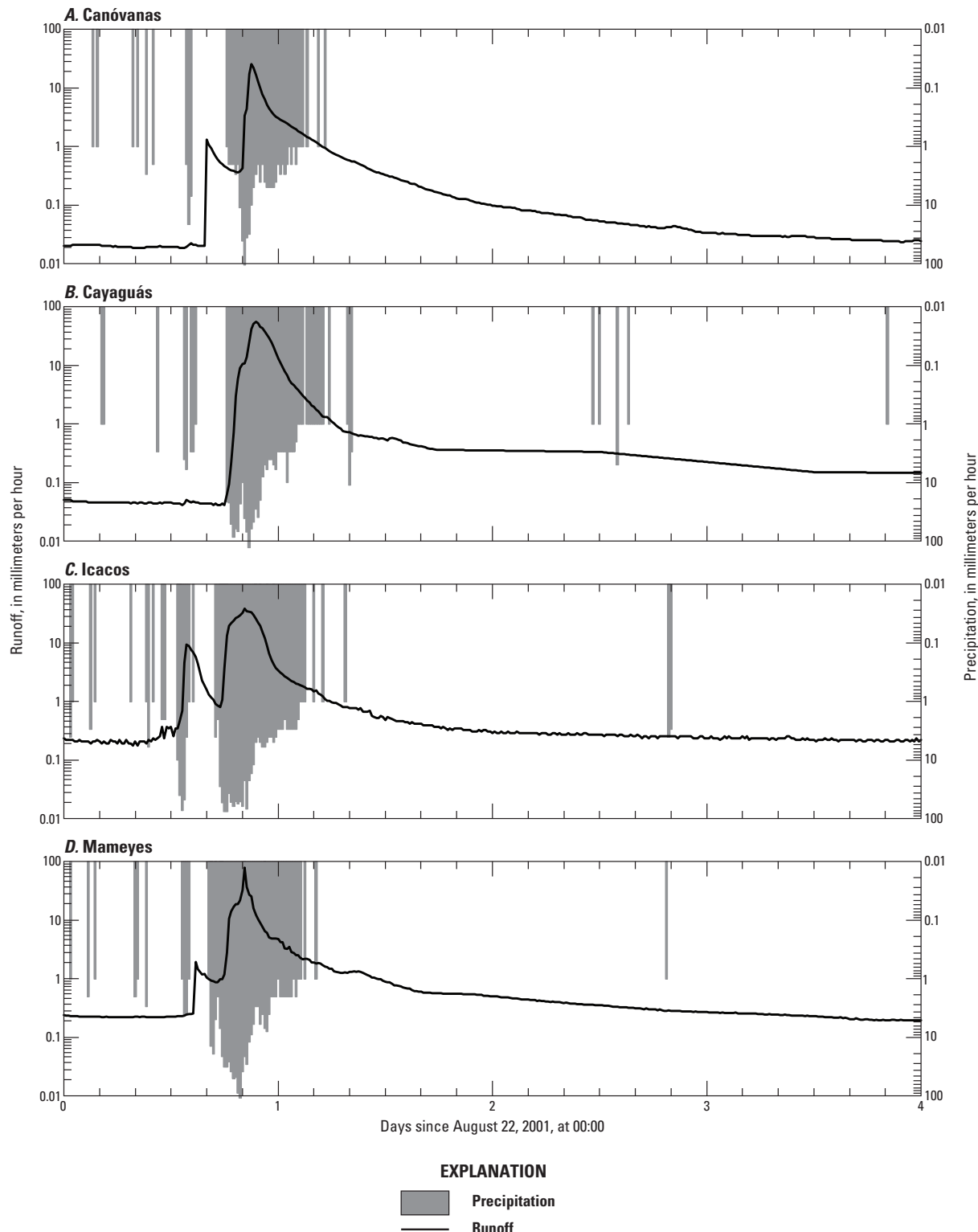


Figure 15. Runoff and precipitation at U.S. Geological Survey stream-gaging stations during and after Tropical Storm Dean, August 2001 (runoff and precipitation shown in 15-minute increments, adjusted to units of millimeters per hour; from U.S. Geological Survey Automated Data Processing System internal data, written commun., 2008; U.S. Geological Survey, 2010).

During the 1991–2005 study period, 130 recessions that lasted 5 days or more, including 7 recessions that lasted longer than 10 days, were identified in the studied watersheds (table 10). Recession models using integrated moving average and simple autoregressive regressions yielded tight 95-percent confidence intervals for recession constants (k) and similar average model recession end runoff rates for each river. Watersheds underlain by granitic rocks (Icacos, Guabá, and Cayaguás) had both higher k_i (subscript i refers to the IMA recession model) and k_A (subscript A refers to the AR(1) recession model) values, suggesting slower drainage and greater storage (table 10). Watersheds underlain by volcaniclastic rocks (Mameyes and Canóvanas) had lower k_i and k_A values, which were 95 percent likely to be different from those of the granitic watersheds; these values were spanned by k_i and k_A values reported for the geologically similar Espíritu Santo and Fajardo Rivers (Rivera-Ramírez and others, 2002), further suggesting that bedrock controls recession properties. Effective groundwater reservoir turnover times, τ_i , and τ_A , were also similar among rock types: shorter in the volcaniclastic watersheds (12 to 19 days, depending on the regression) than in the granitic watersheds (23 to 32 days). These results are consistent with water in the deep-soil environment having about twice the contact time in the granitic watersheds as in the volcaniclastic watersheds.

Field studies have found that surface infiltration was faster and hydraulic conductivities were greater in the Icacos watershed than in the Mameyes watershed (McDowell and others, 1992; Larsen, 1995). In both kinds of soil, macropore flow is likely important; soil pipes are visible along cut banks and steep slopes in hillslope and alluvial soils. Soil pore pressure response measurements by Simon and others (1990) found that granitic soils responded about three times as fast as volcaniclastic soils, suggesting that granitic soils are more permeable to a greater depth than volcaniclastic soils. Dense clays in the volcaniclastic soils likely retard deep infiltration and cause water to follow a shallower trajectory and thus reach streams more quickly (McDowell and others, 1992).

The recession analysis suggested that it would take between 6 and 19 days for runoff in the studied watersheds to drop from a 10-percent runoff rate (which occurs about 28 to 42 percent of the time; table 9) to a 1-percent runoff rate (which occurs about 4 to 7 percent of the time), and an additional 10 to 29 days to drop to minimum observed runoff rates (table 10). The length of time for such decreases was not strongly related to rock type, nor was the effective water column remaining in storage at the lowest flows. This stored water was greatest in the wettest watersheds (Icacos and Guabá) and least in the driest (Canóvanas). The effective water storage at 1-percent runoff rates, which were used to estimate groundwater storage, represents less than 3 percent of mean annual runoff from any watershed (table 10). It is therefore unlikely that long-term storage is a major factor in the interannual water budget. However, there was sufficient storage that none of the rivers completely dried up during the study,

even during the 1993–1995 drought (table 10, fig. 9), when minimum hourly runoff ranged from 0.009 mm h^{-1} (Canóvanas) to 0.059 mm h^{-1} (Icacos). During the periods of record for the gages, lowest daily mean runoff was $0.077 \text{ mm day}^{-1}$ (0.003 mm h^{-1}) or greater (table 5).

Water Budgets for Study Watersheds

Three methods of estimating precipitation in the Icacos and Mameyes watersheds resulted in values within about 5 percent of each other (between 3,980 and 4,160 mm in the Icacos watershed and between 3,660 and 3,830 mm in the Mameyes watershed (table 11)). In the Cayaguás watershed, the elevation-weighted method and PRISM resulted in similar estimates of mean annual precipitation (about 2,350 mm), whereas calculations based on land cover were about 11 percent lower (2,100 mm). Estimates of mean annual precipitation in the Canóvanas watershed ranged widely, from 2,070 mm (elevation-weighted method) to about 3,480 mm (PRISM). PRISM therefore appears to model precipitation in the Cayaguás, Icacos, and Mameyes watersheds effectively, but it does not capture rain-shadow effects in the Canóvanas watershed accurately. Owing to the lack of precipitation data for pasture and lowland forest, the dominant land covers in the Canóvanas and Cayaguás watersheds (Murphy and others, 2012), estimating precipitation from land cover is not likely to be highly accurate in these watersheds. Therefore precipitation based on elevation (adjusted for rain-shadow when necessary) was used in water budgets (table 12).

Rainfall is the dominant input to all watersheds; runoff and ET are the dominant outputs, with differing importance in the watersheds (table 12). Elevation-weighted estimates indicate that cloud drip adds about 1, 2, and 4 percent to the annual precipitation budget in the Canóvanas, Mameyes, and Icacos watersheds, respectively (table 12). Inputs from septic systems, and outputs from withdrawals and groundwater storage, are minor. Runoff is about 47 percent of precipitation plus cloud drip in the Canóvanas watershed, about 70 percent in the Mameyes and Cayaguás watersheds, and about 87 percent in the Icacos watershed. Evapotranspiration values estimated from water budgets ranged from 450 mm yr^{-1} in the Icacos watershed to about $1,070 \text{ mm yr}^{-1}$ in the Canóvanas watershed. Evapotranspiration values estimated from land cover were slightly higher (12 and 15 percent, respectively, of ET estimated from water budgets) in the Mameyes and Canóvanas watersheds, but much higher (77 and 127 percent, respectively) in the Cayaguás and Icacos watersheds (table 12). The high runoff-to-precipitation ratio and substantial discrepancy in ET estimated from water budgets and from land cover in the undeveloped Icacos watershed suggest that evapotranspiration is lower than reported in vegetation-based estimates (table 3), or precipitation is greater than recorded, or both. Most ET studies in the Luquillo Experimental Forest were done in the Espíritu Santo (RES, table 2, fig. 5) and Mameyes watersheds; ET may be lower in the Icacos watershed because

Table 10. Modeled recessions for study watersheds after storm events, eastern Puerto Rico.

[Following Vogel and Kroll (1996) for instantaneous runoff. Includes recessions that lasted 5 days or more; first 2 days excluded from recession. AR(1), autoregressive; h, hour; IMA, integrated moving average; k , recession constant; km^2 , square kilometers; mm, millimeters; mm hr^{-1} , millimeters per hour; mm yr^{-1} , millimeters per year; %, percent]

Watershed	Annual runoff (mm yr^{-1})	Interval (minutes)	Number of recessions	Recession points	Maximum runoff during recessions ² (mm hr^{-1})	Average runoff at recession end (mm hr^{-1})	Minimum runoff during recessions (mm hr^{-1})		Runoff at 10% (mm hr^{-1})	Runoff at 1% (mm hr^{-1})	Minimum observed runoff ³ (mm hr^{-1})
							Average runoff at recession end (mm hr^{-1})	Turnover time ⁴ (days)			
Canóvanas	970	15	34	190	0.24	0.062	0.012	0.041	0.019	0.008	
Cayaguás	1,620	15	29	157	0.20	0.061	0.030	0.073	0.042	0.020	
Guabá	3,630	15	8	19	0.48	0.21	0.13	0.20	0.11	0.040	
Icacos	3,760	15	16	86	0.71	0.22	0.13	0.20	0.13	0.059	
Mameyes	2,750	5	43	228	0.57	0.12	0.039	0.14	0.084	0.025	
Watershed	k (fraction/ day)	95% error in k (fraction/ day)	k (% / day)	Modeled average runoff at recession end (mm hr^{-1})	95% error in modeled average runoff at recession end (%)	Turnover time ⁴ (days)	Time from 10% to 1% of average runoff (days)	Time from 10% to minimum runoff (days)	Linear storage ⁵ at 1% runoff (mm)	Storage at minimum runoff (% of mean annual runoff)	Storage at minimum runoff (% of mean annual runoff)
Canóvanas	0.95	0.007	-5.4	0.067	-7.8	18	14	15	8	4	0.4
Cayaguás	0.97	0.005	-3.2	0.063	-5.3	31	18	23	32	15	0.9
Guabá	0.97	0.014	-3.3	0.21	-2.9	30	19	29	76	29	0.8
Icacos	0.97	0.008	-3.1	0.23	-4.5	32	14	25	100	45	2.6
Mameyes	0.95	0.005	-5.2	0.13	-8.4	19	10	23	37	11	1.2
								7AR(1) regression to determine k_A			
Canóvanas	0.92	0.007	-7.9	0.058	10	12	9	10	6	2	0.2
Cayaguás	0.96	0.006	-3.8	0.061	5.5	26	15	20	27	13	0.8
Guabá	0.96	0.015	-3.5	0.21	3.1	28	17	27	70	26	0.7
Icacos	0.96	0.008	-4.3	0.21	4.9	23	10	18	72	33	0.9
Mameyes	0.92	0.007	-8.1	0.11	12	12	6	14	23	7	0.3

¹1991–2005; from table 5.

²Excluding first 2 days after storm event.

³During 1991–2005 period.

⁴Turnover time (τ in Precipitation and Runoff in Eastern Puerto Rico section) = $1/\ln(k)$.

⁵Water in excess of the field capacity in the soil available for drainage, or aquifer water.

^aThe error for the recession constant, k_i , in the IMA regression, treats the estimate for $\ln(k)$ as a population average.

^bThe error for the recession constant, k_A , in the AR(1) regression, which determines $\ln(k)$ from the slope of a regression forced through 0,0, is based on the error of that slope.

Table 11. Annual precipitation estimated by three methods.

[PRISM, parameter-elevation regressions independent slopes model (Daly and others, 2003). mm yr⁻¹, millimeters per year]

Watershed	Annual precipitation (mm yr ⁻¹)		
	Elevation-weighted regression ¹	PRISM	Calculated from land cover ²
Canóvanas	2,070	3,480	2,770
Cayaguás	2,350	2,350	2,100
Icacos	4,150	3,980	4,160
Mameyes	3,760	3,660	3,830

¹ Rain-shadow-adjusted for Canóvanas and Cayaguás (see Interpretive Approach section).

² Based on 2003 land cover from Gould and others (2008) and land-cover types from literature (table 3).

Table 12. Annual water budgets of study watersheds.

[All values are millimeters per year unless otherwise noted]

Watershed	Inputs					
	Precipitation ¹		Cloud drip ²		Septic ³	
	Estimated	Error	Estimated	Error	Estimated	Error
Canóvanas	2,070	310	22	10	10	10
Cayaguás	2,350	350	0	0	5	5
Icacos	4,150	620	160	72	0	1
Mameyes	3,760	560	84	38	0	1
Watershed	Outputs					
	Runoff ⁴		Withdrawals ³		Groundwater ⁵	
	Estimated	Error	Estimated	Error	Estimated	Error
Canóvanas	980	150	46	46	8	1
Cayaguás	1,620	320	3	3	32	2
Icacos	3,760	560	0	0	100	5
Mameyes	2,750	410	4	4	37	3
Watershed	Outputs/ inputs (percent)	Runoff (as percent of precipitation + cloud drip)	Evapotranspiration			
		From water budget		From land cover ⁶		
	Estimated	Error	Estimated	Error	Estimated	Error
Canóvanas	49	47	1,070	350	1,230	
Cayaguás	70	69	700	470	1,240	
Icacos	90	87	450	840	1,020	
Mameyes	73	72	1,050	700	1,180	

¹Based on elevation-weighted regression; rain-shadow-adjusted for Canóvanas and Cayaguás.

²Based on Schellekens and others (2000), adjusted for elevation.

³From Larsen and Concepción (1998).

⁴U.S. Geological Survey stream-gaging stations, mean of 1991–2005.

⁵From recession calculations (table 10).

⁶Based on 2003 land cover from Gould and others (2008) and land-cover types from literature (table 3).

it less exposed to winds from the east and southeast (Murphy and others, 2012). The high humidity, often completely soaked conditions, and the cloudiness of the cloud-forest zone all contribute to much-reduced rates of evapotranspiration. Studies on nearby Pico del Este (elevation 1,051 m) and El Yunque (elevation 1,059 m; U.S. Geological Survey, 1967) have shown that relative humidity was usually at or near 100 percent, which would cause ET to be very low (Briscoe, 1966; Weaver, 1972). It is possible that precipitation is higher than recorded in this watershed; cloud drip contribution is poorly understood, and the elevation of the watershed is higher than average cloud base. Also, horizontal precipitation during rainstorms is often undermeasured by rain gages; as such, precipitation recorded on windy ridgetops, such as at the Pico del Este station, may underrepresent rainfall accumulation (García-Martino and others, 1996).

In the Cayaguás watershed, the water budget estimate for ET was 700 mm, whereas land cover suggested 1,240 mm (table 12). Although there are few ET data for the dominant land-cover types in this watershed (about 57 percent pasture and 20 percent lowland forest; Murphy and others, 2012), annual ET in lowland tropical forests is typically about 1,400 mm (Leigh, 1999), and nonforested landscapes tend to have lower rates of ET (Lawton and others, 2001). Therefore, the land-cover estimate of ET for this watershed seems more plausible than the lower water budget estimate. The low ET estimated by water budget could be due to greater actual precipitation than is recorded, erroneously high runoff measurements, or under-reported septic system inputs. Substantial differences in two precipitation stations near the mouth of the Cayaguás watershed (Río Cayaguás and San Lorenzo 3S, table 4; CAY and SLZ, fig. 5) indicate considerable short-range variation in precipitation or that some precipitation measurements are erroneous. Runoff data for the Cayaguás stream-gaging station have high uncertainty because of episodic scour and deposition of approximately 1 m in the sandy streambed (Larsen and Santiago-Román, 2001; Díaz and others, 2004). Finally, the Cayaguás watershed has a growing population, so it is possible that septic input is greater than reported, particularly if some households import water from another basin, although this possibility is unlikely.

Summary

Hydrologic regimes in the four U.S. Geological Survey Water, Energy, and Biogeochemical Budgets watersheds in eastern Puerto Rico are dominated by their location relative to the Luquillo Mountains. The Icacos and Mameyes watersheds, located in the eastern half of the mountains, are the wettest of the four watersheds, annually receiving more than 4,300 millimeters and 3,800 millimeters, respectively, of combined rainfall and cloud drip. Precipitation is closely correlated with elevation in these watersheds. The Canóvanas and Cayaguás watersheds, located in the rain shadow to the east and southeast of the mountains, receive roughly half the

precipitation recorded for the Icacos and Mamayes watersheds. Precipitation and watershed elevation are not well correlated in these leeward watersheds, and differences in precipitation are probably related to local topography. Therefore, estimates of watershed-wide precipitation are likely to be much more accurate in windward watersheds (such as the Icacos and Mamayes) than in leeward watersheds (such as the Canóvanas and Cayaguás) in eastern Puerto Rico.

Precipitation and runoff in all watersheds show large interannual variation, which is partly explained by several large-scale climate oscillations. Precipitation and runoff are substantially higher in years when major storms strike Puerto Rico. These large storms typically result in similar runoff in all of the study watersheds, suggesting that higher annual runoff in the Icacos and Mamayes watersheds results from frequent, smaller storms related to orographic precipitation.

Precipitation leaves all of the studied watersheds primarily through runoff and evapotranspiration. Evapotranspiration estimates based on land cover and on water budgets were similar in the Mamayes and Canóvanas watersheds, but they differed substantially in the Icacos and Cayaguás watersheds. In the Icacos watershed, this discrepancy is probably due to reduced actual evapotranspiration caused by high humidity, extensive cloud cover, and reduced wind from eastern and southeastern directions, or greater actual water input than recorded by precipitation stations (owing to cloud drip or horizontal precipitation), or both. In the Cayaguás watershed, the discrepancy is likely due to measurement deficiencies in precipitation, runoff, or septic inputs, leading to low estimates of evapotranspiration by water budgets.

Because of the influence of windward-leeward effects, differences in hydrologic regimes in the four watersheds associated with bedrock geology or land cover are difficult to detect. Groundwater storage is small compared with annual runoff in all watersheds. Geology appears to control the recession characteristics of the rivers; recession is faster in volcanoclastic soils, probably because of impermeable clay layers, than in granitic rocks.

The effects of reforestation or climate change with time are difficult to distinguish from the large interannual variations in weather and the occasional large storm. Similarly, potentially increased evapotranspiration and subsequent decrease in runoff due to ongoing afforestation in the Canóvanas and Cayaguás watersheds would be a small factor compared to the windward-leeward differences. However, climate change may increase Puerto Rico's vulnerability to hurricanes, flooding, and drought, so afforestation remains an important topic for future study. If the effects of climate and land-use change are to be addressed in eastern Puerto Rico, better spatial density of precipitation stations, longer periods of both precipitation and stream-gaging station data, and additional studies of evapotranspiration in different land covers are needed.

Acknowledgments

This chapter would not have been possible without the assistance of Pedro L. Díaz, Angel J. Torres-Sánchez, and others at the U.S. Geological Survey Caribbean Water Science Center. This chapter was greatly improved by suggestions made by Matthew C. Larsen, John A. Moody, Norman E. Peters, and Martha A. Scholl of the U.S. Geological Survey and F.N. Scatena of the University of Pennsylvania.

References

- Alila, Younes, Kura, P.K., Schnorbus, Markus, and Hudson, Robert, 2009, Forests and floods—A new paradigm sheds light on age-old controversies: *Water Resources Research*, v. 45, no. W08416, p. 1–24.
- Ashton, P.S., and CTFS Working Group, 2004, Floristics and vegetation of the forest dynamics plots, in Losos, E.C., and Leigh, E.G., Jr., eds., *Tropical forest diversity and dynamism—Findings from a large-scale plot network*: The University of Chicago Press, p. 90–102.
- Baedeker, M.J., and Friedman, L.C., 2000, Water, energy, and biogeochemical budgets—A watershed research program: U.S. Geological Survey Fact Sheet 165–99, 4 p.
- Barry, R.G., 2008, *Mountain weather and climate* (3d ed.): Cambridge, U.K., Cambridge University Press, 506 p.
- Baynton, H.W., 1969, The ecology of an elfin forest in Puerto Rico—3. Hilltop and forest influences on the microclimate of Pico del Oeste: *Journal of the Arnold Arboretum of Harvard University*, v. 49, no. 4, p. 419–430.
- Bennet, S.P., and Mojica, R., 1998, Hurricane Georges preliminary storm report—From the tropical Atlantic to the United States Virgin Islands and Puerto Rico: National Oceanic and Atmospheric Administration National Weather Service NWSFO San Juan Official Report, October, p. 1–15.
- Beissinger, S.R., Wunderle, J.M., Jr., Meyers, J.M., Saether, B.E., and Engen, S., 2008, Anatomy of a bottleneck—Diagnosing factors limiting population growth in the Puerto Rican parrot: *Ecological Monographs*, v. 78, p. 185–203.
- Birdsey, R.A., and Weaver, P.L., 1982, The forest resources of Puerto Rico: New Orleans, La., U.S. Department of Agriculture Forest Service, Southern Forest Experiment Station Resources Bulletin SO–85, 65 p.
- Bradshaw, C.J.A., Sodhi, N.S., Peh, K.S.-H., and Brook, B.W., 2007, Global evidence that deforestation amplifies flood risk and severity in the developing world: *Global Change Biology*, v. 13, p. 2379–2395.

- Briscoe, C.B., 1966, Weather in the Luquillo Mountains of Puerto Rico: Río Piedras, Puerto Rico, U.S. Department of Agriculture Forest Service International Institute of Tropical Forestry, Forest Service Research Paper ITF-3, 250 p.
- Brown, Sandra, Lugo, A.E., Silander, Susan, and Liegel, Leon, 1983, Research history and opportunities in the Luquillo Experimental Forest: New Orleans, La., U.S. Department of Agriculture Forest Service, Southern Forest Experiment Station General Technical Report SO-44, 128 p.
- Bruijnzeel, L.A., 2004, Hydrological functions of tropical forest—Not seeing the soil for the trees?: Agriculture, Ecosystems and Environment, v. 104, p. 185–228.
- Burrowes, P.A., Joglar, R.L., and Green, D.E., 2004, Potential causes for amphibian declines in Puerto Rico: Herpetologica, v. 60, p. 141–154.
- Calvesbert, R.J., 1970, Climate of Puerto Rico and the U.S. Virgin Islands: U.S. Department of Commerce Climatology of the United States 60–52, 29 p.
- Carter, M.M., 1997, A climatology of tropical cyclone rainfall over Puerto Rico, in Conference on Hurricane and Tropical Meteorology, 22d, Fort Collins, Colo., May 19–23, 1997, Preprints of Conference Proceedings: American Meteorological Society, p. 596–597.
- Center for International Forestry Research, 2005, Forests and floods—Drowning in fiction or thriving on facts?: Bangkok, Thailand, United Nations Food and Agriculture Organization of the United Nations, RAP Publication 2005/03 Forest Perspectives 2, 40 p.
- Chapman, Tom, 1999, A comparison of algorithms for stream flow recession and baseflow separation: Hydrological Processes, v. 13, p. 701–714.
- Christensen, J.H., Hewitson, B., Busuioc, A., Chen, A., Gao, X., Held, I., Jones, R., Kolli, R.K., Kwon, W.-T., Laprise, R., Magaña Rueda, V., Mearns, L., Menéndez, C.G., Räisänen, J., Rinke, A., Sarr, A., and Whetton, P., 2007, Regional climate projections, in Solomon, S., Qin, D., Manning, M., Chen, Z., Marquis, M., Averyt, K.B., Tignor, M., and Miller, H.L., eds., Climate change 2007—The physical science basis, Contribution of Working Group I to the Assessment Report of the Intergovernmental Panel on Climate Change, 4th: Cambridge, U.K., Cambridge University Press, p. 847–940.
- Crook, K.E., Pringle, C.M., and Freeman, M.C., 2009, A method to assess longitudinal riverine connectivity in tropical streams dominated by migratory data: Aquatic Conservation—Marine and Freshwater Ecosystems, v. 19, p. 714–723.
- Crook, K.E., Scatena, F.N., and Pringle, C.M., 2007, Water withdrawn from the Luquillo Experimental Forest, 2004: Río Piedras, Puerto Rico, U.S. Department of Agriculture Forest Service International Institute of Tropical Forestry, General Technical Report IITF-34, 26 p.
- Daly, Christopher, Helmer, E.H., and Quiñones, Maya, 2003, Mapping the climate of Puerto Rico, Vieques and Culebra: International Journal of Climatology, v. 23, p. 1359–1381.
- Díaz, P.L., Aquino, Zaida, Figueroa-Alamo, Carlos, García, René, and Sánchez, A.V., 2004, Water resources data for Puerto Rico and the U.S. Virgin Islands, water year 2002: U.S. Geological Survey Water-Data Report PR-02-1, 652 p.
- Dietrich, W.E., Windsor, D.M., and Dunne, T., 1982, Geology, climate, and hydrology of Barro Colorado Island, in Leigh, E.G., Jr., Rand, A.S., and Windsor, D.M., eds., The ecology of a tropical forest—Seasonal rhythms and long-term changes: Washington D.C., Smithsonian Institution Press, p. 21–46, 468 p.
- Dunion, J.P., and Velden, C.S., 2004, The impact of the Saharan air layer on Atlantic tropical cyclone activity: Bulletin of the American Meteorological Society, v. 85, no. 3, p. 353–365.
- Elsner, J.B., Liu, K.-B., and Kocher, B., 2000, Spatial variations in major U.S. hurricane activity—Statistics and a physical mechanism: Journal of Climate, v. 13, p. 2293–2305.
- Emanuel, Kerry, 2005, Increasing destructiveness of tropical cyclones over the past 30 years: Nature, v. 436, p. 686–688.
- Eugster, Werner, Burkard, Reto, Holwerda, Friso, Scatena, F.N., and Bruijnzeel, L.A., 2006, Characteristics of fog and fogwater fluxes in a Puerto Rican elfin cloud forest: Agricultural and Forest Meteorology, v. 139, p. 288–306.
- Ewel, J.J., Madriz, A., and Tosi, J.A., 1968, Zonas de vida de Venezuela y mapa ecológico de Venezuela: Caracas, Ministerio de Agricultura y Cría, Dirección de Investigación, 265 p. + map.
- Ewel, J.J., and Whitmore, J.L., 1973, The ecological life zones of Puerto Rico and the U.S. Virgin Islands: Río Piedras, Puerto Rico, U.S. Department of Agriculture Forest Service Institute of Tropical Forestry, Forest Service Research Paper, ITF-18, 72 p.
- Frangi, J.L., and Lugo, A.E., 1985, Ecosystem dynamics of a subtropical floodplain forest: Ecological Monographs, v. 55, p. 351–369.
- García-Martino, A.R., Warner, G.S., Scatena, F.N., and Civco, D.L., 1996, Rainfall, runoff, and elevation relationships in the Luquillo Mountains of Puerto Rico: Caribbean Journal of Science, v. 32, p. 413–424.
- Gould, W.A., Alarcón, C., Fevold, B., Jiménez, M.E., Martinuzzi, S., Potts, G., Quiñones M., Solórzano, M., and Ventosa, E., 2008, The Puerto Rico gap analysis project—

- v. 1. Landcover, vertebrate species distributions, and land stewardship: Río Piedras, Puerto Rico, U.S. Department of Agriculture Forest Service International Institute of Tropical Forestry, General Technical Report IITF-GTR-39, 165 p.
- Gould, W.A., Martinuzzi, S., and Parés-Ramos, I.K., 2012, Land use, population dynamics, and land-cover change in eastern Puerto Rico—ch. B, *in* Murphy, S.F., and Stallard, R.F., eds., Water quality and landscape processes of four watersheds in eastern Puerto Rico: U.S. Geological Survey Professional Paper 1789, p. 25–42.
- Granger, R.J., and Gray, D.M., 1989, Evaporation from natural nonsaturated surfaces: *Journal of Hydrology*, v. 111, p. 21–29.
- Gray, S.T., Graumlich, L.J., Betancourt, J.L., and Pederson, G.T., 2004, A tree-ring based reconstruction of the Atlantic Multidecadal Oscillation since 1567 A.D.: *Geophysical Research Letters*, v. 31, no. L12205, p. 1–4.
- Gray, W.M., 1984, Atlantic seasonal hurricane frequency, Part I—El Niño and 30 mb quasibiennial oscillation influences: *Monthly Weather Review*, v. 112, p. 1649–1668.
- Hall, F.R., 1968, Base flow recessions—A review: *Water Resources Research*, v. 4, p. 973–983.
- Heartsill-Scalley, Tamara, Scatena, F.N., Estrada, C., McDowell, W.H., and Lugo, A.E., 2007, Disturbance and long-term patterns of rainfall and throughfall nutrient fluxes in a subtropical wet forest in Puerto Rico: *Journal of Hydrology*, v. 333, p. 472–485.
- Helsel, D.R., and Hirsch, R.M., 2002, Statistical methods in water resources: U.S. Geological Survey Techniques of Water-Resources Investigations, Book 4, ch. A3, 522 p.
- Higuera-Gundy, Antonia, Brenner, Mark, Hodell, D.A., Curtis, J.H., Leyden, B.W., and Binford, M.W., 1999, A 10,300 ¹⁴C yr record of climate and vegetation change in Haiti: *Quaternary Research*, v. 52, p. 159–170.
- Hodell, D.A., Curtis, J.H., Jones, G.A., Higuera-Gundy, A., Brenner, M., Binford, M.W., and Dorsey, K.T., 1991, Reconstruction of Caribbean climate change over the past 10,500 years: *Nature*, v. 352, p. 790–793.
- Holwerda, Friso, Burkard, Reto, Eugster, Werner, Scatena, F.N., Meesters, A.G., and Bruijnzeel, L.A., 2006, Estimating fog deposition at a Puerto Rican elfin cloud forest site—Comparison of the water budget and eddy covariance methods: *Hydrological Processes*, v. 20, p. 2669–2692.
- Howell, T.A., and Evett, S.R., 2004, The Penman-Monteith method—sec. 3, *in* Evapotranspiration—Determination of consumptive use in water rights proceedings: Denver, Continuing Legal Education in Colorado, Inc., 14 p.
- Hurrell, J.W., Kushnir, Y., Visbeck, M., and Ottersen, G., 2003, An overview of the North Atlantic Oscillation, *in* Hurrell, J.W., Kushnir, Y., Ottersen, G., and Visbeck, M., eds., The North Atlantic Oscillation—Climate significance and environmental impact: Geophysical Monograph Series, v. 134, p. 1–35.
- Interagency Wild and Scenic Rivers Council, 2008, National Wild and Scenic Rivers System: accessed April 10, 2008, at <http://www.rivers.gov>
- Jackson, R.B., Jobbágy, E.G., Avissar, R., Roy, S.B., Barrett, D.J., Cook, C.W., Farley, K.A., le Maître, D.C., McCarl, B.A., and Murray, B.C., 2005, Trading water for carbon with biological carbon sequestration: *Science*, v. 310, p. 1944–1947.
- Kennaway, Todd, and Helmer, E.H., 2007, The forest types and ages cleared for land development in Puerto Rico: *GIScience and Remote Sensing*, v. 44, p. 356–382.
- Kerr, R.A., 2000, A North Atlantic climate pacemaker for the centuries: *Science*, v. 288, p. 1984–1986.
- Kerr, R.A., 2005, Atlantic climate pacemaker for millennia past, decades hence?: *Science*, v. 309, p. 41–43.
- Knight, J.R., Folland, C.K., and Scaife, A.A., 2006, Climate impacts of the Atlantic Multidecadal Oscillation: *Geophysical Research Letters*, v. 33, no. L17706, p. 1–4.
- Landsea, C.W., and Gray, W.M., 1992, The strong association between western Sahel monsoon rainfall and intense Atlantic hurricanes: *Journal of Climate*, v. 5, p. 435–453.
- Larsen, M.C., 1995, Use of seismic refraction techniques for investigating recent landslides in a tropical rain forest in Puerto Rico, *in* Miller, R.L., Escalante, J.A., Reinemund, J.A., and Bergin, M.J., eds., Energy and mineral potential of the Central American–Caribbean regions: Berlin, Springer-Verlag, p. 411–414.
- Larsen, M.C., 1997, Tropical geomorphology and geomorphic work—A study of geomorphic processes and sediment and water budgets in montane humid-tropical forested and developed watersheds, Puerto Rico: Boulder, University of Colorado Geography Department, Ph.D. dissertation, 341 p.
- Larsen, M.C., 2000, Analysis of 20th century rainfall and streamflow to characterize drought and water resources in Puerto Rico: Physical Geography, v. 21, p. 494–521.
- Larsen, M.C., 2012, Landslides and sediment budgets in four watersheds in eastern Puerto Rico, ch. F *in* Murphy, S.F., and Stallard, R.F., eds., Water quality and landscape processes of four watersheds in eastern Puerto Rico: U.S. Geological Survey Professional Paper 1789, p. 153–178.
- Larsen, M.C., and Concepción, I.M., 1998, Water budgets of small forested and agriculturally developed montane watershed in eastern Puerto Rico, *in* Segarra-García, R.I.,

- ed., Tropical hydrology and Caribbean water resources, International Symposium on Tropical Hydrology, 3d, and Caribbean Islands Water Resources Congress, 5th, San Juan, Puerto Rico, July 13–16, 1998, Proceedings: American Water Resources Association, p. 199–204.
- Larsen, M.C., and Santiago-Román, A., 2001, Mass wasting and sediment storage in a small montane watershed—An extreme case of anthropogenic disturbance in the humid tropics, in Dorava, J.M., Palcsak, B.B., Fitzpatrick, F., and Montgomery, D., eds., Geomorphic processes and riverine habitat: American Geophysical Union Water Science and Application Series, v. 4, p. 119–138.
- Larsen M.C., and Simon A., 1993, A rainfall intensity-duration threshold for landslides in a humid-tropical environment, Puerto Rico: *Geografiska Annaler*, v. 75A, p. 13–23.
- Larsen, M.C., and Stallard, R.F., 2000, Luquillo Mountains, Puerto Rico—A Water, Energy, and Biogeochemical Budgets program site: U.S. Geological Survey Fact Sheet 163–99, 4 p.
- Larsen, M.C., and Webb, R.M.T., 2009, Potential effects of runoff, fluvial sediment and nutrient discharges on the coral reefs of Puerto Rico: *Journal of Coastal Research*, v. 25, p. 189–208.
- Lawton, R.O., Nair, U.S., Pielke, R.A.S., and Welch, R.M., 2001, Climatic impact of tropical lowland deforestation on nearby montane cloud forests: *Science*, v. 294, 584–587.
- Leigh, E.G., Jr., 1999, Tropical forest ecology—A view from Barro Colorado Island: Oxford, U.K., Oxford University Press, 245 p.
- Long Term Ecological Research Network, 2008, Luquillo LTER data: accessed March 10, 2008, at <http://lug.lternet.edu/data/>
- Longo, A.V., Burrowes, P.A., and Joglar, R.L., 2010, Seasonality of *Batrachochytrium dendrobatidis* infection in direct-developing frogs suggests a mechanism for persistence: *Diseases of Aquatic Organisms*, v. 92, p. 253–60.
- Lugo, A.E., 1986, Water and the ecosystems of the Luquillo Experimental Forest: New Orleans, La., U.S. Department of Agriculture Forest Service, Southern Experiment Station General Technical Report SO-63, 17 p.
- Malmgren, B.A., Winter, A., and Chen, D., 1998, El Niño–Southern Oscillation and North Atlantic Oscillation control of climate in Puerto Rico: *Journal of Climate*, v. 11, p. 2713–2717.
- McDowell, W.H., Bowden, W.B., and Asbury, C.E., 1992, Riparian nitrogen dynamics in two geomorphologically distinct tropical rain forest watersheds—Subsurface solute patterns: *Biogeochemistry*, v. 18, p. 53–75.
- Monteith, J.L., 1965, Evaporation and the environment—The state and movement of water in living organisms, in Society of Experimental Biology, Symposium, 19th: Proceedings, p. 205–234.
- Murphy, S.F., Stallard, R.F., Larsen, M.C., and Gould, W.A., 2012, Physiography, geology, and land cover of four watersheds in eastern Puerto Rico, ch. A in Murphy, S.F. and Stallard, R.F., eds., Water quality and landscape processes of four watersheds in eastern Puerto Rico: U.S. Geological Survey Professional Paper 1789, p. 1–24.
- Musk, L.F., 1988, Weather systems: Cambridge, U.K., Cambridge University Press, 160 p.
- National Oceanic and Atmospheric Administration Coastal Services Center, 2007, Historical north Atlantic and east-central north Pacific tropical cyclone tracks, 1851–2006: accessed October 8, 2007, at <http://maps.csc.noaa.gov/hurricanes/>
- National Oceanic and Atmospheric Administration, 2008, National Climate Data Center: accessed May 16, 2008, at <http://www.ncdc.noaa.gov/oa/ncdc.html>
- National Oceanic and Atmospheric Administration, 2010, Climate indices—Monthly atmospheric and ocean time series: accessed March 1, 2010, at <http://www.esrl.noaa.gov/psd/data/climateindices/list/>
- Odum, H.T., Moore, A.M., and Burns, L.A., 1970, Hydrogen budget and compartments in the rain forest, in Odum, H.T., and Pigeon, R.F., eds., A tropical rain forest: Springfield, Va., National Technical Information Service, p. H-105–H-122.
- Ortiz-Zayas, J.R., and Scatena, F.N., 2004, Integrated water resources management in the Luquillo Mountains, Puerto Rico—An evolving process: *International Journal of Water Resources Development*, v. 20, p. 387–398.
- Peters, N.E., Shanley, J.B., Aulenbach, B.T., Webb, R.M., Campbell, D.H., Hunt, R., Larsen, M.C., Stallard, R.F., Troester, J.W., and Walker, J.F., 2006, Water and solute mass balance of five small, relatively undisturbed watersheds in the U.S.: *Science of the Total Environment*, v. 358, p. 221–242.
- Pringle, C.M., 2000, Threats to U.S. public lands from cumulative hydrologic alterations outside of their boundaries: *Ecological Applications*, v. 10, p. 971–989.
- Quinn, W.H., Neal, V.T., and Antunez de Mayolo, S.E., 1987, El Niño occurrences over the past four and a half centuries: *Journal of Geophysical Research*, v. 92, p. 14,449–14,461.
- Quiñones, Ferdinand, 2010, Disponibilidad, condición y manejo de los recursos de agua de Puerto Rico: accessed May 21, 2012, at <http://recursosaguapuertorico.com/Blank-1.html/>
- Rauber, R.M., Stevens, B., Ochs, H.T., Knight, C., Albrecht, B.A., Blyth, A.M., Fairall, C.W., Jensen, J.B., Lasher-Trapp, S.G., Mayol-Bracero, O.L., Vali, G., Anderson, J.R.,

- Baker, B.A., Bandy, A.R., Burnet, E., Brenguier, J.-L., Brewer, W.A., Brown, P.R.A., Chuang, P., Cotton, W.R., di Girolamo, L., Geerts, B., Gerber, H., Göke, S., Gomes, L., Heikes, B.G., Hudson, J.G., Kollias, P., Lawson, R.P., Krueger, S.K., Lenschow, D.H., Nuijens, L., O'Sullivan, D.W., Rilling, R.A., Rogers, D.C., Siebesma, A.P., Snodgrass, E., Stith, J.L., Thornton, D.C., Tucker, S., Twohy, C.H., and Zuidema, P., 2007, Rain in shallow cumulus over the ocean—The RICO campaign: *Bulletin of the American Meteorological Society*: v. 88, p. 1912–1928.
- Rigau-Pérez, J.G., Vorndam, A.V., and Clark, G.G., 2001, The dengue and dengue hemorrhagic fever epidemic in Puerto Rico, 1994–1995: *American Journal of Tropical Medicine and Hygiene*, v. 64, p., 67–74.
- Rivera-Ramírez, H.D., Warner, G.S., and Scatena, F.N., 2002, Prediction of master recession curves and baseflow recessions in the Luquillo Mountains of Puerto Rico: *Journal of the American Water Resources Association*, v. 38, p. 693–704.
- Roe, G.H., 2005, Orographic precipitation: *Annual Review of Earth and Planetary Sciences*, v. 33, p. 1–31.
- Sauer, V.B., and Meyer, R.W., 1992, Determination of error in individual discharge measurements: U.S. Geological Survey Open-File Report 92–144, 21 p.
- Scatena, F.N., 1995, Relative scales of time and effectiveness of watershed processes in a tropical montane rain forest of Puerto Rico, in Miller, A.J., Potter, K.W., and Wilcock, P.R., eds., *Natural and anthropogenic influences in fluvial geomorphology*: American Geophysical Union Geophysical Monograph, v. 89, p. 103–111.
- Scatena, F.N., 1998, An assessment of climate change in the Luquillo Mountains of Puerto Rico, in Segarra-García, R.I., ed., *Tropical hydrology and Caribbean water resources*, International Symposium on Tropical Hydrology, 3d, and Caribbean Islands Water Resources Congress, 5th, July 13–16, 1998, San Juan, Puerto Rico, Proceedings: American Water Resources Association, p. 193–198.
- Scatena, F.N., 2001, Ecological rhythms and the management of humid tropical forests—Examples from the Caribbean National Forest, Puerto Rico: *Forest Ecology and Management*, v. 5528, p. 1–12.
- Scatena, F.N., and Johnson, S.L., 2001, Instream-flow analysis for the Luquillo Experimental Forest, Puerto Rico—Methods and analysis: Río Piedras, Puerto Rico, U.S. Department of Agriculture Forest Service, International Institute of Tropical Forestry, General Technical Report IITF-GTR-11, 30 p.
- Scatena, F.N., and Larsen, M.C., 1991, Physical aspects of Hurricane Hugo in Puerto Rico: *Biotropica*, v. 23, p. 317–323.
- Schellekens, Jaap, Bruijnzeel, L.A., Scatena, F.N., Bink, N.J., and Holwerda, Friso, 2000, Evaporation from a tropical rain forest, Luquillo Experimental Forest, Puerto Rico: *Water Resources Research*, v. 36, p. 2183–2196.
- Schellekens, Jaap, Bruijnzeel, L.A., Wickel, A.J., Scatena, F.N., and Silver, W.L., 1998, Interception of horizontal precipitation by elfin cloud forest in the Luquillo Mountains, eastern Puerto Rico, in Schemenauer, R.S., and Bridgman, H.A., eds., *International Conference on Fog and Fog Collection*, 1st, Proceedings: Ottawa, Canada, International Development Research Centre, p. 29–32.
- Schellekens, Jaap, Scatena, F.N., Bruijnzeel, L.A., van Dijk, A.I.J.M., Groen, M.M.A., and van Hogenzand, R.J.P., 2004, Stormflow generation in a small rainforest catchment in the Luquillo Experimental Forest, Puerto Rico: *Hydrological Processes*, v. 18, p. 505–530.
- Scholl, M.A., Shanley, J.B., Zegarra, J.P., and Coplen, T.B., 2009, The stable isotope amount effect—New insights from NEXRAD echo tops, Luquillo Mountains, Puerto Rico: *Water Resources Research*, v. 45, no. 12407, p. 1–14.
- Searcy, J.K., 1959, Flow-duration curves, Manual of hydrology—Part 2. Low-flow techniques: U.S. Geological Survey Water-Supply Paper 1542-A, 33 p.
- Shanahan, T.M., Overpeck, J.T., Anchukaitis, K.J., Beck, J.W., Cole, J.E., Dettman, D.L., Peck, J.A., Scholz, C.A., and King, J.W., 2009, Atlantic forcing of persistent drought in West Africa: *Science*, v. 324, p. 377–380.
- Simon, Andrew, Larsen, M.C., and Hupp, C.R., 1990, The role of soil processes in determining mechanisms of slope failure and hillslope development in a humid-tropical forest, eastern Puerto Rico, in Kneuper, P.L.K., and McFadden, L.D., eds., *Soils and landscape evolution: Geomorphology*, v. 3, p. 263–286.
- Smith, J.A., Studevant-Rees, Paula, Baek, M.L., and Larsen, M.C., 2005, Tropical cyclones and the flood hydrology of Puerto Rico: *Water Resources Research*, v. 41, no. W06020, p. 1–16.
- Snodgrass, E.R., Di Girolamo, L., and Rauber, R.M., 2009, Precipitation characteristics of trade wind clouds during RICO derived from radar, satellite, and aircraft measurements: *Journal of Applied Meteorology and Climatology*, v. 48, p. 464–483.
- Stallard, R.F., 2001, Possible environmental factors underlying amphibian decline in eastern Puerto Rico—Analysis of U.S. government data archives: *Conservation Biology*, v. 15, no. 4, p. 943–953.
- Stallard, R.F., 2012, Weathering, landscape equilibrium, and carbon in four watersheds in eastern Puerto Rico, ch. H in Murphy, S.F. and Stallard, R.F., eds., *Water quality and landscape processes of four watersheds in eastern Puerto Rico*: U.S. Geological Survey Professional Paper 1789, p. 199–248.

- Stallard, R.F., and Murphy, S.F., 2012, Water quality and mass transport in four watersheds in eastern Puerto Rico, ch. E in Murphy, S.F., and Stallard, R.F., eds., Water quality and landscape processes of four watersheds in eastern Puerto Rico: U.S. Geological Survey Professional Paper 1789, p. 113–152.
- Still, C.J., Foster, P.N., and Schneider, S.H., 1999, Simulating the effects of climate change on tropical montane cloud forests: *Nature*, v. 389, p. 608–610.
- U.S. Census Bureau, 2000, United States Census 2000: accessed on October 27, 2011, at <http://www.census.gov/main/www/cen2000.html>
- U.S. Geological Survey, 1967, El Yunque quadrangle, Puerto Rico: U.S. Geological Survey topographic map, 7.5 minute series, 1 sheet.
- U.S. Geological Survey, 1994–2006, Water-data reports, Puerto Rico and the U.S. Virgin Islands: accessed June 1, 2009, at <http://pubs.usgs.gov/wdr/>
- U.S. Geological Survey, 2006, Water resources data, Puerto Rico and the U.S. Virgin Islands—Water year 2005 and 2006: accessed June 1, 2009, at <http://pubs.usgs.gov/wdr/>
- U.S. Geological Survey, 2009, Waterwatch: accessed June 1, 2009, at <http://water.usgs.gov/waterwatch/>
- U.S. Geological Survey, 2010, USGS water data for the nation: accessed July 10, 2010, at <http://waterdata.usgs.gov/nwis>
- van der Molen, M.K., 2002, Meteorological impacts of land use change in the maritime tropics: Amsterdam, Netherlands, Vrije Universiteit, Ph.D. dissertation, 262 p.
- van der Molen, M.K., Dolman, A.J., Waterloo, M.J., and Bruijnzeel, L.A., 2006, Climate is affected more by maritime than by continental land use change—A multiple scale analysis: *Global and Planetary Change*, v. 54, p. 128–149.
- van Dijk, A.I.J.M., van Noordwijk, M., Calder, I.R., Bruijnzeel, S.L.A., Schellekens, J., and Chappell, N.A., 2009, Forest-flood relation still tenuous—Comment on “Global evidence that deforestation amplifies flood risk and severity in the developing world” by C.J.A. Bradshaw, N.S. Sodi, K.S.-H. Peh, and B.W. Brook: *Global Change Biology*, v. 15, p. 110–115.
- Vogel, R.M., and Kroll, C.N., 1996, Estimation of baseflow recession constants: *Water Resources Management*, v. 10, p. 303–320.
- Wadsworth, F.H., 1950, Notes on the climax forests of Puerto Rico and their destruction and conservation prior to 1990: *Caribbean Forester*, v. 11, p. 38–56.
- Wadsworth, F.H., 1951, Forest management in the Luquillo Mountains, I—The setting: *Caribbean Forester*, v. 12, p. 93–114.
- Wang, Hongqing, Hall, C.A.S., Scatena, F.N., Fetcher, Ned, and Wu, Wei, 2003, Modeling the spatial and temporal variability in climate and primary productivity across the Luquillo Mountains, Puerto Rico: *Forest Ecology and Management*, v. 179, p. 69–94.
- Warne, A.G., Webb, R.M.T., and Larsen, M.C., 2005, Water, sediment, and nutrient discharge characteristics of rivers in Puerto Rico, and their potential influence on coral reefs: U.S. Geological Survey Scientific Investigations Report 2005–5206, 58 p.
- Weaver, P.L., 1972, Cloud moisture interception in the Luquillo Mountains of Puerto Rico: *Caribbean Journal of Science*, v. 12, p. 129–144.
- Webb, R.M.T., and Soler-López, L.R., 1997, Sedimentation history of Lago Loíza, Puerto Rico, 1953–94: U.S. Geological Survey Water-Resources Investigations Report 97–4108, 18 p. and 9 plates.
- Wu, Wei, Hall, C.A.S., Scatena, F.N., and Quackenbush, L.J., 2006, Spatial modeling of evapotranspiration in the Luquillo Experimental Forest of Puerto Rico using remotely sensed data: *Journal of Hydrology*, v. 328, p. 733–752.
- Zack, Allen, and Larsen, M.C., 1993, Island hydrology—Puerto Rico and the U.S. Virgin Islands: National Geographic Research and Exploration—Water issue, p. 126–134.
- Zeng, Ning, Neelin, J.D., Lau, K.-M., and Tucker, C.J., 1999, Enhancement of interdecadal climate variability in the Sahel by vegetation interaction: *Science*, v. 286, p. 1537–1540.

Atmospheric Inputs to Watersheds of the Luquillo Mountains in Eastern Puerto Rico

By Robert F. Stallard

Chapter D of
**Water Quality and Landscape Processes of Four Watersheds in
Eastern Puerto Rico**

Edited by Sheila F. Murphy and Robert F. Stallard

Professional Paper 1789-D

**U.S. Department of the Interior
U.S. Geological Survey**

Contents

Abstract.....	89
Introduction.....	89
Background—Solute Sources in Tropical Rain	91
Methods Used to Quantify Inputs and Sources of Solutes in Precipitation	92
Grouping Data.....	95
Missing Samples and Big Storms	95
Estimating Source Strengths	99
Seasonality and Trends in Inputs and Sources	107
Conclusions.....	109
Acknowledgments.....	109
References.....	109

Figures

1. Map of Puerto Rico and study watersheds.....	90
2–12. Diagrams showing the following:	
2. Aggregated monthly rainfall, monthly mean concentrations, and monthly mean loading for chemical constituents in rain sampled at the El Verde National Atmospheric Deposition Program site, eastern Puerto Rico.....	97
3. Three samples with the highest chloride concentrations measured for the Río Mameyes, eastern Puerto Rico, during Hurricanes Georges compared with seawater and the first base-flow sample following the hurricane	99
4. Time series of runoff rate and chloride concentrations measured for the Río Mameyes, eastern Puerto Rico, during Hurricanes Hortense and Georges....	100
5. Time series of concentration estimates for the three primary components (marine aerosols, temperate contamination, and desert dust) that contribute to rain chemistry in El Verde, Puerto Rico, and inorganic nitrogen and acidity values.....	101
6. Monthly and annual time series of rainfall, chloride concentrations, and chloride loadings from the National Atmospheric Deposition Program data set for El Verde, Puerto Rico.....	102
7. Time series of monthly and annual loading estimates for the three primary components (marine aerosols, temperate contamination, and desert dust) that contribute to rain chemistry in El Verde, Puerto Rico, and inorganic nitrogen and acidity values.....	106
8. Aggregated monthly concentration estimates for the three primary components (marine aerosols, temperate contamination, and desert dust) that contribute to rain chemistry in El Verde, Puerto Rico	107
9. Aggregated monthly loading estimates for the three primary components (marine aerosols, temperate contamination, and desert dust) that contribute to rain chemistry in El Verde, Puerto Rico.....	107
10. Fractional contribution of the three primary components (marine aerosols, temperate contamination, and desert dust) that contribute to rain chemistry in El Verde, Puerto Rico	108

11. Monthly total acidity concentrations compared to acidity concentration estimates for the three primary components (marine aerosols, temperate contamination, and desert dust) that contribute to rain chemistry in El Verde, Puerto Rico	108
12. Monthly total acidity loadings compared to acidity loading estimates for the three primary components (marine aerosols, temperate contamination, and desert dust) that contribute to rain chemistry in El Verde, Puerto Rico	108

Tables

1. Rainfall-weighted average monthly concentration of various constituents at El Verde, Puerto Rico, 1983 to 2005.....	93
2. Rainfall-weighted average annual concentration of various constituents at El Verde, Puerto Rico, 1983 to 2005.....	94
3. Rainfall-weighted monthly loadings of various constituents at El Verde, Puerto Rico, 1983 to 2005.....	94
4. Rainfall-weighted annual loadings of various constituents at El Verde, Puerto Rico, 1983 to 2005.....	95
5. Constituent correlations for all weekly concentration data (n=818), ranked by correlation with Cl ⁻ , 1983 to 2005	96
6. Constituent correlations for aggregated monthly averaged concentration data (n=12), ranked by correlation with Cl ⁻ , 1983 to 2005.....	96
7. Storms that substantially affected WEBB rivers during the period of study, 1991–2005	98
8. Averaged monthly rain chemistry at El Verde, Puerto Rico, with contributions from different sources identified.....	103
9. Derived properties from monthly data at El Verde, Puerto Rico, with contributions from different sources identified.....	103
10. Rainfall-weighted average monthly concentration of total ionic charge and acidity at El Verde, Puerto Rico, 1983 to 2005.....	104
11. Rainfall-weighted average annual concentration of total ionic charge and acidity at El Verde, Puerto Rico, 1983 to 2005.....	104
12. Rainfall-weighted monthly loadings of total ionic charge and acidity at El Verde, Puerto Rico, 1983 to 2005.....	105
13. Rainfall-weighted average loadings of total ionic charge and acidity at El Verde, Puerto Rico, 1983 to 2005.....	105

Abbreviations Used in This Report

$\mu\text{eq L}^{-1}$	microequivalents per liter
μm	micrometer
$\mu\text{mol L}^{-1}$	micromoles per liter
km	kilometer
km h^{-1}	kilometers per hour
m	meter
mm	millimeter
mm h^{-1}	millimeters per hour
ppmv	parts per million volume
r^2	correlation coefficient, squared
$t \text{ km}^{-2} \text{ yr}^{-1}$	metric tons per square kilometer per year
$\text{Ca}^*, \text{Cl}^*, \text{ or Mg}^*$	calculated nonseasalt concentration of Ca, Cl, or Mg
NADP	National Atmospheric Deposition Program
WEBB	Water, Energy, and Biogeochemical Budgets

Conversion Factors

Multiply	By	To obtain
Length		
micrometer (μm)	0.00003937	inch (in.)
millimeter (mm)	0.03937	inch (in.)
meter (m)	3.281	foot (ft)
kilometer (km)	0.6214	mile (mi)
Flow rate		
millimeters per hour (mm h^{-1})	0.03937	inches per hour (in h^{-1})
Other		
metric tons per square kilometer per year ($t \text{ km}^{-2} \text{ yr}^{-1}$)	2.855	short tons per square mile per year (tons $\text{mi}^{-2} \text{ yr}^{-1}$)

Atmospheric Inputs to Watersheds of the Luquillo Mountains in Eastern Puerto Rico

By Robert F. Stallard

Abstract

Twenty years of precipitation-chemistry data from the National Atmospheric Deposition Program site at El Verde, Puerto Rico, demonstrate that three major sources control the composition of solutes in rain in eastern Puerto Rico. In order of importance, these sources are marine salts, temperate contamination from the Northern Hemisphere, and Sahara Desert dust. Marine salts are a source of roughly 82 percent of the ionic charge in precipitation; marine salt inputs are greatest in January. Evaluation of 15 years of U.S. Geological Survey data for four watersheds in eastern Puerto Rico suggests that large storms, including hurricanes, are associated with exceptionally high chloride concentrations in stream waters. Some of these storms were missed in sampling by the National Atmospheric Deposition Program, and therefore its data on the marine contribution likely underestimate chloride. The marine contribution is a weak source of acidity. Temperate contamination contributes about 10 percent of the ionic charge in precipitation; contaminants are primarily nitrate, ammonia, and sulfate derived from various manmade and natural sources. Peak deposition of temperate contaminants is during January, April, and May, months in which strong weather fronts arrive from the north. Temperate contamination, a strong source of acidity, is the only component that is increasing through time. Sahara Desert dust provides 5 percent of the ionic charge in precipitation; it is strongly seasonal, peaking in June and July during times of maximum dust transport from the Sahara and sub-Saharan regions. This dust contributes, on average, enough alkalinity to neutralize the acidity in June and July rains.

Introduction

A large portion of the dissolved load in near-coastal tropical rivers comes from the atmosphere (Stallard and Edmond, 1981). This load is obtained by several processes such as precipitation, dry deposition (fallout, impaction on surfaces), and chemical fixation by biological processes or chemical-weathering reactions. Precipitation removes aerosols and some gases directly from the atmosphere, while dry deposition transfers aerosols to plant (and other) surfaces to

be washed off by precipitation or condensation. Precipitation and dry deposition are commonly difficult to distinguish chemically, and only precipitation is readily sampled. Dry deposition loadings can be similar to precipitation loadings (Peters and others, 2006). Chemical fixation (the conversion of atmospheric gases into dissolved and solid compounds by chemical or biological means) is the source of much of the dissolved organic and inorganic carbon in surface waters and of considerable dissolved nitrogen. Accordingly, atmospheric inputs to rivers are commonly underestimated. In this report, atmospheric chemical inputs to eastern Puerto Rico were characterized by using relations among chemical constituents to identify constituent sources, and then using constituent deposition rates to estimate source loadings. The rainfall and runoff chemical datasets are from the National Atmospheric Deposition Program (NADP) and the U.S. Geological Survey Water, Energy, and Biogeochemical Budgets (WEBB) program. The NADP record is long (1985 to the present (2010)), but it has several large gaps. The WEBB precipitation data set (1991–1995) is more limited but helps in generalizing the data throughout the region. Runoff data are available for five rivers (Canóvanas, Cayaguás, Guabá, Icacos, and Mameyes) in four study watersheds (fig. 1).

Many of the sources of aerosols and gases that dissolve in precipitation have distinct chemical signatures. In undeveloped tropical regions within about 300 kilometers (km) of the ocean, the ocean is the largest source of solutes in rain (Stallard and Edmond, 1981). Within the ocean, solutes arise in two ways: seasalt from breaking waves and bursting bubbles, and gases emitted, generally from biological activity. The many solutes in seasalt are in characteristic proportions referred to as the “seasalt ratio.” The nutrients nitrate, ammonia, silica, and phosphate are important exceptions and are typically stripped from surface seawater by biological activity. Of the major seawater ions, only sulfate has gaseous sources. Algae release to the atmosphere organic sulfur gases such as methyl sulfide, dimethyl sulfide, and carbon disulfide. Ultraviolet light quickly oxidizes these gases into precursors of sulfuric acid. Thus, the ocean can be a natural source of acid precipitation in the coastal tropics (Stallard and Edmond, 1981).

A variety of nitrogen and sulfur compounds are emitted by natural and human activities. Natural sources of sulfate include emissions from vegetation, anaerobic soils, and

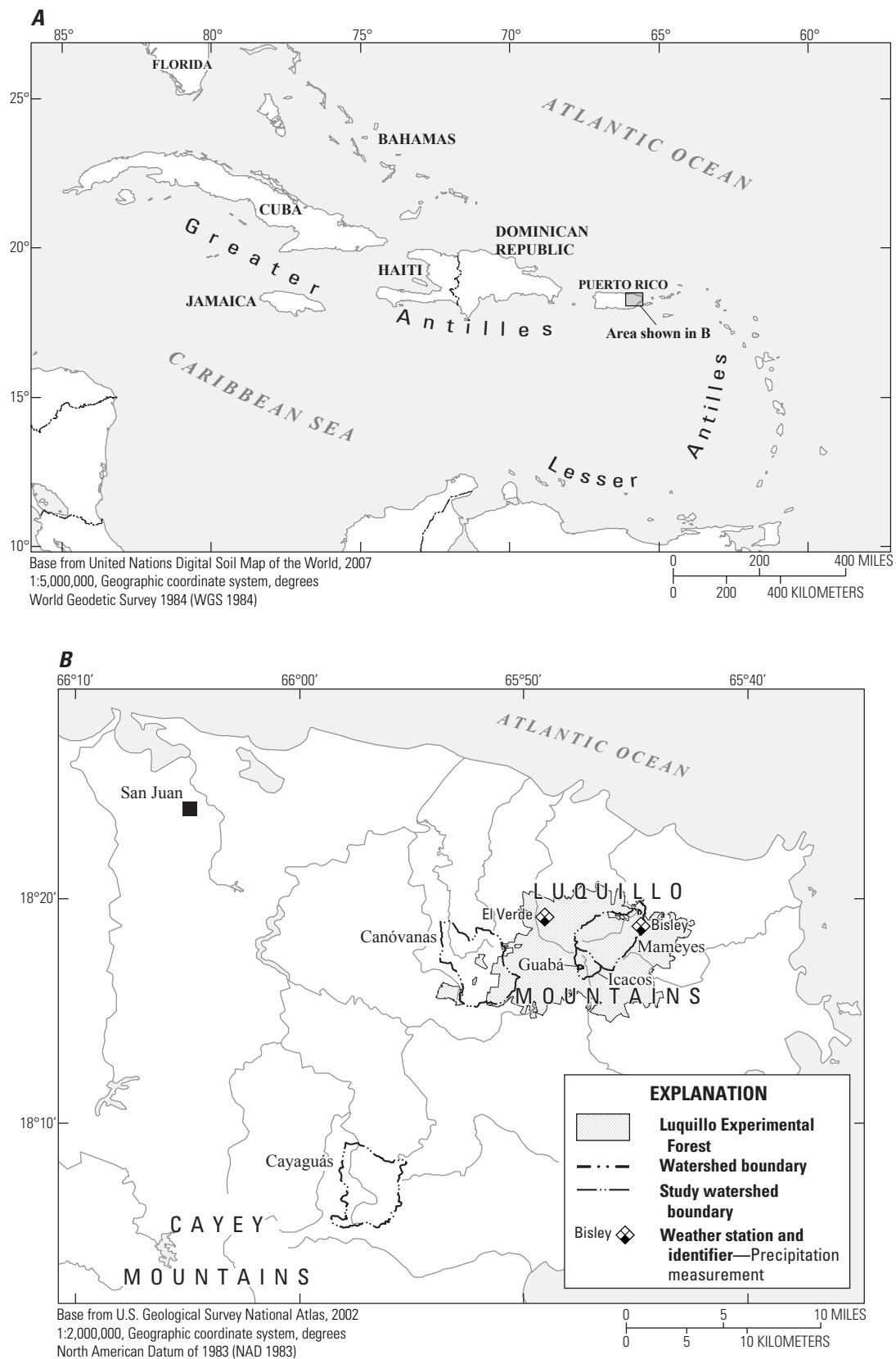


Figure 1. Location of Puerto Rico and study watersheds, eastern Puerto Rico.

volcanoes. Some ammonia and nitrate come from vegetation, biogenic emissions from soils, and from lightning (Junge, 1963). Eastern Puerto Rico is not close to any major terrestrial sources of sulfur or nitrogen, although Soufrière Hills Volcano on Montserrat (an island in the Lesser Antilles about 300 miles east-southeast of Puerto Rico), active 1995 to present, is arguably close enough to have some influence (Heartsill-Scalley and others, 2007). Human activities, especially on lands of the temperate northern hemisphere, are a major and often dominant source of nitrate, ammonia, and sulfate ions in the atmosphere, cloud waters, and precipitation (Junge, 1963; Weathers and others, 1988; Duce and others, 1991; Galloway and others, 1996; Galloway, 1998; Holland and others, 1999; Rasch and others, 2000; Rodhe and others, 2002). The sulfur and nitrogen compounds typically form aerosols that are strong acids, which are the main source of acid rain in polluted regions. Sulfur compounds, which are typically oxidized to form sulfuric acid, come from the burning of fossil fuels. Nitrogen compounds, mainly ammonium and nitrate ions, have a complex mix of sources including burning of fossil fuels and vegetation and biogenic emissions from soils enriched in nitrogen through the use of artificial fertilizers (Junge, 1963). There are no major local sources of such contamination immediately upwind (north and east) of eastern Puerto Rico (Brown and others, 1983; Ortiz-Zayas and others, 2006).

A final major source of solutes in tropical Atlantic coastal regions and islands of the Americas is dust from the Sahara Desert in Africa (Prospero and Carlson, 1972; Stallard, 2001; Reid and others, 2003a,b; Garrison and others, 2003). Fallout of dust from northern Africa blankets a zone from southern North America through Central America and northern South America (Prospero and Carlson, 1972). Seasonally averaged data from a coastal zone color-scanner satellite shows that the biggest desert-dust plume is derived from the Sahara and is carried westward by the trade winds (Stegmann and Tindale, 1999). The structure of this plume is complex and hard to characterize in detail (Reid and others, 2003a). The dust plume typically bathes Puerto Rico from June through August. Farther south, in Costa Rica and Panama, the plume is strong starting in April. The fallout of fine clay and quartz that forms the bulk of the dust is so great that it is the source of soil minerals on carbonate islands such as Bermuda (Herwitz and others, 1996). Although this dustfall has been going on for millions of years (Parkin and Shackleton, 1973), the clearing of land south of the Sahara may provide a new contribution (Lundholm, 1977; Shinn and others, 2000). Recent studies (Dunion and Velden, 2004; Evan and others, 2006) indicate a strong interaction between dry dusty air coming off the Sahara and tropical cyclones, with an inverse relation between dustiness, as measured by satellites, and cyclone activity. Sahara dust may carry pathogens that affect coral (Shinn and others, 2000), amphibians (Stallard, 2001), and people (Kuehn, 2006).

Enough dust comes from the Sahara to affect the strontium isotope composition of water and plants in the Luquillo Mountains (Pett-Ridge and others, 2009a,b) and to be a significant source of phosphate (Pett-Ridge, 2009). (The isotopic

ratios of strontium from the Sahara differ from those ratios in Luquillo rocks and soils.) Pett-Ridge and others (2009b) use the Sr isotopic budget to estimate the long-term average deposition rate for Sahara dust at 21 ± 7 metric tons per square kilometer per year ($t \text{ km}^{-2} \text{ yr}^{-1}$).

Reid and others (2003b) used x-ray fluorescence to analyze 60,500 individual particle aggregates of air-borne Sahara dust collected on a Davis rotating drum collector, which separates the dust into eight particle-size stages from 0.1 to 12 micrometers (μm). Intercorrelations among various elements provide indications of dominant particle sources. The bulk of particles sampled from air-borne Sahara dust are silicate minerals and insoluble oxides; a few percent of the total consists of sodium-chloride, calcium-rich, and calcium-sulfur particles (Reid and others, 2003b). Seasalt is the dominant source of sodium and chloride in the dust. Some salts of desert soils, such as halite (NaCl), are not readily distinguished from seasalt, especially because photochemical processes can slightly shift the original elemental proportions in air-borne seasalt (Stallard and Edmond, 1981; Reid and others, 2003b). Soluble calcium in this dust presumably comes from the calcium carbonate and calcium sulfate minerals that typically accumulate in desert soils (Birkeland, 1999; Reid and others, 2003b). Calcium carbonate reacts with and neutralizes nitric and sulfuric acids, thus generating carbon dioxide.

Elements with especially strong correlations with silicon (correlation coefficient (r^2) > 0.8) were aluminum ($\text{Al/Si}=0.49$, $r^2=0.90$), potassium ($\text{K/Si}=0.059$, $r^2=0.92$), titanium ($\text{Ti/Si}=0.012$, $r^2=0.81$), and iron ($\text{Fe/Si}=0.070$, $r^2=0.92$). Excluding sodium and chlorine, which originate largely from seasalt, the most abundant elements identified by analysis were silicon, aluminum ($\text{Al/Si}=0.49$), calcium ($\text{Ca/Si}=0.13$), sulfur ($\text{S/Si}=0.1$), iron ($\text{Fe/Si}=0.070$), magnesium ($\text{Mg/Si}=0.066$), and potassium ($\text{K/Si}=0.059$). Reid and others (2003b) estimate that more than 70 percent of dust-particle mass can be attributed to aluminosilicate clay minerals such as illite, kaolinite, and montmorillonite. Of these minerals, illite, $\text{K}_{0.6}(\text{H}_3\text{O})_{0.4}\text{Al}_{1.3}\text{Mg}_{0.3}\text{Fe}^{2+}_{0.1}\text{Si}_{3.5}\text{O}_{10}(\text{OH})_2 \cdot (\text{H}_2\text{O})$, is most important. Amorphous silicon and quartz make up the next largest group, composing another 10 to 15 percent. Although these clay minerals and oxides come from desert soils, presumably they were derived from weathering during humid periods, and because these clays are solid weathering products, it is most likely that they contribute to the solid load in the rivers rather than the dissolved load (Herwitz and others, 1996).

Background—Solute Sources In Tropical Rain

The lack of local contamination sources makes the Luquillo Experimental Forest in easternmost Puerto Rico an ideal setting for studying precipitation chemistry (fig. 1). Like the prow of a ship, the Luquillo Mountains meet the east-to-west trade-wind air flow after it transits largely open ocean.

Rainfall for the region is derived from a mix of locally generated showers, tropical systems moving from the east, and frontal systems from the north (McDowell and others, 1990; Lugo and Scatena, 1992; Malmgren and others, 1998). The frontal systems are most important from December to May. Trade winds blow throughout the year but are strongest from June to November (García-Martino and others, 1996). Trade-wind meteorology has been extensively studied in the region east of Puerto Rico (Snodgrass and others, 2009, and references therein). The elevation of the trade-wind cloud base is largely controlled by sea-surface conditions, and it may be as low as 400 meters (m) but is typically around 600 m. Orographic control of rainfall is important (García-Martino and others, 1996; Murphy and Stallard, 2012); about 1,500 millimeters (mm) falls on the coast and more than 4,000 mm falls at highest elevations. More falls on the north and east sides of mountains and less on the south and west. Water from cloud interception provides 10 to 14 percent of the water budget in elfin forests (Baynton, 1968, 1969; Weaver, 1972; Brown and others, 1983; Larsen and Concepción, 1998; Schellekens and others, 1998; Eugster and others, 2006; Holwerda and others, 2006), and it may provide water to the upper portion of palo colorado forest as well.

Several studies have analyzed rain chemistry in the Luquillo Mountains (fig. 1). The best record of rainfall chemistry is from El Verde, which, with few exceptions, has been sampled by the NADP on a weekly basis since early 1985 (National Atmospheric Deposition Program (NRSP-3)/National Trends Network, 2007c, Station PR20). A 2-year gap was sustained from mid-1989 to mid-1991, starting the week that Hurricane Hugo hit, and occasional short gaps have commonly coincided with huge storms.

McDowell and others (1990) used bulk and wet precipitation from the NADP site at El Verde for 1983–1987 to identify three dominant sources of solutes in the rain: (1) marine aerosols (Na^+ , K^+ , Mg^{2+} , Cl^-), (2) temperate contamination (NH_4^+ , SO_4^{2-} , NO_3^-), and (3) Sahara dust (K^+ , Ca^{2+} , Mg^{2+}). Contaminants arrive in frontal systems from North America, and the trade winds carry contaminants from North America, Europe, and Africa. Stallard (2001) extended the analysis by using the NADP data set from 1985 through 1998 and provides a detailed analysis of trends and of the seasonality of these three sources. Stallard (2001) noted that nitrogen loading in precipitation was increasing with time, an observation also later reported by Ortiz-Zayas and others (2006). Stallard (2001) did not observe a significant contribution of K^+ and Mg^{2+} in the desert-dust component.

Heartsill-Scalley and others (2007) examined a 15-year time series, 1988–2002, of chemistry data in precipitation and throughfall sampled at the ridge above the Bisley site in the most northeast part of the Luquillo Experimental Forest (fig. 1). In addition to the constituents determined by the NADP, that study also determined total dissolved nitrogen and PO_4^{3-} . These workers found that for constituents that are common in seasalt and dust (Na^+ , Ca^{2+} , Cl^- , SiO_2 , and SO_4^{2-}), annual rainfall deposition is large compared with

their deposition at other tropical sites, and the enrichment of throughfall by the canopy is small. Plant-active constituents (K^+ , NH_4^+ , NO_3^- , total dissolved nitrogen, and PO_4^{3-}) had lesser deposition in rain (rainout) than was true at many other tropical sites, and enrichment of throughfall by the canopy is large and quite variable. After hurricanes, which destroy canopy, throughfall is a greater fraction of total rainfall but it is less enriched in plant-active constituents because of less interaction with canopy. The enrichment of throughfall by plant-active solutes increased during droughts. Heartsill-Scalley and others (2007) show a weak increase in precipitation fluxes (cations, N, P) that might be associated with the Soufrière Hills Volcano.

The present paper modifies the analytical approach of Stallard (2001) to extend the analysis of the NADP data set though the time period of the WEBB research program. In addition, the effects of data gaps are examined, because the NADP data set used here, from February 12, 1985, through May 15, 2007, contains 123 data gaps ranging from 1 to 89 weeks for a total of 336 weeks out of 1,155 weeks, or 29 percent of the time. The average gap length is 2 weeks, if the four longest gaps of 11, 12, 29, and 89 weeks are excluded. Reasons for the gaps are not given except for the longest, which was caused by a lack of funding. Several gaps coincide with large storms. Large storms, especially hurricanes, defoliate the canopy, carpet the entire landscape with leaves and branches, and topple many trees (Scatena and Larsen, 1991; Schaefer and others, 2000). Collection equipment is commonly compromised, and rain samplers are typically filled with debris. Finally, access roads are sometimes blocked for days to weeks after a storm, and it is often a challenge to recover samples in a timely manner.

Methods Used to Quantify Inputs and Sources of Solutes in Precipitation

Samples at the El Verde NADP Station PR20 are collected weekly from a wet collector and analyzed using a standard protocol (National Atmospheric Deposition Program (NRSP-3)/National Trends Network, 2007a,b). The objective of this standardization is to provide a basis for comparison of major ionic constituents (H^+ , Na^+ , K^+ , Ca^{2+} , Mg^{2+} , NH_4^+ , Cl^- , SO_4^{2-} , NO_3^-) among sites and to identify trends through time. On 11 January 1994, procedures changed slightly, resulting in a slight apparent decrease in concentration of some constituents (National Atmospheric Deposition Program (NRSP-3)/National Trends Network, 2007d); however, this decrease is small compared with concentrations observed for El Verde samples. The NADP data for El Verde are available on the internet (National Atmospheric Deposition Program (NRSP-3)/National Trends Network, 2007a). The largest data gap was almost 2 years (mid-1989 to mid-1991), when samples were not collected. The NADP website provides the raw weekly data as well as monthly and annual digests of the

data. These digests were used and modified as needed for this discussion. Stallard and Edmond (1981), who collected rain samples from a ship on the Amazon River, noted that samples collected close to forest are enriched in nutrients (plant-active constituents) compared with those collected on the river hundreds of meters to kilometers from the forest edge. Accordingly, one would expect some local contamination, by bits of plant debris or insects, of these constituents in the El Verde samples, which are collected close to forest.

The chemical constituents identified by the NADP do not complete a charge balance. The concentration of hydrogen ions in rainwater is controlled by the imbalance of charge between nonreactive anions and cations and equilibration with atmospheric carbon dioxide. Accordingly, two additional constituent concentrations, bicarbonate ion (HCO_3^-) and acidity, were calculated from the hydrogen ion concentration and other constituents. Acidity is the charge difference between nonreactive anions and cations. Acidity is conservative and is the same as the negative of alkalinity (also called acid-neutralization capacity). Organic anions in tropical rainwater are quite unstable (half-lives of only a few hours (Andreae and others, 1990)), and they should not contribute to the acidity of samples that were collected during a week. For the pH range and ionic strength of the NADP samples, at equilibrium with an atmospheric partial pressure of carbon dioxide (P_{CO_2}) of 370 parts per million volume (ppmv), the concentrations of these calculated constituents are given by several equations (Stumm and Morgan, 1981; Stallard, 2001):

$$\text{Hydrogen ion: } \text{H}^+ \text{ in microequivalents per liter} \\ (\mu\text{eq L}^{-1}) = 10^{(6-\text{pH})} \quad (1)$$

$$\text{Bicarbonate ion: } \text{HCO}_3^- = 6.36 / (\text{H}^+) \quad (2)$$

$$\text{Acidity: acidity} = (\text{total anion charge of strong acids}) - (\text{total cation charge of strong bases plus } \text{NH}_4^+) \quad (3)$$

$$\text{Acidity: acidity} \gg \text{H}^+ - \text{HCO}_3^- \quad (4)$$

These two independent calculations of acidity, equations 3 and 4, allow for a quality-control check of the overall analyses. Acidity calculated from laboratory pH is in better agreement with acidity calculated from charge balance than is acidity calculated from field pH, indicating that laboratory pH is of better data quality. When the laboratory pH is used to calculate H^+ and HCO_3^- to complete charge balances, the resultant charge balances are generally within 10 percent. Many of the samples that have excess positive charge also have excess Na^+ relative to that expected from seasalt. Likewise, many of the samples with an excess negative charge also have a sodium deficit. If the pH values are valid, this result points to analytical problems for sodium.

The NADP uses standard procedures to calculate monthly and annual digests of data (National Atmospheric Deposition Program (NRSP-3)/National Trends Network, 2007b). The monthly and annual digests prepared by NADP were used to prepare summary tables of constituent concentrations and loadings (inputs) (tables 1–4). Acidity was calculated from the analyses by using equation 3, and H^+ and HCO_3^- were, in turn, calculated from acidity using equations 2 and 4. This calculation forces a perfect charge balance and leaves problem data, such as the excess Na^+ , just described, intact. The rainfall-volume-weighted averaging (calculated as the sum of weekly volume times concentration divided by total volume) of 4 to 5 weeks for each month and 52 weeks for each year reduces the influence of problem data.

Table 1. Rainfall-weighted monthly average concentration of various constituents at El Verde, Puerto Rico, derived from averaged monthly data of the National Atmospheric Deposition Program for 1983 to 2005.

[mm, millimeter; $\mu\text{mol L}^{-1}$, micromoles per liter]

Month	Rainfall (mm)	H^+ ($\mu\text{mol L}^{-1}$)	Na^+ ($\mu\text{mol L}^{-1}$)	K^+ ($\mu\text{mol L}^{-1}$)	Mg^{2+} ($\mu\text{mol L}^{-1}$)	Ca^{2+} ($\mu\text{mol L}^{-1}$)	NH_4^+ ($\mu\text{mol L}^{-1}$)	Cl^- ($\mu\text{mol L}^{-1}$)	SO_4^{2-} ($\mu\text{mol L}^{-1}$)	NO_3^- ($\mu\text{mol L}^{-1}$)
January	278	9.0	134.7	3.0	15.0	3.7	2.0	153.6	13.3	5.2
February	165	9.2	108.6	2.4	11.5	3.4	2.2	122.5	11.6	5.6
March	193	9.1	82.7	2.0	9.2	3.3	1.8	97.0	9.2	4.4
April	223	13.9	57.4	1.5	6.4	2.8	3.3	67.4	10.0	6.4
May	280	10.6	51.3	1.8	5.9	2.9	2.5	61.0	8.4	5.4
June	226	2.7	64.1	1.9	7.3	6.5	2.1	74.0	8.5	5.0
July	306	2.3	66.1	1.8	7.4	6.6	1.5	75.8	8.7	3.8
August	325	4.9	46.1	1.3	5.2	4.8	1.3	54.7	7.1	3.7
September	287	6.2	70.2	1.8	8.2	4.3	1.6	83.2	8.3	3.9
October	240	7.8	38.0	0.9	4.0	2.1	1.0	44.1	5.7	3.6
November	343	7.4	62.4	1.5	6.7	1.9	0.9	72.3	6.6	2.8
December	246	10.0	90.1	2.0	9.9	2.4	1.1	105.8	9.1	3.3
Total annual	3,113									
Average annual		7.3	71.0	1.8	7.9	3.8	1.7	82.5	8.7	4.3

Table 2. Rainfall-weighted average annual concentration of various constituents at El Verde, Puerto Rico, derived from averaged annual data of the National Atmospheric Deposition Program for 1983 to 2005.[mm, millimeter; $\mu\text{mol L}^{-1}$, micromoles per liter]

Year	Rainfall (mm)	H^+ ($\mu\text{mol L}^{-1}$)	Na^+ ($\mu\text{mol L}^{-1}$)	K^+ ($\mu\text{mol L}^{-1}$)	Mg^{2+} ($\mu\text{mol L}^{-1}$)	Ca^{2+} ($\mu\text{mol L}^{-1}$)	NH_4^+ ($\mu\text{mol L}^{-1}$)	Cl^- ($\mu\text{mol L}^{-1}$)	SO_4^{2-} ($\mu\text{mol L}^{-1}$)	NO_3^- ($\mu\text{mol L}^{-1}$)
1985	3,291	4.2	61.8	1.6	7.4	4.3	0.7	74.4	7.2	1.3
1986	3,345	8.2	53.8	1.5	6.2	3.7	0.6	66.8	7.2	1.9
1987	3,892	6.7	46.5	1.2	5.6	3.7	1.1	56.0	6.9	3.2
1988	3,833	5.3	57.7	1.4	6.7	4.0	0.7	68.2	7.6	2.0
1989 ¹	2,675	8.2	68.1	1.7	7.7	3.7	2.7	81.1	8.6	4.4
1991	1,178	6.9	67.5	1.8	8.1	5.3	1.1	81.2	8.5	4.8
1992	2,930	5.4	69.3	1.8	8.1	3.7	1.7	77.7	8.8	5.2
1993	2,888	7.6	61.9	2.6	7.3	3.0	2.1	73.9	7.6	4.9
1994	2,314	3.9	70.2	1.7	7.9	4.0	2.1	80.0	7.9	4.3
1995	2,624	4.2	74.6	1.7	8.0	3.8	2.9	83.4	8.4	5.2
1996	3,568	4.0	77.6	1.8	7.9	3.1	1.9	84.7	8.3	4.5
1997	2,734	11.6	55.7	1.8	6.1	3.8	1.2	68.8	8.3	4.2
1998	4,400	5.1	83.4	2.1	9.4	3.5	1.1	95.7	8.6	3.4
1999	3,153	2.0	67.2	1.6	7.0	3.8	1.7	70.7	7.7	4.8
2000	2,466	6.9	65.8	1.6	6.9	4.4	1.3	76.4	8.0	4.8
2001	2,825	9.2	67.3	1.7	6.8	4.0	1.9	79.0	8.4	5.3
2002	2,772	12.4	48.4	1.2	5.3	2.9	1.7	61.4	7.0	4.2
2003	3,266	13.6	55.4	1.4	6.1	3.5	2.3	68.6	9.0	5.0
2004	3,794	8.7	77.3	1.9	8.6	4.0	1.8	91.4	9.0	4.8
2005	3,155	9.4	99.9	2.4	11.5	4.0	2.3	113.5	12.4	6.0
2006	3,104	13.9	71.0	1.8	8.0	4.0	2.2	87.2	10.3	4.9

¹Samples were not collected between 12 September 1989 (the day that Hurricane Hugo hit) and 4 June 1991. Rainfall totals in 1989 and 1991 are reduced accordingly.

Table 3. Rainfall-weighted monthly loadings of various constituents at El Verde, Puerto Rico, derived from averaged monthly data of the National Atmospheric Deposition Program for 1983 to 2005.[mm, millimeter; mmol m^{-2} , millimoles per meter squared]

Month	Rainfall (mm)	H^+ (mmol m^{-2})	Na^+ (mmol m^{-2})	K^+ (mmol m^{-2})	Mg^{2+} (mmol m^{-2})	Ca^{2+} (mmol m^{-2})	NH_4^+ (mmol m^{-2})	Cl^- (mmol m^{-2})	SO_4^{2-} (mmol m^{-2})	NO_3^- (mmol m^{-2})
January	278	2.51	37.50	0.84	4.18	1.03	0.55	42.78	3.70	1.45
February	165	1.51	17.92	0.40	1.89	0.55	0.37	20.21	1.92	0.92
March	193	1.75	15.92	0.39	1.78	0.64	0.34	18.68	1.78	0.86
April	223	3.10	12.81	0.33	1.42	0.61	0.74	15.05	2.23	1.44
May	280	2.96	14.37	0.51	1.66	0.80	0.69	17.10	2.34	1.51
June	226	0.62	14.51	0.43	1.64	1.48	0.47	16.75	1.93	1.13
July	306	0.70	20.20	0.55	2.27	2.00	0.47	23.15	2.66	1.15
August	325	1.59	14.98	0.41	1.70	1.57	0.42	17.76	2.29	1.21
September	287	1.78	20.14	0.51	2.35	1.25	0.47	23.88	2.39	1.12
October	240	1.88	9.13	0.22	0.96	0.51	0.25	10.60	1.37	0.87
November	343	2.54	21.39	0.51	2.29	0.64	0.29	24.78	2.27	0.96
December	246	2.47	22.20	0.50	2.43	0.60	0.26	26.06	2.23	0.81
Total annual	3,113	23.4	221.1	5.6	24.6	11.7	5.3	256.8	27.1	13.4

Table 4. Rainfall-weighted annual loadings of various constituents at El Verde, Puerto Rico, derived from averaged annual data of the National Atmospheric Deposition Program for 1983 to 2005.[mm, millimeter; mmol m⁻², millimoles per meter squared]

Year	Rainfall (mm)	H ⁺ (mmol m ⁻²)	Na ⁺ (mmol m ⁻²)	K ⁺ (mmol m ⁻²)	Mg ²⁺ (mmol m ⁻²)	Ca ²⁺ (mmol m ⁻²)	NH ₄ ⁺ (mmol m ⁻²)	Cl ⁻ (mmol m ⁻²)	SO ₄ ²⁻ (mmol m ⁻²)	NO ₃ ⁻ (mmol m ⁻²)
1985	3,291	13.7	203.4	5.4	24.2	14.0	2.4	244.9	23.6	4.4
1986	3,345	27.5	179.8	5.0	20.8	12.4	1.9	223.4	24.1	6.2
1987	3,892	26.0	180.8	4.8	21.6	14.6	4.1	217.8	27.0	12.5
1988	3,833	20.4	221.1	5.3	25.7	15.4	2.8	261.5	29.0	7.6
1989 ¹	2,675	22.0	182.2	4.7	20.6	9.8	7.3	217.0	23.0	11.9
1991	1,178	8.1	79.5	2.1	9.5	6.2	1.3	95.6	10.0	5.7
1992	2,930	15.7	202.9	5.2	23.7	10.7	5.0	227.5	25.8	15.3
1993	2,888	22.0	178.8	7.4	21.1	8.6	5.9	213.4	21.8	14.2
1994	2,314	9.1	162.4	4.0	18.3	9.2	4.9	185.2	18.2	9.9
1995	2,624	11.1	195.8	4.5	20.9	10.0	7.6	218.7	22.1	13.8
1996	3,568	14.2	276.9	6.4	28.3	11.2	6.7	302.2	29.6	16.2
1997	2,734	31.8	152.3	5.0	16.6	10.4	3.2	188.2	22.7	11.4
1998	4,400	22.4	367.1	9.0	41.5	15.5	5.0	421.2	37.8	15.1
1999	3,153	6.4	211.8	5.0	21.9	12.0	5.2	222.8	24.2	15.3
2000	2,466	17.0	162.3	4.0	16.9	10.8	3.3	188.5	19.8	11.8
2001	2,825	26.0	190.1	4.8	19.3	11.2	5.5	223.1	23.7	14.9
2002	2,772	34.4	134.2	3.3	14.7	8.2	4.6	170.2	19.5	11.8
2003	3,266	44.6	181.0	4.6	19.9	11.6	7.4	224.2	29.3	16.2
2004	3,794	33.1	293.4	7.1	32.8	15.1	6.7	346.8	34.2	18.2
2005	3,155	29.8	315.2	7.5	36.2	12.7	7.2	358.1	39.1	19.0
2006	3,104	43.3	220.5	5.6	24.8	12.5	6.9	270.7	31.8	15.1

¹Samples were not collected between 12 September 1989 (the day that Hurricane Hugo hit) and 4 June 1991. Rainfall totals in 1989 and 1991 are reduced accordingly.

Grouping Data

Procedures presented by Stallard and Edmond (1981) and Stallard (2001) were used to quantify the different sources of ions in NADP samples: marine aerosols, temperate contamination, and desert dust. Each source has at least one characteristic marker ion. In marine aerosol, Cl⁻, Na⁺, and Mg²⁺ ions are sufficiently abundant to be marker ions; Cl⁻ is most abundant and was used here. In temperate contamination, NO₃⁻ is the most abundant ion. NH₄⁺ is also attributable to this source. In desert dust, Ca²⁺, after correction for seasalt, is the only marker. A possible fourth source, local vegetation, is considered by using K⁺ after a correction for seasalt.

Constituent groupings can be seen by using cross-correlation tables of constituent concentrations for the entire weekly data set (table 5) and for aggregated monthly mean concentrations (table 6). Rows and columns in these tables are ranked by correlation with Cl⁻. For the entire data set, Cl⁻ correlates well with Na⁺, Mg²⁺, and SO₄²⁻ ($r^2 > 0.5$, indicating that more than half of the variance between Cl⁻ and the other constituent is shared) (Bevington and Robinson, 2003). For monthly mean data, K⁺ joins this group with a strong correlation ($r^2 = 0.89$). The lack of such a strong correlation for weekly K⁺ likely reflects major, but temporally random, local inputs. The intercorrelation among NO₃⁻, NH₄⁺, and SO₄²⁻ is moderate ($r^2 > 0.25$, more than one quarter variance shared) to strong ($r^2 > 0.9$, most variance is shared) in the weekly data

($0.23 < r^2 < 0.49$) and the monthly mean data ($0.29 < r^2 < 0.92$). Finally, Ca²⁺ does not correlate strongly with any parameter in the weekly data but anticorrelates strongly with acidity ($r^2 = 0.67$; $r = -0.82$) in the monthly mean data set. The groupings are illustrated as monthly mean concentrations in figure 2 and table 1 and monthly loadings in figure 2 and table 3.

Missing Samples and Big Storms

A common practice, and one used by the NADP, is to fill gaps in a long time series of data by assuming that missing data resemble data that were collected. During the WEBB Project from 1991 to 2005, in the four study watersheds and one subwatershed described here, 507 hydrologic events were sampled from 263 storms using automated samplers (appendix 1). A total of 4,894 stream-water event samples were analyzed for conductivity, most for chloride, and many for a broad suite of other constituents. Several of the largest storms during which rivers were sampled (table 7) coincide with data gaps in the NADP record. Seven storms produced stream-water chloride concentrations that were substantially greater than typical values in 117 samples. Many of these 117 samples were analyzed for a full suite of constituents, and concentrations of nearly seasalt proportions were observed for all ions that are contained abundantly in seasalt (fig. 3). Heartsill-Scalley and others (2007) note that throughfall is

Table 5. Constituent correlations for all weekly concentration data (number of samples=818), ranked by correlation with Cl⁻, derived from weekly data of the National Atmospheric Deposition Program for 1983 to 2005.[All values are squared correlation coefficients, r²; (), r²<0; --, not relevant]

Constituent	Cl ⁻	Na ⁺	Mg ²⁺	SO ₄ ²⁻	K ⁺	Ca ²⁺	NO ₃ ⁻	NH ₄ ⁺	Acidity
Cl ⁻	1	--	--	--	--	--	--	--	--
Na ⁺	0.97	1	--	--	--	--	--	--	--
Mg ²⁺	0.96	0.97	1	--	--	--	--	--	--
SO ₄ ²⁻	0.51	0.47	0.50	1	--	--	--	--	--
K ⁺	0.32	0.28	0.32	0.20	1	--	--	--	--
Ca ²⁺	0.17	0.16	0.19	0.22	0.11	1	--	--	--
NO ₃ ⁻	0.07	0.07	0.07	0.45	0.05	0.07	1	--	--
NH ₄ ⁺	0.02	0.02	0.02	0.23	0.02	0.01	0.49	1	--
Acidity	0.02	0.01	0.01	0.29	0.00	(0.04)	0.23	0.10	1

Table 6. Constituent correlations for aggregated monthly averaged concentration data (number of samples=12), ranked by correlation with Cl⁻, derived from averaged monthly data of the National Atmospheric Deposition Program for 1983 to 2005.[All values are squared correlation coefficients, r²; (), r²<0; --, not relevant]

Constituent	Cl ⁻	Na ⁺	Mg ²⁺	K ⁺	SO ₄ ²⁻	NO ₃ ⁻	NH ₄ ⁺	Acidity	Ca ²⁺
Cl ⁻	1	--	--	--	--	--	--	--	--
Na ⁺	1.00	1	--	--	--	--	--	--	--
Mg ²⁺	1.00	0.99	1	--	--	--	--	--	--
K ⁺	0.89	0.89	0.92	1	--	--	--	--	--
SO ₄ ²⁻	0.78	0.79	0.80	0.83	1	--	--	--	--
NO ₃ ⁻	0.06	0.06	0.07	0.15	0.41	1	--	--	--
NH ₄ ⁺	0.01	0.01	0.02	0.07	0.29	0.93	1	--	--
Acidity	0.04	0.04	0.03	0.01	0.10	0.19	0.19	1	--
Ca ²⁺	(0.00)	(0.00)	0.00	0.02	0.00	0.01	0.01	(0.68)	1

only slightly enriched in Cl⁻ and other seasalt ions. Because throughfall was collected continuously from 1988 to 2002, it cannot be the source. Similarly, soils and bedrock do not retain substantial Cl⁻ (Stallard, 2012) and base flow is strongly enriched in alkaline ions and calcium, which are both low in concentration in the event samples (Stallard and Murphy, 2012). Groundwater cannot be a source of the high-chloride event samples. The only reasonable source of elevated Cl⁻ and other seasalt ions in these storms is seasalt carried inland by wind and rain. The traditional approach of assuming that missing samples resemble successfully collected samples is therefore invalid for this NADP data set, because several of the data gaps that corresponded to storms were among the nine that had exceptionally high Cl⁻ concentrations. One of these gaps occurred during Hurricane Georges, the largest event during this 15-year study. The second-largest storm, Hurricane Hortense, lacked both a data gap and high chloride.

By assuming that Cl⁻ in the stream water sampled during the storm was derived from the storm, one can integrate water and chloride discharge through the storm hydrograph to calculate total rainfall and the Cl⁻ concentration and loading of that rain. Two contrasting hurricanes, Hortense (September 9–10, 1996) and Georges (September 21, 1998),

had comparable rainfall but show markedly contrasting Cl⁻ behavior (fig. 4). Georges (category 2 on the Saffir-Simpson Hurricane Wind Scale (National Oceanic and Atmospheric Administration, 2010b), winds of 154–177 kilometers per hour (km h⁻¹)) was a shorter and more intense hurricane than Hortense (category 1, winds of 119–153 km h⁻¹ hitting the west of Puerto Rico) (Murphy and others, 2012). Hortense, which was sampled by NADP, was a typical low-Cl⁻ storm, whereas Georges, which was not sampled by NADP, was a high Cl⁻ event. In the Mameyes watershed, the WEBB watershed closest to El Verde, Hurricane Hortense produced 333 mm total runoff with an average stream-water Cl⁻ concentration of 111 micromoles per liter ($\mu\text{mol L}^{-1}$) and a maximum Cl⁻ concentration of 253 $\mu\text{mol L}^{-1}$ in the first few hours of the storm. In contrast, Hurricane Georges produced 317 mm total runoff with an average stream-water Cl⁻ concentration of 455 $\mu\text{mol L}^{-1}$ and a maximum Cl⁻ concentration of 1,567 $\mu\text{mol L}^{-1}$ in the first few hours of the storm. Most of the samples from Hurricane Georges were analyzed for all major constituents. The constituents in these samples are in nearly seasalt proportions, dominated by Na⁺ and Cl⁻, whereas the first base-flow sample collected after the storm is dominated by alkalinity and Ca²⁺ (fig. 3).

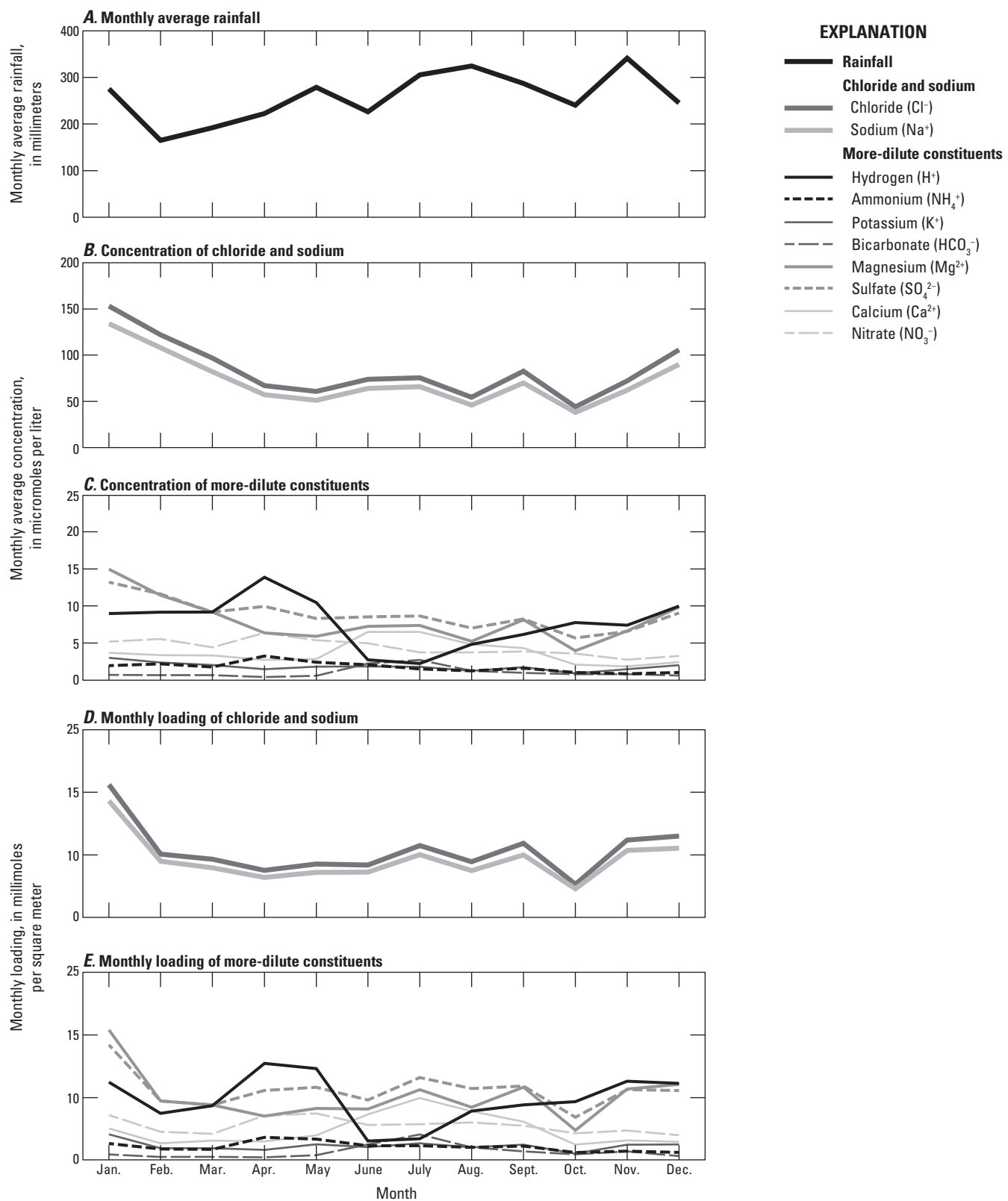


Figure 2. Aggregated monthly rainfall, monthly mean concentrations, and monthly mean loading for chemical constituents in rain sampled at the El Verde National Atmospheric Deposition Program site, eastern Puerto Rico. Light gray lines, constituents with dominantly seawater sources; dark grey lines, constituents strongly influenced by desert-dust inputs; black lines, constituents dominantly influenced by temperate-contamination sources.

Table 7. Storms that substantially affected the Water, Energy, and Biogeochemical Budgets program rivers during the period of study, 1991–2005.

[NADP, National Atmospheric Deposition Program; Can, Canóvanas; Cay, Cayaguás; Gua, Guabá; Ica, Icacos; Mam, Mameyes; n/c, normal chloride; n/g, no gap; n/s, not studied]

Date	Storm ¹	Rivers affected by the storm	Rivers with high-chloride events ²	NADP gaps
1991–11–10	Event	Ica, Mam	n/s	Gap
1992–05–02	Event	Mam	n/c	n/g
1992–07–17	Event	Gua	n/s	n/g
1993–05–01	Event	Gua	n/c	n/g
1994–02–19	Event	Gua, Ica	n/c	n/g
1994–06–03	Minor event	Can	Can	n/g
1995–02–26	Event	Ica	n/c	n/g
1995–09–06	Hurricane Luis	Can	Can	Gap
1996–01–14	Event	Gua, Ica	n/c	n/g
1996–07–09	Hurricane Bertha	Can, Gua, Ica, Mam	Can, Gua, Ica, Mam	Gap
1996–09–10	Hurricane Hortense	Can, Cay, Gua, Ica, Mam	n/c	n/g
1997–09–25	Event	Mam	n/c	n/g
1997–10–14	Event	Gua, Ica, Cay	n/c	n/g
1998–08–25	Event	Cay	n/c	n/g
1998–09–22	Hurricane Georges	Can, Cay, Gua, Ica, Mam	Cay, Gua, Ica, Mam	Gap
1998–10–14	Event	Gua, Ica	Gua, Ica	n/g
1998–10–22	Event	Gua, Cay	Can	n/g
1998–12–02	Event	Gua, Ica	n/c	Gap
1999–11–17	Hurricane Lenny	Gua, Ica	Can	Gap
1999–12–05	Event	Gua, Ica, Mam	n/c	n/g
2000–08–22	Hurricane Debby	Gua	Can	n/g
2001–08–23	Tropical Storm Dean	Cay, Gua, Ica	n/c	n/g
2001–11–08	Cold front	Cay, Gua, Ica, Mam	n/c	n/g
2001–12–23	Event	Gua, Ica, Mam	Can	n/g
2002–05–30	Event	Gua, Ica	n/c	n/g
2003–04–18	Upper-level trough	Gua, Ica, Mam	n/c	n/g
2003–11–13	Tropical wave	Can, Cay, Gua, Ica, Mam	n/c	n/g
2004–09–16	Tropical Storm Jeanne	Can, Cay, Gua, Ica, Mam	n/s	Gap
2004–11–13	Upper-level trough	Gua, Ica, Mam	n/c	n/g
2005–10–03	Event	Cay	n/s	n/g
2005–10–11	Upper-level low	Cay, Gua, Ica	n/s	Gap
2005–10–23	Event	Cay	n/s	n/g

¹Storms that, on the basis of runoff, could have generated landslides in at least one watershed (appendix 1, this volume), except for a minor event on the Rio Canóvanas, which was the only high-chloride event sampled that did not also have substantial runoff.

²As identified in U.S. Geological Survey Water, Energy, and Biogeochemical Budgets program data (appendix 1, this volume).

The source of the seasalt is probably wind-generated spray. In a hurricane, mechanical energy, generated by extracting heat from the ocean, is balanced by frictional dissipation of wind energy, mostly at the sea-air interface (Emanuel, 1991). The Beaufort Scale, developed in 1805, represents a well-established description of sea-surface conditions for a wide range of wind speeds (National Oceanic and Atmospheric Administration, 2010a). For violent storms (winds of 56 to 63 knots or 104 to 117 km h⁻¹), the sea surface is described as “completely covered with long white patches of foam lying along the direction of the wind. Everywhere the edges of the wave crests are blown into froth. Visibility affected.” For hurricane-force winds (at least 64 knots or 117 km h⁻¹) “the

air is filled with foam and spray. Sea completely white with driving spray; visibility very seriously affected.” Some of this airborne spray and foam must be incorporated into the storm. The amount of Cl⁻ deposited by Hurricane Georges over the entire Mameyes Basin is equivalent to 0.3 mm of seawater.

A primary reason that this phenomenon has not been described before is the unique approach used in this research that focused on event sampling (appendix 1). In this study, 332 samples that were collected at runoff rates of greater than 20 millimeters per hour (mm h⁻¹) were later analyzed for suspended sediment and a comprehensive suite of solutes. Globally, no streams have been sampled for later chemical analysis during hurricanes at runoff rates of

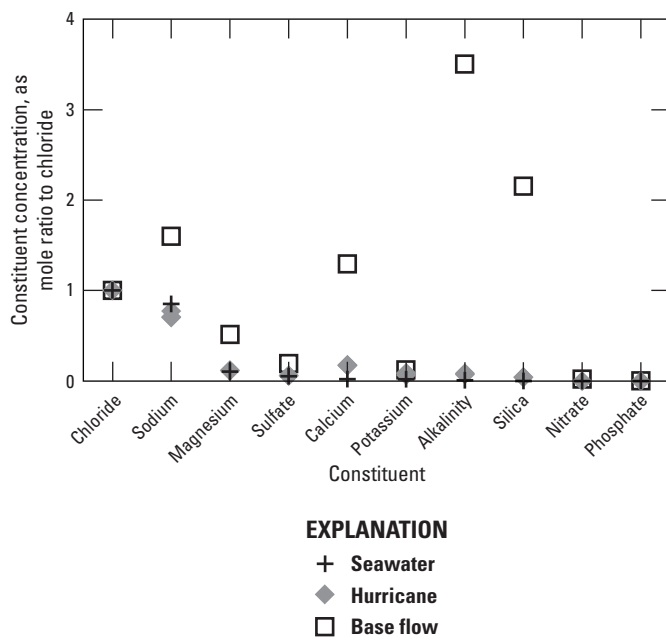


Figure 3. The three samples with the highest chloride concentrations measured for the Río Mameyes, eastern Puerto Rico, during Hurricanes Georges compared with seawater and the first base-flow sample following the hurricane, collected October 7, 1998. Chemical constituent concentrations are normalized to total chloride and are ordered by decreasing seawater concentration. The stormwater constituent proportions are close to those in seawater and are only slightly elevated in calcium, the cation most abundant in base flow.

greater than 20 mm h⁻¹; two samples were collected at about 16 mm h⁻¹ by the U.S. Geological Survey in Puerto Rico in 1970 during a tropical depression (Haire, 1972). Goldsmith and others (2008) collected samples during a Typhoon Mindulle at runoff rates of as much as 7.3 mm h⁻¹, and Hicks and others collected samples during Cyclone Bola at runoff rates of as much as 4.8 mm h⁻¹.

To show the consequences of missing samples, the NADP monthly digests (fig. 5) were adjusted to include Hurricane Georges in the monthly NADP record (fig. 6). The NADP monthly data set constructs September 1998 by using only the first 2 weeks of that month. NADP also reports a total of 467 mm rain for this month; 353 mm was measured in the first 2 weeks. The National Oceanic and Atmospheric Administration rain gage at El Verde reported 730 mm for the same month (National Oceanic and Atmospheric Administration, 2008). It is not obvious why the NADP total is missing 263 mm. The difference between National Oceanic and Atmospheric Administration monthly and NADP 2-week totals is 377 mm. This 377 mm was assigned a Cl⁻ concentration of 455 μmol L⁻¹, the average concentration of Cl⁻ in the

Mameyes River during Georges, along with other common seasalt constituents (Na⁺, K⁺, Ca²⁺, Mg²⁺, SO₄²⁻) in seasalt ratios relative to Cl⁻. A revised monthly average for September 1998 was then reconstructed for the NADP data set (fig. 6).

The reconstructed NADP Cl⁻ time series (fig. 6) demonstrates a prominent spike in September 1998. The only other comparable large spike recorded by the NADP occurred in January 2005. The January 2005 spike appears to record a series of smaller storms associated with cold fronts. Stream water was not sampled by the WEBB Project during these storms. This examination of Hurricanes Hortense and Georges demonstrates that the NADP may undersample Cl⁻ and other seasalt-related ions. This undersampling would be hard to reconstruct. Not only are there other high-Cl⁻ events that were not sampled by NADP (table 7), but two big storms were not sampled by either NADP or WEBB Project, and several storms missed by NADP had high Cl⁻ in some WEBB watersheds and not others (table 7). In the remaining discussion, the above correction for Hurricane Georges, which is the largest, is retained.

Estimating Source Strengths

Partitioning constituents among marine, temperate-contamination, and desert sources requires several steps. First, the marine component of all relevant constituents is calculated. NO₃⁻ and NH₄⁺ are assumed to have zero marine contributions because of their low concentration in surface sea water. Second, nonmarine Ca²⁺ is equated with the desert-dust contribution. Finally, all NO₃⁻ and NH₄⁺ were assumed to come from the temperate (contamination) source, because of the lack of plausible contributions from any other source.

All chloride is initially assumed to be derived from seasalt, and the chloride concentration is used to predict the marine contribution to all other ions. The seasalt contribution was then subtracted from all ions, and seasalt-corrected concentrations were obtained. Following Stallard and Edmond (1981), the concentrations that result from this calculation are designated with a superscript (*): for example, Ca^{*}=Ca²⁺-Cl⁻•(seasalt Ca:Cl). Normally, predicted measured sodium exceeded seasalt sodium, but when the reverse was true (which seldom happens and is most likely due to statistical noise or analytical error), sodium was used to calculate the seasalt contribution and a nonseasalt chloride component was calculated, to avoid negative concentrations. Elevated concentrations of nonseasalt Cl^{*} could indicate volcanic input, as is seen in the rain of La Selva, Costa Rica (Eklund and others, 1997), or long-distance transport and photochemical processing (Stallard and Edmond, 1981). The only recent eruption near Puerto Rico was Soufrière Hills Volcano from 1996 to 1997 (Heartsill-Scalley and others, 2007), and no Cl^{*} anomalies are noted during those times. For the NADP data set, magnesium concentrations seem slightly low and are consistently present in less-than-seasalt proportions, an unlikely situation. When a calculated Mg concentration (Mg^{*}) is negative, again probably from analytical error, it is set to zero.

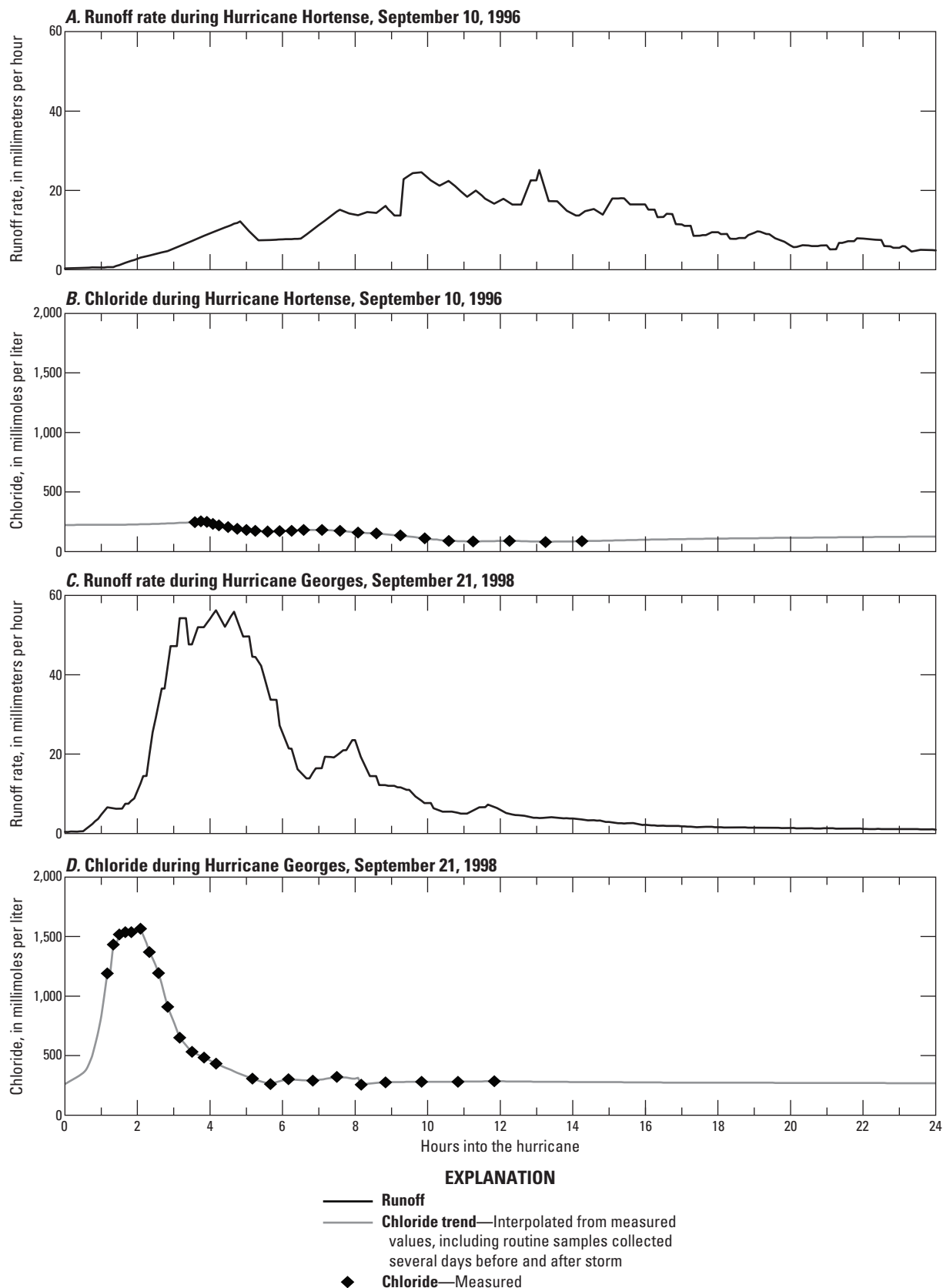


Figure 4. Time series of runoff rate and chloride concentrations measured for the Río Mameyes during Hurricanes Hortense and Georges. (Stallard and Murphy, 2012).

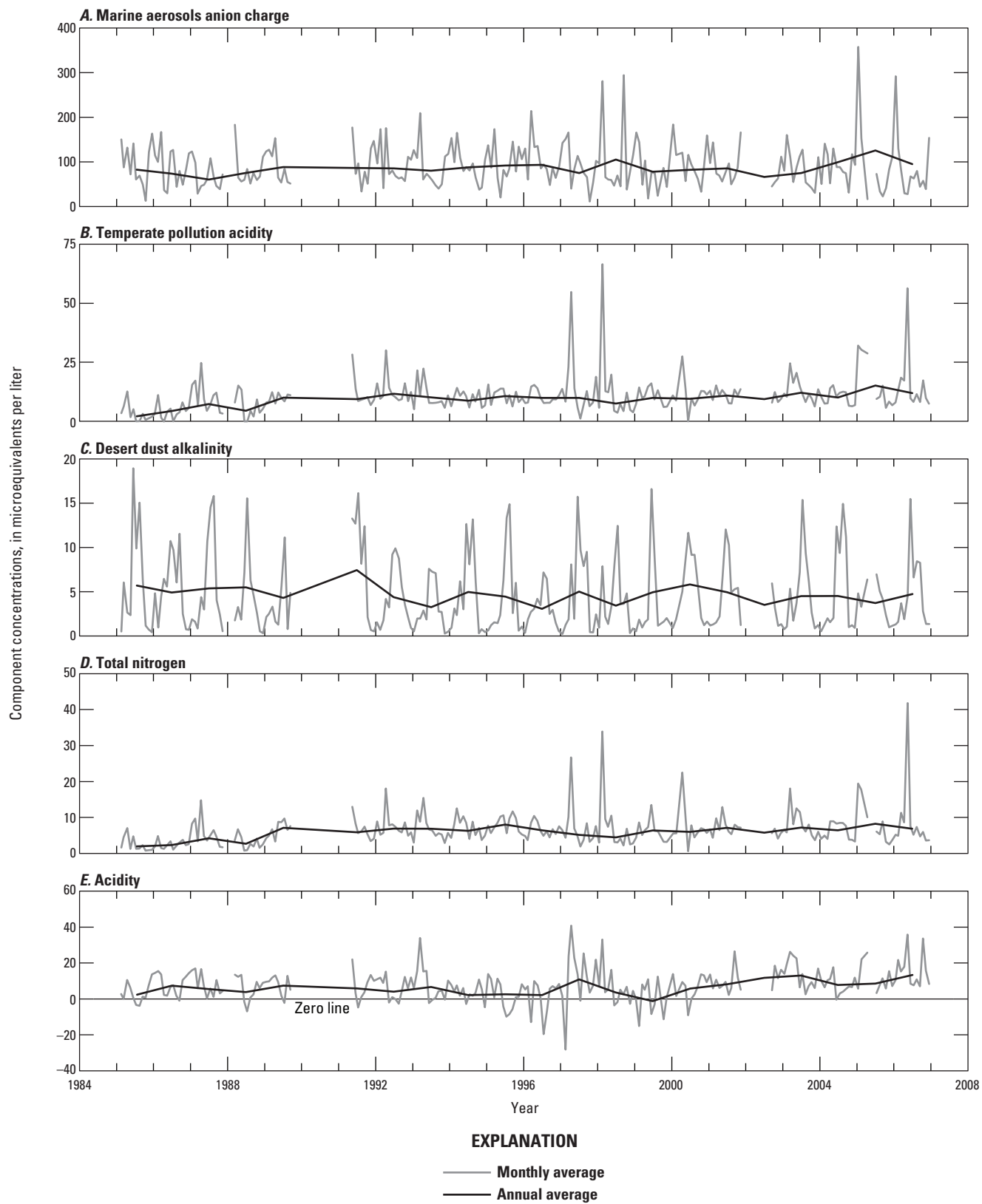


Figure 5. Time series of concentration estimates for the three primary components that contribute to rain chemistry in El Verde, Puerto Rico: *A*, marine aerosols, *B*, temperate contamination, and *C*, desert dust. *D*, total inorganic nitrogen; *E*, acidity. Negative acidity values indicate alkaline rain.

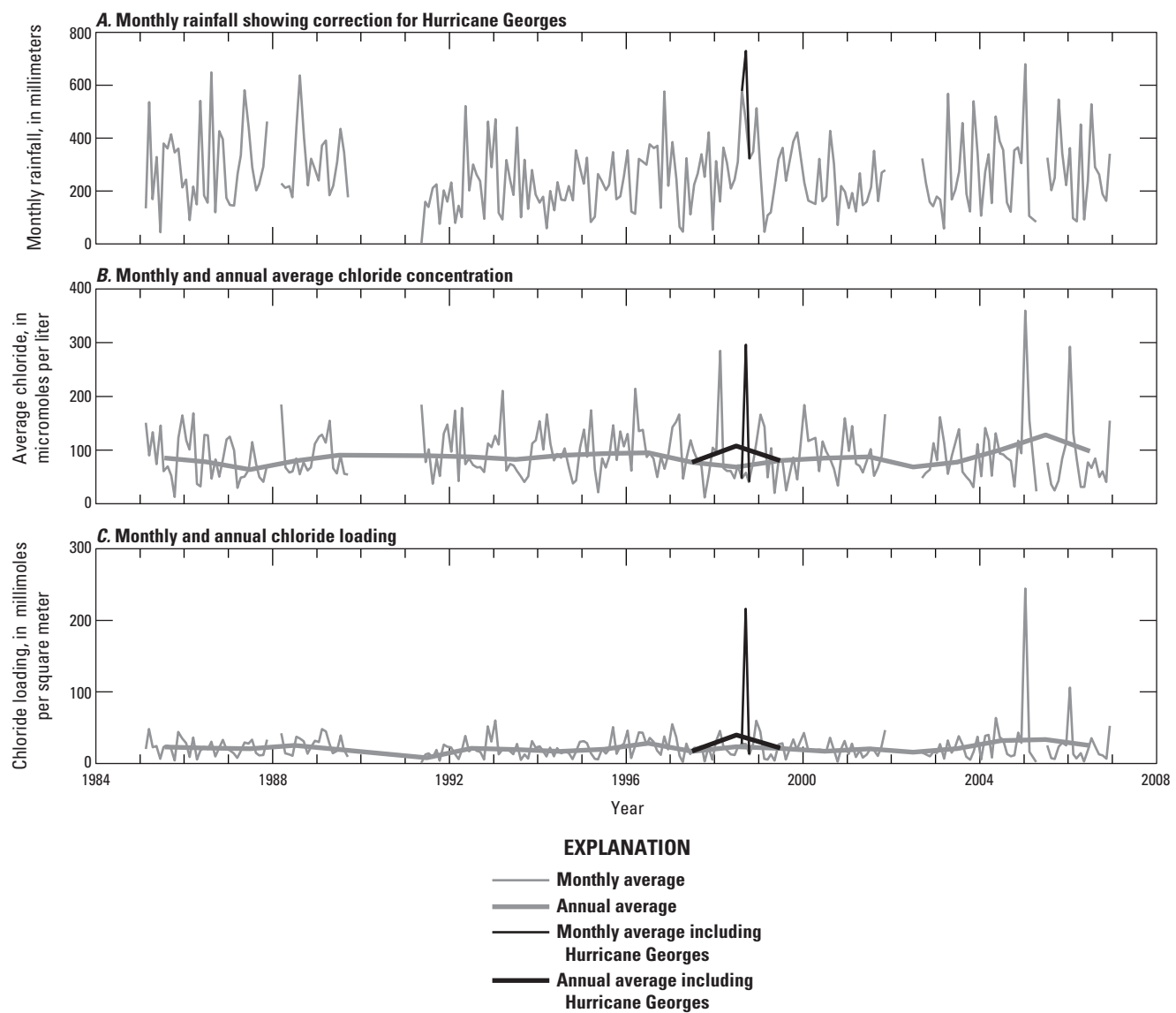


Figure 6. A, Monthly and annual time series of rainfall; B, chloride concentration; and C, chloride loading from the National Atmospheric Deposition Program data set for El Verde, Puerto Rico, showing effects of including data from Hurricane Georges. (Because of sample loss, rainfall amounts and rainfall chemistry were missing from the El Verde dataset for Hurricane Georges. Runoff rates and chemical samples for the Río Mameyes were used to estimate the missing data, as indicated in this graph.)

Geochemically, sulfate ion is associated with seasalt, marine-gas, temperate-contamination, and desert sources. The strong intercorrelations of SO_4^{2-} with both the seasalt (Na^+ , K^+ , Mg^{2+} , Cl^-) and temperate-contamination (NH_4^+ , NO_3^-) groups in tables 5 and 6 support this association. Accordingly, distinguishing among the sources of SO_4^{2-} requires several steps. The marine source for SO_4^{2-} can be separated into seasalt sulfate ($\text{SO}_4^{2-}_{\text{seasalt}}$), for which a seasalt $\text{SO}_4^{2-}:\text{Cl}^-$ ratio can be assumed, and gas emissions ($\text{SO}_4^{2-}_{\text{marine gas}}$). The SO_4^{2-} signatures of the four sources were determined for the weekly data using multiple linear regressions (Bevington and Robinson, 2003). Three

properties were used as dependent variables: seasalt chloride ($\text{Cl}_{\text{seasalt}}$), nitrate (NO_3^-), and Ca^* . In addition, the use of an additive constant, equivalent to assuming a “global” background SO_4^{2-} source, was tested. Most of the variance in SO_4^{2-} is accounted for by $\text{Cl}_{\text{seasalt}}$ and NO_3^- , without an additive constant. Three additional regressions were compared to evaluate whether desert or background sources of SO_4^{2-} might be important. Inclusion of the desert component, Ca^* , was significant at the 76-percent level (f-test comparing a regression using $\text{Cl}_{\text{seasalt}}$ and NO_3^- , with one using $\text{Cl}_{\text{seasalt}}$, NO_3^- , and Ca^*). The inclusion of a background constant was not significant. Thus, the best model is

$$\text{SO}_4^{2-} = 0.060 \cdot \text{Cl}_{\text{seasalt}} + 0.742 \cdot \text{NO}_3^- + 0.229 \cdot \text{Ca}^* \\ (r^2=0.778; n=818). \quad (5)$$

Rather than predicting SO_4^{2-} from each source using each term in equation 5, $\text{SO}_4^{2-}_{\text{seasalt}}$ was assumed to always be present and SO_4^* was calculated as

$$\text{SO}_4^{2-}_{\text{seasalt}} = 0.052 \cdot \text{Cl}_{\text{seasalt}} \quad (6)$$

$$\text{SO}_4^* = \text{SO}_4^{2-} - \text{SO}_4^{2-}_{\text{seasalt}} = 0.008 \cdot \text{Cl}_{\text{seasalt}} + 0.742 \cdot \text{NO}_3^- + 0.229 \cdot \text{Ca}^*. \quad (7)$$

Then SO_4^* was partitioned among the three sources according the proportions below:

$$\text{SO}_4^{2-}_{\text{marine gas}} : \text{SO}_4^{2-}_{\text{temperate contamination}} : \text{SO}_4^{2-}_{\text{desert dust}} = (0.008 \cdot \text{Cl}_{\text{seasalt}}) : (0.742 \cdot \text{NO}_3^-) : (0.229 \cdot \text{Ca}^*). \quad (8)$$

The WEBB Project also collected precipitation between 1991 and 1995 (36 samples from a wet-dry collector in the Bisley area, 42 samples from a wet-dry collector near the Iacosc gage, and 29 samples from a continuous collector in the central Iacosc watershed). When WEBB precipitation samples are added to the regression, the best model was

$$\text{SO}_4^{2-} = 0.062 \cdot \text{Cl}_{\text{seasalt}} + 0.677 \cdot \text{NO}_3^- + 0.247 \cdot \text{Ca}^* \\ (r^2=0.766; n=925). \quad (9)$$

In this regression, somewhat more of the SO_4^{2-} is attributed to a marine gas source, and somewhat less to contamination.

For the entire El Verde NADP record, weekly concentrations of marine, temperate-pollution, and desert-dust components were calculated, as were volume-weighted monthly and annual averages of all rain samples (tables 8–13). Acidity was used to calculate H^+ and HCO_3^- , by using equations 2–4, and pH was calculated from H^+ . Because alkaline desert dust reacts with acid components, thereby neutralizing some H^+ ,

Table 8. Averaged monthly rain chemistry from the National Atmospheric Deposition Program site at El Verde, Puerto Rico, with contributions of various sources.

[$\mu\text{mol L}^{-1}$, micromoles per liter; $\mu\text{eq L}^{-1}$, microequivalents per liter; --, not applicable]

Component	H^* ($\mu\text{mol L}^{-1}$)	Na^+ ($\mu\text{mol L}^{-1}$)	K^+ ($\mu\text{mol L}^{-1}$)	Mg^{2+} ($\mu\text{mol L}^{-1}$)	Ca^{2+} ($\mu\text{mol L}^{-1}$)	NH_4^+ ($\mu\text{mol L}^{-1}$)	Acidity ($\mu\text{eq L}^{-1}$)	Cl^- ($\mu\text{eq L}^{-1}$)	SO_4^{2-} ($\mu\text{mol L}^{-1}$)	NO_3^- ($\mu\text{mol L}^{-1}$)
Average	7.3	71.0	1.8	7.9	3.8	1.7	6.4	82.5	8.7	4.3
Marine										
Seasalt	2.3	68.7	1.4	8.2	1.5	0	-0.5	80.6	4.2	0
Sulfur (sea) gases	3.4	0	0	0	0	0	1.5	0	0.8	0
Temperate	9.7	0	0	0	0	1.7	9.0	0	3.2	4.3
Desert	1.4	0	0	0	2.2	0	-3.3	0	0.6	0
Residual ¹	--	2.3	0.4	-0.3	0.0	0	-0.3	1.9	0	0

¹All constituents not accounted for by other components; H^+ is not included because it is not a conservative constituent.

Table 9. Derived properties from monthly data of the National Atmospheric Deposition Program site at El Verde, Puerto Rico, with contributions of various sources.

[H^+ is reactive and is calculated separately for each source, the average, and the residual. Tz^\pm , total ionic charge; $\mu\text{eq L}^{-1}$, microequivalents per liter; $\mu\text{eq L}^{-1} \text{ yr}^{-1}$, microequivalents per liter per year; -- not applicable]

Component	pH	Tz^\pm ($\mu\text{eq L}^{-1}$)	Percent	Slope ¹ ($\mu\text{eq L}^{-1} \text{ yr}^{-1}$)	Slope, 95 percent error	Probability of trend ² (percent)
Average	5.1	105.1	90	1.22	0.95	76
Marine	5.6	95.2	83	0.94	0.92	68
Seasalt	5.6	91.8	79	--	--	--
Sulfur (sea) gases	5.5	3.4	3	--	--	--
Temperate	5.0	11.4	10	0.33	0.14	97
Desert	5.9	5.8	5	-0.05	0.07	60
Residual ³	5.6	4.5	4	-0.00	--	50

¹Slope of the regression concentration=slope \times year+intercept.

²Probability that the regression slope is non-zero.

³All ionic charge not accounted for by other components.

Table 10. Rainfall-weighted monthly average concentration of total ionic charge and acidity at El Verde, Puerto Rico, derived from averaged monthly data of the National Atmospheric Deposition Program for 1983 to 2005.[mm, millimeter; $\mu\text{eq L}^{-1}$, microequivalents per liter; Tz^\pm , total ionic charge]

Month	Rainfall (mm)	Acidity ($\mu\text{eq L}^{-1}$)			Tz^\pm ($\mu\text{eq L}^{-1}$)				
		Total	Marine	Temperate	Desert	Total	Marine	Temperate	Desert
January	278	8.3	1.3	8.3	-1.3	186.3	172.0	12.6	1.7
February	165	8.5	1.0	9.1	-1.6	154.4	136.4	13.3	2.1
March	193	8.4	0.9	9.9	-2.3	121.4	108.0	10.0	3.0
April	223	13.4	0.7	14.8	-2.1	94.5	75.0	16.5	3.0
May	280	9.9	0.6	11.8	-2.5	84.2	67.9	12.9	3.5
June	226	0.4	0.6	7.9	-8.0	99.3	79.6	9.1	10.3
July	306	-0.5	0.8	6.1	-7.5	101.1	82.7	6.9	10.3
August	325	3.6	0.6	8.8	-5.7	74.8	59.4	7.5	7.7
September	287	5.2	0.8	8.7	-4.3	105.3	91.7	8.0	5.6
October	240	7.0	0.4	8.5	-1.9	60.9	49.0	8.4	2.6
November	343	6.5	0.8	6.5	-0.8	89.5	81.5	6.8	1.0
December	246	9.4	1.1	9.0	-0.7	128.2	118.8	8.2	0.9
Annual	3,113	6.4	0.8	8.9	-3.3	106.1	91.5	9.7	4.4

Table 11. Rainfall-weighted average annual concentration of total ionic charge and acidity at El Verde, Puerto Rico, derived from averaged annual data of the National Atmospheric Deposition Program for 1983 to 2005.[mm, millimeter; $\mu\text{eq L}^{-1}$, microequivalents per liter; Tz^\pm , total ionic charge]

Year	Rainfall (mm)	Acidity ($\mu\text{eq L}^{-1}$)			Tz^\pm ($\mu\text{eq L}^{-1}$)				
		Total	Marine	Temperate	Desert	Total	Marine	Temperate	Desert
1985	3,291	2.6	1.2	5.2	-3.8	91.6	83.6	2.3	5.7
1986	3,345	7.4	1.1	9.5	-3.2	83.9	74.6	4.3	4.9
1987	3,892	5.7	0.6	9.0	-3.9	74.0	61.3	7.4	5.4
1988	3,833	4.1	1.1	6.5	-3.6	86.5	76.5	4.6	5.5
1989 ¹	2,675	7.5	0.7	10.1	-3.4	103.5	89.2	10.0	4.3
1991	1,178	5.9	0.5	11.5	-6.0	103.9	87.0	9.5	7.5
1992	2,930	4.2	0.6	7.0	-3.5	101.7	85.6	11.7	4.4
1993	2,888	6.8	0.4	9.0	-2.7	94.8	81.3	10.2	3.3
1994	2,314	2.3	0.5	5.8	-4.0	101.7	88.0	8.7	5.0
1995	2,624	2.7	0.5	5.9	-3.6	107.0	91.8	10.7	4.5
1996	3,568	2.4	0.6	4.3	-2.5	107.4	94.4	9.9	3.1
1997	2,734	11.1	0.7	14.1	-3.8	90.1	75.3	9.8	5.1
1998	4,400	3.8	0.8	5.7	-2.7	117.6	106.5	7.7	3.5
1999	3,153	-1.1	0.4	2.5	-4.0	94.0	79.0	10.0	5.0
2000	2,466	6.0	0.5	10.3	-4.8	98.2	82.7	9.6	5.9
2001	2,825	8.5	0.5	12.0	-4.0	101.7	85.8	10.9	5.0
2002	2,772	11.9	0.5	14.2	-2.8	80.2	67.1	9.4	3.6
2003	3,266	13.2	0.7	15.8	-3.3	92.0	75.3	12.2	4.5
2004	3,794	8.0	0.6	11.0	-3.6	115.0	100.2	10.2	4.6
2005	3,155	8.8	1.2	10.4	-2.8	145.0	126.1	15.1	3.8
2006	3,104	13.5	1.0	16.0	-3.5	113.0	96.1	12.1	4.8

¹Samples were not collected between 12 September 1989 (the day that Hurricane Hugo hit) and 4 June 1991. Rainfall totals in 1989 and 1991 are reduced accordingly.

Table 12. Rainfall-weighted monthly loadings of total ionic charge and acidity at El Verde, Puerto Rico, derived from averaged monthly data of the National Atmospheric Deposition Program for 1983 to 2005.[mm, millimeter; meq m⁻², milliequivalents per meter squared; Tz[±], total ionic charge]

Month	Rainfall (mm)	Acidity (meq m ⁻²)			Tz [±] (meq m ⁻²)				
		Total	Marine	Temperate	Desert	Total	Marine	Temperate	Desert
January	278	2.31	0.36	2.30	-0.35	51.87	47.89	3.51	0.47
February	165	1.40	0.17	1.50	-0.27	25.48	22.52	2.20	0.35
March	193	1.62	0.17	1.90	-0.45	23.37	20.79	1.93	0.57
April	223	3.00	0.17	3.30	-0.46	21.09	16.74	3.68	0.66
May	280	2.79	0.18	3.31	-0.71	23.57	19.00	3.60	0.97
June	226	0.10	0.14	1.78	-1.82	22.48	18.03	2.06	2.32
July	306	-0.16	0.26	1.88	-2.29	30.88	25.27	2.10	3.14
August	325	1.17	0.18	2.85	-1.86	24.27	19.29	2.45	2.48
September	287	1.48	0.22	2.49	-1.22	30.21	26.32	2.29	1.60
October	240	1.69	0.10	2.04	-0.46	14.65	11.77	2.02	0.61
November	343	2.25	0.27	2.24	-0.26	30.68	27.94	2.32	0.35
December	246	2.31	0.28	2.21	-0.17	31.58	29.27	2.01	0.23
Annual	3,113	19.9	2.5	27.8	-10.3	330.1	284.8	30.2	13.8

Table 13. Rainfall-weighted average loadings of total ionic charge and acidity at El Verde, Puerto Rico, derived from averaged annual data of the National Atmospheric Deposition Program for 1983 to 2005.[mm, millimeter; meq m⁻², milliequivalents per meter squared; Tz[±], total ionic charge]

Year	Rainfall (mm)	Acidity (meq m ⁻²)			Tz [±] (meq m ⁻²)				
		Total	Marine	Temperate	Desert	Total	Marine	Temperate	Desert
1985	3,291	8.7	3.9	17.2	-12.5	301.4	275.0	7.5	18.9
1986	3,345	24.9	3.7	31.9	-10.7	280.5	249.5	14.5	16.5
1987	3,892	22.3	2.4	35.2	-15.3	288.0	238.4	28.6	21.0
1988	3,833	15.8	4.4	25.1	-13.7	331.7	293.1	17.5	21.1
1989 ¹	2,675	19.9	1.8	27.1	-9.0	276.9	238.6	26.7	11.6
1991	1,178	7.0	0.6	13.5	-7.1	122.4	102.5	11.1	8.8
1992	2,930	12.3	1.8	20.6	-10.1	297.9	250.7	34.2	13.0
1993	2,888	19.6	1.2	26.1	-7.7	273.7	234.7	29.5	9.4
1994	2,314	5.3	1.2	13.4	-9.3	235.3	203.6	20.2	11.5
1995	2,624	7.2	1.2	15.4	-9.5	280.7	240.8	28.2	11.7
1996	3,568	8.5	2.1	15.3	-8.8	383.3	336.8	35.4	11.1
1997	2,734	30.3	2.0	38.6	-10.3	246.4	205.7	26.9	13.8
1998	4,400	16.9	3.5	25.2	-11.8	517.5	468.5	33.7	15.3
1999	3,153	-3.4	1.4	7.9	-12.7	296.4	249.1	31.5	15.7
2000	2,466	14.7	1.2	25.3	-11.8	242.1	203.8	23.7	14.6
2001	2,825	24.0	1.4	34.0	-11.4	287.3	242.4	30.9	14.0
2002	2,772	33.0	1.3	39.5	-7.8	222.3	186.1	26.2	9.9
2003	3,266	43.1	2.4	51.5	-10.9	300.5	245.9	39.8	14.7
2004	3,794	30.3	2.4	41.7	-13.8	436.2	380.1	38.7	17.4
2005	3,155	27.6	3.7	32.8	-8.9	457.4	397.9	47.6	11.9
2006	3,104	41.9	3.1	49.6	-10.9	350.8	298.3	37.6	14.9

¹Samples were not collected from 12 September 1989, the week that Hurricane Hugo hit, until 4 June 1991. Rainfall totals in 1989 and 1991 are reduced accordingly.

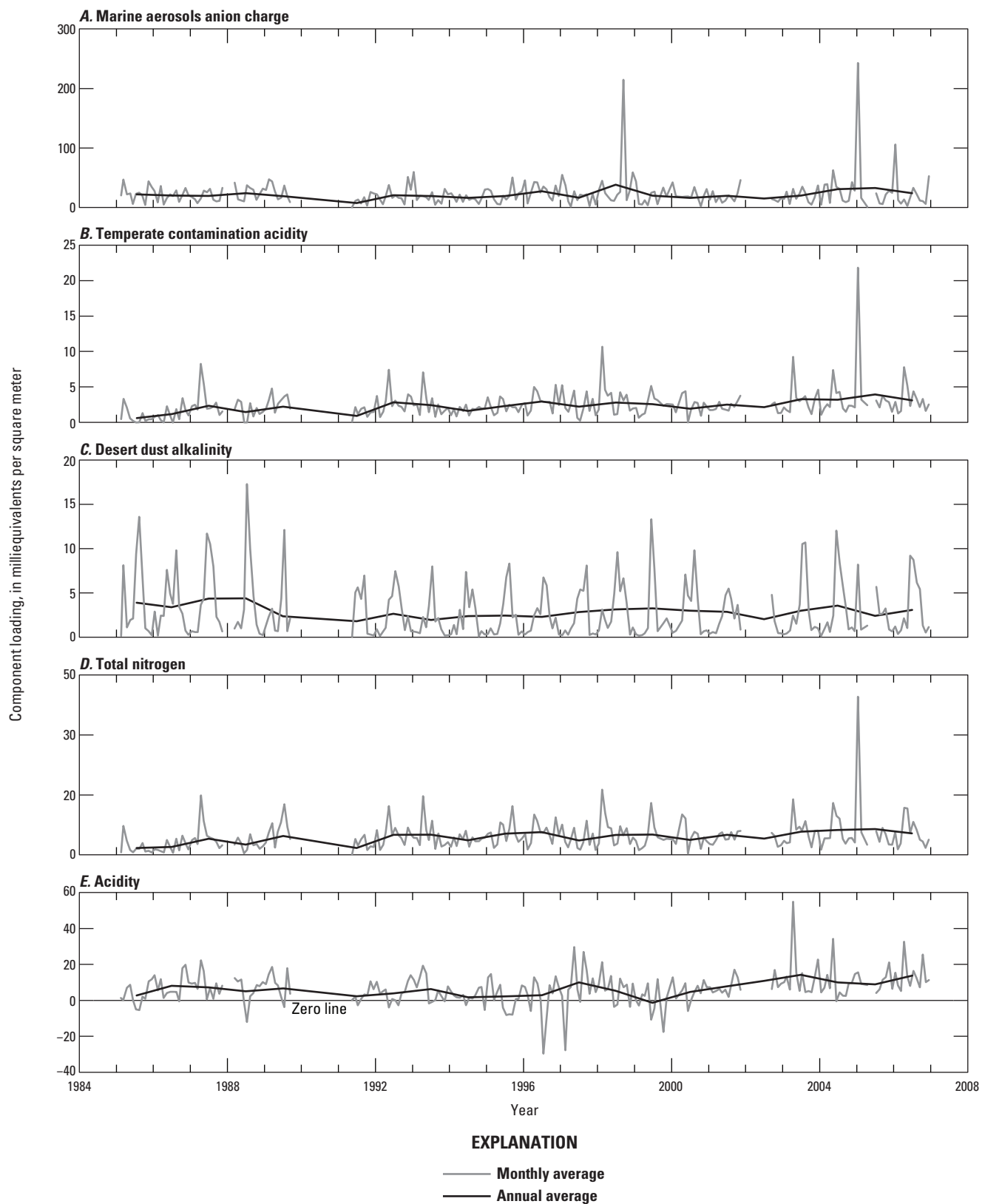


Figure 7. Time series of monthly and annual loading estimates for the three primary components that contribute to rain chemistry in El Verde, Puerto Rico: *A*, marine aerosols, *B*, temperate contamination, and *C*, desert dust. *D*, total inorganic nitrogen; *E*, acidity. Negative acidity values indicate alkaline rain.

total ion charge in rainwater is less than the charge contributed by each component (table 9). Given this caveat, the fractions of total charge attributable to these sources were as follows: marine=83 percent; temperate=10 percent; desert=5 percent; not attributed in this calculation=4 percent.

Of the nonreactive ions, K⁺ has the greatest residual concentration when expressed as a fraction of total input, about 20 percent (table 9). This concentration is followed by acidity at 4 percent. This large residual indicates an additional source of K⁺ beyond the three examined here. Of the constituents analyzed by both NADP and by the study of throughfall chemistry of Heartsill-Scalley and others (2007), throughfall was by far most strongly enriched in K⁺, about 10 times the contribution of rainfall. Potassium was followed by Ca²⁺ and SO₄²⁻, which are each about 1.5 times more abundant in throughfall. Accordingly, the most likely source of the residual K⁺ is wind-blown throughfall or traces of plant matter contaminating the collector, both of which are locally derived.

Seasonality and Trends in Inputs and Sources

The variability in the time series of weekly component concentrations (fig. 5) reflects various types of rainstorms and different air trajectories bringing air from afar into the storm. The 2-year, midrecord gap (1989–1991) was followed by more weeks with especially high concentrations of temperate contaminants, per year, than before. This abundance of especially high concentrations is reflected in the low total cation charge for 1985 to 1988 compared with later years (table 11). Although each component contains high-concentration spikes, there are too few to establish whether they are real or an artifact. When samples are averaged on a monthly basis across all years, all components show seasonality (figs. 5, 7–10). The desert-dust input, which is profoundly seasonal, appears as a major peak in concentration (figs. 5, 8) and loading (figs. 7, 9), centered on July when trade winds are strongest. The peak sea-salt (marine-source) concentration (fig. 8) and loading (input) (fig. 9) is in January. Seasalt makes the smallest fractional contribution from April to July (fig. 10). The peak of hurricane season in Puerto Rico is September (table 7), but it is not reflected in a seasalt maximum. Low-chloride storms, such as Hurricane Hortense (fig. 4), presumably dominate, whereas high-chloride storms, such as Georges (fig. 4), are probably rarer and perhaps substantially undersampled. Temperate contaminants peak in January and in April and May (figs. 8, 9) under the influence of cold fronts from North America. During June to August, when the trade winds are strongest and most sustained, a large volume of contaminants may also be contributed by Europe and Africa.

The only component that shows a well-established long-term trend is temperate contamination. Stallard (2001) and Ortiz-Zayas and others (2006) note an increase in annual total nitrogen concentrations in the NADP data set. To determine

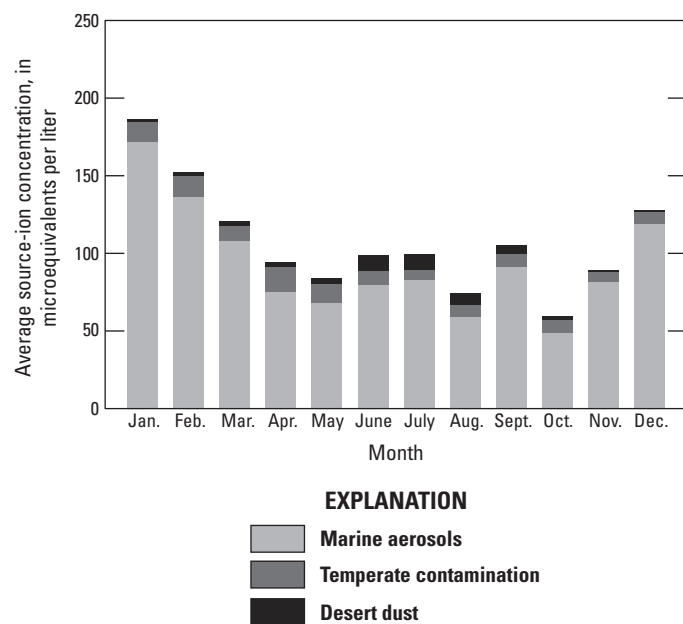


Figure 8. Aggregated monthly concentration estimates for the three primary components that contribute to rain chemistry in El Verde, Puerto Rico—marine aerosols, temperate contamination, and desert dust.

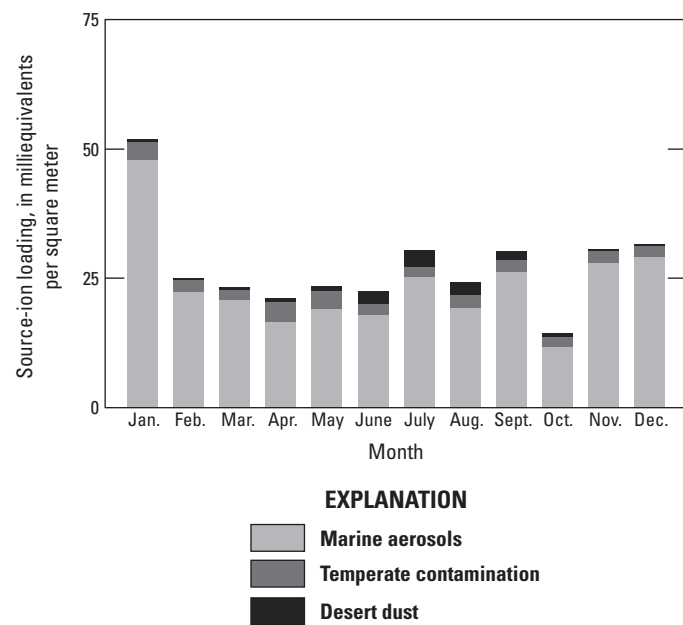


Figure 9. Aggregated monthly loading estimates for the three primary components that contribute to rain chemistry in El Verde, Puerto Rico—marine aerosols, temperate contamination, and desert dust.

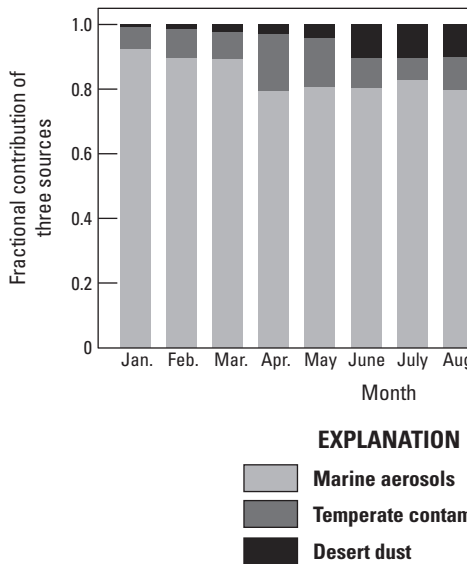


Figure 10. Fractional contribution for the three primary components that contribute to rain chemistry in El Verde, Puerto Rico—marine aerosols, temperate contamination, and desert dust.

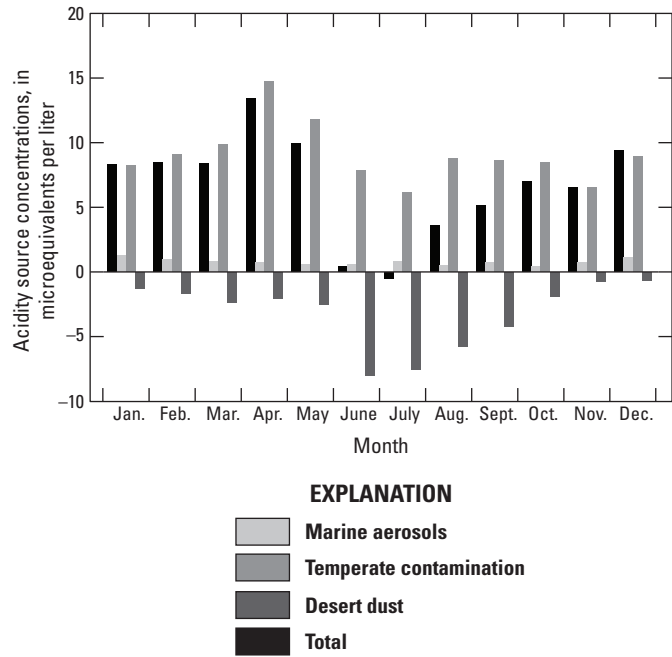


Figure 11. Monthly total acidity concentrations compared to acidity concentration estimates for the three primary components that contribute to rain chemistry in El Verde, Puerto Rico—marine, aerosols, temperate contamination, and desert dust.

significance of trends for the data in this report, the slopes of linear regressions of mean annual source concentrations compared to time were tested against a zero slope using a Student's t-test at a 95 percent confidence level (Stallard, 2001; Bevington and Robinson, 2003). Since sample collection started in 1985, there has been a significant and systematic increase in the mean-annual concentrations of ions presumably coming from the temperate contamination source (figs. 5, 7, table 9). Through time, the ratios of nitrate, ammonia, and nonmarine sulfate in rain from El Verde appear to have fairly characteristic proportions (in moles, $\text{NO}_3^-:\text{NH}_4^+:\text{SO}_4^{2-}=1:0.40:0.74$). Neither marine nor desert sources show significant trends.

Despite the increase in acid-rain components from temperate contamination, on the basis of a t-test, acidity shows no significant trend in for the period of record. Trends in acidity that are small and variable could be obscured by interactions among the three components that effectively introduce noise into the estimates of acidity (figs. 11, 12); the desert-dust input neutralizes some of the acid, and the contributions of marine-source sulfuric acid derived from algae are small and variable. Because acidity is a calculated parameter, the lack of a trend may also be confounded by the anomalous Na^+ analyses mentioned earlier. The greatest acidity, both as a concentration and a loading, develops during April and May, reflecting substantial temperate contamination. The least acidity is in June and July, reflecting reduced contamination inputs and strong loadings of desert dust.

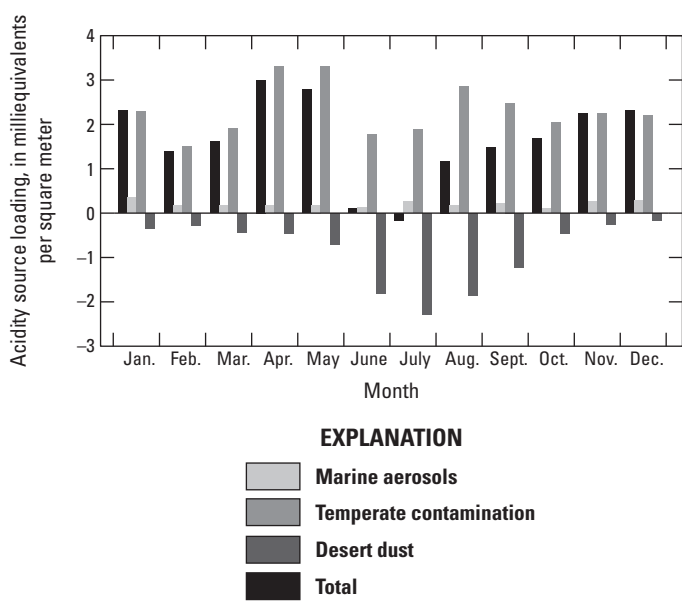


Figure 12. Monthly total acidity loadings compared to acidity loading estimates for the three primary components that contribute to rain chemistry in El Verde, Puerto Rico—marine, aerosols temperate contamination, and desert dust.

Conclusions

Three major sources control the composition of rain in eastern Puerto Rico. In order of importance, these sources are marine salts, temperate contamination, and desert dust.

Marine salts, which produce roughly 83 percent of the ionic charge, are a source of weak acidity. Peak inputs are in January, when weather in Puerto Rico is influenced by fronts and storms of Northern Hemisphere winter. Nine large storms have been associated with exceptionally high chloride concentrations in eastern Puerto Rico stream waters. Five of these storms, including the two largest, were missed in the weekly NADP sampling but not the WEBB Project sampling. Of eight hurricanes and tropical storms that affected the region, all were sampled by WEBB, but only three by NADP; three storms were sampled by neither project, and one high-chloride event, a front, was sampled by NADP but not WEBB. The NADP also did not sample Hurricane Hugo (category 3, winds of $178\text{--}209 \text{ km h}^{-1}$) in 1989, which was larger than Hurricane Georges. Accordingly, the marine input based exclusively on NADP data is underestimated, perhaps substantially, as is indicated by the example of Hurricane Georges explored in this report.

The temperate-contamination source includes nitrate, ammonia, and sulfate derived from anthropogenic and natural sources. Peak deposition is during January, April, and May, months in which storms and cold fronts from the north strongly influence local weather. Trade winds presumably bring contamination from Europe and Africa during the summer months. This source is the only component that is obviously increasing through time, consistent with it being a contamination source. The lesser loadings of the contamination component in the first 4 years of the record correspond with fewer samples with extreme loadings or concentrations for the same period. This trend could reflect greater incursion of contaminated air masses in subsequent years as opposed to an increase in background contamination. Temperate contamination is a strong source of acidity in rain of eastern Puerto Rico and is the chief source of acidity in the rain; by itself it would produce rain with an average pH of 5.0. Combined with other components, rain has an average pH of 5.1 (table 9), and based on application of equations 1–4, without the temperate-contamination component, rain would have an average pH of 5.6. The trend of increasingly acid rain, reflected by the increasing number of especially acid samples, may prove to be deleterious (figs. 6, 7) and by itself would justify continued long-term monitoring at this site.

The desert-dust source is strongly seasonal, peaking in June and July, during times of maximum dust transport from the Sahara and sub-Saharan regions. This dust usually contributes enough alkalinity to neutralize the acidity in June and July rains.

Acknowledgments

This chapter was greatly improved by suggestions made by Jamie B. Shanley and Martha A. Scholl of the U.S. Geological Survey.

References

- Andreae, M.O., Talbot, R.W., Berresheim, H., and Beecher, K.M., 1990, Precipitation chemistry in central Amazonia: *Journal of Geophysical Research* v. 95, p. 16,987–17,000.
- Baynton, H.W., 1968, The ecology of an elfin forest on Puerto Rico—2. The microclimate of Pico del Oeste: *Journal of the Arnold Arboretum of Harvard University*, v. 49, no. 4, p. 419–430.
- Baynton, H.W., 1969, The ecology of an elfin forest on Puerto Rico—3. Hilltop and forest influences on the microclimate of Pico del Oeste: *Journal of the Arnold Arboretum of Harvard University*, v. 50, no. 1, p. 80–92.
- Bevington, P.R., and Robinson, K.D., 2003, Data reduction and error analysis for the physical sciences—2: New York, McGraw Hill, 320 p.
- Birkeland, P.W., 1999, Soils and geomorphology: New York, Oxford University Press, 430 p.
- Brown, Sandra, Lugo, A.E., Silander, S., and Liegel, L., 1983, Research history and opportunities in the Luquillo Experimental Forest: New Orleans, La., U.S. Department of Agriculture Forest Service, Southern Forest Experimental Station General Technical Report SO-44, 128 p.
- Duce, R.A., Liss, P.S., Merrill, J.T., Atlas, E.L., Buat-Menard, P., Hicks, B.B., Miller, J.M., Prospero, J.M., Arimoto, R., Church, T.M., Ellis, W., Galloway, J.N., Hansen, L., Jickells, T.D., Knap, A.H., Reinhardt, K.H., Schneider, B., Soudine, A., Tokos, J.J., Tsunogai, S., Wollast, R., and Zhou, M., 1991, The atmospheric input of trace species to the ocean: *Global Biogeochemical Cycles*, v. 5, no. 3, p. 193–295.
- Dunion, J.P., and Velden, C.S., 2004, The impact of the Saharan air layer on Atlantic tropical cyclone activity: *Bulletin of the American Meteorological Society*, v. 85, no. 3, p. 353–365.
- Eklund, T.J., McDowell, W.H., and Pringle, C.M., 1997, Seasonal variation of tropical precipitation chemistry—La Selva, Costa Rica: *Atmospheric Environment*, v. 31, no. 23, p. 3903–3910.
- Emanuel, K.A., 1991, The theory of hurricanes: *Annual Reviews of Fluid Mechanics*, v. 23, p. 179–196.

- Eugster, Werner, Burkard, R., Holwerda, F., Scatena, F.N., and Bruijnzeel, L.A., 2006, Characteristics of fog and fogwater fluxes in a Puerto Rican elfin cloud forest: Agricultural and Forest Meteorology, v. 139, p. 288–306.
- Evan, A.T., Dunion, J., Foley, J.A., Heidinger, A.K., and Velden, C.S., 2006, New evidence for a relationship between Atlantic tropical cyclone activity and African dust outbreaks: Geophysical Research Letters, v. 33, L19813, p. 1–5.
- Galloway, J.N., 1998, The global nitrogen cycle—Changes and consequences: Environmental Pollution, v. 102, p. 15–24.
- Galloway, J.N., Howarth, R.W., Michaels, A.F., Nixon, S.W., Prospero, J.M., and Dentener, F.J., 1996, Nitrogen and phosphorus budgets of the North Atlantic Ocean and its watershed: Biogeochemistry, v. 35, p. 3–25.
- García-Martino, A.R., Warner, G.S., Scatena, F.N., and Civco, D.L., 1996, Rainfall, runoff, and elevation relationships in the Luquillo Mountains of Puerto Rico: Caribbean Journal of Science, v. 32, no. 4, p. 413–424.
- Garrison, V.H., Shinn, E.A., Foreman, W.T., Griffin, D.W., Holmes, C.W., Kellogg, C.A., Majewski, M.S., Richardson, L.L., Ritchie, K.B., and Smith, G.W., 2003, African and Asian dust—From desert soils to coral reefs: Bioscience, v. 53, no. 5, p. 469–480.
- Goldsmith, S.T., Carey, A.E., Lyons, W.B., Kao, S.-J., Lee, T.-Y., and Chen, J., 2008, Extreme storm events, landscape denudation, and carbon sequestration—Typhoon Mindulle, Choshui River, Taiwan: Geology, v. 36, no. 6, p. 483–486.
- Haire, W.J., 1972, Flood of October 5–10, 1970: Puerto Rico, Commonwealth of Puerto Rico Water-Resources Bulletin 12, 42 p.
- Heartsill-Scalley, Tamara, Scatena, F.N., Estrada, C., McDowell, W.H., and Lugo, A.E., 2007, Disturbance and long-term patterns of rainfall and throughfall nutrient fluxes in a subtropical wet forest in Puerto Rico: Journal of Hydrology, v. 333, p. 472–485.
- Herwitz, S.R., Muhs, D.R., Prospero, J.M., Mahan, S., and Vaughn, B., 1996, Origin of Bermuda's clay-rich Quaternary paleosols and their paleoclimatic significance: Journal of Geophysical Research, v. 101, no. D18, p. 23,389–23,400.
- Holland, E.A., Dentener, F.J., Braswell, B.H., and Sulzman, J.M., 1999, Contemporary and preindustrial global reactive nitrogen budgets: Biogeochemistry, v. 46, p. 7–43.
- Holwerda, Friso, Burkard, R., Eugster, W., Scatena, F.N., Meesters, A.G.C.A., and Bruijnzeel, L.A., 2006, Estimating fog deposition at a Puerto Rican elfin cloud forest site—Comparison of the water budget and eddy covariance methods: Hydrological Processes, v. 20, p. 2669–2692.
- Junge, C.E., 1963, Air chemistry and radioactivity: New York, Academic Press, 382 p.
- Kuehn, B.M., 2006, Desertification called global health threat: Journal of the American Medical Association, v. 295, no. 21, p. 2463–2465.
- Larsen, M.C., and Concepción, I.M., 1998, Water budgets of forested and agriculturally developed watersheds in Puerto Rico, in Segarra-García, R.I., ed., Tropical hydrology and Caribbean water resources, International Symposium on Tropical Hydrology, 3d, and Caribbean Islands Water Resources Congress, 5th, San Juan, Puerto Rico, July 13–16, 1998, Proceedings: American Water Resources Association, p. 199–204.
- Lugo, A.E., and Scatena, F.N., 1992, Epiphytes and climate change research in the Caribbean—A proposal: Selbyana, v. 13, p. 123–130.
- Lundholm, Bengt, 1977, Ecology and dust transport, in Morales, Christer, ed., Saharan dust—Mobilization, transport, deposition; papers and recommendations from a workshop held in Gothenburg, Sweden, 25–28 April 1977: Gothenburg, SCOPE 14, p. 61–68.
- Malmgren, B.A., Winter, A., and Chen, D., 1998, El Niño—Southern oscillation and North Atlantic oscillation control of climate in Puerto Rico: Journal of Climate, v. 11, p. 2713–2717.
- McDowell, W.M., Gines-Sánchez, C., Asbury, C.E., and Pérez, C.R.R., 1990, Influence of sea-salt aerosols and long-range transport on precipitation chemistry at El Verde, Puerto Rico: Atmospheric Environment, v. 24A, p. 2813–2821.
- Murphy, S.F., and Stallard, R.F., 2012, Hydrology and climate of four watersheds in eastern Puerto Rico, ch. C in Murphy, S.F., and Stallard, R.F., eds., Water quality and landscape processes of four watersheds in eastern Puerto Rico: U.S. Geological Survey Professional Paper 1789, p. 43–84.
- Murphy, S.F., Stallard, R.F., Larsen, M.C., and Gould, W.A., 2012, Physiography, geology, and land cover of four watersheds in eastern Puerto Rico, ch. A in Murphy, S.F., and Stallard, R.F., eds., Water quality and landscape processes of four watersheds in eastern Puerto Rico: U.S. Geological Survey Professional Paper 1789, p. 1–24.
- National Oceanic and Atmospheric Administration, 2008, National Climate Data Center, accessed May 16, 2008, at <http://www.ncdc.noaa.gov/oa/ncdc.html>
- National Oceanic and Atmospheric Administration, 2010a, Beaufort Wind Scale, accessed September 30, 2010, at <http://www.srh.noaa.gov/mfl/?n=beaufort>
- National Oceanic and Atmospheric Administration, 2010b, The Saffir-Simpson Hurricane Wind Scale, accessed September 30, 2010, at <http://www.nhc.noaa.gov/pdf/sshws.pdf>

- National Atmospheric Deposition Program (NRSP-3)/ National Trends Network, 2007a, National Atmospheric Deposition Program (NADP/NTN), accessed September 13, 2007, at <http://nadp.sws.uiuc.edu/>
- National Atmospheric Deposition Program (NRSP-3)/ National Trends Network, 2007b, NADP/NTN overview and history, accessed September 13, 2007, at <http://nadp.sws.uiuc.edu/NADP/>
- National Atmospheric Deposition Program (NRSP-3)/ National Trends Network, 2007c, NADP/NTN site list, accessed September 13, 2007, at <http://nadp.sws.uiuc.edu/sites/latlong.asp>
- National Atmospheric Deposition Program (NRSP-3)/ National Trends Network, 2007d, Notification of important change in NADP/NTN procedures on 11 January 1994, accessed September 13, 2007, at <http://nadp.sws.uiuc.edu/documentation/advisory.html>
- Ortiz-Zayas, J.R., Cuevas, E., Mayol-Bracero, O.L., Donoso, L., Trebs, I., Figueroa-Nieves, D., and McDowell, W.H., 2006, Urban influences on the nitrogen cycle in Puerto Rico: Biogeochemistry, v. 79, p. 109–133.
- Parkin, D.W., and Shackleton, N.J., 1973, Trade wind and temperature correlations down a deep-sea core off the Saharan coast: Nature, v. 245, p. 91–92.
- Peters, N.E., Shanley, J.B., Aulenbach, B.T., Webb, R.M., Campbell, D.H., Hunt, R., Larsen, M.C., Stallard, R.F., Troester, J.W., and Walker, J.F., 2006, Water and solute mass balance of five small, relatively undisturbed watersheds in the U.S.: Science of the Total Environment, v. 358, p. 221–242.
- Pett-Ridge, J.C., 2009, Contributions of dust to phosphorus cycling in tropical forests of the Luquillo Mountains, Puerto Rico: Biogeochemistry, v. 96, no. 1, p. 63–80.
- Pett-Ridge, J.C., Derry, L.A., and Barrows, J.K., 2009a, Ca/Sr and $^{87}\text{Sr}/^{86}\text{Sr}$ ratios as tracers of Ca and Sr cycling in the Río Icacos watershed, Luquillo Mountains, Puerto Rico: Chemical Geology, v. 94, no. 1, p. 64–80.
- Pett-Ridge, J.C., Derry, L.A., and Kurtz, A.C., 2009b, Sr isotopes as a tracer of weathering processes and dust inputs in a tropical granitoid watershed, Luquillo Mountains, Puerto Rico: Geochimica et Cosmochimica Acta, v. 73, p. 25–43.
- Prospero, J.M., and Carlson, T.N., 1972, Vertical and areal distribution of Saharan dust over the western equatorial North Atlantic Ocean: Journal of Geophysical Research, v. 77, p. 5255–5265.
- Rasch, P.J., Barth, M.C., Kiehl, J.T., Schwartz, S.E., and Benkovitz, C.M., 2000, A description of the global sulfur cycle and its controlling processes in the National Center for Atmospheric Research Community Climate Model, Version 3: Journal of Geophysical Research, v. 105, p. 1367–1385.
- Reid, J.S., Kinney, J.E., Westphal, D.L., Holben, B.N., Welton, E.J., Tsay, S., Eleuterio, D.P., Campbell, J.R., Christopher, S.A., Colarco, P.R., Jonsson, H.H., Livingston, J.M., Maring, H.B., Meier, M.L., Pilewskie, P., Prospero, J.M., Reid, E.A., Remer, L.A., Russell, P.B., Savoie, D.L., Smirnov, A., and Tanré, D., 2003a, Analysis of measurements of Saharan dust by airborne and ground-based remote sensing methods during the Puerto Rico Dust Experiment (PRIDE): Journal of Geophysical Research, v. 108, no. D19, 8586, p. 1–27.
- Reid, E.A., Reid, J.S., Meier, M.M., Dunlap, M.R., Cliff, S.S., Broumas, A., Perry, K., and Maring, H., 2003b, Characterization of African dust transported to Puerto Rico by individual particle and size segregated bulk analysis: Journal of Geophysical Research, v. 108, no. D19, 8591, p. 1–22.
- Rodhe, Henning, Dentener, F., and Schulz, M., 2002, The global distribution of acidifying wet deposition: Environmental Science and Technology, v. 36, p. 4382–4388.
- Scatena, F.N., and Larsen, M.C., 1991, Physical aspects of hurricane Hugo in Puerto Rico: Biotropica, v. 23, p. 317–323.
- Schaefer, D.A., McDowell, W.H., Scatena, F.N., and Asbury, C.E., 2000, Effects of hurricane disturbance on stream water concentrations and fluxes in eight tropical forest watersheds of the Luquillo Experimental Forest, Puerto Rico: Journal of Tropical Ecology, v. 16, p. 189–207.
- Schellekens, Jaap, Bruijnzeel, L.A., Wickel, A.J., Scatena, F.N., and Silver, W.L., 1998, Interception of horizontal precipitation by elfin cloud forest in the Luquillo Mountains, eastern Puerto Rico, in Schemenauer, R.S., and Bridgman, H.A., eds., International Conference on Fog and Fog Collection, 1st, Vancouver, Canada, July 19–24, 1998, Proceedings: Ottawa, Canada, International Development Research Centre, p. 29–32.
- Shinn, E.A., Smith, G.W., Prospero, J.M., Betzer, P., Hayes, M.L., Garrison, V.H., and Barber, R.T., 2000, African dust and the demise of Caribbean coral reefs: Geological Research Letters, v. 27, no. 19, p. 3029–3032.
- Snodgrass, E.R., di Girolamo, L., and Rauber, R.M., 2009, Precipitation characteristics of trade wind clouds during RICO derived from radar, satellite, and aircraft measurements: Journal of Applied Meteorology and Climatology, v. 84, p. 464–483.
- Stallard, R.F., 2001, Possible environmental factors underlying amphibian decline in eastern Puerto Rico—Analysis of U.S. government data archives: Conservation Biology, v. 15, no. 4, p. 943–953.
- Stallard, R.F., 2012, Weathering, landscape equilibrium, and carbon in the four watersheds in eastern Puerto Rico, ch. H in Murphy, S.F., and Stallard, R.F., eds., Water quality and landscape processes of four watersheds in eastern Puerto Rico: U.S. Geological Survey Professional Paper 1789, p. 199–248.

- Stallard, R.F., and Edmond, J.M., 1981, Geochemistry of the Amazon—1. Precipitation chemistry and the marine contribution to the dissolved load at the time of peak discharge: *Journal of Geophysical Research—Oceans and Atmospheres*, v. 86, no. NC10, p. 9844–9858.
- Stallard, R.F., and Murphy, S.F., 2012, Water quality and mass transport in four watersheds in eastern Puerto Rico, ch. E in Murphy, S.F., and Stallard, R.F., eds., *Water quality and landscape processes of four watersheds in eastern Puerto Rico: U.S. Geological Survey Professional Paper 1789*, p. 113–152.
- Stegmann, P.M., and Tindale, N.W., 1999, Global distribution of aerosols over the open ocean as derived from the coastal zone color scanner: *Global Biogeochemical Cycles*, v. 13, no. 2, p. 383–397.
- Stumm, Werner, and Morgan, J.J., 1981, *Aquatic chemistry*: New York, John Wiley, 780 p.
- Weathers, K.C., Likens, G.E., Bormann, F.H., Bicknell, S.H., Bormann, B.T., Daube, B.C., Jr., Eaton, J.S., Galloway, J.N., Keene, W.C., Kimball, K.D., McDowell, W.H., Sicama, T.G., Smiley, D., and Tarrant, R.A., 1988, Cloud water chemistry from ten sites in North America: *Environmental Science and Technology*, v. 22, p. 1018–1026.
- Weaver, P.L., 1972, Cloud moisture interception in the Luquillo Mountains of Puerto Rico: *Caribbean Journal of Science*, v. 12, no. 3–4, p. 129–144.

Water Quality and Mass Transport in Four Watersheds in Eastern Puerto Rico

By Robert F. Stallard and Sheila F. Murphy

Chapter E of
**Water Quality and Landscape Processes of Four Watersheds in
Eastern Puerto Rico**

Edited by Sheila F. Murphy and Robert F. Stallard

Professional Paper 1789-E

**U.S. Department of the Interior
U.S. Geological Survey**

Contents

Abstract.....	117
Introduction.....	117
Factors Affecting Water Chemistry of Tropical Rivers.....	119
Study Design and Objectives	121
Methods Used to Collect and Interpret Data	122
Sample Collection and Field Measurements	122
Stream Discharge	122
Analytical Procedures.....	123
Discharge, Load, Runoff, and Yield.....	123
Water Quality of Eastern Puerto Rico WEBB Project Watersheds.....	125
Runoff Percentile Classes, Concentration, and Yield	125
Water-Quality Constituents.....	130
Field Measurements.....	130
Silica.....	130
Chloride.....	133
Calcium, Magnesium, and Sodium	135
Dissolved Organic Carbon.....	135
The Nutrients: Nitrate, Ammonia, Phosphate, and Potassium.....	137
Sulfate.....	139
Alkalinity, Carbon Dioxide, and Calcite Saturation	139
Suspended Sediment	141
Conclusions.....	143
Acknowledgements.....	147
References.....	147

Figures

1. Map of Puerto Rico and study watersheds.....	118
2–12. Diagrams showing the following:	
2. Functional classification of tropical forest watersheds according to prevailing hydrological flow paths, based on measured saturated hydraulic conductivities (K_{sat}).....	121
3. Temperature, pH, conductivity, and dissolved oxygen in the eastern Puerto Rico WEBB rivers, 1991–2005.....	131
4. Runoff rate–concentration graphs for dissolved silica.....	133
5. Runoff rate–concentration graphs for chloride	135
6. Runoff rate–concentration graphs for sodium, magnesium, and calcium ions.....	137
7. Runoff rate–concentration graphs for dissolved organic carbon.....	139
8. Runoff rate–concentration graphs for potassium ion	141
9. Runoff rate–concentration graphs for nitrate, ammonium, and phosphate ions ...	143
10. Runoff rate–concentration graphs for sulfate, and sulfate:chloride ratio	144

11. Alkalinity, carbon dioxide saturation, and calcite saturation in the eastern Puerto Rico WEBB rivers, 1991–2005.....	144
12. Runoff rate–concentration graphs for suspended sediment.....	146

Tables

1. Average constituent concentrations and yields for the study period (1991–2005).....	124
2. Runoff rates for WEBB rivers during the study period (1991–2005) at certain thresholds	125
3. Discharge-weighted average concentrations of each percentile class estimated by using LOADEST and hourly discharge	127
4. Percentage of constituent discharged compared with percentage of water discharged (calculated using LOADEST) and comparisons with regressions of log (concentration) to log (runoff rate).....	128

Abbreviations Used in This Report

>	greater than
—	preceding a compound, such as $-PO_4^{3-}$, indicates likelihood of linkage to a cation
μm	micrometer
$\mu S\text{ cm}^{-1}$	microsiemens per centimeter
km	kilometer
km^2	square kilometer
mm	millimeter
$mm\text{ h}^{-1}$	millimeters per hour
$mm\text{ yr}^{-1}$	millimeters per year
$t\text{ km}^{-2}\text{ yr}^{-1}$	metric tons per square kilometer per year
DOC	dissolved organic carbon
SI	saturation index
WEBB	Water, Energy, and Biogeochemical Budgets

Conversion Factors

Multiply	By	To obtain
Length		
micrometer (μm)	0.00003937	inch (in.)
millimeter (mm)	0.03937	inch (in.)
kilometer (km)	0.6214	mile (mi)
Area		
square kilometer (km^2)	0.3861	square mile (mi^2)
Flow rate		
millimeters per hour (mm h^{-1})	0.03937	inches per year (in. h^{-1})
millimeters per year (mm yr^{-1})	0.03937	inches per year (in. yr^{-1})
Specific Conductance		
microsiemens per centimeter ($\mu\text{S cm}^{-1}$)	1.000	micromho per centimeter ($\mu\text{mho cm}^{-1}$)
Other		
metric tons per square kilometer per year ($\text{t km}^{-2} \text{yr}^{-1}$)	2.855	short tons per square mile per year (tons $\text{mi}^{-2} \text{yr}^{-1}$)

Water Quality and Mass Transport in Four Watersheds in Eastern Puerto Rico

By Robert F. Stallard and Sheila F. Murphy

Abstract

Water quality of four small watersheds in eastern Puerto Rico has been monitored since 1991 as part of the U.S. Geological Survey's Water, Energy, and Biogeochemical Budgets program. These watersheds represent a montane, humid-tropical environment and differ in geology and land cover. Two watersheds are located on granitic rocks, and two are located on volcaniclastic rock. For each bedrock type, one watershed is covered with mature rainforest in the Luquillo Mountains, and the other watershed is undergoing reforestation after being affected by agricultural practices typical of eastern Puerto Rico. A subwatershed of the Icacos watershed, the Guabá, was also monitored to examine scaling effects. The water quality of the rivers draining forest, in the Icacos and Guabá (granitic watersheds) and Mameyes (a volcaniclastic watershed), show little contamination by human activities. The water is well oxygenated and has a nearly neutral pH, and nutrient concentrations are low. Concentrations of nutrients in the disturbed watersheds, the Cayaguás (granitic rock) and Canóvanas (volcaniclastic rock), are greater than in the forested watersheds, indicating some inputs from human activities. High in-stream productivity in the Canóvanas watershed leads to occasional oxygen and calcite supersaturation and carbon dioxide undersaturation. Suspended sediment concentrations in all watersheds are low, except during major storms. Most dissolved constituents derived from bedrock weathering or atmospheric deposition (including sodium, magnesium, calcium, silica, alkalinity, and chloride) decrease in concentration with increasing runoff, reflecting dilution from increased proportions of overland or near-surface flow. Strongly bioactive constituents (dissolved organic carbon, potassium, nitrate, ammonium ion, and phosphate) commonly display increasing concentration with increasing runoff, regardless of their ultimate origin (bedrock or atmosphere). The concentrations of many of the bioactive constituents eventually decrease at runoff rates greater than 3 to 10 millimeters per hour, presumably reflecting an increased relative contribution from overland flow. Sulfate behaves like the nonbioactive constituents in the Canóvanas, Cayaguás, and Mameyes watersheds but like a bioactive constituent in the Icacos and Guabá watersheds. Storms resulted in several anomalous sample compositions. Runoff waters from a number of storms—mostly hurricanes,

but also other storms—have exceptionally high chloride concentrations, presumably resulting from windborne seasalt from the ocean, and low nitrate concentrations, reflecting a dominance of maritime air masses contributing moisture to the storms. High-potassium samples, without high chloride, are also associated with some smaller storms that followed Hurricane Georges in 1998; they are likely related to the breakdown of fallen vegetation. Finally, occasional low-silica events are observed in the Icacos and Guabá watersheds in the years prior to Hurricane Georges, but not after; this difference may be related to a change in hydrologic flow paths.

Introduction

The U.S. Geological Survey initiated the Water, Energy, and Biogeochemical Budgets (WEBB) program in 1990 to study water, energy, and biogeochemical fluxes and interactions throughout a range of temporal and spatial scales (Lins, 1994). The WEBB site in eastern Puerto Rico represents a montane, humid-tropical environment with a bedrock geology typical of many parts of the world, and it therefore provides an excellent platform for obtaining a better understanding of processes that control the composition of water in other tropical environments (Larsen and others, 1993). At the Puerto Rico site, four watersheds with different geology and land cover can be compared (Murphy and others, 2012). Two watersheds are located on coarse-grained granitic rocks (Icacos and Cayaguás), and two are located on fine-grained volcanic and volcaniclastic rocks (Mameyes and Canóvanas). For each bedrock type, one watershed is covered with mature forest (Icacos and Mameyes), and the other watershed has been affected by agricultural land use typical of eastern Puerto Rico (Cayaguás and Canóvanas). In addition, a subwatershed of the Icacos watershed, the Guabá, was studied to examine scaling effects.

The warm, wet Luquillo Mountains of eastern Puerto Rico are the headwaters of numerous streams and rivers, including the Río Icacos and Río Mameyes (fig. 1). Visitors to the El Yunque National Forest (which is contiguous with the Luquillo Experimental Forest) typically visit the forest during calm weather, when rivers are clear and gently flowing over their beds. This water has a neutral pH and is well oxygenated,

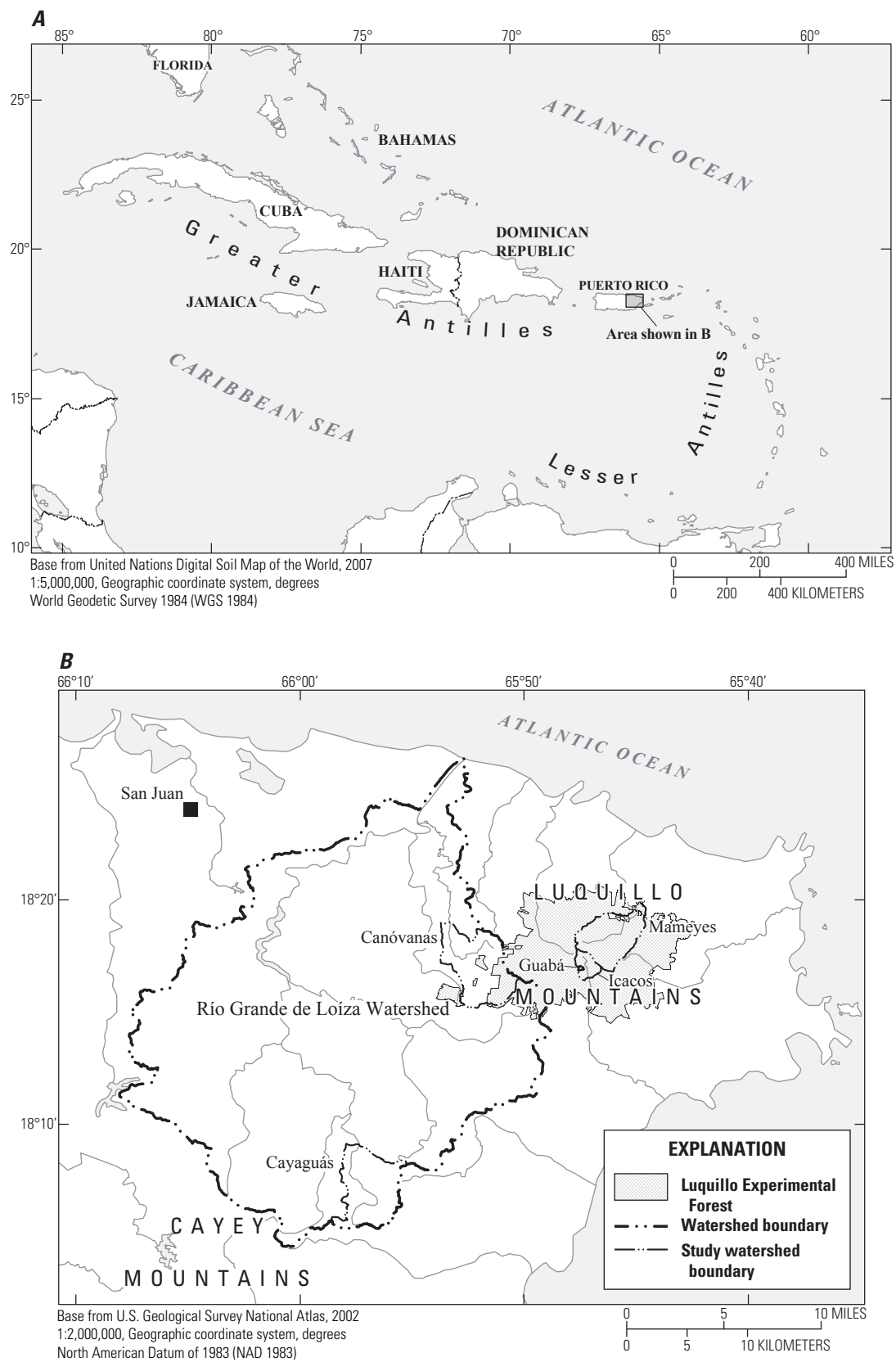


Figure 1. Location of Puerto Rico and study watersheds, eastern Puerto Rico.

and if it is treated to make it potable, it is quite delicious—presumably being flavored by the chemical breakdown of bedrock, a little seasalt, and bit of dissolved organic matter. Most visitors avoid the forest during intense storms, such as hurricanes and major cold fronts, which turn the rivers into muddy, raging torrents that threaten life and infrastructure. Sometimes so much rain falls that entire hillslopes of soil crash down in landslides. Occasionally, winds are so strong that forest vegetation is shredded and large quantities of salt spray from the ocean are blown over the forest. Less visible contributions to the forest are made by atmospheric deposition; nitrogen in rainfall has almost doubled since it was first monitored in 1985 (Stallard, 2012a). A fungus has led to a die-off of some endemic frogs, and droughts and pollution from North America, Europe, and Africa may have increased the virulence of the infection (Stallard, 2001; Burrowes and others, 2004).

The Río Grande de Loíza watershed drains the western flank of the Luquillo Mountains and the flatter area to the west (fig. 1). Deforestation for hundreds of years (Gould and others, 2012; Murphy and others, 2012) and the construction of roads in steep terrain have increased surface runoff and sediment delivery to streams (Larsen and Parks, 1997; Clark and Wilcock, 2000). As Puerto Rico has urbanized during the past half century, much of the island's previously denuded lands, including the Cayaguás and Canóvanas watersheds, are undergoing reforestation; however, stored sediment continues to be released to the reservoirs and the ocean during floods (Webb and Soler-López, 1997; Larsen and Santiago-Román, 2001). The water quality of rivers in the recovering landscape is affected by runoff from remaining agricultural lands and waste from domestic and industrial sources.

Factors Affecting Water Chemistry of Tropical Rivers

The processes by which river waters acquire their composition, as related to the movement of water through soil and its interaction with the overlying vegetation and underlying bedrock, are an area of active research. Previous studies of large tropical rivers (Gibbs, 1967, 1972; Stallard and Edmond, 1981, 1983, 1987; Stallard, 1985, 1988; Lewis and others, 1987; Saunders and Lewis, 1988, 1989; 1990; Fox, 1989, 1993; Lewis and Saunders, 1989; Stallard and others, 1991; Devol and others, 1995; Edmond and others, 1995, 1996; Tardy and others, 2005, 2009) and of the Luquillo Mountains (McDowell and others, 1990, 1996; McDowell, 1991, 1998; Lodge and others, 1994; McDowell and Asbury, 1994; Chestnut and others, 1999; Aitkenhead and McDowell, 2000; Chestnut and McDowell, 2000; Zeigler and others, 2005; Derry and others, 2006; Peters and others, 2006; Bhatt and McDowell, 2007; Heartsill-Scalley and others, 2007; Pett-Ridge, 2009; Pett-Ridge and others, 2009a,b; Shanley and others, 2011) demonstrate that it is possible to classify and organize river-borne chemical constituents on the basis of their primary sources and bioactivity. Constituents that are

largely bedrock derived include calcium (Ca^{2+}), alkalinity, silica (Si(OH)_4), and phosphate ($-\text{PO}_4^{3-}$). Phosphate is susceptible to attaching to aluminum and iron oxides and hydroxides and being lost from solution, and the preceding “–” indicates linkages with other constituents such as iron, aluminum, and organic matter. Chloride (Cl^-) and sulfate (SO_4^{2-}) are largely of seasalt origin; additional SO_4^{2-} comes from the weathering of sulfide minerals, sometimes exposed through mining, and from atmospheric sulfuric acid, which has both natural and combustion sources. The cations sodium (Na^+), potassium (K^+), and magnesium (Mg^{2+}) are predominantly bedrock derived, with lesser seasalt contributions. Siliceous bedrock is a source of all of the bedrock-derived constituents, and Na^+ -bearing and Ca^{2+} -bearing bedrock-forming minerals weather the most rapidly and completely. Where present, carbonate minerals are strong sources of Ca^{2+} , alkalinity, and sometimes Mg^{2+} . Several constituents, such as nitrate (NO_3^-), ammonium ion (NH_4^+), and dissolved organic carbon (DOC), are ultimately derived from atmospheric gases that have chemical, biological, and sometimes anthropogenic origins.

Biological processes associated with the growth and maintenance of a forest can have a considerable effect on the ultimate chemical composition of that water. The classic model of nutrient cycling in tropical rainforests (Herrera and others, 1978a,b; Stark and Jordan, 1978; invoked for Luquillo by McDowell, 1998, 2001) is a tight, vertical, almost-closed cycle where nutrients released from vegetation by throughfall or decay are efficiently recovered by plant roots and reincorporated into vegetation as water moves through the upper soil profile. Of the constituents studied here, K^+ , SO_4^{2-} , DOC, NO_3^- , NH_4^+ , and $-\text{PO}_4^{3-}$, are strongly bioactive, and biological processes, including this internal cycling, can have a profound effect on their distribution in surface waters. The bioactivity of these constituents is manifested by a strong enrichment in throughfall (water that has interacted with leaves and branches) compared with rainfall (Heartsill-Scalley and others, 2007) and in streams following hurricanes (McDowell and others, 1996; Schaefer and others, 2000; Shanley and others, 2011). Sulfate, DOC, NO_3^- , and NH_4^+ can be also be lost to the atmosphere through transformation back into various gases. All of the biologically active constituents have domestic and agricultural sources.

The chemistry of underlying bedrock is a controlling factor of the water chemistry of any river. In Puerto Rico's WEBB program watersheds, the two rock types primarily differ in their quartz content: the granitic rocks typically contain between 20 and 33 percent quartz, whereas the volcaniclastic rocks have little or no quartz (Murphy and others, 2012). The presence of quartz in bedrock leads to a sandy texture in overlying soils and tends to increase their ability to transmit water (Murphy and Stallard, 2012). Where quartz is absent, as in volcanic bedrock, sand-sized grains in associated soils and river sediments are rare (Johnsson and Stallard, 1989; Johnsson, 1990), and soils are typically finer grained and have lower permeability and infiltration rates (Simon and others, 1990).

The presence or absence of quartz in bedrock is clearly evident in the channel forms of eastern Puerto Rico rivers (see cover photograph). The two WEBB study-area rivers that drain quartz-poor, volcaniclastic rocks (Mameyes and Canóvanas) have abundant exposed bedrock, bouldery beds, and poorly developed flood plains and riparian areas. Many nooks and crannies shelter aquatic creatures. In contrast, the rivers that drain granitic rocks (Icacos, Cayaguás, and Guabá) have beds of quartz sand, well-developed flood plains, and extensive riparian areas, especially where their stream gradients are gentler. Their channels support hyporheic flow, and the flood plains and riparian areas can modify water quality.

When quartz chemically weathers, it produces only dissolved silica (Si(OH)_4), which is a common weathering product of many silicate minerals. Therefore, quartz dissolution is difficult to differentiate from other reactions when one examines solute composition alone (pitted quartz surfaces, which have been observed on grains from the Icacos watershed, have been used to identify dissolution; Brantley and others, 1986; Schulz and White, 1999). If quartz is ignored, the remaining minerals in the granitic and volcaniclastic bedrock types are similar, with a slight bias to more Mg- and Ca-rich minerals in the volcaniclastic rocks (Smith and others, 1998, their fig. 3, table 2). Therefore, solute signatures from weathering of the granitic or volcaniclastic rocks should be similar. Differences in solute composition, however, can be caused by other rock types, such as carbonate rocks, sulfide ores, and ultramafic rocks, or by indirect effects, such as different rates and pathways for water movement through soils and the presence or absence of riparian areas.

The interaction between water, soil, and bedrock, as manifested by the relation between concentration (C) and runoff rate (R), appears to be similar in a wide range of rivers, indicating a commonality in the physical and chemical mechanisms that mobilize and export solutes from watersheds. Godsey and others (2009) compare data from the U.S. Geological Survey Hydrologic Benchmark Network for 59 small, geochemically diverse watersheds in the United States in landscapes that are not heavily affected by human activities. They focused on chemical constituents that are derived from bedrock weathering and are not biologically active— Na^+ , Ca^{2+} , Mg^{2+} , and Si(OH)_4 —and looked for crosscutting patterns that would provide insight as to how these constituents were acquired by the streams.

Godsey and others (2009) note that most streams demonstrated a linear relation between $\log(C)$ and $\log(R)$,

$$\log(C) = a + b \cdot \log(R),$$

where a is a constant and b is a slope. A zero slope implies a fixed concentration and is termed a “chemostat,” whereas a slope of -1 implies a constant input rate of the constituent, independent of runoff. A positive slope implies that increasing rainfall and runoff serve to mobilize the constituent. For Na^+ , Ca^{2+} , Mg^{2+} , and Si(OH)_4 , b is typically negative, mostly between -0.05 and -0.15 and is statistically different from

zero. The slightly negative slope is close to being a chemostat, implying that subsoil processes substantially increase the supply of these constituents in response to more water flowing through the soil and that many watersheds respond in a similar way, despite marked differences in geology, vegetation, and climate.

Godsey and others (2009) compared three simple models that each successfully reproduce nearly log-linear relations between runoff and constituent concentration. For two of these models, the Hubbard Brook “working model” of Johnson and others (1969) and the rapid, flow-through-reaction model of Langbein and Dawdy (1964), the model relation has a sigmoidal shape, leveling off at low and high runoff rates. Successful models require that the concentrations of constituents in the input to the soil reservoir greatly exceed those of rainwater and could be thought of as soil-water concentrations. The authors also develop their own strictly log-linear model, the “permeability-porosity-aperture” model. This model assumes that permeability, porosity, and average pore aperture decrease exponentially with depth; precipitation rates are approximately the same across a hillslope; flows through the watershed behave according to Darcy’s Law; minimal flows originate near the divide and the stream; and solute flux is proportional to reactive surface area such that secondary and back-reactions do not control solute fluxes (Godsey and others, 2009). The model handles stored water.

The slope, b , of the permeability-porosity-aperture model is derived from the depth-dependent e -folding lengths of four different structural and chemical properties. The model predicts that b should be the same for all bedrock-derived constituents, although the authors allow that differences for slopes among various constituents could be attributable to differences in the depth distribution of reactive minerals throughout the soil profile. The authors also caution against trying to derive b from field measurements, stating “Any such attempt at direct measurement [of the properties that go into determining the slope] would be complicated by the spatial heterogeneity in subsurface properties, as well as the large differences between field and laboratory weathering rates.”

During big storms, water does not necessarily flow through the soil profile. Storm events play a major, often dominant, role in the mobilization of river-borne materials from hillslopes and stream channels and in the transport of these materials downriver (Wolman and Miller, 1960). In tropical, high-runoff settings, near-surface and overland flow can be more important than soil infiltration during storms (Elsenbeer, 2001, Godsey and others, 2004). Elsenbeer (2001) developed a simplified classification scheme based on infiltration styles (fig. 2). When rainfall intensities for a given locale exceed the hydrologic conductivity (K_{sat}) in the shallow parts of the soil profile, water is shunted into shallower, lateral flow paths or into overland flow. In hilly watersheds with shallow bedrock or impermeable soils (Acrisols), surface lateral flow of water will predominate (fig. 2), because K_{sat} decreases rapidly in the soil profile (a change of 2 or 3 orders of magnitude in the first meter of soil). In contrast, in watersheds with deep, porous

soils (Ferralsols), K_{sat} remains high through the soil profile (a change of 1 order of magnitude or less in the first meter of soil), and deep infiltration is likely. In Acrisols, water and nutrients can both leave the watershed during storms before ever interacting with soil and roots.

For all soils, pipes and macropores (large-diameter connected flow paths characteristically produced by soil cracks, decayed roots, and burrows) can be sufficiently abundant that they dominate infiltration and lateral shallow-soil flow. Shallow-soil, overland, macropore, and pipe flow all provide pathways for water and solutes that modify interaction with plant roots, especially during large storms (Beven and Germann, 1982; Elsenbeer and Cassel, 1990; Elsenbeer and Lack, 1996; Elsenbeer and others, 1996; Godsey and others, 2004; Kinner and Stallard, 2004; Chappell and others, 2005; Larsen and others, 2012). In fact, macropore effects can dominate soil-matrix flow at hillslope scale, considerably changing how a soil might be classified according to figure 2 (Chappell and others 1998, 2005).

The most intense rainfall events in eastern Puerto Rico occur during hurricanes and large frontal storms. These large storms shred and topple vegetation, generate landslides that strip soils and vegetation off slopes, and substantially alter stream-water chemistry (McDowell and others, 1996; Schaefer and others, 2000; Heartsill-Scalley and others, 2007; Larsen, 2012). Although granitic soils have greater groundwater storage and somewhat faster infiltration (Murphy and Stallard, 2012), in both the Mameyes and Icacos watersheds, high runoff rates produce substantial overland flow on forested soils on both granitic and volcaniclastic bedrock as well as on fresh and recovering landslides (Larsen, 2012), indicating Acrisol-type soil hydrology in both types of bedrock.

Study Design and Objectives

This chapter presents water chemistry for thousands of samples collected during the first 15 years (1991–2005) of the Puerto Rico WEBB program. The data, which are available from the U.S. Geological Survey's National Water Information System website (<http://nwis.waterdata.usgs.gov/usa/nwis/qwdata>), provide a unique opportunity to examine the composition of stream water during storms. We are not aware of any published data anywhere in the world for water samples collected at runoff rates greater than 20 millimeters per hour (mm h^{-1}) that have been analyzed for chemistry and suspended sediment (appendix 1). The Hydrologic Benchmark Network dataset examined by Godsey and others (2009) contains comprehensive chemistry for only 30 samples, from 12 rivers, that were sampled at runoff rates greater than 1 mm h^{-1} ; of these, the maximum runoff rate was 5.9 mm h^{-1} . The eastern Puerto Rico WEBB study analyzed comprehensive chemistry in 543 samples collected at runoff rates greater than 1 mm h^{-1} , 256 samples at greater than 10 mm h^{-1} , and 3 samples at greater than 90 mm h^{-1} . Because the soils of the study watersheds generally behave like Acrisols (Murphy and Stallard, 2012), strong, downslope, near-surface water flow and concomitant

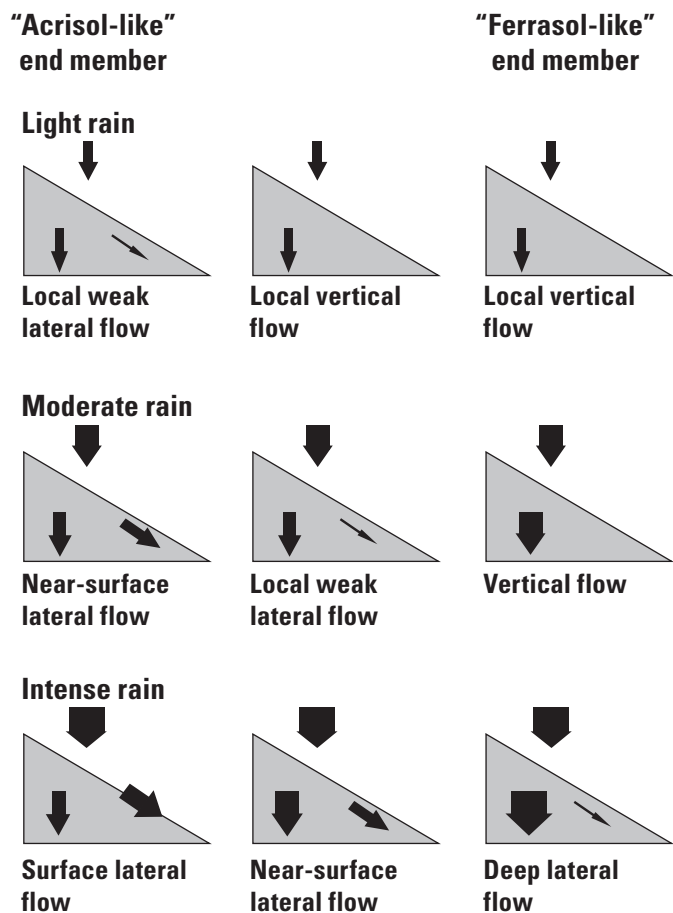


Figure 2. Adaptation of Elsenbeer's (2001) functional classification of tropical forest watersheds according to prevailing hydrological flow paths, based on measured saturated hydraulic conductivities (K_{sat}). Each row represents soil response under different rainfall intensities. Arrows indicate movement of water overland and through soil; thickness of arrows indicates approximate relative proportions. For light rain, much moisture does not get to the stream and is probably lost through transpiration. Surface lateral flow is encountered in hilly watersheds with shallow bedrock or impermeable soils (left diagram), where K_{sat} typically decrease rapidly in the profile and rainfall is intense. Deep lateral flow (right diagram) occurs where K_{sat} do not decrease rapidly in the profile. Note that Acrisols are roughly equivalent to Ultisols in the United States soil classification and Ferralsols are roughly equivalent to Oxisols (Soil Survey Staff, 1995), and that macropores normally complicate the role of matrix porosity (Chappell and others, 1998; Chappell and Sherlock, 2005).

nutrient export are expected during storms. The models presented by Godsey and others (2009) are for water moving through soil; thus, at the high-flow regimes sampled during the WEBB study, deviations from linear trends of $\log(C)$ compared with $\log(R)$ might be expected because different flow paths are active.

In this report, we use the relation between constituent concentration and discharge as a basis for examining processes operating at different flow regimes. Similar to the approach used by Godsey and others (2009), we examined the structure of the primary data graphically and through fitting simple regressions to the data, and we compared these results among study rivers and with the results of other studies. We also estimated continuous rates of watershed export (loads) of each constituent and averaged the loads for ranges of discharge in order to construct averaged constituent-discharge relations. We asked: (1) Do we see nonlinear features in the high-runoff samples in this dataset that are not seen elsewhere, such as in the Hydrologic Benchmark Network's summary of Godsey and others (2009)? (2) How do atmospherically derived and biologically active constituents differ from largely bedrock-derived constituents? And, (3) Do we see features in these data comparisons that can be used to inform the selection of models for describing the biogeochemistry of tropical and other watersheds? To ask these questions, we performed a set of tests:

- Does each constituent show similar behavior among all sites?
- Do all bedrock-derived constituents have nearly linear relations between $\log(C)$ and $\log(R)$?
- For a given river or for rivers with similar watershed geology, are the slopes similar for all bedrock-derived constituents?
- If slopes are not similar, are they arrayed according to the reactivity of the parent minerals in the soil profile, or in some other biogeochemically consistent manner?
- Do differences of slopes in the linear relations between $\log(C)$ and $\log(R)$ among rivers relate to geology, supporting an assumption that soil porosity and pore openings, and their vertical distribution, are controlled by geology?
- Is there a breakdown in the log-linear relation (curvature) at high flow, indicating that other flow paths are active?
- Do bioactive constituents show concentration-runoff relations that reflect their increased abundance in the near-surface environment due to biological activity?

Methods Used to Collect and Interpret Data

Sample Collection and Field Measurements

During the eastern Puerto Rico WEBB program, two principal types of samples were collected: grab samples, which were manually collected on a regular basis from river-banks at well-mixed cross sections near each gage site, and event samples, which were collected by an automated sampler during storm events and retrieved when weather conditions permitted. Conductivity, temperature, pH, and dissolved oxygen (O_2) of grab samples were measured onsite; only conductivity was measured onsite for event samples, because the other field measurements are unstable and thus incorrect if not measured immediately. Depth-integrated samples for suspended sediment were occasionally collected at the same time as a grab sample. All water samples were filtered through 0.2-micrometer (μm) filters as soon as practicable in the laboratory. Sample collection and processing are described in detail in appendix 2.

The automated sampler was programmed to begin sampling when the river rose above a preset stage (appendix 1). Once triggered, all 24 bottles were filled at preset times determined beforehand using representative storm hydrographs. The sampler had to be emptied and restarted manually. Thus, a small storm could prevent the sampling of a subsequent, larger storm and, consequently, trigger levels were gradually raised to ensure sampling of the largest storms. Event samples were a crucial part of the study, because only 20 grab samples were collected in the top 50 percent of runoff, and 2 in the top 10 percent, compared with thousands of event samples. This protocol allowed us to sample several massive storms during the study period, including Hurricane Hortense in September 1996, Hurricane Georges in September 1998, and a powerful upper-level trough in May 2003. Samples from these storms enabled accurate estimation of mass discharge of constituents at high runoff. Owing to the enormous volume of event samples (even after threshold stages were increased), analyses performed on event samples were eventually reduced to stable constituents that are sufficient to assess primary processes (conductivity, Si(OH)_4 , Cl^- , suspended sediment, and usually DOC and K^+).

Stream Discharge

The characterization of mass balances requires high-resolution discharge data to estimate stream discharge at the moment of sampling. The collection frequency was every 5 minutes for the Río Mameyes and every 15 minutes for the remaining rivers, and time stamps were used to match chemistry samples to discharge (appendix 1). All discharge datasets had gaps, ranging from 30 minutes to several months. Commonly the longest gaps were associated with the loss of a streamgage caused by a huge storm, and the length of the gap

reflects the time needed to rebuild the gage. The procedures for determining sample discharge and estimating missing data are described in appendix 1. Estimated data were not used in determining the relation between concentration and discharge discussed below.

Analytical Procedures

The water-quality analytical program was built around a core suite of chemical measurements: field measurements (temperature, conductivity, pH, and dissolved oxygen), major cations (Na^+ , K^+ , Mg^{2+} , and Ca^{2+}), nutrients (nitrite (NO_2^-), nitrate (NO_3^-), ammonium ion (NH_4^+), and phosphate ($-\text{PO}_4^{3-}$)), major anions (Cl^- and SO_4^{2-}), alkalinity, Si(OH)_4 , and DOC. Suspended solids were measured from the weight of filtered material per unit volume following drying to 105°Celsius (C). Sample preservation and analysis are described in appendix 2. Alkalinity, temperature, and pH were used to calculate the partial pressure of carbon dioxide, P_{CO_2} , CO_2 saturation, O_2 saturation, and the saturation index for calcite, $\text{SI}_{\text{calcite}}$, following Stumm and Morgan (1981), in grab samples (appendix 1).

Discharge, Load, Runoff, and Yield

Hydrologic and water-quality data, including several million discharge measurements, thousands of precipitation measurements (from automated rain gages), and almost 10,000 water quality samples were reprocessed for rate calculations as described in appendix 1. Constituent loads were calculated from concentrations by using the computer program LOAD ESTimator (LOADEST; Runkel and others, 2004), which estimates constituent loads in streams and rivers given a time series of stream discharge, constituent concentration, and additional explanatory variables (typically, seasonal cycles (sine and cosine of time in a one-year cycle), and time). LOADEST assists the user in developing a regression model of constituent load (calibration); the model then is used to estimate loads over a specific time interval (estimation).

The construction of the input data files used by LOADEST (Runkel and others, 2004) from our datasets was automated and required some minor adaptations (appendix 1). First, the shortest time step allowed by LOADEST for the time series of explanatory variables is 1 hour, so discharge data were resampled from 5-minute and 15-minute intervals into 1-hour intervals. Estimated Na^+ , K^+ , Mg^{2+} , Ca^{2+} , alkalinity, Cl^- , SO_4^{2-} , Si(OH)_4 , DOC, NO_3^- , NH_4^+ , $-\text{PO}_4^{3-}$, and suspended solid loads are discussed here; several more parameters (including bedrock-derived Na^+ , K^+ , Mg^{2+} , and Ca^{2+} , total dissolved silicate bedrock, total dissolved bedrock cations, suspended bedrock, and particulate organic carbon) are discussed in Stallard (2012b). Complete chemistry was more intensely sampled from 1991 through 2000, whereas Cl^- , Si(OH)_4 , K^+ , and suspended solids were sampled intensively through 2004 (table 5 in appendix 1). These changes in sampling intensity means that for most properties LOADEST is primarily being modeled on the first 10 years of data.

LOADEST is fundamentally a regression, and biases produced by the logarithmic transformation of data and non-normality of the fits to the log-transformed data can produce problems (Runkel and others, 2004). For example, alkalinity loads for the Icacos and Guabá watersheds cannot be estimated directly using LOADEST, because at highest discharge values, alkalinity is sometimes negative (acidity). Discharge, seasonal cycles, and time trends are the core explanatory variables in LOADEST. Some samples have real, but aberrant, concentrations caused by phenomena not strictly related to discharge, time, or seasonality. Some of these measurements, as discussed later in this report, were not included in load estimation; one example is high-chloride storms. These samples are summarized in appendix 1, and the effect of the excluded data on yields is discussed below.

The areas of the study watersheds range from 0.114 square kilometers (km^2) to 26.42 km^2 , so for interwatershed comparisons we converted discharge and loads to runoff rates (discharge/area) and yields (constituent load/area). Average yields were totaled, and average concentrations were calculated from average yield divided by average runoff (table 1). Data are presented both in mass units and molecular units for comparison with other datasets. Concentration data (top two sections, table 1) allow for comparison of water quality, whereas yields (bottom two sections, table 1) allow comparison of rates at which constituents are being released into the rivers.

The forested rivers are wetter (mean annual runoff 2,750 to 3,760 millimeters per year (mm yr^{-1}) than the developed watersheds (970 to 1,620 mm yr^{-1} ; table 1), so to compare samples from equivalent parts of hydrographs, runoff rates were ranked by their overall contribution to annual runoff. All water-quality samples were assigned into runoff-rate percentile classes, similar to the approach used by the U.S. Geological Survey WaterWatch website (<http://water.usgs.gov/waterwatch/>) in monitoring flood and drought conditions throughout the United States. WaterWatch ranks discharge into percentile classes based on the amount of time a river flows in a given discharge range. For this study, however, percentile classes (0–10, greater than (>)10–25, >25–50, >50–75, >75–90, >90–95, >95–99, and >99 percent) are based on runoff (for example, the 10th percentile corresponds to the runoff rate below which 10 percent of the total runoff has been discharged from the watershed; table 2). Rising and falling stage are also distinguished for each sample. The runoff rates and predicted constituent-yield rates for each percentile class of each river were calculated by using all runoff measurements for the 15-year period. Predicted constituent yields and instantaneous runoff were totaled for each percentile class, and a discharge-weighted average concentration for each percentile class was then calculated by dividing total yield for each constituent by total runoff within that class (table 3). When base flow is referred to in this text, it represents the samples in the 0-to-10 percent range. The cumulative fraction of constituent yield that corresponds to each percentile class was also calculated (table 4).

Table 1. Average constituent concentrations and yields of four watersheds during the study period (1991–2005), eastern Puerto Rico.

[DOC, dissolved organic carbon; SSOL, suspended solids; mm yr⁻¹, millimeters per year; -N, as nitrogen; -P, as phosphorus; - not applicable]

Average reporting units and watershed	Years of data	Average runoff (mm yr ⁻¹)	Na ⁺	K ⁺	Mg ²⁺	Ca ²⁺	SiO ₂	SO ₄ ²⁻	Cl ⁻	Alkalinity ¹	DOC	NO ₃ ⁻ -N	NH ₄ ⁺ -N	PO ₄ ³⁻ -P	SSOL
Mass concentration (milligrams per liter)															
Caróvanas	15	970	9.82	1.28	4.81	11.49	10.29	10.90	11.76	4.32	3.86	0.625	0.051	0.012	435
Cayaguás	15	1,620	9.55	2.13	2.05	6.17	11.48	6.95	8.99	4.63	2.88	0.705	0.038	0.018	1,302
Maneyes	15	2,750	5.30	0.72	1.54	6.39	7.54	4.67	9.97	2.95	2.50	0.133	0.010	0.005	118
Iacos	15	3,760	4.40	0.59	0.95	2.76	6.26	2.73	5.42	1.37	2.63	0.163	0.013	0.001	560
Guabá	10	3,630	4.42	0.62	0.78	2.02	6.40	1.98	6.47	1.20	2.02	0.159	0.011	0.002	569
Mole concentration (micromoles per liter)															
Caróvanas	15	970	427	33	198	287	366	908	332	45	321	45	3.7	0.40	--
Cayaguás	15	1,620	415	54	84	154	409	579	254	48	240	50	2.7	0.58	--
Maneyes	15	2,750	230	18	63	159	268	389	197	31	208	9	0.7	0.15	--
Iacos	15	3,760	192	15	39	69	223	227	153	14	219	12	1.0	0.05	--
Guabá	10	3,630	192	16	32	51	228	165	182	12	169	11	0.8	0.05	--
Mass yield (metric tons per square kilometer per year)															
Caróvanas	15	970	9.6	1.2	4.7	11.2	10.0	10.6	11.5	4.2	3.8	0.61	0.05	0.012	424
Cayaguás	15	1,620	15.5	3.4	3.3	10.0	18.6	11.3	14.6	7.5	4.7	1.14	0.06	0.029	2,109
Maneyes	15	2,750	14.6	2.0	4.2	17.6	20.7	12.9	19.2	8.1	6.9	0.37	0.03	0.013	325
Iacos	15	3,760	16.9	2.3	3.6	10.6	24.0	10.4	20.7	5.2	10.0	0.62	0.05	0.006	2,144
Guabá	10	3,630	15.1	2.1	2.7	6.9	21.9	6.8	22.1	4.1	6.9	0.54	0.04	0.006	1,944
Mole yield (kilomoles per square kilometer per year)															
Caróvanas	15	970	417	32	193	280	357	886	324	44	313	44	3.6	0.39	--
Cayaguás	15	1,620	672	88	136	249	662	937	411	78	389	82	4.4	0.94	--
Maneyes	15	2,750	634	51	174	439	739	1,071	541	85	573	26	2.1	0.41	--
Iacos	15	3,760	733	58	150	264	853	869	585	54	837	45	3.7	0.18	--
Guabá	10	3,630	657	54	109	173	779	562	623	43	576	39	2.6	0.18	--

¹Alkalinity mass concentration units are milligrams carbon per liter; alkalinity mole concentration units are microequivalents per liter; alkalinity mass-yield units are metric tons carbon per square kilometer per year; alkalinity mole-yield units are kiloequivalents per square kilometer per year.

Table 2. Runoff rates for Water, Energy, and Biogeochemical Budgets program rivers during the study period (1991–2005) at certain thresholds.

River	Minimum runoff	Percentile of annual runoff volume						Maximum runoff	
		10	25	50	75	90	95		
Runoff rate (millimeters per hour)									
Canóvanas	0.009	0.041	0.083	0.246	1.43	8.10	20.3	43.1	69.0
Cayaguás	0.020	0.073	0.114	0.270	1.79	7.76	17.9	40.6	54.8
Mameyes	0.024	0.141	0.222	0.457	1.49	4.95	11.0	43.3	89.8
Icacos	0.059	0.203	0.290	0.566	2.14	7.51	14.0	36.4	86.0
Guabá	0.036	0.196	0.287	0.477	1.84	10.92	25.5	63.7	118.8

For each constituent for each river the relation between log(concentration) and log(runoff rate) was determined using regressions on the primary data following Godsey and others (2009). In each case, a linear regression,

$$\log(C) = C_0 + C_1 \cdot \log(R)$$

was compared to a quadratic regression,

$$\log(C) = C_0 + C_1 \cdot \log(R) + C_2 \cdot \log(R)^2,$$

where C_0 , C_1 , and C_2 are regression constants. A t-test (Bevington and Robinson, 2003) was used to determine whether the slope of the linear regression, C_1 , was statistically different, with 95 percent confidence, from a zero slope (the chemostat condition). An F-test (Bevington and Robinson, 2003) was used to determine whether the quadratic regression significantly reduced the residual error, with 95 percent confidence, compared to the linear regression or to no regression. The most statistically significant regressions are indicated in table 4. Also, for reference, the constant-input and chemostat conditions of Godsey and others (2009) are provided.

The amount of variance explained by the simple regressions, as compared to LOADEST, was also compared (table 4). In all cases, LOADEST explains more of the data variance than do the simple regressions. An F-test was used to evaluate the likelihood that the LOADEST model results offer a statistically more significant explanation of the dataset.

However, dissolved constituent yields were not very different among watersheds of different geology. Yields of nonbioactive constituents derived largely from bedrock weathering (Ca^{2+} , alkalinity, Si(OH)_4), from seasalt (Cl^-), or from a mix of the two sources (Na^+ , Mg^{2+} and SO_4^{2-}) differed by a factor of less than 2 among all watersheds, showing little relation to land cover, annual runoff, or bedrock type. Nutrient yields were consistently greater in the developed watersheds, despite their lesser runoff. Most dissolved constituents have clearly defined runoff-concentration relations; however, the field measurements and several nutrients (nitrate, ammonium ion, and phosphate) do not.

Runoff Percentile Classes, Concentration, and Yield

Percentile classes correspond to equivalent parts of the hydrograph for each river, so comparing constituent yield per percentile class of runoff provides a means of comparing the relation between runoff and constituent concentration among all watersheds. The percentage of time that runoff is below each threshold in each watershed and the percentage of constituent yield discharged below that threshold are shown in table 4. Constituents are sorted by decreasing yields at 50 percent of runoff. The constituents are therefore ordered from those that are most diluted at higher discharge to those that become most concentrated. For reference, the constant-rate input (equivalent to time) and the “chemostat” input (equivalent to runoff) of Godsey and others (2009) are indicated.

Eighty-five percent of the time, the runoff in the WEBB rivers was less than half of the maximum runoff rate (the constant-rate line in table 4). For example, in the Canóvanas watershed, the lowest 50 percent of runoff rates were recorded, on average, 93.8 percent of the time, or about 342 days' worth of time in a year. The lowest 75 percent of runoff rates were recorded 99.4 percent of the time, or about 363 days' worth of time in a year. In other words, the highest 25th percentile of runoff rates was reached only for 2 days' worth of time in a year, during large storms. The lowest 50 percent of runoff rates corresponds to the export of 70.8 percent of Ca^{2+} from the Canóvanas watershed, but only 38.8 percent of DOC and 4.5 percent of suspended sediment. The lowest 90 percent of runoff rates exports only 53.7 percent of suspended sediment; that is, almost half of suspended sediment is exported when runoff exceeds the 90th percentile, during storm events that total less than 1 day per year.

Water Quality of Eastern Puerto Rico WEBB Project Watersheds

The water quality data produced during the first 15 years of the eastern Puerto Rico WEBB project are available from the U.S. Geological Survey's National Water Information System website (<http://waterdata.usgs.gov/nwis>). The results are summarized and interpreted here. Suspended-sediment yield differed greatly among the study watersheds (table 1). Yields were larger than 1,900 metric tons per square kilometer per year ($\text{t km}^{-2} \text{ yr}^{-1}$) in granitic watersheds (Icacos, Guabá, and Cayaguás), and about one-sixth this value from volcaniclastic watersheds (Mameyes and Canóvanas), independent of land cover and climate (the developed watersheds, Canóvanas and Cayaguás, are drier, having both less rainfall and runoff (Murphy and Stallard, 2012)).

Table 3. Discharge-weighted average concentrations of each percentile class estimated by using LOADEST and hourly discharge.

[DOC, dissolved organic carbon; mm h⁻¹, millimeters per hour; m³ s⁻¹, cubic meters per second; mg L⁻¹, milligrams per liter; $\mu\text{S cm}^{-1}$, microsiemens per centimeter; $\mu\text{mol L}^{-1}$, micromoles per liter; $\mu\text{eq L}^{-1}$, microequivalents per liter; ppmv, parts per million by volume]

Sample percentile class (percent)	Runoff rate (mm h ⁻¹)	Discharge (m ³ s ⁻¹)	Suspended sediment (mg L ⁻¹)	Conductivity ($\mu\text{S cm}^{-1}$)	pH ¹	Na ⁺ ($\mu\text{mol L}^{-1}$)	K ⁺ ($\mu\text{mol L}^{-1}$)	Mg ²⁺ ($\mu\text{mol L}^{-1}$)	Ca ²⁺ ($\mu\text{mol L}^{-1}$)	Si(OH) ₄ ($\mu\text{mol L}^{-1}$)	Alkalinity [$\mu\text{Eq L}^{-1}$] (μmol L ⁻¹)	Cl ⁻ ($\mu\text{mol L}^{-1}$)	SO ₄ ²⁻ ($\mu\text{mol L}^{-1}$)	NO ₃ ⁻ ($\mu\text{mol L}^{-1}$)	NH ₄ ⁺ ($\mu\text{mol L}^{-1}$)	-PO ₄ ³⁻ ($\mu\text{mol L}^{-1}$)	Partial pressure of CO ₂ (ppmv)	Saturation index of calcite	
Cároenas																			
0-10	0.021	0.149	9.8	223	8.34	713	20.6	386	564	580	2,044	459	53.8	164	11.1	2.4	0.36	565	0.21
>10-25	0.061	0.430	29.6	173	8.20	573	25.7	284	422	488	1,450	416	51.3	232	24.3	2.3	0.45	565	-0.17
>25-50	0.158	1.12	87.7	138	8.06	473	30.5	214	318	410	1,035	368	47.8	299	45.3	2.4	0.46	565	-0.55
>50-75	0.765	5.42	448	96	7.82	351	38.5	139	197	292	586	291	42.9	414	66.3	2.9	0.46	556	-1.20
>75-90	4.49	31.8	1,242	66.9	7.69	258	41.3	91.3	118	206	349	208	35.0	420	62.1	5.6	0.28	458	-1.75
>90-95	15.3	108	1,792	53.5	7.67	214	39.6	71.4	83.9	159	282	165	29.9	374	37.2	10.8	0.17	383	-1.98
>95-99	32.0	227	2,042	47.3	7.67	193	37.4	62.2	68.3	138	265	138	26.3	323	25.2	16.1	0.12	366	-2.09
>99-100	59.2	419	2,152	42.9	7.65	179	33.8	55.4	57.0	119	254	122	24.1	266	13.8	21.5	0.07	366	-2.20
Cayaguás																			
0-10	0.041	0.301	13.2	169	7.65	883	36.6	167	312	680	1,395	347	48.7	123	28.9	1.0	1.10	1,932	-0.84
>10-25	0.095	0.698	41.2	135	7.51	651	45.6	137	253	592	997	321	51.4	168	43.4	1.7	0.92	1,932	-1.20
>25-50	0.195	1.43	139.2	106	7.34	499	54.0	103	189	493	669	296	52.4	221	52.4	2.4	0.67	1,932	-1.64
>50-75	0.860	6.31	1,063	65.9	6.94	307	65.3	51.7	91.8	315	250	233	49.8	312	61.0	3.7	0.36	1,831	-2.73
>75-90	4.35	32.0	3,441	41.8	6.66	193	63.3	25.7	44.0	186	80	158	42.2	324	58.1	4.0	0.24	1,117	-3.79
>90-95	12.1	89.0	5,697	31.6	6.70	148	54.7	17.3	29.0	127	48	119	36.0	278	42.8	3.4	0.21	618	-4.14
>95-99	26.2	192	7,184	24.6	6.82	119	46.2	12.1	20.0	91.5	38	93.4	30.5	231	25.9	2.6	0.19	372	-4.28
>99-100	41.0	301	6,984	21.4	6.77	106	42.2	9.9	16.2	78.9	33	80.9	27.7	212	19.7	2.2	0.17	366	-4.46
Mameyes																			
0-10	0.068	0.339	1.6	110	7.97	379	19.1	114	320	571	914	252	43.5	80	7.0	1.0	0.36	617	-0.67
>10-25	0.179	0.884	4.8	82	7.80	295	18.7	85.1	224	372	615	227	36.7	133	7.3	0.7	0.21	617	-1.13
>25-50	0.324	1.61	12.8	68.4	7.68	254	18.4	69.7	176	296	469	209	32.9	178	8.0	0.6	0.16	617	-1.45
>50-75	0.887	4.39	56.4	51.6	7.49	202	18.1	51.0	120	205	297	184	27.8	245	9.7	0.6	0.10	608	-1.98
>75-90	2.81	13.9	217	38.5	7.32	164	18.0	35.6	77.7	139	173	157	23.0	308	12.4	0.7	0.07	526	-2.56
>90-95	7.26	36.0	567	30.9	7.18	142	18.5	26.0	53.3	98.4	106	135	19.3	358	15.2	1.1	0.06	449	-3.05
>95-99	21.2	105	1,275	25.0	7.02	123	19.1	18.6	35.6	69.8	61	114	16.1	347	20.1	1.8	0.06	374	-3.62
>99-100	45.6	226	2,054	22.3	6.87	112	19.5	15.1	27.5	53.6	42	104	14.4	320	22.8	2.6	0.06	366	-4.04

Table 3. Discharge-weighted average concentrations of each percentile class estimated by using LOADEST and hourly discharge.—Continued

[DOC, dissolved organic carbon; mm h^{-1} , millimeters per hour; $\text{m}^3 \text{s}^{-1}$, cubic meters per second; mg L^{-1} , milligrams per liter; $\mu\text{S cm}^{-1}$, microsiemens per centimeter; $\mu\text{mol L}^{-1}$, micromoles per liter; $\mu\text{eq L}^{-1}$, microequivalents per liter; ppmv, parts per million by volume]

Sample percentile class (percent)	Runoff rate (mm h^{-1})	Discharge suspended sediment ($\text{m}^3 \text{s}^{-1}$)	Conductivity ($\mu\text{S cm}^{-1}$)	pH ¹	Na^+ ($\mu\text{mol L}^{-1}$)	Mg^{2+} ($\mu\text{mol L}^{-1}$)	K^+ ($\mu\text{mol L}^{-1}$)	Ca^{2+} ($\mu\text{mol L}^{-1}$)	Si(OH)_4 ($\mu\text{Eq L}^{-1}$)	Alkalinity ($\mu\text{Eq L}^{-1}$)	Cl^- ($\mu\text{mol L}^{-1}$)	NO_3^- ($\mu\text{mol L}^{-1}$)	NH_4^+ ($\mu\text{mol L}^{-1}$)	$-\text{PO}_4^{3-}$ ($\mu\text{mol L}^{-1}$)	Partial pressure of CO_2 (ppmv)	Saturation index of calcite			
Icacos																			
0–10	0.115	0.104	3.7	61.5	6.83	283	16.4	61.7	118	475	426	191	12.2	75	14.6	1.0	0.05	4,053	-2.50
>10–25	0.252	0.228	10.9	52.9	6.72	243	16.4	53.0	97.1	331	332	182	13.6	125	13.5	1.0	0.05	4,053	-2.79
>25–50	0.429	0.389	27.7	45.7	6.62	213	16.2	45.3	80.2	256	265	167	14.3	186	12.3	1.0	0.05	4,053	-3.06
>50–75	1.197	1.08	168.7	35.8	6.46	176	15.5	33.3	55.0	154	165	147	15.5	299	11.1	1.0	0.05	3,677	-3.58
>75–90	3.96	3.59	832	25.6	6.35	135	13.9	21.3	32.5	86.5	79	118	15.7	368	10.0	0.9	0.05	2,293	-4.21
>90–95	9.04	8.18	2,105	20.1	6.31	110	12.6	15.1	21.7	59.1	41	98.7	15.3	349	9.6	0.9	0.05	1,328	-4.70
>95–99	20.8	18.8	5,637	15.6	6.38	89.9	11.1	10.2	13.9	39.8	17	80.6	14.4	285	9.1	0.9	0.05	475	-5.19
>99–100	51.6	46.7	21,372	12.8	5.46	67.6	8.8	6.3	8.0	25.8	-2	61.9	12.8	149	11.3	0.9	0.05	366	-7.37
Guabá																			
0–10	0.104	0.003	5.6	57.0	6.87	295	12.8	51.3	87.4	443	321	224	11.8	79	12.7	0.5	0.05	2,765	-2.70
>10–25	0.250	0.008	16.8	48.7	6.74	257	15.7	40.6	67.1	313	235	212	11.8	120	12.1	0.6	0.05	2,765	-3.08
>25–50	0.383	0.012	37.2	44.5	6.66	237	16.9	35.6	57.0	264	194	203	11.9	142	12.2	0.6	0.06	2,765	-3.30
>50–75	0.950	0.030	198	37.0	6.50	202	18.3	27.2	41.4	171	130	181	12.5	205	11.4	0.8	0.06	2,640	-3.76
>75–90	4.48	0.142	1,460	25.2	6.41	142	15.7	17.2	23.5	83.1	59	130	14.1	265	10.1	1.1	0.05	1,473	-4.42
>90–95	14.48	0.459	3,507	18.9	6.51	110	12.1	12.8	15.9	50.4	30	96.9	15.6	264	9.0	1.3	0.05	604	-4.76
>95–99	33.1	1.05	4,943	14.3	6.46	86.4	9.2	9.5	11.3	33.7	16	69.6	16.1	259	7.8	1.5	0.04	366	-5.22
>99–100	68.6	2.17	6,866	11.1	6.18	69.5	6.9	7.0	7.9	25.0	8	48.6	16.3	223	7.3	1.6	0.03	366	-5.93

¹pH is calculated from CO_2 vapor pressure. Grab samples collected at high runoff rates on the Icacos also indicate equilibration with the atmosphere during high-flow conditions. All rivers were assumed to change from their low-runoff-rate averages to atmospheric equilibrium at high runoff rates. The transition from low runoff rate to high runoff rate values of P_{CO_2} was assigned to the 3 to 20 mm hr^{-1} interval for which the slope of the DOC-runoff relation goes from positive to negative, indicating shallow flowpaths.

Table 4. Percentage of constituent discharged compared with percentage of water discharged (estimated by using LOADEST) and comparisons with regressions of log(concentration) to log(runoff rate).

[Constant rate, a hypothetical constituent introduced at a constant rate, independent of runoff rate; chemostat, a hypothetical constituent introduced at a rate that is proportional to runoff rate. Bold column, 50 percent runoff; bold rows, constant-rate and chemostat models; C_1 , linear regression coefficient relating log(concentration) to log(runoff); C_2 , quadratic coefficient, if quadratic regression is statistically more significant; [], values are not statistically different from zero; F-test, likelihood that the best LOADEST model offers statistically more significant explanation of data set; DOC, dissolved organic carbon; -- not applicable]

Constituent	Percentile of annual runoff volume, in percent estimated using LOAD-EST						Regression on all measurements						Regression on all measurements					
	Yield of each constituent (percent)			C_1			C_1			C_2			C_1			C_2		
	10	25	50	90	95	99	100.0	-1	--	140	1	82	1	82	2	82	2	82
Canóvanas																		
Constant rate	42.8	73.2	93.8	99.4	99.9	100.0	100.0	-1	--	140	1	82	1	82	2	82	2	82
Calcium	18.8	41.6	70.8	90.4	97.3	98.9	99.8	-0.29	--	140	1	82	1	82	2	82	2	82
Magnesium	18.5	40.8	69.3	89.1	96.6	98.5	99.8	-0.26	--	140	1	82	1	82	2	82	2	82
Silica	15.4	35.8	64.9	86.8	95.9	98.2	99.7	-0.20	--	767	1	61	9	62	6	62	6	62
Sodium	15.6	35.9	63.9	85.9	95.5	98.0	99.7	-0.18	--	140	1	80	4	81	4	81	4	81
Chloride	13.9	33.1	61.5	85.2	95.5	98.0	99.7	-0.16	--	739	1	51	9	54	76	76	76	76
Sulfate	12.1	29.5	56.5	81.4	93.8	97.2	99.6	-0.09	--	145	1	61	9	69	78	78	78	78
Phosphate	9.1	25.7	55.9	84.6	96.3	98.7	99.8	[-0.03]	--	133	1	0	8	44	100	100	100	100
Chemostat	10.0	25.0	50.0	75.0	90.0	95.0	99.0	0	--	--	--	--	--	--	--	--	--	--
Potassium	6.6	18.2	41.3	69.4	88.4	94.6	99.2	0.12	--	451	1	39	9	49	99	99	99	99
DOC	5.4	16.0	38.8	69.1	89.2	95.2	99.3	0.10	-0.12	315	2	56	8	59	--	--	--	--
Nitrate	2.8	10.6	34.7	70.2	92.7	97.3	99.7	0.05	-0.27	145	2	67	9	75	--	--	--	--
Ammonium ion	6.0	14.9	30.4	48.0	66.6	79.7	96.0	0.26	--	85	1	21	6	42	100	100	100	100
Sediment	0.2	1.0	4.5	20.4	53.7	75.0	95.8	0.74	-0.24	1,337	2	73	8	75	75	75	75	75
Gayaguás																		
Constant rate	33.9	63.7	91.1	99.0	99.9	100.0	100.0	-1	--	105	1	87	4	89	--	--	--	--
Calcium	18.8	43.3	75.7	93.3	98.3	99.3	99.9	-0.42	--	105	1	88	4	89	--	--	--	--
Magnesium	18.5	42.7	74.9	92.9	98.2	99.2	99.9	-0.40	--	105	1	88	6	43	--	--	--	--
Phosphate	17.8	41.5	72.3	89.9	96.5	98.4	99.7	-0.27	--	91	1	38	6	43	--	--	--	--
Sodium	17.3	39.7	70.7	90.3	97.0	98.7	99.8	-0.31	--	105	1	93	9	94	--	--	--	--
Silica	15.6	37.2	68.2	89.6	97.2	98.8	99.8	-0.31	--	774	1	87	9	88	--	--	--	--
Chloride	13.1	32.0	61.4	85.7	95.7	98.1	99.7	-0.20	--	785	1	78	9	85	89	89	89	89
Sulfate	10.2	26.1	53.0	79.3	93.0	96.8	99.4	-0.08	--	109	1	43	2	56	92	92	92	92
Chemostat	10.0	25.0	50.0	75.0	90.0	95.0	99.0	0	--	--	--	--	--	--	--	--	--	--
Nitrate	6.5	19.3	44.1	73.7	92.5	97.1	99.6	[-0.02]	--	105	1	1	9	31	100	100	100	100
Potassium	7.1	19.5	43.5	72.6	90.5	95.7	99.2	0.04	-0.10	395	2	42	8	44	--	--	--	--
DOC	5.8	16.3	38.1	68.7	89.0	94.9	99.1	0.12	-0.14	98	2	68	8	70	--	--	--	--
Ammonium ion	4.4	13.5	34.2	66.1	88.5	94.9	99.2	0.13	--	62	1	9	2	19	100	100	100	100
Sediment	0.1	0.5	2.5	16.8	50.5	72.4	94.1	1.03	-0.34	991	2	89	8	90	--	--	--	--
Mameyes																		
Constant rate	30.8	58.7	86.0	97.5	99.7	99.9	100.0	-1	--	141	1	42	2	45	--	--	--	--
Phosphate	19.3	41.2	69.1	88.2	96.0	98.1	99.6	-0.35	--	177	1	89	4	89	--	--	--	--
Calcium	17.6	39.1	68.1	88.9	97.0	98.8	99.8	-0.37	--	1,165	1	59	9	62	86	86	86	86
Silica	17.2	38.4	67.3	88.2	96.7	98.7	99.8	-0.34	--	177	1	85	4	86	--	--	--	--
Magnesium	16.1	36.7	65.3	87.1	96.3	98.5	99.8	-0.29	--	177	1	86	8	88	--	--	--	--
Sodium	13.6	32.2	60.1	83.8	94.9	97.8	99.6	-0.19	--	177	1	86	8	87	87	87	87	87
Sulfate	13.2	31.3	58.7	82.3	94.1	97.3	99.5	-0.17	--	179	1	86	8	87	--	--	--	--

Table 4. Percentage of constituent discharged compared with percentage of water discharged (estimated by using LOADEST) and comparisons with regressions of log(concentration) to log(runoff rate).—Continued

[Constant rate, a hypothetical constituent introduced at a constant rate, independent of runoff rate; chemostat, a hypothetical constituent introduced at a rate that is proportional to runoff rate; bold column, 50 percent runoff; bold rows, constant-rate and chemostat models; C_1 , linear regression coefficient relating log(concentration) to log(runoff); C_2 , quadratic coefficient, if quadratic regression is statistically more significant; [], values are not statistically different from zero; F-test, likelihood that the best LOADEST model offers statistically more significant explanation of data set; DOC, dissolved organic carbon; --, not applicable]

Constituent	Percentile of annual runoff volume, in percent estimated using LOAD-EST						Percentile of annual runoff volume, in percent estimated using LOAD-EST						Percentile of annual runoff volume, in percent estimated using LOAD-EST					
	10	25	50	75	90	95	99	all	C_1	C_2	Data count	Regression order	Best LOADEST model ¹	Percent variance explained	Percent variance explained	F-test LOADEST choice		
Yield of each constituent (percent)																		
Chloride	12.4	29.8	56.9	81.1	93.5	97.1	99.5	-0.14	--	1,134	1	33	9	39	100	--	--	
Potassium	10.3	25.5	50.5	75.1	89.8	94.8	98.9	[-0.00]	--	581	1	0	8	5	100	--	--	
Chemostat	10.0	25.0	50.0	75.0	90.0	95.0	99.0	0	--	--	--	--	--	--	--	--	--	
Ammonium ion	10.1	23.0	42.0	60.4	74.4	82.2	94.0	[-0.07]	--	57	1	1	2	10	100	--	--	
Nitrate	7.2	18.7	39.3	63.5	82.1	89.6	97.5	0.24	--	178	1	44	9	54	90	--	--	
DOC	4.8	14.4	34.9	62.4	83.3	91.6	98.4	0.32	-0.18	164	2	82	9	84	--	--	--	
Sediment	0.1	0.6	2.6	10.5	30.9	50.1	84.0	1.18	--	1,248	1	77	8	79	--	--	--	
Mameyes—Continued																		
Constant rate	28.0	56.3	85.6	97.6	99.6	99.9	100.0	-1	--	--	--	--	--	--	--	--	--	
Silica	18.9	42.2	72.4	91.5	97.7	99.1	99.9	-0.54	--	1,074	1	81	4	82	--	--	--	
Calcium	16.1	37.8	67.6	89.2	97.1	98.9	99.8	-0.42	--	238	1	86	6	88	--	--	--	
Magnesium	15.0	35.7	65.1	87.6	96.5	98.6	99.8	-0.35	--	237	1	85	6	88	--	--	--	
Sodium	12.8	31.1	58.9	83.0	94.5	97.6	99.6	-0.19	--	237	1	71	8	78	--	--	--	
Chloride	12.3	30.0	57.6	82.3	94.3	97.5	99.6	-0.16	--	1,104	1	38	9	52	100	--	--	
Nitrate	11.2	28.3	54.8	79.1	92.0	96.1	99.1	-0.13	--	235	1	26	9	31	90	--	--	
Ammonium ion	12.0	28.5	53.5	75.9	89.3	94.1	98.6	[-0.02]	--	136	1	0	1	0	--	--	--	
Potassium	10.7	26.7	53.1	78.5	92.3	96.5	99.4	-0.07	--	607	1	17	9	24	100	--	--	
Chemostat	10.0	25.0	50.0	75.0	90.0	95.0	99.0	0	--	--	--	--	--	--	--	--	--	
Phosphate	9.8	24.6	49.4	74.4	89.7	94.8	99.0	[0.01]	--	196	1	0	1	0	--	--	--	
Sulfate	8.2	21.7	46.2	73.6	90.5	95.6	99.3	0.03	--	238	1	6	6	20	100	--	--	
DOC	4.0	11.8	30.8	61.3	85.8	93.7	99.2	0.44	-0.32	279	2	80	9	81	--	--	--	
Sediment	0.1	0.2	1.0	5.0	19.9	35.2	67.1	1.41	--	1,408	1	89	9	91	--	--	--	
Icacos																		
Constant rate	28.5	54.9	83.5	97.9	99.8	99.9	100.0	-1	--	--	--	--	--	--	--	--	--	
Silica	19.0	41.2	71.1	92.0	98.0	99.2	99.9	-0.52	--	604	1	93	9	94	--	--	--	
Calcium	16.8	37.8	67.1	89.5	97.2	98.9	99.8	-0.34	--	160	1	88	9	90	--	--	--	
Magnesium	15.4	35.4	64.3	87.5	96.5	98.6	99.8	-0.28	--	158	1	84	9	88	--	--	--	
Sodium	14.0	33.0	61.2	85.3	95.5	98.0	99.7	-0.21	--	158	1	81	9	87	--	--	--	
Chloride	13.0	31.1	59.1	84.1	95.2	98.0	99.7	-0.20	--	640	1	60	9	70	98	--	--	
Nitrate	11.0	26.9	53.5	79.0	92.6	96.6	99.4	-0.07	--	156	1	9	7	18	100	--	--	
Potassium	10.4	26.1	52.4	78.3	92.2	96.3	99.3	0.03	-0.16	324	2	39	9	45	89	--	--	
Chemostat	10.0	25.0	50.0	75.0	90.0	95.0	99.0	0	--	--	--	--	--	--	--	--	--	
Phosphate	8.9	23.4	49.1	76.3	92.0	96.5	99.4	[-0.02]	--	112	1	2	2	4	100	--	--	
Sulfate	9.4	23.5	47.0	71.3	87.6	93.7	98.8	0.06	--	155	1	35	7	59	100	--	--	
Ammonium ion	7.0	18.4	39.1	62.8	82.3	90.4	98.0	0.17	--	60	1	18	1	18	--	--	--	
DOC	5.1	15.0	35.0	62.0	84.8	92.6	98.7	0.35	-0.24	120	2	65	9	73	--	--	--	
Sediment	0.1	0.4	1.6	6.8	36.1	62.2	91.8	1.25	--	802	1	86	8	89	--	--	--	

¹For explanation of model number, see Runkel and others, 2004, their table 7.

The increase in percentage yield of constituents listed in table 4 parallels the increase in the value of the linear regression coefficient (or slope), C_1 . The constituents with negative slopes are bedrock-weathering derived, seasalt derived, or a mix of the two (Si(OH)_4 , Ca^{2+} , Mg^{2+} , Na^{2+} , and Cl^-). Although the order varies slightly among rivers, the constituents that are most dominantly of bedrock origin, Si(OH)_4 , Ca^{2+} , and Mg^{2+} , produce more negative slopes than Na^{2+} , which has a large seasalt contribution, and Cl^- , nearly all of which is derived from seasalt. Dissolved organic carbon and suspended sediment always have a positive slope, consistent with surface flow-path inputs. Phosphate has slopes that are either negative or indistinguishable from zero, differing considerably among rivers. All remaining constituents have a mix of slopes that are zero or near zero, close to the slope of the chemostat.

Both LOADEST and simple regression models explained most of the data variance, typically more than 80 percent, in the nonbioactive bedrock-derived constituents (Si(OH)_4 , Ca^{2+} , Mg^{2+} , Na^{2+} , and Cl^- ; table 4). The models generally explained less than half the variance of bioactive constituents (K^+ , NO_3^- , NH_4^+ , and $-\text{PO}_4^{3-}$). The LOADEST model, as compared to simple regressions, significantly improved the explanation of variance for the bioactive constituents, presumably by introducing the influence of seasonality and temporal trends (LOADEST models 3–9). Ammonium ion was modeled poorly in most watersheds. Phosphate was not well modeled in the Icacos and Guabá watersheds, whereas K^+ was not well modeled in the Mameyes watershed. These results parallel similar models by Peters and others (2006) in a comparison of the Río Icacos with the four other Puerto Rico WEBB sites using the first years (1991–1997) of the present dataset. They noted that discharge variations and seasonality explained most of the variance in log(concentration) of alkalinity, Ca^{2+} , Mg^{2+} , Na^+ , Cl^- , and Si(OH)_4 , but less than half of the variance of K^+ , NO_3^- , and SO_4^{2-} ; SO_4^{2-} concentration increased with discharge.

Water-Quality Constituents

The concentration-runoff relations for various constituents (table 3) are consistent with major processes that deliver the constituents to the river—bedrock weathering, seasalt deposition, and biological activity. These relations are reviewed here. Field measurements are presented first, followed by chemical constituents, which are grouped by the major processes that regulate them.

Field Measurements

Water temperature ranges of the rivers were quite narrow (fig. 3), as air temperatures in Puerto Rico do not vary substantially year round. Generally, as runoff increases, temperature decreases. The forested watersheds (Icacos, Guabá, and Mameyes) typically had water temperature values between 18 and 25°C. The developed watersheds (Canóvanas and Cayaguás) generally had higher water temperatures—between 22

and 30°C—because they are located at lower elevations (and hence air temperatures are higher), have less water in streams, and have less riparian vegetation to shade stream channels (see cover photograph).

Dissolved oxygen concentrations of the study rivers were usually close to saturation or slightly undersaturated (fig. 3). Some samples from the Canóvanas watershed were supersaturated; this state is probably due to photosynthesis by aquatic vegetation, which produces oxygen and consumes carbon dioxide during daylight hours (when grab samples were collected). Respiration and decomposition, which continue 24 hours a day, consume oxygen and produce carbon dioxide; therefore, O_2 levels are likely lower at night. The effects of photosynthesis and its relation to carbonate dynamics in the streams are further discussed later in section Alkalinity, Carbon Dioxide, and Calcite Saturation of this chapter.

The pH values of study rivers were typically circumneutral, between 6 and 8. Generally, pH of the study rivers decreases with increasing runoff (fig. 3). The granitic watersheds had the lowest pH values; the forested watersheds (Icacos and Guabá) were of lower pH than the developed watershed (Cayaguás). Highest pH values, as much as 9, were observed in the developed, volcaniclastic Canóvanas. These high pH values are likely related to both the higher alkalinity of the Río Canóvanas (discussed in section Alkalinity, Carbon Dioxide, and Calcite Saturation of this chapter) and to sampling times. Grab samples were always collected during the day, when photosynthesis produces oxygen and consumes carbon dioxide, leading to an increase in pH. Therefore, water likely was sampled when pH values were at a maximum for the day.

Conductivity values, which are affected by all dissolved ions regardless of source, ranged from about 10 to 300 microsiemens per centimeter ($\mu\text{S cm}^{-1}$). Values were generally lowest in the forested watersheds, and values in the granitic watersheds (Icacos and Guabá) were lower than in the volcaniclastic watershed (Mameyes) (fig. 3). Highest conductivity values were observed in the volcaniclastic, developed Canóvanas watershed. This general pattern was repeated for almost all constituents: at a given runoff rate, forested streams were more dilute. In the pH range of the watersheds, conductivity was a conservative property that generally decreased with increasing runoff, as shallower flow paths during storms decrease the concentrations of constituents that dominate conductivity measurements (such as Cl^- and Na^+). High-chloride samples were a notable exception to this trend, as discussed in a later section entitled “Chloride.”

Silica

Dissolved Si(OH)_4 is derived primarily from the weathering of silicate minerals in bedrock and soil. Dissolved Si(OH)_4 concentrations decreased markedly with increasing runoff in all eastern Puerto Rico WEBB rivers (fig. 4). This decrease is consistent with the concept that an ever-larger portion of water moves through shallower flow paths, and they hence have less

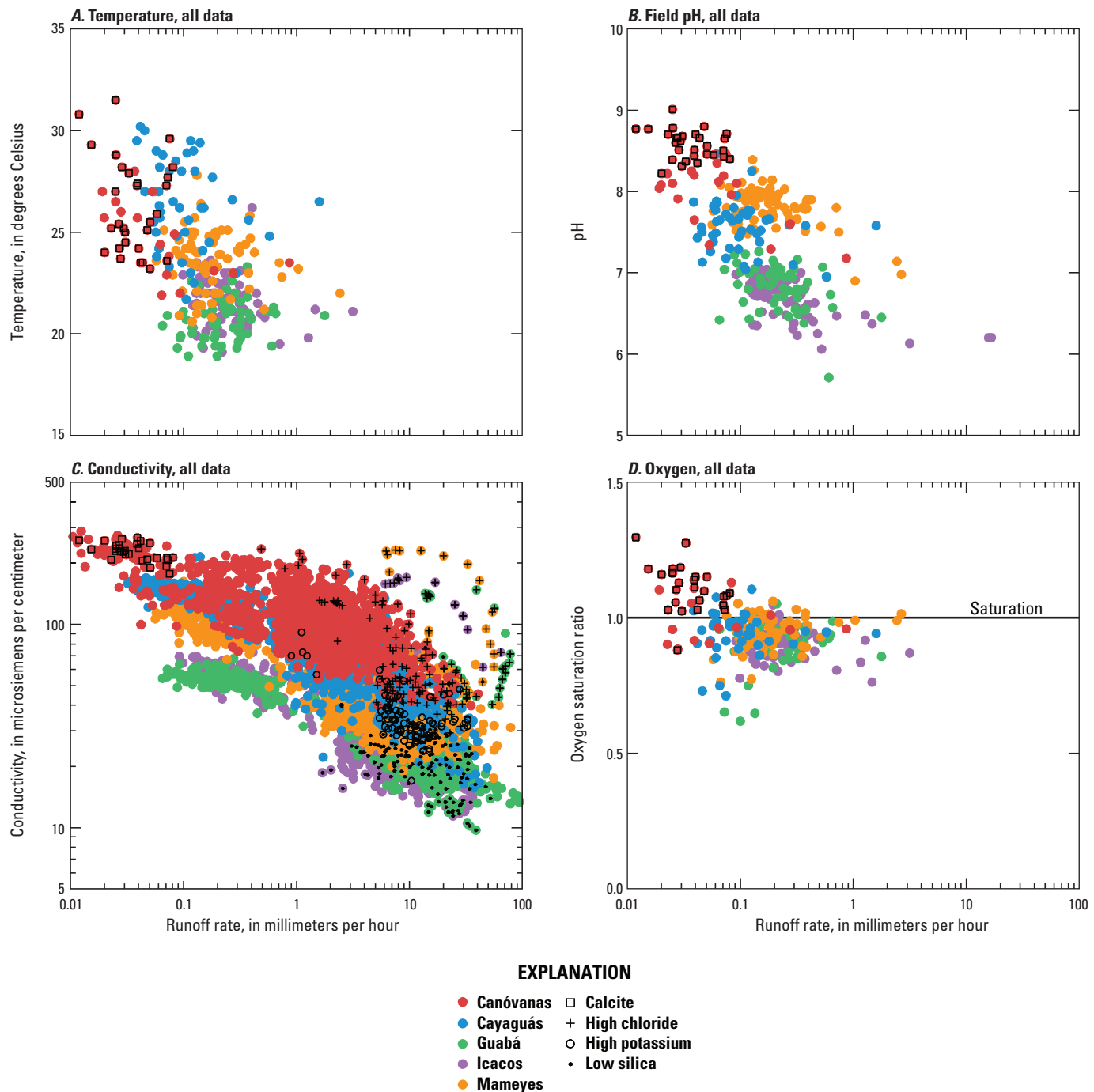


Figure 3. Temperature, pH, conductivity, and dissolved oxygen in the eastern Puerto Rico Water, Energy, and Biogeochemical Budget program rivers, 1991–2005. Additional sample characteristics are indicated with black symbols: calcite, samples supersaturated with respect to calcite; high chloride, samples with exceptionally high chloride concentrations collected during huge storms; high potassium, samples with high potassium but not high chloride; low silica, Icacos and Guabá samples with unusually low silica concentrations for the runoff rate.

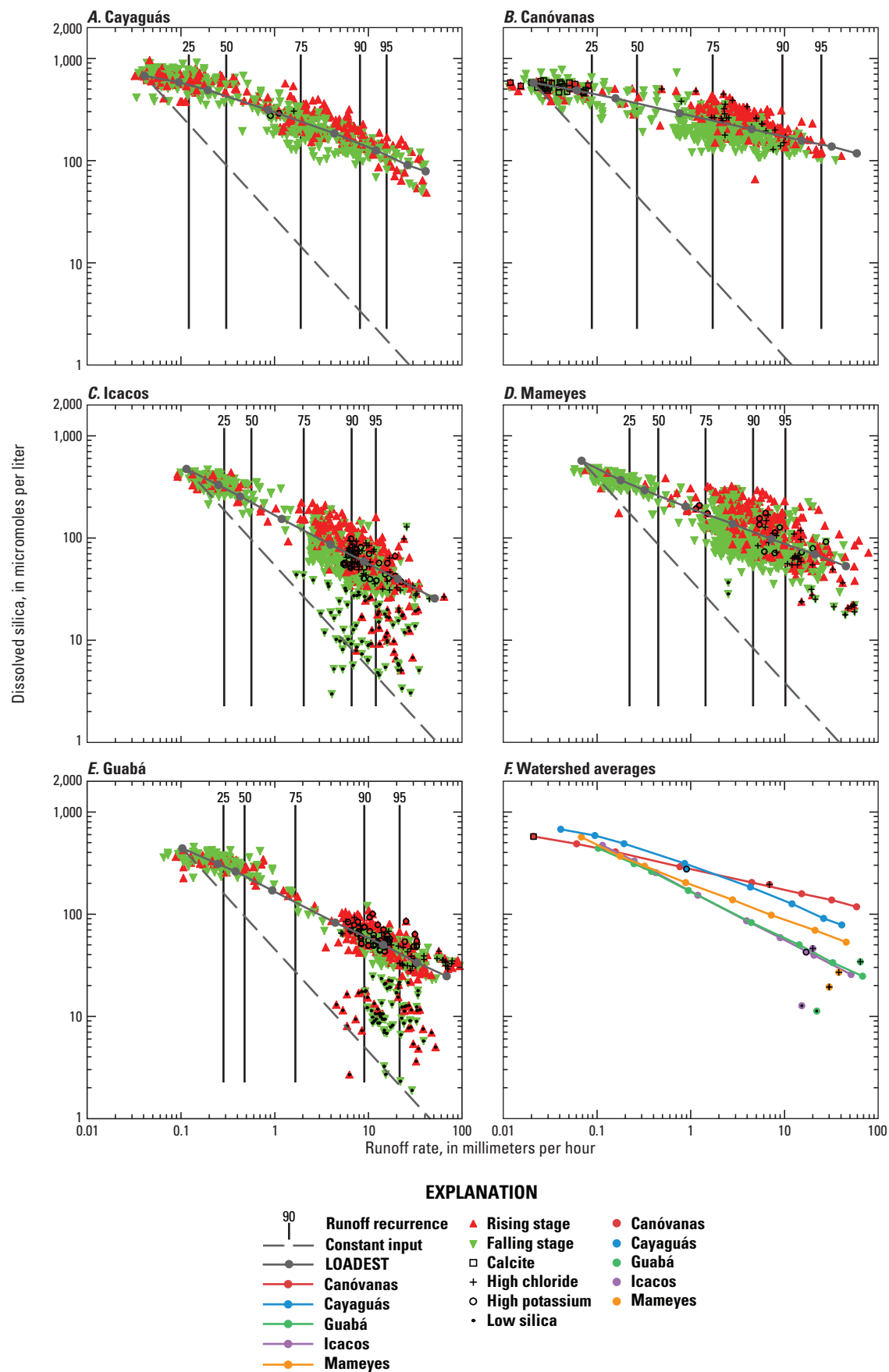


Figure 4 (facing page). Runoff rate-concentration graphs for dissolved silica. Samples in individual rivers are keyed according to runoff percentile class. Averages for runoff percentile class, estimated using LOADEST (see table 3) are indicated in the lower left diagram. Additional sample characteristics are indicated with black symbols: calcite, samples supersaturated with respect to calcite; high chloride, samples with exceptionally high chloride concentrations collected during huge storms; high potassium, samples with high potassium but not high chloride; low silica, Icacos and Guabá samples with unusually low silica concentrations for the runoff rate. The points separated from the watershed-average curves (F) represent the averages of the classes of sample indicated by the superimposed character. These samples are not included in LOADEST models.

contact with deep soil and bedrock, with increasing rainfall and runoff (see Elsenbeer, 2001). Although the Luquillo Mountains receive, on a long-term annual average, about $21 \pm 7 \text{ t km}^{-2} \text{ yr}^{-1}$ of Saharan desert dust (Pett-Ridge and others, 2009b), the dust likely does not contribute substantially to dissolved Si(OH)_4 . More than 85 percent of the dust is composed of aluminosilicate clay minerals (such as illite, kaolinite, and montmorillonite), quartz, and amorphous silicon (Reid and others, 2003), which rather than contributing to dissolved load in rivers would contribute to the solid phases in soils, as has been observed on carbonate islands such as Bermuda (Herwitz and others, 1996). The dust contribution is also small compared to suspended-solid yields, which range from about 320 to $2,100 \text{ t km}^{-2} \text{ yr}^{-1}$ (table 1).

The slope, C_1 , of the regression of the relation of $\log(\text{Si(OH)}_4)$ to $\log(R)$ is least negative in the Canóvanas watershed and most negative in the Icacos and Guabá (table 4) watersheds. These slopes are more negative than the slope (C_1) of most rivers studied by Godsey and others (2009), indicating less of a chemostat-like response (more dilution). Regressions on the primary data demonstrate no curvature.

Unusually low Si(OH)_4 concentrations were observed in the granitic, forested Icacos watershed (and its subwatershed, the Guabá) on the falling stage of some high-runoff hurricanes and frontal storms (fig. 4 and appendix 1, figs. 4, 5). Some samples (which plot below the constant-input line anchored to average base flow; see fig. 4) had Si(OH)_4 yields that were even less than base flow yields, indicating that water that would normally drain from deep in the soil was not doing so during these events. Such low- Si(OH)_4 events were not observed, even during the same storms, in the volcaniclastic watersheds (Mameyes and Canóvanas) or in the granitic watershed with an agricultural land-use history (Cayaguás). Soils on the volcaniclastic rocks are more dense, clay-rich, and less permeable (Murphy and Stallard, 2012), whereas the Cayaguás watershed has been deeply eroded and trampled by cattle (Brown and others, 1998; Larsen and Santiago-Román, 2001); it is possible that the mechanism for low- Si(OH)_4 waters involves soil porosity. Yield reductions indicate that pathways for

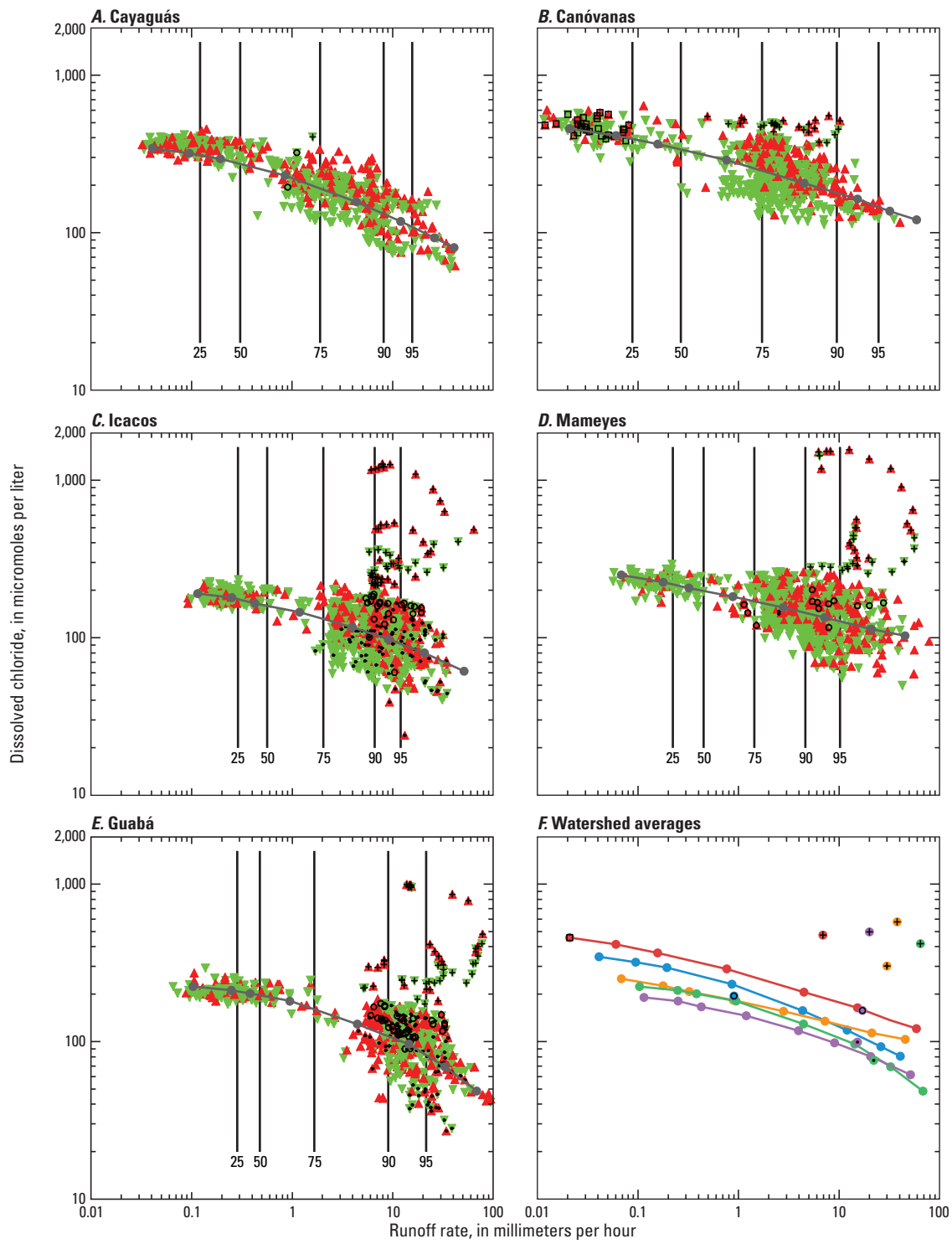
deeper groundwater flow in the forested, granitic watersheds were being restricted or even reversed during such storms. It is possible that sediment or litterfall is mobilized in such a way that shallow soil pore spaces in lower slopes and along channels, including macropores, become clogged. This clogging would lead to decreased groundwater seepage and hence lower Si(OH)_4 concentrations. Most of the low- Si(OH)_4 events occurred prior to the 1998 Hurricane Georges (which was not a low- Si(OH)_4 event). Georges was a category 2 hurricane that struck eastern Puerto Rico directly and caused substantial forest damage (Lugo and Frangi, 2003). This damage may have led to changes in soil properties and flow paths. It is also possible that earthworms, which are quite active in these forests (Larsen and others, 2012) and increase soil porosity, may have had their activity reduced by Georges. Finally, it is possible that low- Si(OH)_4 events may have occurred, but were not sampled, following Georges. Regardless of the reason, because of their occasional and enigmatic nature, the low- Si(OH)_4 events were excluded from the LOADEST calculations.

Chloride

Chloride is derived almost exclusively from seasalt entrained in the atmosphere, and it is primarily deposited as rain (rather than as dry deposition) in the Luquillo Mountains (Heartsill-Scalley and others, 2007; Stallard, 2012a). As with Si(OH)_4 , Cl^- concentrations typically decrease with increasing runoff in all eastern Puerto Rico WEBB rivers (fig. 5), because a greater proportion of stream water is derived from shallow and overland flow paths, rather than from base flow, during large storms. Base flow contains higher Cl^- concentrations than average rainwater (Stallard, 2012a) because evaporation and transpiration concentrate Cl^- in waters moving downward through the canopy, surface soil, and rooting zone. During high-runoff events, water passing quickly overland and through shallow soils is subjected to proportionately less evaporation and transpiration than during small events (fig. 2). Average Cl^- concentrations are typically greatest in the developed Canóvanas and Cayaguás watersheds (fig. 5). These watershed are drier and have a greater ratio of evapotranspiration to runoff (Murphy and Stallard, 2012), which may concentrate the seasalt contribution.

Because Cl^- does not have a bedrock source, the negative slopes (C_1) of the regression of $\log(\text{Cl}^-)$ and $\log(R)$ (table 4) must reflect dilution of the aged, evaporated water by active storms. The range of slopes is quite narrow, -0.20 to -0.14 , presumably reflecting a similar style of mixing among all the watersheds.

Exceptionally high Cl^- concentrations, as much as an order of magnitude greater than average, were recorded in the Mameyes, Icacos, and Guabá watersheds at high runoff rates, primarily during some hurricanes and also during some frontal storms (fig. 5). During Hurricane Georges, a quantity of Cl^- roughly equivalent to 0.3 millimeters (mm) of seawater was deposited over the entire Mameyes watershed (Stallard, 2012a). The Cayaguás watershed, which is leeward of the

**EXPLANATION**

90	Runoff recurrence	▲ Rising stage	● Canóvanas
—●— LOADEST	▼ Falling stage	● Cayaguás	● Cayaguás
—○— Canóvanas	□ Calcite	● Guabá	● Guabá
—●— Cayaguás	+ High chloride	● Icacos	● Icacos
—●— Guabá	○ High potassium	● Mameyes	● Mameyes
—●— Icacos	• Low silica		
—●— Mameyes			

Figure 5 (facing page). Runoff rate-concentration graphs for chloride. Additional sample characteristics are indicated with black symbols: calcite, samples supersaturated with respect to calcite; high chloride, samples with exceptionally high chloride concentrations collected during huge storms; high potassium, samples with high potassium but not high chloride; low silica, Icacos and Guabá samples with unusually low silica concentrations for the runoff rate. The points separated from the watershed-average curves (F) represent the averages of the classes of sample indicated by the superimposed character. These samples are not included in LOADEST models.

Luquillo Mountains and is the farthest inland of the Puerto Rico WEBB watersheds, did not demonstrate any high-Cl⁻ events; the Canóvanas, on the western flank of the mountains, demonstrated subdued events. This pattern suggests that most of the high-Cl⁻ rainwater is deposited on the windward side of the Luquillo Mountains. Substantial atmospheric loadings of Cl⁻ (along with Na⁺, NO₃⁻ and SO₄²⁻) to the Icacos watershed were also noted by Peters and others (2006). Presumably, the high concentrations are related to high winds and breaking waves in the ocean upwind of the watersheds (Stallard, 2012a). Because the high-Cl⁻ events have no relation to the explanatory variables (discharge, time, and seasonality) used in LOADEST, they were excluded from the LOADEST regressions. Our estimates of yields of Cl⁻ and all constituents associated with seasalt are therefore slightly lower than if high-Cl⁻ samples were included. We do not know how much lower, because the National Atmospheric Deposition Program dataset (which was used to estimate Cl⁻ inputs) has major data gaps, many during storms (including Hurricane Georges); however, the overall error appears to be small (Stallard, 2012a).

Calcium, Magnesium, and Sodium

Dissolved Ca²⁺, Mg²⁺ and Na⁺ are dominated by a bedrock weathering source, but they can have appreciable atmospheric inputs from seasalt (Mg²⁺ and Na⁺) or minor soluble desert dust (Ca²⁺) (Stallard, 2012a). The concentrations of Ca²⁺, Mg²⁺, and Na⁺ in all of the study watersheds usually decreased with increasing runoff (fig. 6, table 3), and falling stages tended to have lower concentrations than rising stages. Stream samples from the Mameyes and Canóvanas watersheds contained distinctly elevated Ca²⁺ concentrations compared with the other study watersheds, and the Canóvanas also contains contained elevated Mg²⁺ (fig. 6). The bedrock of these volcaniclastic watersheds is somewhat richer in Ca²⁺-bearing and Mg²⁺-bearing silicate minerals than the granitic watersheds (Jolly and others, 1998; Smith and others, 1998; Stallard, 2012b). Minor bedrock carbonate minerals, which can be a source of abundant Ca²⁺ and sometimes Mg²⁺ (Stallard, 1995a,b), have been documented in the bedrock units underlying the Canóvanas and Mameyes watersheds (Murphy

and others, 2012). Rivers draining carbonate-rich watersheds in western Puerto Rico demonstrated only minor drops in conductivity through major storm events (Haire, 1972) because carbonate rocks dissolve rapidly. All eastern Puerto Rico WEBB watersheds, in contrast, showed decreases in conductivity with increasing runoff (fig. 3), suggesting that the elevated Ca²⁺ and Mg²⁺ were not caused by the carbonate minerals but rather by the silicate minerals.

Sodium concentrations, similar to concentrations of Cl⁻, were typically highest in the developed Canóvanas and Cayaguás watersheds. This pattern may be due to a greater ratio of evapotranspiration to runoff in these drier watersheds (Murphy and Stallard, 2012), which would concentrate the seasalt contribution, or due to domestic inputs (or both). Low-Si(OH)₄ samples tended to also have slightly lower Ca²⁺ (fig. 6), although the effect was not pronounced, indicating that the mechanism causing low Si(OH)₄ may affect other bedrock-derived constituents.

All three cations demonstrate high concentrations during the high-runoff, high-Cl⁻ events discussed earlier in the Chloride section. Accordingly, the cation concentration data for these samples were excluded from the LOADEST calculations and regressions.

For all study watersheds, comparison of the slopes (C_1) of Ca²⁺, Mg²⁺, Na⁺, and Cl⁻ for the regression of log(C) and log(R) demonstrates that the slope of Ca²⁺ is the most negative, followed by Mg²⁺, then Na⁺, and finally Cl⁻ (table 4). This order represents a continuous variation from constituents derived primarily from bedrock weathering to those derived from seasalt, and it is consistent with a mix of the two sources: bedrock weathering deep in the profile, and evaporated rainfall, distributed more widely through the soil profile.

Dissolved Organic Carbon

Dissolved organic carbon is uniquely derived from plant material, either as the product of breakdown or as exudates (Stumm and Morgan, 1981). The ultimate source of DOC is atmospheric carbon dioxide fixed through photosynthesis. DOC was slightly greater in the developed watersheds, perhaps reflecting the differences in land cover or the effects of agricultural on soils. For all watersheds, DOC concentrations increased with increasing runoff rates and reached a rough peak in the 75 to 90 percent or 90 to 95 percent runoff percentiles (table 3). At the very highest runoff rates, DOC concentrations tended to decrease, and differences among the watersheds lessened (fig. 7). This trend was also observed by Shanley and others (2011), who used other sources to extend the present dataset for the Icacos watershed from 1981 to 2008.

The decrease in concentrations at high runoff could imply a supply limitation, whereby the processes that generate and release DOC cannot supply it at a rate that compensates for the increased throughput of water. However, DOC concentrations are highest on falling stages (fig. 7), opposite to what is expected from a supply limitation.

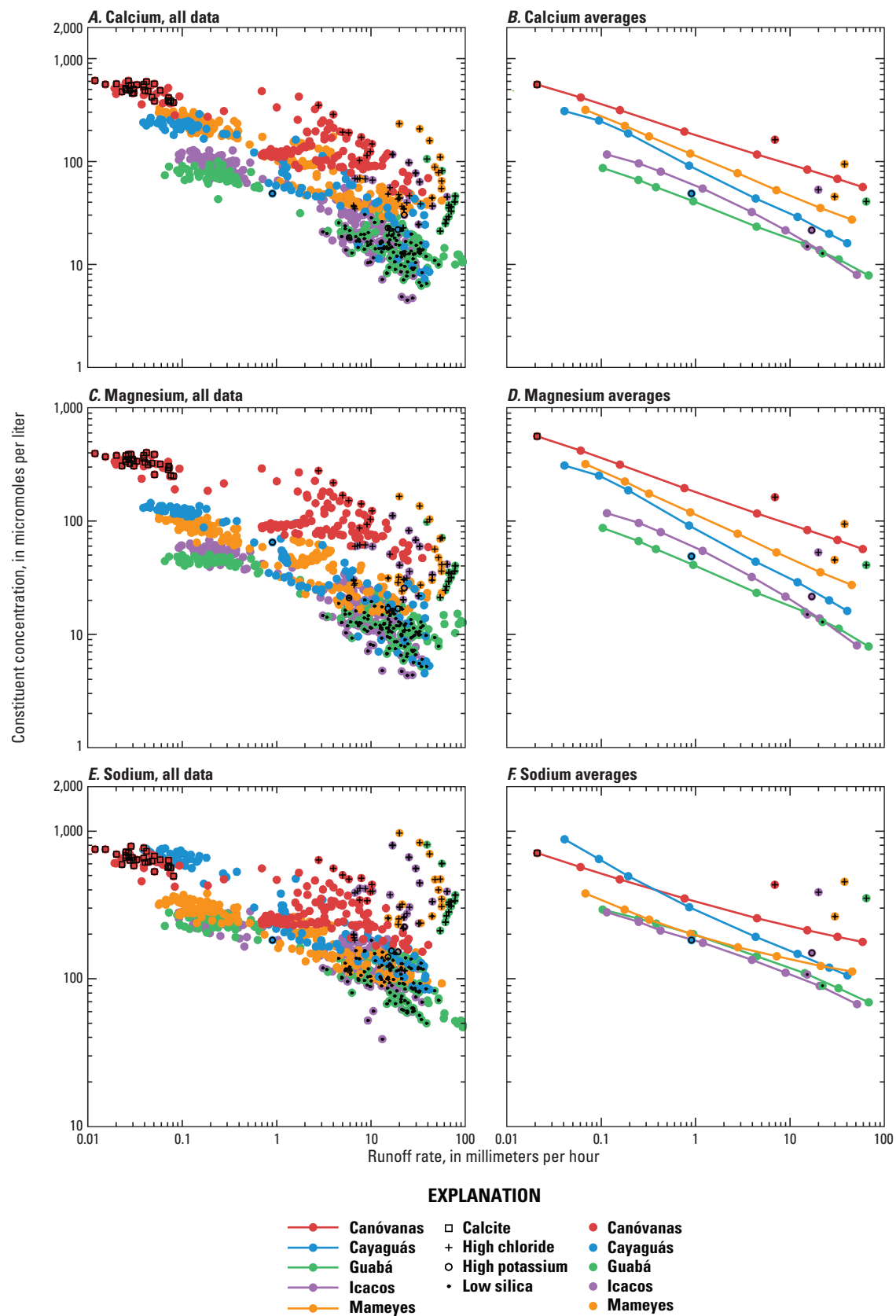


Figure 6 (facing page). Runoff rate-concentration graphs for calcium, magnesium, and sodium ions. The left diagrams represent the Water, Energy, and Biogeochemical Budget program dataset. The right diagrams represent averages calculated from hourly estimates determined using LOADEST. Additional sample characteristics are indicated with black symbols; calcite, samples supersaturated with respect to calcite; high chloride, samples with exceptionally high chloride concentrations collected during huge storms; high potassium, samples with high potassium but not high chloride; low silica, Icacos and Guabá samples with unusually low silica concentrations for the runoff rate. The points separated from the watershed-average curves (B, D, F) represent the averages of the classes of sample indicated by the superimposed character. These samples are not included in LOADEST models.

Alternatively, a DOC decrease with increasing runoff rate may reflect a change to flow paths that involves less interaction and contact time with soil organic matter. At lowest runoff rates, stream water has moved through deep soils, deeper riparian zones, and hyporheic zones (fig. 2). With the exception of the hyporheic zone, these zones contain relatively little organic matter. At intermediate runoff rates, more water is presumably moving through shallow-soil pathways and riparian zones which, if present, are likely to be flooding; this flooding would represent optimum conditions for interacting with shallow-soil organic matter. Finally, at the highest runoff rates, overland flow is important because it reduces the overall interaction of water with organic matter. At runoff rates of roughly 3 to 10 mm h⁻¹ DOC concentrations begin their substantial decline, reflected by the downward curvature of diagrams shown in fig. 7. This decline suggests that this range of runoff rates may mark a transition to a regime where overland flow and associated reduced soil interaction become important. Regardless of the mechanism, these data show that the highest discharge classes (greater than 90 percent) must be included when one calculates DOC loads and yields from watersheds. Without the high-runoff data, yields will be overestimated.

The curves of averaged concentrations based on LOADEST calculations do not always pass through the middle of the concentration-data field at middle-range runoff rates (fig. 7). A likely factor is the lower collection density of middle-range runoff samples (appendix 1), which will not alias the regression residual as strongly.

For every study river, the regression of log(DOC) on log(*R*), using the primary data, has statistically significant downward curvature. The position of the peak is calculated for the zero of the first derivative

$$\text{Peak} = 10^{(-C_1/(2 \cdot C_2))}$$

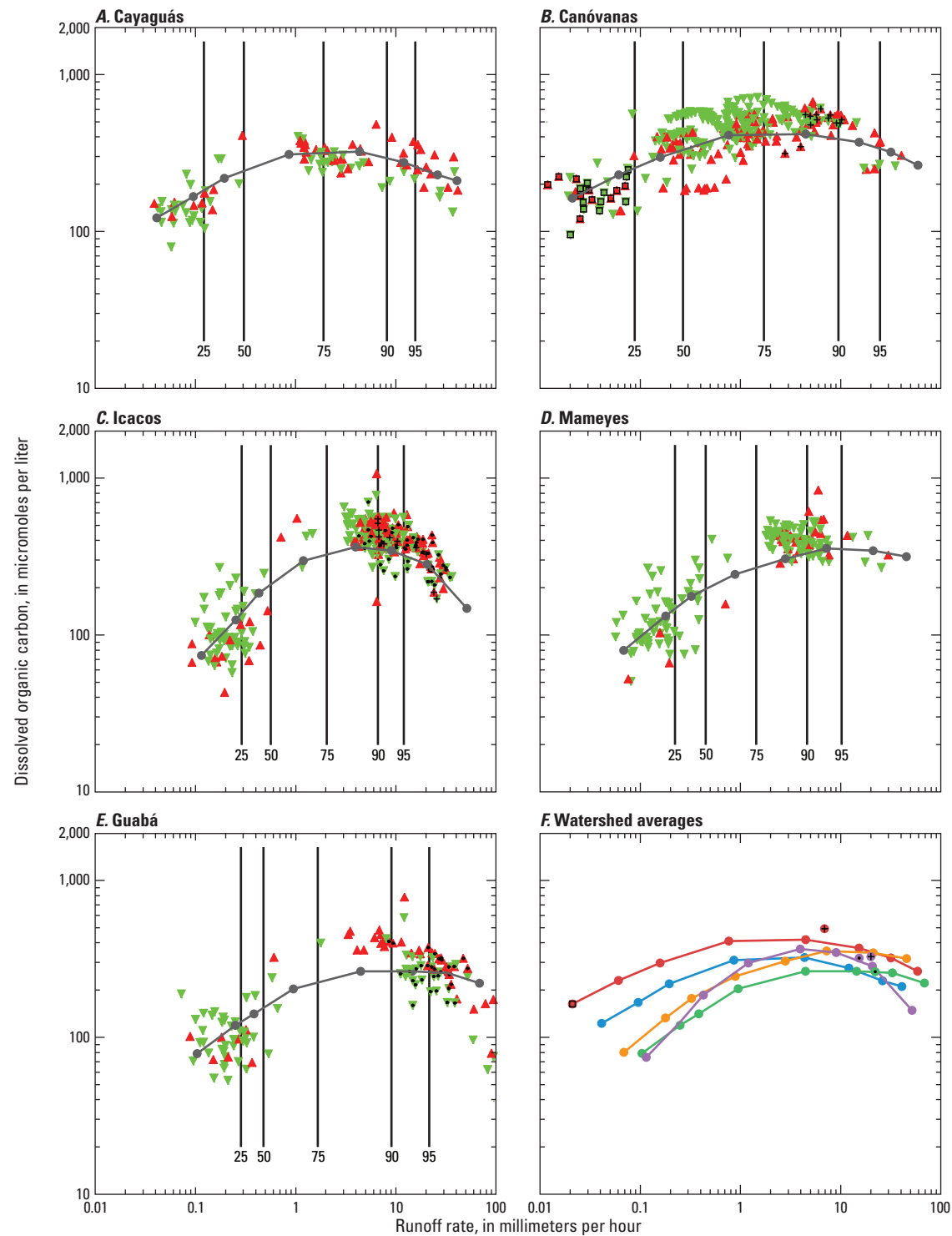
and peaks range from 2.5 mm h⁻¹ to 8.6 mm h⁻¹.

The Nutrients: Nitrate, Ammonium Ion, Phosphate, and Potassium

Nitrate, NH₄⁺, -PO₄³⁻ and K⁺ are considered to be the principal plant nutrients. Of these, throughfall is especially enriched in NH₄⁺, -PO₄³⁻ and K⁺ when compared with rainwater (Heartsill-Scalley, 2007). Nitrate and NH₄⁺ have atmospheric sources, either dissolved in precipitation or as a result of plant fixation. Both can be lost from a watershed by conversion back to gaseous forms. Phosphate is primarily derived from bedrock, but it can also be deposited in eastern Puerto Rico as Saharan dust (Pett-Ridge and others, 2009b). Phosphate is an important plant nutrient that is also easily sequestered by chemical reactions with Al³⁺ or Fe³⁺ ions; distinguishing these two mechanisms of -PO₄³⁻ removal is difficult. Potassium is mostly bedrock derived but can also be atmospherically deposited in seasalt (some K⁺ arrives in Saharan dust, but in the form of insoluble clay minerals; Reid and others, 2003). Potassium and NH₄⁺ can be weakly held on cation-exchange sites in soil. In the developed watersheds, all of these nutrients can be added by manmade products such as fertilizers or by domestic or industrial wastes.

The runoff-concentration relations for K⁺, NO₃⁻, NH₄⁺, and -PO₄³⁻ sometimes demonstrate considerable scatter (figs. 8, 9), and diagrams of these relations do not demonstrate the steeply decreasing curves observed for Si(OH)₄, Cl⁻, Ca²⁺, Mg²⁺, and Na⁺. For each nutrient at almost every runoff rate, the concentration-runoff curves representing the developed watersheds (Canóvanas and Cayaguás) illustrate substantially higher concentrations than those representing the forested watersheds (figs. 8, 9); it is likely that this difference reflects human inputs, such as fertilizers or agricultural and domestic wastes. Precise identification of sources would require detailed surveys that were not part of this study.

A number of high-runoff samples from the Mameyes, Icacos, and Guabá watersheds demonstrated elevated K⁺ concentrations (fig. 8). These samples, however, did not have high concentrations of Cl⁻, so elevated K⁺ probably was not caused by windblown seasalt. These high-K⁺ events were recorded in the Icacos and Guabá watersheds only during the year after Hurricane Georges (1998–1999) and in the Mameyes watershed mostly after Georges (appendix 1, figs. 1–5). After Hurricane Hugo in 1989, stream-water concentrations of K⁺, NO₃⁻, and NH₄⁺ doubled and remained elevated for almost 2 years; K⁺ and NO₃⁻ returned to average concentrations at the same time that the canopy recovered, suggesting biological control on the cycling of these ions (Schaefer and others, 2000; concentrations of Na⁺, Mg²⁺, Ca²⁺, Cl⁻, and SO₄²⁻ showed little effect). The elevated K⁺ concentrations are consistent with other post-Hurricane Georges observations that indicate the release of K⁺ from litter (Ostertag and others, 2003). The high-K⁺ events in this study, however, did not appear to be associated with higher concentrations of either -PO₄³⁻ or NH₄⁺; also, not all the storms in the year following the hurricane resulted in high K⁺ concentrations. It is possible that the absence of high concentrations of either -PO₄³⁻ or NH₄⁺ was a sampling

**EXPLANATION**

- | | | | |
|-----|-------------------|------------------|-------------|
| — | Runoff recurrence | ▲ Rising stage | ● Canóvanas |
| —●— | LOADEST | ▼ Falling stage | ● Cayaguás |
| —○— | Canóvanas | □ Calcite | ● Guabá |
| —●— | Cayaguás | + High chloride | ● Icacos |
| —●— | Guabá | ○ High potassium | ● Mameyes |
| —●— | Icacos | ● Low silica | |
| —●— | Mameyes | | |

Figure 7 (facing page). Runoff rate-concentration graphs for dissolved organic carbon. Additional sample characteristics are indicated with black symbols: calcite, samples supersaturated with respect to calcite; high chloride, samples with exceptionally high chloride concentrations collected during huge storms; high potassium, samples with high potassium but not high chloride; low silica, Icacos and Guabá samples with unusually low silica concentrations for the runoff rate. The points separated from the watershed-average (F) curves represent the averages of the classes of sample indicated by the superimposed character.

artifact, because K^+ was analyzed in considerably more samples than $-PO_4^{3-}$ or NH_4^+ , and analytical errors for K^+ are relatively smaller (appendix 2).

Some samples from the Icacos, Guabá, and Mameyes watersheds demonstrated especially low NO_3^- concentrations (fig. 9). These samples, which were collected during hurricanes, also always have high Cl^- concentrations. Hurricanes derive their energy and moisture from maritime air masses that presumably lack a strong contribution of pollutants, such as NO_3^- , from continents.

Regardless of the reason, because of their occasional and enigmatic nature, the high- K^+ samples and low- NO_3^- samples collected during high- Cl^- events have no obvious relation to the explanatory variables used in LOADEST, so these solutes for these samples were excluded from the LOADEST calculations.

Sulfate

Sulfur derives from a complex array of geologic and atmospheric sources. Geologic sources include reduced sulfur from sulfides, pyrite, and (rarely) elemental sulfur, and from sulfate salts from minerals such as anhydrite and gypsum. Minor sulfides and pyrite are found in small mineralized zones surrounding the Río Blanco intrusion in the Luquillo Mountains (Murphy and others, 2012). Atmospheric sources of sulfur include seasalt, Saharan dust (in the form of anhydrite and gypsum; Reid and others, 2003), volcanic eruptions, burning of fossil fuels, and reduced sulfur gases from marine and terrestrial sources (Stallard and Edmond, 1981; Andreae and Andreae, 1988; Stallard, 2012a). Atmospheric sulfur is deposited as SO_4^{2-} . Sulfur, like organic carbon, NO_3^- , and NH_4^+ , can be lost from a watershed as a gas (Stallard, 2012a).

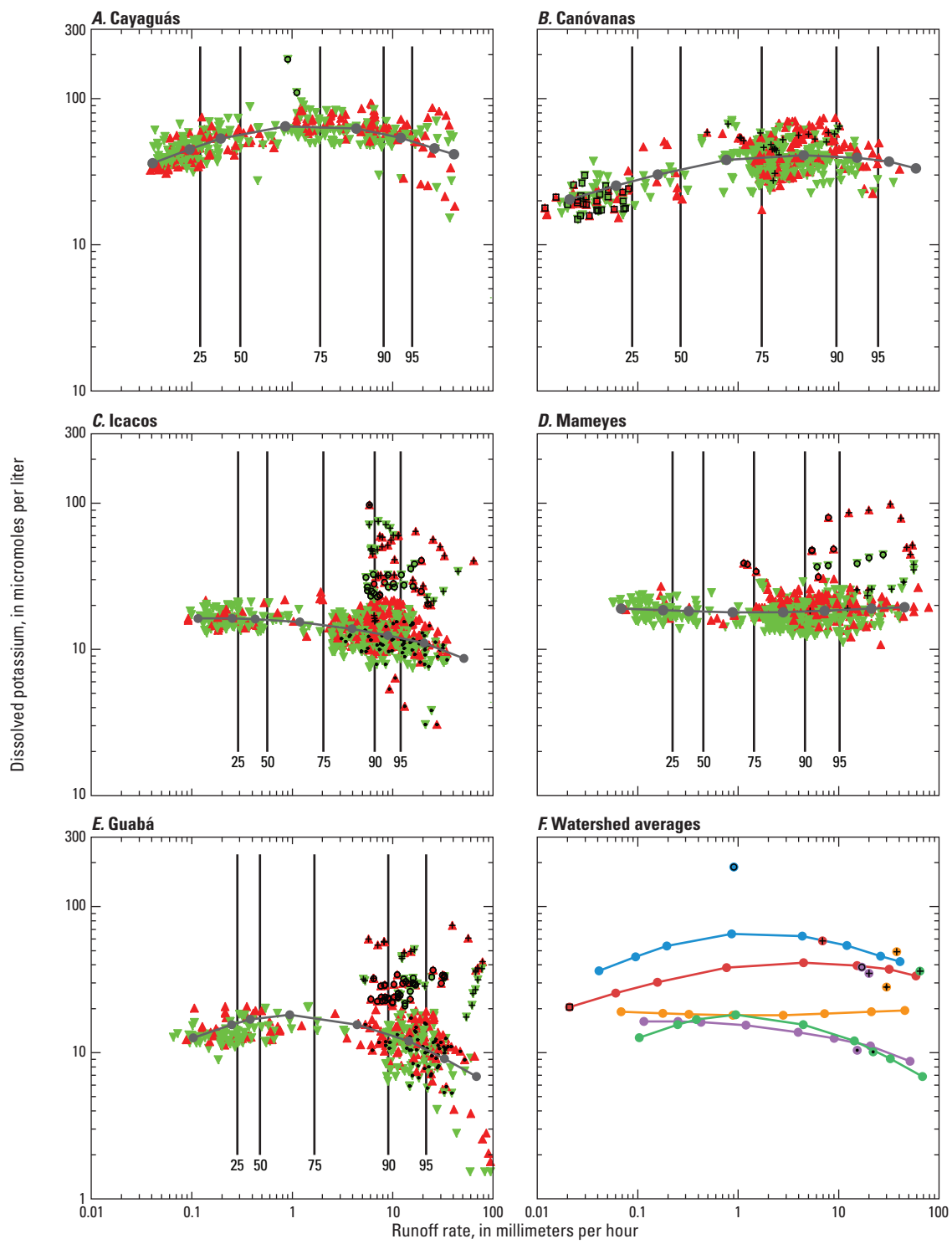
The runoff-concentration relations for SO_4^{2-} in the Puerto Rico WEBB watersheds differed substantially (fig. 10). Sulfate concentrations were generally lowest in the forested, granitic watersheds (Icacos and Guabá) and highest in the developed watersheds (Canóvanas and Cayaguás). Sulfur concentrations in the forested, volcaniclastic Mameyes watershed were similar to those in the developed watersheds at low runoff rates, but at high runoff rates, concentrations were similar to those in the Icacos and Guabá watersheds (fig. 10). The Icacos and Guabá watersheds have runoff-concentration curves that

are relatively flat (similar to the curves of DOC and nutrients), whereas SO_4^{2-} concentrations in the remaining watersheds decrease with increasing runoff (similar to the constituents that are not particularly bioactive and have substantial bedrock and atmospheric sources: Na^+ , Mg^{2+} , and Ca^{2+}). Owing to the low level of human activity in the Mameyes watershed, the high concentrations at low runoff probably reflected a geologic source. It is hard to say whether the high concentrations at low discharge in the Canóvanas and Cayaguás are entirely natural or are influenced by minor contamination, because without detailed investigation, it would be difficult to distinguish an exclusively geologic source from one with added human inputs, such as fertilizers.

Sulfate-to- Cl^- ratios provide information about sources of sulfur (Stallard and Edmond, 1981). The SO_4^{2-} -to- Cl^- mole ratio of seasalt, 0.051, is the lowest of all SO_4^{2-} sources; precipitation in eastern Puerto Rico has a higher average SO_4^{2-} -to- Cl^- ratio (about 0.106), because it contains not only seasalt but also sulfur from gas phase and dust sources (Stallard, 2012a). Sulfate-to- Cl^- ratios in stream samples from the developed, farther-inland watersheds (Canóvanas and Cayaguás) are always greater than the rainfall ratio and increase with runoff, perhaps reflecting an increased contribution of SO_4^{2-} from vegetation or agricultural fertilizers (fig. 10). The forested, volcaniclastic Mameyes watershed also has SO_4^{2-} -to- Cl^- ratios greater than the rainfall ratio (except for high Cl^- events), but these ratios decrease slightly with increasing runoff. The SO_4^{2-} -to- Cl^- ratios in samples from the forested, granitic watersheds (Icacos and Guabá) are exceptionally low (equal to or below the seasalt ratio) at low runoff rates, and they increase to ratios above rainwater at high runoff rates (except for high- Cl^- events). The exceptionally low ratios at low runoff may be due to the transformation of SO_4^{2-} into reduced sulfur gases (such as dimethyl sulfide) in the soil, whereupon the sulfur is emitted to the atmosphere (Stallard and Edmond, 1981). Alternatively, these watersheds may have no substantial geologic source of sulfur, and because sulfur is a nutrient (a part of some amino acids), it should be retained in biomass and organic matter in shallow soils (such as N, P, and K) during lower-runoff conditions only to be subsequently released to the stream during high-runoff events. Soil chemical analyses (Stallard, 2012b), however, show no sulfur in mineral soil or stream sediment.

Alkalinity, Carbon Dioxide, and Calcite Saturation

Alkalinity is the amount of anion charge per unit volume that can be titrated with a strong acid to reach the first equilibrium endpoint for the CO_2 system (Stumm and Morgan, 1981). Alkalinity is a conservative property. The primary source of alkalinity is the weathering of silicate and carbonate minerals; it can be modified by addition or loss of NO_3^- , NH_4^+ , organic acids, and sulfuric acid from sulfide weathering and acid precipitation. Higher alkalinities tend to be associated with higher pH values, but for a given alkalinity, the vapor pressure of CO_2 controls pH.

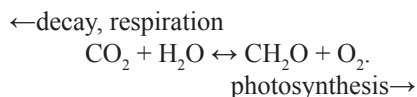
**EXPLANATION**

- | | | |
|-------------------|------------------|-------------|
| Runoff recurrence | ▲ Rising stage | ● Canóvanas |
| LOADEST | ▼ Falling stage | ● Cayaguás |
| —●— Canóvanas | □ Calcite | ● Guabá |
| —●— Cayaguás | + High chloride | ● Icacos |
| —●— Guabá | ○ High potassium | ● Mameyes |
| —●— Icacos | • Low silica | |
| —●— Mameyes | | |

Figure 8 (facing page). Runoff rate-concentration graphs for potassium ion. Additional sample characteristics are indicated with black symbols; calcite, samples supersaturated with respect to calcite; high chloride, samples with exceptionally high chloride concentrations collected during huge storms; high potassium, samples with high potassium but not high chloride; low silica, Icacos and Guabá samples with unusually low silica concentrations for the runoff rate. The points separated from the watershed-average curves (F) represent the averages of the classes of sample indicated by the superimposed character. These samples are not included in LOADEST models.

The study-area rivers draining volcaniclastic rocks tend to have higher alkalinities than rivers draining granitic rocks (fig. 11). Two geologic factors may contribute to this situation: the volcanic rocks have higher concentrations of Ca^{2+} and Mg^{2+} compared with the granitic rocks (Jolly and others, 1998; Smith and others, 1998), and minor calcite is present in some of the volcaniclastic rocks (Murphy and others, 2012). Negative alkalinity (that is, acidity) is observed in event samples collected at the highest runoff rates in the Icacos and Guabá watersheds, reflecting the importance of the various acid inputs, such as acid rain, nitrate formation, and DOC, to these watersheds.

The partial pressure of carbon dioxide (P_{CO_2}), CO_2 saturation, and the saturation index for calcite, $\text{SI}_{\text{calcite}}$, were calculated from alkalinity, temperature, and pH following Stumm and Morgan (1981; appendix 1). These parameters are useful in assessing the state of carbonate-system thermodynamics and, when combined with O_2 , they can be used to identify in-stream respiration. Oxygen is a bioactive gas that is readily exchanged between water and the atmosphere and is linked to CO_2 through photosynthesis, respiration, decay, and combustion. Using CH_2O as chemical shorthand for organic matter, the photosynthesis reaction is simple:



According to this biologically mediated reaction, when the concentration (and hence degree of saturation) of CO_2 rises, O_2 should fall (the reverse is true for combustion, decay, and respiration). The degree of saturation of both gases should rise with an increase in temperature.

The rivers that drain granitic bedrock (Icacos, Guabá, and Cayaguás) have higher degrees of CO_2 saturation, whereas the rivers that drain volcaniclastic bedrock (Mameyes and Canóvanas) are only slightly oversaturated or are even undersaturated (fig. 11). The rivers that drain granitic rocks are less steep and turbulent than those that drain volcaniclastic rocks, and therefore they probably have greater exchange with flood plains and sandy beds. Turbulent flow and rapid gas exchange as rivers cascade over steep rocky beds in the volcaniclastic

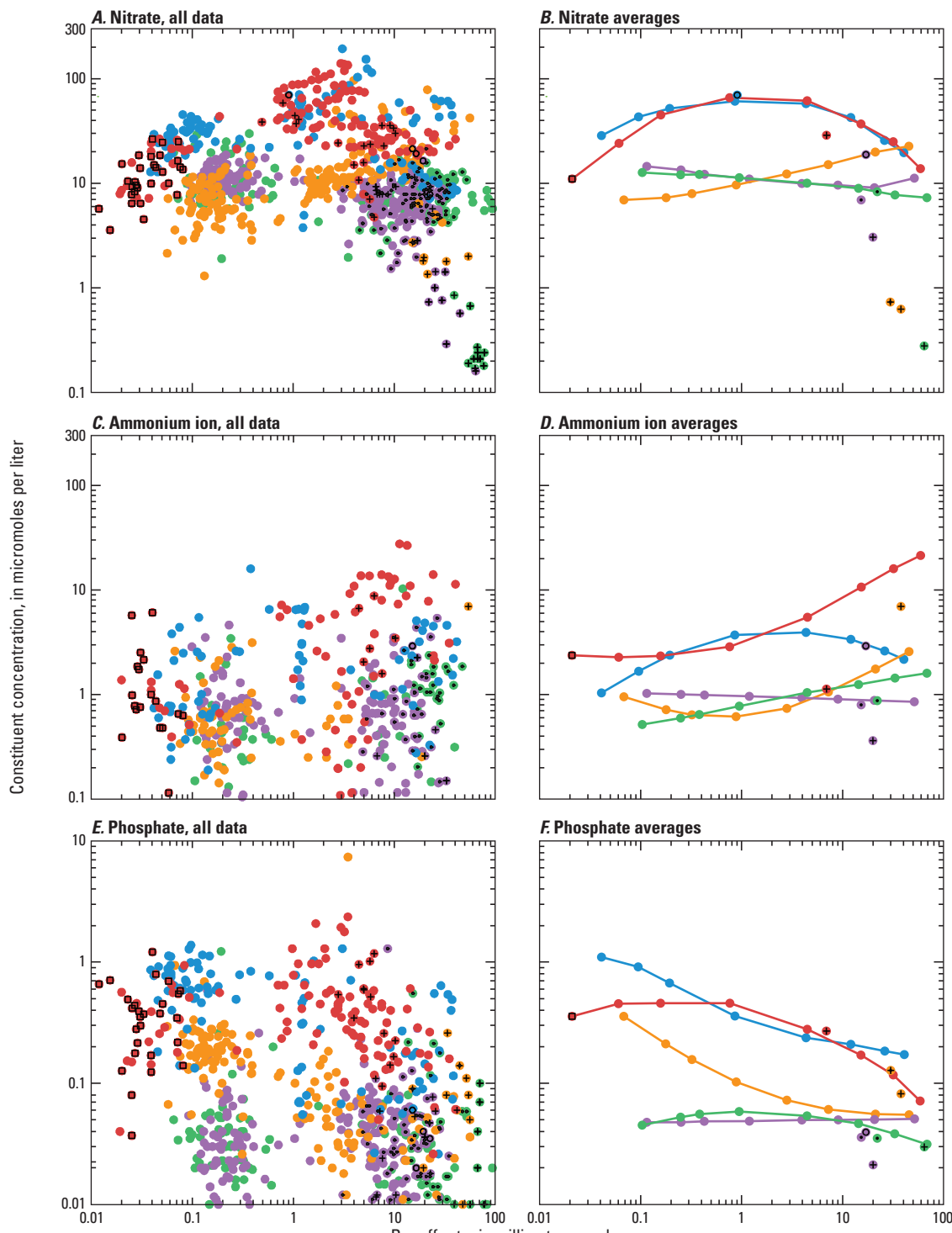
watersheds would drive the water towards equilibrium with the atmosphere. The few grab samples collected from the Icacos watershed at high runoff rates are close to saturation, indicating that this river equilibrates with the atmosphere when the river is quite turbulent. The undersaturation of CO_2 (fig. 11), primarily in the Canóvanas watershed, is probably due to in-channel photosynthesis by aquatic plants, which raises pH and O_2 (fig. 3) and reduces CO_2 . In all the other rivers, CO_2 is usually supersaturated and O_2 undersaturated, indicating a dominance of respiration and decay.

The undersaturation of CO_2 caused by in-stream photosynthesis appears to have driven the high-alkalinity Canóvanas water into supersaturation with respect to calcite at low-runoff conditions (fig. 11). Evidence of calcite precipitation, such as tufa deposits, has not been investigated. The lack of abundant limestone or calcite-bearing bedrock in the Canóvanas watershed suggests that the source of the supersaturated waters is silicate weathering, perhaps accompanied by minor calcite weathering. Soil solutions equilibrate with the high- CO_2 environment of soils and outgas once groundwater enters the channel. The outgassing could lead to calcite supersaturation.

Suspended Sediment

Three sources contribute suspended sediment to the eastern Puerto Rico WEBB watersheds: surficial erosion, landslides, and bed and bank erosion (Larsen, 2012). This sediment can either be transported out of the watershed by rivers or stored in the watershed as colluvium and alluvium. Suspended sediment concentrations in all rivers are low except during major storms when they increase rapidly with runoff rate (fig. 12). All of the LOADEST curves have a slight downward curvature, except for the Icacos watershed. For the Canóvanas and Cayaguás watersheds, runoff must exceed the 50th percentile of runoff rate before concentrations of 100 milligrams per liter are reached; for the Icacos and Guabá, the 75th percentile must be exceeded, and for the Mameyes, the 90th percentile must be exceeded (table 4). A few samples from highest runoff rates in the Cayaguás, Canóvanas, and the Icacos watersheds had exceptionally high concentrations of suspended sediment; one Icacos sample contained more than 100 grams per liter. The cause of these high concentrations is unknown. The Icacos and Cayaguás river beds are very sandy; in fact, sand is extracted commercially in the Río Cayaguás. It is possible that the bed was substantially mobilized and that the water intake nozzle of the sampler, which is not far above the river bed, may have been in the boundary layer. Alternatively, several major events have caused landslides to fall directly into the Icacos channel, so these high concentrations may reflect diluted debris flows.

The suspended-sediment yields reported here are considerably greater than yields reported in all previous estimates (McDowell and Asbury, 1994; Brown and others, 1995; Larsen, 1997; Larsen and Stallard, 2000). The yields reported here reflect the large events captured during the Puerto Rico WEBB program, and they allow the relation between

**EXPLANATION**

- | | | | | | |
|-----|-----------|---|----------------|---|-----------|
| —●— | Canóvanas | □ | Calcite | ● | Canóvanas |
| —●— | Cayaguás | + | High chloride | ● | Cayaguás |
| —●— | Guabá | ○ | High potassium | ● | Guabá |
| —●— | Icacos | • | Low silica | ● | Icacos |
| —●— | Mameyes | ○ | | ● | Mameyes |

Figure 9 (facing page). Runoff rate-concentration graphs for nitrate, ammonium ion, and phosphate ions. Additional sample characteristics are indicated with black symbols; calcite, samples supersaturated with respect to calcite; high chloride, samples with exceptionally high chloride concentrations collected during huge storms; high potassium, samples with high potassium but not high chloride; low silica, Icacos and Guabá samples with unusually low silica concentrations for the runoff rate. The points separated from the watershed-average curves (B, D, F) represent the averages of the classes of sample indicated by the superimposed character. These samples are not included in LOADEST models.

suspended sediment and runoff rate to be characterized at much higher runoff rates than ever before. In addition, the period 1996 to 2005 was a much wetter period than during previous studies.

Sediment yields from all watersheds were considerably greater than Saharan dust loadings of about $21 \pm 7 \text{ t km}^{-2} \text{ yr}^{-1}$ (Pett-Ridge and others, 2009b). This relation indicates that Saharan dust is probably not a major component of the mass budget in this landscape.

Conclusions

The water quality of the eastern Puerto Rico WEBB rivers, in terms of pH, dissolved oxygen, dissolved constituents, and suspended solids, is quite good, despite evidence of amphibian die-offs and increasing atmospheric deposition of nitrate. Despite substantial differences in land cover, annual runoff, or bedrock type, the water quality of these WEBB rivers is not marked by extreme contrasts. The yields of constituents derived largely from bedrock weathering (Ca^{2+} , alkalinity, and Si(OH)_4), from seasalt (Cl^-), or from a mix of the two sources (Na^+ , Mg^{2+} , K^+ , and SO_4^{2-}) differed by a factor of less than 2 among all watersheds, showing little relation to land cover, annual runoff, or bedrock type. Average concentrations of these constituents tended to be higher in the developed, leeward watersheds (Cayaguás and Canóvanas) compared with the forested, windward watersheds (Icacos, Guabá, and Mameyes). The developed watersheds had substantially higher yields of nutrients (NO_3^- , NH_4^+ , and $-\text{PO}_4^{3-}$) than the forested watersheds. In-stream productivity in the Canóvanas watershed is sufficiently great to cause oxygen supersaturation. It is possible that concentrations of some constituents are higher in the rivers draining the developed, leeward watersheds because of lower mean-annual runoff and higher ratios of evapotranspiration to runoff than is true in the forested, windward watersheds. However, the developed watersheds have higher concentrations of Na^+ , Cl^- , SO_4^{2-} , K^+ , NO_3^- , NH_4^+ , and $-\text{PO}_4^{3-}$ at a given discharge; this constituent profile, along with the higher nutrients yields, suggests that additional sources, most likely human activities related to agriculture and

domestic waste rather than to evapotranspiration, are causing the difference. Suspended-sediment yields were generally low during major storms, when a substantial amount of annual sediment export occurred. Suspended sediment yields from the granitic watersheds were about six times as great as from the volcaniclastic watersheds, independent of land cover and mean-annual runoff. The granitic watersheds generated about $2,000 \text{ t km}^{-2} \text{ yr}^{-1}$; this value is greater than previous estimates of sediment yield from these watersheds and may be due to a wetter sampling period or to the sampling of greater runoff events (or both).

Several anomalous types of water-quality samples were identified. Samples with very high Cl^- concentrations were associated with some hurricanes and other large storms. These samples were associated with elevated concentrations of other ions that are abundant in seasalt (Na^+ , K^+ , Mg^{2+} , Ca^{2+} , SO_4^{2-}), and often anomalously low NO_3^- concentrations. This composition reflects windborne seasalt from the ocean and a dominance of maritime, rather than continental, air masses contributing to the storms. Hurricane Georges, the largest storm of our study period, led to short-term and long-term changes in water quality in the forested, windward watersheds. The storm itself, like those described above, produced anomalously high concentrations of seasalt-related constituents and low NO_3^- concentrations. For about 1 to 2 years after the hurricane, occasional high- K^+ event samples were recovered that lacked correspondingly high concentrations of Cl^- and other seasalt-related ions; therefore the K^+ cannot be attributed to seasalt inputs. These samples may indicate the release of potassium from litter deposited by the storm, consistent with post-Hurricane Georges observations (Ostertag and others, 2003). Prior to Hurricane Georges, but not after, samples with anomalously low concentrations of silica were recorded in the forested watersheds. The low-silica events may have been caused by a change in hydrologic pathway during some storms that resulted in shallow flow paths; Georges may have led to the clogging or collapse of such macropores and pipes. These anomalous samples were not included in load and yield regressions.

For most constituents, the rivers show similar trends in runoff-dissolved constituent concentration graphs, suggesting considerable similarity in runoff generation and flow path structuring despite differences in geology, soils, and land cover. The nonbioactive, bedrock-derived and atmospherically derived constituents (Si(OH)_4 , Ca^{2+} , Mg^{2+} , Na^+ , and Cl^-) decrease in concentration with increasing discharge. The trends of the primary data are linear, while some curvature is seen for smoothed data. No trends are sigmoidal. These observations are consistent with the permeability-porosity-aperture model. All the slopes, C_1 , for all the bedrock- and seasalt-derived constituents tend to be lower than for most of the rivers in the Hydrologic Benchmark Network dataset (which are mostly in the -0.15 to -0.05 range). For a given river, the various slopes of bedrock-derived constituents are not statistically identical. The slope of Si(OH)_4 , which is exclusively derived from bedrock weathering, differs considerably from that of the

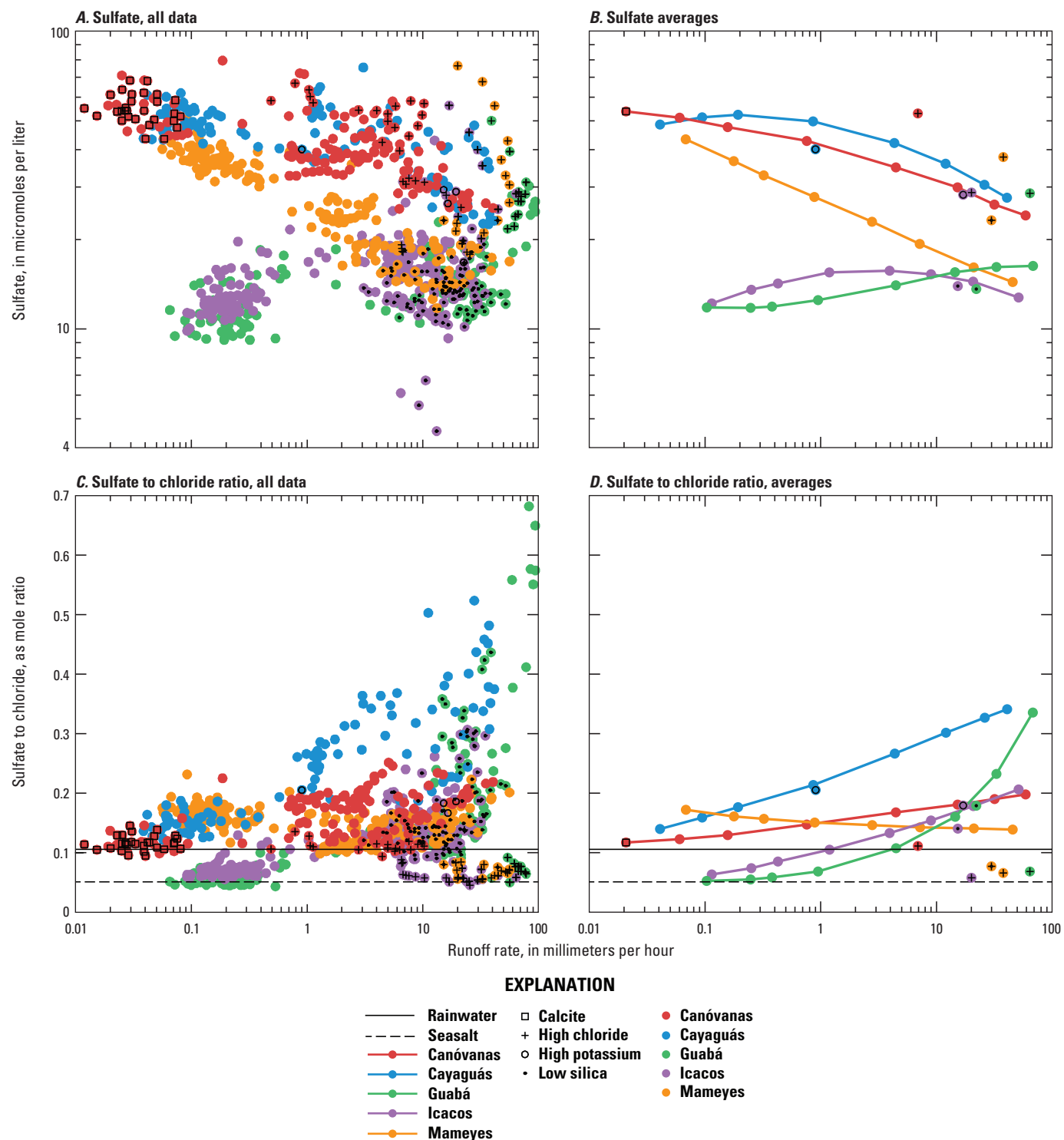


Figure 10. Runoff rate-concentration graphs for sulfate and sulfate:chloride ratio. Additional sample characteristics are indicated with black symbols; calcite, samples supersaturated with respect to calcite; high chloride, samples with exceptionally high chloride concentrations collected during huge storms; high potassium, samples with high potassium but not high chloride; low silica, Icacos and Guabá samples with unusually low silica concentrations for the runoff rate. The points separated from the watershed-average curves (B, D) represent the averages of the classes of sample indicated by the superimposed character. These samples are not included in LOADEST models.

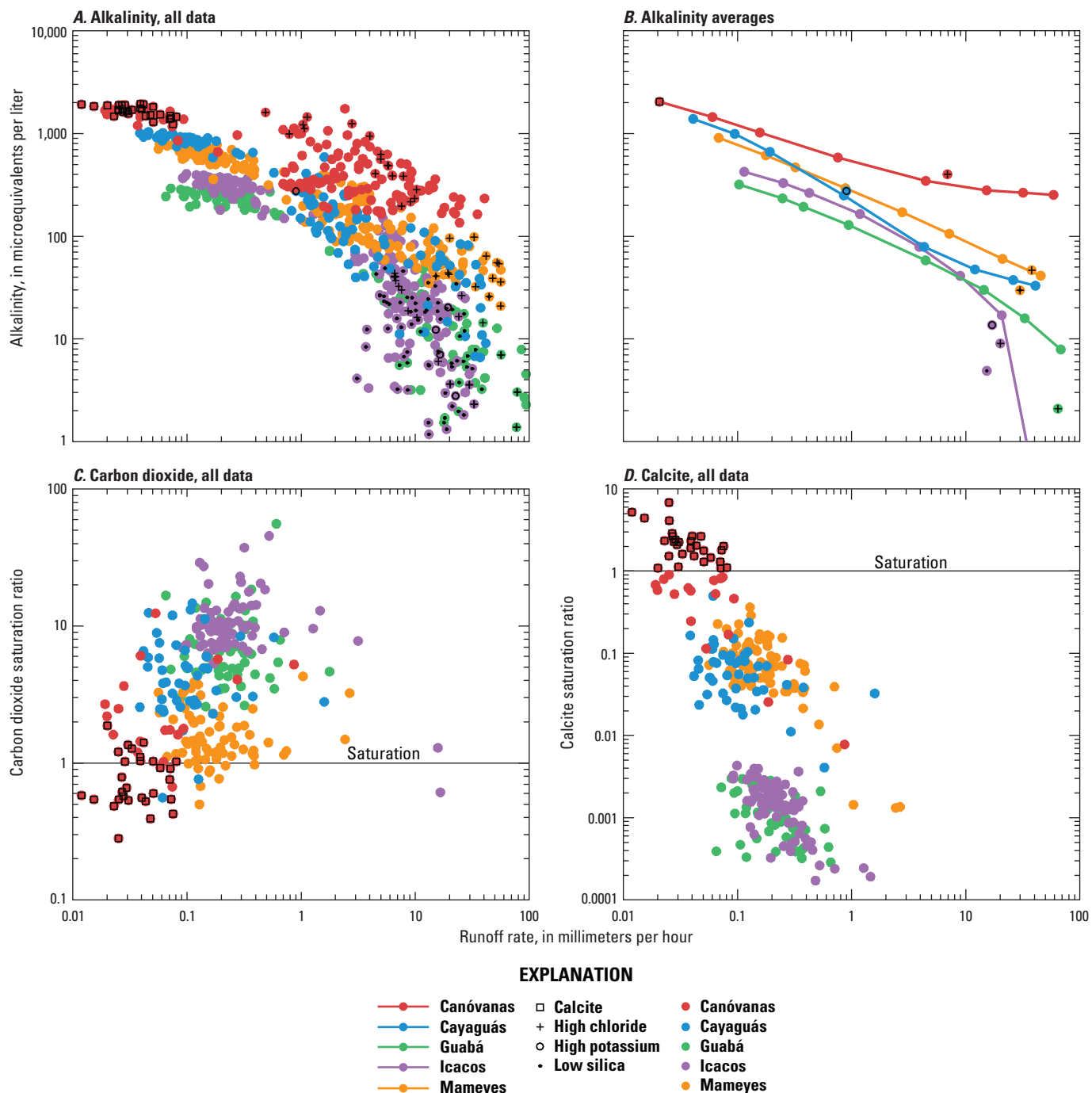
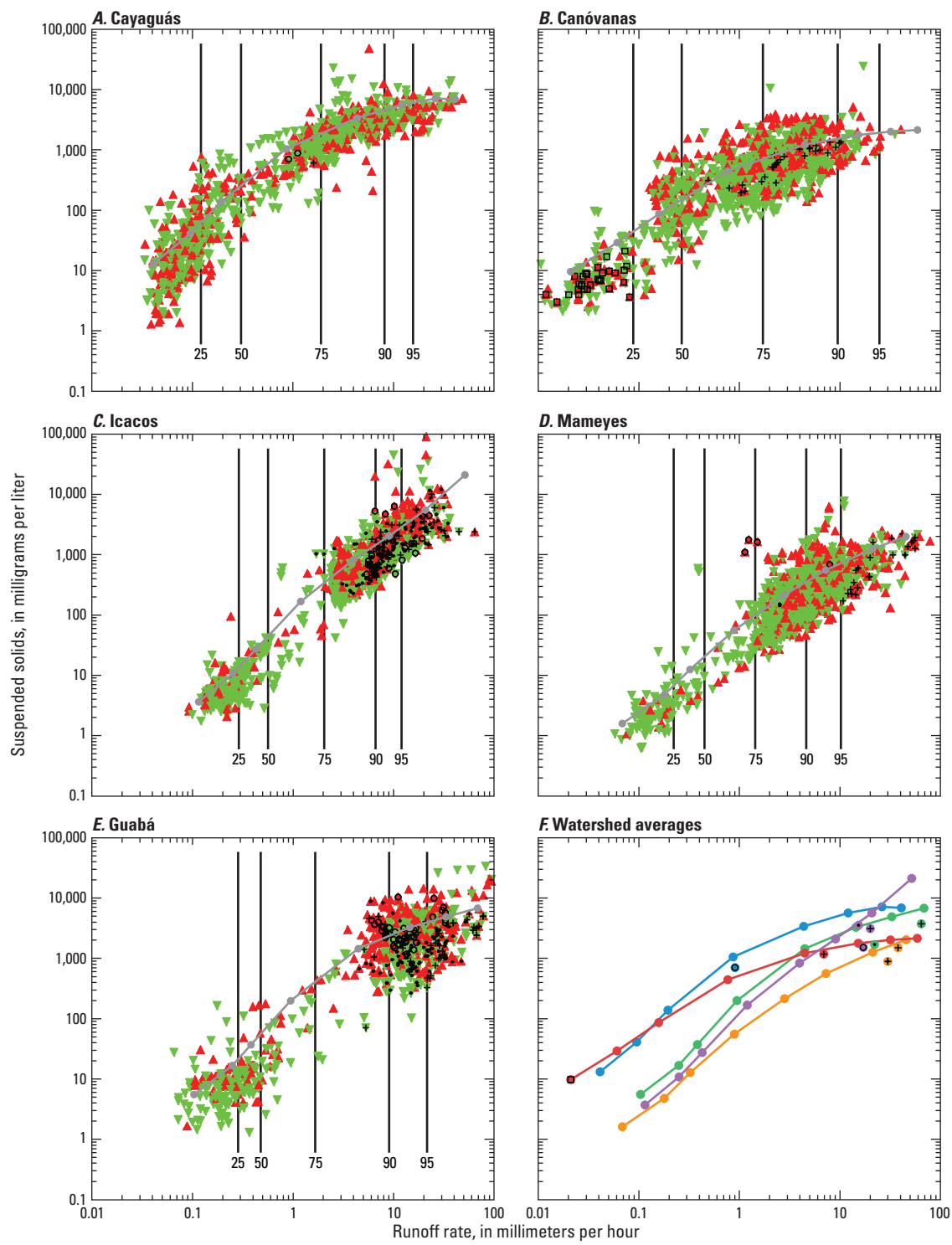


Figure 11. Alkalinity, carbon dioxide saturation, and calcite saturation in the eastern Puerto Rico WEBB rivers, 1991–2005. Additional sample characteristics are indicated with black symbols; calcite, samples supersaturated with respect to calcite; high chloride, samples with exceptionally high chloride concentrations collected during huge storms; high potassium, samples with high potassium but not high chloride; low silica, Icacos and Guabá samples with unusually low silica concentrations for the runoff rate. The points separated from the sample-average curves (B) represent the averages of the classes of sample indicated by the superimposed character. These samples are not included in LOADEST models.



EXPLANATION

90	Runoff recurrence	▲ Rising stage	● Canóvanas
—	LOADEST	▼ Falling stage	● Cayaguás
—	Canóvanas	□ Calcite	● Guabá
—	Cayaguás	+ High chloride	● Icacos
—	Guabá	○ High potassium	● Mameyes
—	Icacos	• Low silica	
—	Mameyes		

Figure 12 (facing page). Runoff rate–concentration graphs for suspended sediment. Additional sample characteristics are indicated with black symbols; calcite, samples supersaturated with respect to calcite; high chloride, samples with exceptionally high chloride concentrations collected during huge storms; high potassium, samples with high potassium but not high chloride; low silica, Icacos and Guabá samples with unusually low silica concentrations for the runoff rate. The points separated from the watershed-average curves (F) represent the averages of the classes of sample indicated by the superimposed character.

most abundant bedrock-derived ion, Ca^{2+} . This finding is not consistent with a single common slope for all bedrock-derived constituents. For each river, however, the slopes of the ionic constituents are ranked according to the relative contribution of bedrock and seasalt, from most negative to least negative, Ca^{2+} , Mg^{2+} , Na^+ , and Cl^- . After excluding the high- Cl^- storms, chloride has a slope of -0.20 to -0.14 . Chloride is atmospherically derived, so this trend must be caused by the mixing of old, evaporated soil waters with younger, typically more dilute rainwater. Focusing on Si(OH)_4 , Ca^{2+} , and Mg^{2+} to limit seasalt effects, the slopes of the linear relations for granitic rivers are consistently less than for the volcaniclastic rivers, suggesting that the physics of water flow through the different soils is slightly different and grouped by geology. A precise physical explanation is limited by the inability to measure, in the field, the parameters that contribute to C_1 in the permeability–porosity-aperture model.

The strongly bioactive constituents typically demonstrate two types of concentration-runoff relations. Some of the bioactive constituents have nearly constant runoff-rate-to-concentration relations (a chemostat), ordinarily with considerable scatter. For DOC, and for some of the remaining bioactive constituents in some rivers, concentrations increase as runoff increases, until runoff rates reach between 3 and 10 mm h^{-1} . At still higher runoff rates, concentrations decrease. This sequence can be interpreted in terms of a simplified soil-hydrology model. At low discharge, most water is presumably arriving through deeper flow paths with less-available bioactive constituents. With increasing runoff, flow paths are more shallow, more-available constituents are removed, and concentrations rise. At the highest runoff, overland flow and macropore flow become important. These paths have less contact with the soil matrix and do not generate waters high in bioactive constituent concentrations; accordingly, stream concentrations drop. An alternate explanation, solute depletion during storms, should cause recessions to have lower concentrations than rises. None of the bioactive constituents show this behavior.

Acknowledgements

This work was supported through the United States Geological Survey Water, Energy, and Biogeochemical Budgets program (Larsen and others, 1993; Lins, 1994). This chapter benefited from reviews by Brent Aulenbach, Alisa Mast, and Jamie Shanley. Without the initial groundwork by Angel Torres-Sánchez in the field and Ellen Axtmann in the lab this report would not have been possible.

References

- Aitkenhead, J.A., and McDowell, W.H., 2000, Soil C : N ratio as a predictor of annual riverine DOC flux at local and global scales: *Global Biogeochemical Cycles*, v. 14, no. 1, p. 127–138.
- Andreae, M.O., and Andreae, T.W., 1988, The cycle of biogenic sulfur-compounds over the Amazon Basin—1. Dry season: *Journal of Geophysical Research—Atmospheres*, v. 93, p. 1487–1497.
- Beven, K.J., and Germann, P., 1982, Macropores and water flows in soils: *Water Resources Research*, v. 18, p. 1311–1325.
- Bevington, P.R., and Robinson, K.D., 2003, Data reduction and error analysis for the physical sciences—2: New York, McGraw Hill, 320 p.
- Bhatt, M.P., and McDowell, W.H., 2007, Controls on major solutes within the drainage network of a rapidly weathering tropical watershed: *Water Resources Research*, v. 43, p. 1–9.
- Brantley, S.L., Crane, S.R., Crerar, D.A., Hellmann, R., and Stallard, R.F., 1986, Dissolution at dislocation etch pits in quartz: *Geochimica et Cosmochimica Acta*, v. 50, p. 2349–2361.
- Brown, E.T., Stallard, R.F., Larsen, M.C., Bourlès, D.L., Raisbeck, G.M., and Yiou, F., 1998, Determination of pre-development denudation rates of an agricultural watershed (Cayaguás River, Puerto Rico) using in-situ-produced ^{10}Be in river-borne quartz: *Earth and Planetary Science Letters*, v. 160, p. 723–728.
- Brown, E.T., Stallard, R.F., Larsen, M.C., Raisbeck, G.M., and Yiou, F., 1995, Denudation rates determined from the accumulation of in situ-produced ^{10}Be in the Luquillo Experimental Forest, Puerto Rico: *Earth and Planetary Science Letters*, v. 129, p. 193–202.
- Burrowes, P.A., Joglar, R.L., and Green, D.E., 2004, Potential causes for amphibian declines in Puerto Rico: *Herpetologica*, v. 60, no. 2, p. 141–154.

- Chappell, N.A., Franks, S.W., and Larenus, J., 1998, Multi-scale permeability estimation for a tropical catchment: *Hydrological Processes*, v. 12, p. 1507–1523.
- Chappell, N.A., and Sherlock, M.D., 2005, Contrasting flow pathways within tropical forest slopes of Ultisol soils: *Earth Surface Processes and Landforms*, v. 30, p. 735–753.
- Chestnut, T.J., and McDowell, W.H., 2000, C and N dynamics in the riparian and hyporheic zones of a tropical stream, Luquillo Mountains, Puerto Rico: *Journal of the North American Benthological Society*, v. 19, p. 199–214.
- Chestnut, T.J., Zarin, D.J., McDowell, W.H., and Keller, M., 1999, A nitrogen budget for late-successional hillslope, Tabonuco Forest, Puerto Rico: *Biogeochemistry*, v. 46, no. 1–3, p. 85–108.
- Clark, J.J., and Wilcock, P.R., 2000, Effects of land-use change on channel morphology in northeastern Puerto Rico: *Geological Society of America Bulletin*, v. 112, p. 1763–1777.
- Derry, L.A., Pett-Ridge, J.C., Kurtz, A.C., and Troester, J.W., 2006, Ge/Si and $^{87}\text{Sr}/^{86}\text{Sr}$ tracers of weathering reactions and hydrologic pathways in a tropical granitoid system: *Journal of Geochemical Exploration*, v. 88, p. 271–274.
- Devol, A.H., Forsberg, B.R., Richey, J.E., and Pimentel, T.P., 1995, Seasonal-variation in chemical-distributions in the Amazon (Solimões) River—A multiyear time-series: *Global Biogeochemical Cycles*, v. 9, no. 3, p. 307–328.
- Edmond, J.M., Palmer, M.R., Measures, C.I., Brown, E.T., and Huh, Y., 1996, Fluvial geochemistry of the eastern slope of the northeastern Andes and its foredeep in the drainage of the Orinoco in Colombia and Venezuela: *Geochimica et Cosmochimica Acta*, v. 60, no. 16, p. 2949–2976.
- Edmond, J.M., Palmer, M.R., Measures, C.I., Grant, B., and Stallard, R.F., 1995, The fluvial geochemistry and denudation rate of the Guayana shield in Venezuela, Colombia, and Brazil: *Geochimica et Cosmochimica Acta*, v. 59, no. 16, p. 3301–3325.
- Elsenbeer, Helmut, 2001, Hydrologic flowpaths in tropical rainforest soilscapes—A review: *Hydrological Processes*, v. 15, p. 1751–1759.
- Elsenbeer, Helmut, and Cassel, D.K., 1990, Surficial processes in the rainforest of western Amazonia, in Ziemer, R.R., and O'Loughlin, C.L.H.L.S., eds., *Research needs and applications to reduce erosion and sedimentation in tropical steep-lands*: International Association of Hydrologic Sciences, p. 289–297.
- Elsenbeer, Helmut, and Lack, A., 1996, Hydrometric and hydrochemical evidence for fast flowpaths at La Cuenca, western Amazonia: *Journal of Hydrology*, v. 180, p. 237–250.
- Elsenbeer, Helmut, Lack, A., and Cassel, K., 1996, The stormflow chemistry at La Cuenca, western Amazonia: *Interciencia*, v. 21, p. 133–138.
- Fox, L.E., 1989, A model for inorganic control of phosphate concentrations in river waters: *Geochimica et Cosmochimica Acta*, v. 53, p. 417–428.
- Fox, L.E., 1993, The chemistry of aquatic phosphate—Inorganic processes in rivers: *Hydrobiologia*, v. 253, p. 1–16.
- Gibbs, R.J., 1967, The geochemistry of the Amazon River system—I. The factors that control the salinity and composition and concentration of suspended solids: *Geological Society of America Bulletin*, v. 78, p. 1203–1232.
- Gibbs, R.J., 1972, Water chemistry of the Amazon River: *Geochimica et Cosmochimica Acta*, v. 36, p. 1061–1066.
- Godsey, S.E., Elsenbeer, H., and Stallard R.F., 2004, Overland flow generation in two lithologically distinct rainforest watersheds: *Journal of Hydrology*, v. 295, p. 276–290.
- Godsey, S.E., Kirchner J.W., and Clow, D.W., 2009, Concentration-discharge relationships reflect chemostatic characteristics of US watersheds: *Hydrological Processes*, v. 23, p. 1844–1864.
- Gould, W.A., Martinuzzi, S., and Parés-Ramos, I.K., 2012, Land use, population dynamics, and land-cover change in northeastern Puerto Rico, ch. B in Murphy, S.F., and Stallard, R.F., eds., *Water quality and landscape processes of four watersheds in eastern Puerto Rico*: U.S. Geological Survey Professional Paper 1789, p. 25–42.
- Haire, W.J., 1972, Flood of October 5–10, 1970, in Puerto Rico: Commonwealth of Puerto Rico Water-Resources Bulletin 12, 42 pages.
- Heartsill-Scalley, Tamara, Scatena, F.N., Estrada, C., McDowell, W.H., and Lugo, A.E., 2007, Disturbance and long-term patterns of rainfall and throughfall nutrient fluxes in a subtropical wet forest in Puerto Rico: *Journal of Hydrology*, v. 333, p. 472–485.
- Herrera, Rafael, Jordan, C., Klinge, H., and Medina, E., 1978a, Amazon ecosystems—Their structure and functioning with particular emphasis on nutrients: *Interciencia*, v. 3, p. 223–232.
- Herrera, Rafael, Merida, T., Stark, N., and Jordan, C., 1978b, Direct phosphorus transfer from leaf litter to roots: *Naturwissenschaften*, v. 65, p. 208–209.
- Herwitz, S.R., Muhs, D.R., Prospero, J.M., Mahan, S., and Vaughn, B., 1996, Origin of Bermuda's clay-rich Quaternary paleosols and their paleoclimatic significance: *Journal of Geophysical Research*, v. 101, no. D18, p. 23,389–23,400.

- Johnson, N.M., Likens, G.E., Bormann, F.H., Fisher, D.W., and Pierce, R.S., 1969, A working model for the variation in stream water chemistry at the Hubbard Brook Experimental Forest, New Hampshire: Water Resources Research, v. 5, p. 1353–1363.
- Johnsson, M.J., 1990, Tectonic versus chemical-weathering controls on the composition of fluvial sands in tropical environments: *Sedimentology*, v. 37, p. 713–726.
- Johnsson, M.J., and Stallard, R.F., 1989, Physiographic controls on sediments derived from volcanic and sedimentary terrains on Barro Colorado Island, Panama: *Journal of Sedimentary Petrology*, v. 59, p. 768–781.
- Jolly, W.T., Lidiak, E.G., Dickin, A.P., and Wu, T.-W., 1998, Geochemical diversity of Mesozoic island arc tectonic blocks in eastern Puerto Rico, in Lidiak, E.G., and Larue, D.K., eds., *Tectonics and geochemistry of the northeastern Caribbean: Geological Society of America Special Paper 322*, p. 67–98.
- Kinner, D.A., and Stallard, R.F., 2004, Identifying storm flow pathways in a rainforest catchment using hydrological and geochemical modeling: *Hydrological Processes*, v. 18, no. 15, p. 2851–2876.
- Langbein, W.B., and Dawdy, D.R., 1964, Occurrence of dissolved solids in surface waters in the United States: U.S. Geological Survey Professional Paper 501–D, p. D115–D117.
- Larsen, M.C., 1997, Tropical geomorphology and geomorphic work—A study of geomorphic processes and sediment and water budgets in montane humid-tropical forested and developed watersheds, Puerto Rico: Boulder, University of Colorado Geography Department, Ph.D. dissertation, 341 p.
- Larsen, M.C., 2012, Landslides and sediment budgets in four watersheds in eastern Puerto Rico, ch. F in Murphy, S.F., and Stallard, R.F., eds., *Water quality and landscape processes of four watersheds in eastern Puerto Rico*: U.S. Geological Survey Professional Paper 1789, p. 153–178.
- Larsen, M.C., Collar, P.D., and Stallard, R.F., 1993, Research plan for the investigation of water, energy, and biogeochemical budgets in the Luquillo Mountains, Puerto Rico: U.S. Geological Survey Open-File Report 92–150, 19 p.
- Larsen, M.C., Liu, Z., and Zou, X., 2012, Effects of earthworms on slopewash, surface runoff, and fine-litter transport on a humid tropical forested hillslope, Luquillo Experimental Forest, Puerto Rico, ch. G in Murphy, S.F., and Stallard, R.F., eds., *Water quality and landscape processes of four watersheds in eastern Puerto Rico*: U.S. Geological Survey Professional Paper 1789, p. 179–198.
- Larsen, M.C., and Parks, J.E., 1997, How wide is a road? The association of roads and mass-wasting disturbance in a forested montane environment: *Earth Surface Processes and Landforms*, v. 22, p. 835–848.
- Larsen, M.C., and Santiago-Román, A., 2001, Mass wasting and sediment storage in a small montane watershed—An extreme case of anthropogenic disturbance in the humid tropics, in Dorava, J.M., Palcsak, B.B., Fitzpatrick, F., and Montgomery, D., eds., *Geomorphic processes and riverine habitat*: American Geophysical Union Water Science and Application Series, v. 4, p. 119–138.
- Larsen, M.C., and Stallard, R.F., 2000, Water, energy, and biogeochemical budgets, Luquillo Mountains, Puerto Rico: U.S. Geological Survey Fact Sheet 163–99, 4 p.
- Lewis, W.M., Jr., Hamilton, S.K., Jones, S.L., and Runnels, D.D., 1987, Major element chemistry, weathering, and element yields for the Caura River drainage, Venezuela: *Biogeochemistry*, v. 4, p. 159–181.
- Lewis, W.M., Jr., and Saunders, J.F., III, 1989, Concentration and transport of dissolved and suspended substances in the Orinoco River: *Biogeochemistry*, v. 7, p. 203–240.
- Lewis, W.M., Jr., and Saunders, J.F., III, 1990, Chemistry and element transport by the Orinoco main stem and lower tributaries, in Weibezaahn, F.H., Alvarez, H., and Lewis, W.M., Jr., eds., *El Río Orinoco como ecosistema / The Orinoco River as an ecosystem*: Caracas, Venezuela, Impresos Rubel, p. 211–239, 430 p.
- Lins, H.F., 1994, Recent directions taken in water, energy, and biogeochemical budget research: *Eos, Transactions, American Geophysical Union*, v. 75, no. 38, p. 433, 438–439.
- Lodge, D.J., McDowell, W.H., and McSwiney, C.P., 1994, The importance of nutrient pulses in tropical forests: *Trends in Ecology & Evolution*, v. 9, p. 384–387.
- Lugo, A.E., and Frangi, J.L., 2003, Changes in necromass and nutrients on the forest floor of a palm floodplain forest in the Luquillo Mountains of Puerto Rico: *Caribbean Journal of Science*, v. 39, no. 3, p. 265–272.
- McDowell, W.H., 1991, Nutrient and major element chemistry of Caribbean rain forests streams: *Internationale Vereinigung für theoretische und angewandte Limnologie*, v. 24, p. 1720–1723.
- McDowell, W.H., 1998, Internal nutrient fluxes in a Puerto Rican rain forest: *Journal of Tropical Ecology*, v. 14, p. 521–536.
- McDowell, W.H., 2001, Hurricanes, people and riparian zones—Controls on nutrient losses from forested Caribbean watersheds: *Forest Ecology and Management*, v. 154, p. 443–451.
- McDowell, W.H., and Asbury, C.E., 1994, Export of carbon, nitrogen, and major ions from three tropical montane watersheds: *Limnology and Oceanography*, v. 39, p. 111–125.

- McDowell, W.H., Gines-Sanchez, C., Asbury, C.E., and Ramos Perez, C.R., 1990, Influence of sea-salt aerosols and long-range transport on precipitation chemistry at El Verde, Puerto Rico: Atmospheric Environment, v. 24A, p. 2813–2821.
- McDowell, W.H., McSwiney, C.P., and Bowden, W.B., 1996, Effects of hurricane disturbance on groundwater chemistry and riparian function in a tropical rain forest: *Biotropica*, v. 28, p. 577–584.
- Murphy, S.F., and Stallard, R.F., 2012, Hydrology and climate of four watersheds in eastern Puerto Rico, ch. C in Murphy, S.F., and Stallard, R.F., eds., Water quality and landscape processes of four watersheds in eastern Puerto Rico: U.S. Geological Survey Professional Paper 1789, p. 43–84.
- Murphy, S.F., Stallard, R.F., Larsen, M.C., and Gould, W.A., 2012, Physiography, geology, and land cover of four watersheds in eastern Puerto Rico, ch. A in Murphy, S.F., and Stallard, R.F., eds., Water quality and landscape processes of four watersheds in eastern Puerto Rico: U.S. Geological Survey Professional Paper 1789, p. 1–24.
- Ostertag, Rebecca, Scatena, F.N., and Silver, W.L., 2003, Forest floor decomposition following hurricane litter inputs in several Puerto Rican forests: *Ecosystems*, v. 6, p. 261–273.
- Peters, N.E., Shanley, J.B., Aulenbach, B.T., Webb, R.M., Campbell, D.H., Hunt, R., Larsen, M.C., Stallard, R.F., Troester, J., Walker, J.F., 2006, Water and solute mass balance of five small, relatively undisturbed watersheds in the U.S.: *Science of the Total Environment*, v. 358, p. 221–242.
- Pett-Ridge, J.C., 2009, Contributions of dust to phosphorus cycling in tropical forests of the Luquillo Mountains, Puerto Rico: *Biogeochemistry*, v. 96, no. 1, p. 63–80.
- Pett-Ridge, J.C., Derry, L.A., and Barrows, J.K., 2009a, Ca/Sr and $^{87}\text{Sr}/^{86}\text{Sr}$ ratios as tracers of Ca and Sr cycling in the Río Icacos watershed, Luquillo Mountains, Puerto Rico: *Chemical Geology*, v. 94, no. 1, p. 64–80.
- Pett-Ridge, J.C., Derry, L.A., and Kurtz, A.C., 2009b, Sr isotopes as a tracer of weathering processes and dust inputs in a tropical granitoid watershed, Luquillo Mountains, Puerto Rico: *Geochimica et Cosmochimica Acta*, v. 73, p. 25–43.
- Reid, E.A., Reid, J.S., Meier, M.M., Dunlap, M.R., Cliff, S.S., Broumas, A., Perry, K., and Maring, H., 2003, Characterization of African dust transported to Puerto Rico by individual particle and size segregated bulk analysis: *Journal of Geophysical Research*, v. 108, no. D19, 8591, p. 1–22.
- Runkel, R.L., Crawford, C.G., and Cohn, T.A., 2004, Load Estimator (LOADEST)—A FORTRAN program for estimating constituent loads in streams and rivers: U.S. Geological Survey Techniques and Methods Book 4, ch. A5, 69 p., program, test files.
- Saunders, J.F., III, and Lewis, W.M., Jr., 1988, Transport of phosphorus, nitrogen, and carbon by the Apure River, Venezuela: *Biogeochemistry*, v. 5, p. 323–342.
- Saunders, J.F., III, and Lewis, W.M., Jr., 1989, Transport of major solutes and the relationship between solute concentrations and discharge in the Apure River, Venezuela: *Biogeochemistry*, v. 8, p. 101–113.
- Schaefer, D.A., McDowell, W.H., Scatena, F.N., and Asbury, C.E., 2000, Effects of hurricane disturbance on stream water concentrations and fluxes in eight tropical forest watersheds of the Luquillo Experimental Forest, Puerto Rico: *Journal of Tropical Ecology*, v. 16, p. 189–207.
- Schulz, M.S., and White, A.F., 1999, Chemical weathering in a tropical watershed, Luquillo Mountains, Puerto Rico. III. Quartz dissolution rates: *Geochimica et Cosmochimica Acta*, v. 63, no. 3–4, p. 337–350.
- Shanley, J.B., McDowell, W.H., and Stallard, R.F., 2011, Long-term patterns and short-term dynamics of stream solutes and suspended sediment in a rapidly weathering tropical watershed: *Water Resources Research*, v. 47, no. W07515, p. 1–11.
- Simon, Andrew, Larsen, M.C., and Hupp, C.R., 1990, The role of soil processes in determining mechanisms of slope failure and hillslope development in a humid-tropical forest, eastern Puerto Rico, in Kneuper, P.L.K., and McFadden, L.D., eds., Soils and landscape evolution. *Geomorphology*, v. 3, p. 263–286.
- Smith, A.L., Shellekens, J.H., and Diaz, A.-L.M., 1998, Batholiths as markers of tectonic change in the northeastern Caribbean, in Lidiak, E.G., and Larue, D.K., eds., *Tectonics and geochemistry of the northeastern Caribbean: Geological Society of America Special Paper 322*, p. 99–122.
- Soil Survey Staff, 1995, Order 1 soil survey of the Luquillo Long-Term Ecological Research Grid, Puerto Rico: Lincoln, Nebraska, U.S. Department of Agriculture Natural Resources Conservation Service, 93 p.
- Stallard, R.F., 1985, River chemistry, geology, geomorphology, and soils in the Amazon and Orinoco basins, in Drever, J.I., ed., *The chemistry of weathering*: Dordrecht, Holland, D. Reidel Publishing Company, NATO ASI Series C—Mathematical and Physical Sciences, v. 149, p. 293–316.
- Stallard, R.F., 1988, Weathering and erosion in the humid tropics, in Lerman, Abraham, and Meybeck, M., eds., *Physical and chemical weathering in geochemical cycles*: Dordrecht, Holland, Kluwer Academic Publishers, NATO ASI Series C—Mathematical and physical sciences 251, p. 225–246.
- Stallard, R.F., 1995a, Relating chemical and physical erosion, in White, A.F., and Brantley, S.L. eds., *Chemical weathering rates of silicate minerals: Reviews in Mineralogy*, v. 31, p. 543–564.

- Stallard, R.F., 1995b, Tectonic, environmental, and human aspects of weathering and erosion—A global review using a steady-state perspective: *Annual Review of Earth and Planetary Sciences*, v. 12, p. 11–39.
- Stallard, R.F., 2001, Possible environmental factors underlying amphibian decline in eastern Puerto Rico—Analysis of U.S. government data archives: *Conservation Biology*, v. 15, p. 943–953.
- Stallard, R.F., 2012a, Atmospheric inputs to watersheds in the Luquillo Mountains of eastern Puerto Rico, ch. D in Murphy, S.F., and Stallard, R.F., eds., Water quality and landscape processes of four watersheds in eastern Puerto Rico: U.S. Geological Survey Professional Paper 1789, p. 85–112.
- Stallard, R.F., 2012b, Weathering, landscape equilibrium, and carbon in four watersheds in eastern Puerto Rico, ch. H in Murphy, S.F., and Stallard, R.F., eds., Water quality and landscape processes of four watersheds in eastern Puerto Rico: U.S. Geological Survey Professional Paper 1789, p. 199–248.
- Stallard, R.F., and Edmond, J.M., 1981, Geochemistry of the Amazon—1. Precipitation chemistry and the marine contribution to the dissolved load at the time of peak discharge: *Journal of Geophysical Research—Oceans and Atmospheres*, v. 86, no. NC10, p. 9844–9858.
- Stallard, R.F., and Edmond, J.M., 1983, Geochemistry of the Amazon—2. The influence of the geology and weathering environment on the dissolved load: *Journal of Geophysical Research—Oceans and Atmospheres*, v. 88, no. NC14, p. 9671–9688, microfiche supplement.
- Stallard, R.F., and Edmond, J.M., 1987, Geochemistry of the Amazon—3. Weathering chemistry and limits to dissolved inputs: *Journal of Geophysical Research—Oceans*, v. 92, no. C8, p. 8293–8302.
- Stallard, R.F., Koehnken, L., and Johnsson, M.J., 1991, Weathering processes and the composition of inorganic material transported through the Orinoco River system, Venezuela and Colombia: *Geoderma*, v. 51, no. 1–4, p. 133–165.
- Stark, Nellie, and Jordan, C.F., 1978, Nutrient retention by the root mat of an Amazonian rain forest: *Ecology*, v. 59, p. 434–437.
- Stumm, Werner, and Morgan, J.J., 1981, *Aquatic chemistry*: New York, John Wiley, 780 p.
- Tardy, Yves, Bustillo, V., Roquin, C., Mortatti, J., and Victoria, R., 2005, The Amazon—Bio-geochemistry applied to river basin management—1. Hydro-climatology, hydrograph separation, mass transfer balances, stable isotopes, and modelling: *Applied Geochemistry*, v. 20, p. 1746–1829.
- Tardy, Yves, Roquin, C., Bustillo, V., Moreira, M., Martinelli, L.A., and Victoria, R., 2009, Carbon and water cycles—Amazon River basin applied biogeochemistry: Biarritz, France, *Atlantica Seguier*, 480 p.
- Webb, R.M.T., and Soler-López, L.R., 1997, Sedimentation history of Lago Loíza, Puerto Rico, 1953–94: U.S. Geological Survey Water-Resources Investigations Report 97-4108, 18 p.
- Wolman, M.G., and Miller, J.P., 1960, Magnitude and frequency of forces in geomorphic processes: *Journal of Geology*, v. 68, p. 54–74.
- Ziegler, Karen, Chadwick, O.A., White, A.F., and Brzezinski, M.A., 2005, $\delta^{30}\text{Si}$ systematics in a granitic saprolite, Puerto Rico: *Geology*, v. 33, no. 10, p. 817–820.

Landslides and Sediment Budgets in Four Watersheds in Eastern Puerto Rico

By Matthew C. Larsen

Chapter F of
**Water Quality and Landscape Processes of Four Watersheds in
Eastern Puerto Rico**

Edited by Sheila F. Murphy and Robert F. Stallard

Professional Paper 1789–F

**U.S. Department of the Interior
U.S. Geological Survey**

Contents

Abstract.....	157
Introduction.....	157
Landslides	159
Slopewash.....	159
Soil Creep	159
Treethrow	159
Suspended Sediment	159
Watershed Sediment Budgets	161
Analysis of Geomorphic Processes.....	161
Landslides	161
Slopewash.....	162
Soil Creep	162
Treethrow	164
Fluvial Sediment.....	165
Sediment Storage	165
Amounts, Rates and Characteristics of Hillslope Erosion, Sediment Storage, and Transport, and Relation to Landform Development	165
Landslides	165
Landslide Frequency	166
Landslide Erosion Rate	167
Slopewash.....	167
Soil Creep	168
Treethrow	168
Fluvial Sediment.....	169
Sediment Storage and Sediment Budgets	170
Sediment Storage in Channel Beds, Bars, and Floodplains	170
Colluvium, Hillslope Sediment, and Core Stones.....	171
Time Scales and Anthropogenic Effects	171
Erosion and Sediment Export: Are They in Balance?	172
Landform Development.....	172
Summary and Conclusions.....	173
Acknowledgments.....	174
References.....	174

Figures

1. Map showing location of Puerto Rico and study watersheds, eastern Puerto Rico	158
2. Photographs of landslides in study watersheds, eastern Puerto Rico.....	160
3. Shaded relief maps of study watersheds showing locations of landslide scars, eastern Puerto Rico.....	163
4. Graph showing fluvial suspended sediment yield versus runoff in study watersheds, eastern Puerto Rico	170

Tables

1. Geologic, geographic, topographic, and hydrologic characteristics of study watersheds, eastern Puerto Rico	164
2. Dimensions of 2,882 landslides mapped from aerial photographs (1937, 1951, 1962, 1972, 1974, 1979, 1990, and 1995) in study watersheds, eastern Puerto Rico	166
3. Types and estimated rates of hillslope erosion in study watersheds, eastern Puerto Rico	168
4. Estimated annual soil creep in study watersheds, eastern Puerto Rico.....	168
5. Annual fluvial suspended sediment, 1991–2005, in study watersheds, eastern Puerto Rico.....	169
6. Estimated sediment in storage in study watersheds, eastern Puerto Rico, in channel beds, bars, floodplains, and Quaternary terraces.....	171

Abbreviations Used in This Report

>	greater than
cm	centimeter
ha	hectare
ha yr ⁻¹	hectares per year
kg km ⁻² h ⁻¹	kilograms per square kilometer per hour
kg km ⁻² mm ⁻¹	kilograms per square kilometer per millimeter
km	kilometer
km ²	square kilometer
km ⁻² century ⁻¹	per square kilometer per century
m	meter
m yr ⁻¹	meters per year
m ²	square meter
m ³	cubic meter
mg L ⁻¹	milligrams per liter

mm	millimeter
mm h ⁻¹	millimeters per hour
mm yr ⁻¹	millimeters per year
t	metric ton
t km ⁻²	metric tons per square kilometer
t km ⁻² yr ⁻¹	metric tons per square kilometer per year
t m ⁻³	metric tons per cubic meter
GIS	geographic information system

Conversion Factors

Multiply	By	To obtain
Length		
millimeter (mm)	0.03937	inch (in.)
centimeter (cm)	0.3937	inch (in.)
meter (m)	3.281	foot (ft)
kilometer (km)	0.6214	mile (mi)
Area		
square meter (m ²)	10.76	square foot (ft ²)
hectare (ha)	0.003861	square mile (mi ²)
square kilometer (km ²)	0.3861	square mile (mi ²)
Volume		
cubic meter (m ³)	35.31	cubic foot (ft ³)
Flow rate		
millimeters per hour (mm h ⁻¹)	0.03937	inches per hour (in. h ⁻¹)
millimeters per year (mm yr ⁻¹)	0.03937	inches per year (in. yr ⁻¹)
meters per year (m yr ⁻¹)	3.281	feet per year (ft yr ⁻¹)
Mass		
milligrams per liter (mg L ⁻¹)	0.058 41	grains per gallon (gr gal ⁻¹)
Other		
metric tons per cubic meter (t m ⁻³)	0.8428	short tons per cubic yard (tons yd ⁻³)
metric tons per square kilometer (t km ⁻²)	2.855	short tons per square mile (tons mi ⁻²)
metric tons per square kilometer per year (t km ⁻² yr ⁻¹)	2.855	short tons per square mile per year (tons mi ⁻² yr ⁻¹)
kilograms per square kilometer per hour (kg km ⁻² h ⁻¹)	5.710	pounds per square mile per hour (lb mi ⁻² h ⁻¹)

Landslides and Sediment Budgets in Four Watersheds in Eastern Puerto Rico

By Matthew C. Larsen

Abstract

The low-latitude regions of the Earth are undergoing profound, rapid landscape change as forests are converted to agriculture to support growing population. Understanding the effects of these land-use changes requires analysis of watershed-scale geomorphic processes to better inform and manage this usually disorganized process. The investigation of hillslope erosion and the development of sediment budgets provides essential information for resource managers.

Four small, montane, humid-tropical watersheds in the Luquillo Experimental Forest and nearby Río Grande de Loíza watershed, Puerto Rico ($18^{\circ} 20' N.$, $65^{\circ} 45' W.$), were selected to compare and contrast the geomorphic effects of land use and bedrock geology. Two of the watersheds are underlain largely by resistant Cretaceous volcaniclastic rocks but differ in land use and mean annual runoff: the Mameyes watershed, with predominantly primary forest cover and runoff of 2,750 millimeters per year, and the Canóvanas watershed, with mixed secondary forest and pasture and runoff of 970 millimeters per year. The additional two watersheds are underlain by relatively erodible granitic bedrock: the forested Icacos watershed, with runoff of 3,760 millimeters per year and the agriculturally developed Cayaguás watershed, with a mean annual runoff of 1,620 millimeters per year.

Annual sediment budgets were estimated for each watershed using landslide, slope wash, soil creep, treethrow, suspended sediment, and streamflow data. The budgets also included estimates of sediment storage in channel beds, bars, floodplains, and in colluvial deposits.

In the two watersheds underlain by volcaniclastic rocks, the forested Mameyes and the developed Canóvanas watersheds, landslide frequency (0.21 and 0.04 landslides per square kilometer per year, respectively), slope wash (5 and 30 metric tons per square kilometer per year), and suspended sediment yield (325 and 424 metric tons per square kilometer per year), were lower than in the two watersheds underlain by granitic bedrock. In these granitic watersheds, landslide frequency, slope wash, and suspended sediment yield were 0.43 landslides per square kilometer per year, 20 metric tons per square

kilometer per year, and 2,140 metric tons per square kilometer per year, respectively, in the forested Icacos watershed and 0.8 landslides per square kilometer per year, 105 metric tons per square kilometer per year, and 2,110 metric tons per square kilometer per year, respectively, in the agriculturally developed Cayaguás watershed. Comparison of sediment budgets from the forested and developed watersheds indicates that human activities increase landslide frequency by as much as a factor of 5 and slope wash by as much as a factor of 6. When the difference in annual runoff is considered, the effect of land use on suspended sediment yields is also notable. Sediment concentration, calculated as sediment yield normalized by runoff, was about 2.3 to 3.7 times as great in the two watersheds in secondary forest and pasture compared with sediment concentration in the watersheds in primary forest. Even in the two watersheds with primary forest cover, the Mameyes and Icacos, located in the Luquillo Experimental Forest, the effects of anthropogenic disturbance were marked: 43 to 63 percent of landslide-related erosion was associated with road construction and maintenance.

Introduction

Erosion and tectonics are continuous processes that shape the surface of the Earth, but our description of the working of these processes is inadequate (Stallard, 1995). The geomorphic activity of humans further complicates our understanding of erosion processes. At present humans may be the most important agent of geomorphic work on the planet (Hooke, 2000). The volume of sediment moved by human activities such as farming, mining, construction, and quarrying may exceed by a factor of 10 the total quantity carried to the sea by the world's rivers (Wolman, 1990) and exceed by a similar amount that moved by all other natural processes operating on the earth's surface.

The humid tropics occupy 25 percent of the Earth's land surface and support approximately 45 percent of the Earth's population (CIA World Factbook, 2005). Development stresses in this region reduce soil resources, water quality, and reservoir storage capacity, and they increase landslide and

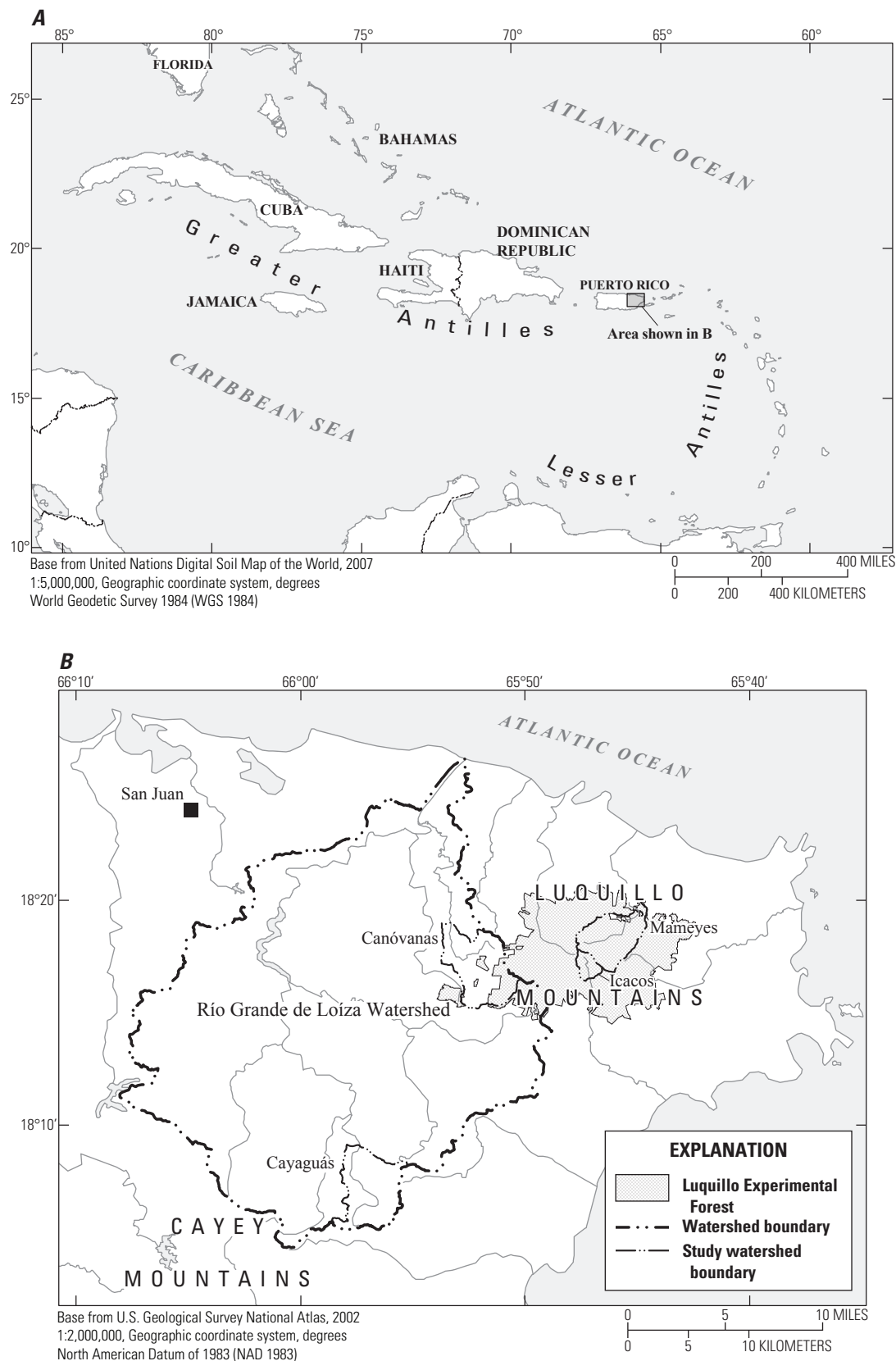


Figure 1. Location of Puerto Rico and study watersheds, eastern Puerto Rico.

flood hazards (Kates and others, 1990). The effect of development pressure is compounded in tropical nations, which tend to have limited resources for planning and carrying out careful economic development. Sustainable development of the tropics, as is true elsewhere, requires improved understanding of the long-term geomorphic effects on soil and water resources of economic development and human activities.

Small watersheds provide an ideal scale for the integrated study of hillslope and fluvial processes because their small size minimizes the spatial variability of lithology, land use, and climate. Paired study of these small watersheds provides a means to isolate and then compare or contrast a variable of interest. Landslide, slopewash, soil creep, treethrow, suspended-sediment, streamflow, and sediment-storage data were used to quantify hillslope and fluvial erosion, transport, and storage processes, and to develop sediment budgets in two relatively undisturbed forested watersheds (Icacos and Mameyes) in the Luquillo Experimental Forest and two agriculturally developed watersheds in the adjacent Río Grande de Loíza watershed (Canóvanas and Cayaguás), Puerto Rico (fig. 1). Geology, climate, hydrology, and land cover of these watersheds are described in Murphy and others (2012), Murphy and Stallard (2012), and Gould and others (2012). The objectives of this work were to quantify and contrast geomorphic processes in relatively undisturbed and developed watersheds in an environment—the montane humid tropics—where relatively little geomorphic research has been done. This study provides sediment budgets that can be compared with budgets in other settings and highlights the importance of landsliding as the dominant mass-wasting process in the montane humid tropics.

Landslides

Landsliding triggered by earthquakes or rainfall is the dominant process of hillslope erosion in many montane humid-tropical environments (Simonett, 1967; Garwood and others, 1979; DeGraff and others, 1989; Maharaj, 1993; Reading and others, 1995; Larsen and Santiago-Román, 2001; Glade and others, 2005; Restrepo and Alvarez, 2006). Rainfall during intense or prolonged storms has been the principal cause of landslides in Puerto Rico during the 20th century (Jibson, 1989; Larsen and Simon, 1993; Larsen and Torres-Sánchez, 1998). Because of the relatively short distances from hillslopes to channels in upland watersheds on the island (fig. 2), hillslope material eroded by landslides is commonly delivered directly to stream channels, resulting in large ratios of sediment delivered to channels compared with that stored on foottslopes or floodplains (Gupta, 1988; Ahmad and others, 1993; Larsen and Parks, 1997). Where hillslope angles are low or foottslopes and floodplains are wide enough, some of the landslide debris or colluvium resides in temporary storage before being entrained by fluvial processes (see example of landslide-debris deposit in fig. 2B). The amount of sediment stored in this buffer area varies both spatially and temporally, complicating quantitative estimates of its volume, residence time, and fluvial transport rate (Trimble, 1977; Larsen and Santiago-Román, 2001).

Slopewash

Slopewash is the movement of hillslope materials by gravity and water not concentrated in channels. Erosion of soil by slopewash is important in humid-temperate and arid areas (Young, 1960; Cerdá and García-Fayos, 1997), but relatively little work on this topic has been published for the forested humid tropics (Ruxton, 1967; Williams, 1973; Chatterjea, 1994; Goudie, 1995; Reading and others, 1995; Larsen and others, 1999; Gellis and others, 2006). Ruxton (1967) observed that slopewash under mature primary rain forest in northern Papua New Guinea was pronounced on steep hillslopes where leaf litter and duff were thin. Rapid rates of litter decomposition and gaps in forest canopy, typical of humid-tropical forest, are important factors that increase slopewash, according to Birot (1966). Slopewash in Puerto Rico can be extremely high in the months immediately following disturbance by landsliding (Shiels and others, 2008).

Soil Creep

Soil creep may be the most common but least studied or quantified process of hillslope soil erosion (Heimsath and others, 2002). Much of the soil-creep research is decades old, so studies using precise measurement techniques are few. Because it is a relatively slow process compared with either landsliding or slopewash, direct quantification of transport rates from soil creep require lengthy field studies. Furthermore, because of complicating processes such as bioturbation and treefall, soil creep is not consistently net downslope parallel to the ground surface (Clarke and others, 1999). As such, estimates of sediment mass transported by soil creep discussed herein must be considered as general at best.

Treethrow

Trees are uprooted by heavy winds during storms. Soil is lifted by roots each time a tree is uprooted and, on hillslopes, some of this soil falls back to the ground surface downslope of its source. Trees that grow on thin soils or on soils with low cohesive strength are generally more susceptible to being uprooted (Lenart, 2003; Osterkamp and others, 2006). Detailed explanations of the process of soil transport by treethrow are provided by Small and others (1990), Gabet and others (2003), Osterkamp and others (2006), and Phillips and Marion (2006).

Suspended Sediment

Mean annual runoff from the entire island of Puerto Rico is estimated at 911 millimeters (mm) (Larsen and Webb, 2009). This runoff results in a mean annual suspended-sediment discharge to surrounding coastal waters estimated to range from 2.7 to 9.0 million metric tons for the water years 1990 to 2000 (Larsen and Webb, 2009). The relation between mean annual sediment yield and mean annual sediment load versus drainage



Figure 2. Landslides in the study watersheds, eastern Puerto Rico. *A*, Roadside slump in the upper Canóvanas watershed. Roadside slumps are an important source of sediment in ephemeral and perennial streams. *B*, Coalesced debris-flow scars estimated to be 10–20 years in age in the Cayaguás watershed, showing recovery of vegetation on scar surface and landslide debris deposited at footslope. *C*, Slump along Río Icacos channel, showing transport of landslide debris directly to river channel. *D*, Aerial view of two large debris-avalanche scars, Icacos watershed, 1989. Debris avalanche to right, triggered by Hurricane Hugo in 1989, measured 33 m wide at the headscarp and had a volume of approximately 30,000 m³. Debris-avalanche scar to left delivered several hundred thousand cubic meters of debris to the Río Icacos channel. It dates to a 1970 tropical depression (rainfall total of 976 mm).

area for Puerto Rico rivers is comparable to that of other rivers of the world draining similar terrain (Larsen and Webb, 2009). However, comparison of mean annual sediment yield to runoff indicates that Puerto Rico rivers are sensitive to the frequent high rainfall associated with tropical storms characteristic of this region (Larsen and Simon, 1993). Furthermore, sediment discharge from the island is highly episodic and spatially uneven because of the variability of tropical storm frequency and topography throughout the island.

Watershed Sediment Budgets

Watershed sediment budgets have been developed for a variety of geographic settings and spatial scales (for example, Trimble, 1977; Dietrich and Dunne, 1978; Meade, 1982; Milliman and Meade, 1983; Caine and Swanson, 1989; Nelson and Booth, 2002; Ramos-Scharron and MacDonald, 2007). These authors discuss the uncertainties of watershed- to regional-scale sediment-budget calculations that are based on relatively short records of sediment flux, and they stress the importance of differentiating between human and “natural” rates of sediment yield. A particularly confounding uncertainty in areas with a history of human disturbance stems from sediment recently eroded (tens to hundreds of years ago) now in temporary storage on lower hillslopes, flood plains, and in aggraded channels, documented by Trimble (1977), Meade (1982), and Larsen and Santiago-Román (2001). These authors emphasize the uncertainties of attempting to use present-day sediment transport rates to estimate long-term watershed denudation rates. In the subtropical Serra do Mar, Brazil, for example, sediment recently eroded (in the 19th and 20th centuries) lies as a colluvial apron at the foot of slopes and, as stated by Haggard (1961), slope conservation efforts may be a century too late.

The work described herein follows the approach outlined by Dietrich and Dunne (1978) that has been widely applied for the development of sediment budgets for small watersheds. Their work describes the quantification of fluvial and hillslope sediment erosion and transport and accounts for debris flows, soil creep, treethrow effects, and the residence time of particles on the valley floor, channel, and hillslope. Because much of the data they required for their budget were unavailable, they used data from nearby or similar watersheds to supplement their work.

Analysis of Geomorphic Processes

For each of the watersheds studied, geomorphic processes were described and sediment budgets were estimated for landslides at the watershed scale. Slopewash, soil creep, and treethrow sediment budgets were estimated at hillslope and plot scale and extrapolated to watersheds. Erosion of channel banks during storms is also a source of sediment and, although such erosion was observed in the four

watersheds, it was not quantified for this study. Generalized land use and the location and extent of landslide scars were mapped using black and white stereo aerial photographs ranging in scale from 1:17,000 to 20,000 for several years between 1937 and 1995 in each of the four study watersheds. Additionally, for the Icacos and Mameyes watersheds, photographs from 1951, 1962–67, 1971–77, and 1990 were used (Larsen and Torres-Sánchez, 1998).

Previously published slopewash data were used to characterize hillslope erosion process, rates, and budgets in the Icacos, Mameyes, and Río Grande de Loíza watersheds (Larsen and others, 1999; Gellis and others, 2006). Soil creep rates were based on work by Lewis (1974) in the Mameyes watershed. Data from Scatena and Lugo (1995) and Larsen (1997) were used to estimate soil eroded by treethrow in the Mameyes watershed. Fluvial sediment data were obtained from U.S. Geological Survey publications (Figueroa-Alamo and others, 2006) and summarized from Larsen (1997), Larsen and Webb (2009) and Stallard and Murphy (2012).

Landslides

Landslides mapped in each of the watersheds were classified by type or movement style (debris flow, slump, shallow soil slip, debris avalanche, earthflow, complex slump–earthflow, and indeterminate) according to scar morphology using the terminology of Campbell (1975) and Cruden and Varnes (1996).

The mapped landslide scars were also classified by apparent age as either “historical” (defined herein as since 1820) or “prehistoric” (defined herein as during the last 1,000 years before 1820). These age classifications are approximate and, in the case of prehistoric scars, are based on size and the presence of mature forest cover, because no precise evidence of landslide scar age exists prior to 1937 aerial photographs. Using their morphology and large dimensions as the key identifying characteristics, prehistoric landslides were identified on aerial photographs. The largest historic scars were assumed to serve as a modern equivalent of landslide scars estimated to have formed before widespread deforestation, which began in the studied watersheds about 1820 (Morales Muñoz, 1943). Debris avalanches triggered by storms caused by a tropical depression in 1970 eroded hillslopes from ridgetops to stream channels and left scars that are comparable in dimension and morphology to numerous hillslope forms in the Luquillo Mountains (Larsen and Torres-Sánchez, 1998). Landslides classified as historical (those that occurred after about 1820) are characterized by bare soil, some vegetation regrowth, head- and side-scarp boundaries that were clear to somewhat subdued at the head, and partially eroded or absent debris deposits. Landslides classified as prehistoric had rounded, gently sloping, eroded head- and side-scarp boundaries, and highly eroded or absent debris deposits. Identification of older scars was based mainly on hillslope morphology that usually showed amphitheater-shaped headscarsps upslope of elongated rectilinear depressions that extended from ridgeline to stream channel.

The identification of prehistoric landslides is biased towards the largest scars, as evidence of small landslides is unlikely to persist for many decades or centuries. The prehistoric age estimate is an approximation and was based on field and photograph observations using two factors: the rate of change of hillslope morphologic features (slopewash processes in this humid-tropical setting, where annual rainfall is measured in meters, subdue most landslide head and side scarps beyond recognition in decades to centuries), and the dimensions of the largest landslides scars (fig. 2D). Debris avalanches (fig. 2D) triggered by a 1970 tropical depression, which substantially exceeded the 100-year-rainfall recurrence interval (Haire, 1972), had a landslide frequency on the order of 0.01 to 0.1 per square kilometer per century ($\text{km}^{-2} \text{ century}^{-1}$) in the Luquillo Mountains (Larsen and Torres-Sánchez, 1998). It is possible that the prehistoric landslides were seismically triggered, but the few data available to evaluate this hypothesis suggest that massive debris avalanches were not associated with seismicity. Rockfalls and river-bank slumps in western Puerto Rico were attributed by Reid and Taber (1919) to a strong 1918 earthquake (modified Mercalli intensity exceeded VII) with an epicenter located approximately 25 km offshore of the northwest coast. However, according to the authors, “in spite of the steep slopes found over most of the island, no important earth-slides were observed.”

All landslides in the Cayaguás watershed were classified as historical—no evidence of prehistoric landslides was visible because of an extremely high rate of historical landslide erosion in this watershed (fig. 2B) (Larsen and Santiago-Román, 2001).

The length, width, and depth of landslide scars were estimated from aerial photographs by using stereo magnifiers (which provide a three-dimensional view) and a 1:20,000-scale calibrated ruler and field measurements (Larsen and Santiago-Román, 2001). Landslide depth was estimated in the Canóvanas and Cayaguás watersheds (fig. 2A, B) from the photographs by comparison with the typical rural Puerto Rico house, which had a height of about 3 meters (m) in 1937, and 6 m in 1995 (see Madej and Ozaki, 1996, for an example of this approach). Landslide depth in the Icacos and Mameyes watersheds (fig. 2C, D), was estimated by comparison with trees, assuming an average tree height of 10 m (Brown and others, 1983). Using the product of the average soil density and individual landslide volume, an eroded mass was estimated for each landslide scar. This value is a minimum estimate because of continued erosion of head and side scarps noted on some scars after the initial failure. These values were summed and divided by the watershed area to normalize the erosion rate.

All visible scars in the Canóvanas, Icacos, and Mameyes watersheds were cataloged (fig. 3). The extreme abundance of landslide scars in the Cayaguás watershed precluded assessment of the entire watershed; scars were cataloged for selected areas which totaled 63 percent of the 26.4- km^2 watershed (fig. 2B) (Larsen and Santiago-Román, 2001). The mapped area represents land use and relief typical of that watershed. General land-use categories (forest, pasture, crops, and anthropogenic modification—highways or other

structures) were noted for the hillslope on which the scar was mapped. Analysis of aerial photographs allowed for examination of extensive areas—the total watershed area for the four watersheds is about 70 km^2 ; however, the technique is limited by the poor quality of some black and white photographs taken between the 1930s and 1950s. Additionally, forest canopy and shadows on steep hillslopes mask landslide features, reducing the total number of identified landslides in such areas. Field reconnaissance in all four watersheds indicated abundant slump, debris-flow, and shallow soil-slip scars along stream channels (fig. 2C). Where concealed by riparian forest cover, these features were not observable on aerial photographs. Landslide erosion rates were expressed as mass per square kilometer per year to compare to fluvial sediment yield, and as mass per square kilometer per century so that whole numbers could be used.

Slopewash

Larsen and others (1999) and Gellis and others (2006) summarized slopewash and surface runoff from unbounded plots on hillslopes instrumented with Gerlach troughs in forest (Icacos and Mameyes watersheds), pasture, crop, and at construction sites (Río Grande de Loíza watershed) in Puerto Rico. A Gerlach trough is a sediment trap designed to retain soil sediment and surface runoff transported downslope by gravity (Gerlach, 1967; Sirvent and others, 1997; Larsen and others, 2012). Uncertainties in slopewash data can be large, resulting from factors such as the varying linear dimensions of the upslope contributing area and the degree to which those dimensions may change in association with variable rainfall and runoff intensity; the effectiveness of runoff and sediment capture by the Gerlach trough; the degree of upslope soil disturbance and time since it occurred; the growth rates, type, and abundance of vegetation or other organic material on the soil surface; and the presence and type of burrowing organisms (Larsen and others 1999; Shiels and others, 2008; Larsen and others, 2012). Additional details of the methods used and results are summarized in Larsen and others (1999), Gellis and others (2006), and Larsen and others (2012).

Soil Creep

Soil creep was measured by Lewis (1974) at several locations in and near the Luquillo Mountains by using Young pits (Young, 1960), in which metal strips are buried vertically in soil and later excavated to measure their downslope deformity. The data were limited to a single pit at each of five sites. Soil creep data from some studies have been shown to correlate poorly with slope angle (Lewis, 1974; Goudie, 1995). However, work using cosmogenic ^{10}Be has shown that creep at a site in California was directly proportional to slope steepness (McKean and others, 1993) as was first suggested by Gilbert (1877). Because of the limited creep estimates published for sites in Puerto Rico, slope angle was not

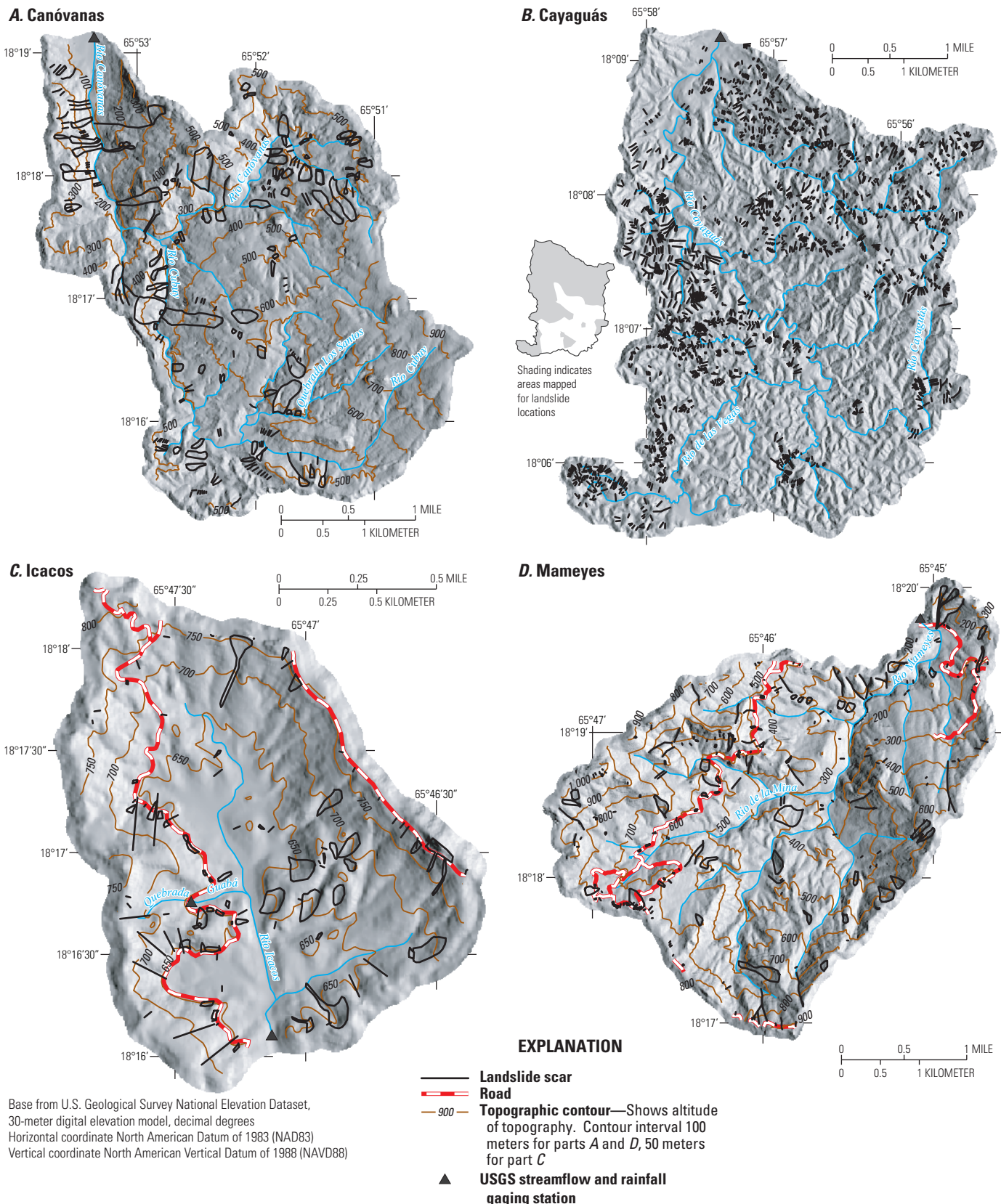


Figure 3. Landslide scars outlined on maps of four study watersheds, eastern Puerto Rico (area examined includes a 100-meter buffer around each watershed). *A*, Canóvanas, *B*, Cayaguás, *C*, Icacos, *D*, Mameyes.

included in the estimates herein. The creep rates ranged from about 0.5 millimeters per year (mm yr^{-1}) to 4 mm yr^{-1} and averaged about 2 mm yr^{-1} in the upper 45 centimeters (cm) of soil (Lewis, 1974). At a Mameyes watershed site in pasture with lower mean annual rainfall than that of the Luquillo Experimental Forest (table 1), the creep rate averaged 3 mm yr^{-1} (Lewis, 1974). As the Cayaguás watershed has annual rainfall that is intermediate between the two sites, a value of 2.5 (mm yr^{-1}) was chosen. In light of published creep rates from other humid-montane settings (1 mm yr^{-1} at Andrews Experimental Forest, Oregon; 3 mm in 7 months at site in the Vosges Mountains, France) the Luquillo Experimental Forest values seem reasonable (Caine and Swanson, 1989; Auzet and Ambroise, 1996). Total soil creep was estimated from the soil creep values discussed above with a simple model described by Dietrich and Dunne (1978):

$$\text{Soil creep} = S_T \cdot D_{\text{soil}} \cdot F_{sc} \cdot L_h / A,$$

where S_T is soil thickness (m), D_{soil} is soil density in metric tons per cubic meter (t/m^3), F_{sc} is creep rate in meters per year (m yr^{-1}), L_h is hillslope length (m), and A is watershed area in square kilometers (km^2). The resulting units are metric tons per square kilometer per year ($\text{t km}^{-2} \text{yr}^{-1}$). To estimate the contribution of soil creep to the total sediment budget, hillslope length in the studied watersheds was estimated to be twice the total channel length (Dietrich and Dunne, 1978).

Treethrow

Treethrow erosion rates were estimated by normalizing the soil mass produced from each uprooted tree to the annual uproot rate for the forested area in each watershed as

$$\text{Soil mass (m}^3\text{)} \cdot \text{uproots (ha}^{-1} \text{yr}^{-1}\text{)} = \text{soil mass uproots (m}^3 \text{ha}^{-1} \text{yr}^{-1}\text{)}.$$

Treecfall gap areas in a 13-hectare (ha) section of the Mameyes watershed were measured (before Hurricane Hugo in 1989) by ground surveys during a 2-year period by Scatena and Lugo (1995). Published data included the depth, area, and location of holes excavated by the root mass as a tree fell to the ground. The mean root area and hole depth were 3.74 m^2 and 1.06 m, respectively. Because of the irregular shape of depressions left by treethrow, the average depression volume (5.32 m^3) was greater than the product of the depth and area. On average, 0.8 gaps $\text{ha}^{-1} \text{yr}^{-1}$ were produced, and 47 percent of gaps were caused by uprooted trees. The gap rate of 0.8 gaps $\text{ha}^{-1} \text{yr}^{-1}$ was therefore multiplied by 0.47 to obtain 0.38 uprooted trees $\text{ha}^{-1} \text{yr}^{-1}$. The mean annual treefall-induced soil bioturbation rates for all watersheds in this study were thus estimated from the average volume of excavated holes (5.32 m^3) and an average soil density of 1 t m^{-3} with the equation:

$$5.32 \text{ t of soil mass/uproot} \cdot 0.38 \text{ uproots ha}^{-1} \text{yr}^{-1} \cdot 100 \text{ ha km}^{-2} = 202 \text{ t km}^{-2} \text{yr}^{-1}.$$

As time passes, most soil lifted by the uprooted tree falls back into the excavated hole, particularly on low-gradient hillslopes (Norman and others, 1995). Lenart (2003) estimated that as slope increases, only about one-third of the soil mass falls downslope of the hole. This reduction is caused by root wads of trees that fall downhill and block a portion of the soil available for downslope transport (Scatena and Lugo, 1995). It was therefore assumed that about two thirds of the total quantity of soil available for downslope movement is held back by each root wad, yielding an estimated rate of total soil transport due to treethrow of 67 $\text{t km}^{-2} \text{yr}^{-1}$.

Table 1. Geologic, geographic, topographic, and hydrologic characteristics of study watersheds, eastern Puerto Rico.

[km^2 , square kilometers; m, meters; mm, millimeters; D_{50} , median particle size]

Characteristic	Watershed			
	Canóvanas	Cayaguás	Icacos	Mameyes
¹ Watershed area, km^2	25.5	26.4	3.26	17.8
² Relief, m	891	293	228	969
² Mean slope of watershed	0.255	0.189	0.222	0.365
¹ Dominant rock type	Volcaniclastic rock	Granitic rock	Granitic rock	Volcaniclastic rock
¹ Principal land use	Pasture, secondary forest	Pasture, secondary forest	Undisturbed forest, secondary forest	Undisturbed forest, secondary forest
³ Annual rainfall, mm	2,070	2,350	4,150	3,760
³ Annual runoff, mm	970	1,620	3,760	2,750
² D_{50} , Channel bed sediment, mm	70	0.5	0.6	110

¹Murphy and others (2012).

²Larsen (1997).

³Murphy and Stallard (2012).

To estimate the net downslope transport of soil due to treethrow for each watershed, the approach of Schaeetzl and others (1990) was used to calculate the total treethrow soil transport rate: the product of average watershed slope (calculated from a 10-m digital elevation model and expressed as the tangent of the topographic slope in degrees). This net downslope rate was then applied to the forested areas of the Icacos and Mameyes watersheds to arrive at total treefall-induced transport rate of soil. The same method was used for forested areas of the Cayaguás and Canóvanas watersheds using the lowest rate ($42 \text{ t km}^{-2} \text{ yr}^{-1}$) determined by Scatena and Lugo (1995). This lower rate is believed to be representative of the secondary forests common in areas of Puerto Rico undergoing afforestation, such as those in the Cayaguás and Canóvanas watersheds (F.N. Scatena, U.S. Department of Agriculture Forest Service, oral communication, 1996).

Fluvial Sediment

The U.S. Geological Survey operates surface-water gaging and sediment stations that use continuous stage recorders and automatic pump samplers at the outlet of each of the four study watersheds (Murphy and Stallard, 2012). Suspended sediment and runoff data from these locations were compiled from Figueroa-Alamo and others (2006), Larsen (1997) and Stallard and Murphy (2012) to summarize annual yield and runoff for the study watersheds for the period 1991 to 2005. Bedload sediment was not analyzed for this study, but Larsen (1997) estimated that the suspended-sediment for the streams draining the watersheds underlain by granitic bedrock (Cayaguás and Icacos watersheds) includes a substantial bedload component, ranging from 6 to 51 percent of suspended sediment load. This bedload component results because these two streams have a median bed material grain size of 0.5 to 0.6 mm (table 1). Sediment with this grain size is entrained from the channel bed into turbulent suspension at even moderate discharge (Dietrich, 1982). In contrast, the much larger median bed material grain size (70 and 110 mm) in the Canóvanas and Mameyes watersheds underlain by volcaniclastic bedrock (volcanic sandstone, mudstone, and breccia) are relatively immobile on an annual basis. As such, suspended-sediment transport underestimates total fluvial sediment transport in time periods greater than 1 or 2 years (Larsen, 1997).

Sediment Storage

Sediment resides in various spatial and temporal storage compartments in a watershed before it is either entrained by fluvial and mass-wasting processes or sequestered for long time periods. These compartments are commonly described as active, semiactive, or inactive depending on how potentially mobile the deposits may be at time scales that range from days to millennia (Madej and Ozaki, 1996). In the study watersheds, channel bars and the channel bed were defined as

active, flood plains and colluvium were defined as semiactive, and Quaternary alluvium was defined as inactive. Watershed sediment storage was estimated by using field surveys and Geographic Information System (GIS) analysis of channel bars, channel width, and flood-plain surface area (Larsen and Santiago-Román, 2001).

Amounts, Rates and Characteristics of Hillslope Erosion, Sediment Storage, and Transport, and Relation to Landform Development

Landslides

Accelerated rates of rainfall-triggered landsliding in eastern Puerto Rico probably began in the early 19th century with the onset of forest clearing for agriculture, particularly in the Canóvanas and Cayaguás watersheds where agricultural development was intense (Larsen and Santiago-Román, 2001; Gellis and others, 2006). Because no historical records of landslides exist, the storms that triggered landslide scars cannot be precisely identified. However, the greatest rainfall intensities and widest distribution of storm rainfall in Puerto Rico are mainly associated with tropical disturbances, which composed 61 percent of the landslide-triggering storms recorded in the central mountains of Puerto Rico between 1960 and 1990 (Larsen and Simon, 1993). Major tropical disturbances struck the island in 1867, 1899, 1928, 1932, 1960, 1970, 1979, and 1989. These storms delivered 24- to 72-hour rainfall totals of 300 to 800 mm, and they are the likely trigger for most of the landslide scars visible in aerial photographs (Scatena and Larsen, 1991; Larsen and Torres-Sánchez, 1998). Field and aerial photographic analyses plus interviews of watershed residents confirm that rainfall associated with hurricanes and other tropical disturbances are commonly the trigger for landslides (Larsen and Torres-Sánchez, 1992).

Historical landslide scars generally affected a small surface area, reflective of the high-intensity but relatively short-duration rainstorms that triggered this style of landslide (Larsen and Simon, 1993) (fig. 2; table 2). In the forested watersheds, historical scars were particularly small (400–600 square meters (m^2)). The larger mean surface area of historical landslide scars in the agriculturally developed watersheds (980–5,000 m^2) indicates that landscape disturbance (forest removal, cropping) by humans can have a profound effect on mass wasting processes. Prehistoric debris avalanche scars are visible on aerial photographs of the Canóvanas, Icacos, and Mameyes watersheds and can be attributed to long-duration storms (Larsen and Simon, 1993). This type of storm occurred in 1970, when a stationary tropical depression released 976 mm of rainfall during a 5-day period, exceeding the 100-year, 7-day storm accumulation and triggering some of the largest debris avalanches observed

Table 2. Dimensions of 2,882 landslides mapped from aerial photographs (1937, 1951, 1962, 1972, 1974, 1979, 1990, and 1995) in four watersheds, eastern Puerto Rico.¹

[m, meter; m², square meter; m² km⁻², square meter per square kilometer; m³, cubic meter; m³ km⁻², cubic meter per square kilometer; t, metric ton; km², square kilometer; t km⁻², metric tons per square kilometer; t km⁻² yr⁻¹, metric tons per square kilometer per year; km² century⁻¹, square kilometers per century]

Characteristic	Watershed and landslide age							
	Canóvanas ²		Cayaguás ²		Icacos ³		Mameyes ³	
	Historical	Prehistoric	Historical	Historical	Prehistoric	Historical	Prehistoric	
Landslides mapped	172	44	2,321	70	24	189	62	
Mean length, m	90	330	53	30	130	30	310	
Mean width, m	30	100	16	20	30	15	53	
Mean depth ⁴ , m	4	20	3.5	2	9	2	12	
Mean surface area, m ²	5,000	49,000	980	600	6,300	400	17,000	
Mean volume, m ³	72,000	935,000	4,700	1,200	71,000	1,200	310,000	
Mean mass, t	94,000	1,234,000	2,300	2,000	93,000	2,300	605,000	
Total surface area, m ²	874,000	2,168,000	2,270,000	42,000	152,000	70,600	1,031,000	
Total volume, m ³	12,314,000	41,159,000	10,900,000	84,000	1,696,000	218,700	19,231,000	
Total mass, t	16,254,000	54,329,000	14,400,000	111,000	2,239,000	426,500	37,501,000	
Landslide scars per km ²	7	2	140	22	7	11	4	
Landslide surface area per watershed area, m ² km ⁻²	34,000	85,000	140,000	13,000	47,000	4,000	58,000	
Percent of basin surface area	3	9	14	1	5	0.4	5.8	
Landslide volume per watershed area, m ³ km ⁻²	483,000	1,615,000	660,000	26,000	520,000	12,000	1,079,000	
Total surface lowering averaged for study area, m	0.5	1.6	0.66	0.03	0.52	0.01	1.08	
Landslide mass, t km ⁻²	638,000	2,132,000	870,000	34,000	687,000	24,000	2,104,000	
Landslide mass, t km ⁻² yr ⁻¹	4,000	2,000	5,000	700	700	480	2,100	
Landslides per km ² per 100 yr	4	0.2	80	43	0.7	21	0.3	

¹Prehistoric landslide scars were estimated to represent as much as 1,000 years of landslide activity. Volume was converted to mass by using an average landslide debris density of 1.3 metric tons per cubic meter. Data for Canóvanas, Icacos, and Mameyes watersheds from Larsen (1997); data for Cayaguás watershed from Larsen and Santiago-Román (2001). Mapped area of Cayaguás watershed was 16.6 square kilometers (63 percent of the total area of the watershed). Other watersheds were fully mapped.

²In Canóvanas and Cayaguás watersheds, historical landslide scars estimated to represent landslide activity since forest clearing for settlement began in the 1820s.

³In forested Icacos and Mameyes watersheds, historical landslide scars estimated to represent landslide activity for a 50 year period (1945–1995).

⁴Calculated as an unweighted average of all landslides.

on the island (fig. 2D; Haire, 1972). In the Cayaguás watershed, the historical landslide frequency is so great that no recognizable evidence of prehistoric landslides persists (fig. 2B). The large size of prehistoric landslide scars (6,300–49,000 m²) mapped in this overall study is mainly a reflection of the operational definition of these features.

Most landslide scars were classified as debris flows; soil slips were the second most common type of scar (Larsen, 1997). Both of these landslide types are characteristic of high-intensity, short-duration storms that result in 24-hour rainfall totals on the order of 200 mm (Larsen and Simon, 1993) and have about a 5-year recurrence interval (U.S. Department of Commerce, 1961). The remaining landslide scars were classified mainly as slumps, debris avalanches, and complex. About 1 percent of landslide scars could not be categorized because of poorly defined features.

Landslide Frequency

Watershed area disturbed by historical landsliding is 1 percent or less in the forested Icacos and Mameyes watersheds. About 3 percent of the Canóvanas watershed surface area was disturbed by historical landsliding, compared with an impressive 19 percent of the Cayaguás watershed (table 2). Historical landslide frequency in the developed Canóvanas and Cayaguás watersheds was estimated to be four landslides km⁻² century⁻¹ and 80 landslides km⁻² century⁻¹, respectively (table 2). The 20-fold difference in the landslide frequency between the two watersheds can be attributed to both the more intensive land-use practices and more erodible bedrock in the Cayaguás watershed (Gould and others, 2012; Murphy and others, 2012). In the well-forested Icacos and Mameyes watersheds, historical landslide frequency was 43 and 21 landslides

km^{-2} century $^{-1}$, respectively. This twofold difference is attributed to the more landslide-prone soil and saprolite weathered from the granitic bedrock of the Icacos watershed compared with the volcaniclastic Mameyes watershed.

Mean annual rainfall in the Icacos watershed is almost double that of the lithologically similar Cayaguás watershed (table 1); therefore, if other factors were equal, the landslide frequency in the Icacos watershed would be expected to be greater than in the Cayaguás watershed. However, historical landslide frequency in the developed Cayaguás watershed was about double that in the forested Icacos watershed (table 2). Note that the dense forest cover of the Icacos watershed reduces the number of visible landslide scars, so the twofold difference may not be as great as estimated here. Evidence of an anthropogenic effect on landslide frequency and location is apparent in the forested watersheds. Forty-three percent of the 189 historical landslides mapped in the Mameyes watershed were associated with road construction and maintenance (fig. 2A; Larsen and Parks, 1997). Most of these landslides were small slumps and shallow soil slips that eroded about $80 \text{ t km}^{-2} \text{ yr}^{-1}$, or approximately one-half of all landslide-derived sediment. In the Icacos watershed, the majority (63 percent) of the 70 historical scars were associated with road construction and maintenance, resulting in $500 \text{ t km}^{-2} \text{ yr}^{-1}$ of hillslope erosion.

Landslide Erosion Rate

The estimated mass wasting rate by historical landsliding in the Canóvanas watershed is about $4,000 \text{ t km}^{-2} \text{ yr}^{-1}$, twice that estimated for the prehistoric period (table 2), suggesting that forest clearing and other agricultural practices have significantly increased hillslope erosion in this watershed. Examination of aerial photography indicates that mass-wasting has been even greater in the Cayaguás watershed, where landslides have eroded approximately $5,000 \text{ t km}^{-2} \text{ yr}^{-1}$ since the watershed was first occupied for subsistence farming (fig. 3; table 2). This mass of material is equivalent to an average watershed surface lowering of 0.66 m in 175 years, comparable to the 0.5-m lowering estimate since European occupation of the region, determined from analysis of cosmogenic ^{10}Be concentration in fluvial sediment in this watershed (Brown and others, 1998).

It is unlikely that the extremely high frequency of historical mass wasting in the Cayaguás watershed existed prior to the period of major land clearing. At present, extensive deposits of the material, apparently eroded during the 19th and 20th centuries, remain in storage throughout the watershed as colluvium as much as 3 m deep on footslopes and as alluvium 1 to 3 m deep along channels and flood plains (Clark and Wilcock, 2000; Larsen and Santiago Román, 2001). Colluvial deposits from groups of small landslide scars coalesce to fill the floors of small zero-order hollows (fig. 2B). Extensive colluvial deposits also mantle the floors of first- and second-order valleys and create poorly drained bog-like soils (Larsen and Santiago Román, 2001).

In the granitic-bedrock Icacos watershed, the rate of historical landslide-induced mass wasting was estimated to be about $700 \text{ t km}^{-2} \text{ yr}^{-1}$. This rate is substantially less than that estimated for the lithologically similar but developed Cayaguás watershed, but about 1.5 times as great as that of the volcaniclastic, forested Mameyes watershed (table 2). Prehistoric landslide scars affected approximately 5 percent of the Icacos watershed surface area, or about 0.5 percent per 100 years, essentially identical to the rate per 100 years determined for the Mameyes watershed (table 2).

A total of 26 of the 70 historical landslides in the Icacos watershed were not associated with roadways because they were distal to road corridors. These landslides had a mean mass of 1,200 t and eroded a total mass of $200 \text{ t km}^{-2} \text{ yr}^{-1}$. This landslide erosion rate probably represents the “natural” rate, or the rate that might be expected for this watershed in the absence of human activity. This rate is less than one-third that estimated for prehistoric landsliding (annual rate of erosion is 700 t km^{-2}), indicating that watershed conditions may have been wetter or storms more frequent during the last 1,000 years. This possibility is supported by work by Donnelly and Woodruff (2007) in which they describe increased tropical storm intensity in the late Holocene near Puerto Rico. Mayewski and others (2004) describe both wetter and drier periods in the Caribbean, but these periods are in the early to middle Holocene. Alternatively, shifting agriculture (known also as “slash and burn”) of pre-European populations may have been actively practiced on hillslopes, resulting in accelerated rates of landsliding (Denevan, 1992). Accounts of Taino Indian population in the Greater Antilles in the 16th century indicate that large numbers of inhabitants resided in these islands; in Puerto Rico, the estimate is as much as 600,000 (Rouse, 1993). A population of this size would likely have occupied at least some hillslope settings and could have altered vegetation, soil stability, and hillslope erosion.

Slopewash

Slopewash erosion rates were estimated to range between 30 and $105 \text{ t km}^{-2} \text{ yr}^{-1}$ in the developed watersheds (Canóvanas and Cayaguás, respectively) and between 5 and $20 \text{ t km}^{-2} \text{ yr}^{-1}$ in the forested Mameyes and Icacos watersheds, respectively (table 3) (Larsen and others 1999; Gellis and others, 2006). Larsen and others (2012) reported a comparable sloopewash rate, $12 \text{ t km}^{-2} \text{ yr}^{-1}$, on a low-gradient hillslope under undisturbed forest canopy in the El Verde section of the Luquillo Experimental Forest. Slopewash was observed as deposits in swales on hillslopes and on footslopes along ephemeral and perennial channels, where it is available for transport into channels. Additionally, other mass wasting processes, including landslides, soil creep, and slumping or erosion of channel banks transport sloopewash into channels where it is entrained as fluvial sediment.

Bruenig (1975) measured average sloopewash rates of $20 \text{ t km}^{-2} \text{ yr}^{-1}$ under virgin forest; sloopewash may be as high as $100 \text{ t km}^{-2} \text{ yr}^{-1}$ for the humid tropics in general (UNESCO/

Table 3. Types and estimated rates of hillslope erosion in study watersheds, eastern Puerto Rico.

[--, not available]

Hillslope erosion process	Average rate (metric tons per square kilometer per year)			
	Canóvanas	Cayaguás	Icacos	Mameyes
Treethrow	11	4	19	29
Soil creep	12	11	11	9
Slopewash	30	105	20	5
Landslide: Historical	4,000	5,000	700	480
Prehistoric	2,000	--	700	2,100
Total hillslope erosion (range varies with landslide rate used)	2,053 to 4,053	5,120	750	523 to 2,143
Suspended-sediment yield ¹	424	2,110	2,140	325
Bedload yield ²	83	--	--	110
Sediment delivery, percent (calculated as suspended sediment yield/ total hillslope erosion; range reflects landslide rates above)	10 to 21	41	285	15 to 62

¹From Stallard and Murphy (2012).²From Larsen (1997).

UNEP/FAO, 1978). Gellis and others (2006) reported slope-wash rates in the Río Grande de Loíza watershed, Puerto Rico, ranging from 10 t km⁻² in secondary forest and pasture, to 31 to 86 t km⁻² on hillslopes in crops, and 288 to 910 t km⁻² at construction sites. Shiels and others (2008) reported remarkably high slopewash rates of 25 to 81 grams per square meter in 1-m² bounded plots (from December 2003 to May 2004) at the center of freshly exposed landslide scars on volcaniclastic and quartz diorite bedrock in the Luquillo Mountains.

Soil Creep

Annual rates of soil creep for each watershed were estimated to be 9–12 t km⁻² yr⁻¹ (table 4). These rates are approximations because of the large uncertainties and variability in creep rate, soil thickness and density, and hillslope lengths within each watershed. Soil creep mobilizes an annual mass of sediment comparable to the contributions of treethrow, but generally less than the slopewash contribution in each watershed. It is assumed that this mass of soil is supplied to channel margins of ephemeral and perennial streams and is entrained by slumping, abrasion, and avulsion of stream banks during high discharge.

In humid-temperate environments, sediment delivery to river channels by soil creep in forested watersheds was estimated at 29 t km⁻² yr⁻¹ from Clearwater River watershed, Washington (Reid, 1981), and at 11 t km⁻² yr⁻¹ from watershed 10, Cascade Range, Oregon (Swanson and others, 1982). In New South Wales, Australia, Heimsath and others (2002) estimated soil creep at 6 mm yr⁻¹ on a hillslope in intermediate to wet sclerophyll forest. Soil creep rates in the Luquillo Experimental Forest averaged about 2 mm yr⁻¹ and ranged from about 0.5 mm yr⁻¹ to 4 mm yr⁻¹ (Lewis, 1974). These rates correlate poorly with slope gradient, indicating that slope angle may not be a limiting factor on most hillslopes. However, the paucity of data makes this difficult to confirm. No other soil creep data are available for the study watershed.

Table 4. Estimated annual soil creep in study watersheds, eastern Puerto Rico.[m yr⁻¹, meters per year; m, meter; t m⁻³, metric tons per cubic meter; km, kilometer; t km⁻² yr⁻¹, metric tons per square kilometer per year]

Watershed	Creep rate (m yr ⁻¹)	Soil thickness (m)	Soil density (t m ⁻³)	Hillslope length (km)	Mean annual soil movement (t km ⁻² yr ⁻¹)
Canóvanas	0.002	0.45	1	332	12
Cayaguás	0.0025	0.25	1.3	342	11
Icacos	0.002	0.45	1	40	11
Mameyes	0.002	0.45	0.8	219	9

Using the annual creep rate of 2 mm and mean slope length of 51 m in the northeastern Luquillo Experimental Forest, Scatena (1995) estimated that creep could remove all hillslope topsoil, absent any soil production from the weathering of bedrock, in a period of 27,000 years.

Treethrow

Estimates of treethrow contribution to hillslope soil movement range from 4 to 29 t km⁻² yr⁻¹ in the study watersheds (table 3). Rates are lower in the developed watersheds owing to less forest cover and because secondary-forest treethrow rates are lower, possibly as a result of lesser tree height. Because the treethrow model is most sensitive to slope, the four watersheds show additional variation as a function of their relative steepness. Bedrock lithology controls treethrow erosion because of relatively greater steeply sloping watershed area. The mean annual treethrow erosion rate for the Canóvanas watershed is reduced because only about 71 percent of the watershed is currently forested (Murphy and others, 2012). Because the Cayaguás watershed has less steep slopes and is only about 42 percent forested, the contribution of treethrow

soil erosion is only $4 \text{ t km}^{-2} \text{ yr}^{-1}$. Comparable values were estimated in North American settings, where sediment delivery to river channels by treethrow was estimated at $9 \text{ t km}^{-2} \text{ yr}^{-1}$ from Clearwater River watershed, Washington (Reid, 1981), and at $1 \text{ t km}^{-2} \text{ yr}^{-1}$ from watershed 10, Cascade Range, Oregon (Swanson and others, 1982).

Fluvial Sediment

Mean suspended sediment yield (or export) ranged from 325 to $2,140 \text{ t km}^{-2} \text{ yr}^{-1}$ in the study watersheds for the period 1991–2005, varying with land use and bedrock lithology (table 5). These values are comparable to island-wide estimates of 570 to $1,900 \text{ t km}^{-2} \text{ yr}^{-1}$ for the period 1990–2000 (Larsen and Webb, 2009). Using a bedload transport equation from Parker and others (1982), Larsen (1997) estimated bedload transport in the Canóvanas and Mameyes rivers for the period 1991–1995 at $83 \text{ t km}^{-2} \text{ yr}^{-1}$ and $110 \text{ t km}^{-2} \text{ yr}^{-1}$, respectively. It should be noted that bedload-sediment transport models are potentially inaccurate by as much as an order of magnitude or more in predicting annual loads, and for the most part they predict maximum potential loads if the various frictional effects of channel obstructions that reduce transport are not considered (Gomez and Church, 1989). With this uncertainty in mind, Larsen (1997) reported that bedload transport was estimated to have occurred for a total of about 7 days during the 5-year (1991–1995) study period in the Canóvanas and Mameyes rivers. The mass of bedload trapped behind wire screens (10-cm mesh) at gaging stations monitored by the U.S. Department of Agriculture Forest Service on two Mameyes tributaries averaged $52 \text{ t km}^{-2} \text{ yr}^{-1}$ (F.N. Scatena, written commun., 1996). This rate is 47 percent of the median rate of $110 \text{ t km}^{-2} \text{ yr}^{-1}$ estimated for the Río Mameyes. The factor-of-2 difference between the two values suggests that the modeled bedload estimates are reasonably accurate, if one considers the coarse screen size used on the Mameyes tributaries and the inherent uncertainties noted above associated with bedload transport models.

Sediment concentration, calculated here as sediment yield normalized by runoff, was about 2.3 to 3.7 times as great in the two watersheds in secondary forest and pasture compared with sediment concentration in the watersheds in primary forest (fig. 4). The influence of lithology was comparable: sediment concentration in granitic-bedrock (quartz diorite and granodiorite) watersheds was 3.0 to 4.7 times as high as sediment concentration in volcaniclastic-bedrock watersheds.

These contrasts highlight the well-known effect of land use on sediment yield, but they also make apparent the strong control of bedrock geology as well.

The relation between suspended-sediment yield and runoff among the four study watersheds is relatively consistent for three orders of runoff, from about 0.1 millimeters per hour (mm h^{-1}) to 30 mm h^{-1} (fig. 4). Yield from the forested Mameyes watershed is the least per unit of runoff, in spite of the great relief (approximately 1 km) of the watershed. The forested Icacos watershed is comparable to the Canóvanas watershed with respect to suspended-sediment yield per unit of runoff. Although relief in the Icacos watershed is much lower than that of the Mameyes watershed, the more easily mobilized sediment in this sandy-bed river makes the Icacos productive. Suspended-sediment yield from the Canóvanas watershed is large, because relief is high and the landscape has been disturbed for agriculture and pasture. Finally, suspended-sediment yield from the Cayaguás watershed is the greatest of the four watersheds, because of the combination of easily mobilized sediment in the sandy-bed river and the great anthropogenic disturbance. Most of the landscape was deforested during the past two centuries for agricultural and pastoral use (Larsen and Santiago-Román, 2001). Mean annual suspended-sediment discharge from Puerto Rico into surrounding coastal waters is estimated to range from 2.7 to 9.0 million metric tons (Larsen and Webb, 2009). Storm runoff transports a substantial part of fluvial suspended sediment from uplands to the coast; for example, the highest recorded daily sediment discharge is 1 to 3.6 times the annual suspended-sediment discharge, and runoff from major storms induces sediment transport 1 to 32 times the median annual sediment load. During this study, suspended-sediment yield (measured as instantaneous concentration) from the four study watersheds extended about nine orders of magnitude, from a low of $0.04 \text{ kg km}^{-2} \text{ h}^{-1}$ in the Canóvanas watershed to a remarkable $2 \text{ million kg km}^{-2} \text{ h}^{-1}$ in the Icacos watershed (fig. 4).

Gellis (1993) described fluvial sediment transported by the discharge related to Hurricane Hugo in the Loíza watershed. He noted that observed suspended-sediment loads were less than expected because high winds caused vegetation and debris to accumulate on hillslopes where it blanketed the soil surface, and in channels where it resulted in local backwater effects that reduced stream velocity. The storm-average suspended sediment concentration in the Río Grande de Loíza was $2,290 \text{ mg L}^{-1}$, the second lowest of 12 storms monitored at the site. In another study, Gellis (1991), again in the Loíza watershed, evaluated the effects of construction on sediment

Table 5. Annual fluvial suspended sediment for the period 1991–2005 in study watersheds, eastern Puerto Rico.¹

[$\text{t km}^{-2} \text{ yr}^{-1}$, metric tons per square kilometer per year; $\text{kg km}^{-2} \text{ mm}^{-1}$, kilograms per square kilometer per millimeter, which is equivalent to milligrams per liter]

Measure of sediment load	Canóvanas	Cayaguás	Icacos	Mameyes
Mean suspended sediment export, $\text{t km}^{-2} \text{ yr}^{-1}$	424	2,110	2,140	325
Mean suspended sediment concentration, $\text{kg km}^{-2} \text{ mm}^{-1}$ of runoff	435	1,300	560	118

¹U.S. Geological Survey data summarized from Stallard and Murphy (2012).

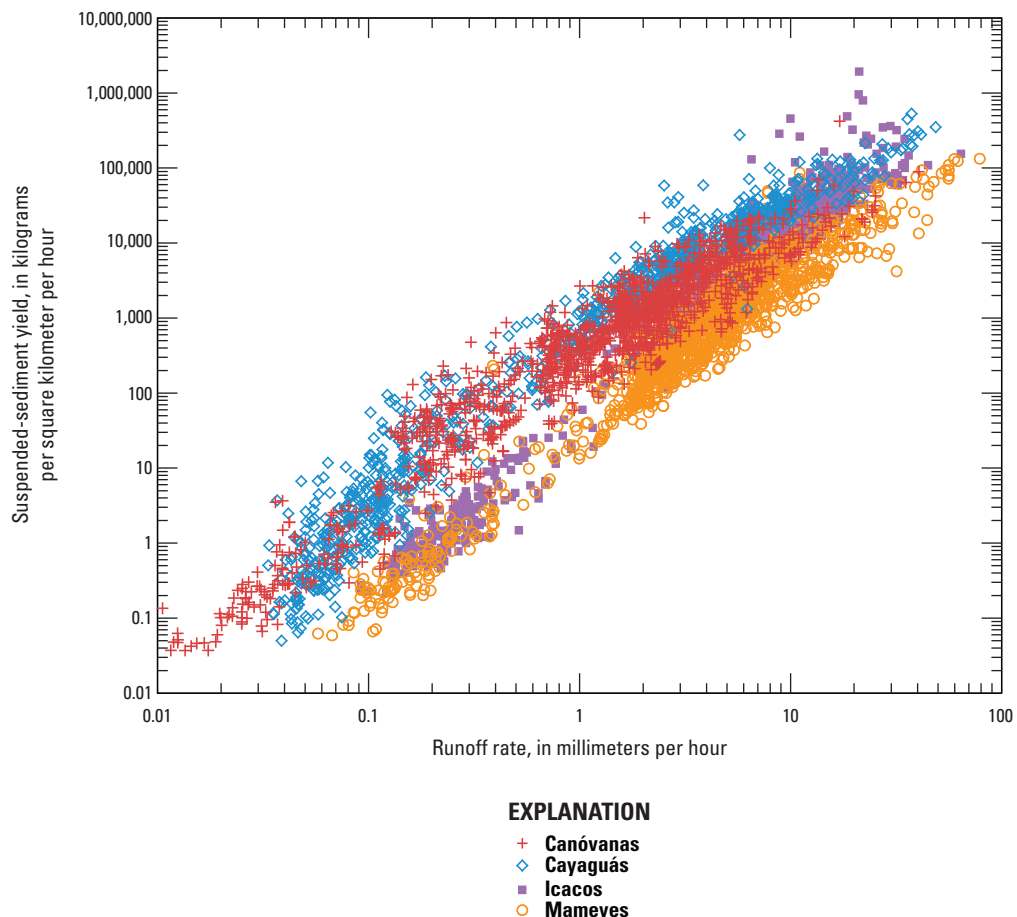


Figure 4. Fluvial transport of suspended-sediment yield compared with runoff rate in the four study watersheds, eastern Puerto Rico.

production. Suspended-sediment concentrations near construction areas were as high as $80,000 \text{ mg L}^{-1}$ with yields ranging from $7,600$ to $11,600 \text{ t km}^{-2} \text{ yr}^{-1}$.

Simon and Guzmán-Ríos (1990) described upland sediment erosion in the Loíza watershed. Using the Yang transport equation (Stevens and Yang, 1989), they estimated bed-material yield from the two principal Río Grande de Loíza tributaries to be $2,900 \text{ t km}^{-2} \text{ yr}^{-1}$. They reported that bed material composed between 34 and 92 percent of the total sediment yield and that the main source of coarse material may have been from the introduction of mass-wasting debris in headwater streams.

Sediment Storage and Sediment Budgets

Hillslope soil and regolith is eroded by continuous low-magnitude processes such as soil creep and slope wash and by episodic high-magnitude processes such as landsliding and (to a lesser extent) treethrow. Once entrained, sediment is exported from the watersheds by fluvial transport (that is,

sediment yield). However, material eroded from hillslopes may reside in several types of storage compartments before leaving the watershed. This element of the sediment budgets was approximated in very general terms and is discussed first.

Sediment Storage in Channel Beds, Bars, and Floodplains

Channel bar mass ranged from a low of 350 t km^{-2} in the Icacos watershed to a maximum of $2,600 \text{ t km}^{-2}$ in the Mameyes watershed (table 6). The estimated mass of sediment composing the beds of rivers ranged from $7,600$ to $12,100 \text{ t km}^{-2}$ of watershed drainage area. Flood-plain and Quaternary alluvium mass ranged from 800 t km^{-2} in the Mameyes watershed to $28,700 \text{ t km}^{-2}$ in the Cayaguás watershed. These values are approximate, as discussed in section Sediment Storage, and probably represent a minimum estimate because many flood-plain deposits in these small watersheds are not easily or accurately identified on 1:20,000-scale maps and aerial photographs.

Table 6. Estimated sediment in storage in study watersheds, eastern Puerto Rico, in channel beds, bars, flood plains, and Quaternary alluvium.

[t km⁻², metric tons per square kilometer]

Storage location	Canóvanas (t km ⁻²)	Cayaguás (t km ⁻²)	Icacos (t km ⁻²)	Mameyes (t km ⁻²)
Channel bed	10,100	11,200	7,600	12,100
Watershed channel bar	720	400	350	2,600
Flood plain and Quaternary alluvium	9,800	28,700	16,300	800
Total	20,620	40,300	24,250	15,500

The channel bed, exposed channel bar, and flood-plain deposits in each watershed were assigned a degree of relative activity as a function of how often particles in each compartment are mobilized (Madej and Ozaki, 1996; Florsheim and others, 2000). The channel bed was defined as active to intermittent, because it is mobilized almost daily in the sand-bed rivers, but only several times per year or less in the boulder-bed rivers. Channel bars were considered to be intermittently mobilized, approximately monthly to annually, in the four watersheds. Flood plains are relatively inactive on an annual basis, although streambank failures were observed following high discharge.

Colluvium, Hillslope Sediment, and Core Stones

A maximum estimate of hillslope colluvial storage can be derived from the volume of historical and prehistoric landslide scars in each watershed (table 2). These values are on the order of 500,000 m³ km⁻² or more in each watershed. The magnitude of total landslide scar volume indicates that colluvial storage of sediment may be the greatest component of watershed-scale sediment storage. In the Icacos watershed, field observation indicates that most of the material eroded by landsliding is not present on footslopes, but rather it has been transported out of the watershed. However, even if only one tenth of landslide-derived colluvial material remains in the watersheds, it still contains more material than all other estimated storage compartments combined (table 6). Colluvium, residing on low-angle footslopes and adjacent flood plains, also represents the least active storage compartment in the watersheds.

Corestones are large bedrock remnants which are exposed gradually as surrounding saprolite is eroded away or episodically by mass wasting (Ruxton, 1967). Corestone boulders are commonly several meters or more in diameter and are abundant in stream channels, where they may remain for thousands of years while being subjected to chemical weathering and to abrasion (Brown and others, 1995). These large boulders represent one end member of the colluvial particle-size distribution.

Abundant corestones are observed in tributaries and in the Icacos main channel. Corestones are observed in the Cayaguás watershed as well, but they are buried by large amounts of modern sandy colluvium and alluvium in the

upland zero- and first-order channel reaches. Excavation of Cayaguás tributary channels reveals their presence within and beneath a matrix of sandy alluvium. In contrast, massive boulders with diameters as large as several meters are commonly exposed in, on, or near the beds of the Canóvanas and Mameyes rivers. The great size and abundance of the boulders present in the Canóvanas and Mameyes channel beds appears to be largely controlled by the massively bedded volcaniclastic sandstone and breccia from which the boulders are derived (Seiders, 1971; Clark and Wilcock, 2000). The large boulders may remain for considerable time in local topographic lows on footslopes, channels, or near-channel areas because of the lack of a transport mechanism once the boulders have reached these locations (Ahmad and others, 1993; Scatena, 1995).

Time Scales and Anthropogenic Effects

The total annual hillslope sediment contribution in the watersheds is dominated by the material derived from landsliding, which highlights a timescale consideration for the budget estimates (table 3). As previously noted in section Analysis of Geomorphic Processes, landslide ages were estimated as historical and prehistoric. The rates of prehistoric landsliding estimated for the Icacos and Mameyes watersheds may be most appropriate for long-term hillslope inputs, because these watersheds have been relatively undisturbed by human influence during the last two centuries. However, this estimation contains uncertainties dependent on climate and land use during the past 1,000 years. In contrast, historical rates should be more appropriate in the Canóvanas and Cayaguás watersheds because they reflect changes in hillslope processes that have resulted from human influence.

Ultimately, the episodic nature of mass wasting by landslides dictates that sediment budgets (in an environment where landslides dominate hillslope erosive processes) are best estimated at decadal- to century-scale time steps, rather than annually as described here. This longer time step serves to reduce the great difference in magnitude between geomorphically continuous and episodic processes. The landslide-dominated hillslope sediment inputs listed in table 3 are not necessarily expected to compare closely with fluvial export, because much of the colluvium may be long retained in sediment storage sites before transport from the watershed. The storage sites act as an enormous buffer, periodically receiving

large pulses of hillslope-derived sediment and losing it at a more continuous rate. Nonetheless, the fluvial sediment export rates are multiyear averages from a period that included a drought and several large hurricanes and should, therefore, represent long-term conditions. These variations in geomorphic process considerations, timescales, and land use notwithstanding, the approximate sediment budgets provide insights into the geomorphology of each watershed.

Erosion and Sediment Export: Are They in Balance?

Hillslope erosion in the Canóvanas watershed exceeds fluvial suspended-sediment export (yield) (table 3). If all hillslope inputs are included, this watershed has a sediment delivery ratio of 10 to 21 percent (13 to 25 percent if bedload yield estimates are included). However, because little landslide activity has been noted in the watershed during recent decades, most of the current annual sediment export was probably derived from nonlandslide inputs (slopewash, soil creep, and treethrow). The annual landslide input of 2,000 to 4,000 t km⁻² can therefore be left out of the budget for recent decades. Accordingly, at least for the period 1991 to 2005, the difference between the sum of the annual nonlandslide inputs and annual fluvial export could have been derived from the extensive active and intermittent storage compartments (tables 3, 5, and 6).

In the Cayaguás watershed, hillslope erosion is more than double the estimate of fluvial sediment export. As discussed in the Landslide Frequency section, this highly modified landscape can yield sediment in large quantities. Much of the sediment in this low-gradient watershed resides in temporary storage in and near channels where it is available for export during storms.

The estimate of hillslope erosion in the Icacos watershed is less than half the fluvial export rate; however, if one considers the inherent uncertainties of each element, this difference may not be important (table 3). Hillslope-derived inputs were calculated to be 750 t km⁻² yr⁻¹, while the mean annual fluvial export was 2,140 t km⁻². The high annual rainfall, minimal anthropogenic disturbance, and sand-dominated particle size lead to a high transport-rate, high-efficiency geomorphic system. The large amount of material available for transport from active storage in the channel bars and the channel bed, 7,950 t km⁻² (table 6), means that most storms should be able to transport substantial sediment loads. Field observations and GIS analysis of the watershed indicates that extensive flat areas (flood plains and Quaternary alluvium) total approximately 36,000 m² in the Icacos watershed (Larsen, 1997). Sediment storage in these areas is 16,300 t km⁻² (table 6). This area provides an additional source of sediment, although deposits in this area are probably rarely entrained because of the low channel gradient and small contributing area of the watershed (0.88 km²) upstream of most of the deposits. Finally, historical landslides not associated with roads in the Icacos watershed were estimated to have eroded 200 t km⁻²

yr⁻¹. This volume indicates that two thirds of all hillslope erosion, 500 t km⁻² yr⁻¹, is attributable to road construction and maintenance. Anthropogenic disturbance in this watershed may be responsible for the majority of fluvial sediment yield.

Hillslope erosion in the Mameyes watershed exceeds fluvial sediment export. If all hillslope inputs are included, the Mameyes has a sediment delivery ratio of 15 to 62 percent (20 to 83 percent if bedload yield estimates are included). This ratio indicates a more efficient linkage between hillslopes and river channels than in the anthropogenically disturbed Canóvanas watershed. A total of 43 percent of the 189 historical landslides mapped in the Mameyes watershed were associated with road construction and maintenance. Most of these landslides were small slumps and shallow soil slips that eroded about 80 t km⁻² yr⁻¹, or approximately half of all landslide-derived sediment. Most of the total fluvial sediment yield may therefore be derived from landslide activity associated with roads.

Landform Development

A conceptual geomorphic model of landform development for the Greater Antilles was proposed by Ahmad and others (1993). This model postulates that landsliding is the major contributor of sediment to stream channels. A similar landslide-dominated model was proposed earlier for the island of Dominica by Reading (1986). These models are supported by the work described in the four Puerto Rican study watersheds.

A total of 41 landslide-triggering storms occurred between 1960 and 1991 in the central mountains of Puerto Rico (Larsen and Simon, 1993), an average of 1.3 landslide-triggering storms per year. This rate demonstrates that geomorphic work by mass wasting is a regular and important process in much of the island. With respect to mass wasting, landslides, for the most part, move orders of magnitude more material than other modes of hillslope erosion. The annual mass of combined slopewash, treefall, and soil creep is dwarfed by the amount of material eroded by landsliding. At decadal or longer time scales, landslides deliver orders of magnitude more sediment to footslopes, flood plains, and stream channels than all other hillslope-erosion processes combined, although the frequency and magnitude of landsliding differs strongly with lithology and land use.

Once the sediment is delivered to riparian areas and stream channels, the rate and manner of its evacuation are also variable, and both depend on, and contribute to, channel morphology. In the watersheds underlain by volcaniclastic bedrock (Canóvanas and Mameyes) this evacuation of sediment can be seen as an autocontrolled feedback loop in which a period of accelerated mass wasting (caused in the short term by anthropogenic disturbance, climate perturbation (a period of increased tropical disturbances), winter storms, or other heavy rainfall) introduces large amounts of sediment, including massive boulders, into the river channels. The increased number of large particles armors the channel bed, temporarily reduces sediment transport, and reduces channel incision.

As incision is slowed, the rate of mass wasting of hillslopes may be reduced and theoretically remain so until chemical weathering, abrasion, or sufficient high-magnitude flows are able to reduce the mass of large particles and transport enough channel sediment to allow further incision. Thus starts another cycle of potentially increased mass wasting.

In the watersheds underlain by granitic bedrock (Cayaguás and Icacos), the much higher rate of chemical weathering of the coarsely crystalline rocks limits channel armoring with boulders, compared with the volcaniclastic bedrock of other watersheds. The explanation lies in the highly erodible nature of granitic rock in the humid tropics (White and others, 1998). The granitic bedrock weathers to saprolite to depths of as much as tens of meters (Douglas, 1967; Simon and others, 1990). As feldspars and other minerals are weathered in the year-round wet ($>2,000$ mm annual rainfall) and warm ($>19^{\circ}\text{C}$ mean annual temperature) environment, the rock matrix disaggregates, and easily transported grus develops at the ground surface (Gerrard, 1994; Buss and White, 2012). Therefore, landsliding and slopewash are more effective agents of erosion in granitic bedrock terrain than in the volcaniclastic terrain. Although large corestones are abundant in some channel reaches in the granitic bedrock, the resulting material delivered to drainage channels is mainly sand sized. Consequently, fluvial erosion is highly effective and promotes channel extension. This extension is manifested, in part, as active slumping at the heads of tributaries in zero-order valleys, leading to higher watershed drainage density in the watersheds underlain by granitic bedrock (1.87 km km^{-2} in the Cayaguás watershed and 2.54 km km^{-2} in the Icacos watershed), compared with those in volcaniclastic bedrock (about 1.35 km km^{-2} in both the Canóvanas and Mameyes watersheds). Moreover, channel heads that are extended by erosion during large storms tend to pirate neighboring drainages observable in the field or on topographic maps as unusual confluences in southern portion of Cayaguás watershed. Outward expansion resulting from mass wasting on valley sides also leads to widening of main channel valleys. This rapid erosion has lowered channel gradients in the granitic watersheds to the point where the Icacos watershed forms, on average, a relatively low-relief landscape in the central part of the watershed (fig. 3). The contact between the erodible granitic bedrock and resistant volcaniclastic bedrock downstream of the Icacos gaged outlet is a prominent nickpoint, downstream of which the stream descends from 610 m to 50 m elevation above mean sea level in a distance of only 3 km. This nickpoint limits erosion and downcutting of the Río Icacos upstream of the gaging station. The Río Cayaguás has eroded its watershed similarly, such that low-gradient tributaries predominate and their headward extension has enabled the stream system to approach within 12 km of the south (Caribbean) coast of the island, in spite of being part of a north-coast-draining river that crosses a straight-line distance of more than 50 km to reach the Atlantic Ocean. However, substantial erosion and downcutting of the Río Cayaguás upstream of the gaging station is limited by its relatively low elevation, only 150 m above sea level (Figueroa-Alamo and others, 2006).

The rates of mass-wasting erosion and fluvial sediment transport estimated for the Cayaguás and Icacos watersheds are high for Puerto Rico. Even on geologic time scales, landscape denudation in the Cayaguás and Icacos watersheds appears to have been extreme. Evidence of this denudation can be seen on topographic maps, where watersheds underlain by granitic bedrock appear anomalously low compared with surrounding nongranitic bedrock terrain. The granitic rocks are easily identified on topographic maps as eroded areas of the otherwise high-elevation Luquillo Mountains and Cayey Mountains.

Summary and Conclusions

The montane humid tropics are a geomorphologically dynamic environment that hosts a range of continuous to episodic hillslope erosion processes. The warm, moist setting promotes rapid development of soil and subsequent growth of vegetation. Steep hillslopes and heavy, intense rainfall result in active hillslope erosion.

The four forested and agriculturally developed watersheds located in eastern Puerto Rico that were investigated in this study hold numerous possibilities for geomorphological comparison, only a few of which were examined here. Hillslope erosional processes—landslides, slopewash, soil creep, and treethrow—are important mass wasting mechanisms in all four study watersheds. The intensity of these processes is closely related to land use, bedrock geology, and rainfall. In all watersheds, episodic landslide activity, calculated at annual, decadal, or greater time scales, is far more important than any other form of mass wasting with respect to the mass of earth materials moved downslope. Landslide activity is estimated to have eroded about 500 to $5,000 \text{ t km}^{-2} \text{ yr}^{-1}$ in the four watersheds, whereas the combined totals of estimated slopewash, soil creep, and treethrow ranged from 43 to $120 \text{ t km}^{-2} \text{ yr}^{-1}$. Nonetheless, the low-intensity, more continuous processes of erosion (slopewash, soil creep, treethrow) provide a steady stream of sediment to fluvial systems that is sufficient to make up the bulk of fluvial sediment export during some years.

In contrast, anthropogenic disturbance plays a conspicuous role in mass wasting that is most apparent in the developed Cayaguás watershed. Much of the landslide-caused erosion in the forested watersheds was associated with highway corridors: road-related landslides composed 63 percent and 43 percent of the total contribution of historical landslides in the Icacos and Mameyes watersheds, respectively. The differing timescales upon which the landslide data were based require cautious comparison of annual mass wasting rates. However, the order of magnitude difference in rates between the forested and developed watersheds implies that human modification of hillslopes has increased landslide frequency and consequent availability of sediment for fluvial transport. The large proportion of rapid mass movements associated with road construction and maintenance in the forested watersheds further demonstrates the great sensitivity of these hillslopes to human disturbance.

Suspended sediment yield from the four watersheds ranged from 325 to 2,140 t km⁻² yr⁻¹. Expressed as metric tons per square kilometer of sediment per millimeter of runoff per year, yield was 2.3 to 3.7 times as high in the anthropogenically disturbed watersheds (Canóvanas and Cayaguás) as in the forested watersheds (Icacos and Mameyes) and, similarly, 3.0 to 4.7 times as high in the watersheds underlain by granitic bedrock (Cayaguás and Icacos) as in the watersheds underlain by volcaniclastic bedrock (Canóvanas and Mameyes). These comparisons highlight the importance of both land use and bedrock geology on fluvial sediment transport.

The quantification of the principal hillslope and fluvial processes and sediment budgets provides a means for evaluating small montane humid-tropical watersheds from a geomorphological perspective and for comparing them with other small watersheds. More important, the contrasting of watersheds with differing land use history provides insights into what present-day development strategies may bring in future decades or even centuries. Based on storage of colluvium and annual fluvial sediment yields, hillslope processes that were triggered as long ago as the early 19th century by the onset of forest clearing will likely affect fluvial sediment transport for more decades to come and possibly into the late 21st century.

Acknowledgments

This work was supported through the United States Geological Survey Water, Energy, and Biogeochemical Budgets program (Larsen and others, 1993; Lins, 1994). Many of the data used in this study were collected and compiled by U.S. Geological Survey Caribbean Water Science Center staff Angel Torres-Sánchez and Iris Margarita Concepción. The manuscript was greatly improved by thoughtful review comments received from Allen Gellis, and Jonathan Godt, both of the U.S. Geological Survey.

References

- Ahmad, Rafi, Scatena, F.N., and Gupta, Avijit, 1993, Morphology and sedimentation in Caribbean montane streams—Examples from Jamaica and Puerto Rico: *Sedimentary Geology*, v. 85, p. 157–169.
- Auzet, Anne-Veronique, and Ambroise, Bruno, 1996, Soil creep dynamics, soil moisture and temperature conditions on a forested slope in the granitic Vosges Mountains, France: *Earth Surface Processes and Landforms*, v. 21, p. 531–542.
- Briot, Pierre, 1966, General physical geography: London, Harrap, 360 p.
- Brown, E.T., Stallard, R.F., Larsen, M.C., Bourlès, D.L., Raisbeck, G.M., and Yiou, F., 1998, Determination of predevelopment denudation rates of an agricultural watershed (Cayaguás River, Puerto Rico) using in situ-produced ¹⁰Be in river-borne quartz: *Earth and Planetary Sciences Letters*, v. 160, p. 723–728.
- Brown, E.T., Stallard, R.F., Larsen, M.C., Raisbeck, G.M., and Yiou, F., 1995, Denudation rates determined from the accumulation of in-situ produced ¹⁰Be in the Luquillo Experimental Forest, Puerto Rico: *Earth and Planetary Science Letters*, v. 129, p. 193–202.
- Brown, Sandra, Lugo, A.E., Silander, Susan, and Liegel, Leon, 1983, Research history and opportunities in Luquillo Experimental Forest: New Orleans, La., U.S. Department of Agriculture Forest Service, Southern Forest Experimental Station General Technical Report SO-44, 128 pages.
- Bruenig, E.F., 1975, Tropical ecosystems—State and targets of research into the ecology of humid tropical systems: *Plant Research and Development*, v. 1, p. 22–38.
- Buss, H.L., and White, A.F., 2012, Weathering processes in the Río Icacos and Río Mameyes watersheds in eastern Puerto Rico, ch. I in Murphy, S.F., and Stallard, R.F., eds., *Water quality and landscape processes of four watersheds in eastern Puerto Rico*: U.S. Geological Survey Professional Paper 1789, p. 249–262.
- Caine, Nel, and Swanson, F.J., 1989, Geomorphic coupling of hillslope and channel systems in two small mountain basins: *Zeitschrift für Geomorphologie* N.F., v. 33, no. 2, p. 189–203.
- Campbell, R.H., 1975, Soil slips, debris flows and rainstorms in the Santa Monica Mountains and vicinity, southern California: *U.S. Geological Survey Professional Paper* 851, 51 p.
- Cerdà, Artemi, and García-Fayos, Patricio, 1997, The influence of slope angle on sediment, water and seed losses on badland landscapes: *Geomorphology*, v. 18, p. 77–90.
- Chatterjea, Kalyani, 1994, Dynamics of fluvial and slope processes in the changing geomorphic environment of Singapore: *Earth Surface Processes and Landforms*, v. 19, p. 585–607.
- CIA World Factbook, 2005, at url <http://www.cia.gov/cia/publications/factbook/index.html>, ISSN 1553–8133, accessed November 11, 2005.
- Clark, J.J., and Wilcock, P.R., 2000, Effects of land-use change on channel morphology in northeastern Puerto Rico: *Geological Society of America Bulletin*, v. 112, p. 1763–1777.
- Clarke, M.F., Williams, M.A.J., and Stokes, T., 1999, Soil creep—Problems raised by a 23-year study in Australia: *Earth Surface Processes and Landforms*, v. 24, p. 151–175.

- Cruden, D.M., and Varnes, D.J., 1996, Landslide types and processes, in Turner, A.K., and Schuster, R.L., eds., *Landslides, investigation and mitigation—Transportation Research Board Special Report 247*: Washington, D.C., National Academy Press, p. 36–75.
- DeGraff, J.V., Bryce, R., Jibson, R.W., Mora, Sergio, and Rogers, C.T., 1989, Landslides—Their extent and significance in the Caribbean, in Brabb, E.E., and Harrod, B.L., eds., *Landslides—Extent and economic significance, International Geological Symposium on Landslides, 28th*, Washington, D.C., 1989, Proceedings: Rotterdam, The Netherlands, Balkema Publishers, p. 51–80.
- Denevan, W.M., 1992, The pristine myth—The landscape of the Americas in 1492: *Annals of the Association of American Geographers*, v. 82, no. 3, p. 369–385.
- Dietrich, W.E., 1982, Settling velocity of natural particles: *Water Resources Research*, v. 18, no. 6, p. 1615–1626.
- Dietrich, W.E., and Dunne, Thomas, 1978, Sediment budget for a small catchment in mountainous terrain: *Zeitchrift für Geomorphologie N.F.*, Supplementband 29, p. 191–206.
- Donnelly, J.P., and Woodruff, J.D., 2007, Intense hurricane activity over the past 5,000 years controlled by El Niño and the West African monsoon: *Nature*, v. 447, p. 465–468.
- Douglas, Ian, 1967, Natural and man-made erosion in the humid tropics of Australia, Malaysia, and Singapore: *International Association of Scientific Hydrology*, v. 75, p. 31–39.
- Figueroa-Alamo, Carlos, Aquino, Zaida, Guzmán-Ríos, Senén, and Sánchez, A.V., 2006, Water resources data—Puerto Rico and the U.S. Virgin Islands, water year 2004: U.S. Geological Survey Water-Data Report PR-04-1, 577 p.
- Florsheim, J.L., Mount, J.F., and Rutten, L.T., 2000, Effect of base level change on floodplain and fan sediment storage and ephemeral tributary channel morphology, Navarro River, California: *Earth Surface Processes and Landforms*, v. 26, p. 219–232.
- Gabet, E.J., Reichman, O.J., and Seabloom, E.W., 2003, The effects of bioturbation on soil processes and sediment transport: *Annual Review of Earth and Planetary Sciences*, v. 31, p. 249–273.
- Garwood, N.C., Janos, D.P., and Brokaw, Nicholas, 1979, Earthquakecaused landslides—A major disturbance to tropical forests: *Science*, v. 205, p. 997–999.
- Gellis, Allen, 1991, Construction effects on sediment for two basins in Puerto Rico, in Fan, Shou-Shan, and Kuo, Yung-Huang, eds., *Interagency Sedimentation Conference, 5th*, Las Vegas, Nevada, March 18–21, 1991, Proceedings: Federal Energy Regulatory Commission, ch. 4: p. 72–78.
- Gellis, Allen, 1993, The effects of Hurricane Hugo on suspended-sediment loads, Lago Loíza Basin, Puerto Rico: *Earth Surface Processes and Landforms*, v. 18, p. 505–517.
- Gellis, A.G., Webb, R.M.T., McIntyre, S., and Wolfe, W.J., 2006, Land-use effects on erosion, sediment yields, and reservoir sedimentation—A case study in the Lago Loíza Basin, Puerto Rico: *Physical Geography*, v. 27, p. 39–69.
- Gerlach, T., 1967, Hillslope troughs for measuring sediment movement: *Revue de Géomorphologie Dynamique*, v. 17, p. 173–174.
- Gerrard, John, 1994, Weathering of granitic rocks—Environment and clay mineral formation, in Robinson, D.A., and Williams, R.B.G., eds., *Rock weathering and landform evolution*: New York, John Wiley, p. 3–20.
- Gilbert, G.K., 1877, Report on the geology of the Henry Mountains, Utah: Washington, D.C., U.S. Geographic and Geologic Survey, Rocky Mountain Region, 160 p.
- Glade, Thomas, Anderson, M.G., and Crozier, M.J., 2005, *Landslide hazard and risk*: New York, John Wiley, 824 p.
- Gomez, Basil, and Church, Michael, 1989, An assessment of bed load sediment transport formulae for gravel bed rivers: *Water Resources Research*, v. 25, no. 6, p. 1161–1186.
- Goudie, Andrew, 1995, *The changing earth, rates of geomorphological processes*: Oxford, United Kingdom, Blackwell Publishers, 302 p.
- Gould, W.A., Martinuzzi, S., and Parés-Ramos, I.K., 2012, Land use, population dynamics, and land-cover change in northeastern Puerto Rico, ch. B in Murphy, S.F., and Stallard, R.F., eds., *Water quality and landscape processes of four watersheds in eastern Puerto Rico: U.S. Geological Survey Professional Paper 1789*, p. 25–42.
- Gupta, A., 1988, Large floods as geomorphic events in the humid tropics, in Baker, V.R., Kochel, R.C., and Patton, P.C., eds., *Flood geomorphology*: New York, John Wiley, p. 301–315.
- Haggett, Peter, 1961, Land use and sediment yield in an old plantation tract of the Serra do Mar, Brazil: *Geographical Journal*, v. 27, p. 50–59.
- Haire, W.J., 1972, Flood of October 5–10, 1970, in Puerto Rico: Commonwealth of Puerto Rico Water Resources Bulletin 12, 38 p.
- Heimsath, A.M., Chappell, John, Spooner, N.A., and Questiaux, D.G., 2002, Creeping soil: *Geology*, v. 30, no. 2; p. 111–114.
- Hooke, R.L., 2000, On the history of humans as geomorphic agents: *Geology*, v. 28, no. 9, p. 843–846.
- Jibson, R.W., 1989, Debris flows in southern Puerto Rico: *Geological Society of America Special Paper* 236, p. 29–55.

- Kates, R.W., Turner, B.L., and Clark, W.C., 1990, The great transformation, in Turner, B.L., Clark, W.C., Kates, R.W., Richards, J.F., Mathews, J.T., and Meyer, W.B., The Earth as transformed by human action—Global and regional changes in the biosphere over the past 300 years: New York, Cambridge University Press, p. 1–17.
- Larsen, M.C., 1997, Tropical geomorphology and geomorphic work—A study of geomorphic processes and sediment and water budgets in montane humid-tropical forested and developed watersheds, Puerto Rico: Boulder, University of Colorado Geography Department, unpublished Ph.D. dissertation, 341 p.
- Larsen, M.C., Collar, P.D., and Stallard, R.F., 1993, Research plan for the investigation of water, energy, and biogeochemical budgets in the Luquillo Mountains, Puerto Rico: U.S. Geological Survey Open-File Report 92–150, 19 p.
- Larsen, M.C., Liu, Z., and Zou, X., 2012, Effects of earthworms on slopewash, surface runoff, and finelitter transport on a humidtropical forested hillslope, Luquillo Experimental Forest, Puerto Rico, ch. G in Murphy, S.F., and Stallard, R.F., eds., Water quality and landscape processes of four watersheds in eastern Puerto Rico: U.S. Geological Survey Professional Paper 1789, p. 179–198.
- Larsen, M.C., and Parks, J.E., 1997, How wide is a road? The association of roads and mass-wasting disturbance in a forested montane environment: Earth Surface Processes and Landforms, v. 22, p. 835–848.
- Larsen, M.C., and Santiago-Román, Abigail, 2001, Mass wasting and sediment storage in a small montane watershed—An extreme case of anthropogenic disturbance in the humid tropics, in Dorava, J.M., Palcsak, B.B., Fitzpatrick, F., and Montgomery, D., eds., Geomorphic processes and riverine habitat: American Geophysical Union Water Science and Application, v. 4, p. 119–138.
- Larsen, M.C., and Simon, Andrew, 1993, Rainfall-threshold conditions for landslides in a humid-tropical system, Puerto Rico: Geografiska Annaler, v. 75A (1–2), p. 13–23.
- Larsen, M.C., and Torres-Sánchez, A.J., 1992, Landslides triggered by the rainfall associated with Hurricane Hugo, eastern Puerto Rico, September 1989: Caribbean Journal of Science, v. 28, no. 3–4, p. 113–120.
- Larsen, M.C., and Torres-Sánchez, A.J., 1998, The frequency and distribution of recent landslides in three montane tropical regions of Puerto Rico: Geomorphology, v. 24, p. 309–331.
- Larsen, M.C., Torres-Sánchez, A.J., and Concepción, I.M., 1999, Slopewash, surface runoff, and finelitter transport in forest and landslide scars in humidtropical steeplands, Luquillo Experimental Forest, Puerto Rico: Earth Surface Processes and Landforms, v. 24, p. 481–506.
- Larsen, M.C., and Webb, R.M.T., 2009, Potential effects of runoff, fluvial sediment and nutrient discharges on the coral reefs of Puerto Rico: Journal of Coastal Research, v. 25, p. 189–208.
- Lenart, M.T., 2003, A comparative study of soil disturbance from uprooted trees, and mound and pit decay, in Puerto Rico and Colorado: Tucson, University of Arizona, unpublished Ph.D. dissertation, 175 p.
- Lewis, L.A., 1974, Slow movements of earth under tropical rainforest conditions: Geology, v. 2, p. 9–10.
- Lins, H.F., 1994, Recent directions taken in water, energy, and biogeochemical budget research: EOS, Transactions, American Geophysical Union, v. 75, no. 38, p. 433–439.
- Madej, M.A., and Ozaki, Vicki, 1996, Channel response to sediment wave propagation and movement, Redwood Creek, California, USA: Earth Surface Processes and Landforms, v. 21, no. 10, p. 911–928.
- Maharaj, R.J., 1993, Landslide processes and landslide susceptibility analysis from an upland watershed—A case study from St. Andrew, Jamaica, West Indies: Engineering Geology, v. 34, p. 53–79.
- Mayewski, P.A., Rohling, E.E., Stager, J.C., Karlén, Wibjörn, Maasch, K.A., Meeker, L.D., Meyerson, E.A., Gassef, Francoise, van Kreveld, Shirley, Holmgren, Karin, Lee-Thorp, Julia, Rosqvist, Gunhild, Rack, Frank, Staubwasser, Michael, Schneider, R.R., and Steig, E.J., 2004, Holocene climate variability: Quaternary Research, v. 62, p. 243–255.
- McKean, J.A., Dietrich, W.E., Finkel, R.C., Southon, J.R., and Caffee, M.W., 1993, Quantification of soil production and downslope creep rates from cosmogenic ¹⁰Be accumulations on a hillslope profile: Geology, v. 21, p. 343–346.
- Meade, R.H., 1982, Sources, sinks, and storage of river sediment in the Atlantic drainage of the United States: Journal of Geology, v. 90, p. 235–252.
- Milliman, J.D., and Meade, R.H., 1983, World-wide delivery of river sediment to the oceans: Journal of Geology, v. 91, p. 1–21.
- Morales Muñoz, G.E., 1943, Orígenes históricos de San Miguel de Hato Grande—Actual pueblo de San Lorenzo: Hato Rey, Puerto Rico, Esmaco Printers Corp., 333 p.
- Murphy, S.F., and Stallard, R.F., 2012, Hydrology and climate of four watersheds in eastern Puerto Rico, ch. C in Murphy, S.F., and Stallard, R.F., eds., Water quality and landscape processes of four watersheds in eastern Puerto Rico: U.S. Geological Survey Professional Paper 1789, p. 43–84.
- Murphy, S.F., Stallard, R.F., Larsen, M.C., and Gould, W.A., 2012, Physiography, geology, and land cover of four watersheds in eastern Puerto Rico, ch. A in Murphy, S.F., and

- Stallard, R.F., eds., Water quality and landscape processes of four watersheds in eastern Puerto Rico: U.S. Geological Survey Professional Paper 1789, p. 1–24.
- Nelson, E.J., and Booth, D.B., 2002, Sediment sources in an urbanizing, mixed land-use watershed: *Journal of Hydrology* 264, p. 51–68.
- Norman, S.A., Schaetzl, R.J., and Small, T.W., 1995, Effects of slope angle on mass movement by tree uprooting: *Geomorphology*, v. 14, no. 1, p. 19–27.
- Osterkamp, W.R., Toy, T.J., and Lenart, M.T., 2006, Development of partial rock veneers by root throw in a subalpine setting: *Earth Surface Processes and Landforms*, v. 31, p. 1–14.
- Parker, Gary, Klingeman, P.C., and McLean, D.C., 1982, Bedload and size distribution in paved gravel-bed streams: *Journal of the Hydraulics Division of the American Society of Civil Engineers*, v. 108, no. HY4, p. 544–571.
- Phillips, J.D., and Marion, D.A., 2006, Biomechanical effects of trees on soil and regolith—Beyond treethrow: *Annals of the Association of American Geographers*, v. 96, p. 233–247.
- Ramos-Scharrón, C.E., and MacDonald, L.H., 2007, Development and application of a GIS-based sediment budget model: *Journal of Environmental Management*, v. 84, p. 157–172.
- Reading, A.J., 1986, Landslides, heavy rainfalls, and hurricanes in Dominica, West Indies: Aberystwyth, United Kingdom, University of Wales, unpublished Ph.D. dissertation, 545 p.
- Reading, A.J., Thompson, R.D., and Millington, A.C., 1995, Humid tropical environments: Cambridge, Mass., Blackwell Publishers, 429 p.
- Reid, H.F., and Taber, Stephen, 1919, The Puerto Rico earthquakes of October–November 1918: *Bulletin of the Seismological Society of America*, v. 9, no. 4, p. 94–127.
- Reid, L.M., 1981, Sediment production from gravel-surfaced forest roads, Clearwater Basin, Washington: Seattle, University of Washington Fisheries Research Institute publication FRI-UW8108, 247 p.
- Restrepo, Carla, and Alvarez, Nora, 2006, Landslides and their contribution to land-cover change in the mountains of Mexico and Central America: *Biotropica*, v. 38, p. 446–457.
- Rouse, Irving, 1993, The Tainos—Rise and decline of the people who greeted Columbus: New Haven, Conn., Yale University Press, 211 p.
- Ruxton, B.P., 1967, Slope wash under mature primary rainforest in northern Papua, in Jennings, J.N., and Mabbutt, J.A., eds., *Landform studies from Australia and New Guinea*: Cambridge, United Kingdom, Cambridge University Press, p. 85–94.
- Scatena, F.N., and Larsen, M.C., 1991, Physical aspects of Hurricane Hugo in Puerto Rico: *Biotropica*, v. 23, no. 4A, p. 317–323.
- Scatena, F.N., 1995, Relative scales of time and effectiveness of watershed processes in a tropical montane rain forest of Puerto Rico, in Costa, J.E., Miller, A.J., Potter, K.W., and Wilcock, Peter, eds., *Natural and anthropogenic influences in fluvial geomorphology*: American Geophysical Union Geophysical Monograph 89, p. 103–111.
- Scatena, F.N., and Lugo, A.E., 1995, Geomorphology, disturbance, and the soil and vegetation of two subtropical wet steepland watersheds of Puerto Rico: *Geomorphology*, v. 13, p. 199–213.
- Schaetzl, R.J., Burns, S.F., Small, T.W., and Johnson, D.L., 1990, Tree uprooting—Review of types and patterns of soil disturbance: *Physical Geography*, v. 11, p. 277–291.
- Seiders, V.M., 1971, Geologic map of the El Yunque quadrangle, Puerto Rico: U.S. Geological Survey Miscellaneous Geologic Investigations Map I-658, scale 1:20,000.
- Shiels, A.B., West, C.A., Weiss, Laura, Klawinski, P.D., and Walker L.R., 2008, Soil factors predict initial plant colonization on Puerto Rican landslide: *Plant Ecology*, v. 195, p. 165–178.
- Simon, Andrew, and Guzmán-Ríos, Senén, 1990, Sediment discharge from a montane basin, Puerto Rico—Implications of erosion processes and rates in the humid tropics, in Ziemer, R.R., O'Loughlin, C.L., and Hamilton, L.S., eds., *Research needs and applications to reduce erosion and sedimentation in tropical steppes*: International Association of Hydrologic Science Publication 192, p. 35–47.
- Simon, Andrew, Larsen, M.C., and Hupp, C.R., 1990, The role of soil processes in determining mechanisms of slope failure and hillslope development in a humid-tropical forest—Eastern Puerto Rico, in Kneuper, P.L.K., and McFadden, L.D., eds., *Soils and landscape evolution*: *Geomorphology*, v. 3, p. 263–286.
- Simonett, D.S., 1967, Landslide distribution and earthquakes in the Bewani and Torricelli Mountains, New Guinea, in Jennings, J.N., and Mabbutt, J.A., eds., *Landform studies from Australia to New Guinea*: Cambridge, United Kingdom, Cambridge University Press, p. 64–84.
- Sirvent, Jaume, Desir, Gloria, Gutierrez, M., Sancho, Carlos, and Benito, Gerardo, 1997, Erosion rates in badland areas recorded by collectors, erosion pins and profilometer techniques (Ebro Basin, northeast Spain): *Geomorphology*, v. 18, p. 61–75.
- Small, T.W., Schaetzl, R.J., and Brixie, J.M., 1990, Redistribution and mixing of soil gravels by tree uprooting: *The Professional Geographer*, v. 42, p. 445–457.

- Stallard, R.F., 1995, Tectonic, environmental, and human aspects of weathering and erosion—A global review using a steady-state perspective: *Annual Reviews of Earth and Planetary Science*, v. 13, p. 11–39.
- Stallard, R.F., 2012, Weathering, landscape equilibrium, and carbon in four watersheds in eastern Puerto Rico, ch. H in Murphy, S.F., and Stallard, R.F., eds., *Water quality and landscape processes of four watersheds in eastern Puerto Rico*: U.S. Geological Survey Professional Paper 1789, p. 199–248.
- Stevens, H.H., and Yang, C.T., 1989, Summary and use of selected fluvial sediment-discharge formulas: U.S. Geological Survey Water Resources Investigation Report 89–4026, 62 p.
- Swanson, F.J., Fredriksen, R.L., and McCorison, F.M., 1982, Material transfer in a western Oregon forested watershed, in R.L. Edmonds, ed., *Analysis of coniferous forest ecosystems in the western United States*: Stroudsburg, Pa., Hutchinson Ross Publishing Company, p. 233–266.
- Trimble, S.W., 1977, The fallacy of stream equilibrium in contemporary denudation studies: *American Journal of Science*, v. 277, p. 876–887.
- UNESCO/UNEP/FAO [United Nations Educational, Scientific, and Cultural Organization, United Nations Environmental Programme, United Nations Food and Agriculture Organization], 1978, *Tropical forest ecosystems*: Paris, UNESCO, 683 p.
- U.S. Department of Commerce, 1961, Generalized estimates of probable maximum precipitation and rainfall frequency data for Puerto Rico and the Virgin Islands: U.S. Department of Commerce Technical Report 52, 94 p.
- White, A.F., Blum, A.E., Schulz, M.S., Vivit, D.V., Stonestrom, D.A., Larsen, Matthew, Murphy, S.F., and Eberl, D., 1998, Chemical weathering in a tropical watershed, Luquillo Mountains, Puerto Rico—I. Longterm versus shortterm weathering fluxes: *Geochimica et Cosmochimica Acta*, v. 62, no. 2, p. 209–226.
- Williams, M.A.J., 1973, The efficacy of creep and slopewash in tropical and temperate Australia: *Australian Geographical Studies*, v. 11, p. 62–78.
- Wolman, M.G., 1990, The impact of man: EOS, Transactions, American Geophysical Union, v. 71, no. 52, p. 1884–1886.
- Young, A., 1960, Soil movement by denudational processes on slopes: *Nature*, v. 188, p. 120–122.

Effects of Earthworms on Slopewash, Surface Runoff, and Fine-Litter Transport on a Humid-Tropical Forested Hillslope in Eastern Puerto Rico

By Matthew C. Larsen, Zhigang Liu, and Xiaoming Zou

Chapter G of
**Water Quality and Landscape Processes of Four Watersheds in
Eastern Puerto Rico**

Edited by Sheila F. Murphy and Robert F. Stallard

Professional Paper 1789-G

**U.S. Department of the Interior
U.S. Geological Survey**

Contents

Abstract.....	183
Introduction.....	183
Purpose and Scope	184
Site Description.....	184
Preparation and Observation of Study Plots.....	187
Data Characteristics and Limitations	187
Effects of Earthworms on Slopewash, Surface Runoff, and Fine-Litter Transport	188
Summary and Conclusions.....	193
Acknowledgments.....	195
References.....	195

Figures

1. Map showing location of Puerto Rico and study area	185
2. Photographs of study site, El Verde, eastern Puerto Rico, 1998.....	186
3. Annotated sketch of idealized soil cross section and a Gerlach trough.....	188
4. Diagrams of rainfall and runoff per sampling period at control and experimental plots, El Verde, eastern Puerto Rico	190
5. Diagrams of daily rainfall and transported soil and organic matter at control and experimental plots, El Verde, eastern Puerto Rico.....	191
6. Diagrams of daily rainfall and transported soil and transported mineral soil at control and experimental plots, El Verde, eastern Puerto Rico	192
7. Diagrams of daily rainfall and transported soil and transported organic material at control and experimental plots, El Verde, eastern Puerto Rico	194

Table

1. Rainfall, runoff, and transported material by sampling period, El Verde, eastern Puerto Rico	189
---	-----

Abbreviations Used in This Report

cm	centimeter
cm s ⁻¹	centimeters per second
g m ⁻²	grams per square meter
h	hour
kg ha ⁻¹	kilograms per hectare
kg m ⁻² yr ⁻¹	kilograms per square meter per year
m	meter
m ²	square meter
mm	millimeter
mm 1,000 yr ⁻¹	millimeters per thousand years
r ²	correlation coefficient
t ha yr ⁻¹	metric tons per hectare per year

Conversion Factors

Multiply	By	To obtain
Length		
millimeter (mm)	0.03937	inch (in.)
centimeter (cm)	0.3937	inch (in.)
meter (m)	3.281	foot (ft)
Area		
square meter (m ²)	10.76	square foot (ft ²)
Flow rate		
centimeters per second (cm s ⁻¹)	0.3937	inches per second (in. s ⁻¹)
millimeters per 1,000 years (mm 1,000 yr ⁻¹)	0.03937	inches per year (in. 1,000 yr ⁻¹)
Other		
grams per square meter (g m ⁻²)	8.922	pounds per acre (lb acre ⁻¹)
kilograms per hectare (g ha ⁻¹)	0.8922	pounds per acre (lb acre ⁻¹)
kilograms per square meter per year (kg m ⁻² yr ⁻¹)	1.843	pounds per square yard per year (lb yd ⁻² yr ⁻¹)

Effects of Earthworms on Slopewash, Surface Runoff, and Fine-Litter Transport on a Humid-Tropical Forested Hillslope in Eastern Puerto Rico

By Matthew C. Larsen,¹ Zhigang Liu,² and Xiaoming Zou^{2,3}

Abstract

Rainfall, slopewash (the erosion of soil particles), surface runoff, and fine-litter transport were measured in tropical wet forest on a hillslope in the Luquillo Experimental Forest, Puerto Rico, from February 1998 until April 2000. Slopewash data were collected using Gerlach troughs at eight plots, each 2 square meters in area. Earthworms were excluded by electroshocking from four randomly selected plots. The other four (control) plots were undisturbed. During the experiment, earthworm population in the electroshocked plots was reduced by 91 percent. At the end of the experiment, the electroshocked plots had 13 percent of earthworms by count and 6 percent by biomass as compared with the control plots.

Rainfall during the sampling period (793 days) was 9,143 millimeters. Mean and maximum rainfall by sampling period (mean of 16 days) were 189 and 563 millimeters, respectively. Surface runoff averaged 0.6 millimeters and 1.2 millimeters by sampling period for the control and experimental plots, equal to 0.25 and 0.48 percent of mean rainfall, respectively. Disturbance of the soil environment by removal of earthworms doubled runoff and increased the transport (erosion) of soil and organic material by a factor of 4.4. When earthworms were removed, the erosion of mineral soil (soil mass left after ashing) and the transport of fine litter were increased by a factor of 5.3 and 3.4, respectively. It is assumed that increased runoff is a function of reduced soil porosity, resulting from decreased burrowing and reworking of the soil in the absence of earthworms. The background, or undisturbed, downslope transport of soil, as determined from the control plots, was 51 kilograms per hectare and the “disturbance” rate, determined from the experimental plots, was 261 kilograms per hectare. The background rate for

downslope transport of fine litter was 71 kilograms per hectare and the disturbance rate was 246 kilograms per hectare. Data from this study indicate that the reduction in soil macrofauna population, in this case, earthworms, plays a key role in increasing runoff and soil erosion and, therefore, has important implications for forest and water management.

Introduction

The hydrological role of tropical forests as compared with deforested landscapes has been a source of considerable controversy during the past century because forests, although they are recognized to have many benefits, such as carbon storage, biodiversity, and landscape aesthetics, almost universally consume more water than deforested landscapes (Bruijnzeel, 2004; Jackson and others, 2005). In seasonal-climate regions, this excess consumption of water can be mitigated if pedogenic processes characteristic of forests promote sufficient infiltration such that groundwater reserves under forests exceed those under deforested landscapes—the “sponge effect” of Bruijnzeel (2004).

One characteristic of forested environments is macroporosity and soil structure created by burrowing animals. We examined the generation of macroporosity by earthworms in forests of eastern Puerto Rico. Eastern Puerto Rico represents an excellent setting for such an experiment because it hosts fewer types of burrowing organisms than mainland tropical forests, where burrowing mammals, leaf-cutter ants, and cicadas are common. Earthworms at the Puerto Rico site can easily be excluded using electroshock techniques.

Soil erosion is a widespread problem in the humid tropics (Douglas, 1967; Haantjens, 1969; Lal, 1990; Nooren and others, 1995). Rates of soil erosion are high in part because of abundant, deep, highly weathered regolith and soils typical of the warm, moist environment and high rainfall intensity associated with convective storms and tropical disturbances such as hurricanes (Ruxton, 1967; Hastenrath, 1991; Reading and others, 1995). The rate of soil erosion is influenced by the character, abundance, and decomposition of plant litter, which is, in turn, strongly affected by soil fauna, including

¹U.S. Geological Survey, 436 National Center, Reston, Va., 20192, USA

²Institute for Tropical Ecosystem Studies, University of Puerto Rico, P.O. Box 21910, Rio Piedras, Puerto Rico, 00931–1910, USA

³Xishuangbanna Tropical Botanical Garden, Chinese Academy of Sciences, 88 Xuefu Road, Kunming, Yunnan, China

earthworms (Hazelhoff and others, 1981; Haria, 1995; Chauvel and others, 1999; Heneghan and others, 1999; Lavelle and others, 1999; Liu and Zou, 2002; Six and others, 2004).

Land degradation has been defined as a substantial decrease in either or both of an area's biological productivity or usefulness due to human interference (Johnson and Lewis, 1995). One aspect of landscape degradation is increased runoff, which in disturbed environments has been thought to be largely a function of such factors as soil compaction, loss of the soil A horizon, loss of vegetative cover, decreased evapotranspiration, and decreased leaf litter (Johnson and Lewis, 1995). In contrast, the burrowing of earthworms increases soil porosity, resulting in greater rainfall infiltration. As they burrow, earthworms exert pressure on surrounding soil and deposit mucus on the burrow walls; additionally, the burrow walls may be lined with oriented clays (Six and others, 2004). These two features of earthworm burrows can provide stable, efficient conduits of near-surface throughflow. Earthworms ingest organic and inorganic materials that are mixed in the gut and excreted as a cast (Six and others, 2004). Deposition of surface casts on the ground surface creates surface roughness, which can itself reduce rainfall runoff and soil erosion (Le Bayon and Binet, 2001). Additionally, field observations by the authors and others (Le Bayon and Binet, 2001) indicate that earthworm casts, if abundant, can increase soil surface area at the microtopographic scale. The comminuting, feeding, burrowing, and casting activities of earthworms regulate soil processes and are well recognized for their influence on the decomposition of plant materials (Darwin, 1892; Lee, 1985). Darwin (1892) was the first to quantify the geomorphic work accomplished by earthworms, calculating that in Staffordshire, England, they brought to the soil surface 1.7 kilograms per square meter per year ($\text{kg m}^{-2} \text{ yr}^{-1}$) (17 metric tons per hectare per year ($\text{t ha}^{-1} \text{ yr}^{-1}$)) of dry earth. Chauvel and others (1999) estimated that earthworms in a humid-tropical area of Brazil produced 100 metric tons per hectare per year of casts.

Earthworms generally represent the greatest portion of macrofauna biomass in moist and wet tropical forests (Camilo and Zou, 2001). In tropical wet forest in the Luquillo Experimental Forest, eastern Puerto Rico, earthworms compose as much as one third of the fauna biomass (Odum and Pigeon, 1970). In agroecosystems, Parmelee and others (1990) showed that earthworms increase plant litter decomposition rates by 20 to 50 percent. This substantial effect is reduced in disturbed landscapes or when forests are converted to other uses such as pasture (Liu and Zou, 2002). Where natural forest in Puerto Rico was replaced by Caribbean pine and mahogany plantations, earthworm richness and density were shown to be reduced by half, possibly as a result of differences in soil water content, soil pH, organic matter content, and nutrient availability associated with the quantity and quality of litter inputs (González and others, 1996; Liu and Zou, 2002). Exclusion of tropical earthworms *P. corethrurus* in the study forest was associated with a reduction in soil respiration rates (Liu and Zou, 2002).

Purpose and Scope

Soil fauna populations are known to be affected by land use change, but the ecological consequences of changing soil fauna have not been extensively evaluated in tropical ecosystems (Blanchard and others, 1997). Nonetheless, many studies demonstrate that tropical soil macrofauna speed the decomposition of plant litter (Bouché, 1977; Chauvel and others, 1999; Heneghan and others, 1999; González and Seastedt, 2001). The published literature describing the role of soil macrofauna in soil erosion and runoff processes in the humid tropics is limited (Baidgett and others, 2001). Because human population pressure on the natural environment has increased substantially in the humid tropics in recent decades, baseline studies are needed to better understand these process and to improve land-management practices (Johnson and Lewis, 1995; Grau and others, 2003).

In an effort to quantify the association of earthworms with several basic physical soil and hydrological processes, in the present study we asked the following questions: do earthworms affect slopewash, the amount of surface rainfall runoff, and the transport of fine litter? A simple field experiment was designed to measure these quantities.

Site Description

A gentle hillslope 350 meters (m) above sea level, sloping 10° to the northwest (azimuth 310°) in the El Verde section of the Luquillo Experimental Forest ($18^\circ 20' \text{ N.}$, $66^\circ 49' \text{ W.}$) was selected for the experiment (fig. 1). The site is classified as tropical wet forest (Ewel and Whitmore, 1973) and is dominated by tabonuco trees (*Dacryodes excelsa*), a broad-leaved evergreen (fig. 2). Mean monthly temperature ranges from 20.8 to 24.4°C (Brown and others, 1983). Mean annual rainfall is 3,536 millimeters (mm), and it was 4,035 mm during the study period (Schaefer and Melendez, 2001). Mean daily rainfall was 12 mm during the study period; maximum daily rainfall was 160 mm, recorded on April 16, 1998, in association with a local convective storm. The soil is classified as a deep, moderately well-drained Oxisol with a high clay content (89 percent; Soil Survey Staff, 1995). Surficial soil is highly permeable, and little rainfall becomes surface runoff; Larsen and others (1999) reported runoff values of 0.2 to 0.5 percent of monthly rainfall and soil infiltration rates of 0.001 centimeters per second (cm s^{-1}) to 0.46 cm s^{-1} in the Luquillo Experimental Forest. Vegetation covers 80 percent of the forest, and a layer of leaf litter several centimeters thick covers the soil surface (fig. 2). The mean fresh weight of earthworms in the forest is 25 grams per square meter (g m^{-2}), and earthworm density ranges from 32 to 137 m^{-2} ; the mean is 89 worms per square meter (Liu and Zou, 2002). Earthworms are dominated by nonendemic species *P. corethrurus* and *Amynthas rodericensis*, but the native species *Estherella gatesi* also is present (Zou and González, 1997; González and others, 1999). In mature forest, *P. corethrurus* is the most abundant species, but biomass

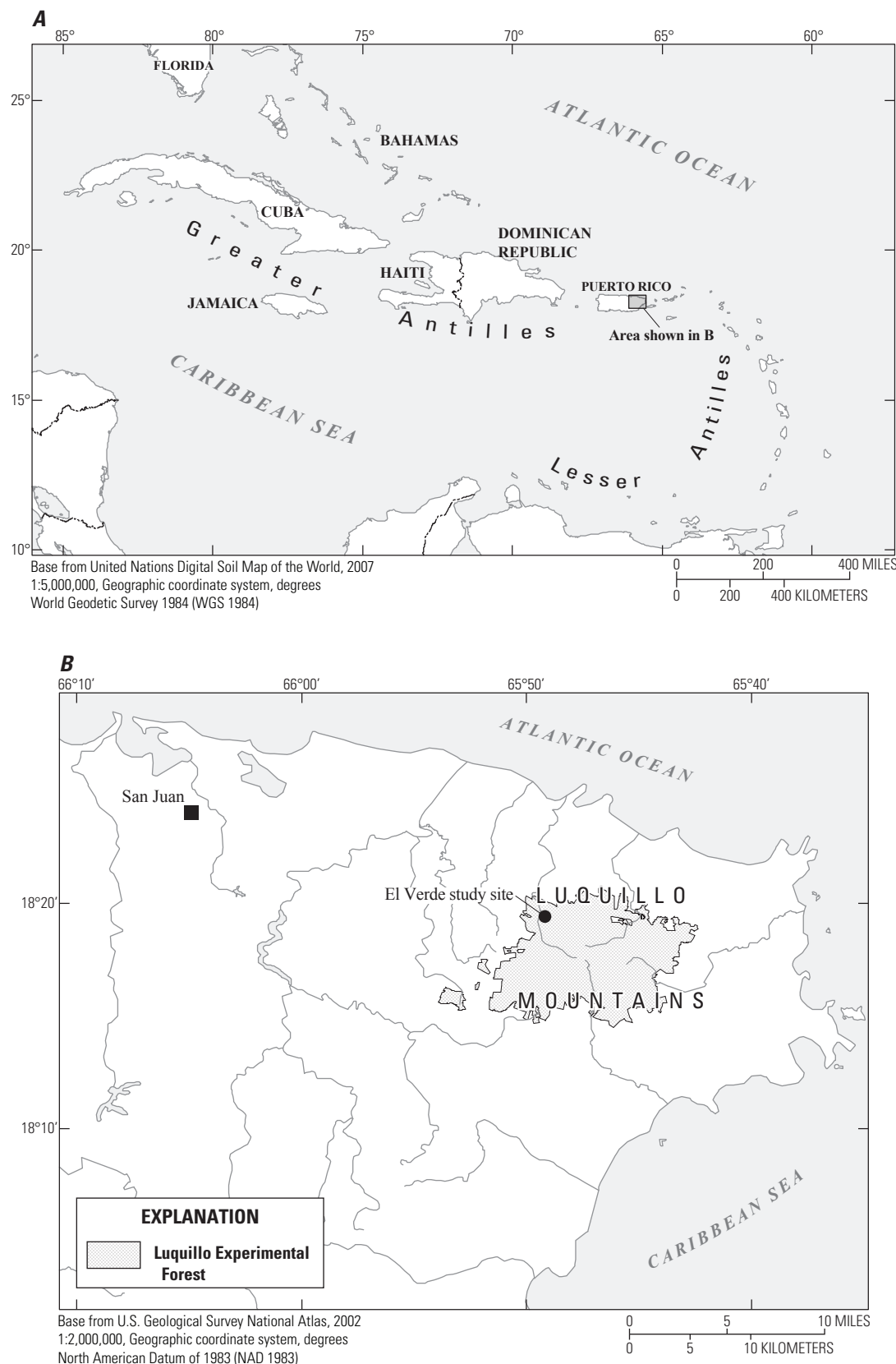


Figure 1. Location of Puerto Rico and study area, eastern Puerto Rico.



Figure 2. Study site, El Verde, eastern Puerto Rico, 1998. *A*, tabonuco forest; *B*, one of eight 2-square-meter measurement plots prior to installation of Gerlach trough at downslope end; *C*, understory; and *D*, closeup of forest floor and litter layer. In *D*, note worm castings (*w*), fine rootlets (*f*), and small anthills (*a*); scale in inches (top) and centimeters.

of native earthworms is higher (Zou and González 1997; Sanchez and others, 2003). Earthworms are not highly active during the relative dry season between January and April.

In general, three morphoecological groups of earthworms are described by Bouché (1977): epigeic species, anecic species, and endogeic species. Epigeic species inhabit the litter layer of forest soils above the mineral soil surface and have little effect on soil structure. Anecic species form a network of burrows that penetrate deep into the mineral soil, feed on decayed surface litter, and transport organic material from the surface into their burrows. Endogeic species live in mineral soil horizons and feed on soil enriched with organic matter. *P. corethrurus* and *E. gates* are endogeic species and *A. rodericensis* is an anecic species.

Preparation and Observation of Study Plots

A forested hillslope at the El Verde study site was sampled from February 26, 1998, to April 28, 2000 (fig. 1). Eight rectilinear plots each 2 square meters (m^2) in area (1 m wide, 2 m long) were bounded along their margins with plastic sheeting attached to steel rods for 26 months. The plastic sheets were buried to a depth of 0.5 m; 0.15 m was exposed above the surface to prevent runoff and earthworms from crossing the plot boundaries. Earthworms were removed from four of these plots by electroshocking, by using a 240 volt alternating electrical current (supplied by a portable generator) to bring earthworms to the surface. Once at the surface, earthworms were removed by hand. Each of the four plots from which earthworms were removed was treated with the electrical current for 1.5 hours (h) every 3 months. Electroshocking is an effective technique for removing earthworms; it has been shown to result in minimal soil disturbance and no appreciable effects on microarthropods and nematodes, and it does not persist in the soil, unlike chemicals that can affect soil's biological properties (Blair and others, 1995). At the end of the 26-month experiment, a 0.25- by 0.25-m quadrant in the center of each of the eight plots was excavated to a depth of 0.5 m, and all earthworms were removed and sorted for counting and weighing in a laboratory.

At the start and end of the experiment, Liu and Zou (2002) collected soil samples from six cores (19 mm in diameter) in each plot. They determined soil bulk density by oven-drying at 105°C for 48 h and soil pH by using a 1:1 mixture of soil and deionized water (Liu and Zou, 2002).

Surface-water runoff and slopewash were trapped at the downslope end of each plot by using Gerlach troughs (Gellis and others, 1999; Larsen and others, 1999). A Gerlach trough is a sediment trap designed to retain soil particles, organic material, and surface runoff transported downslope by gravity (Young, 1960; Gerlach, 1967). The Gerlach troughs were fabricated with materials available from a standard hardware

store, using a plastic section of household rain gutter with a hinged metal lid to prevent direct interception of rainfall, rainsplash-transported sediment, and direct litterfall (fig. 3). A rectangular metal strip was attached to the upslope side of the trough and imbedded in the soil to allow slopewash, surface runoff, and fine litter to enter the trough. A 13-mm-diameter plastic tube connected the side of the trough to a 20-liter closed bucket anchored downslope to allow excess runoff and fine sediment to be trapped. Regular sampling of each trap included scooping out sediment and fine litter caught in the trough and measuring the volume of the water-sediment mixture in the buckets. Runoff for each of the eight plots was defined as the total volume of water in the Gerlach trough and 20-liter bucket, divided by the 2- m^2 drainage area. Slopewash samples were collected from each Gerlach trough on average every 16 days (range 8 to 34 days), oven dried at 100°C for 24 h, weighed, then ashed at 550°C for 1 h, and reweighed to determine loss on ignition. Average daily flux of material was calculated for the total mass of oven-dried soil and organic material; for the total mass of mineral soil (soil mass left after ashing); and for the total mass of organic material, defined as the portion of oven-dried soil and organic material that was lost on ignition. Daily rainfall data were collected at the El Verde field station, located approximately 0.4 kilometers south of the study site (Schaefer and Melendez, 2001). Rainfall data were expressed as average daily amounts for each sampling period. All data were expressed as totals for the study period; as mean, median, and maximum by sampling period; and as time series and scatter plots. Least-squares linear regression models (Helsel and Hirsch, 2002) were developed for each data set with model confidence limits set at 95 percent and number of samples (n)=50.

Data Characteristics and Limitations

Although Gerlach troughs provide an inexpensive means for quantifying surface runoff and slopewash, their limitations should be noted. Occasional decoupling of the Gerlach troughs from the soil resulted in the diversion of slopewash and runoff and undermeasurement of the sample. Reseating the trough sometimes resulted in a temporary increase in the mass of soil particles and organic debris transported into the trough. The use of bounded plots for Gerlach troughs defines the contributing area, in this study, 2 m^2 each, but ultimately the contributing area for each trough is controlled by such factors as the soil heterogeneity, intensity of a rainstorm, antecedent soil moisture, and the subsequent surface runoff. The uncertainty of these factors increases scatter in the data. Odum and others (1970) measured an average of five rainfall events per day in their study of climate in the Luquillo Experimental Forest. The difficulty of sampling at the end of every rainfall event prevented the precise determination of the relation between rainfall, runoff, and transport of soil and organic material.

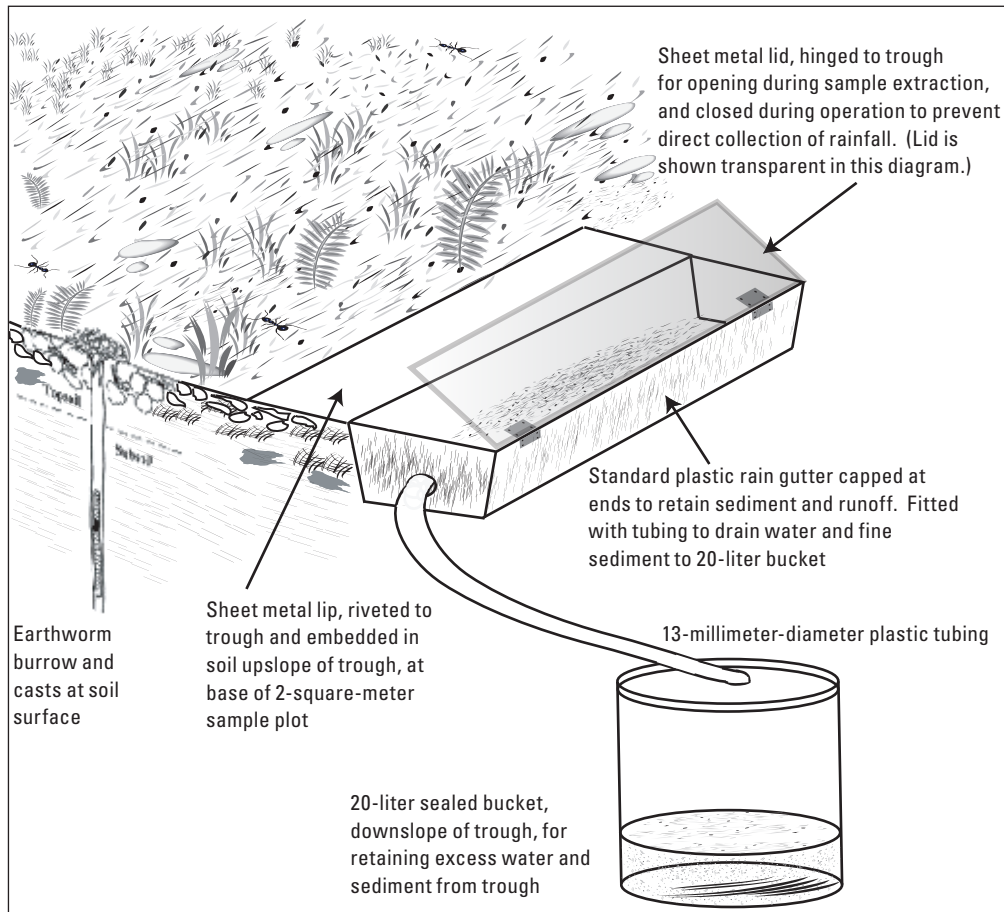


Figure 3. Idealized soil cross section and Gerlach trough showing hinged lid, which covers trough to prevent direct interception of rainfall and permits removal of sediment and water during sampling. Sheet metal lip embedded in soil upslope of trough allows soil particles, debris, and runoff to enter trough. Plastic tubing and bucket are attached downslope to collect overflow water and sediment from trough.

Effects of Earthworms on Slopewash, Surface Runoff, and Fine-Litter Transport

Earthworm population in the experimental (electroshocked) plots was reduced by 91 percent by the end of the 26-month experiment, compared with the population prior to shocking. When the experiment was terminated, the electroshocked plots had 13 percent of earthworms by count and 6 percent by biomass as compared with the control plots (Liu and Zou, 2002). Electroshocking had no effect on soil bulk density or pH (Liu and Zou, 2002).

A total of 9,423 mm of rainfall was recorded during the 793-day study period (table 1). Mean and maximum rainfall by sampling period (mean of 16 days) were 189 and 563 mm, respectively. Runoff averaged 0.6 mm and 1.2 mm

by sampling period for the control and experimental plots, respectively. The mean runoff (calculated using the runoff percent for each of the 50 sample periods) was 0.25 percent and 0.48 percent of rainfall for the control and experimental plots, respectively (table 1). Runoff from the control plots was nearly identical to earlier results using Gerlach troughs in other parts of the study area (Larsen and others, 1999), where runoff was 0.2 percent of rainfall on the same soil type in an undisturbed setting but with steeper slopes. Comparable runoff data were obtained by Chandler and Walter (1988) at tropical upland watersheds in Leyte, Philippines, where surface hydrologic response of forest, tilled land, slash and mulch, and pasture were compared; the forested site had the lowest annual runoff—less than 3 percent of rainfall.

At the El Verde site, time series of rainfall and runoff show generally increased runoff from the experimental plots compared with runoff from the control plots throughout the

Table 1. Rainfall, runoff, and transported material by sampling period, El Verde, eastern Puerto Rico.

[transported material, grams transported from each 2×2-meter plot; 50 sampling periods with a mean of 16 days each; g, gram; mm, millimeter; SD, standard deviation]

Sampling period (days)	Rainfall (mm)	Mean runoff (mm)		Runoff (percent of rainfall)		Mean soil and organic material (g)		Mean mineral soil (g)		Mean organic material portion (g)		
		Control	Experimental	Control	Experimental	Control	Experimental	Control	Experimental	Control	Experimental	
Mean	16	189	0.6	1.2	0.25	0.48	1.1	4.6	0.40	2.30	0.60	2.20
Median	15	167	0.2	0.5	0.03	0.16	0.7	3.5	0.30	1.00	0.40	1.70
Maximum	34	563	4.8	6.6	1.22	2.07	5.9	36.1	3.10	27.00	2.80	9.10
Minimum	8	1.3	0.0	0.0	0.0	0.0	0.2	0.7	0.05	0.25	0.03	0.35
SD	4.0	143	1.0	1.6	0.20	0.40	1.1	5.7	0.50	4.40	0.70	1.70
Total	793	9,423	31	59	0.33	0.62	53	231	22 ¹	114 ¹	31 ¹	107 ¹

¹Totals for mean mineral soil and mean organic portion do not sum to soil and organic material because data are missing in one sample set.

experiment (fig. 4A). This tendency is also indicated by the greater slope, 0.0099 as compared with 0.0065, of the curves representing the dependency of runoff on rainfall (fig. 4B). The approximately two-fold difference in runoff between the experimental and control plots increased slightly as daily rainfall increased (fig. 4B). As expected, daily rainfall was a reasonably good predictor of runoff; the least-squares linear regression models had correlation coefficient (r^2) values of 0.67 and 0.60, respectively, for the experimental and control plots. In this and each of the other data sets that were analyzed, r^2 values were greater for the experimental plots, suggesting that the absence of earthworms reduces some of the natural heterogeneity in the hydrological response to rainfall. Soil fauna such as earthworms and termites can substantially increase rates of infiltration through soil by creating macropores and channels during their feeding and burrowing activities (Baidgett and others, 2001). Removal of earthworms reduces porosity and eliminates earthworm casting activity, resulting in more microtopographic uniformity and a reduction of total surface area of the soil surface.

Daily rainfall and daily transported soil and organic material expressed as a time series showed a clear difference between the experimental and control plots (fig. 5A). Transport of total soil and organic material from the experimental plots was 4.4 times as great as from the control plots, totaling 231 and 53 g, respectively, for the duration of the experiment (table 1). Shuster and others (2002) also reported increased transport of soil in an experiment in which earthworm populations were reduced in a tilled corn agroecosystem; they attributed the increase in sediment flux to incorporated residue levels, reduction of the earthworm population, and reduced macropore and midden density. In our experiment, mean transport of total soil and organic material was 4.6 and 1.1 g per sampling period, respectively, from the experimental and control plots. The transport of soil and organic material from the experimental plots was variable, but it showed a general correlation with rainfall (slope, 0.018 and r^2 value, 0.35 (fig. 5B). Control plots showed no correlation with rainfall, presumably because of their greater heterogeneity in hydrologic response as noted above.

Chauvel and others (1999) also reported increased soil erosion in tropical pastures by *P. corethrurus* owing to surface casting associated with soil compaction due to cattle grazing. At El Verde, the background, undisturbed downslope transport of soil, as determined from the control plots, was 51 kilograms per hectare (kg ha^{-1}) and the “disturbance” rate, determined from the experimental plots, was 261 kg ha^{-1} . The background rate for downslope transport of fine litter was 71 kg ha^{-1} and the disturbance rate was 246 kg ha^{-1} .

On steep hillslopes, earthworm casts may become detached and roll downslope, possibly contributing to net soil erosion (Larsen and others, 1999). However, when earthworm casts are dried or aged, they become quite stable (Shipitalo and Protz, 1988), and on a gentle slope such as the one studied here, casting activity in and of itself was not observed to contribute directly to net downslope movement of soil, at least by movement of detached casts.

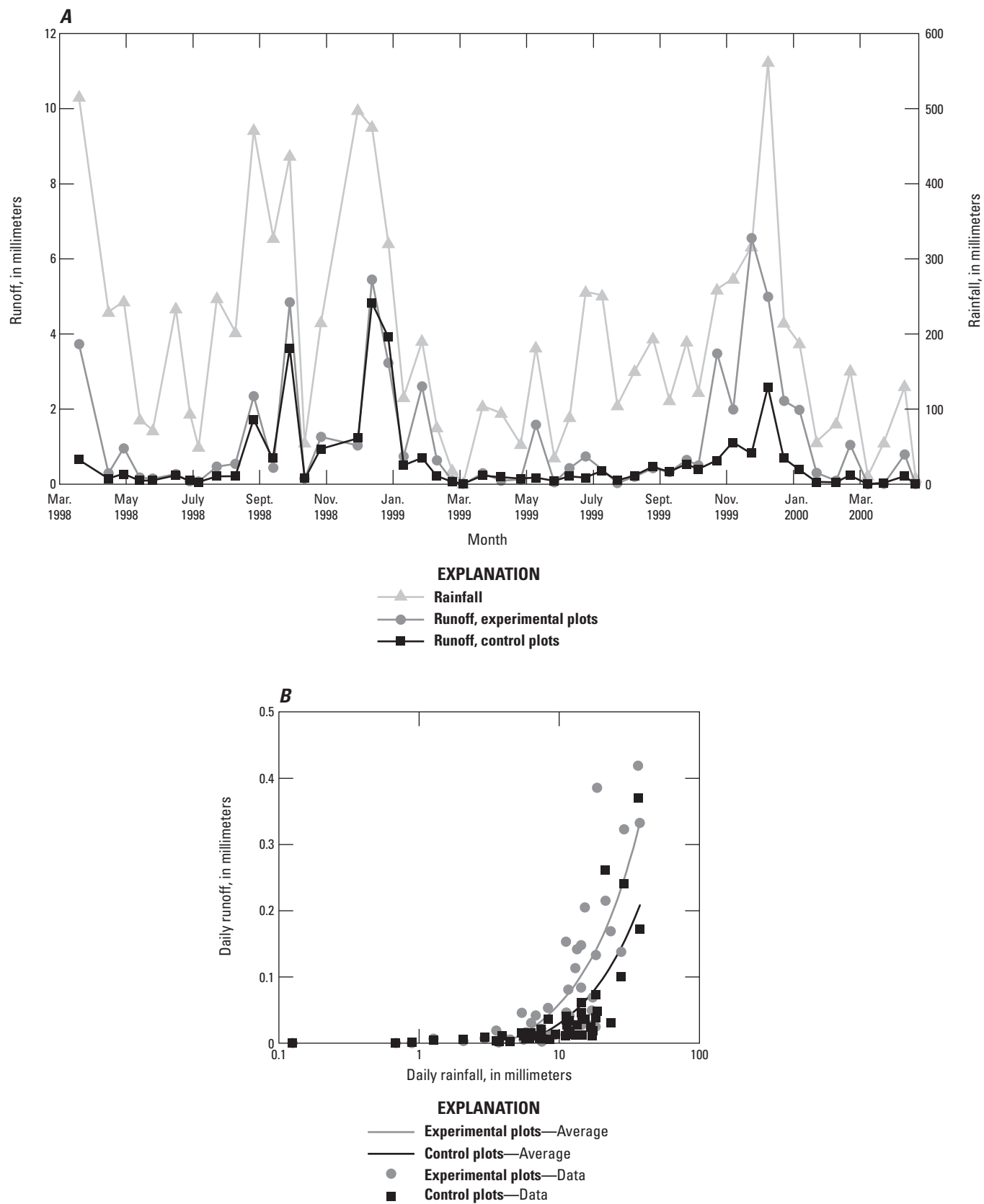


Figure 4. Rainfall and runoff per sampling period (mean of 16 days) at control and experimental plots, El Verde, eastern Puerto Rico. A, Time series; B, Scatterplot (control: daily runoff = $0.0065 \cdot$ daily rainfall – 0.0353, correlation coefficient (r^2) = 0.60; experimental: daily runoff = $0.0099 \cdot$ daily rainfall – 0.0407, r^2 = 0.67).

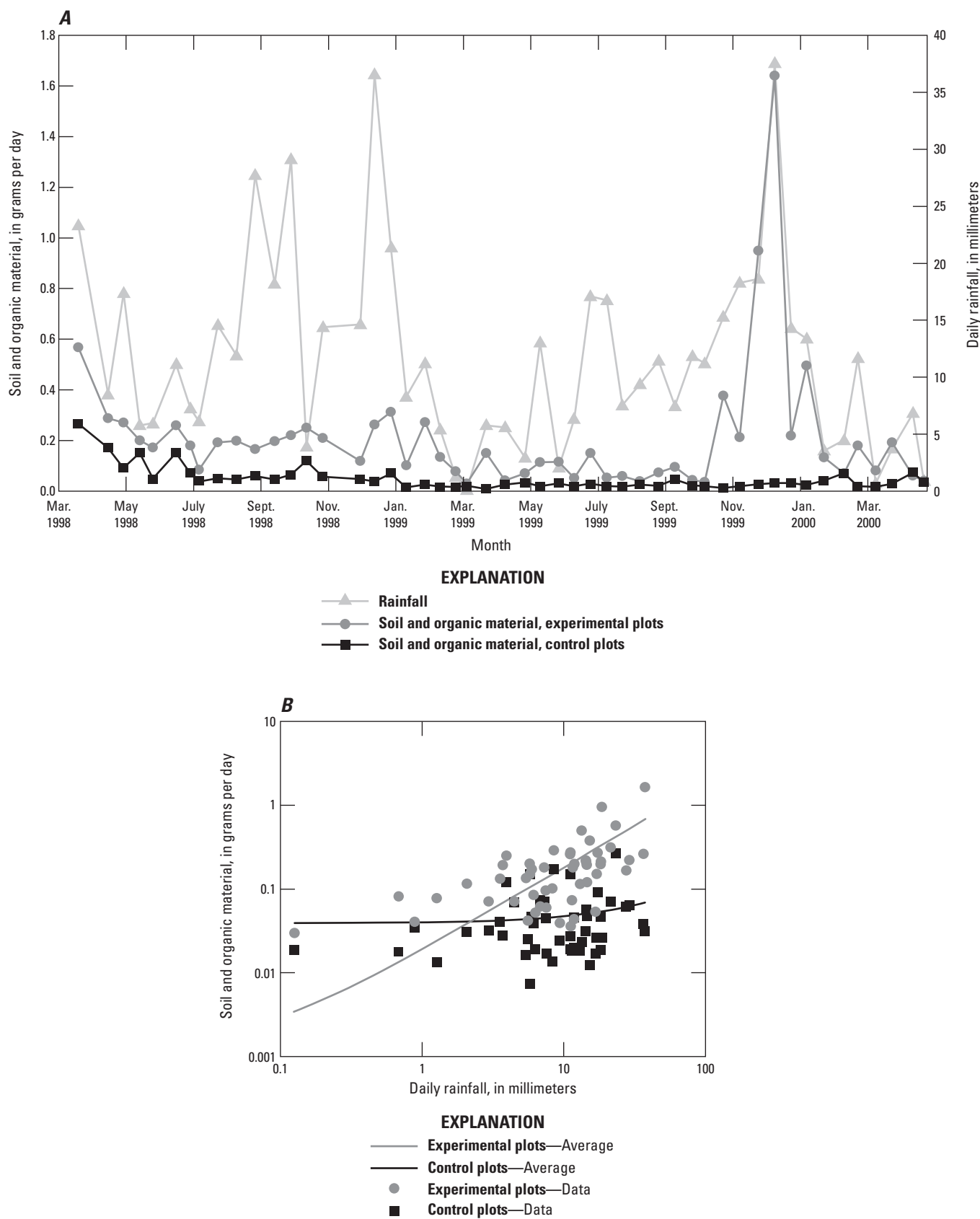


Figure 5. Daily rainfall and transported soil and organic matter at control and experimental plots, El Verde, eastern Puerto Rico. A, Time series; B, Scatterplot (control: $\text{soil and organic material} = 0.0008 \cdot \text{daily rainfall} + 0.0391$, correlation coefficient (r^2) = 0.02; experimental: $\text{soil and organic material} = 0.018 \cdot \text{daily rainfall} + 0.0012$, $r^2 = 0.35$).

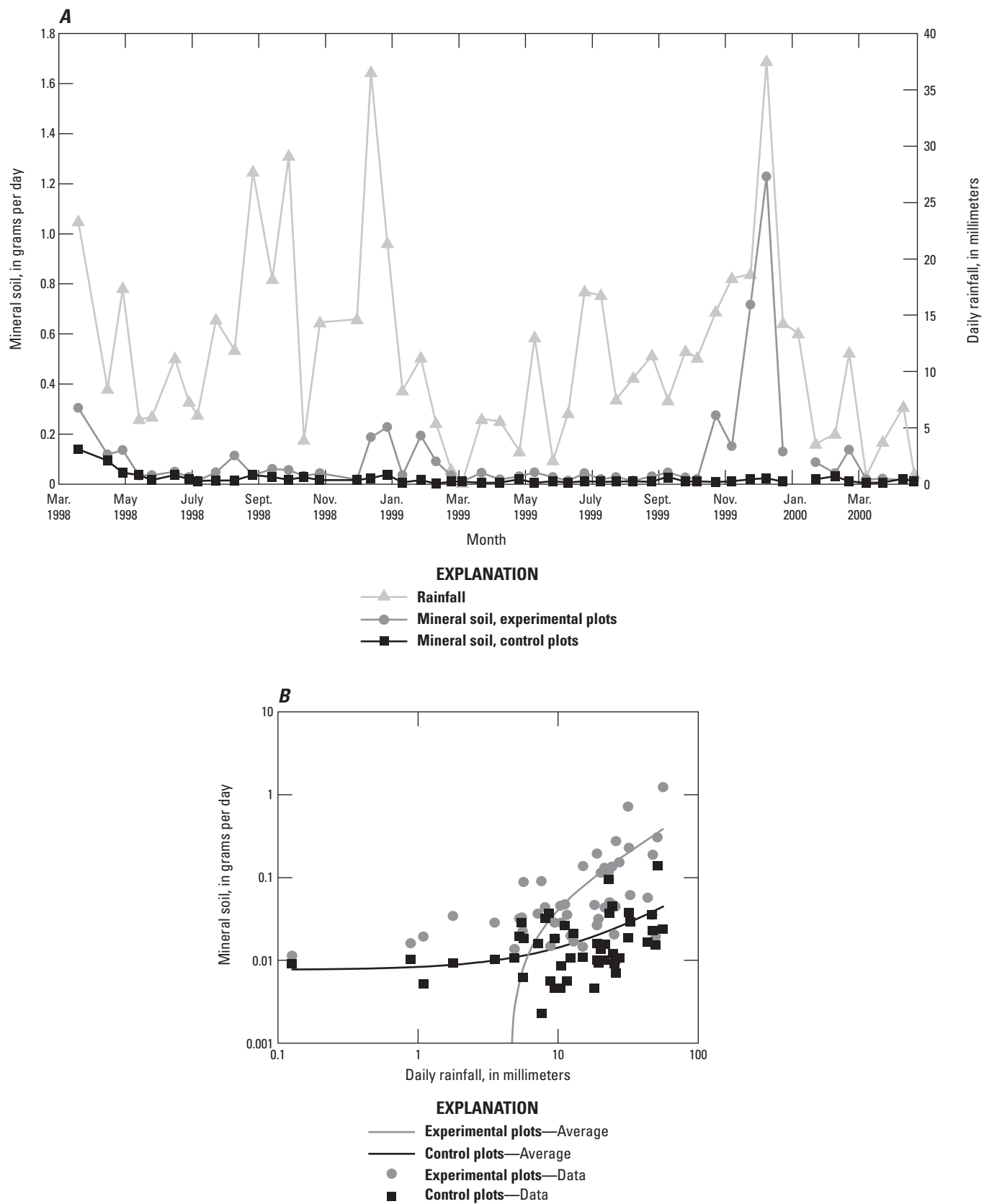


Figure 6. Daily rainfall and transported soil and transported mineral soil at control and experimental plots, El Verde, eastern Puerto Rico. *A*, Time series; *B*, Scatterplot (control: mineral soil = $7 \times 10^{-5} \cdot$ daily rainfall + 0.0077, correlation coefficient (r^2) = 0.17; experimental: mineral soil = $0.0007 \cdot$ daily rainfall – 0.0335, r^2 = 0.28).

Earthworm casts on the soil surface may mitigate soil erosion by increasing surface roughness (Le Bayon and Binet, 2001). Additionally, field observations by the authors indicate that earthworm casts, if abundant, increase soil surface area at the microtopographic scale. The increased surface area can be estimated by calculating the area of the one half of a spherical cast that is exposed to direct rainfall and summing the surface area of all casts per square meter. The worm castings shown in figure 2D are roughly spherical and on the order of 1 centimeter (cm) in diameter. Using an estimate of a single 1-cm cast produced by each of the average of 89 earthworms per square meter, the increase in surface area would be 280 cm², approximately 3 percent of a 1-m² area. At another humid-tropical site, Henrot and Brussaard (1997) describe *P. corethrurus* surface casts up to 3 cm thick. The increase in surface area at this site would be approximately 840 cm², or approximately 8 percent of a square meter. These effects of casting would be expected to reduce runoff and enhance infiltration during low-to moderate-intensity rainfall.

The pattern of daily rainfall and daily transport of mineral soil was comparable to that of total soil and organic material (figs. 5A, 6A). The transport of mineral soil was 5.2 times as great from the experimental plots as from the control plots, totaling 114 and 22 g, respectively, for the duration of the experiment (table 1). Mean transport of mineral soil was 2.3 and 0.4 g per sampling period, respectively, from the experimental and control plots. The least-squares linear regression models developed for daily transport of mineral soil as compared with daily rainfall had r² values that were similar to those developed for the total soil and organic material (figs. 5B, 6B). Transport of organic material was calculated using a residual value (loss on ignition), so the magnitude and frequency of mineral-soil transport was similar to that discussed above (see fig. 5) for total-soil and organic-material transport (fig. 7). On average, organic-material transport from the experimental plots was 46 percent of the total material collected, compared with 59 percent in the case of the control plots (table 1).

The three-fold increase in fine litter trapped in Gerlach troughs at the experimental plots likely reflects the greater availability of fine litter—the result of a decrease in fine-litter decomposition associated with the lowered earthworm population (Liu and Zou, 2002). The relatively lower rate of fine-litter export in the control plots may also be due to the gluing effect of earthworm casts (Chauvel and others, 1999). Shipitalo and Protz (1988) report that clay minerals and organic material become encrusted with mucus when they are mixed in the earthworm gut, contributing to microaggregate (cast) formation. It is possible that the bonding of cast material may also inhibit litter transport downslope.

The results of our study at El Verde indicate that the reduction of earthworm populations in a managed tropical forest with moderate-gradient hillslopes can substantially increase soil erosion, from a background rate (defined by the control plots) of 51 kg ha⁻¹ to the disturbance rate (defined by the experimental plots) of 261 kg ha⁻¹. These rates of

soil erosion are equal to a background surface-lowering rate of 9 millimeters per thousand years (mm 1,000 yr⁻¹) and a disturbance surface-lowering rate of 48 mm 1,000 yr⁻¹. The background rate for downslope transport of fine litter was 71 kg ha⁻¹ and the disturbance rate was 246 kg ha⁻¹. The increased mass of soil and fine litter moving downslope may be temporarily sequestered in local swales or depressions on the hillslope as well as at the footslope; however, no measurements were made to test this assumption. In the highly dissected Luquillo Experimental Forest, however, upland hillslopes have limited flood plain or other low-gradient surfaces. As a result, most of the soil and fine litter is presumed to be delivered to ephemeral and perennial channels, where it is easily entrained and incorporated by streamflow into the suspended-sediment load.

The effect of reduced earthworm population on hillslope hydrology is evident in the runoff rate, which more than doubled in the plots within which earthworm populations were reduced (table 1). If extended across a landscape, this association indicates that in areas where widespread changes in land use also markedly reduce earthworm population, streamflow peaks may be greater and may rise and fall more quickly in response to storms. Such earthworm reduction may increase downstream channel scour and flash-flood risk. Additionally, lower rates of rainfall infiltration (more than a 50 percent decline) in areas where earthworm populations have been greatly reduced would be expected to diminish soil moisture and groundwater recharge. Although we were not able to measure rates of infiltration below the rooting depth of 15 to 30 cm (Brown and others, 1983), earthworm burrows in the mineral horizon would serve to divert near-surface flow (in the meaning used by Elsenbeer, 2001; see fig. 2 in chapter E of this report) into deeper groundwater where it would contribute to higher dry-season base flow. This possibility is a potential area for future research. It is clear that the effects of reducing earthworm population on hydrologic and soil properties could be substantial in the montane humid tropics, where effective management of these critical natural resources is often a challenging task (Larsen, 2000; Bruijnzeel, 2004).

Summary and Conclusions

Disturbance of the soil environment by removal of earthworms doubled runoff and increased the erosion of soil and downslope transport of fine litter. This doubling can be attributed to two factors: reduced soil porosity resulting from decreased burrowing and reworking of the soil, and decreased soil surface area and surface roughness from a reduction in earthworm casting activity. Earthworm casts increase soil surface area and roughness at the microtopographic scale, thereby reducing runoff, at least during light- to moderate-intensity rainfall. Increased runoff in disturbed environments has been thought to be largely a function of such factors as soil compaction, loss of the soil A horizon, loss of vegetative cover, decreased evapotranspiration, and decreased leaf litter. In

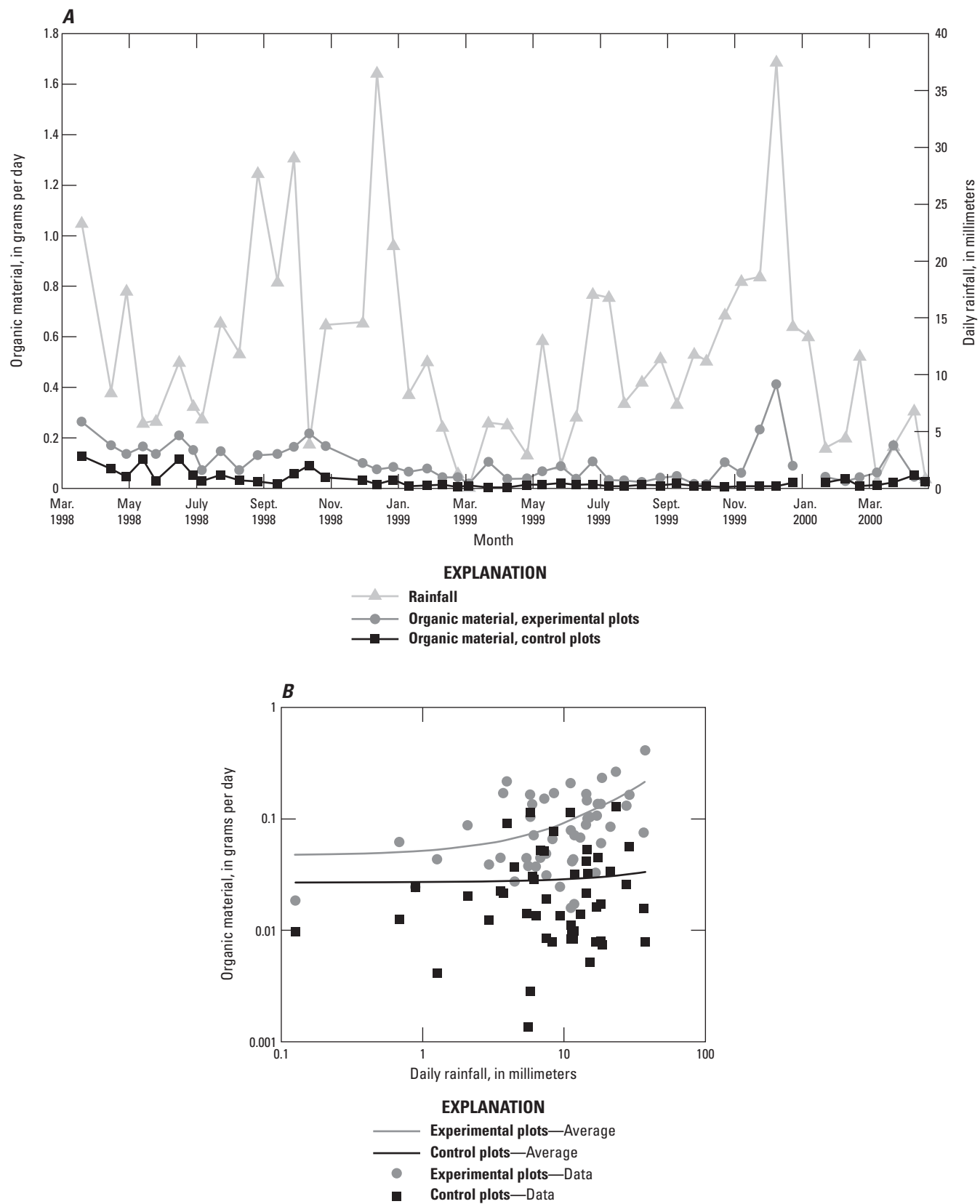


Figure 7. Daily rainfall and transported soil and transported organic material at control and experimental plots, El Verde, eastern Puerto Rico. *A*, Time series; *B*, Scatterplot (control: organic material = $0.0002 \cdot$ daily rainfall + 0.0269, correlation coefficient (r^2) = 0.003; experimental: organic material = $0.0045 \cdot$ daily rainfall + 0.0471, r^2 = 0.25).

the Luquillo Experimental Forest, and presumably in similar humid tropical forests, a decrease in burrowing soil macrofauna should be added to this list.

Land degradation has been defined as a substantial decrease in either or both of an area's biological productivity or usefulness due to human interference. Anthropogenic reduction in earthworm population, whether intentional (as in this experiment) or unplanned (as the result of the disturbance of soil or vegetative cover) is a form of land degradation that has unanticipated consequences. The data from this study indicate that the reduction in soil macrofauna population, in this case earthworms, can substantially alter soil physical properties, resulting in the degradational processes of markedly reduced rainfall infiltration, increased runoff, and increased soil erosion. As land and ecosystem management strategies become increasingly complex, improved understanding of the role of macrofauna on soil and water resources is needed.

Acknowledgments

This work was supported by National Science Foundation grant DEB-9705814, National Aeronautics and Space Administration grant NAGW 4059, and the U.S. Geological Survey Water, Energy, and Biogeochemical Budgets program (Larsen and others, 1993; Lins, 1994). Special thanks to Angel J. Torres Sánchez and Iris M. Concepción, U.S. Geological Survey, and to Joel Martinez and Marcelle Fabregas, University of Puerto Rico, for laboratory processing of sample material. Helpful manuscript review suggestions were offered by Robert F. Stallard, Cliff R. Hupp, and Allen C. Gellis, U.S. Geological Survey, and by two anonymous reviewers.

References

- Baidgett, R.D., Anderson, J.M., Behan-Pelletier, V., Brus-
saard, L., Coleman, D.C., Ettema, C., Moldenke, A.,
Schimel, J.P., and Wall, D.H., 2001, The influence of soil
biodiversity on hydrological pathways and the transfer of
materials between terrestrial and aquatic ecosystems: Eco-
systems, v. 4, p. 421–429.
- Blair, J.M., Bohlen, P.J., Stinner, B.R., and Edwards, C.A., 1995,
Manipulation of earthworm populations in field experiments
in agroecosystems: *Acta Zoologica Fennica*, v. 196, p. 48–51.
- Blanchart, E., Lavelle, P., Braudeau, E., Le Bissonnais,
Y., and Valentin, C., 1997, Regulation of soil structure
by geophagous earthworm activities in humid savannas
of Côte D'Ivoire: *Soil Biology and Biochemistry*, v. 29,
p. 431–439.
- Bouché, M.B., 1977, Stratégies lombriciennes, *in* Lohm, U.,
and Persson, E., eds., Soil organisms as components of
ecosystems—Ecological Bulletins: Stockholm, Swedish
Natural Science Research Council, p. 122–132.
- Brown, Sandra, Lugo, A.E., Silander, Susan, and Liegel,
Leon, 1983, Research history and opportunities in Luquillo
Experimental Forest: U.S. Department of Agriculture U.S.
Forest Service General Technical Report SO-44, 128 p.
- Bruijnzeel, L.A., 2004, Hydrological functions of tropical
forests—Not seeing the forests for the trees: *Agriculture,
Ecosystems and Environment*, v. 104, p. 185–228.
- Camilo, G.R., and Zou, X.M., 2001, Soil fauna in managed
forests, *in* Fimbrel, R.A., Grajal, A., and Robinson, J.G.,
eds., The cutting edge—Conserving wildlife in logged
tropical forest: New York, Columbia University Press,
p. 289–303.
- Chandler, D.G., and Walter, M.F., 1998, Runoff responses
among common land uses in the uplands of Matalom,
Leyte, Philippines: *Transactions of the ASAE (American
Association of Agricultural Engineers)*, v. 41,
p. 1635–1641.
- Chauvel, Armand, Grimaldi, Michael, Barros, Eleusa,
Blanchart, Eric, Desjardins, Thierry, Sarrazin, Max, and
Lavelle, Patrick, 1999, Pasture damage by an Amazonian
earthworm: *Nature*, v. 398, p. 32–33.
- Darwin, Charles, 1892, The formation of vegetable mould,
through the action of worms, with observations on their
habits: New York, D. Appleton, 326 p.
- Douglas, Ian, 1967, Erosion of granite terrains under tropical
rain forest in Australia, Malaysia, and Singapore: Interna-
tional Union of Geodesy and Geophysics, and International
Association of Scientific Hydrology Symposium on River
Morphology, Berne, Switzerland, 25 Sept.–7 Oct 1967,
Proceedings, v. 75, p. 31–39.
- Elsenbeer, Helmut, 2001, Hydrologic flowpaths in tropical
rainforest soilscapes—A review: *Hydrological Processes*,
v. 15, p. 1751–1759.
- Ewel, J.J., and Whitmore, J.L., 1973, The ecological life
zones of Puerto Rico and the U.S. Virgin Islands: U.S.
Department of Agriculture Forestry Service Research Paper
ITF-18, 72 p.
- Gellis, A.C., Webb, R.M.T., Wolfe, W.J., and McIntyre, S.C.I.,
1999, Effects of land use on upland erosion, sediment trans-
port and reservoir sedimentation, Lago Loíza Basin, Puerto
Rico: U.S. Geological Survey Water-Resources Investiga-
tions Report 99-4010, 60 p.
- Gerlach, T., 1967, Hillslope troughs for measuring sedi-
ment movement: *Revue de Geomorphologie Dynamique*,
special edition to the International Hydrological Decade,
v. 4, p. 173–174.
- González, Grizelle, and Seastedt, T.R., 2001, Soil fauna and
plant litter decomposition in tropical and subalpine forests:
Ecology, v. 82, p. 955–964.

- González, Grizelle, Zou, Xiaoming, and Borges, Sonya, 1996, Earthworm abundance and species composition in abandoned tropical croplands—Comparisons of tree plantations and secondary forests: *Pedobiologia*, v. 40, p. 385–391.
- González, Grizelle, Zou, Xiaoming, Sabat, Alberto, and Fetter, Ned, 1999, Earthworm abundance and distribution pattern in contrasting plant communities within a tropical wet forest in Puerto Rico: *Caribbean Journal of Science*, v. 35, p. 93–100.
- Grau, H.R., Aide, T.M., Zimmerman, J.K., Thominson, J.R., Helmer, E., and Zou, X.M., 2003, The ecological consequences of socioeconomic and land-use changes in postagriculture Puerto Rico: *BioScience*, v. 53, p. 1159–1168.
- Haantjens, H.A., 1969, Fire and wind erosion, or earthworms as the cause of microrelief in the lower Sepik plains, New Guinea: *Australian Journal of Science*, v. 32, p. 52–54.
- Haria, A.H., 1995, Hydrological and environmental impact of earthworm depletion by the New Zealand flatworm (*Artioposthia triangulata*): *Journal of Hydrology*, v. 171, p. 1–3.
- Hastenrath, Stefan, 1991, Climate dynamics of the tropics: Boston, Kluwer Academic Publishers, 488 p.
- Hazelhoff, L., Van Hoof, P., Imeson, A.C., and Kwaad, F.J.P.M., 1981, The exposure of forest soil to erosion by earthworms: *Earth Surface Processes and Landforms*, v. 6, p. 235–250.
- Helsel, D.R., and Hirsch, R.M., 2002, Statistical methods in water resources: U.S. Geological Survey Techniques of Water-Resources Investigations, Book 4, Ch. A3, 522 p.
- Heneghan, Liam, Coleman, D.C., Zou, X.M., Crossley, D.A., Jr., and Haines, B.L., 1999, Soil microarthropod contributions to decomposition dynamics—Tropical-temperate comparisons of a single substrate: *Ecology*, v. 80, p. 1873–1882.
- Henrot, Jacqueline, and Brussaard, Lijbert, 1997, Abundance, casting activity, and cast quality of earthworms in an acid Ultisol under alley-cropping in the humid tropics: *Applied Soil Ecology*, v. 6, p. 169–179.
- Jackson, R.B., Jobbágy, E.G., Avissar, R., Roy, S.B., Barrett, D.J., Cook, C.W., Farley, K.A., le Maitre, D.C., McCarl, B.A., and Murray, B.C., 2005, Trading water for carbon with biological carbon sequestration: *Science*, v. 310, p. 1944–1947.
- Johnson, D.L., and Lewis, L.A., 1995, Land degradation—Creation and destruction: Oxford, Blackwell Publishers, 335 p.
- Lal, Rattan, 1990, Soil erosion in the tropics—Principles and management: New York, McGrawHill, 580 p.
- Larsen, M.C., 2000, Analysis of 20th century rainfall and streamflow to characterize drought and water resources in Puerto Rico: *Physical Geography*, v. 21, p. 494–521.
- Larsen, M.C., Collar, P.D., and Stallard, R.F., 1993, Research plan for the investigation of water, energy, and biogeochemical budgets in the Luquillo Mountains, Puerto Rico: U.S. Geological Survey Open-File Report 92–150, 19 p.
- Larsen, M.C., Torres-Sánchez, A.J., and Concepción, I.M., 1999, Slopewash, surface runoff, and finelitter transport in forest and landslide scars in humidtropical steeplands, Luquillo Experimental Forest, Puerto Rico: *Earth Surface Processes and Landforms*, v. 24, p. 481–506.
- Lavelle, P., Brussaard L., and Hendrix, P.F., 1999, Earthworm management in tropical agroecosystems: London, Oxford University Press, 320 p.
- Le Bayon, R.-C., and Binet, F., 2001, Earthworm surface casts affect soil erosion by runoff water and phosphorus transfer in a temperate maize crop: *Pedobiologia*, v. 45, p. 430–442.
- Lee, K.E., 1985, Earthworms—Their ecology and relationships with soils and land use: Sidney, Australia, Academic Press, 412 p.
- Lins, H.F., 1994, Recent directions taken in water, energy, and biogeochemical budgets research: *EOS, Transaction of the American Geophysical Union*, v. 75, p. 433–439.
- Liu, Z.G., and Zou, X.M., 2002, Exotic earthworms accelerate plant litter decomposition in a tropical pasture and a wet forest of Puerto Rico: *Ecological Applications*, v. 12, 1406–1417.
- Nooren, C.A.M., van Breemen, N., Stoorvogel, J.J., and Jongmans, A.G., 1995, The role of earthworms in the formation of sandy surface soils in a tropical forest in Ivory Coast: *Geoderma*, v. 65, p. 135–148.
- Odum, H.T., Drewry, G., and Kline, J.R., 1970, Climate at El Verde, in Odum, H.T., and Pigeon, R.F., eds., A tropical rain forest—A study in irradiation and ecology at El Verde, Puerto Rico: Springfield, Va., U.S. Department of Commerce National Technical Information Service, p. B347–B418.
- Odum, H.T., and Pigeon, R.F., eds., 1970, A tropical rain forest—A study in irradiation and ecology at El Verde, Puerto Rico: National Technical Information Service, Springfield, 1970, 1678 p.
- Parmelee, R.W., Beare, M.H., Cheng, W., Hendrix, P.F., Rider, S.J., Crossley, D.A., Jr., and Coleman, D.C., 1990, Earthworms and enchytraeids in conventional and no-tillage agroecosystems—A biocide approach to assess their role in organic matter breakdown: *Biology and Fertility of Soils*, v. 10, p. 1–10.

- Reading, A.J., Thompson, R.D., and Millington, A.C., 1995, Humid tropical environments: Cambridge, Mass., Blackwell Publishers, 429 p.
- Ruxton, B.P., 1967, Slopewash under mature primary rainforest in northern Papua, in Jennings, J.N., and Mabbutt, J.A., eds., Landform studies from Australia and New Guinea: Cambridge, United Kingdom, Cambridge University Press, p. 85–94.
- Sanchez, Yaniria, Zou, Xiaoming, Borges, Sonya, and Ruan, H.H., 2003, Recovery of native earthworms in abandoned tropical pastures: Conservation Biology, v. 17, p. 999–1006.
- Schaefer, Douglas, and Melendez, Eda, 2001, Annual rainfall data, El Verde, Puerto Rico: accessed December 2001 at <http://luq.lternet.edu/data/>
- Shipitalo, M.J., and Protz, R., 1988, Factors influencing the dispersibility of clay in worm casts: Soil Science Society of America Journal, v. 52, p. 764–769.
- Shuster, W.D., McDonald, L.P., McCartney, D.A., Parmelee, R.W., Studer, N.S., and Stinner, B.R., 2002, Nitrogen source and earthworm abundance affected runoff volume and nutrient loss in a tilled-corn agroecosystem: Biology and Fertility of Soils, v. 35, p. 320–327.
- Six, Johan, Bossuyt, Heleen, Degryze, S., and Denef, Karolien, 2004, A history of research on the link between (micro) aggregates, soil biota, and soil organic matter dynamics: Soil and Tillage Research, v. 79, p. 7–31.
- Soil Survey Staff, 1995, Order 1 soil survey of the Luquillo Long Term Ecological Research Grid, Puerto Rico: Lincoln, Neb., U.S. Department of Agriculture Natural Resources Conservation Service, 181 p.
- Young, A., 1960, Soil movement by denudational processes on slopes: Nature, v. 188, p. 120–122.
- Zou, X.M., and González, G., 1997, Changes in earthworm density and community structure during secondary succession in abandoned tropical pastures: Soil Biology Biochemistry, v. 29, p. 627–629.

Weathering, Landscape Equilibrium, and Carbon in Four Watersheds in Eastern Puerto Rico

By Robert F. Stallard

Chapter H of
**Water Quality and Landscape Processes of Four Watersheds in
Eastern Puerto Rico**

Edited by Sheila F. Murphy and Robert F. Stallard

Professional Paper 1789–H

**U.S. Department of the Interior
U.S. Geological Survey**

Contents

Abstract.....	205
Introduction.....	205
Research Setting.....	207
Purpose and Scope	207
Weathering, Erosion, and the Carbon Cycle	209
Solute Loads and Chemical Erosion in Eastern Puerto Rico	209
Solid Loads and Physical Erosion in Eastern Puerto Rico	210
Steady-State Erosion	211
Carbon, Weathering, and Erosion	211
Landslides, Erosion, and Carbon	212
Methods Used to Assess the Effects of Weathering and Erosion in the Carbon Cycle.....	213
Chemical Analyses of Dissolved and Solid Phases	213
Estimation of Constituent Yields.....	215
Data Manipulation and Processing of Dissolved Constituents.....	217
Correction for Atmospherically Derived Contributions to the Dissolved and Solid Load	217
Total Dissolved Bedrock	219
Equilibrium Model: Calculating Steady-State Erosion from Dissolved Bedrock.....	219
Suspended Bedrock, Loss on Ignition, and Particulate Organic Carbon.....	224
Projection to a Common Intermediate Yield.....	224
Suspended Bedrock and Runoff	225
Solid Loads for Individual Years	225
Calculating the Long-Term Average for Nonlinear Sediment-Yield Models.....	233
Interpretation of Projections to a Common Yield.....	233
Results, Comparison of Constituent Yields, and Assessment of Landscape Equilibrium	235
Constituent-Yield Comparisons	235
Landscape Equilibrium.....	237
Summary and Conclusion: General Landscape Disequilibrium and the Carbon Cycle	239
Acknowledgments.....	241
References.....	241

Figures

1.	Map showing location of Puerto Rico and study watersheds	208
2–13.	Diagrams showing the following:	
2.	Carbon accumulation on a chronosequence of landslides from the Luquillo Mountains, eastern Puerto Rico	213
3.	Concentration of dissolved silicate bedrock and two dissolved constituents used in calculating bedrock denudation rates and in estimating equilibrium physical denudation rates, eastern Puerto Rico	219
4.	Concentration of the three major components of carbon transport in tropical rivers, eastern Puerto Rico	221
5.	Concentration of an operationally derived constituent, suspended bedrock, used in calculating physical denudation rates, eastern Puerto Rico.....	221
6.	Percent loss on ignition of sediment collected in eastern Puerto Rico	222
7.	Time series of annual runoff and annual yields of chloride, sodium, calcium, and of bedrock-derived sodium and calcium, eastern Puerto Rico	226
8.	Time series of annual yields of magnesium, potassium, sulfate, nitrate, ammonia, and phosphate, eastern Puerto Rico	227
9.	Time series of annual yields of constituents that best characterize erosion and the carbon cycle, eastern Puerto Rico	228
10.	Annual runoff compared with annual yields of silica, chloride, sodium, calcium, and bedrock-derived sodium and calcium for five rivers, eastern Puerto Rico	229
11.	Annual runoff compared with annual yields of magnesium, potassium, sulfate, nitrate, ammonia, and phosphate for five rivers, eastern Puerto Rico	230
12.	Annual runoff compared with annual yields of constituents that best characterize erosion and the carbon cycle, eastern Puerto Rico	231
13.	A model-based comparison of annual runoff compared with annual yields of bedrock, eastern Puerto Rico	235

Table

1.	X-ray fluorescence and wet-chemical analysis of geologic materials and water from the Luquillo Mountains, eastern Puerto Rico.....	214
2.	Discharge-weighted average concentrations for each percentile class estimated by using LOADEST and hourly discharge from study watersheds, eastern Puerto Rico.....	215
3.	Average annual net, atmospheric, and bedrock inputs to study watersheds, 1991 to 2005, eastern Puerto Rico	216
4.	Parameters and coefficients used in modeling equilibrium erosion in study watersheds, eastern Puerto Rico, by using Na-Si and Ca-Si pairs.....	223
5.	Analysis of loss on ignition for a discharge-weighted average sample of solid load from study rivers, eastern Puerto Rico.....	224
6.	Coefficients of power-law model relating annual suspended-bedrock yield to runoff in study watersheds, eastern Puerto Rico.....	225
7.	Coefficients of model relating annual suspended-bedrock yield to runoff and landslide day runoff in study watersheds, eastern Puerto Rico.....	232

8.	Coefficients that predict landslide-day runoff given annual runoff in study watersheds, eastern Puerto Rico	232
9.	Convolution information used to represent interannual variability.....	233
10.	Yields in study watersheds as observed and adjusted to a common intermediate runoff, eastern Puerto Rico	236
11.	Interpretation of changes in yields of study watersheds as observed and adjusted to a common intermediate runoff, eastern Puerto Rico	237
12.	Summary of landscape equilibrium properties in study watersheds, eastern Puerto Rico	238
13.	Observed mean-annual runoff compared with equilibrium runoff for power-law and landslide day erosion models in study watersheds, eastern Puerto Rico	238
14.	Total denudation compared with equilibrium denudation for current mean-annual runoff and projected to a common runoff in study watersheds, eastern Puerto Rico..238	
15.	Excess particulate organic carbon yields from the equilibrium model of study watersheds, eastern Puerto Rico	238

Abbreviations Used in This Report

*	calculated bedrock-derived constituent
<	less than
>	greater than
μm	micrometer
$\mu\text{mol L}^{-1}$	micromoles per liter
eq mol^{-1}	equivalents of charge per mole
h	hour
kmol	kilomole
$\text{kmol km}^{-2} \text{yr}^{-1}$	thousand moles per square kilometer per year
m	meter
mg L^{-1}	milligrams per liter
mm	millimeter
mm h^{-1}	millimeters per hour
mm k.y.^{-1}	millimeters per thousand years
mm yr^{-1}	millimeters per year
pg yr^{-1}	petagrams per year (1 petagram=1 gram ¹⁵)
ppm	parts per million
$\text{t km}^{-2} \text{yr}^{-1}$	metric tons per square kilometer per year
DBrx	dissolved bedrock
DIC	dissolved inorganic carbon
DOC	dissolved organic carbon
LOI	loss on ignition

PIC	particulate inorganic carbon
POC	particulate organic carbon
SBrx	suspended bedrock
SSol	suspended solids
WEBB	Water, Energy, and Biogeochemical Budgets
ZBrx	total bedrock-derived cation charge

Conversion Factors

Multiply	By	To obtain
Length		
micrometer (μm)	0.00003937	inch (in.)
millimeter (mm)	0.03937	inch (in.)
meter (m)	3.281	foot (ft)
Flow rate		
millimeters per hour (mm h^{-1})	0.03937	inches per hour (in. h^{-1})
millimeters per year (mm yr^{-1})	0.03937	inches per year (in. yr^{-1})
millimeters per 1,000 years (mm k.y.^{-1})	0.03937	inches per 1,000 year (in. k.y.^{-1})
Mass		
milligrams per liter (mg L^{-1})	0.05841	grains per gallon (gr gal^{-1})
Other		
petagrams per year	1.102	billions of short tons per year (t yr^{-1}) ⁹
metric tons per square kilometer per year ($\text{t km}^{-2} \text{ yr}^{-1}$)	2.855	short tons per square mile per year ($\text{tons mi}^{-2} \text{ yr}^{-1}$)

Weathering, Landscape Equilibrium, and Carbon in Four Watersheds in Eastern Puerto Rico

By Robert F. Stallard

Abstract

The U.S. Geological Survey's Water, Energy, and Biogeochemical Budgets (WEBB) program research in eastern Puerto Rico involves a double pair-wise comparison of four montane river basins, two on granitic bedrock and two on fine-grained volcaniclastic bedrock; for each rock type, one is forested and the other is developed. A confounding factor in this comparison is that the developed watersheds are substantially drier than the forested (runoff of 900–1,600 millimeters per year compared with 2,800–3,700 millimeters per year). To reduce the effects of contrasting runoff, the relation between annual runoff and annual constituent yield were used to estimate mean-annual yields at a common, intermediate mean-annual runoff of 1,860 millimeters per year. Upon projection to this intermediate runoff, the ranges of mean-annual yields among all watersheds became more compact or did not substantially change for dissolved bedrock, sodium, silica, chloride, dissolved organic carbon, and calcium. These constituents are the primary indicators of chemical weathering, biological activity on the landscape, and atmospheric inputs; the narrow ranges indicate little preferential influence by either geology or land cover. The projected yields of biologically active constituents (potassium, nitrate, ammonium ion, phosphate), and particulate constituents (suspended bedrock and particulate organic carbon) were considerably greater for developed landscapes compared with forested watersheds, consistent with the known effects of land clearing and human waste inputs. Equilibrium rates of combined chemical and physical weathering were estimated by using a method based on concentrations of silicon and sodium in bedrock, river-borne solids, and river-borne solutes. The observed rates of landscape denudation greatly exceed rates expected for a dynamic equilibrium, except possibly for the forested watershed on volcaniclastic rock. Deforestation and agriculture can explain the accelerated physical erosion in the two developed watersheds. Because there has been no appreciable deforestation, something else, possibly climate or forest-quality change, must explain the accelerated erosion in the forested watersheds on granitic rocks. Particulate organic carbon yields are closely linked to sediment yields. This relation implies that much of the particulate organic carbon transport in the four rivers is being caused by this enhanced erosion aided by landslides and fast carbon recovery. The

increase in particulate organic carbon yields over equilibrium is estimated to range from 300 kilomoles per square kilometer per year (6 metric tons carbon per square kilometer per year) to 1,700 kilomoles per square kilometer per year (22 metric tons carbon per square kilometer per year) and is consistent with human-accelerated particulate-organic-carbon erosion and burial observed globally. There is no strong evidence of human perturbation of silicate weathering in the four study watersheds, and differences in dissolved inorganic carbon are consistent with watershed geology. Although dissolved organic carbon is slightly elevated in the developed watersheds, that elevation is not enough to unambiguously demonstrate human causes; more work is needed. Accordingly, the dissolved organic carbon and dissolved inorganic carbon yields of tropical rivers, although large, are of secondary importance in the study of the anthropogenically perturbed carbon cycle.

Introduction

The humid tropics presently occupy about 25 percent of the Earth's land surface, and the warm temperatures, moist conditions, and luxuriant vegetation promote especially rapid biological and chemical processes—photosynthesis, respiration, decay, and chemical weathering—making the region particularly important at a global scale from the perspective of weathering, erosion, and carbon cycling. Tropical forests alone cover only 12 to 13 percent of the Earth's land surface, but they contain 45 to 52 percent of terrestrial biomass carbon and 11 to 17 percent of soil carbon, and they account for 23 to 35 percent of net primary productivity (Prentice and others, 2001). This productivity equates to between 780 and 1,250 metric tons per square kilometer per year of carbon ($t \text{ km}^{-2} \text{ yr}^{-1}$ C). Other widespread humid-tropical land cover includes grasslands, wetlands, and various types of agricultural lands. According to Meybeck (1979), rivers in the humid tropics supply about 65 percent of the dissolved silica and 38 percent of the ionic load delivered by rivers to the ocean. Data compiled by Milliman and Meade (1983) and Milliman and Syvitski (1992) indicate that the humid tropics contribute about 50 percent of the total solid load delivered by rivers to the ocean. These and related studies demonstrate that about 30 percent of the solid load comes from steep, undammed,

coastal rivers that drain active orogenic belts and island arcs in the tropics (Lyons and others, 2002). These rivers are an especially strong source of particulate organic carbon (POC) in the ocean (Ver and others, 1999; Lyons and others, 2002; Syvitski and others, 2005; Galy and others; 2007; Hilton and others, 2008a,b).

When examined at both human and geologic time scales, today's world is in a state of exceptionally rapid change caused by human activities (Science Magazine, 2011). For the last several thousand years, we humans have been modifying the Earth's landscape with fire and tools for food and agriculture, and for the past few hundred years, we humans have remodeled the Earth's surface and altered biogeochemical cycles with a technology fueled by geologic and biospheric energy sources, a time period commonly referred to as the Anthropocene. Associated with this remodeling is a vast mobilization and redistribution of soils, sediments, and rock at a scale comparable to that of natural erosion (Hooke, 1994, 2000). Rivers and materials transported by rivers have been profoundly affected by human activities related to hydraulic engineering, water consumption, waste introduction, and land-cover modification (Meybeck, 2003).

Human impacts motivate one of the great developing themes of contemporary biogeochemistry, that of describing the anthropogenically modified carbon cycle and understanding how it relates to changes in atmospheric and seawater composition, land use, and land cover. The ongoing accumulation of carbon dioxide in the atmosphere, derived from fossil-fuel burning, deforestation, and land clearing, is now a major concern, because of potentially severe consequences on climate (Schneider, 2009). Examination of natural and technological mechanisms that limit CO₂ accumulation in the atmosphere through sequestration has become a global research focus. This theme is now a major thrust of the current U.S. Geological Survey Strategic Plan (U.S. Geological Survey, 2007). For reference, current characterizations of the global carbon budget (Denman and others, 2007) estimate that the combined emissions from fossil fuels and cement release 7.2±0.3 petagrams of carbon per year (pg C yr⁻¹). Of this total, 4.1±0.1 pg C yr⁻¹ accumulate in the atmosphere; 2.2±0.5 pg C yr⁻¹ enter the ocean, and 0.9±0.6 pg C yr⁻¹ are stored on land. The large error in the terrestrial carbon sink reflects the relative difficulty in accounting for all carbon on land.

Studies of terrestrial CO₂ sequestration normally take place at a landscape scale, because the size of the technological perturbation of the carbon cycle is so large that any substantial sequestration must be either quite strong or quite widely distributed. For a suite of processes to be prominent in the technologically perturbed carbon cycle, it must affect about 1 pg C yr⁻¹ globally. Distributed over the Earth's land surface (149•10⁶ km²), this amount corresponds with about 6.7 t km⁻² yr⁻¹ C. Forest regrowth and densification of woody vegetation are clearly important at this scale (Pacala and others, 2001; summaries in Denman and others, 2007). The land area of humid tropical mountains is not large, about 4•10⁶ km² (United Nations Environment Programme World

Conservation Monitoring Centre, 2002). If a process capable of sequestering 1 pg C yr⁻¹ were to be confined to just humid tropical mountains, it would need to sequester 250 t km⁻² yr⁻¹ C; this mass is about one third to one fifth of tropical forest net primary productivity.

Weathering and erosion have a smaller effect on the carbon cycle than do plant growth and decay. The combined fluvial transport to the ocean of dissolved inorganic carbon (DIC), dissolved organic carbon (DOC), and POC is less than 1 pg C yr⁻¹ (Sarmiento and Sundquist, 1992). It is difficult to envision changes caused by human activities that could alter current dissolved-carbon fluxes on the order of 1 pg C yr⁻¹. Particulate carbon fluxes to the ocean have increased somewhat because of human activities despite the interception of considerable masses of sediment behind artificial reservoirs (Syvitski and others, 2005), and vast quantities of POC are stored on land as soils, colluvium, alluvium, and lacustrine deposits. Stallard (1998) estimated that globally averaged upland physical erosion caused by human activities has increased twofold to sixfold as compared with preagricultural rates and has increased erosion by 10 to 50 pg yr⁻¹ sediment; most of this eroded sediment is stored in terrestrial sediments rather than being transported to the ocean. This deposition results in long-term storage of carbon in terrestrial sediments on the order of 0.6 to 1.5 pg C yr⁻¹. Stallard (1998) asserted that much of this carbon is being replaced through the creation of new POC at the sites of erosion, and that carbon stores in depositional sites may also be augmented with additional POC from autochthonous production in surface waters and wetlands. Considerable work has gone into estimating the POC fluxes in the landscape and testing whether the deposited carbon is stable and whether the deposited carbon is being replaced by newly produced POC (Berhe and others, 2007; Van Oost and others, 2007, 2008; Harden and others, 2008; Lal and Pimentel, 2008; Quinton and others, 2010). The most recent estimate of the amount of carbon being removed from the atmosphere by erosion, deposition, and replacement is about 0.5 pg C yr⁻¹; increased erosion produces about 35 pg yr⁻¹ sediment (Quinton and others, 2010). This estimate does not include the contribution of carbon to fluvial and lacustrine sediments by autochthonous production.

The U.S. Geological Survey's Water Energy and Biogeochemical Budgets (WEBB) program research in eastern Puerto Rico, described herein, provided a unique opportunity to examine major biogeochemical processes in headwater river systems in humid tropical mountains, to examine their role in the carbon cycle, and to judge whether climate change or human activities have pushed these systems out of equilibrium. Up to now, research into the biogeochemical functioning of headwater river systems in such settings has been limited despite their obvious importance in erosion and biogeochemical processes. The fieldwork is quite challenging. To assess the importance of interannual variations, years of monitoring are required, and huge storms, which are extremely difficult and can be dangerous to sample, have a dominant role in transport processes.

Research Setting

The U.S. Geological Survey initiated the WEBB program in 1991. The WEBB site in eastern Puerto Rico (Larsen and others, 1993), one of five sites, was chosen because it is in a montane humid-tropical environment having a bedrock geology that is representative of many parts of the world. Puerto Rico is part of the volcanically inactive Greater Antilles island arc (fig. 1) that has been moderately to deeply eroded in a humid tropical climate. The qualities of geology, climate, land cover, and land use make Puerto Rico similar to vast swaths of the humid tropics, including the remainder of the Greater Antillean island arc, much of Central America, many island arcs extending from the southwest Pacific to the eastern Indian Ocean such as the Indonesian Archipelago, and considerable portions of the Southeast Asian mainland. These landscapes are agriculturally productive and support large human populations (Bot and others, 2000; Webb, 2006; Foley and others, 2011).

Puerto Rico has undergone a rapid transformation in the past several centuries from pre-European conditions of relatively undisturbed forest, to intensive agriculture in the 19th and early 20th century, to a post-1950 industrial economy. In the past 60 years land cover has shifted from almost entirely deforested to forest covering about half of the island (Brandeis, 2007; Kennaway and Helmer, 2007). For further background, see Murphy and others (2012).

The Puerto Rico WEBB work involves a double pair-wise comparison of montane streams on granitic bedrock compared with fine-grained volcaniclastic bedrock and of forested compared with agricultural landscapes (Murphy and others, 2012, their table 1). Unlike some island-arc regions, Puerto Rico has not had active volcanoes for tens of millions of years. Its soils lack abundant allophane, which is commonly derived from tephras in younger volcanic landscapes. Allophane stabilizes soil organic matter and is associated with especially productive agricultural soils (Parfit, 2009). The selection of the two types of geology was predicated on the idea that the abundance of coarse-grained quartz in the granitic rocks would result in soils with sufficiently different properties from soils on the quartz-poor volcanic rocks that the differences would be manifested in the erosional styles, water flow paths, and solute-load chemical composition. The soils of the volcanic watersheds are, for instance, richer in secondary clay minerals and in base cations. For each bedrock type, one watershed is covered with mature rainforest (drained by Río Icacos and Río Mameyes), and the other watershed is affected by land use typical of eastern Puerto Rico (drained by Río Cayaguás and Río Canóvanas). Two watersheds are located on coarse-grained granitic rocks (Icacos and Cayaguás), and two are located on fine-grained volcanic rocks and volcaniclastic sedimentary rocks derived from closely allied magmas (Mameyes and Canóvanas). Data from the Quebrada Guabá, a tributary of the Icacos which was monitored for 10 years (1993–2002), is included in many calculations and tables as a surrogate for the Icacos (the Guabá streamgaging station failed in April 2003 during a large storm (appendix 1 of this report; Murphy and Stallard, 2012)).

The double pair-wise comparison of physical and chemical weathering processes has been a major objective of the Puerto Rico WEBB program since its inception (Larsen and others, 1993). To this end, the program depended upon the collection of time-series of meteorologic, hydrologic, soil-water, and groundwater samples and data. Long-term monitoring of biogeochemical budgets of the four major watersheds included water, major dissolved constituents, nutrients, carbon, and sediment. Weathering and mass-wasting processes were to be examined in each rock type and land cover by comparing budgets calculated for each. Sampling major hydrologic events was especially important. A benefit of working in Puerto Rico is that at a given altitude and rainfall, similar natural vegetation exists on all types of bedrock (see Murphy and others, 2012), presumably because as an island, Puerto Rico lacks high floral diversity (Ashton and others, 2004). A confounding factor in this comparison, however, is that both agricultural watersheds are substantially drier than the forested watersheds (runoff of 900–1,600 millimeters per year (mm yr^{-1}) as compared with 2,800–3,700 mm yr^{-1}).

An initial snapshot of a four-way comparison, covering 1991 to 1995, was published by Larsen and Stallard (2000). Four-way sediment budgets have been examined by Larsen (1997, 2012). Detailed descriptions of the regional geography (Murphy and others, 2012), atmospheric inputs (Stallard, 2012), the study watersheds and intercomparisons of their hydrology (Murphy and Stallard, 2012), physical erosion (Larsen, 2012), and water quality (Stallard and Murphy, 2012) are found elsewhere in this volume.

Purpose and Scope

The present chapter focuses on a four-way comparison of the rates of chemical and physical erosion as related to carbon transport and in turn to rates of runoff. Simple models are used to project annual constituent-yield data for each river basin to a single intermediate runoff, thereby circumventing the confounding factor of having different mean-annual runoff between forested and developed pairs. The same models are also used to consider the consequences of climate change on chemical and physical weathering and on fluvial carbon transport. Six questions are asked:

1. What are the measured rates of chemical and physical denudation and how do these relate to runoff in each watershed?
2. How do watersheds compare in weathering, erosion, carbon export, and nutrient export with regard to geology and land cover? Do geology and land cover matter?
3. Is the forested landscape in a steady state? In essence, are the Luquillo Mountains a model of a quiescent, stable, natural landscape, or are they changing?
4. What does the present dynamic state of the landscape imply regarding past and future response to climate change?

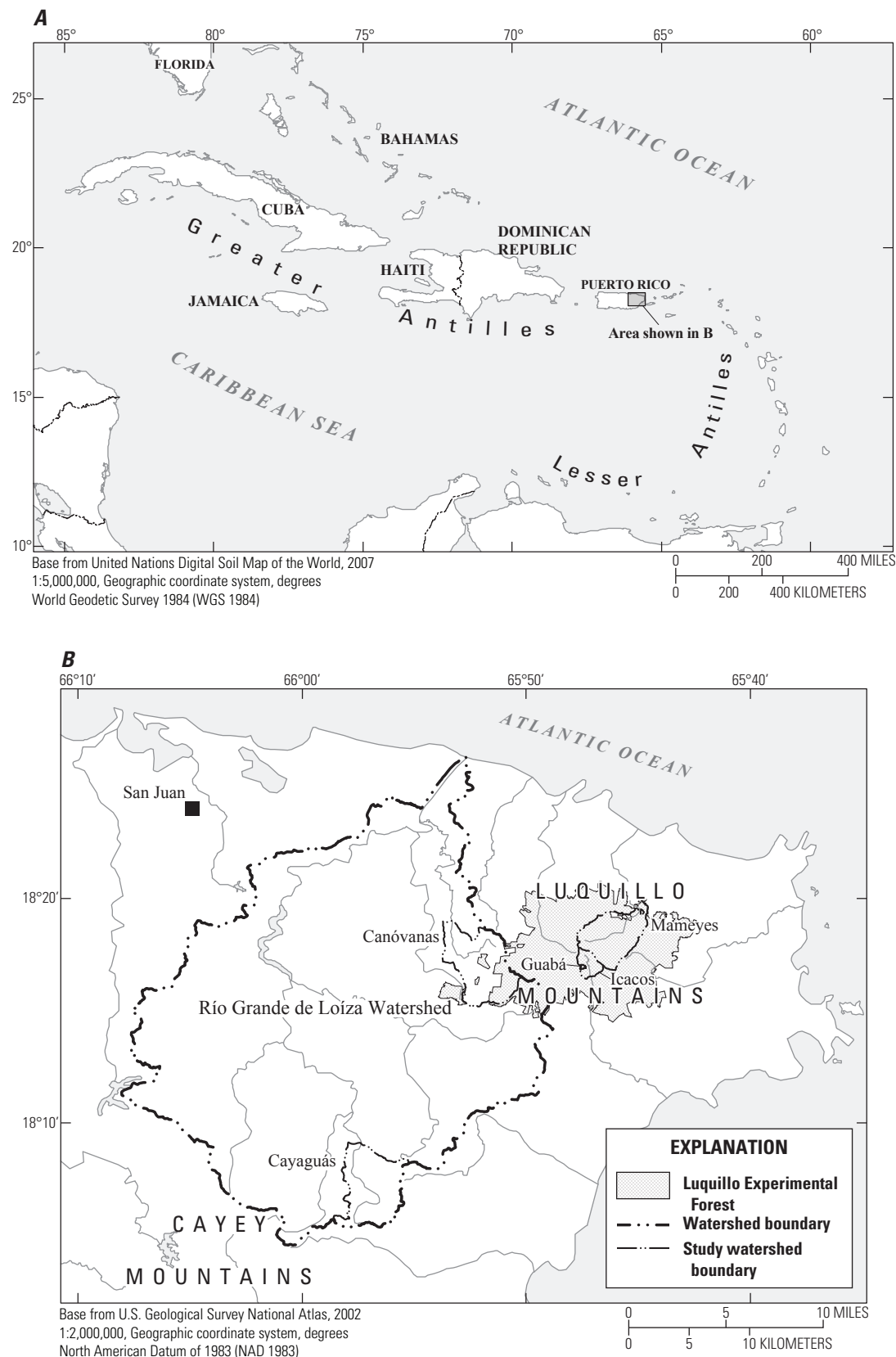


Figure 1. Location of Puerto Rico and study watersheds.

5. What are the rates of export of carbon in its various forms; how do these rates relate to runoff, and is this exported carbon being replaced by new photosynthetically fixed carbon?
6. Are rates of carbon processing through the landscape notable on the time scales of human-induced climate change?

The models used in this paper with minor modifications, as noted, were developed in parallel with the WEBB data-collection program. Stallard (1995a,b) introduced the concept of dissolved and solid bedrock and how major-element compositional information can be rigorously used to characterize steady-state erosion. Brown and others (1995, 1998) expanded on the concept of steady state and perturbed landscapes as determined by measurements of cosmogenic ^{10}Be in bedrock, soils, and sediments. Stallard (1998) developed tools that link physical erosion that has been greatly accelerated by human activities to the anthropologically modified carbon cycle. Carbon dioxide is removed from the atmosphere through accelerated soil loss and subsequent deposition and burial of the eroded soil and associated particulate organic carbon. The buried soil carbon is replaced by new soil carbon at the site of erosion, thereby creating a net carbon-dioxide sink. Stallard (1999) and Stallard and Kinner (2005) formulated models to include landslide-producing events in characterizations of annual sediment yields.

Weathering, Erosion, and the Carbon Cycle

Soils, river-borne solutes, and sediments are all derived from weathering processes that produce both dissolved and solid products. Most parent material must weather before becoming soil or being transported by flowing water. During chemical weathering, some minerals react congruently to produce only dissolved weathering products. Common minerals that always weather congruently are halite, anhydrite, gypsum, aragonite, calcite, dolomite, and quartz. Halite, anhydrite, and gypsum are so unstable that they almost never occur in the solid load of rivers. Calcite and dolomite sometimes occur in alkaline rivers that are supersaturated with respect to these minerals; for example, rivers within the Yukon River system in Alaska (Striegl and others, 2007). Quartz (crystalline SiO_2) is the most persistent of all common primary minerals and is typically abundant in river sediments. Most silicate and sulfide minerals weather incongruently to produce both dissolved cations (Na^+ , K^+ , Mg^{2+} , Ca^{2+}), silica (Si(OH)_4), sulfate (SO_4^{2-}) and sometimes minor constituents along with solid products that are depleted in cations and usually in silica. Minerals that contain aluminum and iron typically weather incongruently to produce clays and aluminum/iron sesquioxides (oxides and hydroxides of Al^{3+} and Fe^{3+}). Magnesium, potassium and, to a lesser extent, calcium and sodium are retained in cation-rich clays such

as the smectites, vermiculites, illites, and chlorites (Stallard, 1985, 1988; Stallard and Edmond, 1983, 1987; Stallard and others, 1991; Stallard, 1995a).

To this point, most studies of weathering associated with the WEBB program in eastern Puerto Rico have focused on the Río Icacos watershed, because of its homogenous granitic bedrock. As White and Blum (1995) state, “the pristine Icacos watershed in the Luquillo Mountains in eastern Puerto Rico has the fastest documented weathering rate of silicate rocks on the Earth’s surface.” The earliest biogeochemical work in the Icacos watershed was associated with the Luquillo Long-Term Ecological Research program (McDowell and others, 1992; McDowell and Asbury, 1994; McDowell, 1998; Bhatt and McDowell, 2007). Brown and others (1995) examined denudation rates using cosmogenic ^{10}Be in exposed bedrock, soils, and fluvial quartz and concluded that denudation rates calculated from ^{10}Be match those determined from solid and solute loads. Various aspects of chemical weathering have been examined by White and Blum (1995), Dong and others (1998), Murphy and others (1998), White and others (1998, 1999a,b), Schulz and White (1999), White (2002), Turner and others (2003), Buss and others (2004, 2005, 2008), Derry and others (2006); Fletcher and others (2006), Pett-Ridge and others (2008, 2009), Pett-Ridge (2009), and Buss and White (2012). Water quality of the measured river-borne constituents is discussed in chapter E of this report (Stallard and Murphy, 2012). McDowell and Asbury (1994) compared mass balances of the Icacos with two other rivers in the Luquillo Mountains that drain volcaniclastic rocks, the Sonadora and Toronja. Peters and others (2006) compared mass balances for 1991 to 1996 for the Icacos with rivers from each of the other four WEBB sites in the conterminous United States. Shanley and others (2011) examined 25 years of data from the Icacos starting in 1983.

Solute Loads and Chemical Erosion in Eastern Puerto Rico

Virtually all dissolved constituents in surface waters either arrive in rainfall or are acquired as water falls through vegetation and moves through soil and bedrock. Soils on the quartz-rich granitic rocks tend to be considerably thicker than soils on the volcanic and volcaniclastic rocks (see Murphy and others, 2012). Infiltration in all soils tends to be slow, and water infiltration to depths below 0.5 meters (m) takes many hours to several days, although rates are about three times as fast in soils on the granitic rocks as in soils on volcaniclastic rocks (Simon and others, 1990). At the lowest rainfall rates, water in all soils flows vertically into deeper soils, through deeper riparian zones, and then as hyporheic discharge. Water moving through these deep-soil environments typically flows past some unweathered primary minerals and relatively little organic matter. Studies of weathering in the granitic Icacos watershed demonstrate the importance of deep-flowing water in the weathering process (Turner and others, 2003; Buss and others, 2004, 2005, 2008; Fletcher and others, 2006; Buss and White, 2012). Silicon and strontium isotopes confirm

that deep-flowing water, emerging as base flow, interacts with primary minerals (Ziegler and others, 2005; Derry and others, 2006; Pett-Ridge and others, 2009). Shallow flow paths increase in relative importance with increasing rates of runoff (Derry and others, 2006; Stallard and Murphy, 2012). Similar patterns are recorded in volcaniclastic rocks (Larsen and others, 1999; Schellekens and others, 2004). At intermediate runoff rates, water also moves through shallow-soil pathways, and riparian zones are typically saturated. Shallow flow paths commonly have abundant organic matter and plant roots, but little unweathered primary minerals except for quartz. Finally, at the highest runoff rates, overland flow can become increasingly important, reducing the overall interactions of water with plant roots and deeper soil while also entraining higher particulate loads (Larsen and others, 1999; Schellekens and others, 2004; Larsen, 2012; Stallard and Murphy, 2012).

The relation between runoff and concentration of the various measured constituents is discussed in Stallard and Murphy (2012). Briefly, constituents that are not particularly bioactive and are derived from bedrock weathering or precipitation decrease in concentration with increasing runoff, reflecting the decreasing relative importance of flow paths that pass deep into the soil. Water that enters deeper soil generally passes through shallow-soil roots and is subject to more transpiration. Such constituents include sodium (Na^+), magnesium (Mg^{2+}), calcium (Ca^{2+}), silica (Si(OH)_4), alkalinity, and (Cl^-). Strongly bioactive constituents commonly display steady or increasing concentration with increasing runoff rates. These constituents include dissolved organic carbon (DOC), potassium (K^+), nitrate (NO_3^-), ammonium ion (NH_4^+), and phosphate (PO_4^{3-}). The concentrations of many of the bioactive constituents eventually decrease at runoff rates greater than 3 to 10 millimeters per hour (mm h^{-1}), presumably reflecting an increased dilution by rain and less-concentrated overland flow; DOC consistently increases and then decreases with increasing runoff rates. Note, however, that water interactions with vegetation (throughfall and stemflow) affect stream composition even in intense storms (Heartsill-Scalley and others, 2007). Sulfate (SO_4^{2-}) behaves like a bedrock-derived constituent in the Canóvanas, Cayaguás, and Mameyes rivers but like a bioactive constituent in the Icacos and Guabá (Stallard and Murphy, 2012).

Solid Loads and Physical Erosion in Eastern Puerto Rico

The most stable primary minerals are usually physically eroded before they have a chance to chemically decompose. Minerals that decompose contribute to the dissolved load in rivers, and their solid chemical-weathering products contribute to the secondary minerals in the solid load. The secondary minerals and the more stable primary minerals are the most important constituents of clastic sedimentary rocks. If physical erosion processes are weak, most of the erosion products are dissolved, and stable primary minerals and secondary minerals accumulate on top of bedrock to form soil (Stallard, 1985, 1988).

Landslides are a dominant component of physical erosion in steeper landscapes of eastern Puerto Rico (see Larsen, 2012), and the volume moved by landslides exceeds the volume moved by surficial erosion through mechanisms such as direct impaction by raindrops on soil, sheet wash, rill formation, and gullying. On the basis of 60 years of aerial photography, shallow landslides appear to affect approximately 1 percent of the forested eastern Puerto Rican landscape per century (Guariguata, 1990; Larsen and Torres-Sánchez, 1998). This rate is equivalent to a recurrence interval of about 10,000 years for landslides at a given site. Landslides erode remarkable quantities of solids in an exceedingly short time, typically in association with extreme rainfall events. Landslides in the Luquillo Mountains occupy a continuum from simple slumps to slides and debris flows, and most are entirely composed of soil produced by chemical weathering of bedrock.

Human activities greatly exacerbate landsliding. Aerial photographs demonstrate that landslides are much more common on deforested lands in eastern Puerto Rico (Larsen and Torres-Sánchez, 1998; Larsen and Santiago-Román, 2001). Of particular note is the agriculturally developed basin of the Río Cayaguás, on granodiorite. Here the thick soils that had developed under forest conditions were consumed by massive, regional, shallow-soil landsliding related to land clearing that lowered the landscape on average about 660 millimeters (mm) since 1820 (Larsen and Santiago-Román, 2001). This study of aerial photographs suggests that optimal factors promoting landslides are moderate to steep ($>12^\circ$) slopes, sufficient rainfall, typically greater than some threshold, and nonnatural land cover, notably construction sites and roads. Road building alone increases rates of landslides sixfold to eightfold in an 85-m swath bordering the roads (Larsen and Parks, 1997).

Typical prerequisites for landslides are steep slopes and bedrock that is structurally unstable (relatively noncohesive, sheared, or fractured) or, in the case of stable bedrock, the formation of unstable soils through chemical or physical weathering. Landslides typically come in clusters that are triggered by events such as large amounts of precipitation, typically exceeding some regional slide-inducing threshold (Starkel, 1972; Caine, 1980; Scatena and Larsen, 1991; Larsen and Simon, 1993; Montgomery and Dietrich, 1994; Crosta, 1998; Reid, 1998; Molnia and Hallam, 1999; Montgomery and others, 2000; Larsen and others, 2001) or earthquakes (Simonett, 1967; Garwood and others, 1979; Keefer, 1984).

Work in the Puerto Rico WEBB program (Larsen, 2012) has focused on the landslide process and emphasizes the importance of shallow-soil landslides in physical erosion. Tropical disturbances and northern-hemisphere, wintertime cold fronts trigger most of the landslides in the Puerto Rico WEBB watersheds (Scatena and Larsen, 1991; Larsen and Simon, 1993; Larsen and Torres-Sánchez, 1998). Larsen and Simon (1993) derived an empirical landslide threshold relation, relating rainfall, P (in millimeters), to storm duration and to T (in hours) that must be exceeded for landslides to happen:

$$P \geq 91.46 \cdot T^{0.18}. \quad (1)$$

The essence of this relation is that if more than the requisite rain falls in specified time, and if the terrain is sufficiently steep ($>12^\circ$ slope), then there may be landslides. This relation was field tested in Puerto Rico after Hurricane Hugo in 1989 and found to be valid (Larsen and Torres-Sánchez, 1992). For storms with a duration of 24, 48, and 72 hours, the threshold rainfall is 162, 184, and 197 mm respectively, or roughly 200 mm. Stallard (1999) and Stallard and Kinner (2005) note that in the Panama Canal watershed (where runoff variation among rivers was similar to that of the Puerto Rico WEBB rivers), the transition to landslide-driven erosion is in the range of 800 mm to 1,000 mm mean-annual runoff, but that this transition might be lower in basins subjected to intense storms such as hurricanes. Accordingly, attempts to predict solid yields for wetter and drier conditions need to explicitly account for the presence or absence of landslide-producing storms at higher runoff regimes.

Without chemical weathering, there would be few landslides. Shallow-soil landslides typically occur near the interface between hard and soft saprolite, commonly on zones of weakness formed on former exfoliation surfaces that had become conduits for soil water (Simon and others, 1990). The thickness of the soil that slides is about 1 to 4 m (Simon and others, 1990; Larsen and Torres-Sánchez, 1992; Larsen and Simon, 1993; Larsen, 1997, 2012; Larsen and Santiago-Román, 2001). Landslide erosion can enrich the solute load in cations that are largely leached out of hard saprolite (Na^+ and Ca^{2+}) compared with those that partially leach (K^+ and Mg^{2+}) (Stallard, 1985, 1988). In the Icacos watershed, which is underlain by granitic rocks, an analysis of in-place-produced cosmogenic ^{10}Be in quartz as a function of grain size shows that the fine material in the river is largely derived from surficial erosion, whereas the coarse material is derived from deep erosion, presumably landslides (Brown and others, 1995). Sediment-discharge calculations indicate that about half of the river-borne quartz is derived from deep erosion.

Vegetation regrowth and succession following a landslide are quite rapid—perhaps 100 to 200 years (Guariguata, 1990; Walker and others, 1996), starting with the bare slip face. Soon after, a characteristic sequence of vegetation grows on the slide (lichens and moss, then ferns and grass, then second-growth trees, and finally mature forest), anchoring the soil. Similarly, soil development and restoration of soils to preslide nutrient conditions is on the same time scale (Zarin, 1993; Zarin and Johnson, 1995a,b). Conditions in Puerto Rico appear to be especially favorable to the rapid regrowth of vegetation; in the nearby Blue Mountains of Jamaica, plant succession appears to be much slower (Dalling and Tanner, 1995).

In addition to delivering sediment directly to rivers during storms, landslides are strong secondary sources of sediments. First, landslides normally deliver far more debris to a valley than rivers can remove in a single flood. This debris is then eroded by subsequent storms. Second, the bare slip face itself becomes a source of sediment (Larsen, 1997, 2012).

Initially, sediment yield from the slip face was more than ten-fold as great as yield from the adjacent forest, but after 4 to 5 years, sediment yields dropped to less than those of the forest.

Steady-State Erosion

Erosion under steady-state conditions, or dynamic equilibrium, is a useful frame of reference for studying a river system (Stallard, 1995a,b, 1998), especially in a landscape with such varied and intense physical erosion as eastern Puerto Rico. The core idea is that the geomorphic properties of the landscape are not changing substantially through time. Steady-state erosion also implies a chemical mass balance, such that the sum of the fluxes of all solid and dissolved weathering products leaving a landscape should equal the mass of bedrock being degraded by weathering. When rates of physical erosion are less than rates of the production of loose material by weathering, soils thicken. When the opposite holds true, there is net soil erosion. Human activities, mostly land clearing and agriculture, have substantially accelerated upland erosion as compared with presumed steady-state rates, causing greatly increased carbon burial in sediments (Stallard, 1998). When chemical weathering reactions control the rate of production of erodible solid materials, rates of chemical weathering and the composition of weathering products can be used to calculate yields of dissolved constituents and thus predict equilibrium yields of solids (Stallard, 1995a,b).

For the Icacos watershed, Brown and others (1995) compared rates of erosion estimated by using cosmogenic ^{10}Be to rates estimated by using chemical and sediment data for 1983–1986 from McDowell and Asbury (1994) and from the earliest years of the Puerto Rico WEBB program. The data indicated that the Icacos landscape is near a dynamic equilibrium. Chemical mass balance calculations by White and others (1998) supported this assertion. In contrast, studies of ^{10}Be in the sediments transported by the Río Cayaguás indicate that erosion rates today are considerably greater than they were in the past (Brown and others, 1998).

Carbon, Weathering, and Erosion

The largest export of carbon from watersheds is not fluvial; it is the conversion of carbon fixed into organic matter by net primary productivity back into atmospheric carbon dioxide by respiration and decay. Fluvial transport typically exports the next largest amount of carbon from a watershed (excluding agricultural and timber harvest), and this transport is tightly linked to weathering and erosion. Rivers export carbon from watersheds in four broad classes of material (Meybeck, 1993): dissolved inorganic carbon (DIC), dissolved organic carbon (DOC), and particulate organic carbon (POC) are important in the streams of Puerto Rico, whereas particulate inorganic carbon (PIC), which consists of calcium-magnesium carbonates, is not typically present in

tropical rivers because tropical waters are typically strongly undersaturated with respect to these minerals (Stallard and Edmond, 1987; Stallard and others, 1991; Stallard, 1995a). The fluvial export of carbon may be related to either inventory changes or new transfers from the atmosphere.

Carbon transport by rivers is tightly coupled with chemical and physical erosion processes. Dissolved inorganic carbon is derived from dissolved carbon dioxide that is converted to bicarbonate and carbonate ions through the chemical weathering of most silicate rocks and all carbonate rocks. In these weathering reactions, hydrogen ions are consumed and soluble cations (Na^+ , K^+ , Mg^{2+} , Ca^{2+}) are released (Garrels and Mackenzie, 1971). The weathering of sulfide minerals, which generates mostly insoluble sesquioxides and sulfuric acid, has the reverse effect, converting bicarbonate and carbonate ions into dissolved carbon dioxide (Garrels and Lerman, 1984).

The weathering of carbonate rocks is a source of non-atmospheric DIC (Garrels and Mackenzie, 1971; Garrels and Lerman, 1984; Meybeck, 1993). Minor carbonates are present in the granitic and volcaniclastic rocks in the study watersheds (see Murphy and others, 2012). Trace carbonate weathering in the granitic rocks in the Luquillo Mountains appears to be limited by the general advance of weathering fronts into the rocks (White and others, 1999b). My own observations suggest that no geomorphic evidence indicates preferential weathering of extensive carbonate rocks in the Luquillo Mountains, such as one sees in karst limestone landscapes of north-central Puerto Rico.

Igneous rocks do not contain fossil carbon, a conspicuous research advantage in constructing carbon budgets in the Puerto Rico WEBB watersheds. Many rivers in island arcs and orogenic belts erode organic-rich shales, and in determining POC loads, it is important to distinguish between eroded fossil carbon (kerogen) and young (soil) carbon, because the reburial of fossil carbon does not affect atmospheric carbon budget (Leithold and Blair, 2001; Blair and others, 2003; Galy and others, 2007; Hilton and others, 2008a). Carbon budget calculations for such rivers are further complicated by the oxidation of fossil carbon and pyrite during weathering, which effectively releases carbon dioxide to the atmosphere (Petsch and others 2000, 2001). In the study WEBB watersheds, we can assume that all eroded carbon is geologically young.

The export of DIC from a watershed is operationally defined and is best compared with the export of alkalinity, which is commonly equated with the bicarbonate ion in streamwater. Alkalinity is strictly the amount of anion charge per unit volume that can be titrated with a strong acid to reach the first equilibrium endpoint for the carbon dioxide system (Stumm and Morgan, 1981). Another name for alkalinity is acid-neutralization capacity. Alkalinity is a conservative property and is also equal to the total charge of nontitratable cations (which include ammonium ion at $\text{pH} < 9.3$) minus the total charge of nontitratable anions (including NO_3^-). Alkalinity is also independent of the pH

and the carbon-dioxide vapor pressure (P_{CO_2}) of the sample. If a strong base is required to titrate to the endpoint, then the alkalinity is negative and is sometimes referred to as acidity. In this report DIC is treated as equal to alkalinity.

Dissolved organic carbon (DOC) is derived from carbon dioxide that has been “fixed” into soluble organic compounds through photosynthesis by plants and has been released as plant, fungal, or algal exudates or by the decay of biomass (Meybeck, 1993; Hedges and others, 2000; Aufdenkampe and others, 2001, 2007; Striegl and others, 2007).

Particulate organic carbon (POC) comes mostly from fragments of plant material in various stages of decay and from DOC that has become bound to surfaces of mineral grains (Hedges and others, 2000; Aufdenkampe and others, 2001, 2007). Grain-surface POC and fine-grained POC form a large component of total POC. Clay-size (<0.2 micrometer (μm)) mineral grains, including aggregated grains, have an especially large surface-area-to-volume ratio; they are most important in stabilizing organic carbon as POC. In headwater streams, such as those described here, organic carbon is largely allochthonous (soil and plant debris). In eastern Puerto Rico, surface soils in the agricultural watershed are 1 to 3 percent carbon, whereas soil carbon in the forested landscape is somewhat greater (Beinroth and others, 1992). The estimated POC yields for many mountainous rivers having high runoff and smaller drainage areas greatly exceed the global-average POC yield of $2\text{--}3 \text{ t km}^{-2} \text{ yr}^{-1}$ C (Stallard, 1998). Organic-carbon molecules range considerably in size, so the transition between DOC and POC is operational, based on the effective pore size of the filters that were used to process the sample. Most Puerto Rico WEBB samples were filtered through 0.2- μm membrane filters that rapidly clogged (appendix 2).

Landslides, Erosion, and Carbon

Landslides, including those induced by tropical disturbances, probably have a major role in the erosional export of young organic carbon to the ocean (Hilton and others, 2008a,b). Landslide erosion has many parallels with accelerated agricultural erosion, which is a substantial component of the technologically modified carbon cycle, provided that carbon eroded from agricultural lands is buried and then replaced at the site of erosion with new photosynthetic carbon (Stallard, 1998). Landslides are even more effective than agricultural erosion at removing the entire soil profile along with all of its organic carbon (Simon and others, 1990; Zarlin, 1993; Zarlin and Johnson, 1995a,b; Walker and others, 1996). Zarlin (1993) and Zarlin and Johnson (1995a,b) have documented the regeneration of soils in chronosequences of slide scars in and around the Icacos watershed. A zero-order accumulation, first-order-loss model of soil carbon for soils (Stallard, 1998, equation 5) can be applied to the soil organic carbon data of Zarlin (1993) (fig. 2). It is assumed that little physical erosion occurs on the slide scar once it is stabilized by pioneer plants. It is

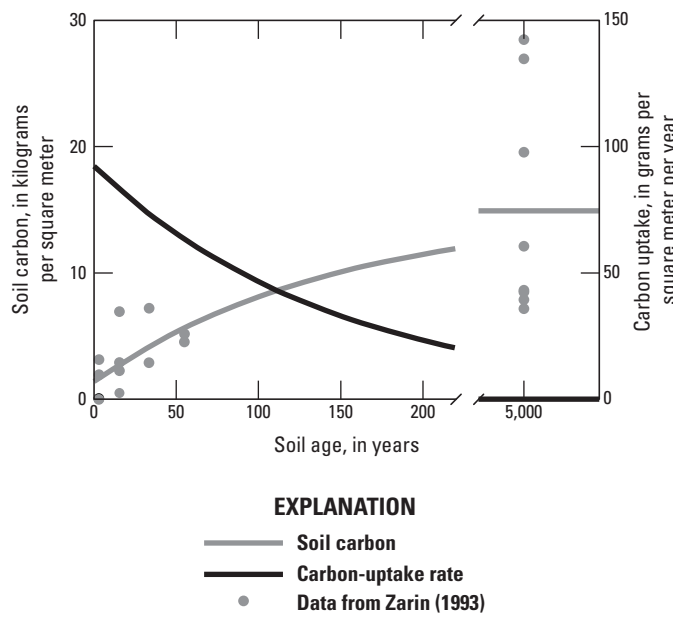


Figure 2. A zero-order accumulation, first-order-loss model of soil carbon accumulation on a chronosequence of landslides from the Luquillo Mountains based on data from Zarin (1993). This version of the model includes initial carbon on the slide face.

also assumed that the age of old soils in this dataset is a large fraction of 10,000 years, the approximate landslide recurrence interval calculated for the Luquillo Mountains. The variability of the old-soil carbon values reflects the several types of forest that eventually develop following landslides (Guariguata, 1990). The initial model soil-carbon accumulation rate for landslide scars is about $80 \text{ t km}^{-2} \text{ yr}^{-1}$ C or 6,700 kilomoles moles per square kilometer per year ($\text{kmol km}^{-2} \text{ yr}^{-1}$ C), if one assumes minor initial carbon on the fresh scars. If the fresh slide faces are assumed to be carbon-free, initial rates are $150 \text{ t km}^{-2} \text{ yr}^{-1}$ C or 12,000 $\text{kmol km}^{-2} \text{ yr}^{-1}$ C. These fluxes represent upper limits on rates of POC generation for the eastern Puerto Rico landscape. This rate is 10 to 20 percent of net primary productivity for tropical forests, in general. The rapid regeneration of soil carbon, about half in 80 years, indicates that all POC removed from the watersheds by landslides and subsequent fluvial transport is rapidly being replaced by new carbon.

Methods Used to Assess the Effects of Weathering and Erosion in the Carbon Cycle

An analysis of weathering and erosion of bedrock and its relation to fluvial-carbon transport requires the introduction of several properties derived from the concentrations of

measured constituents. For simplicity, these are referred to as “derived constituents.” Two important derived constituents are dissolved bedrock and suspended bedrock, concepts that were introduced by Stallard (1995b). Dissolved bedrock (DBrx) is derived using the concentrations of various solutes to determine the quantity of original bedrock that this represents, which is then expressed as a concentration. Similarly, suspended bedrock (SBrx) is the concentration of original bedrock represented by solids in suspension. To determine DBrx and SBrx, one models atmospheric contributions to the dissolved and solid load using mass balances and reconstructions of weathering reactions. These and other derived constituents can then be used to formulate erosion models and yield-estimation procedures that can be compared among the four watersheds.

Chemical Analyses of Dissolved and Solid Phases

During 1991 to 2005 in the five rivers of the Puerto Rico WEBB program, automated samplers collected data on 507 hydrologic events from 263 storms, including all major hurricanes (Stallard and Murphy, 2012; appendix 1 of this report). A total of 4,894 samples were sufficiently analyzed to determine dissolved and solid denudation rates, and 860 of these were analyzed for a comprehensive suite of chemical constituents. Of samples analyzed for comprehensive chemistry and sediment, 543 were collected at runoff rates greater than 1 mm h^{-1} , 256 at rates exceeding 10 mm h^{-1} , and three that exceed 90 mm h^{-1} . Globally, few samples have been collected and analyzed for chemistry and suspended solids at runoff rates exceeding 1 mm h^{-1} (appendix 1). In terms of process studies, these data represents a new realm of water-quality data.

The analysis of dissolved constituents and sediment is discussed by Stallard and Murphy (2012) and in appendix 2 of this report.

Samples of soil, sediment, and bedrock, selected on the basis of freshness of exposure, were analyzed for chemical composition. Solid samples were ground using a chrome steel grinder such that they could pass through a 250 mesh (65 micrometer) stainless steel sieve. Samples were analyzed as a lithium-metaborate fused disk by X-ray fluorescence and reported as oxides (table 1). Analyses included SiO_2 , Al_2O_3 , CaO , MgO , Na_2O , K_2O , Fe_2O_3 , MnO , TiO_2 , and P_2O_5 , and loss on ignition (LOI) with a detection limit of 0.01 percent, and Ba, Nb, Rb, Sr, Y, and Zr with a detection limit of 10 parts per million (ppm). Cr_2O_3 was analyzed to check for grinder contamination, which proved negligible. Ba and Nb were generally below detection and are not included in table 1. In addition, some samples were analyzed for ferrous iron (FeO in table 1), CO_2 , H_2O^+ , and H_2O^- by wet chemistry and for sulfur and chloride by pressed-pellet X-ray fluorescence. Analyses were performed at XRAL Activations Services, Ann Arbor, Michigan.

Table 1. X-ray fluorescence and wet-chemical analysis of geologic materials and water from the Luquillo Mountains, eastern Puerto Rico.

[Units are percent unless otherwise noted; LOI, loss on ignition; -, not analyzed]

Description	SiO ₂	Al ₂ O ₃	CaO	MgO	Na ₂ O	K ₂ O	Fe ₂ O ₃	MnO	TiO ₂	P ₂ O ₅	S	Cl ⁻	LOI	H ₂ O ⁺	CO ₂	FeO	Rb ⁺	Sr ²⁺	Zr ⁴⁺
Solids																			
Quartz diorite, Icacos Route 191, lower road	61.1	17.6	7.18	2.50	3.36	1.23	6.85	0.14	0.56	0.09	--	--	0.69	--	--	--	37	223	62
Quartz diorite, landslide 43 ²	64.2	16.6	6.17	2.13	3.56	1.39	5.96	0.13	0.44	0.09	--	--	0.60	--	--	--	37	220	76
Quartz diorite, landslide 43	63.4	16.9	6.04	2.10	3.53	1.25	6.53	0.14	0.471	0.12	0.06	0.05	0.34	0.8	0.2	0.01	4.0	38	78
Quartz diorite, landslide 43	62.4	16.8	6.05	2.27	3.42	1.22	6.60	0.14	0.47	0.12	0.1	0.05	0.46	0.7	0.2	0.0	4.1	39	79
Xenolith in quartz diorite, landslide 43	55.2	12.0	6.19	6.00	2.11	1.97	14.70	0.36	1.156	0.24	0.06	0.09	0.72	1.4	0.2	0.02	9.4	84	164
Xenolith in quartz diorite, landslide 43	56.6	15.3	7.21	5.30	3.30	1.20	9.17	0.27	0.78	0.21	0.2	0.06	0.82	1.2	0.2	0.0	6.6	34	145
Aplitic vein in quartz diorite, landslide 43	64.4	20.1	3.01	0.14	5.72	4.56	1.19	0.02	0.097	0.02	0.22	0.02	0.39	0.3	0.2	0.01	0.7	49	230
Volcanic rock, landslide 8 ³	49.1	17.4	8.93	6.64	3.84	0.52	9.78	0.14	0.83	0.11	--	--	3.47	--	--	--	0	615	60
Volcanic rock, landslide 8	50.9	14.4	9.82	7.82	2.00	0.43	8.11	0.12	0.78	0.14	0.1	0.01	4.27	4.1	0.4	0.6	6.1	0	402
Volcanic rock, landslide 8	51.4	14.1	9.19	7.78	2.10	0.45	8.02	0.12	0.822	0.16	0.09	0.01	4.00	3.9	0.3	0.50	6.0	19	416
Volcanic rock, landslide 8	50.4	14.1	10.10	7.80	1.99	0.47	8.27	0.12	0.76	0.15	0.1	0.01	4.46	3.8	0.3	1.1	6.3	19	406
Granitic rock, surface soil, on divide, landslide 43	70.3	11.7	0.03	0.12	0.08	0.25	0.91	0.03	0.48	0.03	--	--	14.35	--	--	--	31	0	226
Granitic rock, surface soil, mid-slope, landslide 43	63.2	14.4	0.25	0.20	0.00	0.23	4.65	0.03	0.52	0.04	0.0	0.02	15.34	10.0	1.8	0.0	0.9	9	256
Icacos gage, sand sample	79.3	6.9	0.98	1.00	0.33	0.41	7.55	0.10	0.54	0.03	--	--	2.99	--	--	--	24	9	557
Icacos gage, overbank sediment	36.6	28.1	0.58	0.76	0.22	0.46	12.90	0.17	0.890	0.13	--	--	20.40	--	--	--	16	39	140
Volcaniclastic rock, surface soil, landslide 8	46.8	19.6	0.34	0.44	0.04	0.27	10.25	0.02	1.527	0.09	0.03	0.02	20.64	13.2	3.1	0.00	1.7	19	43
Dissolved bedrock oxide concentrations, calculated as described in the text																			
Canóvanas, dissolved bedrock	43.6	--	30.5	13.2	9.45	2.49	--	--	0.06	0.69	--	--	--	--	--	--	--	--	--
Cayaguás, dissolved bedrock	54.3	--	18.0	5.67	15.1	5.20	--	--	0.09	1.67	--	--	--	--	--	--	--	--	--
Mameyes, dissolved bedrock	54.0	--	28.8	6.39	7.25	2.35	--	--	0.04	1.17	--	--	--	--	--	--	--	--	--
Icacos, dissolved bedrock	64.9	--	17.5	5.13	9.65	2.84	--	--	0.02	0.00	--	--	--	--	--	--	--	--	--
Guabá, dissolved bedrock	71.0	--	12.9	3.30	9.92	2.88	--	--	0.02	0.0	--	--	--	--	--	--	--	--	--

¹Parts per million.²Landslide 43 of Guariguata and Larsen (1990) is located in the Icacos watershed, at the first large stream crossing on Route 191, west side.³Landslide 8 of Guariguata and Larsen (1990) is located on Route 988, about 1 kilometer west of the Mameyes gage site.

Estimation of Constituent Yields

The loads and yields (loads divided by watershed area) of most constituents, including derived constituents, were calculated using LOADEST (load estimator; Runkel and others, 2004) as described in Stallard and Murphy (2012) and in appendix 1. The process involved merging thousands of chemical measurements with nearly continuous discharge

measurements calculated from stage recordings. LOADEST was used to estimate constituent yields for hourly and yearly intervals and for the entire study period (15 years in the Canóvanas, Cayaguás, Mameyes, and Icacos rivers and 10 years in the Guabá; tables 2, 3; figs 3–6).

Alkalinity can have negative values because of addition of organic acids from soil process and sulfuric and nitric acids from rain. LOADEST, because it works with

Table 2. Discharge-weighted average concentrations of each percentile class estimated by using LOADEST and hourly discharge from study watersheds, eastern Puerto Rico.

[DIC, dissolved inorganic carbon; DOC, dissolved organic carbon; POC, particulate organic carbon; LOI, loss on ignition; mm h⁻¹, millimeters per hour; mg L⁻¹, milligrams per liter; µmol L⁻¹, micromoles per liter]

Sample percentile class	Runoff rate (mm hr ⁻¹)	SiO ₂ (mg L ⁻¹)	Bedrock Na ₂ O (mg L ⁻¹)	Dissolved bedrock (mg L ⁻¹)	Suspended bedrock (mg L ⁻¹)	DIC (µmol L ⁻¹)	DOC (µmol L ⁻¹)	POC (µmol L ⁻¹)	LOI (percent of suspended solids)	POC (percent of suspended solids)
Canóvanas										
0–10 percent	0.021	34.8	9.9	90	8	2,044	164	19	23	2.3
>10–25 percent	0.061	29.3	6.8	70	24	1,450	232	51	20	2.1
>25–50 percent	0.158	24.7	4.9	55	72	1,035	299	139	18	1.9
>50–75 percent	0.765	17.5	3.2	37	380	586	414	647	15	1.7
>75–90 percent	4.49	12.4	2.5	26	1,050	349	420	1,786	15	1.7
>90–95 percent	15.3	9.6	2.3	20	1,489	282	374	2,669	17	1.8
>95–99 percent	32.0	8.3	2.3	18	1,669	265	323	3,141	18	1.8
>99–100 percent	59.2	7.1	2.3	16	1,723	254	266	3,457	20	1.9
Cayaguás										
0–10 percent	0.041	40.9	18.2	83	12	1,395	123	14	11	1.3
>10–25 percent	0.095	35.6	11.7	67	37	997	168	37	10	1.1
>25–50 percent	0.195	29.6	7.6	53	128	669	221	116	8	1.0
>50–75 percent	0.860	18.9	3.4	31	995	250	312	806	6	0.9
>75–90 percent	4.35	11.2	1.8	19	3,237	80	324	2,580	6	0.9
>90–95 percent	12.1	7.6	1.4	13	5,366	48	278	4,287	6	0.9
>95–99 percent	26.2	5.5	1.2	10	6,727	38	231	5,391	6	0.9
>99–100 percent	41.0	4.7	1.1	9	6,484	33	212	5,015	7	0.9
Mameyes										
0–10 percent	0.068	34.3	5.1	61	1	914	80	5	35	3.5
>10–25 percent	0.179	22.3	3.2	41	3	615	133	13	32	3.2
>25–50 percent	0.324	17.8	2.3	32	9	469	178	30	28	2.8
>50–75 percent	0.887	12.3	1.4	22	43	297	245	111	23	2.4
>75–90 percent	2.81	8.3	0.9	15	176	173	308	362	19	2.0
>90–95 percent	7.26	5.9	0.8	11	479	106	358	835	15	1.8
>95–99 percent	21.2	4.2	0.8	8	1,101	61	347	1,692	14	1.6
>99–100 percent	45.6	3.2	0.7	6	1,778	42	320	2,540	13	1.5
Icacos										
0–10 percent	0.115	28.6	3.7	41	3	426	75	9	30	2.8
>10–25 percent	0.252	19.9	2.7	30	8	332	125	24	27	2.7
>25–50 percent	0.429	15.4	2.2	24	21	265	186	58	24	2.5
>50–75 percent	1.197	9.3	1.6	15	139	165	299	269	18	1.9
>75–90 percent	3.96	5.2	1.1	9	728	79	368	983	12	1.4
>90–95 percent	9.04	3.6	0.8	6	1,901	41	349	1,998	10	1.1
>95–99 percent	20.8	2.4	0.7	4	5,291	17	285	3,830	6	0.8
>99–100 percent	51.6	1.5	0.5	3	21,372	-2	149	7,811	3	0.4
Guabá										
0–10 percent	0.104	26.6	3.2	36.1	4	321	79	14	29	2.9
>10–25 percent	0.250	18.8	2.4	26.1	12	235	120	38	27	2.7
>25–50 percent	0.383	15.8	2.0	22.1	28	194	142	76	25	2.5
>50–75 percent	0.950	10.28	1.5	15.0	161	130	205	326	19	2.0
>75–90 percent	4.48	5.00	1.0	8.0	1,275	59	265	1,801	13	1.5
>90–95 percent	14.48	3.03	0.8	5.3	2,956	30	264	3,621	11	1.3
>95–99 percent	33.1	2.03	0.8	3.9	4,484	16	259	4,998	9	1.2
>99–100 percent	68.6	1.50	0.9	3.1	6,299	8	223	6,667	8	1.2

Table 3. Average annual net, atmospheric, and bedrock inputs in 1991 to 2005 to study watersheds, eastern Puerto Rico.

[DOC, dissolved organic carbon; POC, particulate organic carbon; DBrx, dissolved bedrock; SBrx, suspended bedrock; mm yr⁻¹, millimeters per year; kmol km⁻² yr⁻¹, kilomoles per square kilometer per year; kEq km⁻² yr⁻¹, kiloequivalents per square kilometer per year; t km⁻² yr⁻¹, metric tons per square kilometer per year; -- not analyzed]

Watershed	Runoff (mm yr ⁻¹)	Na ⁺	K ⁺	Mg ²⁺	Ca ²⁺	Si(OH) ₄	Cl ⁻	SO ₄ ²⁻	NO ₃ ⁻	NH ₄ ⁺	-PO ₄ ³⁻	Alkalinity (kEq km ⁻² yr ⁻¹)	DOC (kmol km ⁻² yr ⁻¹)	POC (kmol km ⁻² yr ⁻¹)	DBrx (t km ⁻² yr ⁻¹)	SBrx (t km ⁻² yr ⁻¹)	
Annual net yields																	
Annual atmospheric inputs																	
Canóvanas	970	276	5.8	31	13	280	357	324	43.8	43.5	3.6	0.39	918	313	627	47.0	355
Cayaguás	1,620	672	88.1	136	249	662	411	78.1	81.5	4.4	0.94	865	389	1,594	72.6	1,979	
Mameyes	2,750	634	50.7	174	439	739	541	84.5	26.1	2.1	0.41	1,137	573	503	87.3	270	
Icacos	3,760	733	58.1	150	264	853	585	54.4	44.5	3.7	0.18	800	837	1,787	78.0	1,983	
Guabá	3,630	657	54.0	109	173	779	623	42.7	38.9	2.6	0.18	502	576	2,282	67.0	1,717	
Canóvanas	970	350	7.4	40	14	0	411	41.7	23.9	9.1	--	--	-32	313	627	0.0	21
Cayaguás	1,620	461	9.7	52	17	0	541	54.9	31.5	12.0	--	-61	-44	389	1,594	0.0	21
Mameyes	2,750	498	10.5	57	17	0	585	59.3	34.0	13.0	--	-67	-61	573	503	0.0	21
Icacos	3,760	531	11.2	60	18	0	623	63.2	36.3	13.8	--	-73	-67	837	1,787	0.0	21
Guabá	3,630	531	11.2	60	18	0	623	63.2	36.3	13.8	--	-73	-73	576	2,282	0.0	21
Canóvanas	970	141	26.0	162	267	357	0	11.0	24.7	-3.6	--	950	0	0	47.0	334	
Cayaguás	1,620	322	80.8	96	235	662	0	36.4	57.6	-4.7	--	908	0	0	72.6	1,958	
Mameyes	2,750	173	41.0	122	422	739	0	29.6	-5.4	-9.9	--	1,199	0	0	87.3	249	
Icacos	3,760	235	47.7	93	246	853	0	-4.9	10.5	-9.3	--	867	0	0	78.0	1,962	
Guabá	3,630	126	42.9	49	154	779	0	-20.6	2.6	-11.2	--	574	0	0	67.0	1,696	
Atmospheric inputs as percentage of net yield																	
Canóvanas	970	66	18	16	4	0	100	75	43	201	--	-3	100	100	0	6	
Cayaguás	1,620	52	8	29	6	0	100	53	29	207	--	-5	100	100	0	1	
Mameyes	2,750	73	19	30	4	0	100	65	121	582	--	-5	100	100	0	8	
Icacos	3,760	68	18	38	7	0	100	109	76	353	--	-8	100	100	0	1	
Guabá	3,630	81	21	55	11	0	100	148	93	534	--	-14	100	100	0	1	

¹Negative values indicate that atmospheric input exceeds river export.

logarithmic transforms of the data, cannot handle situations with legitimate negative values. Instead, alkalinity loads and average concentrations were calculated using the loads and concentrations of other constituents as estimated by LOADEST (concentrations in mole units):

$$\text{alkalinity} = \text{Na}^+ + \text{K}^+ + \text{NH}_4^+ + 2 \cdot (\text{Mg}^{2+} + \text{Ca}^{2+} + \text{Sr}^{2+}) - (\text{Cl}^- + \text{NO}_3^- + 2 \cdot \text{SO}_4^{2-} + Z_{\text{DOC}}) \quad (2)$$

where Z_{DOC} is the negative charge per carbon atom in DOC. For each river, Z_{DOC} was calculated by adjusting predicted alkalinity to measured alkalinity such that the ratio of averages was 1:1. The range of estimated values was 0.5 equivalents of charge per mole (eq mol⁻¹) to 0.8 eq mol⁻¹ (appendix 1). For reference, Tardy and others (2005) found an optimal Z_{DOC} of 0.64 eq mol⁻¹ for Amazonian lowland rivers.

Data Manipulation and Processing of Dissolved Constituents

One of the main motivations for introducing derived constituents is the need to subtract atmospherically derived contributions to the dissolved load, much of it seasalt, from bedrock-derived contributions. This subtraction is also termed a cyclic-salt correction (Stallard and Edmond, 1981, 1983). Once such a subtraction is accomplished, it is possible to calculate DBrx, which when combined with SBrx, can be used to accurately estimate erosion and determine whether erosion is in disequilibrium.

Correction for Atmospherically Derived Contributions to the Dissolved and Solid Load

A substantial portion of the dissolved load in rivers is derived from the atmosphere. Historically, estimates of denudation have not corrected for this component. One atmospheric source is precipitation; another is direct transfer from the atmosphere to plant and ground surfaces by impaction and dry deposition. Another pathway is “fixation” from the gas phase into a solid or soluble form by biological processes, mostly photosynthesis and nitrogen fixation. Finally, chemical weathering involves fixation of water and carbon dioxide from the atmosphere into dissolved ionic forms and into soil minerals as structural or bound water. In the eastern Puerto Rico watersheds, which are underlain almost entirely by igneous rocks, virtually all the inorganic and organic carbon is atmospherically derived. The same is true for all forms of nitrogen. Almost all river-borne Cl⁻ has a seasalt origin, and almost all ions that are abundant in surface seawater make considerable atmospheric contributions to the dissolved load. Biogenic gases and pollution contribute SO₄²⁻, NO₃⁻, and NH₄⁺. Desert dust contributes notable amounts of soluble calcium (see Stallard, 2012).

Atmospheric sources also contribute to the solid load. All of the organic carbon and much of the water bound into

clays in river-borne sediment has an atmospheric origin (table 1, LOI, H₂O⁺, H₂O⁻). For reference, kaolinite and halloysite (Al₂Si₂O₅(OH)₄) are 14.0 percent by weight water. Clays and other minerals in desert dust also make a minor contribution to the solid load (Pett-Ridge, 2009; Stallard, 2012).

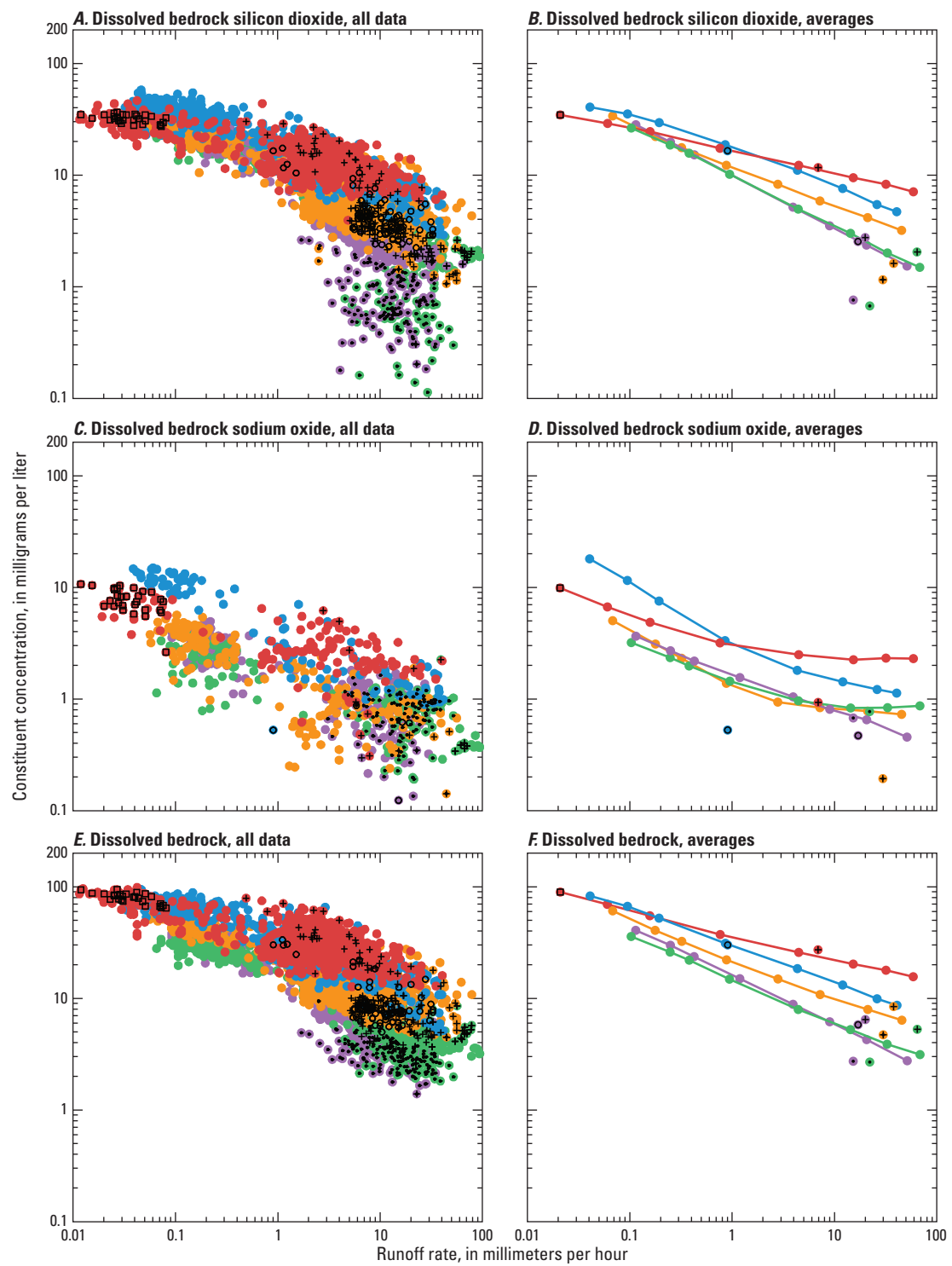
In order to estimate bedrock contributions to the dissolved load, the major cations (Na⁺, K⁺, Mg²⁺, Ca²⁺), and SO₄²⁻ require corrections for atmospheric inputs. For Na⁺, K⁺, and Mg²⁺, the correction involves subtracting a seasalt contribution on the basis of the ratio of that ion to Cl⁻ either in rain or in seasalt. If we use Na⁺ as an example, the Na⁺:Cl⁻ mole ratio for seasalt is 0.8525:

$$\text{Na}^* = \text{Na}^{2+} - (\text{Na}^+:\text{Cl}^-) \cdot \text{Cl}^- \quad (3)$$

The “*” designates a calculated bedrock-derived constituent. The Mg²⁺:Cl⁻ ratio in rain is 0.09689, less than the seasalt ratio of 0.10145 (Stallard, 2012). The seasalt SO₄^{2-":Cl⁻ ratio is 0.052, and in some storms, especially high-chloride events, the rain and runoff are near this ratio (Stallard and Murphy, 2012, their fig. 10). However, additional sulfur comes from pollution and emissions of organic sulfur compounds (dimethyl sulfide and methyl sulfide) from the marine environment. To further complicate matters, the forest environment may also emit organic sulfur compounds back to the atmosphere (Stallard and Edmond, 1981; Stallard and Murphy, 2012). The overall SO₄^{2-":Cl⁻ ratio is 0.10614 in rain, and this ratio was used in calculations. The K⁺:Cl⁻ ratio in rain is 0.02306, whereas the seasalt ratio is 0.0179. Because throughfall is so rich in K⁺ (Heartsill-Scalley and others, 2007), the greater rain ratio is seen as reflecting local, minor plant contamination, so the seasalt ratio was used. The Ca^{2+":Cl⁻ ratio is 0.01876, and seasalt is a minor contributor to the calcium budget.}}}

In individual samples, the atmospheric-correction calculation occasionally yields a negative value. This result may be due to real processes, such as cation exchange in soil that can alter cation proportions, or it may be due to true variations in the ratios to Cl⁻ for individual storms, as happens with SO₄²⁻. In constructing annual and long-term budgets, the atmospheric corrections incorporate calculated yields using the Cl⁻ yield as the basis for the correction. The calculation was checked against LOADEST calculations of Na* and Ca*.

Constituent yields estimated using LOADEST were compared with atmospheric inputs (Stallard, 2012) (table 3). Several constituents (Na⁺, Cl⁻, SO₄²⁻, and NO₃⁻ plus NH₄⁺, DOC, and POC) are largely atmospheric in origin. Potassium and Mg²⁺ receive a contribution of about 10 to 50 percent from the atmosphere. Calcium, silica, dissolved bedrock, and suspended bedrock receive minor atmospheric contributions, 0 to about 10 percent. Alkalinity has a small negative atmospheric contribution; in essence, acidity in rain is titrating the landscape. The atmospheric contribution for phosphate, which is quite large (Pett-Ridge, 2009), was not included in table 3; phosphate is biologically and chemically quite reactive, and without more information it would be hard to apportion atmospheric inputs to the dissolved or solid load.

**EXPLANATION**

- | | | |
|---------------|------------------|-------------|
| —●— Canóvanas | □ Calcite | ● Canóvanas |
| —●— Cayaguás | + High chloride | ● Cayaguás |
| —●— Guabá | ○ High potassium | ● Guabá |
| —●— Icacos | • Low silica | ● Icacos |
| —●— Mameyes | | ● Mameyes |

Figure 3. (facing page) The concentration of dissolved silicate bedrock (DBrx) and two dissolved constituents, bedrock Na₂O and silicon dioxide, Na₂O, used in calculating DBrx and in estimating equilibrium physical denudation rates in eastern Puerto Rico. Bedrock Na₂O is dissolved sodium ion, Na⁺, corrected for seasalt sodium, and then expressed as an oxide. SiO₂ is dissolved silica, Si(OH)₄, expressed as an oxide. DBrx is the sum of all bedrock-derived cations, expressed as oxides or sulfide, after correction for atmospheric inputs. The left panels represent the WEBB dataset. The right panels represent averages calculated from hourly estimates determined using LOADEST. For a number of samples, additional sample characteristics are indicated with black symbols. These categories are discussed in detail in Stallard and Murphy (2012): calcite, samples supersaturated with respect to calcite; high chloride, samples with exceptionally high chloride concentrations collected during huge storms; high potassium, samples with high potassium but not high chloride; low silica, Icacos and Guabá samples with unusually low silica concentrations for the runoff rate. The points separated from the sample-average curves represent the averages of the classes of sample indicated by the superimposed character. These samples are not included in LOADEST models.

Sahara dust brings in additional Ca²⁺ and insoluble clays (Stallard, 2012). Because this Ca²⁺ is also a minor part of the overall Ca²⁺ budget, and because the dust fallout comes from variable long-range transport, a uniform dust correction (6.4 kmol km⁻² Ca) was subtracted from the final Ca²⁺ budget for each watershed. All silicon, aluminum, and iron in Sahara dust were assumed to reside in nonreactive clays and sesquioxides and therefore to be insoluble (Stallard, 2012; Stallard and Murphy, 2012). Sahara dust deposition rates of 21 t km⁻² yr⁻¹ estimated by Pett-Ridge and others (2009) were subtracted equally from the solid bedrock yields for all study watersheds.

Total Dissolved Bedrock

Solute denudation rates were calculated using the approach of Stallard (1995a,b) that expresses the concentrations of most bedrock-derived constituents as dissolved oxides for mass-balance calculations. Silica and each cation, after correction for atmospheric inputs, were converted into a mass concentration of the corresponding bedrock oxide. For example, the calculation of dissolved sodium concentration expressed as an oxide (Na₂O[d]) (table 2) from bedrock-derived sodium, Na*, was performed as follows:

$$\text{Na}_2\text{O}[d] (\text{mg L}^{-1}) = 0.03098 \cdot \text{Na}^* (\mu\text{mol L}^{-1}), \quad (4)$$

where mg L⁻¹ is milligrams per liter, and μmol L⁻¹ is micro-moles per liter.

Dissolved SO₄²⁻ was converted into sulfide. The concentrations of the dissolved oxides and sulfide were summed to get total dissolved bedrock (DBrx) (fig. 3; tables 2, 3). If the bedrock of a watershed were to contain abundant carbonate rocks, for which the charge of Ca²⁺ and Mg²⁺ is balanced by carbonate ions (CO₃²⁻) rather than oxygen (O²⁻), the amount of dissolved bedrock would be markedly underestimated.

In addition to calculating DBrx of samples with complete chemistry (about 870 samples), DBrx was also estimated in all samples for which conductivity, Cl⁻, and Si(OH)₄ were measured (about 3,780 samples). This calculation involved three steps. First, the bedrock contribution to conductivity was estimated by subtracting an atmospheric contribution, which was calculated by using a factor determined by estimating the conductivity of water having ions in the atmospheric-correction ratios to Cl⁻ just indicated, and by using the specific conductivities of each ion (appendix 1):

$$\text{conductivity}^* = \text{conductivity} - 0.13028 \cdot \text{Cl}^-. \quad (5)$$

The relation between conductivity* and total bedrock-derived cation charge, ZBrx, is estimated through a regression that used the 1,040 completely analyzed samples. A single set of regression coefficients worked for all Puerto Rico WEBB rivers:

$$\text{ZBrx} = a \cdot (\text{conductivity}^*)^b, \quad (6)$$

where *a* (1.08612) and *b* (0.83239) were regression coefficients (coefficient of determination (*r*²) = 0.96). Using ZBrx, an estimated total dissolved bedrock, DBrx', was determined by

$$\text{DBrx}' = c \cdot (\text{ZBrx})^d + \text{SiO}_2[d], \quad (7)$$

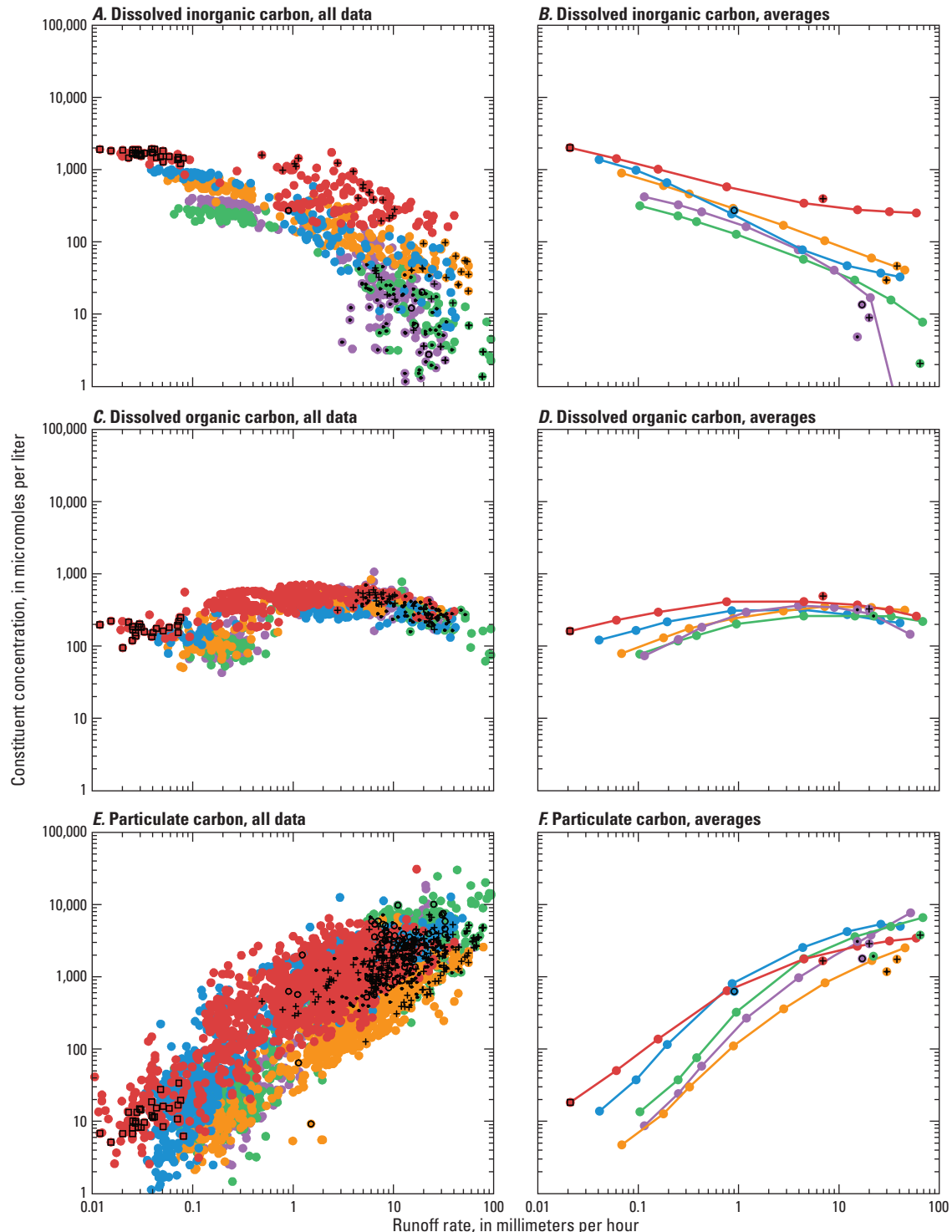
where *c* and *d* are regression coefficients determined for each river (table 3 in appendix 1), and SiO₂[*d*] is the dissolved silica concentration expressed as an oxide (table 2, fig. 3):

$$\text{SiO}_2[d] (\text{mg L}^{-1}) = 0.06008 \cdot \text{Si(OH)}_4 (\mu\text{mol L}^{-1}). \quad (8)$$

The correlation between DBrx' and DBrx for all 1,040 samples is *r*² = 0.990; between log(DBrx') and log(DBrx), *r*² = 0.986. About 4,650 samples were used in load calculations for both DBrx and DBrx', providing a rigorous estimate of dissolved bedrock erosion (table 2).

Equilibrium Model: Calculating Steady-State Erosion from Dissolved Bedrock

When chemical weathering reactions control the rate of production of solid materials, the yields of dissolved constituents can be used to predict equilibrium yields of solids (Stallard, 1995a,b). The sodium-to-silica ratio of the dissolved and solid load compared with the ratio in bedrock (after correction for atmospheric inputs) is especially useful.

**EXPLANATION**

- | | | | | | |
|-----|-----------|---|----------------|-----|-----------|
| —●— | Canóvanas | □ | Calcite | —●— | Canóvanas |
| —○— | Cayaguás | + | High chloride | —○— | Cayaguás |
| —●— | Guabá | ○ | High potassium | —●— | Guabá |
| —●— | Icacos | • | Low silica | —●— | Icacos |
| —○— | Mameyes | | | —○— | Mameyes |

Figure 4. (facing page) The concentration of the three major components of carbon transport in tropical rivers in eastern Puerto Rico: dissolved inorganic carbon (DIC = alkalinity), dissolved organic carbon (DOC), and particulate organic carbon (POC). The left panels represent the WEBB dataset. The right panels represent averages calculated from hourly estimates determined using LOADEST. For a number of samples, additional sample characteristics are indicated with black symbols: calcite, samples supersaturated with respect to calcite; high chloride, samples with exceptionally high chloride concentrations collected during huge storms; high potassium, samples with high potassium but not high chloride; low silica, Icacos and Guabá samples with unusually low silica concentrations for the runoff rate. The points separated from the sample-average curves represent the averages of the classes of sample indicated by the superimposed character. These samples are not included in LOADEST models.

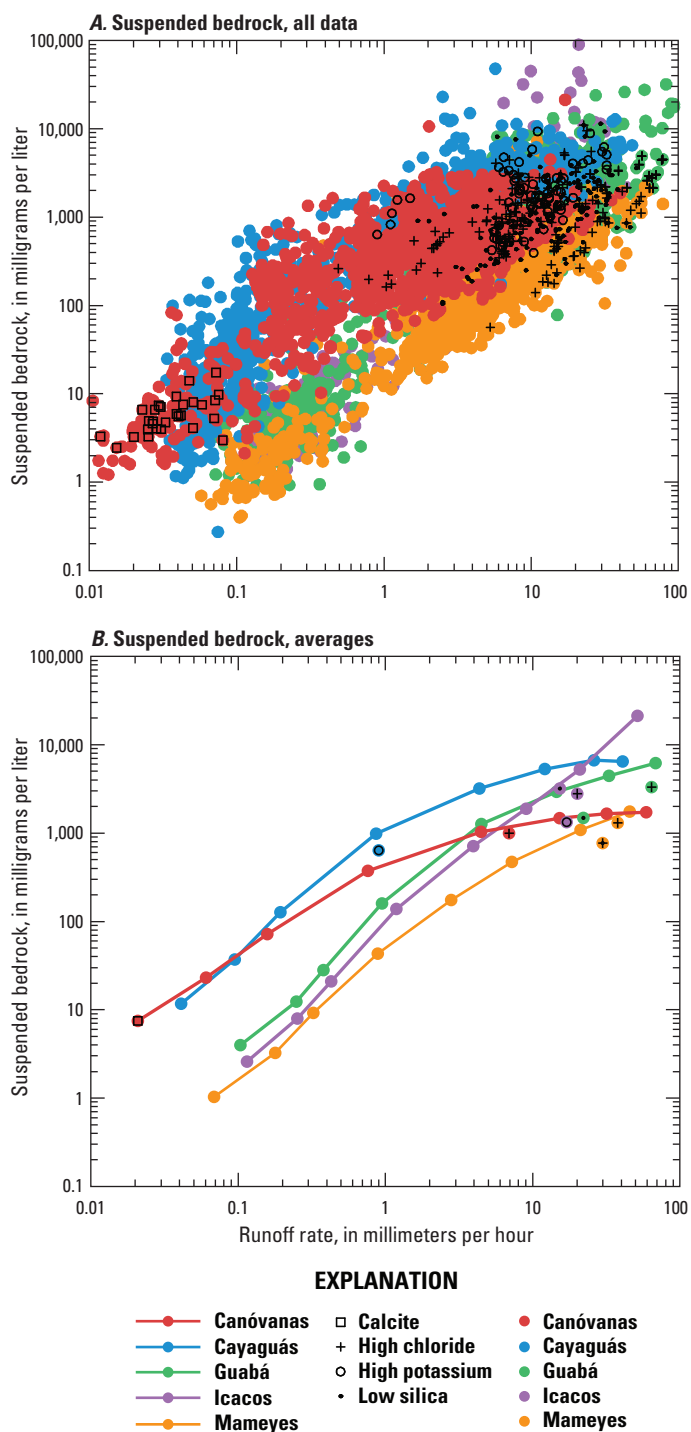


Figure 5. The concentration of an operationally derived constituent, suspended bedrock (SBrx) used in calculating physical denudation rates in eastern Puerto Rico. SBrx is the mass of the sample after heating to 550°C. For a number of samples, additional sample characteristics are indicated with black symbols: calcite, samples supersaturated with respect to calcite; high chloride, samples with exceptionally high chloride concentrations collected during huge storms; high potassium, samples with high potassium but not high chloride; low silica, Icacos and Guabá samples with unusually low silica concentrations for the runoff rate. The points separated from the sample-average curves represent the averages of the classes of sample indicated by the superimposed character. These samples are not included in LOADEST models.

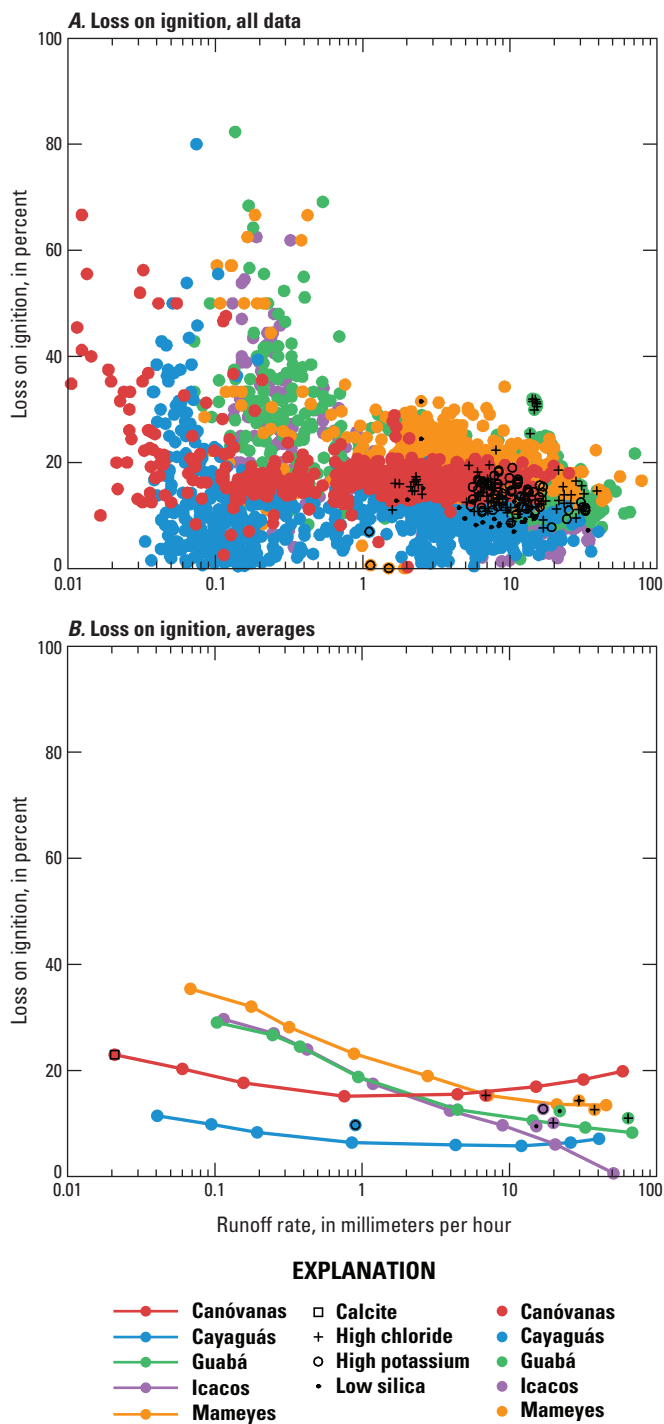


Figure 6. Percent loss on ignition (LOI). For a number of samples, additional sample characteristics are indicated with black symbols: calcite, samples supersaturated with respect to calcite; high chloride, samples with exceptionally high chloride concentrations collected during huge storms; high potassium, samples with high potassium but not high chloride; low silica, Icacos and Guabá samples with unusually low silica concentrations for the runoff rate. The points separated from the sample-average curves represent the averages of the classes of sample indicated by the superimposed character. These samples are not included in LOADEST models.

In headwater streams, such as those studied in eastern Puerto Rico, neither sodium nor silica are particularly bioactive; igneous and metamorphic rocks have a narrow range of sodium-to-silica ratios, and sodium weathers out of bedrock sufficiently early in the weathering process, such that the sodium-to-silica ratios of solid weathering products are quite low (table 1) throughout the soil profile and as river-borne sediments. Calcium shares most of these characteristics, except that the calcium-to-silica ratio ranges more widely in igneous and metamorphic rocks and is influenced by carbonate rocks (Stallard, 1995a).

To calculate the proportions of dissolved and solid weathering products that are being produced, one needs to express the compositions of bedrock, river-borne solids, and bedrock-derived solutes as weight-percent oxides. This goal is simple for the solid phases, because bulk analyses are normally reported this way (table 1). For solutes, the concentration of dissolved bedrock oxides, calculated as described earlier (for example, equation 4), must be normalized to total 100 percent (table 4):

$$\text{Na}_2\text{O}[d'] = 100 \cdot \text{Na}_2\text{O}[d] / \text{DBrx} . \quad (9)$$

Following Stallard (1995a, equations 3 and 5 of that report), the leaching efficiency of bedrock, W , is the ratio of the yield of bedrock weathered into solution, Y_{DBrx} , to the yield of total bedrock weathered, $Y_{\text{DBrx}} + Y_{\text{SBrx}}$:

$$W = Y_{\text{DBrx}} / (Y_{\text{DBrx}} + Y_{\text{SBrx}}) . \quad (10)$$

The hypothetical yield of solid weathering products, Y'_{SBrx} , expressed in terms of the observed yield of dissolved weathering products, Y_{DBrx} , is given by

$$Y'_{\text{SBrx}} = Y_{\text{DBrx}} \cdot (1-W) / W . \quad (11)$$

Similarly, the efficiency of leaching of silica, W_{Si} , is given by

$$W_{\text{Si}} = W \cdot \text{SiO}_2[d'] / \text{SiO}_2[b] , \quad (12)$$

where $[d']$ refers to the weight percent oxide in the dissolved load and $[b]$ to the weight percent oxide in bedrock. When one has a constituent pair, such as sodium paired with silica, W_{Si} can also be expressed in terms of concentrations of both constituents ($[s]$ refers to weathered solids):

$$W_{\text{Si}}(\text{Si}, \text{Na}) = ((\text{Na}_2\text{O}[b] / \text{SiO}_2[b]) - (\text{Na}_2\text{O}[s] / \text{SiO}_2[s])) / ((\text{Na}_2\text{O}[d'] / \text{SiO}_2[d']) - (\text{Na}_2\text{O}[s] / \text{SiO}_2[s])) . \quad (13)$$

With this equation, Y'_{SBrx} is expressed in terms of measurable or easily estimated parameters, all of which are concentration ratios. The use of ratios limits the effect of many shared errors, such as errors in discharge measurements. Finally, from equations 11 and 13,

Table 4. Parameters and coefficients used in modeling equilibrium erosion in study watersheds, eastern Puerto Rico, by using sodium-silicon and calcium-silicon pairs.
[A and B are dimensionless coefficients defined in equations 16–18]

Description	Bedrock			Sediment			Dissolved			Sodium model			Calcium model		
	SiO ₂	Na ₂ O	CaO	SiO ₂	Na ₂ O	CaO	SiO ₂	Na ₂ O	CaO	A	B	A	B	A	B
Canóvanas, dissolved bedrock	53.8	3.31	8.12	50.3	0.03	1.31	43.6	9.45	30.5	30.5	0.018	14.9	0.388		
Cayagüas, dissolved bedrock	62.9	3.84	6.07	58.0	0.27	0.78	54.3	15.09	18.0	28.3	0.134	19.1	0.258		
Mameyes, dissolved bedrock	53.8	3.31	8.12	50.3	0.03	1.31	54.0	7.25	28.8	30.5	0.018	14.9	0.388		
Icacos, dissolved bedrock	61.4	3.45	6.90	58.0	0.27	0.78	64.9	9.65	17.5	31.6	0.150	16.5	0.222		
Guabá, dissolved bedrock	61.4	3.45	6.90	58.0	0.27	0.78	71.0	9.92	12.9	31.6	0.150	16.5	0.222		

$$Y'_{SBrx} = Y_{DBrx} \cdot (\text{SiO}_2[d'] / \text{SiO}_2[b]) \cdot (1 - W_{Si}(\text{Si}, \text{Na})) \\ / W_{Si}(\text{Si}, \text{Na}) . \quad (14)$$

When the observed weathered bedrock yield equals the steady-state weathering yield, $Y_{SBrx} = Y'_{SBrx}$, the denudation of the landscape is in equilibrium. If $Y_{SBrx} > Y'_{SBrx}$, solid weathering products are accumulating on the landscape as soils, alluvium, and colluvium, and if $Y_{SBrx} < Y'_{SBrx}$, physical erosion exceeds the generation of solids, and there must be net loss of soil or stored sediment.

Equations 13 and 14 have a number of terms that, in a given watershed, are constant for all calculations, such as the bedrock and solid-load compositions. These constants allow the equations to be simplified into a form that involves either measured or easily estimated parameters. For example, the concentrations of dissolved bedrock oxides (equation 9), expressed as percent, can also be calculated from solute yields. Using sodium as an example:

$$\text{Na}_2\text{O}[d'] = 100 \cdot Y_{\text{Na}_2\text{O}[d]} / Y_{DBrx} . \quad (15)$$

Accordingly,

$$Y'_{SBrx} = (A \cdot Y_{\text{Na}_2\text{O}[d]} - B \cdot Y_{\text{SiO}_2[d]}) - Y_{DBrx} , \quad (16)$$

where

$$A = 100 \cdot \text{SiO}_2[s] / (\text{Na}_2\text{O}[b] \cdot \text{SiO}_2[s] - \\ \text{Na}_2\text{O}[s] \cdot \text{SiO}_2[b]) , \quad (17)$$

and

$$B = 100 \cdot \text{Na}_2\text{O}[s] / (\text{Na}_2\text{O}[b] \cdot \text{SiO}_2[s] - \\ \text{Na}_2\text{O}[s] \cdot \text{SiO}_2[b]) . \quad (18)$$

Note that the denominators (the terms in parentheses) in equations 17 and 18 are the same; accordingly, A is more sensitive to errors in estimating SiO₂[s], and B, which is quite a small term, is more sensitive to errors in Na₂O[s]. In fact, so long as Na₂O[s] is small, even with considerable error, this equation is quite robust. Moreover, in the equations for A and B, the numerator represents a concentration of river-borne solids and the difference terms in the denominator are multiplied by concentrations of river-borne solids. This combination of terms eliminates any need to correct for LOI, despite the assumption that LOI is atmospherically derived water and organic matter.

By using equation 16, LOADEST-based yield estimates were used to calculate equilibrium denudation rates and test whether erosion is in equilibrium and how equilibria may respond to changes in average long-term runoff; this method is referred to as the equilibrium model. Denudation rates were calculated using calcium, as a check, but because of the caveats regarding variability of bedrock CaO[s]:SiO₂[s] ratios and the influence of possible calcite inputs, the sodium calculations are much preferred.

Table 4 presents the concentrations of solids and solutes needed to calculate equilibrium yields, using either sodium or calcium, along with respective coefficients A and B . In addition to analyses of samples collected for this study (table 1), table 4 is based on averaged data that includes published analyses of volcanic rocks from other sources. For the bedrock of the Mameyes and Canóvanas watersheds, analyses of volcanic rocks from Jolly and others (1998; samples DG–12, DG–14, DG–16; FG–17, FG–7, FG–9; INF–7, J–77, LOM–12) were averaged with the volcanic samples in table 1. For the Icacos and Guabá, data from the Río Blanco stock from Smith and others (1998, Río Blanco samples 6513, PRP–4, PRP–5, PRP–6, PRP–12, PRP–14, PRP–16, PRP–17) were averaged with quartz-diorite samples from table 1, excluding xenoliths and aplite. For the Cayaguás, data from Smith and others (1998; San Lorenzo samples PP–1, PRP–1, PRP–2, PRP–10, PRP–11; PRP–100, PRP–103, PRP–104, PRP–105; SL–1) were averaged.

Suspended Bedrock, Loss on Ignition, and Particulate Organic Carbon

River-borne solids are composed of material from three sources: primary and secondary mineral matter derived from the weathering of bedrock, water that has been incorporated into secondary minerals during weathering, and organic matter. For about two-thirds of the measurements of suspended sediment (see Stallard and Murphy, 2012, and appendices 1, 2), we also measured loss on ignition (LOI), which involves measuring the mass loss upon heating to 550°C samples that have been dried at temperatures of 105°C. Studies summarized in Mackenzie (1957) and Mackenzie and Caillère (1979) show that in heating to 550°C, all of the clays and sesquioxides lose nonstructural water (most below 200°C). In addition, all sesquioxides, most kaolins, and substantial illites and vermiculites lose lattice water below 550°C; however, smectites, talcs, and chlorites do not. Nonmineral organic carbon and most mineral carbon (coal and graphite) are also oxidized in this range. Carbonate rocks are generally stable.

In this work, the mass of the sample after heating to 550°C was equated with SBrx (fig. 5). The sample dried to 105°C is referred to as suspended solids or suspended sediment (SSol). For samples in which suspended bedrock was not measured, regressions for each river related SBrx to SSol and LOI:

$$\text{SBrx} = \text{SSol} \cdot (a + b \cdot \log(\text{SSol})), \quad (19)$$

and

$$\text{LOI} = \text{SSol} - \text{SBrx}, \quad (20)$$

where a and b are regression coefficients. Values for a and b for each river are given in appendix 1. At lowest runoff rates, LOI is elevated in the forested rivers (Mameyes, Icacos, and Guabá; fig. 6). Given that LOI for kaolinite and halloysite is 14.0 percent, values greater than 14.0 percent likely reflect organic matter. At low runoff rates, the overall contribution of

sediments to the net sediment load is very small (Stallard and Murphy, 2012). At highest runoff rates, LOI values of sediment in rivers that drain granitic rocks are low because of the large contribution of quartz sand to these samples.

POC was not measured on most of the sediment samples; instead, LOI (fig. 6) is used as a surrogate measurement. LOI is commonly equated with organic matter; however, the study samples are rich in kaolinite, halloysite, or iron and aluminum sesquioxides. Instead, it is assumed here that POC is a fixed fraction of LOI for all study samples. This fraction was determined such that the 15-year yield of SSol for the Río Icacos consisted of 1 percent carbon, a value that is typical of world rivers (Stallard, 1998). The result is that LOI for the study rivers consists of 11 percent carbon. For reference, pure organic matter is about 50 percent carbon by mass (Stallard, 1998). The water contribution to average LOI never exceeds the value of 14.0 percent of pure kaolinite (table 5). The average POC of forested rivers, at low runoff rates of less than 1 mm h⁻¹, is 2 to 3.5 percent SSol (table 2), similar to values reported elsewhere (McDowell and Asbury, 1994). For estimates of LOI, POC, and organic matter, see table 5.

Table 5. Analysis of loss on ignition for a discharge-weighted average sample of solid load from study rivers, eastern Puerto Rico.

[LOI, loss on ignition; POC, particulate organic carbon]

River	LOI	Weight percent of suspended solids		
		Water	Organic matter ¹	POC
Canóvanas	16.3	12.8	3.5	1.8
Cayaguás	6.1	4.3	1.8	0.9
Mameyes	16.9	13.2	3.7	1.9
Icacos	7.5	5.5	2.0	1.0
Guabá	11.7	8.9	2.8	1.4

¹Organic matter is assumed to be twice POC.

Projection to a Common Intermediate Yield

The principal confounding issue in the comparison of constituent yields of the various Puerto Rico WEBB watersheds is that among them, the long-term, mean-annual runoff differs markedly. The forested watersheds are considerably wetter (Mameyes—2,750 mm yr⁻¹, Icacos—3,760 mm yr⁻¹, Guabá—3,630 mm yr⁻¹) than the developed watersheds (Canóvanas—970 mm yr⁻¹, Cayaguás—1,620 mm yr⁻¹). To compare sites, regressions between annual runoff and constituent yields were used to project annual yields to an annual intermediate runoff, 1,860 mm yr⁻¹, about halfway between the runoff for the Canóvanas and the Mameyes. This value is within the observed range of annual runoffs for the Mameyes and Cayaguás and represents an extrapolation for the Canóvanas, Icacos, and Guabá. These relations were also used to establish whether these landscapes are in a state of dynamic equilibrium such that the yield of solid bedrock is the same as the rates at which solid weathering products are being generated (equation 16).

Annual constituent yields, including derived constituents, were calculated using LOADEST (appendix 1). Annual runoff varied considerably from year to year (fig. 7). The highs and lows were mirrored by constituent yields (figs. 7–9).

The relation between annual runoff and annual dissolved constituent yields was a simple linear relation for all dissolved constituents (figs. 10–12). Many rivers produce linear relations such as these (6 rivers, White and Blum, 1995; 57 rivers, Godsey and others, 2009). The buffering or “chemo-static” behavior can be explained by many mechanisms, such as ion exchange, buffering with amorphous phases, large soil reservoirs of solutes, or weathering reactions that respond proportionally to the water flux passing through the soil. Godsey and others (2009) presented a “permeability-porosity-aperture model” that predicts that in a given watershed, the relation between log(concentration) and log(runoff) should be linear and with the same slope for all bedrock-derived constituents. The authors allow that differences for slopes among various constituents could be attributable to differences in the depth distribution of reactive minerals throughout soil profiles.

Suspended Bedrock and Runoff

Unlike solute erosion, for which a linear relation between annual runoff and annual solute yield agrees well with the data, physical erosion is decidedly nonlinear, and concentrations of solid constituents typically increase markedly with discharge. Two issues must be addressed with respect to solid loads. First is selecting the relation between runoff and solid yield for individual years. Landslides add complexity, because landslide-producing storms do not occur every year. The second is the problem of averaging the effects of variation in interannual runoff. Long-term averages reflect a mix of drier and wetter years. For linear processes the average solute yield of many years is the same as the solute yield of the average runoff for all the same years. For solid yields, years that have high runoff and abundant high-runoff storms heavily influence long-term averages, and computational procedures need to capture this increased weighting of wet-year contributions.

Solid Loads for Individual Years

Surficial erosion, the combined effects of direct impaction by raindrops on soil, sheet wash, rill formation, and gullying, is driven by flowing water and tends to increase exponentially with increasing discharge. Physical erosion is most simply described using power-law formulations relating annual suspended solids yield, Y_{SSol} , to annual runoff, R :

$$Y_{SSol}(\text{year}) = a \cdot R(\text{year})^b, \quad (21)$$

where a and b are regression coefficients. For the eastern Puerto Rico rivers, the coefficients were estimated iteratively by means of nonlinear regressions as opposed to regressions on log-transformed data (table 6). Landslides, which typically are caused by only the largest storms, distort this relation.

Table 6. Coefficients of power-law model relating annual suspended-bedrock yield to runoff ($\text{Yield} = a \cdot \text{Runoff}^b$) in study watersheds, eastern Puerto Rico.

River	Coefficient		Percent variance explained	Years
	<i>a</i>	<i>b</i>		
Canóvanas	0.002	1.72	43	15
Cayaguás	$9.2 \cdot 10^{-5}$	2.21	79	15
Mameyes	$5.6 \cdot 10^{-11}$	3.64	54	15
Icacos	$4.4 \cdot 10^{-8}$	2.93	40	15
Guabá	$1.9 \cdot 10^{-6}$	2.52	48	10

Stallard (1999) and Stallard and Kinner (2005) developed an approach for quantifying annual sediment yields in landslide-dominated watersheds; this approach empirically distinguishes surficial and landslide erosion by using datasets for rivers in the Panama Canal watershed that had a decade or more of daily sediment data. The Puerto Rico WEBB dataset does not have such daily measurements, but because of the emphasis on storm sampling, the yield estimations done using LOADEST are a reasonable substitute. A key assumption of this approach is that annual sediment discharge from each watershed is considerably greater than interannual storage. The volcaniclastic watersheds do not store fine-grained sediments in their riverbeds, so the assumption is valid in these watersheds. For the granitic watersheds, flood plain storage can be extensive (Brown and others, 1995, 1998; Larsen and Santiago-Román, 2001; Larsen, 2012). My repeated visits to many sites along the channels of the Río Icacos and the Quebrada Guabá during this project revealed little change, suggesting little net storage or loss, and that Quebrada Guabá has no floodplain. The Río Cayaguás channel, however, changed considerably in appearance, but it would be difficult to assess storage or loss.

As discussed earlier, rainfall must exceed some threshold before landslides occur (equation 1). Rather than use rainfall, which requires interpolation and is especially ambiguous in the Canóvanas watershed (see Murphy and Stallard, 2012), this analysis follows Stallard (1999) and Stallard and Kinner (2005) and uses daily runoff, R , calculated from the daily discharge (D).

A day is defined as a landslide day if

$$R(24, 48, \text{ or } 72 \text{ h}) > F \cdot 91.46 \cdot D^{0.18} \quad (D = 24, 48, \text{ or } 72 \text{ h}), \quad (22)$$

where h is hour, F is an empirical coefficient between 0 and 1 that adjusts the threshold for three factors that reduce runoff relative to local rainfall, in essence stating $R = F \cdot$ precipitation for big storms. These three factors are evapotranspiration, infiltration, and rainfall patchiness, where in parts of a watershed rainfall will exceed the threshold but in other parts not do so. Stallard (1999) and Stallard and Kinner (2005) determined that $F=0.85$ for the Panama Canal watershed by using 10 to 16 years of daily sediment data on six rivers.

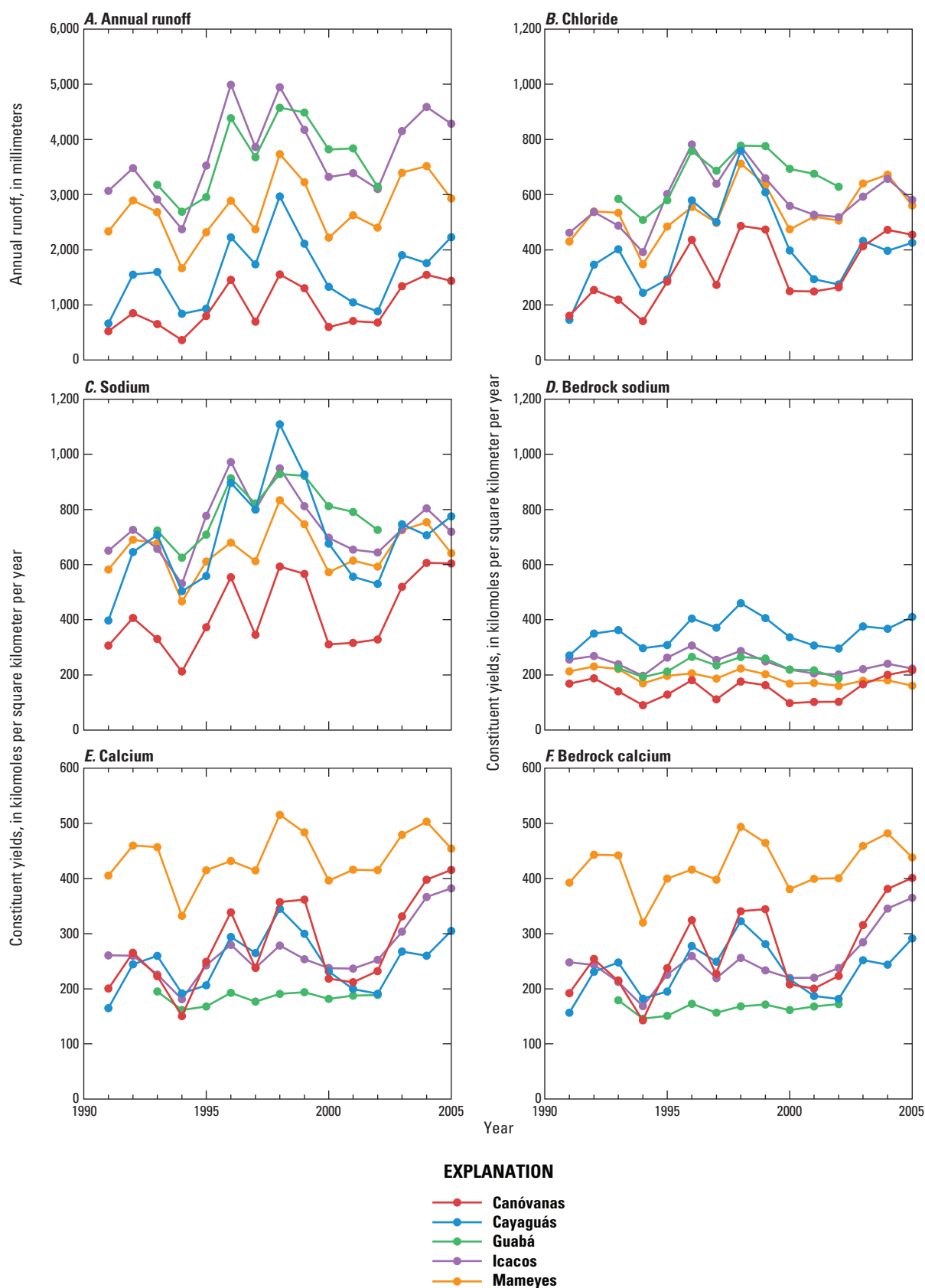


Figure 7. Time series of annual runoff (upper left) and the annual yields of chloride, sodium, calcium, and bedrock-derived sodium and calcium, eastern Puerto Rico.

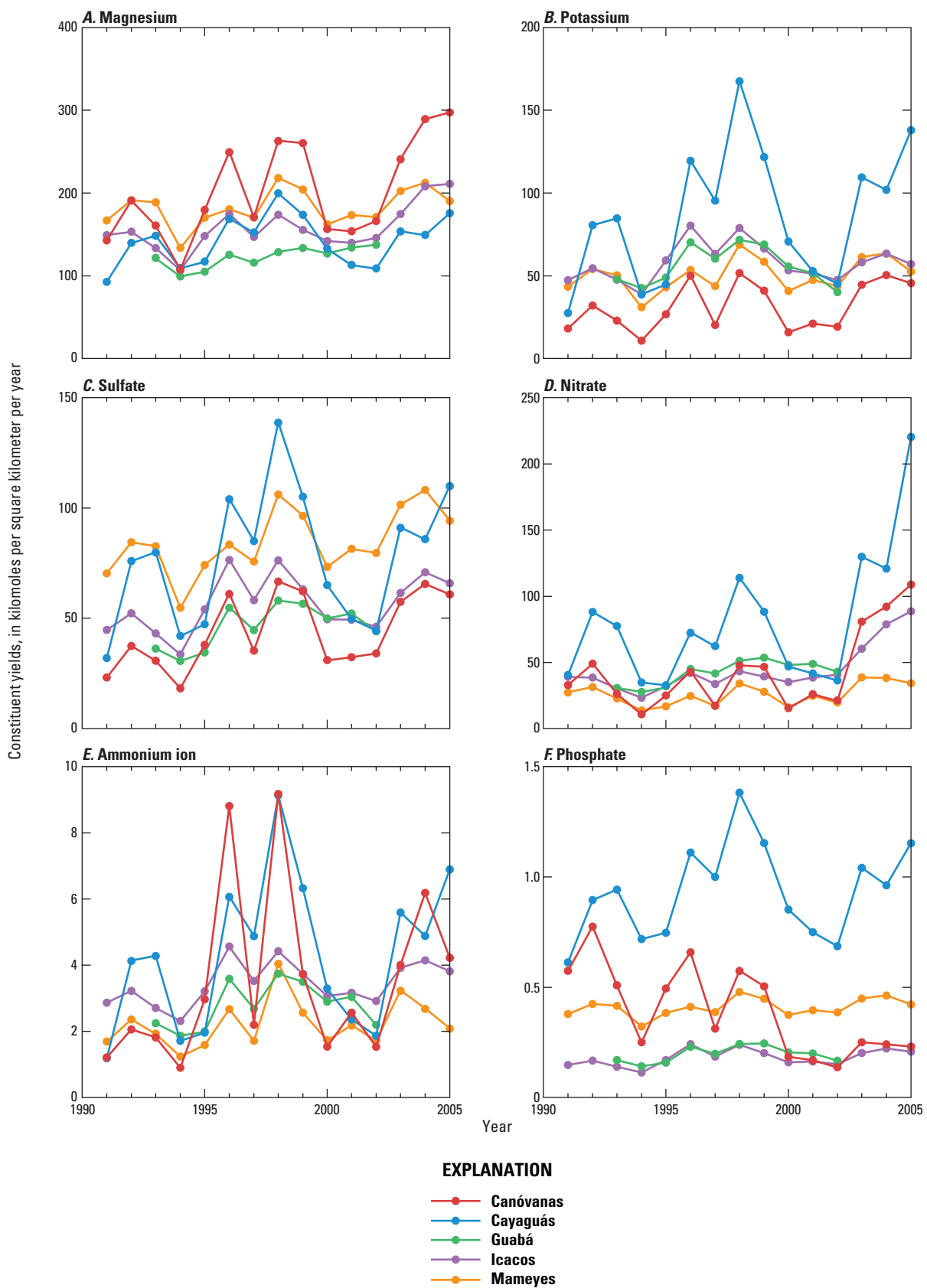


Figure 8. Time series of the annual yields of magnesium, potassium, sulfate, nitrate, ammonium ion, and phosphate, eastern Puerto Rico. Magnesium is mostly influenced by weathering and atmospheric inputs. The remaining constituents in this graph are strongly influenced by biological activities and in some cases by human activities such as fertilizer applications and domestic waste.

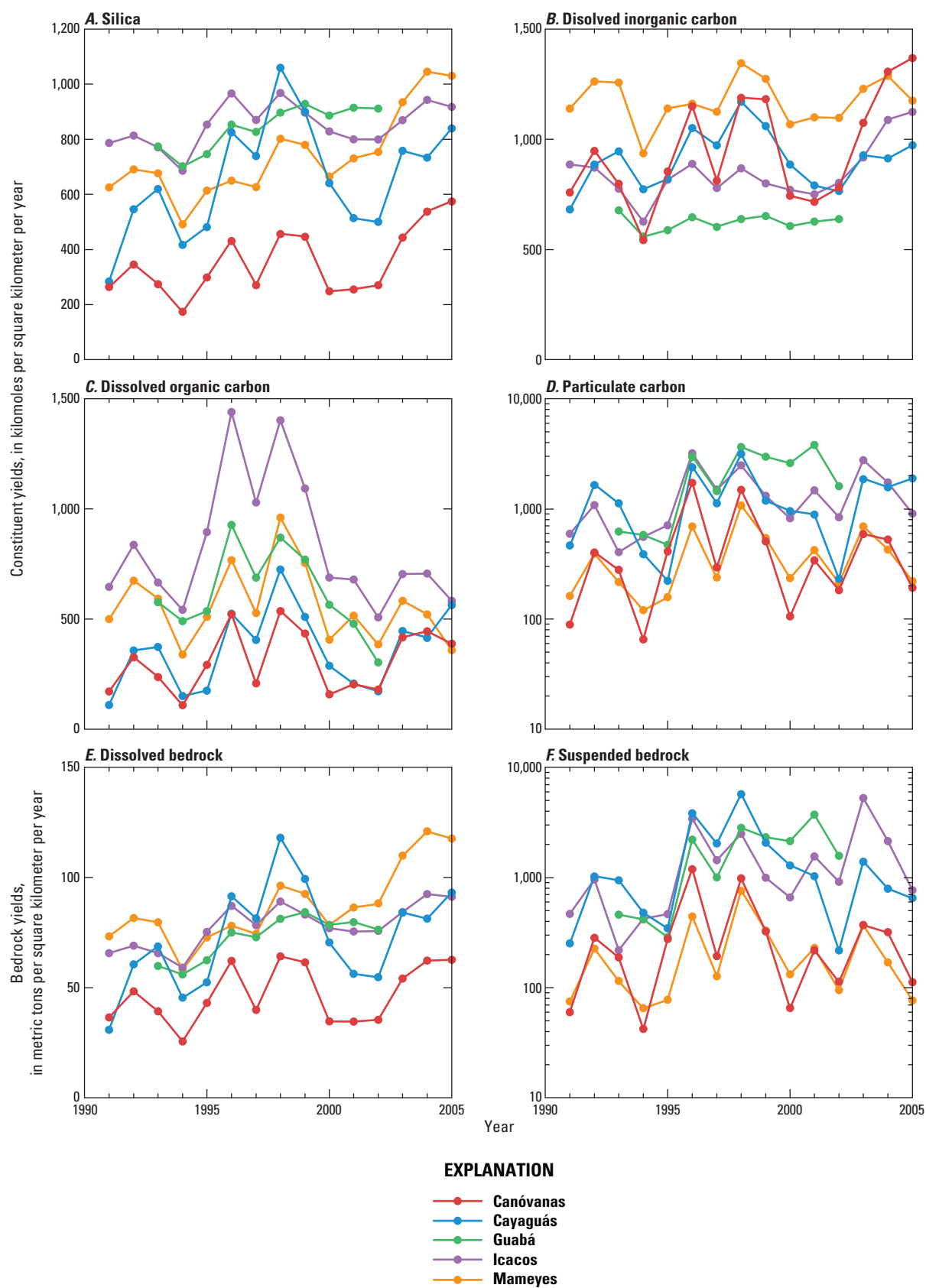


Figure 9. Time series of the annual yields of important constituents in characterizing erosion and the carbon cycle in eastern Puerto Rico: silica, dissolved inorganic carbon, dissolved organic carbon, particulate organic carbon, dissolved bedrock, and suspended bedrock.

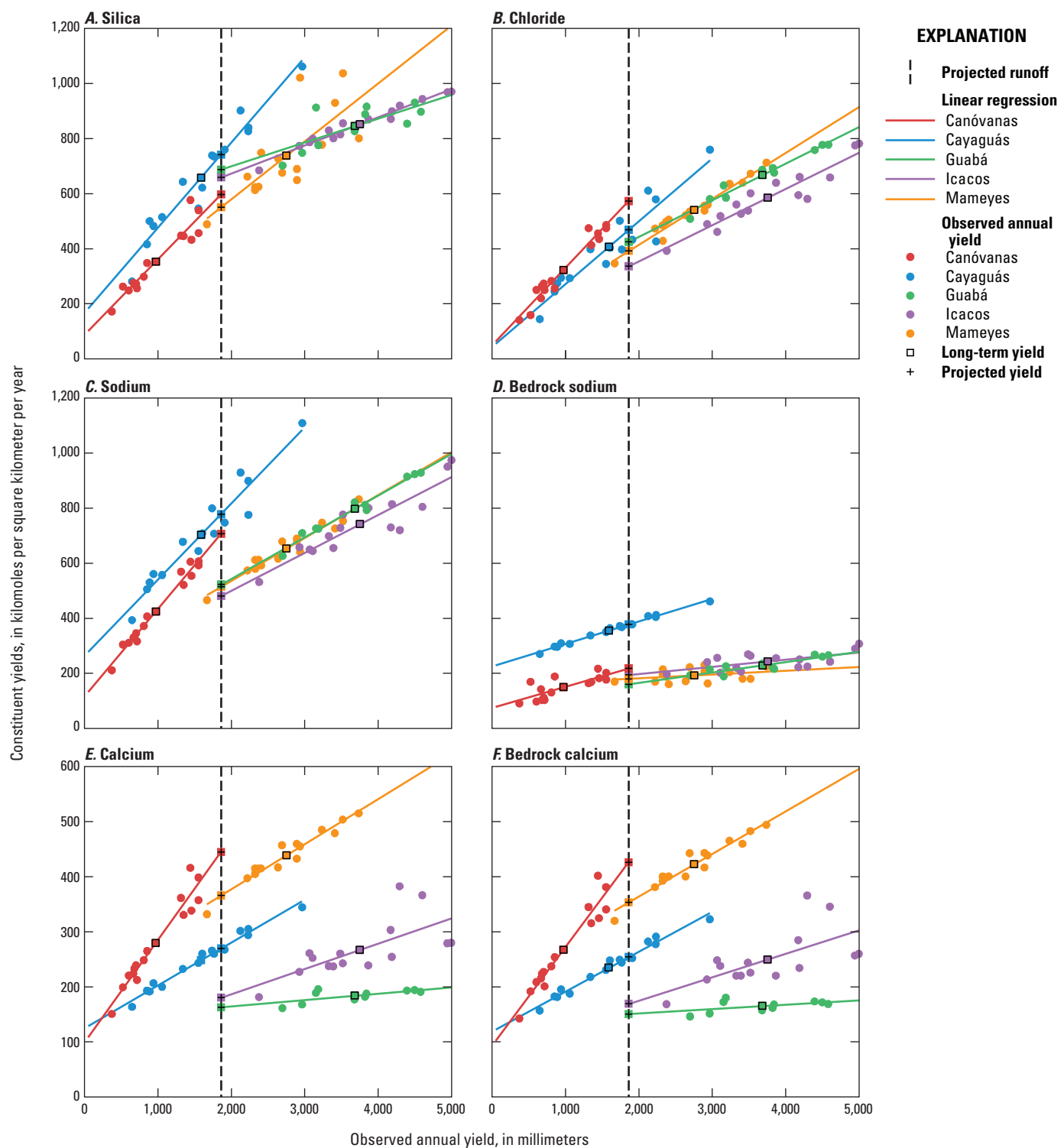


Figure 10. Annual runoff compared with the annual yields of silica, chloride, sodium, calcium, and bedrock-derived sodium and calcium for the five rivers studied, eastern Puerto Rico. The vertical gray line corresponds with 1,860 millimeters per year, and the solid squares with black plus symbols correspond with the projected annual yields. The points are observed annual yields; lines are linear regressions based on the assumption that annual yield responds linearly with changing runoff.

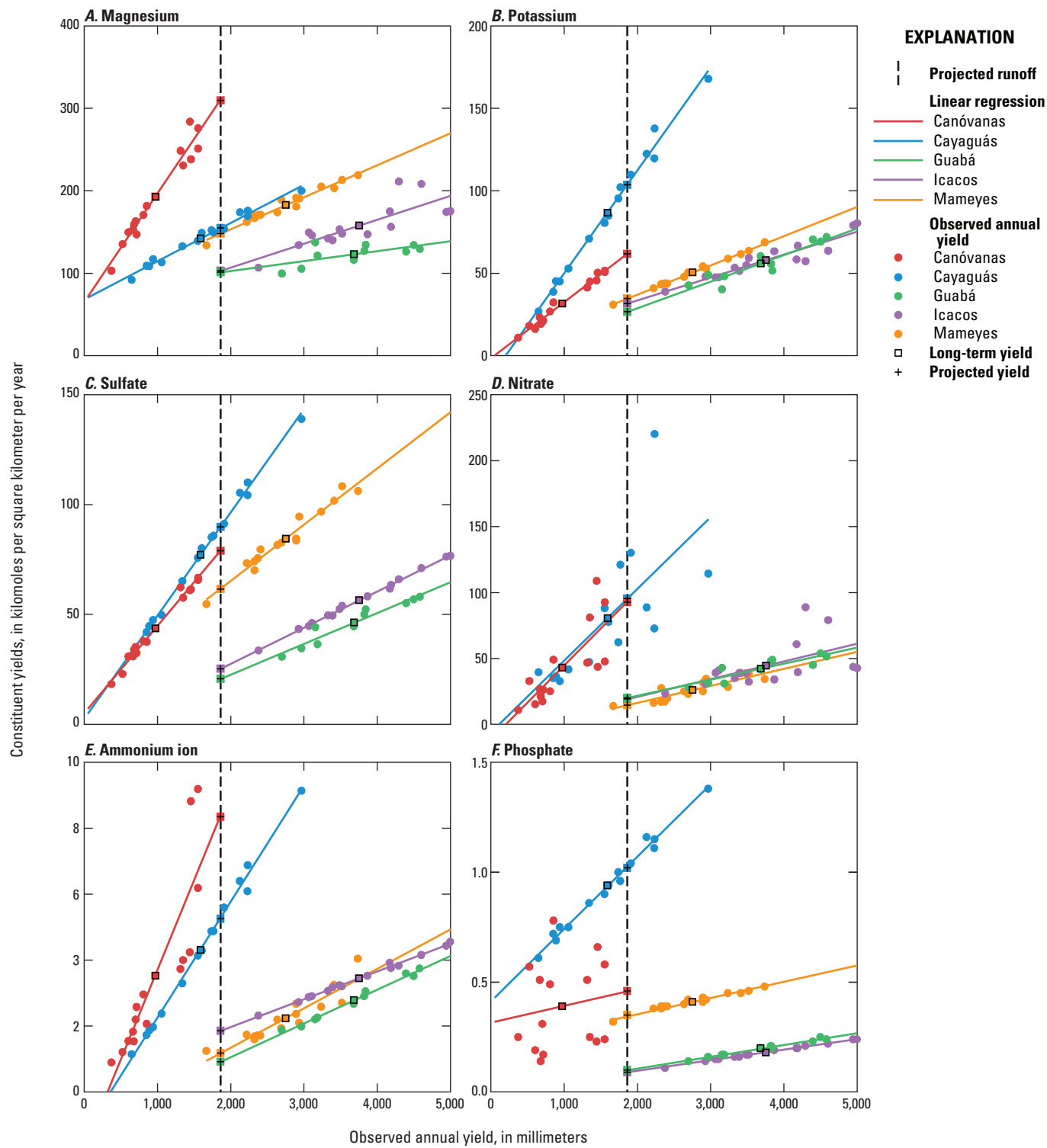


Figure 11. Annual runoff compared with the annual yields of magnesium, potassium, sulfate, nitrate, ammonium ion, and phosphate for the five rivers studied, eastern Puerto Rico. The vertical gray line corresponds with 1,860 millimeters per year, and the solid squares with black plus symbols correspond with the projected annual yields. The points are observed annual yields; lines are linear regressions based on the assumption that annual yield responds linearly with changing runoff. Except for magnesium, the constituents in this graph are strongly influenced by biological activities and in some cases by human activities such as fertilizer applications and domestic waste. Yields of potassium, nitrate, ammonium ion, and phosphate have bedrock sources. Yields of potassium, nitrate, ammonium ion, and phosphate are especially elevated in the developed watersheds indicating additional agricultural or domestic sources.

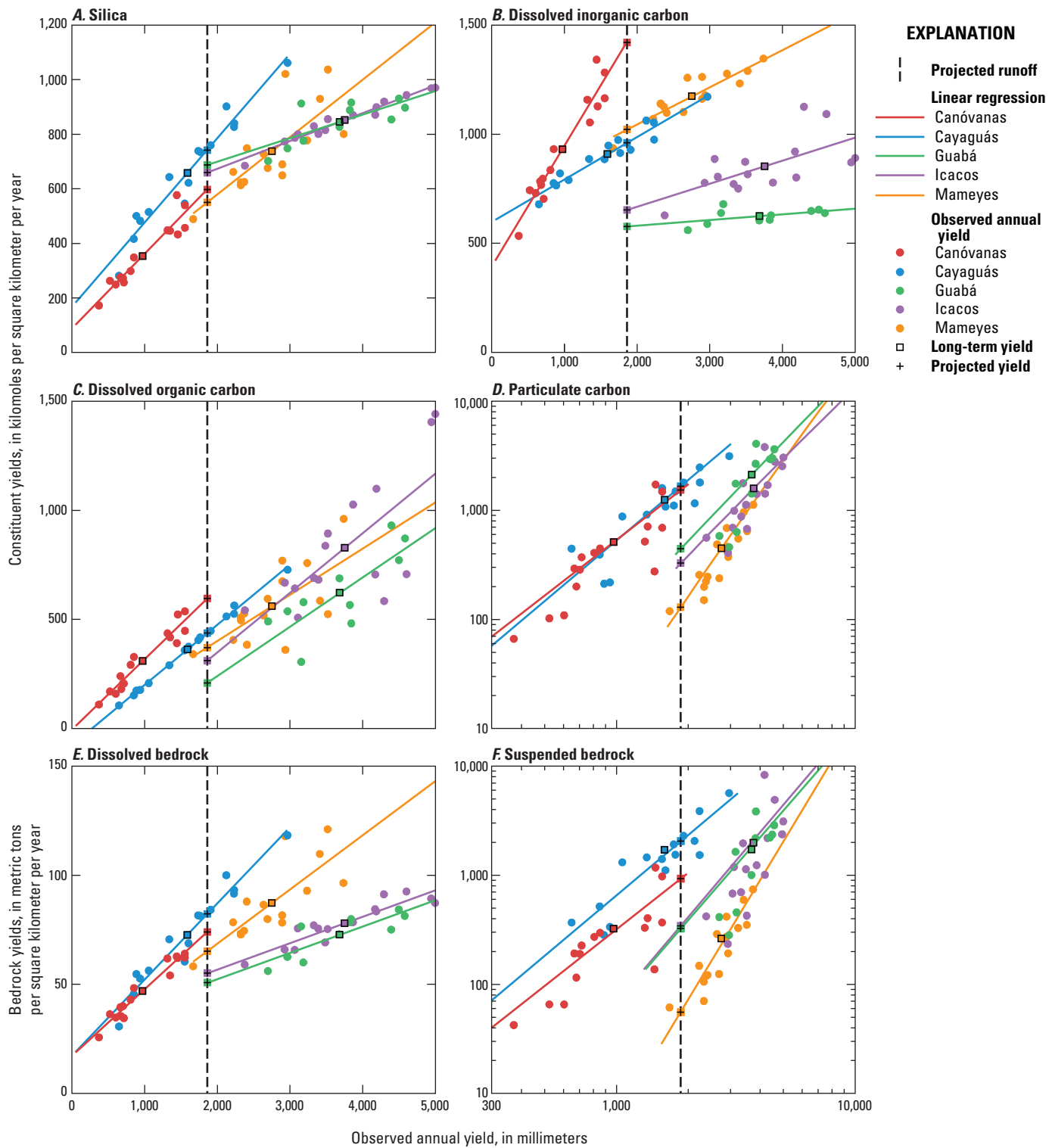


Figure 12. Annual runoff compared with annual yields of important constituents in characterizing erosion and the carbon cycle in eastern Puerto Rico: silica, dissolved inorganic carbon, dissolved organic carbon, particulate organic carbon, dissolved bedrock and suspended bedrock. The vertical gray line corresponds with 1,860 millimeters per year, and the solid squares with black plus symbols correspond with the projected annual yields. The points are the observed annual yields. The lines in parts A-C and E are linear regressions based on the assumption that annual yield responds linearly with changing runoff. The lines in parts D and F were produced by power-law models, on the basis of equation 21, which plot as lines on graphs with log-log scales. Because these power-law curves are being used to predict trends for a changing climate, and because of the variability of climate, a convolution, equation 26, was used to smooth the power-law curves. Such convolutions have no effect on linear models.

For each river and each year of the dataset, the number of landslide days, as defined by equation 22, were totaled as landslide days per year, $N_s(\text{year})$; successive landslide days were assigned to a single day. The resulting combined surface erosion–landslide erosion model is

$$Y_{SSol}(\text{year}) = a \cdot R(\text{year})^b + c \cdot N_s(\text{year}), \quad (23)$$

where a , b , and c are regression coefficients. This first term on the right is a traditional sediment transport model (equation 21). The second term is a statement that each landslide day dumps a certain quantity of sediment into the river.

$N_s(\text{year})$ does not distinguish between small and large landslide-producing events, so in the present paper, the net runoff for landslide days is totaled to determine the landslide-day runoff per year, $R_s(\text{year})$.

$$Y_{SSol}(\text{year}) = a \cdot R(\text{year})^b + c \cdot R_s(\text{year}) \quad (24)$$

where a , b , and c are regression coefficients. The second term on the right side of equation 24 assumes that the amount of slide material dumped into rivers on landslide days is directly proportional to the runoff on those days.

There are four adjustable parameters in this surface-erosion–landslide-erosion model (equation 23). The landslide threshold adjustment parameter, F , is assumed to be the same for all of the watersheds. Because daily sediment data are not available for eastern Puerto Rico, a value of 0.85, as determined by Stallard (1999) and Stallard and Kinner (2005), was used. The remaining coefficients were estimated iteratively by means of nonlinear regressions. The first terms, a and b , were estimated for each river using data for years lacking landslide days; then the second term, c , was estimated using only those years with landslide days (table 7). When compared with the power-law model (equation 21) and on the basis of an F-test of model variance (Bevington and Robinson, 2003), the models that used landslide runoff, $R_s(\text{year})$, generally were statistically more significant (tables 6, 7), except for the Mameyes watershed, where the landslide model and the power-law model were indistinguishable. From 1991 through 2005, we observed landslides in the Mameyes watershed associated with large storms. The similarity of the two models may imply that, currently, landslides make a relatively small contribution to the sediment load of the Mameyes.

Table 7. Coefficients of model relating annual suspended-bedrock yield to runoff and landslide day runoff in study watersheds, eastern Puerto Rico.

[Yield = $a \cdot \text{Annual runoff}^b + c \cdot \text{Slide-day runoff}$]

River	Coefficient			Percent variance explained	Years	F-test compared to power-law model ¹
	<i>a</i>	<i>b</i>	<i>c</i>			
Canóvanas	1.6	0.67	1.77	91	15	98
Cayaguás	$8.2 \cdot 10^{-4}$	1.87	2.84	94	15	86
Mameyes	$1.2 \cdot 10^{-10}$	3.53	0.13	74	15	52
Iacós	$8.7 \cdot 10^{-8}$	2.63	4.13	86	15	93
Guabá	0.059	1.17	3.20	84	10	78

¹F-test gives the probability that this model is better than the power-law model (table 6); 50 percent implies that the models are indistinguishable.

To adapt the landslide model to a continuum of runoff it is necessary to predict landslide-producing runoff, R_s (annual runoff), as a function of annual runoff, R_{annual} . The form used here was the simplest possible, a linear relation. Only years having landslide days are considered. The relation is:

$$R_s(R_{\text{annual}}) = a \cdot (R_{\text{annual}} - R_{s0}), R_{\text{annual}} > R_{s0}, \quad (25)$$

where a and $a \cdot R_{s0}$ are regression coefficients (table 8). This equation defines an annual runoff threshold, $R_{s0} = 0$, below which landslides should not occur. This threshold is $R_{s0} = 1,272 \text{ mm yr}^{-1}$ for the Canóvanas, $R_{s0} = 1,656 \text{ mm yr}^{-1}$ for the Cayaguás, $R_{s0} = 2,440 \text{ mm yr}^{-1}$ for the Mameyes, $R_{s0} = 2,857 \text{ mm yr}^{-1}$ for the Iacós, and $R_{s0} = 3,098 \text{ mm yr}^{-1}$ for the Guabá. The increasing threshold with increasing runoff among the five watersheds appears reasonable, because differences in interannual runoff appear to be primarily driven by orographic precipitation and numerous small storms, which do not produce landslides, and not by the number or size of the biggest storms (see Murphy and Stallard, 2012).

Table 8. Coefficients used to predict landslide-day runoff given annual runoff in study watersheds, eastern Puerto Rico.

[Landslide-day runoff = $a \cdot (\text{annual runoff} - \text{runoff threshold})$, provided annual runoff is greater than the runoff threshold]

River	Runoff threshold	Coefficient <i>a</i>	Percent variance explained	Years
Canóvanas	1,272	1.18	73	15
Cayaguás	1,656	0.58	85	15
Mameyes	2,440	0.32	68	15
Iacós	2,857	0.31	80	15
Guabá	3,098	0.45	77	10

Calculating the Long-Term Average for Nonlinear Sediment-Yield Models

Because river-borne-solid yields are strongly nonlinear with respect to runoff, the effects of interannual variation must be assessed and adjusted in order to estimate average yields.

Only one river in eastern Puerto Rico, the Río Fajardo, has a sufficiently long record, 45 years, to characterize the range and nature of interannual variation (see Murphy and Stallard, 2012). The annual discharge distribution is log normal with a standard deviation of 0.142 log units. For the purposes of data smoothing, this same log-normal distribution was assumed to apply to all the rivers, and to speed calculation, the effects of interannual variations were handled computationally as a convolution (see appendix 1). The Fajardo runoff data were ranked by increasing annual runoff and separated into seven roughly equivalent bins of 7, 6, 6, 7, 6, 6, and 7 years, successively. The average of log(runoff) for all the years of data was subtracted from each log(runoff), and the resultant values of log(runoff) minus average(log(runoff)) were, in turn, averaged for each bin (table 9). A 7-point, B-spline convolution (Jupp, 1976, that report's table 6, $m=4$, $k=2$) was used such that the values of the model function were averaged using the B-spline coefficients for the runoff under consideration and three equally spaced log(runoff) values before and after (table 9). SBrx(r) is suspended bedrock as predicted by either the power-law model (equation 21) or the landslide model (equations 21, 24, 25). The convolved SBrx(r) at a given runoff, r , SBrcx(r), is given by

$$\begin{aligned} \text{SBrcx}(r) = & w_1 \cdot \text{SBrx}(c_1 \cdot r) + w_2 \cdot \text{SBrx}(c_2 \cdot r) + w_3 \cdot \\ & \text{SBrx}(c_3 \cdot r) + w_4 \cdot \text{SBrx}(c_4 \cdot r) \\ & + w_5 \cdot \text{SBrx}(c_5 \cdot r) + w_6 \cdot \text{SBrx}(c_6 \cdot r) + w_7 \cdot \text{SBrx}(c_7 \cdot r), \quad (26) \end{aligned}$$

where $c_1 \dots c_7$ are logarithmic convolution factors and $w_1 \dots w_7$ are weighting factors (table 9). The log(runoff) interval, 0.069, was adjusted so that the seven convolution points best matched the Río Fajardo bin averages (table 9). Presumably, SBrcx(r) captures the effect of interannual variation.

Table 9. Convolution information used to represent interannual variability.

[7-point convolution around a reference runoff such that $\text{SBrcx}(r) = w_1 \cdot \text{SBrx}(c_1 \cdot r) + w_2 \cdot \text{SBrx}(c_2 \cdot r) + w_3 \cdot \text{SBrx}(c_3 \cdot r) + w_4 \cdot \text{SBrx}(c_4 \cdot r) + w_5 \cdot \text{SBrx}(c_5 \cdot r) + w_6 \cdot \text{SBrx}(c_6 \cdot r) + w_7 \cdot \text{SBrx}(c_7 \cdot r)$, where r is runoff; w is runoff weighting factor; and c is convolution weighting factor]

Convolution point	Relative position	Normalized runoff bin for Río Fajardo	w	c
1	-3	0.60	0.62	0.010
2	-2	0.77	0.73	0.083
3	-1	0.88	0.85	0.240
4	0	0.99	1	0.333
5	1	1.16	1.17	0.240
6	2	1.31	1.37	0.083
7	3	1.68	1.61	0.010

The relation between annual runoff and particulate constituents is best portrayed using log-log graphs (fig. 12, POC and SBrx). Power-law (equation 21) and landslide (equations 21, 24, 25) models, after convolution (equation 26), are represented separately (fig. 13). Note that the landslide models display a distinct hump in the Canóvanas and Iacos. These are the rivers for which the landslide model best represents the annual sediment-yield data when compared to power-law representations (tables 6, 7).

Interpretation of Projections to a Common Yield

It is assumed that constituents with yields that become more alike when projected to a common intermediate runoff are not strongly controlled by either geology or land cover. Atmospheric inputs, such as chloride, fall into this category because the source is external to the watersheds. Accordingly, to characterize the significance of projecting mean-annual yields to a common intermediate runoff (table 10), tests were designed to characterize the compactness of the projection and the degree of overlap in the two pair-wise comparisons: forested compared with developed landscape and granitic compared with volcanic bedrock. For each constituent, the compactness of the range of yields was compared though a simple test involving the minimum and maximum yields for constituent X , $Y_{X:\min}$, and $Y_{X:\max}$, respectively:

$$\text{Range ratio as a percent} = 200 \cdot \frac{(Y_{X:\max} - Y_{X:\min})}{(Y_{X:\max} + Y_{X:\min})}. \quad (27)$$

The more compact the data range, the smaller this ratio. This range ratio for the averaged observed annual-mean yields was compared with the ratio of the projected yields for a common intermediate mean-annual runoff. Range reduction or no change was assumed to indicate that differences in geology or land cover did not strongly influence yields. Five rivers were too few to develop strong statistical comparisons; however, range is a reasonable surrogate for standard deviation and confidence intervals (Dean and Dixon, 1951). Accordingly, extreme examples of range reduction or extension are probably meaningful.

Overlap was characterized by using a simple ranking in which the maximum yields for a class of geology or land cover are compared to the minimum yields of the alternative class: forest compared to developed and granitic compared to volcanic (table 11). Increasing degrees of overlap were interpreted as reinforcing the effects of range reduction, and loss of overlap or major overlap reversals was interpreted as reinforcing the effects of range extension.

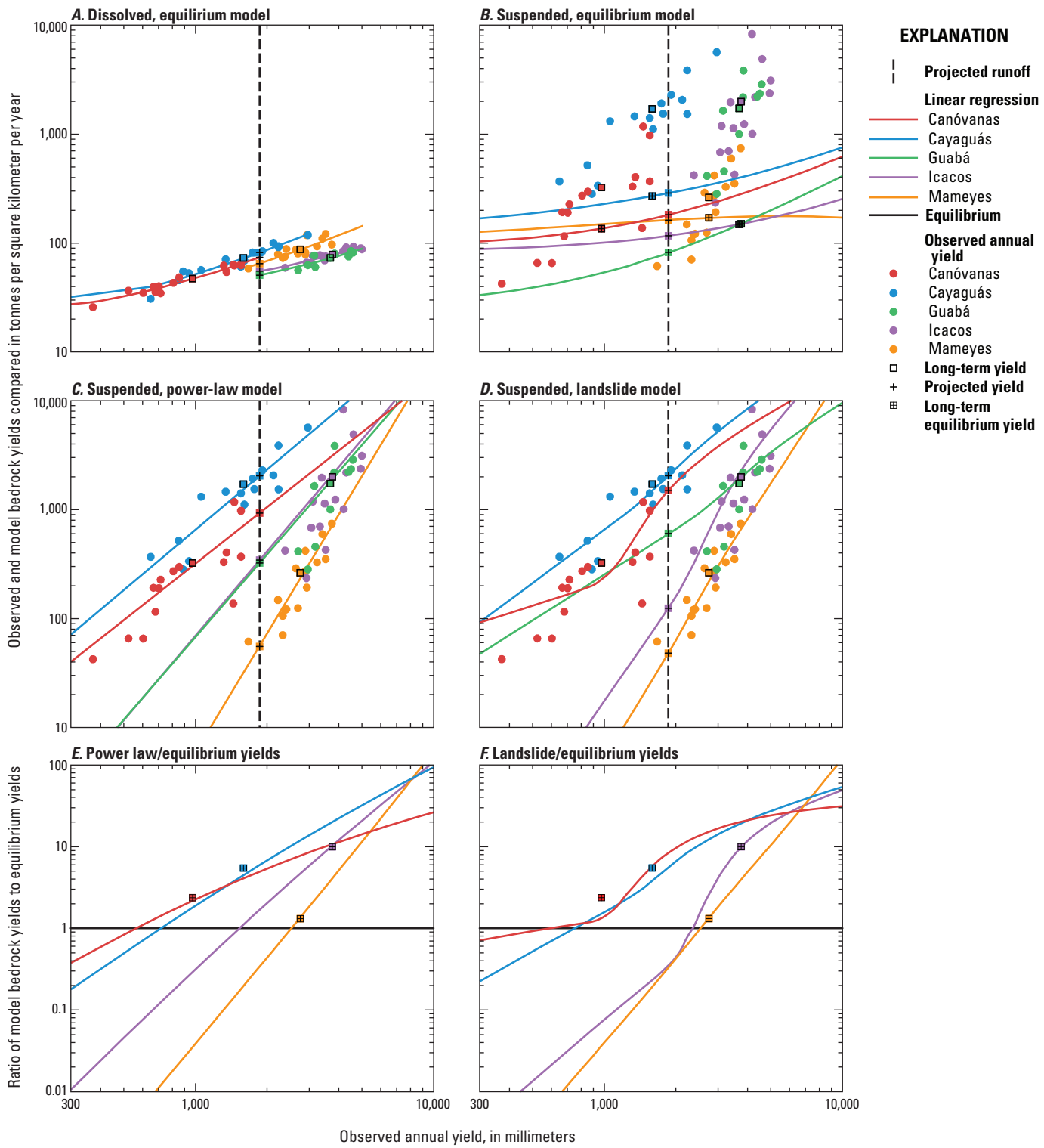


Figure 13. A model-based comparison of annual runoff compared with the annual yields of dissolved bedrock (part A) and suspended bedrock (parts B, C, D), eastern Puerto Rico. The vertical gray line in parts A–D corresponds with 1,860 millimeters per year, solid squares with black plus symbols correspond to the projected annual yields, and points are the observed annual yields. The curves in part A are linear regressions based on the assumption that the annual yield of dissolved bedrock responds linearly with changing runoff. The curves in part B relate dissolved bedrock to suspended bedrock through an equilibrium model discussed in the section Calculating Steady-State Erosion from Dissolved Bedrock. This relation is derived from the curves in figures 13A, 10A, and 10D using equation 16. The relation is almost linear and there has been no convolution smoothing. The lines in part C are power-law models, based on equation 21, which plot as lines on graphs with log-log scales. The curves in part D are derived from the landslide model, equations 24 and 25. Curves in parts C and D were smoothed by using equation 26 to account for climate variability. The ratio of the power-law model of suspended bedrock to equilibrium model and landslide model to the equilibrium model are presented in parts E and F, respectively. Note that observed suspended-bedrock yields are typically far greater than yields calculated by equilibrium models (part B). Compared with expected equilibrium yield, yield in the Mameyes watershed is slightly elevated and in the Canóvanas more so; the Cayaguás, Icacos, and Guabá are physically eroding at rates that greatly exceed expected equilibrium (parts E and F).

the reverse was true for the forested rivers. For some constituents such as $\text{Si}(\text{OH})_4$, however, the projected yields formed a more compact group than did the averaged observed mean-annual yields; for other constituents, such as POC, the projected yields became more widely dispersed.

The ranges for Na^+ , $\text{Si}(\text{OH})_4$, Cl^- , and dissolved bedrock became more compact upon projection to a common intermediate runoff (figs. 10, 12; table 11). This observation also applied to Na^* (fig. 10), which is not included in the table. The wider ranges for DOC and calcium were slight and not significant (Dean and Dixon, 1951). The elevated DOC yield on the Canóvanas might be an anthropogenic effect; more research is needed. The constituents associated with compact ranges are also the principal constituents used to describe and assess inputs from chemical weathering, atmospheric sources, and biological processes. This compactness indicates that these three classes of inputs operated in a similar way in all four study watersheds. In particular, overall rates of chemical weathering cannot be strongly distinguished when they are compared in terms of land cover or bedrock type. Some slight differences may relate to bedrock geology. Yields of Na^* and $\text{Si}(\text{OH})_4$ from the Cayaguás watershed are distinctly greater than in the other three rivers, and Ca^* yields from the Canóvanas and Mameyes watersheds were elevated. These latter watersheds are both on volcaniclastic rocks, which contain more calcium-bearing silicate minerals than do the granitic rocks, and the watersheds might also leach some calcium from minor sedimentary carbonate bedrock.

The ranges for the remaining constituents (Mg^{2+} , DIC, bioactive constituents, and particulate constituents) increased, most by large amounts (table 11; figs. 11, 12). In this group of constituents, developed watersheds tended to demonstrate a large increase in mean-annual yield relative to the forested watersheds once data were projected to a common mean-annual runoff. The only exception was DIC, for which developed and nondeveloped projected yields were intermingled. With the exception of SO_4^{2-} , Mg^{2+} , and DIC, the behavior of this group of constituents was consistent with our understanding of developed landscapes. Fertilizers and domestic wastes can contribute additional nutrients to developed watersheds, and increased erosion of deforested and agricultural landscapes can contribute to the particulate load.

Differences among watersheds for yields of sulfate, Mg^{2+} , and DIC (alkalinity) may have geologic causes. DIC is elevated in the Canóvanas watershed (figs. 4, 12). Note the similarity in diagrams of Mg^{2+} (fig. 11) and DIC (fig. 12). Carbonate rocks, which weather more rapidly than most silicate rocks, are a potential source of elevated alkalinity. A small amount of carbonate rock is found in the volcaniclastic rocks within the Canóvanas watershed (Murphy and others, 2012), and Ca^* yields (fig. 10) are not especially elevated; however, Mg^{2+} yields (fig. 11) are exceptionally high. Perhaps bedrock contains abundant, easily weathered mafic minerals, such as serpentine. Serpentinites are found in Puerto Rico, but none have been described within the

Results, Comparison of Constituent Yields, and Assessment of Landscape Equilibrium

Constituent-Yield Comparisons

Projection of annual yields to a common runoff, 1,860 mm yr^{-1} , brings several features to the fore (figs. 10–13, table 11). A characteristic of the linear relations for dissolved constituents (figs. 10–12) is that all have positive slopes and most have positive intercepts. In contrast to $\text{Si}(\text{OH})_4$ in the study rivers, the linear relations between $\text{Si}(\text{OH})_4$ and runoff presented by White and Blum (1995) all had negative intercepts. Annual solute yields must go to zero if annual runoff goes to zero (which would mean a profound desert), so these linear relations with nonzero intercepts must eventually reorganize as annual runoff approaches zero. For developed rivers, for which mean-annual runoff was below the projected runoff, all yields increased for all constituents following projection;

Table 10. Watershed yields as observed in eastern Puerto Rico and adjusted to a common intermediate runoff ($1,860 \text{ mm yr}^{-1}$), on the basis of the relation between runoff and annual yield.

[DIC, dissolved inorganic carbon; DOC, dissolved organic carbon; POC, particulate organic carbon; DBrx, dissolved bedrock; SBrx, suspended bedrock; mm yr^{-1} , millimeters per year; kmol $\text{km}^{-2} \text{ yr}^{-1}$, kilomoles per square kilometer per year; *, derived bedrock contribution]

Watershed	Runoff (mm yr^{-1})	Na^+	K^+	Mg^{2+}	Ca^{2+}	Si(OH)_4	Cl^-	SO_4^{2-}	NO_3^-	NH_4^+	PO_4^{3-}	DIC	DOC	POC	DBrx	SBrx	Na*	Ca*	
								(kmol $\text{km}^{-2} \text{ yr}^{-1}$)							(t $\text{km}^{-2} \text{ yr}^{-1}$)		(kmol $\text{km}^{-2} \text{ yr}^{-1}$)		
Annual net yields																			
Canóvanas	970	426	32	193	280	357	323	44	43	3.6	0.39	927	313	627	47	753	150	267	
Cayaguás	1,620	707	88	143	250	662	411	78	82	4.4	0.94	913	389	1,595	73	1,916	357	235	
Mameyes	2,750	654	51	183	439	739	542	85	26	2.1	0.41	1,174	573	503	87	604	193	423	
Iacos	3,760	745	58	157	264	854	585	54	45	3.7	0.18	868	837	1,788	78	2,148	246	246	
Guabá	3,630	735	51	113	170	778	615	43	39	2.6	0.18	587	574	1,954	67	2,347	211	152	
Annual net yields, adjusted to a common runoff																			
Canóvanas	1,860	713	63	312	448	607	578	80	94	8.5	0.47	1,424	605	1,729	74	2,076	221	429	
Cayaguás	1,860	786	106	156	271	748	476	92	97	5.4	1.03	967	475	1,910	82	2,295	380	256	
Mameyes	1,860	515	35	148	366	552	393	62	15	1.3	0.35	1,023	380	155	65	186	180	354	
Iacos	1,860	486	32	104	183	652	342	25	19	1.9	0.09	666	323	253	55	304	195	172	
Guabá	1,860	504	27	95	152	645	411	21	20	1.0	0.10	541	227	196	49	236	153	140	
Projected change in net annual yields from current mean-annual runoff to a common mean-annual runoff																			
Canóvanas	888	287	31	119	168	250	254	36	51	4.9	0.08	498	292	1,102	27	1,323	71	162	
Cayaguás	271	78	18	13	22	87	65	13	15	1.0	0.09	54	86	315	9	379	23	20	
Mameyes	-891	-139	-16	-35	-73	-187	-149	-23	-11	-0.8	-0.06	-151	-194	-348	-22	-418	-12	-69	
Iacos	-1,891	-259	-26	-53	-81	-202	-243	-29	-25	-1.8	-0.09	-203	-514	-1,535	-23	-1,844	-51	-75	
Guabá	-1,531	-231	-24	-18	-18	-133	-204	-21	-19	-1.6	-0.08	-47	-346	-1,758	-18	-2,112	-58	-12	
Watershed	Runoff (mm yr^{-1})	Na^+	K^+	Mg^{2+}	Ca^{2+}	Si(OH)_4	Cl^-	SO_4^{2-}	NO_3^-	NH_4^+	PO_4^{3-}	DIC	DOC	POC	DBrx	SBrx	Na*	Ca*	
Percent change in net annual yields from current mean-annual runoff to a common mean-annual runoff																			
Canóvanas	91	67	97	62	60	70	79	82	117	137	21	54	93	176	58	176	47	61	
Cayaguás	17	11	21	9	9	13	16	17	19	23	10	6	22	20	13	20	6	9	
Mameyes	-32	-21	-31	-19	-17	-25	-27	-27	-44	-38	-16	-13	-34	-69	-25	-69	-6	-16	
Iacos	-50	-35	-45	-34	-31	-24	-42	-54	-56	-48	-51	-23	-61	-86	-29	-86	-21	-30	
Guabá	-45	-31	-47	-16	-10	-17	-33	-50	-48	-61	-45	-8	-60	-90	-28	-90	-27	-8	

Table 11. Interpretation of changes in watershed yields as observed in eastern Puerto Rico and adjusted to a common intermediate mean-annual runoff.

* calculated bedrock contribution; DIC, dissolved inorganic carbon; DOC, dissolved organic carbon; POC, particulate organic carbon; DBrx, dissolved bedrock; SBrx, suspended bedrock; < less than

¹Before after -2-2^{*}maximum forest≤minimum developed; -1- maximum forest≤minimum developed; 0- range overlap; 1- maximum developed≤minimum forest; 2- maximum developed≤minimum forest.

²Before, after: -2, 2•maximum granitic<minimum volcanic; -1=maximum granitic<minimum volcanic; 0, range overlap; 1, maximum granitic<minimum volcanic; 2, 2•maximum granitic< minimum volcanic. Change: -1 from nonoverlap to overlay; 0 overlay before and after; 1 similar look of overprint before and after; 2 a reversal or loss in look of overprint

Canóvanas watershed. The high SO_4^{2-} in the Mameyes, Canóvanas, and Cayaguás rivers is likely influenced by bedrock, because SO_4^{2-} yields of these watersheds exceed atmospheric inputs (table 3). Sulfide ores are found in the region (see Murphy and others, 2012). Additional inputs from human activities cannot be discounted, however, in the developed watersheds.

Landscape Equilibrium

The relation between annual runoff and annual yields of suspended bedrock are modeled in three ways: a standard power-law physical-erosion model (equation 21), a landslide physical-erosion model (equations 22, 24, 25), and as the result of equilibrium erosion (the equilibrium model, equation 16) (fig. 13). The landslide model provides a superior representation of erosion in the Icacos and Canóvanas watersheds, compared with the power-law model, and it is a somewhat more accurate model in the Cayaguás (fig. 13E,F). Neither model is superior in describing the Mameyes watershed. The equilibrium model bears little resemblance to observations or other models (fig. 13B). Observed annual suspended-bedrock yields were considerably in excess of expected equilibrium yields, except for the Mameyes (table 12, fig. 13B).

Contemporary observed suspended-bedrock yields in all study watersheds exceeded equilibrium rates calculated by using Na₂O (table 12). In the Mameyes watershed, physical erosion is modeled to be twice equilibrium when Na₂O is paired with SiO₂, which is the preferred pairing, but it is modeled to be at equilibrium when CaO is paired with SiO₂ (table 12). The two models of physical erosion can be used to estimate the mean-annual runoff for which yields would be in equilibrium (fig. 13, table 13). In all watersheds, current mean-annual runoff is in excess of the equilibrium runoff. Such an excess could imply either that climate has become wetter or stormier, pushing the watersheds out of equilibrium, or that erosion processes have changed owing to land-cover changes.

In the case of the volcanic watersheds, the Canóvanas and the Mameyes, the current mean-annual runoff deviates from equilibrium by less than 600 mm (table 13), and suspended-bedrock yields are considerably smaller than in the granitic watersheds (table 12). This smaller runoff is within the range of annual runoff variation for the Mameyes, and a climatic explanation is possible, although it is contrary to presumed long-term drying trends (Zack and Larsen, 1993). Although substantial parts of the Canóvanas are now in second growth (Murphy and others, 2012), much of the watershed has been deforested, farmed, and grazed, and its somewhat larger deviation from equilibrium could be caused by this history of land-cover change.

The Cayaguás and Iacos watersheds, both on granitic rocks, are much further from equilibrium. We know that deforestation and agriculture have accelerated physical erosion in the Cayaguás; however, the Iacos, which has similar

Table 12. Summary of landscape equilibrium properties, eastern Puerto Rico.[DBrx, dissolved bedrock; SBrx, suspended bedrock; mm yr⁻¹, millimeters per year; t km⁻² yr⁻¹, metric tons per square kilometer per year]

River	Observed mean annual runoff (mm yr ⁻¹)	Observed DBrx yield (t km ⁻² yr ⁻¹)	Observed SBrx yield (t km ⁻² yr ⁻¹)	Power-law SBrx yield (t km ⁻² yr ⁻¹)	Landslide-day SBrx yield (t km ⁻² yr ⁻¹)	Equilibrium SBrx yield based on Na ₂ O (t km ⁻² yr ⁻¹)	Ratio of observed to equilibrium SBrx yields based on Na ₂ O	Equilibrium SBrx yield based on CaO (t km ⁻² yr ⁻¹)	Ratio of observed to equilibrium SBrx yields based on CaO
Canóvanas	970	47.0	355	299	184	89	3.99	154	2.30
Cayaguás	1,620	72.7	1,981	1,219	1,031	233	8.48	162	12.22
Mameyes	2,750	87.3	270	230	228	106	2.56	265	1.02
Icacos	3,760	78.1	1,985	1,555	1,481	154	12.91	130	15.22
Guabá	3,630	67.0	1,590	1,648	1,428	137	11.58	60	26.69

Table 13. Observed mean-annual runoff compared with equilibrium runoff for power-law and landslide day erosion models in study watersheds, eastern Puerto Rico.[mm yr⁻¹, millimeters per year]

River	Observed mean annual runoff (mm yr ⁻¹)	Equilibrium runoff, power-law model (mm yr ⁻¹)	Equilibrium runoff, landslide model (mm yr ⁻¹)	Runoff in excess of equilibrium for power-law model (mm yr ⁻¹)	Runoff in excess of equilibrium for landslide model (mm yr ⁻¹)
Canóvanas	970	430	270	540	700
Cayaguás	1,620	670	690	950	930
Mameyes	2,750	2,220	2,240	530	510
Icacos	3,760	1,540	2,370	2,220	1,390
Guabá	3,630	820	200	2,810	3,430

Table 14. Total denudation compared with equilibrium denudation for current mean-annual runoff and projected to a common runoff in study watersheds, eastern Puerto Rico.[mm yr⁻¹, millimeters per year; m Ma⁻¹, meters per mega annum (10⁶ years)]

River	Observed mean annual runoff (mm yr ⁻¹)	Observed total denudation (m m.y. ⁻¹)	Equilibrium denudation, modeled (m m.y. ⁻¹)	Projected total denudation at 1,860 mm yr ⁻¹ annual runoff (m m.y. ⁻¹)	Projected equilibrium denudation at 1,860 mm yr ⁻¹ annual runoff (m m.y. ⁻¹)	Equilibrium denudation at equilibrium annual runoff (m m.y. ⁻¹)
Canóvanas	970	152	51	614	72	36
Cayaguás	1,620	775	116	643	125	84
Mameyes	2,750	135	73	45	65	68
Icacos	3,760	779	87	36	66	72
Guabá	3,630	625	77	157	49	72

Table 15. Excess particulate organic carbon yields from the equilibrium model of study watersheds, eastern Puerto Rico.[DOC, dissolved organic carbon; POC, particulate organic carbon; mm yr⁻¹, millimeters per year; kmol km⁻² yr⁻¹, kilomoles per square kilometer per year]

River	Observed mean annual runoff (mm yr ⁻¹)	Observed DOC yield (kmol km ⁻² yr ⁻¹)	Observed POC yield (kmol km ⁻² yr ⁻¹)	Equilibrium POC yield (kmol km ⁻² yr ⁻¹)	POC yield in excess of equilibrium (kmol km ⁻² yr ⁻¹)	POC yield in excess of equilibrium (percent)
Canóvanas	970	313	627	157	470	300
Cayaguás	1,620	389	1,595	188	1,407	750
Mameyes	2,750	573	503	197	306	160
Icacos	3,760	837	1,788	139	1,650	1,190
Guabá	3,630	574	1,954	169	1,786	1,060

bedrock and is forested, is even further from equilibrium. For both rivers, the current mean-annual runoff deviates from equilibrium by 900 mm to 2,200 mm. Denudation rates (table 14) that are projected to a common runoff value produce equilibrium rates for the forested watersheds that exceed the predicted denudation rate; these conditions are those needed to develop thicker soils.

Excess POC yields are calculated by assuming that the equilibrium POC yield is in the same proportions compared with equilibrium solid yield as the observed POC yield is to the observed solid yield (table 15). The excess POC yield, which reflects presumed landscape disequilibrium, is the largest part of the organic carbon budget in all study watersheds except the Mameyes.

Summary and Conclusion: General Landscape Disequilibrium and the Carbon Cycle

The biogeochemistry and physical erosion of four research watersheds were examined through the development of simple models that relate observed annual runoff to annual yields for various constituents. Several derived constituents were developed, including the bedrock-derived yields of all measured constituents, dissolved silicate bedrock, suspended silicate bedrock, and the equilibrium production of bedrock-derived solids. Several constituents are largely atmospheric in origin (table 3)— Na^+ , Cl^- , SO_4^{2-} , NO_3^- plus NH_4^+ , DOC, and POC. Between 10 and 50 percent of K^+ and Mg^{2+} originate in the atmosphere. Less than 10 percent of Ca , Si(OH)_4 , dissolved bedrock, and suspended bedrock originates in the atmosphere. Conductivity, Cl^- , and Si(OH)_4 proved to be an excellent surrogate suite of measurements to use for estimating dissolved bedrock.

At the beginning of the paper, six questions are asked; they can now be answered.

What are the measured rates of chemical and physical denudation and how do these relate to mean-annual runoff in each watershed?

Rates of chemical and physical denudation are summarized in table 14. For dissolved constituents, the relation between annual runoff and annual yields is linear (figs. 10–12). This relation is consistent with results of other studies (White and Blum (1995) and Godsey and others (2009)). Intercepts do not intersect zero, an indication that processes must change as mean-annual runoff approaches zero. Suspended bedrock and particulate organic carbon can be modeled either by a power-law relation or by a model based on accounting for the total runoff of all days having storms large enough to produce landslides (fig. 13C, D).

How do watersheds compare in weathering, erosion, carbon export, and nutrient export with regard to geology and land cover? Do geology and land cover matter?

Watersheds were compared in two ways, at their current conditions of mean-annual runoff and by using the relation between annual runoff and annual yield to estimate mean-annual yields at a common, intermediate, mean-annual runoff of $1,860 \text{ mm yr}^{-1}$. Current mean-annual runoffs differ widely among the watersheds, because the forested watersheds are relatively wet and the developed watersheds are considerably drier.

Before projection to a common runoff, dissolved bedrock yields, about 47 to $87 \text{ t km}^{-2} \text{ yr}^{-1}$, differed by a factor of less than 2 among all watersheds but were greater for the wetter watersheds. Silica, Cl^- , and DOC also demonstrated little relation to land cover, mean-annual runoff, or bedrock type. Before projection to a common yield, suspended-bedrock yields, ranging from 600 to $2,350 \text{ t km}^{-2} \text{ yr}^{-1}$, were threefold to fourfold as great for the watersheds draining granitic rocks.

Upon projection to a common mean-annual runoff, the yield ranges of dissolved bedrock, Na^+ , Si(OH)_4 , and Cl^- became more compact, whereas the yield ranges of DOC and Ca^{2+} changed little. These constituents are primary measures of chemical weathering, seasalt input, and biological activity on the landscape. Narrow ranges indicate that differences in bedrock and land cover did not exert a strong influence on how these constituents were processed in this landscape. DIC, Mg^{2+} , SO_4^{2-} , and Na^* showed systematically greater yields in a few watersheds (figs. 10–12), probably for geological reasons. The projected yields of biologically active constituents (K^+ , NO_3^- , NH_4^+ , PO_4^{3-}), and particulate constituents (suspended bedrock and POC) were considerably greater on developed landscapes (table 10, figs. 11–13), consistent with the effects of land clearing, fertilizer application, and minor domestic or industrial waste inputs. DOC may show a slight human effect in that concentrations in the developed watersheds were greater than in the forested ones; the difference is not as pronounced as with the previous constituents.

Is the landscape in a state of dynamic equilibrium? In essence, are the Luquillo Mountains a model of a quiescent natural landscape or are they changing?

The calculation of equilibrium denudation rates by using measurements of silica, sodium, and total dissolved bedrock appears to be robust (Stallard, 1995a). A notable feature of the approach was the use of conductivity, Cl^- , and Si(OH)_4 measurements, when they were appropriately calibrated, to estimate total dissolved bedrock in samples for which it could not be measured because of staff and laboratory limitations. This use of surrogates allowed thousands of additional estimates of total dissolved bedrock. Adding Na^+ to this suite, which now

also includes suspended sediment, K⁺, and DOC, would allow especially rigorous characterizations of chemical and physical erosion and carbon export from certain watersheds—those where chemical weathering generates erodible solids, and those solids have low ratios of Na₂O to SiO₂ compared with ratios in bedrock. Such settings would be environments with moderate to intense chemical weathering. Use of total dissolved solids rather than total dissolved bedrock erroneously doubles estimates of solute erosion, and use of suspended sediments (dried at 105°C) rather than suspended bedrock (heated to 550°C) overestimates physical erosion by about 10 percent.

Except possibly for the Mameyes watershed, the current landscape is not in a state of dynamic equilibrium as estimated using the method of Stallard (1995a,b), based on concentrations of silicon and sodium in bedrock, in river-borne solids, and in solution (fig. 12, tables 12–14). The estimates of equilibrium rates are consistent, but slightly greater than, estimates obtained by using cosmogenic ¹⁰Be for the Icacos (Brown and others, 1995) and for the Cayaguás (Brown and others, 1998). Observed suspended-bedrock yields are fivefold to tenfold as great as equilibrium yields on the granitic rocks and only slightly elevated on the volcanic rocks. The Mameyes watershed appears to be relatively close to equilibrium.

Brown and others (1995) observed that the Icacos watershed is in a state of dynamic equilibrium, on the basis of a cosmogenic ¹⁰Be denudation rate of 43 millimeters per thousand years (mm k.y.⁻¹) that matched an estimate of denudation of 75 mm k.y.⁻¹, based on limited data. The 75 mm k.y.⁻¹ denudation rate is clearly too low, given rates estimated from the Puerto Rico WEBB dataset of 780 mm k.y.⁻¹. It is more likely that the Icacos recently departed from equilibrium and that the cosmogenic ¹⁰Be in sediments and ridge-crest soils of the Icacos record its former equilibrium denudation rate much as Brown and others (1998) demonstrated for the Cayaguás, where the preagricultural equilibrium rate recorded in sediments is estimated to be 85 mm k.y.⁻¹.

The equilibrium denudation rates at the annual runoff rates where the physical-erosion models match the equilibrium rates of sediment production in the Icacos (table 12) are somewhat greater than those based on cosmogenic ¹⁰Be, indicating that the denudation rates recorded by ¹⁰Be for the Icacos were established under even drier or more quiescent conditions. Clearly, the ridgetops in the Icacos watershed that were sampled for ¹⁰Be in soils must still reflect the old equilibrium conditions as evidenced by the clean bioturbation profiles reported in Brown and others (1995). The watershed as a whole, however, is not in this quiescent state.

What does the present dynamic state of the landscape imply regarding past and future response to climate change?

Deforestation and agriculture can easily explain disequilibrium erosion in the two developed watersheds. The disequilibrium is so great for the forested watershed on

granitic rock (the Icacos) that other explanations are needed. The equilibrium denudation rates at the annual runoff rates where the models predict equilibrium (table 14) are somewhat greater than those based on cosmogenic ¹⁰Be for the Icacos, indicating that the thick soils of this watershed were developed under especially quiescent conditions of physical erosion, compared with today. If the rate change is to be attributed to human activities, trails to mines have crossed the landscape for perhaps 500 years, and paved roads were built into the Icacos watershed in the middle 20th century (Larsen, 2012; Murphy and others, 2012). Alternatively, the forest in the Icacos may be degrading, perhaps from increased nitrogen loading (Stallard, 2012) or invasion by species such as bamboo (Murphy and others, 2012), thereby failing to inhibit erosion, particularly through an increasing rate of landsliding. Climate change, perhaps by increasing the frequency of huge landslide-generating storms, could have caused such a change in erosional style in the forested granitic watersheds; the weather record is not long enough to test this suggestion.

What are the rates of export of carbon in its various forms; how do these rates relate to runoff, and is this carbon being replaced by new photosynthetically fixed carbon?

Rates of carbon export as dissolved-inorganic, dissolved-organic, and particulate-organic carbon are summarized as yields in table 15. The POC yields exceed combined dissolved carbon yields in the granitic watersheds, but they are considerably less than the dissolved yields in the volcanic watersheds. Annual yields of DIC and DOC relate linearly to annual runoff, whereas POC has a steep power-law-style increase with increasing runoff. The POC yields are tied to sediment yields that are, in turn, far in excess of equilibrium yields. This excess implies that much of the present carbon transport in eastern Puerto Rico is the result of erosion in excess of equilibrium rates as hypothesized by Stallard (1998). In essence, soils that have developed for thousands of years are eroding more rapidly than they are now forming. Carbon accumulation is quite rapid, however, and in a landslide scar half of the carbon is regenerated in 80 years and all of it in about 200 years (fig. 2). Thus, eroding carbon is being replaced with new photosynthetic carbon from the atmosphere.

Are rates of carbon processing through the landscape notable on the time scales of human-induced climate change?

Estimates of the combined yields of all forms of carbon from the WEBB watersheds (table 3) range from about 1,800 kmol km⁻² yr⁻¹ (22 t km⁻² yr⁻¹ C) to 3,300 kmol km⁻² yr⁻¹ (40 t km⁻² yr⁻¹ C). The largest observed yield of organic carbon (DOC+POC), 2,600 kmol km⁻² yr⁻¹ (31 t km⁻² yr⁻¹ C), is 2.5 to 4 percent of net primary productivity for tropical

forests, an amount that is relatively small and sustainable. For reference, these POC yields from the granitic watersheds are about half of those estimated by Hilton and others (2008a) for a landslide-prone shaly landscape in New Zealand. For a process to be important to the carbon cycle, it would have to scale to about $6.7 \text{ t km}^{-2} \text{ yr}^{-1}$ C for a global terrestrial phenomenon, or about $250 \text{ t km}^{-2} \text{ yr}^{-1}$ C if confined to humid tropical mountains. The perturbed POC yields (table 15), $300 \text{ kmol km}^{-2} \text{ yr}^{-1}$ ($6 \text{ t km}^{-2} \text{ yr}^{-1}$ C) to $1,700 \text{ kmol km}^{-2} \text{ yr}^{-1}$ ($22 \text{ t km}^{-2} \text{ yr}^{-1}$ C), are close to and greater than $6.7 \text{ t km}^{-2} \text{ yr}^{-1}$ C but far less than $250 \text{ t km}^{-2} \text{ yr}^{-1}$ C.

Human-accelerated POC burial is a global phenomenon (Stallard, 1998), and these excess POC yields are consistent with it. The lack of evidence in eastern Puerto Rico of human effects for either DOC production or silicate weathering suggests that although the DIC and DOC yields of tropical rivers are large, they are of secondary interest to research of the anthropogenically perturbed carbon cycle at a century time scale.

Eastern Puerto Rico contains a fascinating landscape for examining biogeochemical processes operating at maximal rates. The models presented here, however, represent considerable simplifications of these complex interacting processes. It is hoped that these results inspire others to develop physically based models and geochemical tests that better define the processes and how they respond to environmental and climate change. It is a setting that may have been important to the climate history of our planet, and it probably is representative of the sources of a huge fraction of the clastic sediments that form the geologic record. From the perspective of observation, this landscape, except perhaps for the Mameyes watershed, is far from equilibrium and probably is more representative of conditions during major erosion cycles in the Earth's history than the more quiescent times in between.

Acknowledgments

This work was supported through the United States Geological Survey Water, Energy, and Biogeochemical Budgets program (Larsen and others, 1993; Lins, 1994). This chapter benefited from reviews by Troy Baisden, Alex Blum, and Jamie Shanley. During the last 22 years, management support of this long-term study, from concept to integrated product, has been greatly appreciated.

References

- Ashton, P.S., Brokaw, N., Bunyavechewin, S., Condit, R., Chuyong, G., Co, L., Dattaraja, H.S., Davies, S., Esufali, S., Ewango, C.E.N., Foster, R., Gunatilleke, N., Gunatilleke, S., Hernandez, C., Hubbell, S., Itoh, A., John, R.,

Kanzaki, M., Kenfack, D., Kiratiprayoon, S., LaFrankie, J., Lee, H.S., Liengola, I., Lao, S., Losos, E.C., Makana, J.R., Manokaran, N., Navarrete, H., Okhubo, T., Pérez, R., Pongpattannanurak, N., Samper, C., Sri-ngernyuang, K., Sukumar, R., Sun, I.F., Suresh, H.S., Tan, S., Thomas, D., Thompson, J., Vallejo, M., Villa Muñoz, G., Valencia, R., Yamakura, T., and Zimmerman, J., 2004, Floristics and vegetation of the forest dynamics plots, in Losos, E.C., and Leigh, E.E., Jr., eds., Tropical forest diversity and dynamism—Findings from a large-scale plot network: Chicago, The University of Chicago Press, p. 90–102.

Aufdenkampe, A.K., Hedges, J.I., Richey, J.E., Krusche, A.V., and Llerena, C.A., 2001, Sorptive fractionation of dissolved organic nitrogen and amino acids onto fine sediments within the Amazon Basin: Limnology and Oceanography, v. 46, no. 8, p. 1921–1935.

Aufdenkampe, A.K., Mayorga, E., Hedges, J.I., Llerena, C., Quay, P.D., Gudeman, J., Krusche, A.V., and Richey, J.E., 2007, Organic matter in the Peruvian headwaters of the Amazon—Compositional evolution from the Andes to the lowland Amazon mainstem: Organic Geochemistry, v. 38, p. 337–374.

Beinroth, F.H., Hernández, P.J., Esnard, A.-M., Acevedo, G., and Dubee, B.C., 1992, Organic carbon content of the soils of Puerto Rico, in Beinroth, F.H., ed., Organic carbon sequestration in the soils of Puerto Rico—A case study of a tropical environment: Mayagüez, Puerto Rico, University of Puerto Rico Department of Agronomy and Soils, and U.S. Department of Agriculture Soil Conservation Service, p. 57–62, 69 pages.

Berhe, A.A., Harte, J., Harden, J.W., and Torn, M.S., 2007, The significance of the erosion-induced terrestrial carbon sink: BioScience, v. 57, no. 4, p. 337–346.

Bevington, P.R., and Robinson, K.D., 2003, Data reduction and error analysis for the physical sciences—2: New York, McGraw Hill, 320 p.

Bhatt, M.P., and McDowell, W.H., 2007, Controls on major solutes within the drainage network of a rapidly weathering tropical watershed: Water Resources Research, v. 43, p. 1–9.

Blair, N.E., Leithold, E.L., Ford, S.T., Peeler, K.A., Holmes, J.C., and Perkey, D.W., 2003, The persistence of memory—The fate of ancient sedimentary organic carbon in a modern sedimentary system: Geochimica et Cosmochimica Acta, v. 67, no. 1, p. 63–73.

Bot, A.J., Nachtergaele, F.O., and Young, A., 2000, Land resource potential and constraints at regional and country levels: Rome, Land and Water Development Division Food and Agriculture Organization of the United Nations, 214 p.

Brandeis, T.J., Helmer, E.H., and Oswalt, S.N., 2007, The status of Puerto Rico's forests, 2003: U.S. Department of Agriculture Forest Service, Southern Forest Experiment Station Resources Bulletin SRS-119, 75 pages.

- Brown, E.T., Stallard, R.F., Larsen, M.C., Bourlès, D.L., Raisbeck, G.M., and Yiou, F., 1995, Pre-anthropogenic denudation rates of a perturbed watershed (Cayaguás River, Puerto Rico) estimated from in-situ-produced ^{10}Be in river-borne quartz: *Eos, Transactions, American Geophysical Union*, v. 76, no. 46 supplement, p. F685–F686.
- Brown, E.T., Stallard, R.F., Larsen, M.C., Bourlès, D.L., Raisbeck, G.M., and Yiou, F., 1998, Determination of pre-development denudation rates of an agricultural watershed (Cayaguás River, Puerto Rico) using in-situ-produced ^{10}Be in river-borne quartz: *Earth and Planetary Science Letters*, v. 160, p. 723–728.
- Buss, H.L., Brantley, S.L., Sak, P.B., and White, A.F., 2004, Mineral dissolution at the granite-saprolite interface, in Wanty, R.B., and Seal, R.R.I., eds., *International Symposium on Water-Rock Interaction*, 11th, Saratoga Springs, N.Y., July 2004, Proceedings: London, Taylor and Francis, p. 819–823.
- Buss, H.L., Bruns, M.A., Schulz, M.S., Moore, J., Mathur, C.F., and Brantley, S.L., 2005, The coupling of biological iron cycling and mineral weathering during saprolite formation, Luquillo Mountains, Puerto Rico: *Geobiology*, v. 3, p. 247–260.
- Buss, H.L., Sak, P.B., Webb, S.M., and Brantley, S.L., 2008, Weathering of the Río Blanco quartz diorite, Luquillo Mountains, Puerto Rico—Coupling oxidation, dissolution, and fracturing: *Geochimica et Cosmochimica Acta*, v. 72, p. 4488–4507.
- Buss, H.L., and White, A.F., 2012, Weathering processes in the Río Iacos and Río Mameyes watersheds in eastern Puerto Rico, ch. I in Murphy, S.F., and Stallard, R.F., eds., *Water quality and landscape processes of four watersheds in eastern Puerto Rico*: U.S. Geological Survey Professional Paper 1789, p. 249–262.
- Caine, Nelson, 1980, The rainfall intensity-duration control of shallow landslides and debris flows: *Geografiska Annaler*, v. 62A, p. 23–27.
- Crosta, G.B., 1998, Regionalization of rainfall thresholds—An aid to landslide hazard evaluation: *Environmental Geology*, v. 35, no. 2–3, p. 131–145.
- Dalling, J.W., and Tanner, E.V.J., 1995, An experimental study of regeneration on landslides in montane rain forest in Jamaica: *Journal of Ecology*, v. 83, no. 1, p. 55–64.
- Dean, R.B., and Dixon, W.J., 1951, Simplified statistics for small numbers of observations: *Analytical Chemistry*, v. 23, no. 4, p. 636–638.
- Denman, K.L., Brasseur, G., Chidthaisong, A., Ciais, P., Cox, P.M., Dickinson, R.E., Hauglustaine, D., Heinze, C., Holland, E., Jacob, D., Lohmann, U., Ramachandran, S., da Silva Dias, P.L., Wofsy, S.C., and Zhang, X., 2007, Couplings between changes in the climate system and biogeochemistry, in Solomon, Susan, Qin, D., Manning, M., and others, eds., *Climate change 2007—The physical science basis. Contribution of Working Group I to the fourth assessment report of the Intergovernmental Panel on Climate Change*: Cambridge, United Kingdom, Cambridge University Press, p. 499–587.
- Derry, L.A., Pett-Ridge, J.C., Kurtz, A.C., and Troester, J.W., 2006, Ge/Si and $^{87}\text{Sr}/^{86}\text{Sr}$ tracers of weathering reactions and hydrologic pathways in a tropical granitoid system: *Journal of Geochemical Exploration*, v. 88, p. 271–274.
- Dong, Hailiang, Peacor, D.R., and Murphy, S.F., 1998, TEM study of progressive alteration of igneous biotite to kaolinite throughout a weathered soil profile: *Geochimica et Cosmochimica Acta*, v. 62, no. 11, p. 1881–1887.
- Fletcher, R.C., Buss, H.L., and Brantley, S.L., 2006, A spheroidal weathering model coupling porewater chemistry to soil thicknesses during steady-state denudation: *Earth and Planetary Science Letters*, v. 244, p. 444–457.
- Foley, J.A., Ramankutty, Navin, Brauman, K.A., Cassidy, E.S., Gerber, J.S., Johnston, Matt, Mueller, N.D., O'Connell, Christine, Ray, D.K., West, P.C., Balzer, Christian, Bennett, E.M., Carpenter, S.R., Hill, Jason, Monfreda, Chad, Polasky, Stephen, Rockström, Johan, Sheehan, John, Siebert, Stefan, Tilman, David, and Zaks, D.P.M., 2011, Solutions for a cultivated planet: *Nature*, v. 478, p. 337–342.
- Galy, Valier, France-Lanord, C., Beyssac, O., Faure, P., Kudrass, H., and Palho, F., 2007, Efficient organic carbon burial in the Bengal fan sustained by the Himalayan erosional system: *Nature*, v. 450, p. 407–410.
- Garrels, R.M., and Lerman, A., 1984, Coupling of the sedimentary sulfur and carbon cycles—An improved model: *American Journal of Science*, v. 284, p. 989–1007.
- Garrels, R.M., and Mackenzie, F.T., 1971, *Evolution of sedimentary rocks*: New York, W.W. Norton and Company, 397 p.
- Garwood, N.C., Janos, D.P., and Brokaw, N.V.L., 1979, Earthquake-caused landslides—A major disturbance to tropical forests: *Science*, v. 205, p. 997–999.
- Godsey, S.E., Kirchner, J.W., and Clow, D.W., 2009, Concentration-discharge relationships reflect chemostatic characteristics of U.S. watersheds: *Hydrological Processes*, v. 23, p. 1844–1864.
- Guariguata, M.R., 1990, Landslide disturbance and forest regeneration in the upper Luquillo Mountains of Puerto Rico: *Journal of Ecology*, v. 78, no. 3, p. 814–832.
- Guariguata, M.R., and Larsen, M.C., 1990, Preliminary map showing landslides in El Yunque quadrangle, Puerto Rico: U.S. Geological Survey Open-File Report 89–257, 1 map sheet, scale 1:20,000, text.

- Harden, J.W., Berhe, A.A., Torn, M., Harte, J., Liu, S., and Stallard, R.F., 2008, Soil erosion—Data say C sink: *Science*, v. 320, no. 5873, p. 178–179.
- Heartsill-Scalley, Tamara, Scatena, F.N., Estrada, C., McDowell, W.H., and Lugo, A.E., 2007, Disturbance and long-term patterns of rainfall and throughfall nutrient fluxes in a subtropical wet forest in Puerto Rico: *Journal of Hydrology*, v. 333, p. 472–485.
- Hedges, J.I., Mayorga, E., Tsamakis, E., McClain, M.E., Aufdenkampe, A.K., Quay, P., Richey, J.E., Benner, R., Opsahl, S., Black, B., Pimentel, T., Quintanilla, J., and Maurice, L., 2000, Organic matter in Bolivian tributaries of the Amazon River—A comparison to the lower mainstream: *Limnology and Oceanography*, v. 45, no. 7, p. 1449–1466.
- Hilton, R.G., Galy, A., and Hovius, N., 2008a, Riverine particulate organic carbon from an active mountain belt: Importance of landslides: *Global Biogeochemical Cycles*, v. 22, no. GB1012, p. 1–2.
- Hilton, R.G., Galy, A., Hovius, N., Chen, M.-C., Horng, M.-J., and Chen, H., 2008b, Tropical-cyclone-driven erosion of the terrestrial biosphere from mountains: *Nature Geoscience*, v. 1, p. 769–772.
- Hooke, R.L., 1994, On the efficacy of humans as geomorphic agents: *GSA Today*, v. 4, p. 218, 224–225.
- Hooke, R.L., 2000, On the history of humans as geomorphic agents: *Geology*, v. 28, no. 9, p. 843–846.
- Jolly, W.T., Lidiak, E.G., Schellekens, J.H., and Santos, J., 1998, Volcanism, tectonic and stratigraphic correlations in Puerto Rico, in Lidiak, E.G., and Larue, D.K., eds., *Tectonics and geochemistry of the northeastern Caribbean: Geological Society of America Special Paper 322*, p. 1–34.
- Jupp, D.L., 1976, B-splines for smoothing and differentiating data sequences: *Mathematical Geology*, v. 8, no. 3, p. 243–266.
- Keefer, D.K., 1984, Landslides caused by earthquakes: *Geological Society of America Bulletin*, v. 95, p. 406–421.
- Kennaway, Todd, and Helmer, E.H., 2007, The forest types and ages cleared for land development in Puerto Rico: *GIScience and Remotely Sensing*, v. 44, no. 4, p. 356–382.
- Lal, Rattan, and Pimentel, D., 2008, Soil erosion—A carbon sink or source?: *Science*, v. 319, p. 1040–1041.
- Larsen, M.C., 1997, Tropical geomorphology and geomorphic work—A study of geomorphic processes and sediment and water budgets in montane humid-tropical forested and developed watersheds, Puerto Rico: Boulder, University of Colorado Department of Geography, Ph.D. dissertation, 244 p.
- Larsen, M.C., 2012, Landslides and sediment budgets in four watersheds in eastern Puerto Rico, ch. F in Murphy, S.F., and Stallard, R.F., eds., *Water quality and landscape processes of four watersheds in eastern Puerto Rico: U.S. Geological Survey Professional Paper 1789*, p. 153–178.
- Larsen, M.C., Collar, P.D., and Stallard, R.F., 1993, Research plan for the investigation of water, energy, and biogeochemical budgets in the Luquillo Mountains, Puerto Rico: U.S. Geological Survey Open-File Report 92–150, 19 p.
- Larsen, M.C., and Parks, J.E., 1997, How wide is a road? The association of roads and mass-wasting in a forested montane environment: *Earth Surface Processes and Landforms*, v. 22, p. 835–848.
- Larsen, M.C., and Santiago-Román, A., 2001, Mass wasting and sediment storage in a small montane watershed—An extreme case of anthropogenic disturbance in the humid tropics, in Dorava, J.M., Palcsak, B.B., Fitzpatrick, F., and Montgomery, D., eds., *Geomorphic processes and riverine habitat: American Geophysical Union Water Science & Application Series*, v. 4, p. 119–138.
- Larsen, M.C., and Simon, A., 1993, A rainfall intensity-duration threshold for landslides in a humid-tropical environment, Puerto Rico: *Geografiska Annaler*, v. 75A, p. 13–23.
- Larsen, M.C., and Stallard, R.F., 2000, Luquillo Mountains, Puerto Rico—A Water, Energy, and Biogeochemical Budgets program site: U.S. Geological Survey Fact Sheet 163–99, 4 p.
- Larsen, M.C., and Torres-Sánchez, A.J., 1992, Landslides triggered by Hurricane Hugo in eastern Puerto Rico, September 1989: *Caribbean Journal of Science*, v. 28, no. 3–4, p. 113–125.
- Larsen, M.C., and Torres-Sánchez, A.J., 1998, The frequency and distribution of recent landslides in three montane tropical regions of Puerto Rico: *Geomorphology*, v. 24, no. 4, p. 309–331.
- Larsen, M.C., Torres-Sánchez, A.J., and Concepcion, I.M., 1999, Slopewash, surface runoff and fine-litter transport in forest and landslide scars in humid-tropical steeplands, Luquillo Experimental Forest, Puerto Rico: *Earth Surface Processes and Landforms*, v. 24, no. 6, p. 481–502.
- Larsen, M.C., Vásquez Conde, M.T., and Clark, R.A., 2001, Landslide hazards associated with flash-floods, with examples from the December 1999 disaster in Venezuela, in Grunfest, Eve, and Handmer, J., eds., *Coping with flash floods: Dordrecht, Holland, Kluwer Academic Publishers, NATO ASI Series C: Mathematical and Physical Sciences*, p. 259–275.
- Leithold, E.L., and Blair N.E., 2001, Watershed control on the carbon loading of marine sedimentary particles: *Geochimica et Cosmochimica Acta*, v. 54, no. 14, p. 2231–2240.

- Lyons, W.B., Nezat, C.A., Carey, A.E., and Hicks, D.M., 2002, Organic carbon fluxes to the ocean from high-standing islands: *Geology*, v. 30, no. 5, p. 443–446.
- Mackenzie, R.C., ed., 1957, Differential thermal analysis of clays: London, Mineralogical Society, 389 p.
- Mackenzie, R.C., and Caillère, S., 1979, Thermal analysis, DTA, TG, DTG, in Van Olphen, Hendrik, and Fripiat, J.J., eds., *Data handbook for clay material and other non-metallic minerals*: New York, Pergamon, p. 243–284.
- McDowell, W.H., 1998, Internal nutrient fluxes in a Puerto Rican rain forest: *Journal of Tropical Ecology*, v. 14, p. 521–536.
- McDowell, W.H., and Asbury, C.E., 1994, Export of carbon, nitrogen, and major ions from three tropical montane watersheds: *Limnology and Oceanography*, v. 39, no. 1, p. 111–125.
- McDowell, W.H., Bowden, W.B., and Asbury, C.E., 1992, Riparian nitrogen dynamics in two geomorphologically distinct tropical rain-forest watersheds—Subsurface solute patterns: *Biogeochemistry*, v. 18, no. 2, p. 53–75.
- Meybeck, Michel, 1979, Concentration des eaux fluviales en éléments majeurs et apports en solution aux océans: *Revue de Géologie Dynamique et de Géographie Physique*, v. 21, no. 3, p. 215–246.
- Meybeck, Michel, 1993, Riverine transport of atmospheric carbon—Sources, global typology, and budget: *Water, Air, and Soil Pollution*, v. 70, p. 443–463.
- Meybeck, Michel, 2003, Global analysis of river systems—From earth system controls to anthropocene syndromes: *Philosophical Transactions of the Royal Society [London] Series B—Biological Sciences*, v. 358, no. 1440, p. 1935–1955.
- Milliman, J.D., and Meade, R.H., 1983, World-wide delivery of river sediment to the oceans: *Journal of Geology*, v. 91, p. 1–21.
- Milliman, J.D., and Syvitski, J.P.M., 1992, Geomorphic/tectonic control of sediment discharge to the ocean—The importance of small mountainous rivers: *Journal of Geology*, v. 100, p. 525–544.
- Molnia, B.F., and Hallam, C.A., 1999, Open skies aerial photography of selected areas in Central America affected by Hurricane Mitch: U.S. Geological Survey Circular 1181, 82 p., 1 CD-ROM.
- Montgomery, D.R., and Dietrich, W.E., 1994, A physically based model for the topographic control on shallow landsliding: *Water Resources Research*, v. 30, no. 4, p. 1153–1171.
- Montgomery, D.R., Schmidt, K.M., Greenberg, H.M., and Dietrich, W.E., 2000, Forest clearing and regional landsliding: *Geology*, v. 28, no. 4, p. 311–314.
- Murphy, S.F., Brantley, S.L., Blum, A.E., White, A.F., and Dong, H., 1998, Chemical weathering in a tropical watershed, Luquillo Mountains, Puerto Rico—II. Rate and mechanism of biotite weathering: *Geochimica et Cosmochimica Acta* v. 62, p. 227–243.
- Murphy, S.F., and Stallard, R.F., 2012, Hydrology and climate of four watersheds in eastern Puerto Rico, ch. C in Murphy, S.F., and Stallard, R.F., eds., *Water quality and landscape processes of four watersheds in eastern Puerto Rico: U.S. Geological Survey Professional Paper 1789*, p. 43–84.
- Murphy, S.F., Stallard, R.F., Larsen, M.C., and Gould, W.A., 2012, Physiography, geology, and land cover of four watersheds in eastern Puerto Rico, ch. A in Murphy, S.F., and Stallard, R.F., eds., *Water quality and landscape processes of four watersheds in eastern Puerto Rico: U.S. Geological Survey Professional Paper 1789*, p. 1–24.
- Pacala, S.W., Hurt, G.C., Baker, D., Peylin, P., Houghton, R.A., Birdsey, R.A., Heath, L., Sundquist, E.T., Stallard, R.F., Ciais, P., Moorcroft, P., Caspersen, J.P., Shevliakova, E., Moore, B., Kohlmaier, G., Holland, E., Gloor, M., Harmon, M.E., Fan, S.M., Sarmiento, J.L., Goodale, C.L., Schimel, D., and Field, C.B., 2001, Consistent land- and atmosphere-based U.S. carbon sink estimates: *Science*, v. 292, no. 5525, p. 2316–2320.
- Parfitt, R.L., 2009, Allophane and imogolite—Role in soil biogeochemical processes: *Clay Minerals*, v. 44, p. 135–155.
- Peters, N.E., Shanley, J.B., Aulenbach, B.T., Webb, R.M., Campbell, D.H., Hunt, R., Larsen, M.C., Stallard, R.F., Troester, J., and Walker, J.F., 2006, Water and solute mass balance of five small, relatively undisturbed watersheds in the U.S.: *Science of the Total Environment*, v. 358, p. 221–242.
- Petsch, S.T., Berner, R.A., and Eglington, T.I., 2000, A field study of the chemical weathering of ancient sedimentary organic matter: *Organic Geochemistry*, v. 31, p. 475–487.
- Petsch, S.T., Eglington, T.I., and Edwards, K.J., 2001, ¹⁴C-dead living biomass—Evidence for microbial assimilation of ancient organic carbon during shale weathering: *Science*, v. 292, p. 1127–1131.
- Pett-Ridge, J.C., 2009, Contributions of dust to phosphorus cycling in tropical forests of the Luquillo Mountains, Puerto Rico: *Biogeochemistry*, v. 96, no. 1, p. 63–80.
- Pett-Ridge, J.C., Derry, L.A., and Barrows, J.K., 2009, Ca/Sr and ⁸⁷Sr/⁸⁶Sr ratios as tracers of Ca and Sr cycling in the Río Icacos watershed, Luquillo Mountains, Puerto Rico: *Chemical Geology*, v. 94, no. 1, p. 64–80.
- Pett-Ridge, J.C., Derry, L.A., and Kurtz, A.C., 2008, Sr isotopes as a tracer of weathering processes and dust inputs in a tropical granitoid watershed, Luquillo Mountains, Puerto Rico: *Geochimica et Cosmochimica Acta*, v. 73, p. 25–43.

- Prentice, I.C., Farquhar, G.D., Fasham, M.J.R., Goulden, M.L., Heimann, M., Jaramillo, V.J., Kheshgi, H.S., Le Quéré, C., Scholes, R.J., and Wallace, D.W.R., 2001, The carbon cycle and atmospheric carbon dioxide, *in* Houghton, J.T., Ding, Y., Griggs, D.J., Noguer, M., van der Linden, P.J., Dai, X., Maskell, K., and Johnson, C.A., eds., Climate change 2001—The scientific basis. Contribution of Working Group I to the third assessment report of the Intergovernmental Panel on Climate Change: Cambridge, United Kingdom, Cambridge University Press, p. 183–237.
- Quinton, J.N., Govers, G., Van Oost, K., and Bardgett, R.D., 2010, The impact of agricultural soil erosion on biogeochemical cycling: *Nature Geoscience*, v. 3, p. 1–4; doi 10.1038/ngeo838.
- Reid, L.M., 1998, Calculation of average landslide frequency using climatic records: *Water Resources Research*, v. 34, no. 4, p. 869–877.
- Runkel, R.L., Crawford, C.G., and Cohn, T.A., 2004, Load Estimator (LOADEST)—A FORTRAN program for estimating constituent loads in streams and rivers: U.S. Geological Survey Techniques and Methods Book 4–A5, 75 p.; program, test files.
- Sarmiento, J.L., and Sundquist, E.T., 1992, Revised budget for the oceanic uptake of anthropogenic carbon dioxide: *Nature*, v. 356, p. 389–393.
- Scatena, F.N., and Larsen, M.C., 1991, Physical aspects of Hurricane Hugo in Puerto Rico: *Biotropica*, v. 23, p. 317–323.
- Schellekens, Jaap, Scatena, F.N., Bruijnzeel, L.A., van Dijk, A.I.J.M., Groen, M.M.A., and van Hogenzand, R.J.P., 2004, Stormflow generation in a small rainforest catchment in the Luquillo Experimental Forest, Puerto Rico: *Hydrological Processes*, v. 18, p. 505–530.
- Schneider, S.H., 2009, The worst-case scenario: *Nature*, v. 459, p. 1104–1105.
- Schulz, M.S., and White, A.F., 1999, Chemical weathering in a tropical watershed, Luquillo Mountains, Puerto Rico—III. Quartz dissolution rates: *Geochimica et Cosmochimica Acta*, v. 63, no. 3–4, p. 337–350.
- Science Magazine, 2011, News focus—A global perspective on the Anthropocene: *Science*, v. 334, p. 34–35.
- Shanley, J.B., McDowell, W.H., and Stallard, R.F., 2011, Long-term patterns and short-term dynamics of stream solutes and suspended sediment in a rapidly weathering tropical watershed: *Water Resources Research*, doi no. 10.1029/2010WR009788.
- Simon, Andrew, Larsen, M.C., and Hupp, C.R., 1990, The role of soil processes in determining mechanisms of slope failure and hillslope development in a humid-tropical forest, eastern Puerto Rico: *Geomorphology*, v. 3, p. 263–286.
- Simonett, D.S., 1967, Landslide distribution and earthquakes in the Bewani and Torricelli Mountains, New Guinea—A statistical analysis, *in* Jennings, J.N., and Mabbutt, J.A., eds., Landform studies from Australia and New Guinea: Canberra, Australian National University Press, p. 64–84.
- Smith, A.L., Schellekens, J.H., and Diaz, A.-L.M., 1998, Batholiths as markers of tectonic change in the northeastern Caribbean, *in* Lidiak, E.G., and Larue, D.K., eds., Tectonics and geochemistry of the northeastern Caribbean: Geological Society of America Special Paper 322, p. 99–122.
- Stallard, R.F., 1985, River chemistry, geology, geomorphology, and soils in the Amazon and Orinoco Basins, *in* Drever, J.I., ed., The chemistry of weathering: Dordrecht, Holland, D. Reidel Publishing Co., NATO ASI Series C—Mathematical and Physical Sciences, v. 149, p. 293–316.
- Stallard, R.F., 1988, Weathering and erosion in the humid tropics, *in* Lerman, Abraham, and Meybeck, M., eds., Physical and chemical weathering in geochemical cycles: Dordrecht, Holland, Kluwer Academic Publishers, NATO ASI Series C—Mathematical and Physical Sciences, v. 251, p. 225–246.
- Stallard, R.F., 1995a, Relating chemical and physical erosion, *in* White, A.F., and Brantley, S.L., eds., Chemical weathering rates of silicate minerals: Washington, D.C., Mineralogical Society of America Reviews in Mineralogy and Geochemistry, v. 31, p. 543–564.
- Stallard, R.F., 1995b, Tectonic, environmental, and human aspects of weathering and erosion—A global review using a steady-state perspective: *Annual Review of Earth and Planetary Sciences*, v. 12, p. 11–39.
- Stallard, R.F., 1998, Terrestrial sedimentation and the carbon cycle—Coupling weathering and erosion to carbon burial: *Global Biogeochemical Cycles*, v. 12, no. 2, p. 231–252.
- Stallard, R.F., 1999, Erosion and the effects of deforestation in the Panama Canal Basin, *in* Panama Canal Watershed Monitoring Project, ed., Report of the Panama Canal Watershed Monitoring Project: Panama City, Panama, Smithsonian Tropical Research Institute, ch. II.8, 8 volumes, 21 CD-ROMs.
- Stallard, R.F., 2012, Atmospheric inputs to watersheds in the Luquillo Mountains of eastern Puerto Rico, ch. D *in* Murphy, S.F., and Stallard, R.F., eds., Water quality and landscape processes of four watersheds in eastern Puerto Rico: U.S. Geological Survey Professional Paper 1789, p. 85–112.
- Stallard, R.F., and Edmond, J.M., 1981, Geochemistry of the Amazon 1. Precipitation chemistry and the marine contribution to the dissolved load at the time of peak discharge: *Journal of Geophysical Research—Oceans and Atmospheres*, v. 86, p. 9844–9858.

- Stallard, R.F., and Edmond, J.M., 1983, Geochemistry of the Amazon 2. The influence of the geology and weathering environment on the dissolved load: *Journal of Geophysical Research—Oceans and Atmospheres*, v. 88, p. 9671–9688, microfiche supplement.
- Stallard, R.F., and Edmond, J.M., 1987, Geochemistry of the Amazon 3—Weathering chemistry and limits to dissolved inputs: *Journal of Geophysical Research*, v. 92, p. 8293–8302.
- Stallard, R.F., and Kinner, D.A., 2005, Estimation of landslide importance in hillslope erosion within the Panama Canal watershed, in Harmon, R.S., ed., *The Rio Chagres, Panama—A multidisciplinary profile of a tropical watershed*: Dordrecht, The Netherlands, Springer Water Science and Technology Library, v. 52, p. 281–295.
- Stallard, R.F., Koehnken, L., and Johnsson, M.J., 1991, Weathering processes and the composition of inorganic material transported through the Orinoco River system, Venezuela and Colombia: *Geoderma*, v. 51, p. 133–165.
- Stallard, R.F., and Murphy, S.F., 2012, Water quality and mass transport in four watersheds in eastern Puerto Rico, ch. E in Murphy, S.F., and Stallard, R.F., eds., *Water quality and landscape processes of four watersheds in eastern Puerto Rico*: U.S. Geological Survey Professional Paper 1789, p. 113–152.
- Starkel, Leszek, 1972, The role of catastrophic rainfall in the shaping of the relief of the Lower Himalaya (Darjeeling Hills): *Geographia Polonica*, v. 21, p. 103–147.
- Striegl, R.G., Dornblaser, M.M., Aiken, G.R., Wickland, K.P., and Raymond, P.A., 2007, Carbon export and cycling by the Yukon, Tanana, and Porcupine rivers, Alaska, 2001–2005: *Water Resources Research*, v. 43, p. W02411.
- Stumm, Werner, and Morgan, J.J., 1981, *Aquatic chemistry*: New York, John Wiley, 780 p.
- Syvitski, J.P.M., Vörösmarty, C.J., Kettner, A.J., and Green, P., 2005, Impact of humans on the flux of terrestrial sediment to the global coastal ocean: *Science*, v. 308, p. 376–380.
- Tardy, Yves, Bustillo, V., Roquin, C., Mortatti, J., and Reynaldo, R., 2005, The Amazon—Bio-geochemistry applied to river basin management, part I. Hydro-climatology, hydrograph separation, mass transfer balances, stable isotopes, and modelling: *Applied Geochemistry*, v. 20, p. 1746–1829.
- Turner, B.F., Stallard, R.F., and Brantley, S.L., 2003, Investigation of *in situ* weathering of quartz diorite bedrock in the Río Icacos Basin, Luquillo Experimental Forest, Puerto Rico: *Chemical Geology*, v. 202, no. 3–4, p. 313–341.
- U.S. Geological Survey, 2007, Facing tomorrow's challenges—U.S. Geological Survey science in the decade 2007–2017: U.S. Geological Survey Circular 1309, x + 70 p.
- United Nations Environment Programme World Conservation Monitoring Centre, 2002, *Mountain Watch, 2002—Environmental change and sustainable development in mountains*: Cambridge, United Kingdom, United Nations Environment Programme World Conservation Monitoring Centre, 80 p.
- Van Oost, Kristof, Quine, T.A., Govers, G., De Gryze, S., Six, J., Harden, J.W., Ritchie, J.C., McCarty, G.W., Heckrath, G., Kosmas, C., Giraldez, J.V., Marques da Silva, J.R., and Merckx, R., 2007, The impact of agricultural soil erosion on the global carbon cycle: *Science*, v. 318, p. 626–629.
- Van Oost, Kristof, Six, J., Govers, G., Quine, T.A., and De Gryze, S., 2008, Soil erosion—A carbon sink or source? Response: *Science*, v. 319, p. 1040.
- Ver, L.M.B., Mackenzie, F.T., and Lerman, A., 1999, Carbon cycle in the coastal zone—Effects of global perturbations and change in the past three centuries: *Chemical Geology*, v. 159, p. 283–304.
- Walker, L.R., Zarin, D.J., Fetcher, N., Myster, R.W., and Johnson, A.H., 1996, Ecosystem development and plant succession on landslides in the Caribbean: *Biotropica*, v. 28, no. 4a, p. 566–576.
- Webb, Richard, 2006, Cartography—A popular perspective: *Nature*, v. 439, p. 800.
- White, A.F., 2002, Determining mineral weathering rates based on solid and solute weathering gradients and velocities—Application to biotite weathering in saprolites: *Chemical Geology*, v. 190, p. 69–89.
- White, A.F., and Blum, A.E., 1995, Effects of climate on chemical weathering in watersheds: *Geochimica et Cosmochimica Acta*, v. 59, no. 9, p. 1729–1747.
- White, A.F., Blum, A.E., Bullen, T.D., Vivit, D.V., Schulz, M.S., and Fitzpatrick, J., 1999a, The effect of temperature on experimental and natural chemical weathering rates of granitoid rocks: *Geochimica et Cosmochimica Acta*, v. 63, no. 19–20, p. 3277–3291.
- White, A.F., Blum, A.E., Schulz, M.S., Vivit, D.V., Stonestrom, D.A., Larsen, M.C., Murphy, S.F., and Eberl, D., 1998, Chemical weathering in a tropical watershed, Luquillo Mountains, Puerto Rico—I. Long-term versus short-term weathering fluxes: *Geochimica et Cosmochimica Acta*, v. 62, no. 2, p. 209–226.
- White, A.F., Blum, A.E., Schulz, M.S., Vivit, D.V., Clow, D.W., and Bullen, T.D., 1999b, The role of disseminated calcite in the chemical weathering of granitoid rocks: *Geochimica et Cosmochimica Acta*, v. 63, no. 13–14, p. 1939–1953.
- Zack, A.L., and Larsen, M.C., 1993, Island hydrology—Puerto Rico and the U.S. Virgin Islands: *National Geographic Research and Exploration—Water Issue*, p. 126–134.

- Zarin, D.J., 1993, Nutrient accumulation during succession in subtropical lower montane wet forests, Puerto Rico: Philadelphia, University of Pennsylvania, Ph.D. dissertation, 182 p.
- Zarin, D.J., and Johnson, A.H., 1995a, Base saturation, nutrient cation, and organic matter increases during early pedogenesis on landslide scars in the Luquillo Experimental Forest, Puerto Rico: *Geoderma*, v. 65, no. 3–4, p. 317–330.
- Zarin, D.J., and Johnson, A.H., 1995b, Nutrient accumulation during primary succession in a montane tropical forest, Puerto Rico: *Soil Science Society of America Journal*, v. 59, no. 5, p. 1444–1452.
- Ziegler, Karen, Chadwick, O.A., White, A.F., and Brzezinski, M.A., 2005, $\delta^{30}\text{Si}$ systematics in a granitic saprolite, Puerto Rico: *Geology*, v. 33, no. 10, p. 817–820.

Weathering Processes in the Icacos and Mameyes Watersheds in Eastern Puerto Rico

By Heather L. Buss and Arthur F. White

Chapter I of
**Water Quality and Landscape Processes of Four Watersheds in
Eastern Puerto Rico**

Edited by Sheila F. Murphy and Robert F. Stallard

Professional Paper 1789-I

**U.S. Department of the Interior
U.S. Geological Survey**

Contents

Abstract.....	253
Introduction.....	253
Weathering Processes at the Bedrock Interface	256
Weathering Processes in the Saprolite and Soil	260
Summary.....	260
References.....	260

Figures

1. Map showing location and geology of Icacos and Mameyes watersheds.....255
2. Photograph showing a corestone of Río Blanco quartz diorite that is weathering spheroidally.....256
3. Schematic diagram of the weathering profile in the Icacos watershed.....257
4. Backscattered electron images of thin sections taken from a corestone-rindlet complex, Icacos watershed.....258

Abbreviations Used in This Report

≈	nearly equal to
^{30}Si	ratio of stable isotopes of silicon, $^{30}\text{Si}/^{28}\text{Si}$, relative to a standard
Å	angstrom
$\mu\text{mol mol}^{-1}$	micromoles per mole
cm	centimeter
km^2	square kilometer
m	meter
Ma	million years old
m m.y.^{-1}	meters per million years
$\text{mol m}^{-2} \text{s}^{-1}$	moles per square meter per second
ICP–OES	inductively coupled plasma–atomic emission spectroscopy
WEBB	Water, Energy, and Biogeochemical Budgets
XRD	X-ray diffraction

Conversion Factors

Multiply	By	To obtain
Length		
centimeter (cm)	0.3937	inch (in.)
meter (m)	3.281	foot (ft)
Area		
square kilometer (km^2)	0.3861	square mile (mi^2)
Weathering rate		
meters per million years (m m.y.^{-1})	3.281	feet per million years (ft m.y.^{-1})

Weathering Processes in the Icacos and Mameyes Watersheds in Eastern Puerto Rico

By Heather L. Buss and Arthur F. White

Abstract

Streams draining watersheds of the two dominant lithologies (quartz diorite and volcaniclastic rock) in the Luquillo Experimental Forest of eastern Puerto Rico have very high fluxes of bedrock weathering products. The Río Blanco quartz diorite in the Icacos watershed and the Fajardo volcaniclastic rocks in the Mameyes watershed have some of the fastest documented rates of chemical weathering of siliceous rocks in the world. Rapid weathering produces thick, highly leached saprolites in both watersheds that lie just below the soil and largely isolate subsurface biogeochemical and hydrologic processes from those in the soil. The quartz diorite bedrock in the Icacos watershed weathers spheroidally, leaving large, relatively unweathered corestones that are enveloped by slightly weathered rock layers called rindlets. The rindlets wrap around the corestones like an onionskin.

Within the corestones, biotite oxidation is thought to induce the spheroidal fracturing that leads to development of rindlets; plagioclase in the rindlets dissolves, creating additional pore spaces. Near the rindlet-saprolite interface, the remaining plagioclase dissolves, hornblende dissolves to completion, and precipitation of kaolinite, gibbsite, and goethite becomes pervasive. In the saprolite, biotite weathers to kaolinite and quartz begins to dissolve. In the soil layer, both quartz and kaolinite dissolve. The volcaniclastic bedrock of the Mameyes watershed weathers even faster than the quartz diorite bedrock of the Icacos watershed, leaving thicker saprolites that are devoid of all primary minerals except quartz. The quartz content of volcaniclastic bedrock may help to control watershed geomorphology; high-quartz rocks form thick saprolites that blanket ridges.

Hydrologic flow paths within the weathering profiles vary with total fluid flux, and they influence the chemistry of streams. Under low-flow conditions, the Río Icacos and its tributaries are fed by rainfall and by groundwater from the fracture zones; during storm events, intense rainfall rapidly raises stream levels and water is flushed through the soil as shallow flow. As a result, weathering constituents that shed into streamwaters are dominated by rindlet-zone weathering processes during base flow and by soil weathering processes during stormflow. The upper reaches of the Mameyes watershed are characterized by regolith more than 35 meters thick

in places that contains highly fractured rock embedded in its matrix. Weathering contributions to stream chemistry at base flow are predicted to be more spatially variable in the Mameyes watershed than in the Icacos watershed owing to the more complex subsurface weathering profile of the volcaniclastic bedrocks of the Mameyes watershed.

Introduction

Biogeochemical and physical weathering processes in tropical watersheds produce most of the solutes and sediments discharged to the oceans. These watersheds contribute 50 percent of the water, 38 percent of the dissolved ions, and 65 percent of the dissolved silica in the oceans, despite covering only about 25 percent of the terrestrial surface (Stallard and Edmond, 1983; Meybeck, 1987). Thus, relative to their area, tropical systems are disproportionately important in terms of weathering, erosion, and global CO₂ cycles. In addition to influencing stream and ocean chemistry and sediment loads, weathering processes exert control over chemical transport through soils and regolith (such as saprolite), soil and saprolite formation rates, mineral nutrient availability, and microbial growth rates. Weathering processes are complex phenomena comprising coupled chemical, physical, and microbial processes, driven by water and oxygen fluxes. These coupled processes also control the shape, position, stability, and rate of retreat of the bedrock weathering interface, which in turn affect topography and erosion.

To date (2012), the majority of research into weathering processes in the four U.S. Geological Survey Water, Energy, and Biogeochemical Budgets program (WEBB) watersheds in eastern Puerto Rico has focused on the Icacos watershed. This watershed is an ideal site for studying tropical weathering processes, because it is relatively pristine, small (3.3 square kilometers (km²)), and lithologically homogeneous (99 percent Río Blanco quartz diorite; Murphy and others, 2012). Thick saprolite profiles on ridge tops allow analysis of deep weathering and the cycling of chemical elements—processes that are not directly coupled with the surficial environment. The homogeneity of the quartz diorite (relative to the volcaniclastic units that dominate the Mameyes watershed) also considerably simplifies interpretation of the weathering profiles. Currently, a subwatershed of the

Mameyes watershed, Bisley 1 (fig. 1), is being investigated and compared with the Icacos watershed in order to better understand the influence of lithology on weathering processes, weathering fluxes, and mineral nutrient availability.

Weathering processes within the Bisley 1 watershed are spatially more variable than in the Icacos watershed owing to the more varied lithology of the parent rock. The Bisley 1 watershed is underlain by the Fajardo Formation, a marine-bedded volcaniclastic bedrock that is mapped as having several units: an upper thin-bedded tuffaceous siltstone and sandstone, an upper thick-bedded tuff, a lower thin-bedded tuffaceous sandstone and siltstone, a lower thick-bedded tuff, and an undivided unit (Briggs and Aguilar-Cortés, 1980). Bed thicknesses differ, and coarse tuff, breccias, and cherty or calcareous siltstone beds are found in some units. Although the few bedrock exposures in the Bisley watershed appear homogeneous, the watershed is underlain by the upper thick-bedded tuff unit, which includes some breccias, lithic andesitic clasts, calcareous siltstone, and some pumice and red scoria. Spheroidally weathered, marine-bedded, volcaniclastic sandstones are occasionally exposed by landslides. Weathered, quartz-rich clasts, which may be relict quartz veins, are found in the Bisley regolith.

In contrast to the high quartz content of the Río Blanco quartz diorite (\approx 20–30 percent by weight; White and others, 1998; Turner and others, 2003; Buss and others, 2008), which creates a weathering-resistant matrix that supports isovolumetric weathering to form saprolite, the bluish-gray tuffaceous rock commonly found in the Bisley streambeds contains very little quartz (\approx 7 percent, as analyzed by X-ray diffraction (XRD) and quantified using the program Rock-Jock as described by Eberl, 2003). Without a quartz matrix to support the volume during chemical weathering, these volcaniclastic rocks likely dissolve completely or collapse in volume during weathering. However, quartz-rich saprolites (as much as 65 percent) greater than 35 meters (m) deep are found in the Bisley watershed, indicating formation from a parent rock with a higher quartz content than the rocks commonly encountered in the Bisley watershed today. Similar rocks, but with higher quartz content (\approx 22–27 percent) may be exposed after relatively deep landslides in the Bisley 1 watershed and within a few kilometers to the east. These rocks may have been hydrothermally altered by infiltrating Si-rich fluids during intrusion of the Río Blanco stock. Thus, saprolite-mantled ridges in the Bisley watershed likely formed from these relatively quartz-rich rocks.

Both the quartz-rich and quartz-poor volcaniclastic rocks in the Bisley watershed contain similar amounts of chlorite (20–25 percent) and pyroxene (5–10 percent), but they diverge in feldspar content: about 35 and 50 percent, respectively. The Bisley saprolite contains \approx 15–65 percent microcrystalline quartz into which are embedded sparse, small, weathered, quartz-rich clasts (as much as \approx 80 percent quartz) that may represent relict quartz veins. Typically, quartz content by weight is higher in weathered materials, such as saprolite, relative to the parent rock. When other minerals weather and

elements such as Ca, Na, Mg, and K are lost from the system, quartz makes up a larger proportion of the remaining mass than it did originally. Similarly, elements that are relatively immobile during chemical weathering, such as Ti and Zr, are also more abundant in saprolite relative to parent rock in both the Bisley watershed (bulk chemistry measured by inductively coupled plasma–atomic emission spectroscopy (ICP–OES) after lithium metaborate fusion) and Icacos watershed (White and others, 1998; Buss and others, 2005, 2008).

The Fajardo Formation, which underlies the Bisley watershed, is older than the granitic intrusion underlying the Icacos watershed, \approx 100 million years old (Ma) as compared with 47 Ma, respectively (Jolly and others, 1998; Smith and others, 1998). Regolith in the Bisley 1 watershed is also thicker than in the Icacos watershed: about 10–20 m and 5–9 m on ridge tops in the Bisley and Icacos watersheds, respectively (White and others, 1998; Schellekens and others, 2004; Buss and others, 2005). Borehole drilling on a road in the Bisley 1 watershed recovered regolith cores more than 35 m deep, within which were embedded highly fractured rock in varying stages of weathering. These cores may contain a combination of transported material (such as from old landslides) and saprolite (which is formed in place, by definition). A 29-m-deep borehole on a road in the Icacos watershed passed through 5 m of saprolite, followed by a fractured-bedrock zone less than 1 m thick, and finally through 23 m of solid, unfractured, quartz diorite bedrock. A saprolite-production rate (or bedrock-weathering rate) of 211 meters per million years ($m\ m.y.^{-1}$) has been estimated for a Bisley ridgeline (Dosseto and others, 2011), which is considerably faster than the 43–58 $m\ m.y.^{-1}$ rate estimated for the Icacos watershed (Brown and others, 1995; White and others, 1998; Riebe and others, 2003, 2004). The bedrock weathering rates of both watersheds are also high relative to weathering rates of siliceous bedrock (such as basalts, andesites, granitoids, and schists) in watersheds around the world (White and others, 1998; Freyssinet and Farah, 2000; Navarre-Sitchler and Brantley, 2007; Dosseto and others, 2011).

The Bisley saprolite is about 60–80 weight percent clay (primarily microcrystalline, disordered kaolinite) and is completely devoid of primary minerals except quartz, indicating an advanced stage of weathering (mineralogy analyzed by XRD). The kaolinite contains impurities of Mg, Fe, and K that are released as the kaolinite itself dissolves with time. The Icacos saprolite contains primary biotite, which releases appreciable Mg, K, and Fe during transformation to kaolinite throughout the saprolite (Murphy and others, 1998).

The remainder of this chapter discusses weathering processes in the Icacos watershed (fig. 1), which has been studied in much greater detail than the Mameyes watershed. The Río Blanco quartz diorite weathers in place along joint planes, forming rounded bedrock corestones (as much as about 2 m diameter), which then weather spheroidally (fig. 2). Onionskin-like layers (rindlets) form on the corestones during spheroidal weathering; continued weathering of the corestones produces a thick (about 2–8 m) saprolite overlain by

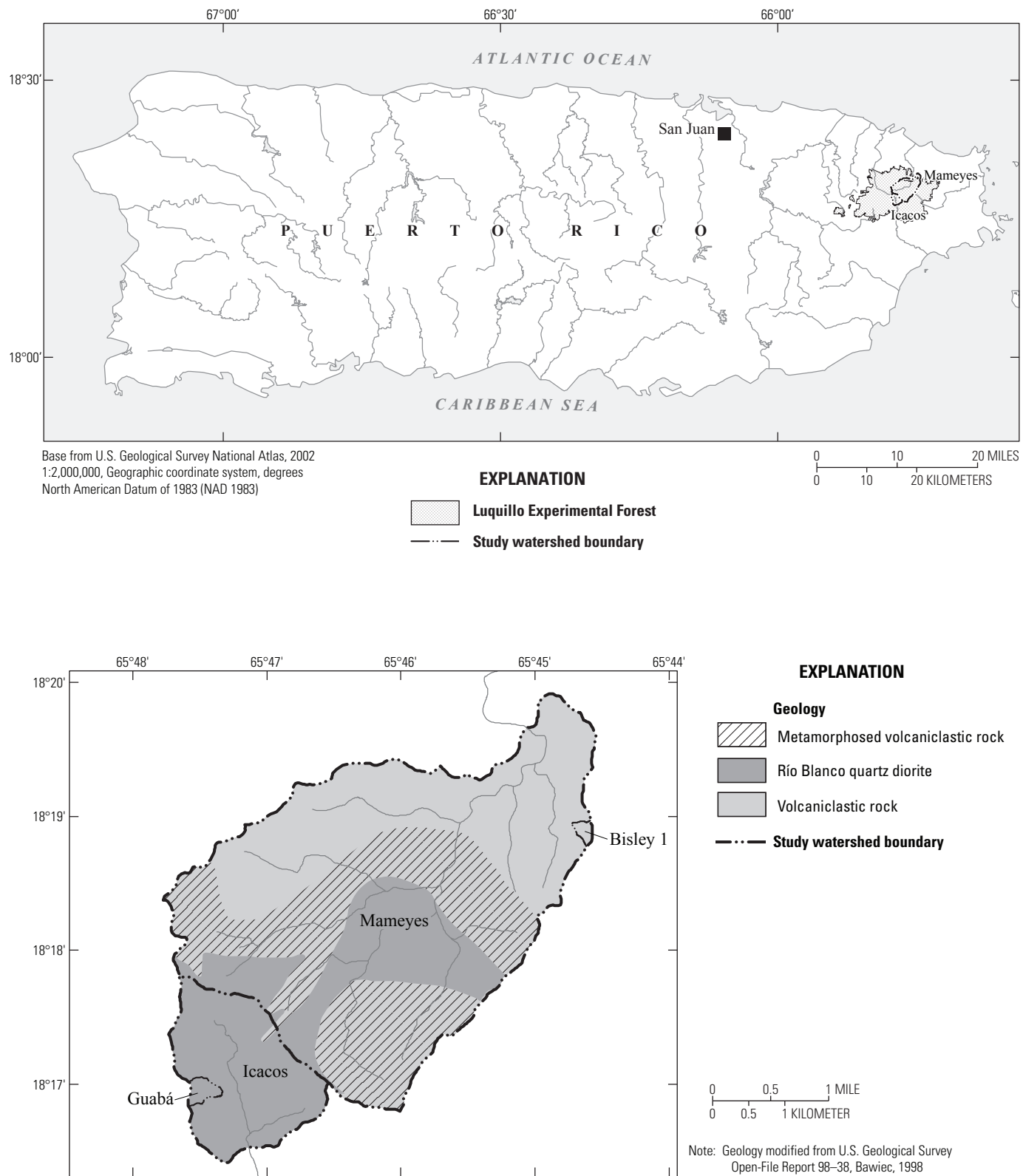


Figure 1. Location and geology of Icacos and Mameyes watersheds. (Geology adapted from Bawiec (1998); metamorphic contact from Seiders (1971) and Briggs and Aguilar-Cortés (1980), with digital interpretation by F.N. Scatena and Miguel Leon, University of Pennsylvania Luquillo Critical Zone Observatory; Bisley 1 watershed boundary courtesy Miguel Leon, University of Pennsylvania; Guabá watershed boundary courtesy Sheila Murphy, U.S. Geological Survey.)



Figure 2. Sampled roadcut 600 meters southeast of the mouth of the Icacos watershed showing a 2-meter diameter corestone of Río Blanco quartz diorite that is weathering spheroidally. A 49-centimeter-thick zone of partially weathered rock layers called rindlets surrounds the corestone. The string grid (at an angle to the camera) partitions the outcrop into 1-square-meter blocks.

thin (about 0.5–1 m) soils. The resulting weathering profile is characterized by multiple interfaces that define distinct zones in which weathering processes differ and, in some cases, operate independently of the processes operating within the other zones. Here we will discuss weathering processes in individual zones from the fresh bedrock upward to the surface soil.

Weathering Processes at the Bedrock Interface

Weathering of fresh, intact bedrock is the initial step in the soil-forming process and is the primary contributor of chemical solutes to the hydrosphere—groundwater, streams, precipitation, and oceans. Interfaces where intact bedrock weathers to disaggregated material, such as saprolite, are controlled by coupled chemical, physical, and microbial processes driven by the flux of reactants to the fresh rock. The rate at

which the bedrock weathers determines the rate at which the interface moves downward, the rate of formation of the saprolite, the flux of mineral nutrients to the biosphere, and the flux of solutes to the hydrosphere.

A spheroidally weathering interface, such as in the Río Blanco quartz diorite, provides a model environment for studying the coupling of physical and chemical processes involved in rock weathering and saprolite formation. Spheroidal weathering is a well-known, but poorly understood, form of exfoliation that has been linked to chemical weathering (for example, Farmin, 1937; Ollier, 1971; Fletcher and others, 2006; Buss and others, 2008). Spheroidal weathering begins when bedrock joint planes are exposed to weathering, which rounds off corners in place to form boulders called corestones. Corestones then fracture parallel to and just below their surface, forming concentric layers called rindlets (Bisdom, 1967; Ollier, 1971; Fritz and Ragland, 1980; Turner and others, 2003; Buss and others, 2005, 2008). A complete set of rindlets (from corestone to saprolite) comprise a rindlet zone (fig. 3).

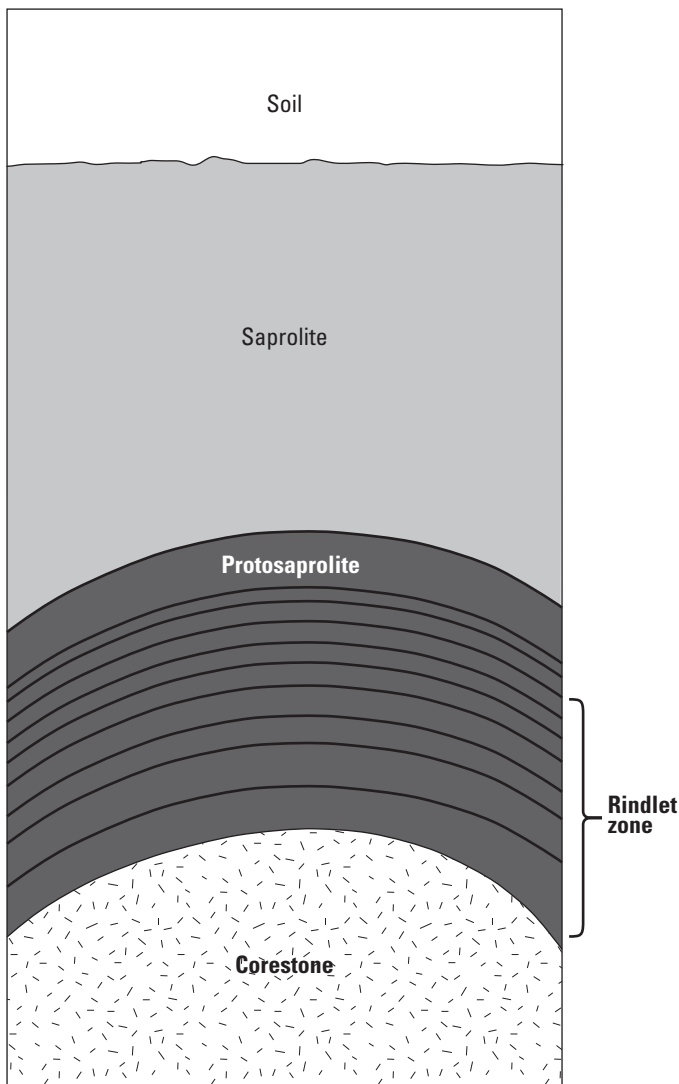


Figure 3. Generalized view of the weathering profile in the Icacos watershed. Quartz diorite bedrock corestones weather spheroidally, producing a zone of concentric layers called rindlets. Rindlets transform into saprolite in a zone called protosaprolite or saprock, where weathering processes differ from those in either the rindlet zone or saprolite (Buss and others, 2008).

Rindlets are slightly weathered, but most are still relatively hard. The hand-friable outer rindlets (at the saprolite interface) are sometimes referred to as *saprock*, a material intermediate between saprolite and bedrock. Where rindlet zones are exposed by erosion (which is dominated by landslides; Larsen and Torres-Sánchez, 1998), they tend to slough off, leaving bare corestones. Corestone-rindlet complexes that remain in place at depth eventually weather to saprolite.

Expansion of a mineral during chemical weathering has been identified as a possible cause of spheroidal fracturing (for example, Larsen, 1948; Simpson, 1964; Eggler and others,

1969; Isherwood and Street, 1976; Begle, 1978; Chatterjee and Raymahashay, 1998; Fletcher and others, 2006; Buss and others, 2008). Although isovolumetric weathering is required to produce the overlying saprolite, Fletcher and others (2006) demonstrated quantitatively that only a very small net volume change is required to generate sufficient elastic strain energy to produce spheroidal fracturing as observed in the Río Blanco quartz diorite.

The rindlet zone in the Río Blanco quartz diorite is composed of a sequence of rindlets each about 2.5 centimeters (cm) thick, which are slightly weathered relative to the parent corestones (fig. 4). Within the rindlet zone, the transformation from bedrock to saprolite is accomplished. This transformation includes development of pore space, essentially complete loss (\approx 99 percent) of the primary minerals plagioclase, hornblende, chlorite, and apatite; oxidation of biotite; and formation of the secondary minerals kaolinite, gibbsite, and goethite (Buss and others, 2008, 2010). These weathering processes occur at different points within the rindlet zone but are interrelated. The transformation of bedrock to saprolite begins within the corestones. Aqueous oxygen contained in pore waters diffuses into the unweathered corestone and oxidizes Fe(II) in the biotite (Buss and others, 2008), which then expands in the $d(001)$ direction from 10.0 angstroms (\AA) to 10.5 \AA (Dong and others, 1998; Murphy and others, 1998). This modest expansion builds up elastic strain energy within the rock (Buss and others, 2008). When the elastic-strain-energy density reaches fracture surface energy, fracturing occurs, creating a rindlet (Fletcher and others, 2006). The oxidation of Fe(II) in biotite is initiated when dissolved oxygen diffuses into the corestones; thus the weathering rate depends on the concentration of oxygen in pore waters. This concentration is expected to decrease with increasing saprolite thickness, creating a positive feedback between erosion and weathering rates that may maintain profiles at steady state throughout geologic time (Fletcher and others, 2006).

A weathering front is a boundary layer, or zone, that separates weathered material from fresh rock. It is often defined in terms of a weathering reaction (for example, dissolution of a given mineral) such that the weathering front encompasses the entire zone where the weathering reaction occurs. For a mineral weathering reaction, the mineral becomes progressively more altered (or changes in abundance) within the weathering front. Turner and others (2003) conceptualized the spheroidal weathering system in the Río Blanco quartz diorite as consisting of many parallel weathering fronts that move inward toward each of the rindlet centers from their edges as well as inward towards the centers of the corestones. However, in detailed analyses of a complete rindlet sequence, Buss and others (2008) did not detect a trend in chemical weathering intensity within individual rindlets and proposed an alternative model. In this model, the entire rindlet zone and corestone is a single weathering front controlled by only two interfaces: the bedrock-rindlet interface and the rindlet-saprolite interface, which are coupled by the pore-space-forming processes of mineral dissolution and fracturing.

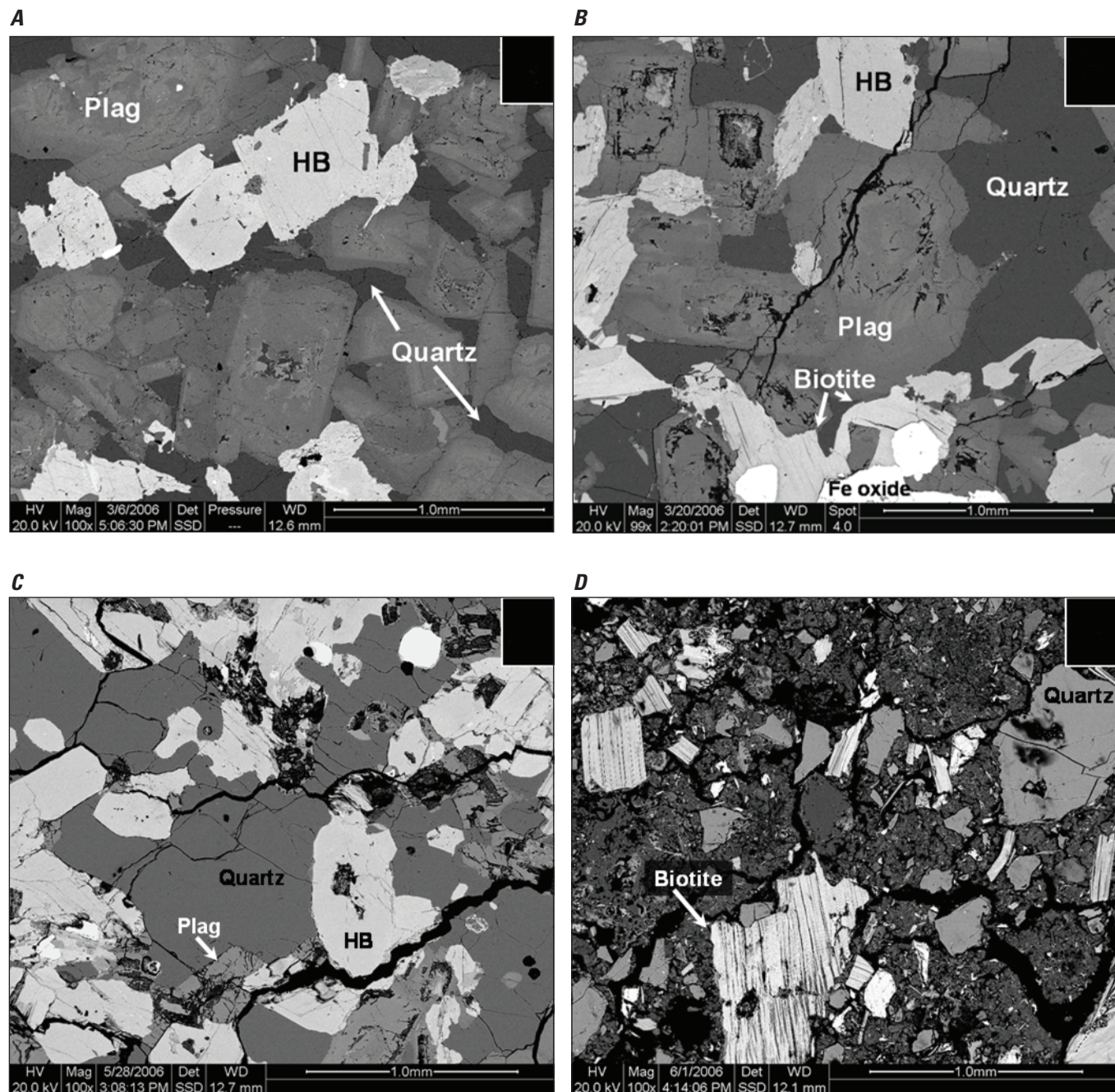


Figure 4. Backscattered electron images of thin sections taken from a corestone-rindlet complex exposed at a roadcut 600 meters southeast of the mouth of the Icacos watershed. *A*, Corestones are relatively unweathered and unfractured and are dominated by large zoned plagioclase crystals. *B*, A typical rindlet sampled from about 20 centimeters above the corestone (the entire rindlet sequence was 49 centimeters thick) contains microcracks, unaltered hornblende (HB), and pore space within plagioclase (Plag) crystals where calcic cores are weathering before sodic edges. *C*, Within the protosaprolite zone, a rindlet sampled from about 2 centimeters below the visible rindlet-saprolite interface contains unaltered quartz, highly weathered plagioclase (Plag) with gibbsite and kaolinite within the pore spaces, and slightly weathered hornblende (HB). *D*, Also within the protosaprolite zone, a sample taken from about 0.5 centimeter above the visible rindlet-saprolite interface contains quartz and visibly altered biotite; hornblende and plagioclase crystals are no longer visible. Large areas are filled with gibbsite and kaolinite (after Buss, 2006; Buss and others, 2008).

In a one-dimensional, steady-state profile, the loss of a mobile element or dissolving mineral can be modeled as a linear decrease with decreasing depth from the parent rock composition to some weathered composition. This linear decrease, or weathering gradient, is composed of two vectors: the weathering velocity (which equals rate of advance of the weathering front in a solid-state profile or the fluid flux in an aqueous profile) and the rate of loss of the individual mineral or element that defines the gradient (White, 2002). Solid-state gradients in Na, Fe(II), and P within a rindlet zone were used to calculate weathering rates for plagioclase dissolution (Na), biotite oxidation (Fe(II)), and apatite dissolution (P) (Buss and others, 2008, 2010).

Within the bulk of the rindlet zone, hornblende is relatively stable, whereas plagioclase dissolves at a rate of 90×10^{-14} moles per square meter per second ($\text{mol m}^{-2} \text{s}^{-1}$), biotite is oxidized at a rate of $3.1 \times 10^{-14} \text{ mol m}^{-2} \text{s}^{-1}$, and apatite dissolves at a rate of $6.8 \times 10^{-14} \text{ mol m}^{-2} \text{s}^{-1}$ (Buss and others, 2008, 2010). Concurrent with these mineral weathering reactions, the rindlets are further fractured by microcracks. Additional pore space develops by the dissolution of plagioclase; some of the dissolved constituents precipitate within the pore space as kaolinite and gibbsite (Murphy and others, 1998; Turner and others, 2003; Buss and others, 2004, 2008), whereas other constituents, notably Na and Ca, are lost from the profile. Sodium and calcium are abundant in all stream waters within the Icacos Basin (Bhatt and McDowell, 2007), reflecting plagioclase dissolution. The precipitation of kaolinite following plagioclase dissolution leads to an isotopically heavy $\delta^{30}\text{Si}$ signature (+0.8 per mil; ratio of stable isotopes of silicon, $^{30}\text{Si}/^{28}\text{Si}$, relative to international standard NBS-28) in pore waters from the deepest saprolite, because isotopically light Si is preferentially sequestered in the kaolinite (Ziegler and others, 2005). Similarly, Ge/Si ratios in deep saprolite pore waters are low ($\approx 1.0\text{--}2.0$ micromoles per mole ($\mu\text{mol mol}^{-1}$)) reflecting the dissolution of plagioclase ($\text{Ge/Si} = 1.5 \mu\text{mol mol}^{-1}$) and the formation of kaolinite enriched in Ge ($\text{Ge/Si} = 4.8\text{--}6.1 \mu\text{mol mol}^{-1}$, Lugolobi and others, 2010). Because plagioclase weathers only in the rindlet zone (White and others, 1998; Turner and others, 2003) and at the rindlet-saprolite interface (Buss and others, 2008), weathering at this interface is the primary control on Si flux into the deep saprolite pore waters. The low Ge/Si ratios of the deep saprolite pore waters are also reflected in stream waters in the Icacos and Guabá watersheds during base flow ($\text{Ge/Si} \approx 0.29 \mu\text{mol mol}^{-1}$), indicating that weathering at the rindlet zone is the primary contributor to stream-water Si during base flow (Lugolobi and others, 2010; Kurtz and others, 2011). Likewise, the isotopic composition of Si in stream waters in the Icacos watershed ($\delta^{30}\text{Si} = +1.2$ to $+1.5$ per mil during base flow) reflects weathering reactions (plagioclase and hornblende dissolution) that occur at the bedrock-saprolite interface (Ziegler and

others, 2005). During storm events, however, stream-water Ge/Si ratios are higher ($2.3 \mu\text{mol mol}^{-1}$) and $\delta^{30}\text{Si}$ values lower (+0.8 per mil), consistent with the shallow saprolite and soil zone Ge/Si ratios (2.3 to 3.3 and $4.6 \mu\text{mol mol}^{-1}$, respectively) and $\delta^{30}\text{Si}$ values (-0.8 and -1.4 to -1.7 per mil, respectively), indicating rapid flow of storm waters overland and through shallow subsurface zones (Ziegler and others, 2005; Kurtz and others, 2011).

The removal of soil and saprolite from bedrock and corestone-rindlet assemblages by landslides enhances access of reactants (such as oxygen, carbonic acid, and organic acids) to primary minerals such as plagioclase, hornblende, biotite, and apatite (Frizano and others, 2002; Bhatt and McDowell, 2007). This effect is more pronounced at higher elevations and is revealed in stream waters draining higher elevations (Bhatt and McDowell, 2007). Enhanced access to mineral nutrients contained in primary minerals also aids in the rapid restoration of vegetation on landslide scarps in the Icacos watershed (Frizano and others, 2002).

At the rindlet-saprolite interface, the rindlets finally disaggregate and transform into saprolite (figs. 3, 4). The narrow zone (≈ 7 cm at the rindlet sequence studied) surrounding the visible interface has been called the protosaprolite zone (Buss and others, 2008) or saprock zone (Minyard and others, 2011). Within this zone, plagioclase and apatite completely dissolve and biotite achieves the oxidized composition found within the saprolite. Also within this zone, hornblende begins to weather and rapidly dissolves to completion at a rate of $1.4 \times 10^{-12} \text{ mol m}^{-2} \text{s}^{-1}$, calculated from the solid-state gradient in Fe(II) within the protosaprolite zone (Buss and others, 2008). Thus hornblende provides the dominant flux of Fe(II) to the saprolite and the deep saprolite biota (Buss and others, 2005).

In the deep saprolite, microbial communities are relatively isolated from the biogeochemical cycling near the surface. Nutrients, such as organic carbon and phosphorous, do not infiltrate to the deep saprolite (Murphy, 1995; Buss and others, 2005, 2010). Therefore, the deep communities depend directly upon nutrients and energy sources derived from the rock-forming minerals during weathering of the rindlets and corestones. Apatite dissolution across the rindlet zone and at the rindlet-saprolite interface produces sufficient flux of phosphorous to support the needs of the deep microbial community (Buss and others, 2010). This community includes autotrophic microorganisms that fix CO_2 to produce organic carbon from inorganic carbon. At least some of these autotrophs are also iron oxidizers, which derive energy by oxidizing the Fe(II) that is rapidly released at the rindlet-saprolite interface during hornblende dissolution (Buss and others, 2005, 2008). Iron-oxidizing bacteria contribute to the formation of secondary Fe(III)-oxide minerals (goethite) in the saprolite and potentially affect the rate of spheroidal weathering by decreasing the concentration of dissolved oxygen in pore water (Buss and others, 2005, 2008).

Weathering Processes in the Saprolite and Soil

Saprolite is, by definition, an isovolumetric weathering product (Bates and Jackson, 1984), and this characteristic has been confirmed for the Icacos saprolite by calculations of volumetric strain with respect to Ti (White and others, 1998; Buss and others, 2008) that are close to zero. The 50 percent porosity and visible primary granitic texture of the saprolite is also consistent with isovolumetric weathering (White and others, 1998).

Weathering reactions within the saprolite include the replacement of biotite by kaolinite, quartz dissolution, oxidation of Fe(II) and Mn(II), and precipitation of Fe and Mn oxides (Murphy and others, 1998; White and others, 1998; Buss and others, 2005). These reactions are revealed in gradients in pore-water and solid-state chemistry, in petrographic and electron microscopy of thin sections, and in microbiological assays. Concentrations of K, Mg, and Si in Icacos saprolite pore waters increase with depth, defining weathering gradients (White and others, 1998). Weathering rates for biotite alteration to kaolinite (10^{-15} mol m⁻² s⁻¹) and for quartz dissolution ($10^{-14.8}$ mol m⁻² s⁻¹) were calculated from these gradients (Murphy and others, 1998; Schulz and White, 1999).

In the Icacos weathering profile, biotite weathers in two stages. As mentioned earlier, biotite in the corestones and rindlets oxidizes to form an “altered biotite” phase, which is characterized by a d(001) spacing of ≈ 10.5 Å, and higher Al/Si ratios and lower Fe, Mg, and K contents than fresh biotite (Dong and others, 1998; Murphy and others, 1998; Buss and others, 2008). In the saprolite, altered biotite weathers further to form kaolinite by either of two mechanisms: direct epitaxial overgrowth of two layers of kaolinite onto one layer of altered biotite, or formation of one layer of kaolinite per layer of altered biotite after the formation of an intermediate halloysite layer (Dong and others, 1998; Murphy and others, 1998). The weathering of biotite to kaolinite controls Mg and Si concentrations in pore waters in all but the shallowest and deepest saprolite.

Quartz dissolution in the soil is reflected in Si concentrations (Schulz and White, 1999) and Si isotope ratios (Ziegler and others, 2005) in the pore waters. Quartz dissolution rates under natural conditions are extremely slow, and thus residual quartz is the major structural component of many weathering profiles, including the Icacos saprolite, where quartz abundances and grain size distributions are approximately constant with depth. However, these quartz grains are not inert but show evidence of dissolution in the form of etch pits (Schulz and White, 1999). Quartz dissolution rates, calculated from silica concentrations in the pore waters, are fastest at shallow depths (2.8×10^{-15} mol m⁻² s⁻¹ at 1.5 m depth), where quartz-grain etch pits are the most abundant (Schulz and White, 1999). Silica concentrations in the saprolite pore waters increase linearly with depth, whereas quartz weathering rates decrease with depth. Quartz dissolution also controls the $\delta^{30}\text{Si}$

signature in the soil pore waters (-1.4 to -1.7 per mil, Ziegler and others, 2005). Some kaolinite in the shallow soil dissolves in association with lower pH and elevated concentrations of Al and dissolved organic carbon in the soil pore waters (White and others, 1998). Dissolution by organic acids and other organic ligands produced by soil microorganisms and vegetation are likely responsible for the loss of kaolinite in the soil layer, as has been observed in laboratory studies (for example, Maurice and others, 2001) and in other tropical soils (for example, Chorover and Sposito, 1995). However, despite the influence of quartz and kaolinite dissolution, pore-water chemistry in the soil and shallow saprolite is dominated by atmospheric deposition and biological cycling (White and others, 1998; Pett-Ridge and others, 2009; Lugolobi and others, 2010) rather than mineral weathering processes.

Summary

Calculated bedrock weathering rates for the Icacos and Mameyes watersheds are high compared with watersheds around the world that are underlain by siliceous bedrock. Rapid weathering produces thick, highly leached saprolites in both watersheds that decouple subsurface processes from those in the soil. The quartz diorite bedrock in the Icacos watershed weathers spheroidally, forming relatively unweathered bedrock corestones that are surrounded by concentric layers of rock called rindlets. The spheroidal weathering process produces two controlling weathering interfaces. First, disaggregation of the intact rock is initiated at the bedrock-rindlet interface, where biotite oxidation within the corestones leads to spheroidal fracturing. The second controlling interface is the rindlet-saprolite boundary, where the rindlets disintegrate into saprolite owing to the development of extensive pore space and the complete dissolution of plagioclase and hornblende. Stream-water chemistry at base flow within the Río Icacos and its tributaries reflects these rindlet-zone weathering processes. Within the saprolite, biotite is replaced by kaolinite and quartz dissolves. The geochemistry of the overlying soil layer is dominated by the biological recycling of mineral nutrients, but it is also influenced by the dissolution of quartz and kaolinite. These shallow weathering processes are reflected in stream-water chemistry during storm events.

References

- Bates, R.L., and Jackson, J.A., 1984, Dictionary of geological terms: Falls Church, Va., The American Geological Institute, 571 p.
- Bawiec, W. J., 1998, Geology, geochemistry, geophysics, mineral occurrences, and mineral resource assessment for the commonwealth of Puerto Rico: U.S. Geological Survey Open-File Report 98-38, CD-ROM.

- Begle, E.A., 1978, The weathering of granite, Llano region, central Texas: Austin, The University of Texas at Austin, 163 p.
- Bhatt, M.P., and McDowell, W.H., 2007, Controls on major solutes within the drainage network of a rapidly weathering tropical watershed: *Water Resources Research*, v. 43, n. W11402, p. 1–9.
- Bisdom, E.B.A., 1967, The role of micro-crack systems in the spheroidal weathering of an intrusive granite in Galicia (NW Spain): *Geologie en Mijnbouw*, v. 46, p. 333–340.
- Briggs, R.P., and Aguilar-Cortés, E., 1980, Geologic map of the Fajardo and Cayo Icacos quadrangles, Puerto Rico: U.S. Geological Survey Miscellaneous Geologic Investigations Map I-1153, scale 1:20000, 1 sheet.
- Brown, E.T., Stallard, R., Larsen, M.C., Raisbeck, G.M., and Yiou, F., 1995, Denudation rates determined from the accumulation of in situ-produced ^{10}Be in the Luquillo Experimental Forest, Puerto Rico: *Earth and Planetary Science Letters*, v. 129, p. 193–202.
- Buss, H.L., Bruns, M.A., Schultz, M.J., Moore, J., Mathur, C.F., and Brantley, S.L., 2005, The coupling of biological iron cycling and mineral weathering during saprolite formation, Luquillo Mountains, Puerto Rico: *Geobiology*, v. 3, p. 247–260.
- Buss, H.L., Mathur, R., White, A.F., and Brantley, S.L., 2010, Phosphorus and iron cycling in deep saprolite, Luquillo Mountains, Puerto Rico: *Chemical Geology*, v. 269, p. 52–61.
- Buss, H.L., Sak, P.B., Webb, S.M., and Brantley, S.L., 2008, Weathering of the Rio Blanco quartz diorite, Luquillo Mountains, Puerto Rico—Coupling oxidation, dissolution, and fracturing: *Geochimica et Cosmochimica Acta*, v. 72, p. 4488–4507.
- Buss, H.L., Sak, P.B., White, A.F., and Brantley, S.L., 2004, Mineral dissolution at the granite-saprolite interface, in Wanty, R.B., and Seal, R.R.I., eds., International Symposium on Water-Rock Interaction, 11th: Saratoga Springs, N.Y., 27 June–2 July 2004, Taylor and Francis, p. 819–823.
- Chatterjee, A., and Raymahashay, B.C., 1998, Spheroidal weathering of Deccan Basalt—A three-mineral model: *Quarterly Journal of Engineering Geology*, v. 31, p. 175–179.
- Chorover, Jon, and Sposito, G., 1995, Surface charge characteristics of kaolinitic tropical soils: *Geochimica et Cosmochimica Acta*, v. 59, p. 875–884.
- Dong, Hailiang, Peacor, D.R., and Murphy, S.F., 1998, TEM study of progressive alteration of igneous biotite to kaolinite throughout a weathered soil profile: *Geochimica et Cosmochimica Acta*, v. 62, p. 1881–1887.
- Dosseto, Anthony, Buss, H., and Suresh, P.O., 2011, The delicate balance between soil production and erosion, and its role on landscape evolution: *Applied Geochemistry*, v. 26, S24–S27.
- Eberl, D.D., 2003, User guide to RockJock—A program for determining quantitative mineralogy from X-ray diffraction data: U.S. Geological Survey Open-File Report 03–78, 36 p.
- Eggerl, D.H., Larson, E.E., and Bradley, W.C., 1969, Granites, grusses, and the Sherman erosion surface, southern Laramie Range, Colorado-Wyoming: *American Journal of Science*, v. 267, p. 510–522.
- Farmin, Rollin, 1937, Hypogene exfoliation in rock masses: *Journal of Geology*, v. 45, p. 625–635.
- Fletcher, R.C., Buss, H.L., and Brantley, S.L., 2006, A spheroidal weathering model coupling porewater chemistry to soil thicknesses during steady-state denudation: *Earth and Planetary Science Letters*, v. 244, p. 444–457.
- Freyssinet, Phillippe, and Farah, A.S., 2000, Geochemical mass balance and weathering rates of ultramafic schists in Amazonia: *Chemical Geology*, v. 170, p. 133–151.
- Fritz, S.J., and Ragland, P.C., 1980, Weathering rinds developed on plutonic igneous rocks in the North Carolina piedmont: *American Journal of Science*, v. 280, p. 546–559.
- Frizano, Jacqueline, Johnson, A.H., and Vann, D.R., 2002, Soil phosphorus fractionation during forest development on landslide scars in the Luquillo Mountains, Puerto Rico: *Biotropica*, v. 34, p. 17–26.
- Isherwood, Dana, and Street, A., 1976, Biotite-induced grussification of the Boulder Creek Granodiorite, Boulder County, Colorado: *Geological Society of America Bulletin*, v. 87, p. 366–370.
- Jolly, W.T., Lidiak, E.G., Schellekens, J.H., and Santos, J., 1998, Volcanism, tectonic and stratigraphic correlations in Puerto Rico, in Lidiak, E.G., and Larue, D.K., eds., Tectonics and geochemistry of the northeastern Caribbean: *Geological Society of America Special Paper* 322, p. 1–34.
- Kurtz, A.C., Lugolobi, F., and Salvucci, G., 2011, Germanium-silicon as a flowpath tracer—Application to the Río Icacos watershed: *Water Resources Research*, v. 47, W06516.
- Larsen, E.S., 1948, Batholith and associated rocks of Corona, Elsinore and San Luis Rey quadrangles, southern California: *Geological Society of America Memoir*, v. 29, p. 114–119.
- Larsen, M.C., and Torres-Sánchez, A.J., 1998, The frequency and distribution of recent landslides in three montane tropical regions of Puerto Rico: *Geomorphology*, v. 24, p. 309–331.

- Lugolobi, Festo, Kurtz, A.C., and Derry, L.A., 2010, Germanium-silicon fractionation in a tropical, granitic weathering environment: *Geochimica et Cosmochimica Acta*, v. 74, p. 1294–1308.
- Maurice, P.A., Vierkorn, M.A., Hersman, L.E., and Fulghum, J.E., 2001, Dissolution of well and poorly ordered kaolinites by an aerobic bacterium: *Chemical Geology*, v. 180, p. 81–97.
- Meybeck, Michel, 1987, Global chemical weathering of surficial rocks estimated from dissolved river loads: *American Journal of Science*, v. 287, p. 401–428.
- Minyard, M.L., Bruns, M.A., Martinez, C.E., Liermann, L.J., Buss, H.L., and Brantley, S.L., 2011, Halloysite nanotubes and bacteria at the saprolite-bedrock interface, Rio Icacos watershed, Puerto Rico: *Soil Science Society of America Journal*, v. 75, p. 348–356.
- Murphy, S.F., 1995, The weathering of biotite in a tropical forest soil, Luquillo Mountains, Puerto Rico: State College, Pennsylvania State University Master's thesis, 100 p.
- Murphy, S.F., Brantley, S.L., Blum, A.E., White, A.F., and Dong, H., 1998, Chemical weathering in a tropical watershed, Luquillo Mountains, Puerto Rico—II. Rate and mechanism of biotite weathering: *Geochimica et Cosmochimica Acta*, v. 62, p. 227–243.
- Murphy, S.F., Stallard, R.F., Larsen, M.C., and Gould, W.A., 2012, Physiography, geology, and land cover of four watersheds in eastern Puerto Rico, ch. A in Murphy, S.F., and Stallard, R.F., eds., *Water quality and landscape processes of eastern Puerto Rico*: U.S. Geological Survey Professional Paper 1789, p. 1–24.
- Navarre-Sitchler, Alexis, and Brantley, S., 2007, Basalt weathering across scales: *Earth and Planetary Science Letters*, v. 261, p. 321–334.
- Ollier, C.D., 1971, Causes of spheroidal weathering: *Earth-Science Reviews*, v. 7, p. 127–141.
- Pett-Ridge, J.C., Derry, L.A., and Kurtz, A.C., 2009, Sr isotopes as a tracer of weathering processes and dust inputs in a tropical granitoid watershed, Luquillo Mountains, Puerto Rico: *Geochimica et Cosmochimica Acta*, v. 73, p. 25–43.
- Riebe, C.S., Kirchner, J.W., and Finkel, R.C., 2003, Long-term rates of chemical weathering and physical erosion from cosmogenic nuclides and geochemical mass balance: *Geochimica et Cosmochimica Acta*, v. 67, p. 4411–4427.
- Riebe, C.S., Kirchner, J.W., and Finkel, R.C., 2004, Erosional and climatic effects on long-term chemical weathering rates in granitic landscapes spanning diverse climate regimes: *Earth and Planetary Science Letters*, v. 224, p. 547–562.
- Schellekens, Jaap, Scatena, F.N., Bruijnzeel, L.A., van Dijk, A.I.J.M., Groen, M.M.A., and van Hogenzand, R.J.P., 2004, Stormflow generation in a small rainforest catchment in the Luquillo Experimental Forest, Puerto Rico: *Hydrological Processes*, v. 18, p. 505–530.
- Schulz, M.S., and White, A.F., 1999, Chemical weathering in a tropical watershed, Luquillo Mountains, Puerto Rico—III. Quartz dissolution rates: *Geochimica et Cosmochimica Acta*, v. 63, p. 337–350.
- Seiders, V.M., 1971, Geologic map of the El Yunque quadrangle, Puerto Rico. U.S. Geological Survey Miscellaneous Geological Investigation I-658, 1 sheet, scale 1:20,000; available at <http://pubs.er.usgs.gov/publication/i658>
- Simpson, D.R., 1964, Exfoliation of the Upper Pocohontas sandstone, Mercer County, West Virginia: *American Journal of Science*, v. 242, p. 545–551.
- Smith, A.L., Schellekens, J.H., and Diaz, A.M., 1998, Batholiths as markers of tectonic change in the northeastern Caribbean: *Geological Society of America Special Paper*, v. 322, p. 99–122.
- Stallard, R.F., and Edmond, J.M., 1983, Geochemistry of the Amazon—2. The influence of geology and weathering environment on the dissolved load: *Journal of Geophysical Research*, v. 88, p. 9671–9688.
- Turner, B.F., Stallard, R.F., and Brantley, S.L., 2003, Investigation of in situ weathering of quartz diorite bedrock in the Río Icacos Basin, Luquillo Experimental Forest, Puerto Rico: *Chemical Geology*, v. 202, p. 313–341.
- White, A.F., 2002, Determining mineral weathering rates based on solid and solute weathering gradients and velocities—Application to biotite weathering in saprolites: *Chemical Geology*, v. 190, p. 69–89.
- White, A.F., Blum, A.E., Schulz, M.S., Vivit, D.V., Stonestrom, D.A., Larsen, M., Murphy, S.F., and Eberl, D., 1998, Chemical weathering in a tropical watershed, Luquillo Mountains, Puerto Rico—I. Long-term versus short-term weathering fluxes: *Geochimica et Cosmochimica Acta*, v. 62, p. 209–226.
- Ziegler, Karen, Chadwick, O.A., White, A., and Brzezinski, M.A., 2005, $\delta^{30}\text{Si}$ systematics in a granitic saprolite, Puerto Rico: *Geology*, v. 33, p. 817–820.

Appendix 1. Data Processing and Computation to Characterize Hydrology and Compare Water Quality of Four Watersheds in Eastern Puerto Rico

By Robert F. Stallard

Introduction

This appendix summarizes procedures used to characterize hydrology and to compare water quality among four watersheds studied as part of the U.S. Geological Survey's Water, Energy, and Biogeochemical Budgets (WEBB) research program in Puerto Rico and parallel work in Panama. The four comparative watersheds were the Canóvanas, Cayaguás, Icacos, and Mameyes (fig. 1). An additional small watershed within the Icacos watershed, the Guabá, was examined to study scaling effects; therefore, data from five stream-gaging stations were available (fig. 1). Data from the first 15 years (1991–2005) of the Puerto Rico component were processed for this report, an undertaking that entailed working with several million discharge measurements, thousands of measurements from automated rain gages, and several thousand samples analyzed for some aspect of water quality (from suspended sediment and electrical conductivity to comprehensive chemical analyses). Discharge records from stream-gaging stations and water-quality datasets were processed separately to check for errors and to fill in discharge-data gaps with estimated values. The hydrologic and water-quality datasets were then merged into two types of master files. One contains all primary hydrology data and interpretive information about hydrologic processes, such as calculating trends and tagging recessions and exceptional storms; one hydrologic-data file was compiled for each gage site. The other file type holds primary water-quality data, chemical parameters derived from the primary data, and an abbreviated hydrological characterization of each sample; analyses of samples from all sites and sources were compiled into a single water-quality data file. This water-quality-data file, which contains about 6,400 records for 15 years of data, can be manipulated in conventional spreadsheets.

This appendix is divided into seven sections. The first discusses the computational procedures used to handle this large dataset. The second covers hydrological data processing. The third describes processing of the water-quality data, including calculated parameters such as saturation indices, cyclic-salt correction, and dissolved bedrock. The fourth describes the constituent-load computations built around the program LOADEST (Runkel and others, 2004). The fifth details how runoff and yield percentile ranges are calculated. The sixth presents summaries of the dataset. The last compares this dataset with other large datasets assembled by the U.S. Geological Survey, in terms of the range of process rates measured.

Computational Procedures to Interpret and Merge Hydrology and Chemistry Datasets

This data-processing exercise required the design of computational procedures to handle files that exceed the capacity of many databases and spreadsheets and to link data records on the basis of time stamps and sample identifications. Multimillion-record datasets are well beyond the size normally handled by conventional spreadsheets. Each discharge-data record represents an independent measurement, and subsequent modeling and interpretation is typically based on watershed conditions at or immediately before the time of measurement. A major objective was to prepare the database for models presented in Murphy and Stallard (2012), Stallard (2012b), and Stallard and Murphy (2012).

For much of this work, the program "gawk," GNU Operating System's implementation of a selection program "awk," was used (<http://www.gnu.org/software/gawk/gawk.html>) to process data files. Programs that read and process single records at a time are well suited to handling time-series datasets; records are read in chronological order, calculations are made, statistical information is accumulated, and where necessary a short, running history is stored in memory. As processing is completed, the modified records, with computed statistics, are written into a new file. In this manner, complex calculations can be undertaken without having the entire dataset resident in computer memory at once. The "gawk" program has excellent text-parsing capabilities and adequate math and array processing. These features permit the creation of programs that combine data archives in many individual text-based formats into a single standardized text-based format. Capabilities include error recognition, complex renaming, unit conversions, data testing, and more advanced calculations. The "gawk" scripts are compiled when they are called, allowing for fast and effective debugging.

An important feature of an integrated computational package is its ability to reprocess data when appreciable changes are made. The procedures described in this chapter are controlled by a small number of batch-processing scripts. As new data were added or whenever notable changes were made, such as acquisition of better estimates of watershed areas, the entire dataset was rebuilt from primary data sources. In this manner, partial implementation of changes and retention of errors was avoided.

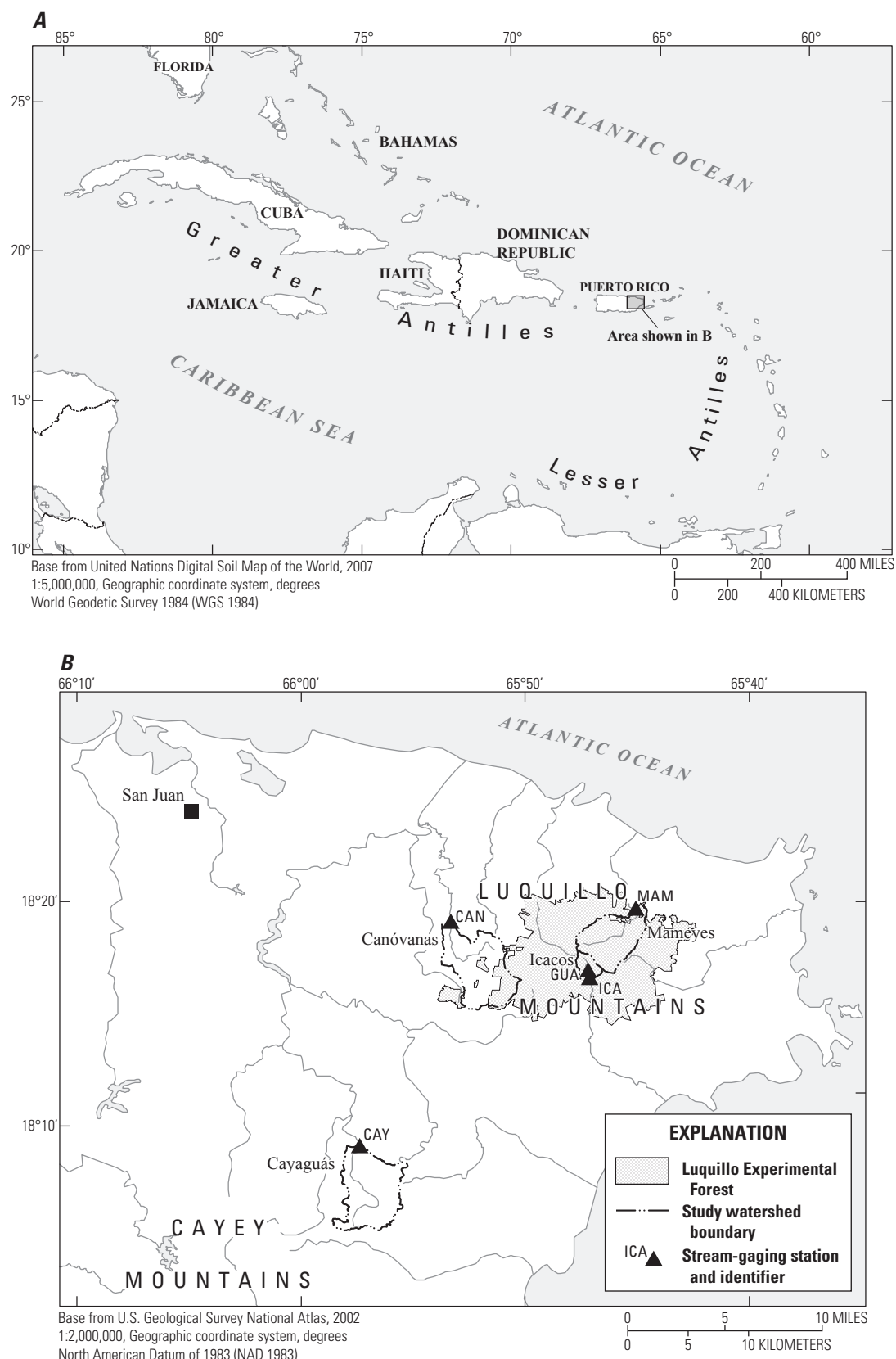


Figure 1. Location of Puerto Rico, study watersheds, and stream-gaging stations (CAN, Río Canóvanas near Campo Rico; CAY, Río Cayaguás at Cerro Gordo; GUA, Quebrada Guabá near Naguabo; ICA, Río Icacos near Naguabo; MAM, Río Mameyes near Sabana).

Noise Reduction, Smoothing, and Derivatives

All hydrologic data contain measurement noise, which complicates calculations such as the rate of change in discharge (the derivative of discharge with respect to time, dQ/dt). Time derivatives are used to characterize many hydrologic phenomena, such as the description of rises and recessions (Vogel and Kroll, 1996; Geyer and others, 2008). In general, these characterizations should not make restrictive assumptions about the mathematical functions that are used to describe the data, because such assumptions can bias subsequent modeling. The huge files evaluated here required that simplified calculation tools be used for smoothing data and estimating derivatives. The primary assumption made here is that data, which are expected to match real-world observations, are smoothly varying; step functions and isolated sharp peaks are not physically realistic and indicate faulty data. The filling of intermittent or extended data gaps is discussed in the section “Filling Data Gaps.” Spline functions are ideal computational tools for examining smoothly varying data, and two types of spline procedures were used in the data processing here: the relaxed cubic spline and the B-spline convolution (table 1).

The relaxed cubic spline (Reinsch, 1967) is a piecewise, continuous (connecting without gaps) set of cubic polynomials fit through the data, with one polynomial for each data segment. These polynomials are also piecewise continuous in the first and second derivatives. Moreover, in a relaxed cubic spline, the residual error of the regression can be specified beforehand. Data points do not need to be equally spaced along the ordinate axis (time). The time ordinate must increase monotonically, and no two points can have the same ordinate value. The cubic-spline regression uses an array that is seven times as large as the number of data pairs, and when the error is specified, the derivation of spline coefficients is iterative, making it difficult to apply a relaxed cubic spline to an entire time series of millions of measurements.

The B-spline convolution (Jupp, 1976) requires that points be evenly spaced. The advantage of a convolution is that only a few points in the convolution calculation have to be in memory during any computational step. The B-spline both smooths the data and calculates derivatives of the smoothed data at the central point in the convolution. Smoothing is especially useful in reducing measurement noise, which can be recorded during low-flow conditions. Accordingly, smoothed data were used in low-flow estimates, in describing recession curves, and in characterizing data noise. To estimate the derivative of the data during nonlow-flow conditions, a fourth-order function was forced through the central point and two adjacent points on each side, resulting in no smoothing. This procedure was also completed as a convolution.

Processing Hydrologic Data

Water-stage levels are recorded every 5 minutes at the Río Mameyes stream-gaging station and every 15 minutes for the remaining stations (on Río Canóvanas, Río Cayaguás,

Quebrada Guabá, Río Icacos). Stage levels are subsequently converted into real-time discharge by using a stage-discharge relation. The real-time data are stored in the U.S. Geological Survey’s Automated Data Processing System at the Caribbean Water Science Center. For Río Mameyes, the 15-year dataset represented roughly 1.6 million measurements. Real-time-discharge measurements were downloaded from this data processing system and were converted into a more compact format that uses a spreadsheet-style Julian date (days since December 30, 1899) and metric units. Four parameters were generated (table 1): Julian time, raw stage (in meters), corrected stage (in meters), and discharge (in cubic meters per second). Corrected stage refers to documented corrections made in processing the data before acquiring data from the data processing system; normally this category is blank.

The secondary source of discharge data is the official tabulation of daily-mean discharges reported through the U.S. Geological Survey’s National Water Information System (NWIS), publicly available on the Web site (<http://waterdata.usgs.gov/nwis>). NWIS data are calculated by using the data in the Automated Data Processing System, and when data are missing in the latter, Water Science Center hydrologists estimate the NWIS data using data from other stream-gaging stations and rainfall. The NWIS data were used to check the efficacy of calculations by the programs described here, and where primary data from the Automated Data Processing System were missing, estimated NWIS daily mean discharge data were used to calculate estimated values to fill those gaps (by using procedures described in the next section).

All data assembly calculations used primary discharge (Q) data. Because the drainage areas of the watersheds are different, however, subsequent comparisons used area-normalized properties, specifically runoff rates of water (R) and yields of constituents (Y_x), which are calculated from water discharge ($R = Q / \text{area}$) and constituent loads ($Y_x = \text{Load}_x / \text{area}$), respectively. Annual runoff also differs among the sites, and discharge-weighted concentrations are used for runoff-normalized comparisons (average concentration of $X = \text{average yield of } X / \text{average runoff}$).

Site-Specific Issues

A datum shift for the Río Icacos stream-gaging station was identified in 2003 (Matthew Larsen, Caribbean Water Science Center Chief, written commun., January 15, 2003; Díaz and others, 2004), whereby the elevation datum (reference mark (RM)-1) on an old rock stilling well (the original stage measurement recording site, since replaced) shifted downward through subsidence of the manmade structure. From 1979 to 1987, the RM-1 elevation decreased by 0.083 feet (ft); from 1987 to 1995, by 0.111 ft; and from 1995 to 1999, by 0.268 ft. All datums are tied to RM-1, the base reference mark for this station. The Caribbean Water Science Center corrected the record. As a result of this instability, discharge data had been too high (a 0.2-ft change is equal to 10 to 20 cubic feet per second ($\text{ft}^3 \text{ s}^{-1}$) at base-flow conditions). All discharge data for

Table 1. Parameters input and calculated in the real-time discharge-data file used to characterize the hydrology of five rivers, eastern Puerto Rico.

Field	Variable	Header	Parameter
Primary data fields			
1	JULIAN	Julian_Time	Julian time in spreadsheet format
2	RAW_ST	Stage_Raw	Raw stage data in meters or coding for missing data. Codes: “--”, good discharge, no stage; “==”, estimated discharge. Derivatives and several other derived parameters were not calculated for stream samples when discharges were estimated.
3	STAGE	Stage_Fin	Corrected stage data in meters.
4	QQ	Q_cms	Discharge, Q , in cubic meters per second. If discharge was estimated, the raw stage (RAW_ST) is coded accordingly.
Data fields calculated by the smoothing routine			
5	SMTH_QQ	Smooth_Q	Smoothed discharge, Q_s , in cubic meters per second. Used in low-flow estimates, determining recession curves, and in characterization of data noise.
6	DQ_DT	dQ/dt	The derivative of discharge with respect to time, dQ/dt , in cubic meters per second per hour.
7	SMTH_DQDT	Smooth_dQ/dt	The derivative of smoothed discharge with respect to time, dQ_s/dt , in cubic meters per second per hour.
8	DL10Q_DT	d(log(Q))/dt	The derivative of $\log(Q)$ with respect to time, $d\log(Q)/dt$, in log(fraction) per hour.
9	SM_DL10QT	Sm_dlogQ/dt	The derivative of $\log(Q_s)$ with respect to time, $d\log(Q_s)/dt$, in log(fraction) per hour.
Data fields calculated by the antecedent-conditions routine			
10	AVG_Q_1	Avg(Q)_day	Running average discharge for the prior day, in cubic meters per second, for characterization of antecedent conditions.
11	AVG_Q_7	Avg(Q)_week	Running average discharge for the prior week, in cubic meters per second, for characterization of antecedent conditions.
12	AVG_Q14	Avg(Q)_window	Running average discharge for the prior 2-week period, in cubic meters per second, for characterization of antecedent conditions.
13	MAX_Q14	Max(Q)_window	Maximum discharge for the prior 2-week period, in cubic meters per second, for characterization of antecedent conditions.
14	MAX_J14	Max(Q)_julian	Julian time off the maximum discharge for the prior 2-week period for characterization of antecedent conditions.
Baseflow data field calculated by the baseflow routine			
15	BASEFLOW	Baseflow	Baseflow estimate, in cubic meters per second.
Data fields calculated by the recession and landslide routine			
16	RECESS	Quick_Recess	Quick-recession curve (monotonic decrease of Q_s), in successive measurements.
17	RECSLO	Slow_Recess	Slow-recession curve (steady drop of AVG_1Q to AVG_1Q to AVG_1Q) in successive measurements. This procedure for calculating recession is similar to most published methods, which are based on mean daily discharge.
18	AVQ_1Q	One-day_Q	Running daily convolution of average flow, in cubic meters per second. For any moment this is an average discharge of one-half day back and one-half day forward in time.
19	OVER_TH	Over-Threshold	If the runoff in the previous 1, 2, or 3 days exceeds the landslide threshold, this runoff is coded in binary: +=1 is 1 day; +=2 is 2 days; +=4 is 3 days.
20	PAST_SD	Slide-day JT	Days since the end of the last period for which runoff in the previous 1, 2, or 3 days exceeds the landslide threshold. If this number is zero, then the observation is within the period where the threshold has been exceeded.

the Río Icacos station were subsequently revised in the Automated Data Processing System and in the NWIS to correct for the datum shift.

The useable record for the Quebrada Guabá stream-gaging station is only 10 years long (1993 through 2002) and ends with gage failure on April 17, 2003, during a large frontal storm that produced several landslides upstream of the gage. A site inspection in August 2010 indicated that pulses of coarse sediment derived from these landslides continue to move through the channel and create a time-varying cross section. Although data for the station were reported by the U.S. Geological Survey after that date, we consider these data to be flawed.

Filling Data Gaps

Each of the real-time-discharge datasets has gaps ranging from 30 minutes to several months. Commonly, the longest gaps are associated with the loss of a streamgage caused by a huge storm; the length of the gap reflects the time needed to rebuild the gage. These gaps introduce two problems. First, a gap represents a missing water volume that must be estimated to complete annual water and constituent budgets. Second, the computational procedures require evenly spaced, gap-free data. The objective of data interpolation was to calculate estimated discharge in gaps in real-time Automated Data Processing

System data, such that there is either an observed or an estimated discharge for each possible measurement time. Fulfilling this objective makes the smoothing algorithms far more rapid, because convolutions can be used. Gaps were filled by using a cubic spline calculation such that (1) daily mean discharges of the estimated data matched the daily mean discharges in the NWIS, and (2) estimated data were calculated at the same time intervals and are continuous with respect to real data and to first and second derivatives. These discharge estimates are used in daily, monthly, and annual mass balance calculations, but they are flagged as estimated data so that they would not be used to determine discharges of individual samples.

For data gaps of less than a day, discharge values were linearly interpolated from the adjacent data. For gaps too long to be filled by interpolation, both the stage and discharge fields are filled with a no-data code, to ensure that there are no time gaps. For gaps equal to or longer than a day, discharge values were estimated at the same time steps as the real-time data by using NWIS mean-daily discharge; on a few occasions when NWIS estimates were not available, mean-daily discharge values were estimated by using adjacent sites. Daily discharge estimates were downloaded from the NWIS and converted to a simpler format, similar to that described for Automated Data Processing System files.

For gap-filling calculations, mean-daily-discharge files also had to be gap free. The NWIS does not have measured or estimated daily values for the full 15-year record for Río Canóvanas (743 days missing) or Quebrada Guabá (1,541 days missing, including all days after April 17, 2003). For the Canóvanas and Guabá gaps, daily values were estimated by using relations determined from regressions (Bevington and Robinson, 2003) on all combinations of one or more daily-mean-discharge data from nearby gages. For Río Canóvanas, the Río Cayaguás was selected as the independent variable. For Quebrada Guabá, the Río Iacacos was the independent variable. The selected regression equations are as follows:

$$Q_{\text{Canóvanas}} = 0.573 \cdot Q_{\text{Cayaguás}} - 0.068 \quad (r^2=0.806)$$

$$Q_{\text{Guabá}} = 0.0298 \cdot Q_{\text{Iacacos}} - 0.00102 \quad (r^2=0.872),$$

where Q is the daily mean discharge at the station indicated by the subscript of the variable, and r^2 is the coefficient of determination and is the fraction of the variance accounted for by the regression (Bevington and Robinson, 2003). A cubic spline was used to fill the gaps. Julian day is the independent variable. For each gapless daily-value file, cumulative total daily discharge in cubic meters is calculated and assigned to the next day; this cumulative total becomes the dependent variable. A nonrelaxed cubic spline (nonrelaxed goes through the data points) is fit through the cumulative data such that at the end of each day, the discharge total calculated by summing the mean-daily discharge data matches the value of the cubic spline. The derivative of this spline is calculated for each time step of the real-time discharge record. This derivative is converted to cubic meters per second and, where real-time discharge data are lacking, these estimates provide a smoothly

varying substitute. The estimated real-time data are used for discharge-related calculations involving time resolution of a day or more, but they are not used to calculate instantaneous-flow statistics or instantaneous mass fluxes.

The final file assembled for all discharge-related calculations was constructed by merging the real-time discharge data from the Automated Data Processing System with the estimated real-time data from the NWIS. These estimates vary smoothly and have the same daily mean-discharge values as the NWIS dataset. The estimated data have no time or discharge gaps, but there are no estimates of stage. The merging process looked for gaps that are greater than a day, because shorter gaps were already filled through interpolation. First, the appropriate discharge estimates were extracted from the smoothed data files derived from daily mean values. A fourth-order polynomial having zero slope at each end and zero area was added to the estimated discharge; this addition adjusted the estimated data to the real data such that all data connect without any abrupt steps or slope breaks. For short gaps of less than 1.5 days, a single adjustment curve is used. For longer gaps, two adjustment curves (of no more than one day in length) were applied, one at each end of the gap. Between the two curves the discharge estimates are not adjusted.

For computational simplicity, the fourth-order polynomial is calculated by assuming that the gap, or the part of the gap that is being adjusted, is normalized such that it starts at zero and has a length of one day. The difference between the observed discharge at the beginning of the gap (Q_{o1}) and the estimated discharge (Q_{e1}) is D_{o1} . D_{o2} is calculated the same way at the end of the gap.

$$D_{o1} = Q_{o1} - Q_{e1}, \text{ and } D_{o2} = Q_{o2} - Q_{e2}.$$

To simplify the calculation, the duration of the adjustment period was normalized to 1, and a dimensionless time, X , $0 \leq X \leq 1$, is defined (t is the time of the adjusted observation, the adjustment start time is t_{start} , and the adjusted end is t_{end}):

$$X = (t - t_{start}) / (t_{end} - t_{start}).$$

If the beginning or the end of the polynomial is within the gap, then the respective D_{o1} or D_{o2} is assigned a zero value. The fourth-order polynomial is given by the following:

$$D_o(X) = D_{o1} + c \cdot X^2 + d \cdot X^3 + e \cdot X^4, \quad 0 \leq X \leq 1$$

$$c = -(18 \cdot D_{o1} + 12 \cdot D_{o2})$$

$$d = 32 \cdot D_{o1} + 28 \cdot D_{o2}$$

$$e = -15 \cdot (D_{o1} + D_{o2}).$$

X and $D_o(X)$ is calculated for every time step in the adjustment period, and $D_o(X)$ is added to the smoothed data.

The resulting gap-filled real-time discharge files are of the following form: Julian time, raw stage (in meters), corrected stage (in meters), and discharge (in cubic meters per second). If the discharge was estimated for gaps of more than a day, a “==” was coded into the raw stage.

Processing Real-Time-Discharge Data

Sixteen parameters were calculated from gap-filled, real-time discharge data. These parameters, in addition to the four primary measurements, were recorded in a single flat file for subsequent access by other data-characterization programs (table 1). These other programs include graphing programs, a program that links discharges, runoff rates, and rates of change of discharge to individual samples, a program that summarized flow statistics, a program that characterizes recurrence, and a program that does recession analyses. The procedures for estimating these 16 parameters are described below.

The Smoothing Routine

A variety of processes related to whether samples are collected on the rising or falling limbs of the hydrograph can affect the concentrations of constituents. Whether discharge is increasing or decreasing is determined by the derivative of discharge with respect to time. Measurement errors can produce noise that, if not damped, can make the calculations of derivatives quite difficult. To provide such information for data interpretation, the entire discharge record, including filled gaps, is smoothed by using a B-spline convolution (Jupp, 1976) to calculate a smoothed discharge (Q_s) and its derivative (dQ_s/dt). Because the errors of $\log(Q)$ are approximately normally distributed, the calculations used log-transformed data, $\log(Q)$. The convolution coefficients (Jupp, 1976, that report's table 6, m=4, k=2) are as follows:

for the smoothing convolution, $\log(Q_s)$: (1, 8, 23, 32, 23, 8, 1)/96

for the derivative, $d\log(Q_s)/dt$: (5, 4, 1, 0, -1, -4, -5)/(32•seconds per interval).

Smoothed Q_s and dQ_s/dt are calculated from $\log(Q_s)$ and $d\log(Q_s)/dt$, respectively:

$$Q_s = 10^{\log(Q_s)}$$

$$dQ_s/dt = (Q_s \cdot d((\log(Q_s))/dt)) / \ln(10)$$

The nonsmoothed derivative of the data is also calculated by using a five-point convolution that is equivalent to fitting a fourth-order polynomial through five consecutive points:

for the derivative, $d\log(Q)/dt$: (8, 1, 0, -1, -8)/(12•seconds per interval).

Five fields of data are added after the original four fields (table 1): Q_s , dQ/dt , dQ_s/dt , $d\log(Q)/dt$, and $d\log(Q_s)/dt$ to produce a smoothed-data file.

Antecedent-Conditions Routine

Antecedent conditions in a watershed are usually assumed to influence the chemistry of streams, and more recent conditions are assumed to be more important than those of the more distant past. To provide information about prior watershed wetness, additional discharge information is extracted from the antecedent data (table 1). Data are

summarized for three time windows: one day, one week, and two weeks. Five new fields of data are appended to the previous nine: a one-day average discharge, a one-week average discharge, a two-week average discharge, the maximum discharge in the previous two weeks, and the Julian time of the maximum discharge in the previous two weeks. In addition, a temporary file of the minimum smoothed discharge, Q_s , in the previous two weeks, along with the Julian time of this minimum discharge, is generated in order to delineate base flow.

Base Flow Calculation Routines

When a considerable amount of time had passed after storm events, the water in the channel was assumed to be entirely base flow or else water that was contributed to the river from deeper flow paths (Vogel and Kroll, 1996). A low-flow envelope was defined for the dataset (table 1) of the real-time data (including filled gaps). This envelope was developed iteratively. The table of minimum discharge in the previous two weeks (table 1) and the Julian time of this minimum discharge were used to delineate an envelope of minimum flows. For simplicity the minimums were connected by linear interpolation. This envelope was compared with observed flows, Q_s , and points below the curve that had been defined by linear interpolation were added to refine the envelope. This procedure was repeated three times, and the base-flow estimate was appended to the data table.

Recession-Curve and Landslide-Day-Extraction Routines

Two types of phenomena examined in this report, recession curves and landslide-producing storms, rely on characterization of hydrographs of storms. Both of these determinations represent a characterization of antecedent conditions, recession curves for dry periods following storms, and landslide-producing storms, here termed “landslide days,” for especially wet events (slide-day in table 1). These routines identify recession curves and landslide days, but do no further calculations.

Recession calculations normally use daily mean discharge (see reviews and model summaries by Hall, 1968; Tallaksen, 1995; Vogel and Kroll, 1996; and Chapman, 1999). Daily mean discharge is used in part because a large body of daily means is available, but it was also used because during low flows, at time scales of less than a day, processes that produce minor fluctuations in discharge (such as transpiration or floating debris) do not substantially affect daily means. Accordingly, two types of recession are identified. In a quick-recession curve, the smoothed discharge, Q_s , steadily decreases. In a slow-recession curve, daily mean discharge calculated by the antecedent-conditions routine steadily decreases. Each discharge measurement is tagged as being part of neither, one, or both recessions.

Much of the work in the Puerto Rico Water, Energy, and Biogeochemical Budgets (WEBB) program has focused on the landslide process and emphasizes the importance of shallow-soil landslides in physical erosion (Larsen, 2012). Stallard (1999) and Stallard and Kinner (2005) formulated models that include landslide-producing events in characterizations of annual sediment yields; the models are based on an empirical

landslide threshold derived by Larsen and Simon (1993). This landslide threshold relates a rainfall threshold, P (in millimeters), that must be exceeded for landslides to be initiated, to storm duration, D (in hours):

$$P(\text{millimeters}) \geq 91.46 \cdot D(\text{hours})^{0.18}. \quad (1)$$

The essence of this relation is that if more than the requisite rain falls in the requisite time, and if the terrain is sufficiently steep ($>12^\circ$ slope), then landslides may be initiated. For storms with durations of 24, 48, and 72 hours (h), the threshold rainfall is 162, 184, and 197 millimeters (mm) respectively.

Stallard (1999) and Stallard and Kinner (2005) modified this threshold relation to accommodate runoff, rather than rainfall, because many river basins lack adequate rain-gage networks. These reports describe rivers in the Panama Canal watershed for which a decade or more of combined daily-discharge and daily-sediment-load data had been recorded in a terrane with exhumed island-arc geology, topography, and annual rainfall similar to that of eastern Puerto Rico. The daily runoff value, R , needed to exceed the landslide threshold was calculated from the daily discharge data. A day was defined as a landslide day if the amount of runoff indicates that rainfall during that day exceeded the landslide threshold

$$R(\text{millimeters in } 24, 48, 72 \text{ h}) > F \cdot 91.46 \cdot D^{0.18} \\ (D = 24, 48, 72 \text{ h}), \quad (2)$$

where F is a catchall empirical coefficient between 0 and 1 that adjusts the threshold for three factors that reduce runoff relative to local rainfall. These three factors are (1) evapotranspiration, (2) infiltration, and (3) rainfall patchiness, whereby parts of a watershed will be over or under the threshold. Because daily sediment data were not available for eastern Puerto Rico, an F value of 0.85, as determined empirically by Stallard (1999) and Stallard and Kinner (2005) for central Panama watersheds, was used. For storms with a duration of 24, 48, and 72 hours, the threshold runoff is 138, 156, and 167 mm respectively. Calculations were based on whole days, because many sites elsewhere do not have real-time data, and because we could use estimated discharges during real-time data gaps.

Landslide days were identified by comparing runoff totals for the previous 24, 48, and 72 h with the threshold values. The threshold-exceedence state of the river was coded as a binary value. A value of one was added if the threshold is exceeded for the previous day; two was added if the threshold is exceeded for the previous 2 days, and four was added if thresholds were exceeded for the previous 3 days. In addition, the number of days since the landslide threshold was last exceeded was tabulated. This value is zero when the discharge measurement was within a period in which the threshold was exceeded.

Processing Water-Quality Data

During the eastern Puerto Rico WEBB Program, two principal types of samples were collected: grab samples, which were manually collected on a regular basis from riverbanks

at well-mixed cross sections near each gage site, and event samples, which were collected by an automated sampler during storm events and retrieved when weather conditions permitted. Conductivity, temperature, pH, and dissolved oxygen (O_2) of grab samples were measured onsite; only conductivity was measured onsite for event samples, because the other field parameters are unstable if not measured promptly. Depth-integrated samples for suspended sediment were occasionally collected at the same time as a grab sample. All water samples were filtered through 0.2- micrometer (μm) filters as soon as practicable in the laboratory. Sample collection and processing are described in detail in appendix 2.

Measured Water-Quality Parameters

This section describes how water-quality measurements were processed to characterize each water sample and to estimate constituent loads. Constituent measurements include the following:

1. Field properties: sample time, temperature, pH, conductivity, and dissolved oxygen (O_2).
2. Major cations: sodium (Na^+), potassium (K^+), magnesium (Mg^{2+}), and calcium (Ca^{2+}).
3. Major anions: chloride (Cl^-) and sulfate (SO_4^{2-}).
4. Alkalinity: (alkalinity = $HCO_3^- + 2 \cdot CO_3^{2-} + OH^- - H^+$).
5. Dissolved silica: ($Si(OH)_4$).
6. Dissolved organic carbon (DOC).
7. Nutrient ions: nitrite (NO_2^-), nitrate (NO_3^-), ammonium ion (NH_4^+), and phosphate ($-PO_4^{3-}$: preceding “-” refers to the tendency for phosphate to bind with other constituents).
8. Suspended solids: weight of material filtered onto a 0.2-micrometer (μm) filter per unit volume following drying to 105°C.
9. Suspended bedrock: weight of material filtered onto a 0.2- μm filter per unit volume following ashing at 550°C. This process is referred to as ashing, and the weight loss is referred to as loss on ignition (LOI).
10. Suspended sand: weight of sand sieved out of the sample using a 65- μm sieve prior to filtration and dried at 105°C. The weight of this sand is added into measurements of suspended solids. Inspection of sand samples indicated very little clay pellets or organic matter.
11. Trace constituents: strontium (Sr^{2+}), aluminum ($-Al^{3+}$), manganese ion (Mn^{2+}), reduced iron (Fe^{2+}), total iron ($Fe_{total} = Fe^{2+} + -Fe^{3+}$), boric acid ($B(OH)_3$), fluoride (F^-) and bromide (Br^-). Trace constituents were analyzed in a reduced suite of samples.

12. Dissolved organic nutrients: dissolved organic nitrogen and dissolved organic phosphorus were analyzed in some samples in the last years of the program (appendix 2).

These constituents were analyzed at several laboratories and by several types of analytical equipment (appendix 2). The data formats from these laboratories differed, and analyses were often reported in different units. For example, SO_4^{2-} was reported variously as micromoles per liter, microequivalents per liter, milligrams of sulfur per liter, and milligrams of sulfate per liter. All constituent concentrations were converted to micromoles per liter, except alkalinity, which was converted to microequivalents per liter, and suspended solids, sand, and ashed solids, which were converted to milligrams per liter. Data were standardized iteratively because of typographical errors in transcribing field and laboratory data and ambiguous reporting units. The tracking of anomalous results commonly required consultation of the original field and laboratory notes. Data processing was programmed in the “awk” (“gawk”) language because of its portability and its simplicity in handling both numeric and character data. The final data files were converted into a format suitable for upload into the NWIS.

Derived Water-Quality Parameters

The interpretation of the analytical results required the calculation of additional, derived, parameters. Table 2 gives constituent properties that were used in deriving some of these parameters. Derived parameters used in developing this report are grouped as follows:

1. Error checking: Total cation and total anion charge, net charge, and predicted conductivity (Miller and others, 1988)
2. Thermodynamic calculations: Ionic strength, ionic strength correction (gamma), hydrogen ion (H^+), hydroxide ion (OH^-), carbon-dioxide vapor pressure (P_{CO_2}), dissolved carbon dioxide ($\text{H}_2\text{CO}_3 = \text{CO}_2[\text{d}] + \text{H}_2\text{CO}_3[\text{d}]$), bicarbonate ion (HCO_3^-), carbonate ion (CO_3^{2-}), the saturation index of calcite ($\text{SI}_{\text{calcite}}$), and oxygen saturation (S_{O_2}).
3. Cyclic salt corrections: Large fractions of some constituents are derived from marine solutes blown inland, cyclic salts. Because we assumed that all chloride is cyclic, a marine-derived cyclic salt component was subtracted from various constituents, leaving an estimated bedrock-derived concentration. Following Stallard and Edmond (1981), estimated bedrock-derived constituents are designated with a “*”—for example, Na^* . Cyclic-salt corrections were determined for Na^* , K^* , Mg^* , Ca^* , Sr^* , Cl^* , and SO_4^{2-} . Other constituents were assumed to have no marine inputs.
4. Dissolved bedrock erosion: dissolved bedrock (DBrx).
5. Suspended bedrock (SBrx) and particulate organic carbon.

Error Checking

Two types of error checking were used in quality control of the water-quality data. Charge balance was calculated from the sum of concentrations times valence states (table 2) for the various chemical constituents. To check for errors, total positive and negative charges were compared; major disparities, greater than 5 percent, indicated potential problems. Predicted conductivity was calculated from the equivalent conductivity for each ion (table 2). To check for errors, observed and predicted conductivities were compared (Miller and others, 1988). Because conductivity is a field measurement, this check proved a robust way to track down improperly recorded or handled samples.

Thermodynamic Calculations

For thermodynamic calculations involving the carbon-dioxide system, equilibrium constants were tabulated as a function of temperature (Stumm and Morgan, 1981). Some of these tabulations were in the form of equations, but many were table entries. Table entries were converted into equations as a function of temperatures and are given below. To correct for the effects of ionic strength, the Davies equation was used to calculate the ionic-strength correction, gamma. Stumm and Morgan (1981) present all equations used in the thermodynamic calculations. Oxygen saturation is given by an equation developed by Elmore and Hayes (1960).

Equilibrium constants (K) are given by the following equations (K refers to temperature in degrees Kelvin; the subscripts of K refer to different reactions, where “W” refers to the deprotonation of water, “H” refers to Henry’s law for total dissolved carbon dioxide, “1” and “2” refer to the first and second deprotonations of carbonic acid, respectively, and “sp” refers to the solubility product of calcite; T refers to temperatures in degrees Celsius; and mg L^{-1} , milligrams per liter):

1. Reaction $\text{H}_2\text{O} \leftrightarrow \text{H}^+ + \text{OH}^-$,
 $K_W = -4470.99/\text{K} + 6.0875 - 0.01706 \cdot \text{K}$
2. Reaction $\text{CO}_2[\text{g}] + \text{H}_2\text{O} \leftrightarrow \text{H}_2\text{CO}_3^*$,
 $K_H = 2201.32/\text{K} - 12.60325 + 0.01258 \cdot \text{K}$
3. Reaction $\text{H}_2\text{CO}_3^* \leftrightarrow \text{H}^+ + \text{HCO}_3^-$,
 $K_1 = -3406.15/\text{K} + 14.844 - 0.03277 \cdot \text{K}$
4. Reaction $\text{HCO}_3^- \leftrightarrow \text{H}^+ + \text{CO}_3^{2-}$,
 $K_2 = -2910.82.15/\text{K} + 6.54767 - 0.02386 \cdot \text{K}$
5. Reaction $\text{CaCO}_3 \leftrightarrow \text{Ca}^{2+} + 2\text{CO}_3^{2-}$,
 $K_{\text{sp}} = -3000/\text{K} + 13.543 - 0.04001 \cdot \text{K}$
6. Reaction $\text{O}_2[\text{g}] \leftrightarrow \text{O}_2[\text{d}]$,
 $\text{O}_2 \text{ saturation in mg L}^{-1} = 14.652 - 0.41022 \cdot \text{T} + 0.007991 \cdot \text{T}^2 - 0.00007777 \cdot \text{T}^3$

Table 2. Measured constituent properties used in calculating interpretive parameters and derived constituents in five rivers, eastern Puerto Rico.

[g mol^{-1} , grams per mole; $\mu\text{S cm}^{-1} \text{mEq L}^{-1}$, microsiemens per centimeter per milliequivalent per liter; $\mu\text{mol L}^{-1}$, micromoles per liter; $\mu\text{Eq L}^{-1}$, microequivalents per liter; mg L^{-1} , milligrams per liter; DOC, dissolved organic carbon; --, not relevant]

Constituent	Database units	Molecular weight (g mol^{-1})	Valence	Equivalent conductivity ($\mu\text{S cm}^{-1} \text{mEq L}^{-1}$)	Ratio in seawater, constituent to chloride	Cyclic-salt-correction ratio to chloride	Bedrock chemical form	Conversion factor to bedrock (g mol^{-1})
Measured constituents								
Na^+	$\mu\text{mol L}^{-1}$	22.9898	1	50.1	0.85251	0.85251	Na_2O	30.99
K^+	$\mu\text{mol L}^{-1}$	39.102	1	73.5	0.01790	0.01790	K_2O	47.1
Mg^{2+}	$\mu\text{mol L}^{-1}$	24.312	2	53.1	0.10145	0.09689	MgO	40.31
Ca^{2+}	$\mu\text{mol L}^{-1}$	40.08	2	59.5	0.01876	0.01876	CaO	56.08
Sr^{2+}	$\mu\text{mol L}^{-1}$	87.62	2	59.4	0.00016	0.00016	SrO	103.62
Si(OH)_4	$\mu\text{mol L}^{-1}$	96.115	0	0	0	0	SiO_2	60.08
Alkalinity	$\mu\text{Eq L}^{-1}$	61.0173	-1	44.5	0.00714	-0.10992	--	--
Cl^-	$\mu\text{Eq L}^{-1}$	35.453	-1	76.4	1	1	--	--
SO_4^{2-}	$\mu\text{mol L}^{-1}$	96.06	-2	80	0.052	0.10597	S	32.06
NO_3^-	$\mu\text{mol L}^{-1}$	62.0049	-1	71.5	0	0	--	--
NO_2^-	$\mu\text{mol L}^{-1}$	46.0055	-1	71.5	0	0	--	--
NH_4^+	$\mu\text{mol L}^{-1}$	18.0388	1	73.4	0	0	--	--
$-\text{PO}_4^{3-}$	$\mu\text{mol L}^{-1}$	94.9714	-2	57.4	0	0	P_2O_5	70.97
Oxygen	mg L^{-1}	31.9988	0	0	--	--	--	--
DOC	$\mu\text{mol L}^{-1}$	12.0111	-0.07	40.9	0	0	--	--
$-\text{Al}_{3+}$	$\mu\text{mol L}^{-1}$	26.9815	0	68.4	0	0	Al_2O_3	50.98
$-\text{Fe}_{3+}$	$\mu\text{mol L}^{-1}$	55.847	0	68.4	0	0	$\text{FeO} + \text{Fe}_2\text{O}_3$	71.73
B	$\mu\text{mol L}^{-1}$	10.811	0	--	0.00076	0.00076	--	--
F ⁻	$\mu\text{mol L}^{-1}$	18.9984	-1	55.4	0.00012	0.00012	--	--
Br ⁻	$\mu\text{mol L}^{-1}$	79.909	-1	78.1	0.00153	0.00153	--	--
Derived constituents								
H ⁺	$\mu\text{mol L}^{-1}$	1.00797	1	349.8	--	--	--	--
OH^-	$\mu\text{mol L}^{-1}$	17.0074	-1	198.6	--	--	--	--
H_2CO_3	$\mu\text{mol L}^{-1}$	62.0253	0	0	--	--	--	--
HCO_3^-	$\mu\text{mol L}^{-1}$	61.0173	-1	44.5	--	--	--	--
CO_3^{2-}	$\mu\text{mol L}^{-1}$	60.0093	-2	80	--	--	--	--

Cyclic Salt Corrections

In order to estimate bedrock contributions to the dissolved load, the major cations (Na^+ , K^+ , Mg^{2+} , Ca^{2+}), and sulfate (SO_4^{2-}) require corrections for atmospheric inputs. For Na^+ , K^+ , and Mg^{2+} , the correction involves subtracting a seasalt contribution based either on the ratio of that ion to chloride (Cl^-) in rain or on the seasalt ratio (table 2). If we use sodium as an example, the $\text{Na}^+:\text{Cl}^-$ mole ratio for seasalt is 0.8525:

$$\text{Na}^* = \text{Na}^{2+} - (\text{Na}^+:\text{Cl}^-) \cdot \text{Cl}^- \quad (3)$$

Following Stallard and Edmond (1981), the “*” designates an estimated bedrock-derived constituent. Note that the seasalt correction, based on measured chloride, also effectively removes NaCl derived from human activities. The $\text{Mg}^{2+}:\text{Cl}^-$ ratio in rain is 0.09689, less than the seasalt ratio of 0.10145 (see discussion in Stallard, 2012a). The seasalt $\text{SO}_4^{2-}:\text{Cl}^-$ ratio is 0.052, and in some storms, especially high-chloride events, the rain and runoff are near this ratio (Stallard and Murphy, 2012, their fig. 10). However, additional

sulfur comes from pollution and from emissions of organic sulfur compounds (dimethyl sulfide and methyl sulfide) from the marine environment (Stallard and Edmond, 1981). To further complicate matters, forests may also emit organic sulfur compounds back to the atmosphere and sulfur may also be sequestered in vegetation (Stallard and Murphy, 2012). The overall rain $\text{SO}_4^{2-}:\text{Cl}^-$ ratio is 0.10597, and this ratio was used in calculations. Potassium was handled differently. The $\text{K}^+:\text{Cl}^-$ ratio in rain is 0.0231, whereas the seasalt ratio is 0.0179. Because plant material is so rich in potassium, the greater rain ratio is seen as reflecting local, minor plant contamination, so the seasalt ratio was used. The $\text{Ca}^{2+}:\text{Cl}^-$ ratio in rain is 0.01876, and seasalt is therefore a minor contribution to the calcium budget. Sahara dust brings in additional soluble calcium (Stallard, 2012a). Because this calcium is also a minor part of the overall calcium budget, and because the dust fallout comes from long-range transport, a uniform dust correction was subtracted from the final calcium budget rather than from individual samples. All silicon, aluminum, and iron in Sahara dust was assumed to be in nonreactive clays and sesquioxides and is therefore insoluble (Stallard, 2012a). Owing

to biological activity, surface seawater has low concentrations of $\text{Si}(\text{OH})_4$, NO_2^- , NO_3^- , NH_4^+ , and $-\text{PO}_4^{3-}$, and essentially zero ratios of these constituents to Cl^- .

For individual samples, the atmospheric-correction calculation occasionally yields a negative value. This value may be due to real processes, such as cation exchange in soil that can alter cation proportions, or it may be due to true variations in the ratios to chloride during individual events, as happens with sulfate. With sodium and magnesium, the calculations calculate the differences of large numbers, so analytical errors can produce negative values. This large-number problem is quite severe for high-chloride events (see Stallard, 2012a; Stallard and Murphy, 2012), so high-chloride events are not included in the bedrock-contribution calculations. Regardless of the reason, if the result of the calculation is negative, it was reassigned a zero value, essentially indicating that the sample contained no effective bedrock contribution of that constituent. Mg^* and SO_4^* calculations result in many zero values; Na^* and K^* rarely do; and Ca^* never.

Dissolved-Bedrock Erosion

Conventionally, solute denudation rates are calculated by using the concentration of total dissolved solids, defined as the total of the mass concentration of all dissolved constituents. This total is multiplied by discharge to get load, and then divided by drainage area to get the yield of dissolved solids, which is in turn equated with solute denudation. This calculation fails to correct for atmospheric inputs which, in addition to all chloride present and a considerable portion of the major cations, also includes the bicarbonate and carbonate ions that balance most of the bedrock-derived cation charge. Moreover, it fails to recognize that silicate rocks, particularly igneous and metamorphic rocks, are essentially a mixture of complex oxides (table 2), for which the charge of all the soluble cations and silicon was once balanced by oxygen (O^{2-}).

Stallard (1995a,b) uses a different approach that expresses the concentrations of most bedrock-derived constituents as dissolved oxides for mass-balance calculations. Silica and each cation, after correction for atmospheric inputs, are converted into a mass concentration of the corresponding bedrock oxide (table 2). For example, the calculation of dissolved sodium concentration expressed as an oxide ($\text{Na}_2\text{O}[d]$) (table 2) from bedrock-derived sodium, Na^* , was performed as follows (mg L⁻¹, milligrams per liter; $\mu\text{mol L}^{-1}$, micromoles per liter, 30.98, conversion factor in g mol⁻¹ from table 2):

$$\text{Na}_2\text{O}[d] (\text{mg L}^{-1}) = 0.001 \cdot 30.98 \cdot \text{Na}^* (\mu\text{mol L}^{-1}). \quad (4)$$

Dissolved sulfate is converted into sulfide. The concentrations of the dissolved oxides and sulfide are summed to get total dissolved bedrock (DBrx). For the WEBB watersheds, DBrx estimates were approximately half of the total dissolved solids, an indication of the serious degree of error introduced by estimating bedrock solute yields on the basis of total dissolved solids. Obviously, if the bedrock of a watershed includes substantial carbonates (Stallard,

1995a), for which the charge of calcium and magnesium is balanced by carbonate ions (CO_3^{2-}) rather than by oxygen (O^{2-}), DBrx will underestimate the amount of dissolved bedrock.

In addition to calculating DBrx for samples with complete chemistry (about 870 samples), it was estimated in all samples for which conductivity, chloride, and silica were measured (about 3,780 samples). High-chloride events were excluded, because of the problems of calculating the differences of large numbers. This calculation involves three steps. First, the bedrock contribution to conductivity is estimated by subtracting an atmospheric contribution. The atmospheric contribution is calculated by using the equivalent conductivities of each ion (table 2) to estimate conductivity of a solution that has the chloride concentration of the sample with each ion in the atmospheric-correction ratio to chloride just indicated:

$$\text{conductivity}^* = \text{conductivity} - 0.13028 \cdot \text{Cl}^- \quad (5)$$

The assumption is that the “acid” rain caused by additional sulfate in the rain is mixed with soil and groundwaters that have positive alkalinity. The excess H^+ in the rain is neutralized by this positive alkalinity, and although a negative alkalinity is used in cyclic-salt correction (table 2), the hydrogen-ion contribution to rainwater conductivity is ignored. Interestingly, this correction is very close to the sea-salt correction (0.13142) without excess sulfate.

The relation between conductivity* and total bedrock-derived cation charge, ZBrx, is estimated through a regression involving the 1,040 completely analyzed samples. A single set of regression coefficients worked for all Puerto Rico WEBB rivers:

$$\text{ZBrx} = a \cdot (\text{conductivity}^*)^b \quad (6)$$

where a (1.08612) and b (0.83239) are regression coefficients ($r^2 = 0.963$). Using ZBrx, estimated total dissolved bedrock, DBrx', is determined:

$$\text{DBrx}' = c \cdot (\text{ZBrx})^d + \text{SiO}_2[d] \quad (7)$$

where c and d are regression coefficients determined for each river (table 3), and $\text{SiO}_2[d]$ is the dissolved silica concentration expressed as an oxide:

$$\text{SiO}_2[d] (\text{mg L}^{-1}) = 0.06008 \cdot \text{Si} (\mu\text{mol L}^{-1}). \quad (8)$$

The correlation between DBrx' and DBrx for all 1,040 samples is $r^2 = 0.990$, and between $\log(\text{DBrx}')$ and $\log(\text{DBrx})$, $r^2 = 0.986$. Accordingly, both DBrx and DBrx', about 4,650 samples (figs. 2–6), were used in load calculations. Instantaneous dissolved-bedrock erosion rate is the product of either DBrx or DBrx' and instantaneous runoff rate. The large number of determinations of either DBrx or DBrx' gives considerably more rigor to estimates of long-term bedrock erosion through leaching.

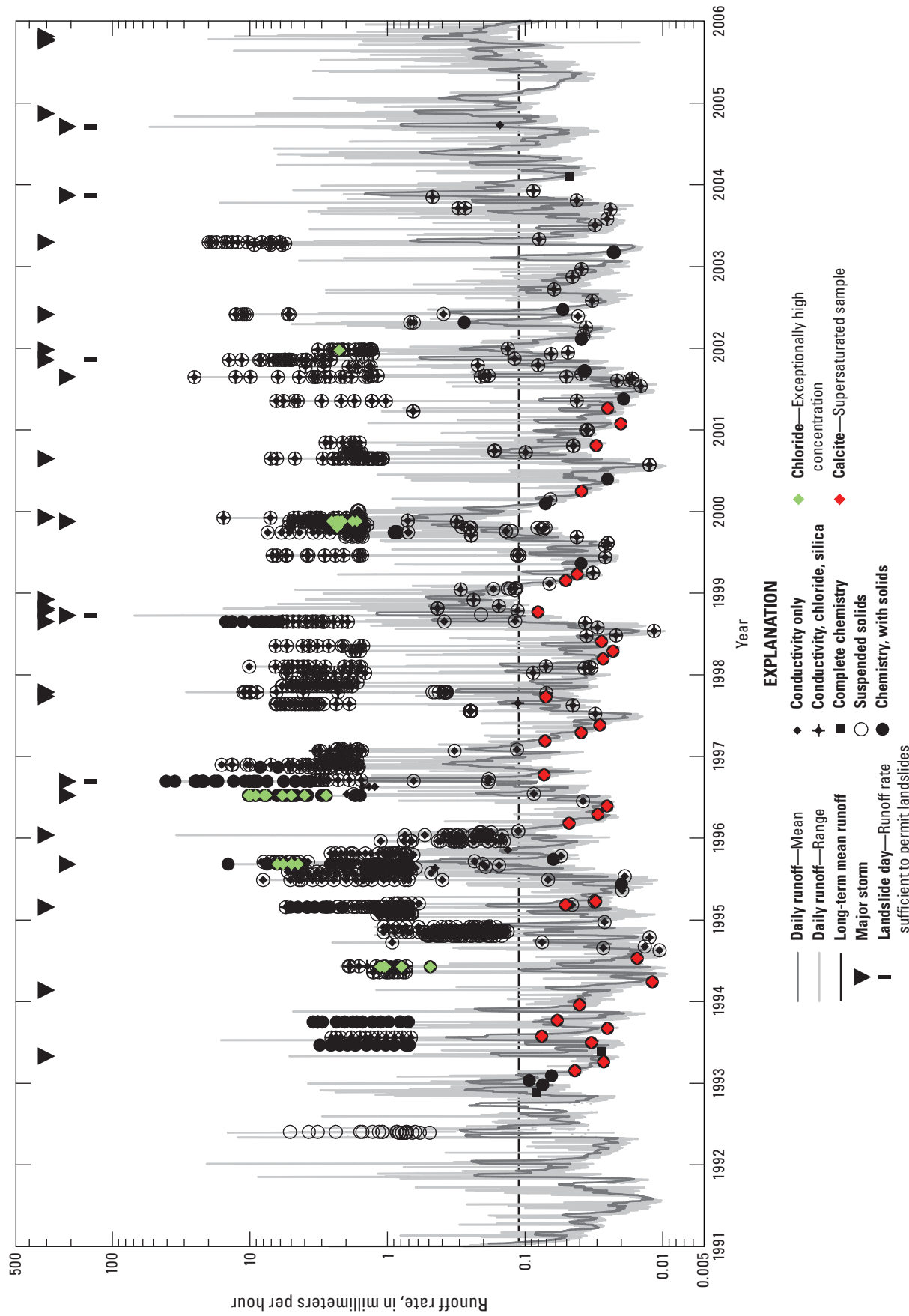


Figure 2. Data record for stream-gaging station Rio Canóvanas near Campo Rico, Puerto Rico, station number 50061800. Daily range of runoff (real-time data), daily mean runoff, and date on which water sample collected and type of analysis (Stallard and Murphy, 2012).

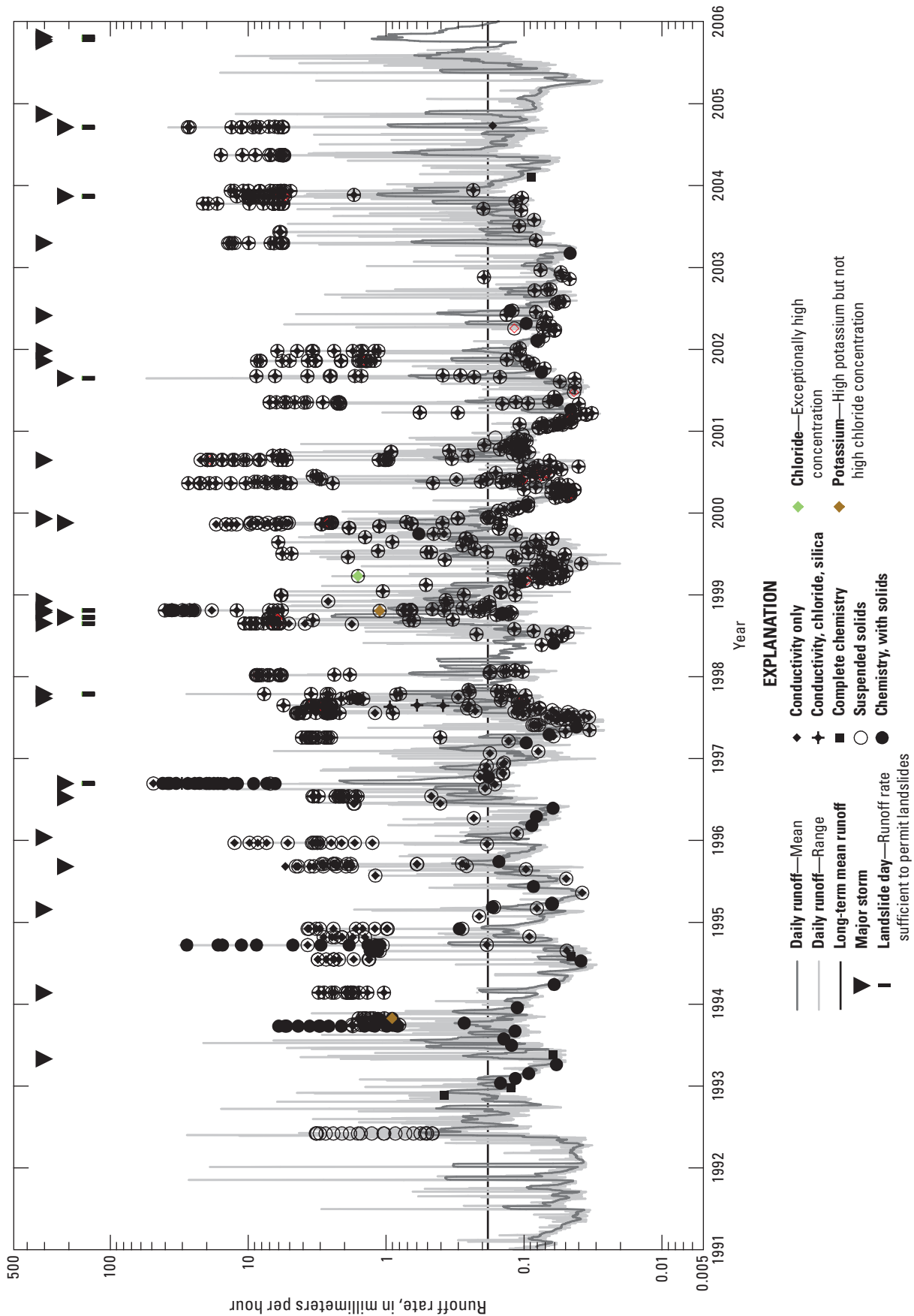


Figure 3. Data record for stream-gaging station Río Cayaguás at Cerro Gordo, Puerto Rico, station number 50051310. Daily range of runoff (real-time data), daily mean runoff, and date on which water sample collected and type of analysis (Stallard and Murphy, 2012).

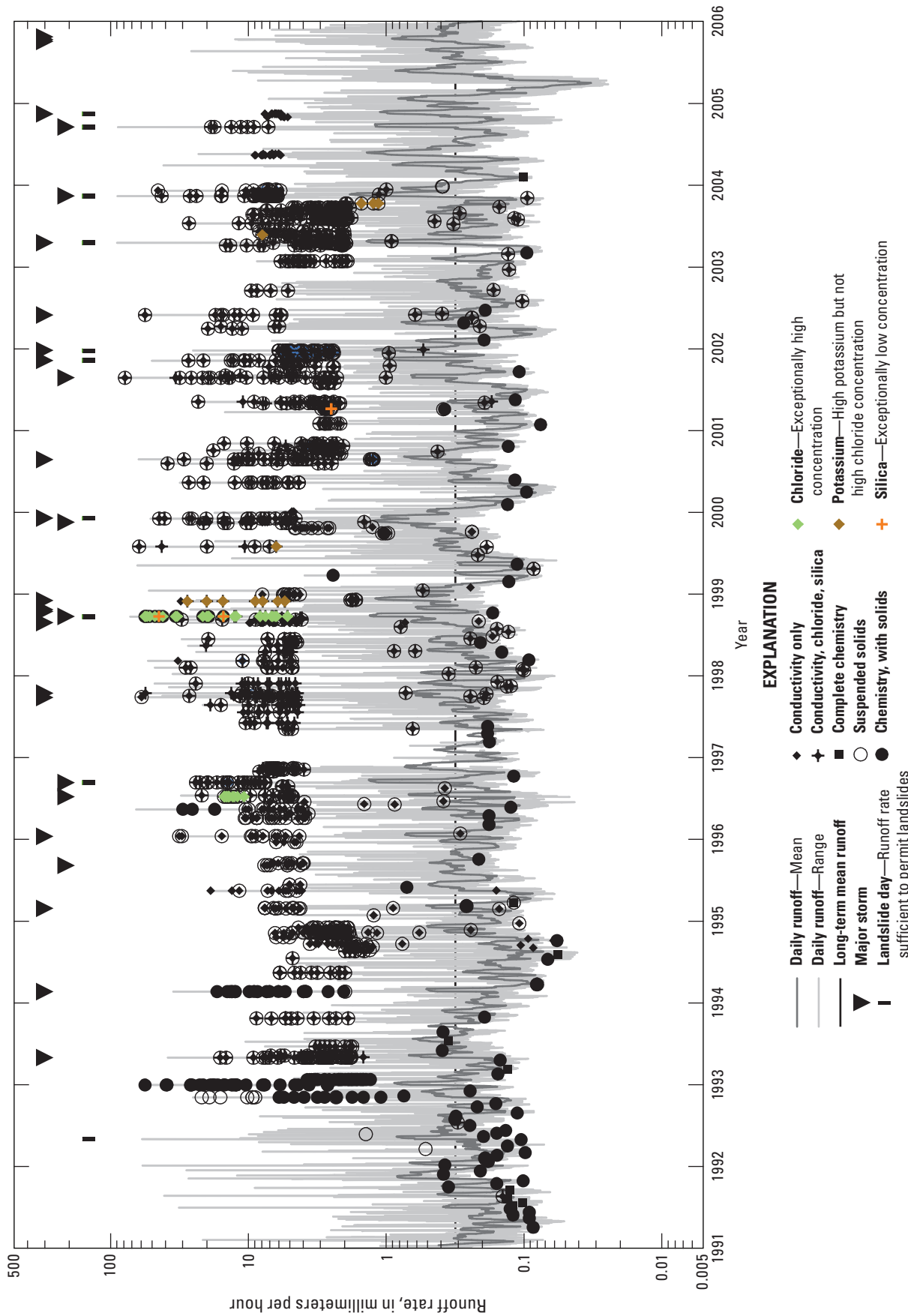


Figure 4. Data record for stream-gaging station Rio Mameyes near Sabana, Puerto Rico, station number 50065500. Daily range of runoff (real-time data), daily mean runoff, and date on which water sample collected and type of analysis (Stallard and Murphy, 2012).

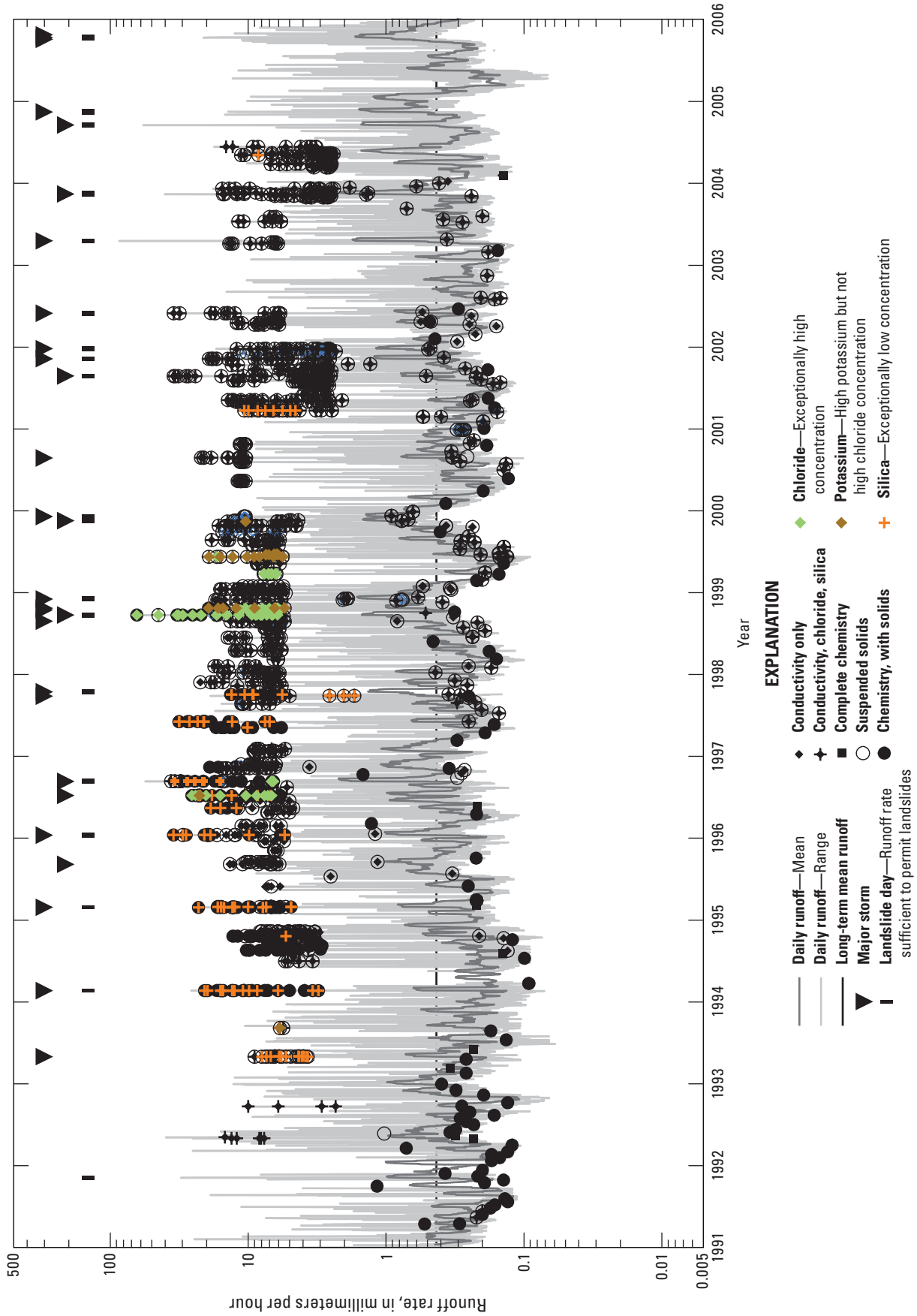


Figure 5. Data record for stream-gaging station Río Icacos near Naguabo, Puerto Rico, station number 50075000. Daily range of runoff (real-time data), daily mean runoff, and date on which water sample collected and type of analysis (Stallard and Murphy, 2012).

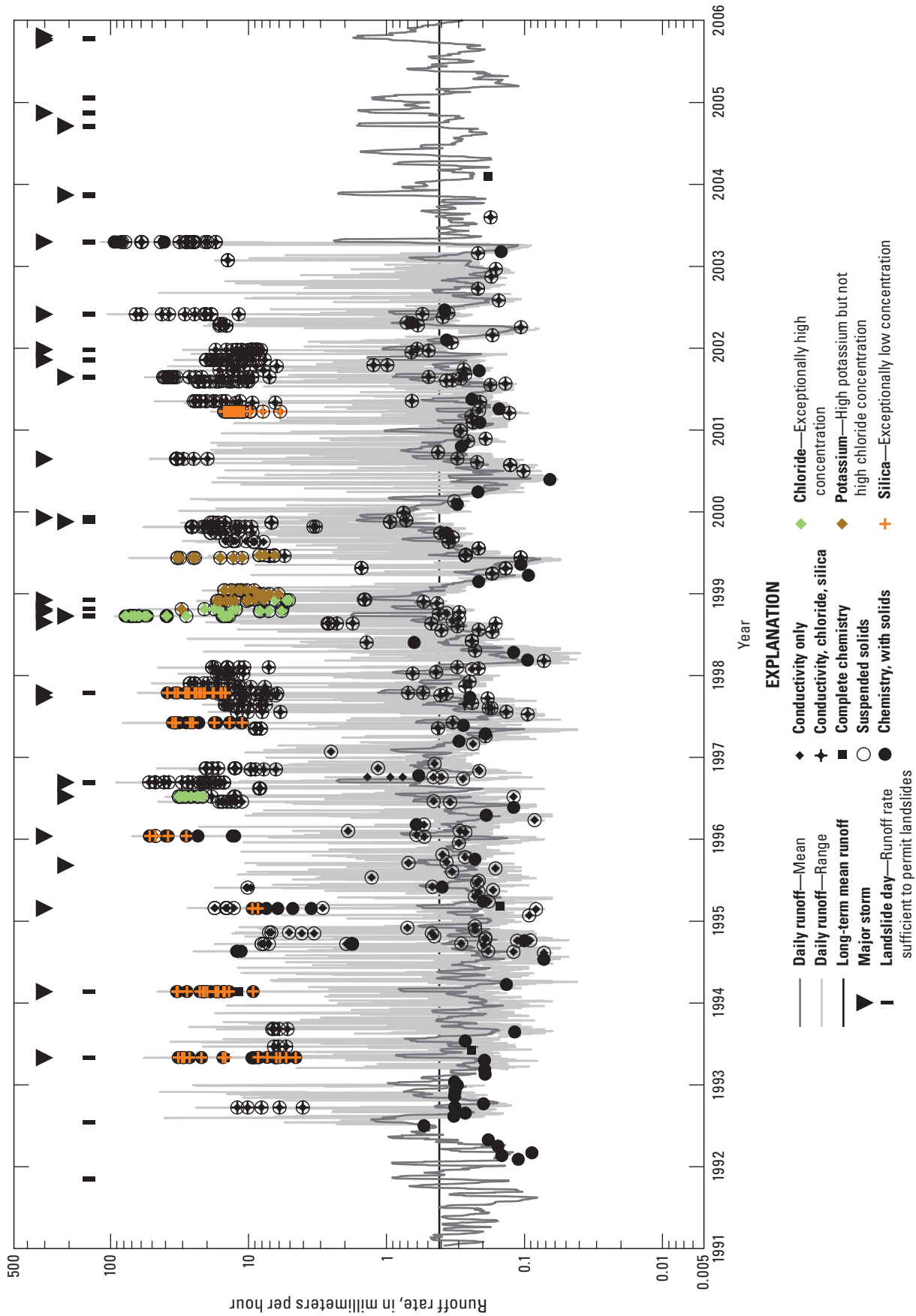


Figure 6. Data record for stream-gaging station Quebrada Guabá near Naguabo, Puerto Rico, station number 50074950. Daily range of runoff (real-time data), daily mean runoff, and date on which water sample collected and type of analysis (Murphy and Stallard, 2012). First 1.6 and final 2.7 years of daily runoff were estimated using the Rio Icacos data record.

Table 3. Coefficients of a model relating bedrock-derived cation charge, ZBrx, to dissolved bedrock, DBrx ($DBrx = c \cdot ZBrx^d + SiO_2$) in five watersheds, eastern Puerto Rico.

Watershed	Coefficient <i>c</i>	Coefficient <i>d</i>	Correlation ¹	Count
Canóvanas	-1.431	0.955	1.000	163
Cayaguás	-1.279	0.914	1.000	127
Mameyes	-1.348	0.958	1.000	177
Icacos	-1.393	0.941	0.999	249
Guabá	-1.398	0.941	0.997	156

¹Correlation between log(DBrx) and predicted log(DBrx).

Suspended Bedrock and Particulate Organic Carbon

River-borne sediment is composed of material from three sources: primary and secondary mineral matter derived from the weathering of bedrock, water that has been incorporated by secondary minerals during weathering, and organic matter. For about two-thirds of the measurements of suspended sediment (see Stallard and Murphy, 2012, and appendix 2), we also measured loss on ignition (LOI)—the weight loss of samples that were dried (at 105°C) upon heating up to 550°C. Studies summarized in Mackenzie (1957) and Mackenzie and Caillère (1979) show that in heating to 550°C, all of the clays and sesquioxides lose nonstructural water (most below 200°C). In addition, all sesquioxides, most kaolins, and substantial illites and vermiculites lose lattice water below 550°C; however, smectites, talcs, and chlorites do not. Talc and chlorites are not reported from soils or sediments; smectites are rare. Nonmineral organic carbon and most mineral carbon (coal and graphite) are also oxidized in this range. Carbonates, which are absent in humid-tropical soils and sediment, are generally stable.

In this study, the weight of the sample after heating to 550°C is equated with “suspended bedrock” (SBrx). The sample dried to 105°C is referred to as suspended solids or suspended sediment (SSol). For samples in which suspended bedrock was not measured, regressions for each river relate SBrx to SSol:

$$LOI = SSol - SBrx, \quad (11)$$

and

$$SBrx = SSol \cdot (a + b \cdot \log(SSol)), \quad (12)$$

where *a* and *b* are regression coefficients (table 4).

Table 4. Coefficients for a model relating suspended bedrock, SBrx, to suspended solids, SSol ($SBrx = SSol \cdot (a + b \cdot \log(SSol))$) in five watersheds, eastern Puerto Rico.

Watershed	Coefficient <i>a</i>	Coefficient <i>b</i>	Correlation ¹	Count
Canóvanas	0.809	0.0126	1.000	873
Cayaguás	0.905	-0.0007	1.000	802
Mameyes	0.647	0.0709	1.000	133
Icacos	0.720	0.0477	1.000	646
Guabá	0.651	0.0696	1.000	1,035

¹Correlation between log(SBrx) and log(SSol).

Particulate organic carbon was not measured on most of the sediment samples; instead, LOI was used as a surrogate measurement. LOI is often equated with organic matter; however, this procedure is not used with samples that are rich in kaolinite, halloysite, or iron and aluminum sesquioxides such as the WEBB samples. Instead, it was assumed here that particulate organic carbon is a fixed fraction of LOI for all the WEBB samples. This fraction was determined such that the 15-year yield of SSol for the Río Icacos consisted of 1 percent carbon, a value that is typical of rivers elsewhere in the world (Stallard, 1998). The result is that LOI for the WEBB rivers consists of 11 percent carbon. Because pure organic matter is about 50 percent carbon by mass (Stallard, 1998), 11 percent of LOI is the noncarbon elements in organic matter, and 78 percent is water. For the forested rivers, at low runoff rates of less than 1 millimeter per hour, the average particulate organic carbon is 2 to 3.5 percent of SSol (Stallard, 2012b, its tables 2, 5).

Calculation of Discharge, Constituent Loads, Runoff, and Constituent Yields

In order to calculate yields, the real-time discharge and water-quality datasets needed to be merged. This merger matched timestamps in the water-quality dataset with those in the real-time-discharge dataset, and interpolated where necessary. In addition to pairing water quality with discharge, additional properties were appended to each record in the water-quality dataset. These properties included runoff rate (*R*), days since the last landslide day, estimated base flow, and $d\log(Q_s)/dt$. Runoff rate was typically used for comparison, because it is area-normalized.

Of the variety of approaches that could be used to estimate constituent loads, the load estimator program LOADEST (Runkel, and others, 2004) was chosen. LOADEST estimates constituent loads in streams and rivers given a time series of streamflow, additional independent variables, and a constituent concentration. LOADEST assists the user in developing a regression model of constituent load (calibration). The explanatory variables normally used in LOADEST are discharge, seasonal cycles (sine and cosine of time), and time. The formulated regression model is then used to estimate loads throughout a user-specified time interval (estimation).

The construction of the input data files used by LOADEST from our two types of datasets was automated. For each river, the LOADEST calibration file is derived from relevant entries in the water-quality file, and the LOADEST estimation file is derived from the real-time discharge-data file. LOADEST requires only minor adaptations of these two datasets. First, the shortest time step allowed for the time series of discharge and other data in the estimation file is one hour. This time step requirement requires subsampling of eastern Puerto Rico real-time discharge data into one-hour intervals (which creates a small (less than 0.1 percent) difference with

the runoff values calculated using all runoff measurements). Second, model run times allowed use of only the simplest option for standard-error calculation (defined by LOADEST parameter SEOPT).

The SEOPT parameter allows selections of increasingly rigorous calibration options. The calibration and estimation procedures within LOADEST are based on three statistical estimation methods: adjusted maximum likelihood estimation, maximum likelihood estimation, and least absolute deviation, an alternative to maximum likelihood estimation that can be used when residuals are not normally distributed. The simplest option for calculating standard error, SEOPT=1, calculates standard error for an adjusted-maximum-likelihood-estimation-based linear approximation; standard error is not calculated for maximum likelihood estimation and least absolute deviation. The data processing for the eastern Puerto Rico dataset required one hour of computer time. The next-level option, SEOPT=2, additionally calculates standard errors for maximum likelihood estimation and least absolute deviation. That option, SEOPT=2, was run for 2 weeks on an otherwise unused computer. On the basis of the number of calculations that had been completed at the end of 2 weeks, more than 150 days of computer time would have been required to calculate standard errors for maximum likelihood estimation and least absolute deviation for all parameters of interest. Therefore, running the model while using SEOPT=2 or 3 was not viable.

To examine the eastern Puerto Rico dataset, a variety of yield models was tested in LOADEST. The user can define the model to be used in LOADEST; alternatively, LOADEST comes with a suite of regression options (defined by LOADEST parameter MODNO). If MODNO is set to zero, then LOADEST automatically selects the best model from a set of nine models (MODNO=1 to 9; Runkel, and others, 2004). This suite of models combines linear and quadratic fits to the natural log of discharge ($\ln[\text{discharge}]$) and time and to the sine or cosine of time ($\sin[\text{time}]$ or $\cos[\text{time}]$). A regression to time and to time squared implies a systematic drift in chemistry. The effects of increased runoff may be adequately represented by the $\ln(\text{discharge})$ part of the regression. Accordingly, five model options were chosen. LOADEST was allowed to select the best option (MODNO=0), which could be a model with systematic drift. In addition, all options that did not include systematic drift (MODNO=1, 2, 4, and 6) were run separately and compared with the selected model. In reporting average yields, the results of MODNO=0 and the best driftless model are tabulated.

LOADEST was used to calculate the loads of Na^+ , K^+ , Mg^{2+} , Ca^{2+} , Cl^- , SO_4^{2-} , Si(OH)_4 , DOC, NO_3^- , NH_4^+ , $-\text{PO}_4^{3-}$, and suspended sediment (Stallard and Murphy, 2012). LOADEST was also used to calculate the yields of DBrx, SBrx, Na^* , and particulate organic carbon (Stallard, 2012b). Alkalinity was calculated from the other models as described below.

Fundamentally, LOADEST is a regression, and biases produced by the logarithmic transformation of data and non-normality of log-transformed data produce problems that can

invalidate results (Runkel and others, 2004). In particular, zero values complicate LOADEST calculations. Mg^* and SO_4^* calculations result in many zero values; Na^* and K^* rarely; and Ca^* never. Of these, K^+ acts as a nutrient, and Ca^{2+} is primarily bedrock derived. Accordingly, only Na^* yield, derived using LOADEST, is used directly in budget calculations. For all other bedrock constituents, the atmospheric-input corrections are made afterwards on calculated constituent yields, by using the calculated chloride yields, and in the case of Ca^* , on additional deposition from Saharan dust (Stallard, 2012b).

Alkalinity loads cannot be estimated directly using LOADEST, because in samples collected at highest discharge values in the Icacos and Guabá watersheds, alkalinity is frequently negative (acidity). The primary source of alkalinity is the weathering of silicate and carbonate minerals. This weathering consumes hydrogen ions from the water, releasing nontitratable cations but essentially no nontitratable anions. Organic acids, sulfuric acid, and nitric acid can cause negative alkalinites. In load estimates, alkalinity was calculated from the concentrations of all other constituents (concentrations in mole units):

$$\text{Alkalinity} = (\text{Na}^+ + \text{K}^+ + \text{NH}_4^+ + 2 \cdot (\text{Mg}^{2+} + \text{Ca}^{2+} + \text{Sr}^{2+}) - (\text{Cl}^- + \text{NO}_3^- + 2 \cdot \text{SO}_4^{2-} + Z_{\text{DOC}} \cdot \text{DOC})) \quad (9)$$

where Z_{DOC} is the negative charge per carbon (equivalents per mole). For each river, Z_{DOC} was calculated by adjusting predicted alkalinity in the water-quality data file to measured alkalinity such that the ratio of averages was 1:1. For the Canóvanas, calculated $Z_{\text{DOC}} = 0.08$ equivalents per mole (eq mol⁻¹); Cayaguás, $Z_{\text{DOC}} = 0.06$ Eq mol⁻¹; Mameyes, $Z_{\text{DOC}} = 0.07$ Eq mol⁻¹; Icacos, $Z_{\text{DOC}} = 0.05$ Eq mol⁻¹, and Guabá, $Z_{\text{DOC}} = 0.05$ Eq mol⁻¹. For comparison, Tardy and others (2005) estimate an optimum Z_{DOC} of 0.064 Eq mol⁻¹ for Amazonian lowland rivers.

Other samples showed anomalous trends on plots of concentration against runoff rate (figs. 2–6). Some of these anomalies were caused by processes that are exceptional, such as high-chloride storms, that are not related to the explanatory variables normally used by LOADEST—discharge, seasonal cycles, and time trends. Statistically these samples are outside a normal distribution, and they were not included in load estimation. High-chloride samples are caused when winds during major storms blow exceptionally large amounts of seasalt inland (Stallard, 2012a). Samples collected during high-chloride events were censored for major seawater constituents (Na^+ , K^+ , Mg^{2+} , Ca^{2+} , Cl^- , SO_4^{2-}). These same samples also had exceptionally low NO_3^- , perhaps reflecting rainwater composition (Stallard and Murphy, 2012), and NO_3^- was also censored. Following Hurricane Georges, a high-chloride event, a number of subsequent events demonstrated high potassium, but not high concentrations of chloride and other seasalt constituents. The elevated potassium is likely attributed to the decay of downed vegetation (Stallard and Murphy, 2012). High-potassium samples were censored only for potassium. A few events affecting the

Icacos River during the first several years of the program had exceptionally low silica concentrations (Stallard and Murphy, 2012). Because silica concentrations in most event samples during this same time interval were not low, silica concentrations in low-silica samples were also censored.

Calculation of Runoff and Yield Percentile Ranges

To compare equivalent samples among rivers, runoff rates were ranked by their overall contribution to annual runoff. This ranking allowed equivalent classes of samples to be compared among the five rivers despite differences in annual runoff. All water-quality samples were assigned into runoff-rate percentile classes, similar to the approach used by the U.S. Geological Survey Water Watch Web site (<http://water.usgs.gov/waterwatch/>) in monitoring flood and drought conditions in the United States. Water Watch ranks discharge into percentile classes based on the amount of time a river flows in a given discharge range and compares daily discharge to this ranking. For this report, where the focus is on mass balance, percentile classes (0–10, >10–25, >25–50, >50–75, >75–90, >90–95, >95–99, and >99 percent) are based on runoff and yields. For example, the tenth percentile corresponds to a runoff rate below which 10 percent of the total runoff has been discharged from the basin. Likewise, the tenth percentile in sediment yield corresponds to a runoff rate below which 10 percent of the total sediment mass has been discharged from the basin. When we compared rivers based in percentile classes, our implicit assumption was that each class is hydrologically equivalent in each river (see Stallard and Murphy, 2012). When base flow is referred to in this text, it typically represents the samples in the 0-to-10-percent range.

To calculate percentile classes, the volume of water or mass of a constituent being discharged at a particular runoff was assigned to and totaled in a logarithmic runoff bin, with 20 bins per log cycle. For runoff, the real-time discharge-data files were used, whereas for constituent yields, the individual output load files of LOADEST were used. The bins were cumulatively totaled and normalized by the total volume of water or constituent mass discharged from the watershed for the period 1991–2005. Percentile classes for each constituent were then calculated from the normalized mass-accumulation curve for that constituent. Each sample in the water-quality database was then assigned to a runoff percentile class and rising and falling stages were distinguished on the basis of $d\log(Q_s)/dt$. Predicted constituent yields and instantaneous runoff were totaled for each percentile class, and an average concentration for each percentile class was then calculated by dividing total yield for each constituent by total runoff within that class.

Dataset Features and Characteristics

The combined datasets are presented in two ways: a graphical time series of daily mean runoff (figs. 2–6), simplified sample information (tables 5, 6), and annual summaries of the same information. The simple classification is used to assess the degree of completeness of sample analyses and unusual chemical characteristics. The degree of completeness includes a chemistry characterization and a sediment characterization. In terms of increasing degrees of analysis for chemistry, we distinguished among (1) samples with only conductivity measured, (2) samples with at least conductivity, Cl^- , and Si(OH)_4 measured, and (3) samples with complete chemistry. We also distinguished the presence or absence of suspended sediment data. Special chemical characteristics are included because of the way several of these were handled in load-estimation calculations and because their biogeochemical significance is discussed in other chapters of this report. These special chemical characteristics are (1) high-chloride samples, (2) normal-chloride, high-potassium samples, (3) low-silica samples, and (4) samples that are supersaturated with respect to calcite.

The sampling design used in the Puerto Rico WEBB program is clearly evident by the distribution of sample-data points in figures 2 through 6. Two primary types of samples were collected, manual “grab” samples and automated “event” samples (appendix 2). Grab samples were collected by researchers or a field crew who visited each site at regular intervals. Most samples collected during low runoff (figs. 2–6) were grab samples, whereas samples collected during high runoff were event samples. At intermediate runoff, relatively fewer samples were collected, an artifact of the sampling protocol. Owing to the large volume of samples collected by automated sampling, the stage threshold for event sampling was adjusted, typically by an increase, first in 1994 and again in 1997, with the objective of sampling the biggest events. This increase is reflected by upward shifts in the event-data distribution evident in figures 2 through 6. Samples in the intermediate zone were typically collected during multipeak events and during falling stage after single events.

Comparison of Hydrologic Sampling in the Eastern Puerto Rico Large-Scale Study with Hydrologic Sampling in Other Large-Scale Studies

In many settings, rare, high-energy hydrologic events play a major, often dominant, role in the mobilization of river-borne materials from hillslopes and stream channels and in the transport of these materials downriver (Wolman and Miller, 1960). In the WEBB watersheds described in this report, work on water quality emphasized event sampling. From 1991

Table 5. Annual hydrologic characteristics, data quality, and sampling effort in five watersheds, eastern Puerto Rico.[mm, millimeters; mm h^{-1} , millimeters per hour; km^2 , square kilometers; --, no samples]

Annual runoff total (mm)	Year	Minimum daily runoff rate (mm h ⁻¹)	Minimum daily runoff rate (mm h ⁻¹)	Average runoff rate (mm h ⁻¹)	Maximum daily runoff rate (mm h ⁻¹)	Maximum runoff rate (mm h ⁻¹)	Number of landslide day periods	Total of landslide day runoff (mm)	Days of gaps	Sediment day runoff (mm)	Conductivity, chloride, silica, sediment			
Canóvanas (station 50061800, area 25.49 km ²)														
1991	471	0.010	0.011	0.054	1.51	8.7	--	28.2	--	--	--	--	--	--
1992	907	0.008	0.013	0.103	1.58	20.6	--	86.3	24	--	--	1	1	--
1993	667	0.014	0.014	0.076	2.79	16.2	--	21.6	--	--	13	1	37	--
1994	371	0.009	0.010	0.042	0.71	2.5	--	2.5	8	136	2	16	8	--
1995	810	0.011	0.012	0.092	3.45	14.7	--	--	27	258	--	1	31	--
1996	1,449	0.021	0.021	0.165	16.98	40.5	1	449	25.7	5	38	55	46	1
1997	697	0.014	0.015	0.080	2.72	29.0	--	--	2	1	37	74	4	--
1998	1,547	0.010	0.010	0.177	8.09	69.0	1	370	--	--	4	77	14	--
1999	1,314	0.021	0.022	0.150	2.12	16.2	--	--	7	5	54	--	176	4
2000	600	0.010	0.011	0.068	1.49	7.1	--	--	1.4	--	20	--	46	4
2001	710	0.011	0.012	0.081	3.85	25.3	--	--	--	1	1	99	--	4
2002	678	0.017	0.018	0.077	2.98	12.7	--	--	--	5	--	13	--	3
2003	1,416	0.014	0.015	0.162	5.99	20.0	1	242	12.9	--	--	28	--	1
2004	1,539	0.030	0.032	0.175	6.76	53.6	1	215	--	--	2	--	--	1
2005	1,448	0.015	0.032	0.165	2.62	20.0	--	--	5.3	--	--	--	--	--
Total	974	0.008	0.010	0.111	16.98	69.0	4	1,276	183.8	33	46	555	9	598
Cayaguás (station 50051310, area 26.42 km ²)														
1991	652	0.033	0.035	0.074	3.71	27.0	--	--	--	--	--	--	--	--
1992	1,546	0.032	0.033	0.176	3.25	27.8	--	--	22	--	--	--	2	--
1993	1,603	0.050	0.051	0.183	4.37	21.2	--	--	--	--	--	19	1	24
1994	852	0.030	0.030	0.097	3.55	31.4	--	--	19.3	--	35	1	15	--
1995	939	0.035	0.035	0.107	1.96	13.4	--	--	10.1	2	44	--	4	--
1996	2,240	0.030	0.049	0.255	19.86	48.7	1	551	41.3	1	--	--	23	2
1997	1,759	0.026	0.032	0.201	6.79	28.0	1	196	41.0	--	38	4	4	7
1998	3,297	0.033	0.053	0.376	15.86	43.3	3	1,024	156.5	2	19	--	133	9
1999	2,123	0.020	0.033	0.242	4.03	17.1	--	--	--	23	1	89	--	4
2000	1,339	0.037	0.041	0.152	4.61	27.4	--	--	15.9	3	--	33	--	4
2001	1,061	0.028	0.032	0.121	5.52	54.8	1	42	3.1	--	4	--	101	4
2002	904	0.041	0.042	0.103	2.09	5.5	--	--	18.5	--	1	--	24	2
2003	1,913	0.042	0.043	0.218	5.55	21.2	1	220	--	--	2	--	68	--
2004	1,768	0.055	0.058	0.201	5.71	37.9	1	105	--	2	--	28	--	1
2005	2,237	0.027	0.029	0.255	3.72	16.0	2	78	134.0	--	--	--	--	--
Total	1,615	0.020	0.029	0.184	19.86	54.8	10	2,217	439.7	28	4	220	13	704
Maneiyés (station 50055500, area 17.82 km ²)														
1991	2,329	0.051	0.053	0.266	3.66	40.8	--	--	1.0	--	--	2	4	11
1992	2,901	0.071	0.091	0.330	4.29	60.6	1	52	12.1	10	--	1	--	58
1993	2,690	0.071	0.095	0.307	3.02	38.5	--	--	45.2	--	7	74	2	37
1994	1,677	0.041	0.043	0.191	2.90	35.1	--	--	4.1	--	17	17	2	24
1995	2,323	0.060	0.065	0.265	1.86	18.8	--	--	--	15	42	--	1	3
1996	2,929	0.043	0.068	0.333	10.72	65.2	1	308	47.5	--	10	53	12	--
1997	2,428	0.060	0.063	0.277	3.01	65.3	--	--	64.0	3	1	67	39	3
1998	3,646	0.079	0.087	0.416	8.42	72.0	1	316	--	21	14	35	53	18
1999	3,247	0.058	0.075	0.371	3.70	63.9	--	--	--	16	13	37	4	--
2000	2,218	0.059	0.062	0.253	4.04	62.5	--	--	--	5	6	3	91	4

Table 5. Annual hydrologic characteristics, data quality, and sampling effort in five watersheds, eastern Puerto Rico.—Continued[mm, millimeters; mm h⁻¹, millimeters per hour; km², square kilometers; --, no samples]

Year	Annual runoff total (mm)	Minimum runoff rate (mm h ⁻¹)	Maximum daily runoff rate (mm h ⁻¹)	Average runoff rate (mm h ⁻¹)	Maximum daily runoff rate (mm h ⁻¹)	Number of landslides day periods (mm h ⁻¹)	Total of landslides day runoff (mm)	Days of gaps	Sediment runoff of gaps (mm)	Conductivity only	Conductivity and sediment	Conductivity, chloride, silica, sediment	Conductivity, chloride, silica, sediment	Conductivity, chloride, silica, sediment	Lacking runoff data																
		Year	Minimum runoff rate (mm h ⁻¹)	Maximum daily runoff rate (mm h ⁻¹)	Average runoff rate (mm h ⁻¹)	Maximum daily runoff rate (mm h ⁻¹)	Number of landslides day periods (mm h ⁻¹)	Total of landslides day runoff (mm)	Days of gaps	Conductivity only	Conductivity and sediment	Conductivity, chloride, silica, sediment	Conductivity, chloride, silica, sediment	Conductivity, chloride, silica, sediment	Lacking runoff data																
2001 2,633 0.067 0.072 0.301 4.20 78.8 2 234 -- -- 29 13 138 -- 4 --																															
2002 2,405 0.059 0.063 0.275 3.41 56.2 -- -- -- -- -- -- -- -- --	2003 3,400 0.073 0.077 0.388 9.57 89.8 2 575 -- 3 -- -- -- --	2004 3,553 0.053 0.060 0.405 8.01 88.6 2 397 -- -- -- -- -- --	2005 2,929 0.025 0.027 0.334 2.19 26.0 -- -- -- -- -- -- -- --	Total 2,753 0.025 0.027 0.314 10.72 89.8 9 1,883 -- -- -- -- -- -- --	Mameyes (station 50065500, area 17.32 km ²)—Continued	Icacos (station 50075000, area 3.26 km ²)	176.3 13 87 298 140 835 9 178 2	138 -- 4 --	28 -- 3 --	275 -- 1 --	7 -- 1 --	19 -- 1 --	5 2 5 --	-- -- --																	
1991 3,089 0.113 0.113 0.353 4.76 30.7 1 147 -- -- -- -- -- -- --	1992 3,552 0.066 0.077 0.404 5.04 39.4 -- -- -- -- -- -- --	1993 2,935 0.059 0.097 0.335 2.13 12.5 -- -- -- -- -- -- --	1994 2,384 0.071 0.088 0.272 3.65 25.8 -- -- -- -- -- -- --	1995 3,512 0.119 0.134 0.401 3.95 24.6 -- -- -- -- -- -- --	1996 4,989 0.109 0.122 0.568 17.93 55.6 2 674 -- 1 -- --	1997 3,934 0.117 0.130 0.449 5.07 32.7 1 135 37.6 -- 1 --	1998 4,960 0.100 0.114 0.566 7.48 64.1 2 539 12.6 -- 11 40 --	1999 4,193 0.090 0.099 0.470 5.91 19.7 2 256 -- -- -- -- -- --	2000 3,328 0.101 0.126 0.379 4.53 22.7 -- -- -- -- -- -- --	2001 3,395 0.116 0.121 0.388 5.89 37.9 3 483 -- -- -- --	2002 3,102 0.130 0.142 0.354 6.38 35.1 1 180 3.2 -- -- --	2003 4,169 0.119 0.131 0.476 13.86 86.0 3 807 -- -- -- -- --	2004 4,606 0.123 0.134 0.524 10.97 57.5 2 685 -- -- -- -- --	2005 4,295 0.067 0.076 0.490 5.11 21.1 1 301 5.9 -- -- --	Total 3,762 0.059 0.076 0.429 17.93 86.0 18 4,307 206.8 4 37 285 15 919 10 241 32	71.6 -- -- --	16.5 1 -- --	11.2 6 --	48.3 57 --	17 49 --	5 53 --	4 2 --	5 1 70 --	5 4 21 --	46 1 48 --	84 -- 34 --	1 151 14 --	137 1 4 --	2 19 1 --	5 2 5 1 --	13 4 21 1 --
1991 2,701 0.074 0.074 0.308 4.44 5.0 1 149 -- -- -- -- -- -- --	1992 4,211 0.068 0.076 0.479 4.71 43.9 1 38 201.7 -- -- --	1993 2,962 0.063 0.104 0.338 3.50 57.2 1 53 67.7 -- -- --	1994 2,512 0.041 0.079 0.287 5.36 45.6 1 206 9.1 -- 24 --	1995 2,764 0.063 0.096 0.315 2.89 27.6 -- -- -- -- -- --	1996 4,114 0.063 0.090 0.468 20.26 91.0 3 735 18.5 -- 2 24 --	1997 3,384 0.041 0.074 0.398 4.52 82.1 1 107 -- 2 11 24 --	1998 4,247 0.040 0.069 0.485 12.60 93.3 3 714 -- 1 10 10 --	1999 4,117 0.055 0.055 0.470 7.10 73.2 2 475 -- -- -- --	2000 3,487 0.057 0.061 0.397 4.14 52.0 -- -- -- -- -- --	2001 3,523 0.094 0.115 0.402 6.79 56.2 3 637 15.9 -- 2 2 26 --	2002 2,963 0.079 0.084 0.338 7.89 105.1 1 232 20.0 -- -- --	2003 4,453 0.090 0.096 0.508 18.57 118.8 3 1052 258.0 -- 1 1 1 26 --	2004 4,588 0.107 0.110 0.522 11.36 13.1 2 769 366.0 -- 11 1 78 --	2005 4,255 0.047 0.060 0.486 5.27 5.8 2 422 365.0 -- 8 1 17 --	Total 3,624 0.040 0.055 0.414 20.26 118.8 24 5588 1,691.2 2 10 143 1 575 4 159 73	365.0 1 -- --	38 1 -- --	53 1 -- --	31 2 59 --	2 1 64 1 --	1 1 94 11 --	1 1 9 11 --	5 1 59 12 --	8 2 48 12 --	1 1 64 38 --	30 1 36 11 --	1 1 94 11 --	17 1 59 12 --	2 1 52 12 --	1 1 23 23 1 --	18 5 38 38 23 1 --

Table 6. Number and types of samples collected in different discharge classes and special sample types in five rivers, eastern Puerto Rico.

[--, no samples]

Discharge classes and special sample types	Number of samples	Sediment only	Conductivity only	Conductivity and sediment	Conductivity, chloride, silica	Conductivity, chloride, silica, sediment	Full chemistry	Full chemistry, sediment
Canóvanas								
0–10 percent, rising	26	--	--	2	--	15	--	9
0–10 percent, falling	45	--	--	9	--	19	1	16
>10–25 percent, rising	16	--	--	3	--	5	--	8
>10–25 percent, falling	33	1	--	9	--	13	1	9
>25–50 percent, rising	53	3	3	38	--	9	--	--
>25–50 percent, falling	100	3	3	65	1	26	--	2
>50–75 percent, rising	136	10	11	83	--	28	--	4
>50–75 percent, falling	384	12	22	215	2	110	--	23
>75–90 percent, rising	223	2	2	47	2	146	--	24
>75–90 percent, falling	307	2	5	78	3	189	--	30
>90–95 percent, rising	24	--	--	2	1	13	--	8
>90–95 percent, falling	19	--	--	1	--	12	--	6
>95–100 percent, rising	3	--	--	--	--	1	--	2
>95–100 percent, falling	1	--	--	--	--	--	--	1
High chloride	29	--	--	2	--	11	--	16
High potassium	--	--	--	--	--	--	--	--
Low silica	--	--	--	--	--	--	--	--
No runoff	2	--	--	1	--	1	--	--
Cayaguás								
0–10 percent, rising	60	--	--	14	--	40	1	5
0–10 percent, falling	87	--	--	18	1	56	1	11
>10–25 percent, rising	50	2	--	11	--	32	--	5
>10–25 percent, falling	68	--	--	17	1	40	--	10
>25–50 percent, rising	37	--	--	9	--	24	--	4
>25–50 percent, falling	80	2	--	21	--	50	1	6
>50–75 percent, rising	55	4	--	8	1	32	1	9
>50–75 percent, falling	119	11	--	23	5	69	--	11
>75–90 percent, rising	130	3	2	32	1	88	--	4
>75–90 percent, falling	192	5	--	41	1	136	--	9
>90–95 percent, rising	37	--	1	5	--	26	--	5
>90–95 percent, falling	39	--	1	8	--	27	--	3
>95–100 percent, rising	24	--	--	5	--	5	--	14
>95–100 percent, falling	23	1	--	4	3	10	--	5
High chloride	1	--	--	--	--	1	--	--
High potassium	2	--	--	--	--	1	--	1
Low silica	--	--	--	--	--	--	--	--
No runoff	59	--	--	4	--	53	--	2
Mameyes								
0–10 percent, rising	6	--	3	--	--	2	--	1
0–10 percent, falling	50	--	1	4	--	11	7	27
>10–25 percent, rising	8	--	1	1	--	2	--	4
>10–25 percent, falling	32	--	--	3	1	9	--	19
>25–50 percent, rising	3	--	--	2	--	1	--	--
>25–50 percent, falling	33	2	1	6	--	11	1	12
>50–75 percent, rising	10	--	--	1	1	7	--	1
>50–75 percent, falling	39	2	4	19	--	9	--	5
>75–90 percent, rising	161	1	10	32	6	93	--	19
>75–90 percent, falling	446	--	15	98	17	285	--	31
>90–95 percent, rising	202	1	22	37	23	113	1	5
>90–95 percent, falling	344	4	20	80	52	179	--	9
>95–100 percent, rising	86	1	3	7	8	52	--	15
>95–100 percent, falling	87	2	7	7	9	47	--	15
High chloride	34	--	--	1	14	7	--	12
High potassium	13	--	--	--	9	4	--	--
Low silica	4	--	--	--	--	2	--	2
No runoff	3	--	1	--	--	1	--	1

Table 6. Number and types of samples collected in different discharge classes and special sample types in five rivers, eastern Puerto Rico.—Continued

[--, no samples]

Discharge classes and special sample types	Number of samples	Sediment only	Conductivity only	Conductivity and sediment	Conductivity, chloride, silica	Conductivity, chloride, silica, sediment	Full chemistry	Full chemistry, sediment
Icacos								
0 to 10 percent, rising	19	--	--	1	--	9	--	9
0 to 10 percent, falling	55	--	--	5	1	19	1	28
>10 to 25 percent, rising	12	--	--	2	--	9	--	1
>10 to 25 percent, falling	49	1	--	10	--	22	4	12
>25 to 50 percent, rising	12	--	--	2	--	5	1	4
>25 to 50 percent, falling	47	1	--	14	2	16	1	13
>50 to 75 percent, rising	9	1	--	--	--	7	--	1
>50 to 75 percent, falling	22	--	--	6	--	13	--	3
>75 to 90 percent, rising	171	--	1	44	1	112	--	13
>75 to 90 percent, falling	330	1	11	65	2	229	--	22
>90 to 95 percent, rising	222	--	16	53	3	134	--	16
>90 to 95 percent, falling	196	--	5	49	3	126	--	13
>95 to 100 percent, rising	83	--	2	17	3	45	1	15
>95 to 100 percent, falling	67	--	2	13	--	44	1	7
High chloride	62	--	--	--	--	42	--	20
High potassium	24	--	--	1	--	20	--	3
Low silica	89	--	--	1	--	28	1	59
No runoff	32	--	1	2	--	27	--	2
Guabá								
0–10 percent, rising	16	--	--	1	--	13	1	1
0–10 percent, falling	43	--	--	12	--	13	--	18
>10–25 percent, rising	9	--	--	1	--	6	--	2
>10–25 percent, falling	49	--	1	15	1	18	1	13
>25–50 percent, rising	19	--	--	8	--	8	--	3
>25–50 percent, falling	43	--	--	12	--	20	--	11
>50–75 percent, rising	18	--	4	3	--	9	--	2
>50–75 percent, falling	23	--	--	4	--	16	--	3
>75–90 percent, rising	63	--	1	16	--	42	--	4
>75–90 percent, falling	22	1	--	5	--	14	--	2
>90–95 percent, rising	104	--	2	22	--	74	1	5
>90–95 percent, falling	126	--	2	22	--	93	--	9
>95–100 percent, rising	57	--	--	3	--	44	--	10
>95–100 percent, falling	56	--	--	1	--	50	--	5
High chloride	50	--	--	--	--	42	--	8
High potassium	40	--	--	--	--	40	--	--
Low silica	83	--	--	--	--	25	1	57
No runoff	72	--	--	18	--	48	--	6

through 2005, 507 hydrologic events were sampled by automated samplers in five rivers during 263 storms, including all major hurricanes during that period (figs. 2–6). Although the climate of eastern Puerto Rico is weakly seasonal (more rain in May and in August through December) large storms occur throughout the year in response to cold fronts from November to May and tropical disturbances from June to October. In this study, 332 samples that were analyzed for suspended sediment and chemistry were collected at runoff rates greater than 20 millimeters per hour (mm h^{-1}), and some chemical samples were even collected at runoff rates of almost 100 mm h^{-1} .

Without comparison with other sampling programs, it is difficult for the reader to assess sampling effort necessitated

by the need to accurately describe storm-related processes at the eastern Puerto Rico WEBB site. For such a comparison, a large data collection assembled by Alexander and others (1996a, 1996b, 1998) was chosen. This collection contains data describing rivers from the U.S. Geological Survey Hydrologic Benchmark Network for 1962 to 1995 and from the U.S. Geological Survey National Stream Quality Accounting Network (NASQAN) for 1973 to 1995. This combined database is referred to here as Water Quality Network–1996 (WQN96). The average record duration per site in the WQN96 database is 18.36 years, comparable to the 15 years of the WEBB dataset. Watersheds from these networks represent a broad cross section of rivers in the

United States, including 8 in Hawaii, 6 in Puerto Rico, and 1 in Guam. Most of the rivers are described by a set of chemical and physical measurements that match those sampled in the Puerto Rico WEBB rivers. The programs that produced the WQN96 database sampled extreme flows in many of the rivers. To compare sampling efforts with the eastern Puerto Rico WEBB program, all sites lacking discharge measurements or having ambiguous drainage areas (lakes, canals, and diversion—total of 24) and all sites without a body of comparable chemical and physical measurements (less than 4 suspended-sediment measurements or less than 10 complete chemical analyses for a total of 20) were eliminated from comparison. A total of 53 rivers were excluded from the comparison, leaving 626 rivers.

When compared with the 626 rivers in the WQN96 database, the eastern Puerto Rico rivers are among those that are wettest and have the greatest runoff. The watersheds with the greatest mean-annual runoff in our study are the Mameyes, Icacos, and Guabá, which are forested. Only three rivers in the WQN96 database had comparable mean-annual runoff (the Queets River and North Fork of the Quinault, both in Washington; and Honolii Stream, Hawaii). Mean annual runoff of the Cayaguás is exceeded by 11 rivers from California, Hawaii, and Washington. Mean annual runoff for the Río Canóvanas is exceeded by 26 other rivers.

A runoff rate of 1 mm h⁻¹ was set as the dividing line between low- and high-runoff samples in the eastern Puerto Rico WEBB and the WQN96 databases. In the WEBB rivers, 30 to 37 percent of the total annual runoff occurs when runoff rates exceed 1 mm h⁻¹ (0.2778 cubic meters per second per square kilometer (m³ s⁻¹ km⁻²), or 25.41 cubic feet per second per square mile (ft³ s⁻¹ mi⁻²)). A higher runoff rate might have been chosen, but very few samples in the combined WQN96 database were collected at high runoff rates. Only samples that had enough chemical analyses to calculate bedrock denudation (table 7) or a charge balance (comprehensive chemistry, table 8) were included. For samples with a full charge balance, the WEBB dataset also recorded suspended solids; the WQN96 samples usually did not. The sampling effort for comprehensive chemistry, expressed as samples per river per year (table 8), was about five times as great for eastern Puerto Rico WEBB rivers as compared with the overall combined WQN96 database. For tropical rivers, the WEBB effort was less than three-fold as great. For samples collected at rates less than 1 millimeter per hour (mm h⁻¹), there was a comparable effort; however, for runoff rates greater than 1 mm h⁻¹, the eastern Puerto Rico effort was 50-fold as great; 543 samples were collected as compared with 149 for the entire combined database or 38 for the tropical rivers in the database. The maximum runoff rates sampled for chemistry in the combined WQN96 database were 12.79 mm h⁻¹ for Biscuit Brook, New York, and 9.77 mm h⁻¹ for Honolii Stream, Hawaii. The eastern Puerto Rico database has 125 samples with runoff rates that exceed 20 mm h⁻¹ and 3 that even exceed 90 mm h⁻¹. Basin area might be a factor in this comparison, and in terms of basin

Table 7. Number of samples in three river-hydrology datasets that have sufficient data to calculate total denudation rates.

[WQN96, database that combines data of the Hydrologic Benchmark and National Assessment of the Quality of Water Networks (Alexander and others, 1996b); WEBB, Water, Energy, and Biogeochemical Budgets; <, less than; >, more than; mm h⁻¹, millimeters per hour]

Runoff rate of sample	Number of rivers in class	Number of samples	Samples per river	Samples per river per year
All rivers in WQN96 with chemistry or sediment data				
Total	679	211,281	311	16.73
All rivers in WQN96 with sufficient data to calculate total denudation rates				
<1 mm h ⁻¹	548	30,187	55	2.96
>1 mm h ⁻¹	43	96	2	0.12
>10–20 mm h ⁻¹	0	0	—	—
>20 mm h ⁻¹	0	0	—	—
Total	548	30,283	55	2.97
All tropical rivers in WQN96 with sufficient data to calculate total denudation rates				
<1 mm h ⁻¹	15	980	65	3.51
>1 mm h ⁻¹	11	35	3	0.17
>10–20 mm h ⁻¹	0	0	—	—
>20 mm h ⁻¹	0	0	—	—
Total	15	1,015	68	3.64
Eastern Puerto Rico WEBB samples with sufficient data to calculate total denudation rates				
<1 mm h ⁻¹	5	922	184	13
>1 mm h ⁻¹	5	3,398	680	49
>10–20 mm h ⁻¹	5	932	186	13
>20–30 mm h ⁻¹	5	303	61	4.3
>30–40 mm h ⁻¹	5	124	25	1.8
>40–50 mm h ⁻¹	5	53	11	0.76
>50–60 mm h ⁻¹	3	32	11	0.76
>60–70 mm h ⁻¹	3	20	7	0.48
>70–80 mm h ⁻¹	2	11	6	0.39
>80–90 mm h ⁻¹	1	5	5	0.36
>90 mm h ⁻¹	1	3	3	0.21
Total	5	4,320	864	62

area, the WQN96 rivers overlap all the WEBB rivers, except the Guabá which has a 0.114-km² watershed at the stream-gaging station.

Globally, few other event samples of streams have been collected and analyzed for sediment and chemistry at runoff rates of greater than 5 mm h⁻¹. In the tropics, two samples were collected at about 16 mm h⁻¹ by the U.S. Geological Survey in Puerto Rico in 1970 during a tropical depression (Haire, 1970). Goldsmith and others (2008) collected samples in Taiwan during Typhoon Mindulle at runoff rates of as much as 7.3 mm h⁻¹, and Hicks and others (2000) collected samples in New Zealand during Cyclone Bola at runoff rates of as much as 4.8 mm h⁻¹.

The eastern Puerto Rico WEBB sampling program represents the opportunity to assess how physical and biogeochemical processes affect small watersheds at extremely high runoff conditions. Because of the extensive sampling of

Table 8. Number of samples in three river-hydrology datasets that have comprehensive chemistry.

[WQN96, combined dataset of the Hydrologic Benchmark and National Assessment of the Quality of Water Networks (Alexander and others, 1996b); WEBB, Water, Energy, and Biogeochemical Budgets program; <, less than; >, greater than; mm h⁻¹, millimeters per hour]

Runoff rate of sample	Number of rivers in class	Number of samples	Samples per river	Samples per river per year
All rivers in WQN96 with chemistry or sediment data				
All	679	211,281	311	16.73
All rivers in WQN96 with runoff and comprehensive chemistry				
<1 mm h ⁻¹	548	26,568	48	2.61
>1 mm h ⁻¹	54	149	3	0.15
>10–20 mm h ⁻¹	1	1	1	0.05
>20 mm h ⁻¹	0	0	—	—
All	548	26,717	49	2.62
All tropical rivers in WQN96 with runoff and comprehensive chemistry				
<1 mm h ⁻¹	15	1,167	78	4.18
>1 mm h ⁻¹	13	38	3	0.16
>10–20 mm h ⁻¹	0	0	—	—
>20 mm h ⁻¹	0	0	—	—
All	15	1,205	80	4.32
Eastern Puerto Rico WEBB samples with runoff and comprehensive chemistry				
<1 mm h ⁻¹	5	314	63	4.5
>1 mm h ⁻¹	5	543	109	7.8
>10–20 mm h ⁻¹	5	256	51	3.7
>20–30 mm h ⁻¹	5	125	25	1.8
>30–40 mm h ⁻¹	5	56	11	0.80
>40–50 mm h ⁻¹	5	24	5	0.34
>50–60 mm h ⁻¹	3	18	6	0.43
>60–70 mm h ⁻¹	3	9	3	0.21
>70–80 mm h ⁻¹	2	6	3	0.21
>80–90 mm h ⁻¹	1	3	3	0.21
>90 mm h ⁻¹	1	3	3	0.21
All	5	857	171	12

high-runoff-rate events, these data are unique: they represent a seldom-examined realm of process-related water-quality studies. The extensive sampling for suspended sediment, combined with the use of surrogate parameters to calculate dissolved bedrock, means that the WEBB database is much better poised than most other long-term studies for evaluating denudation processes (table 7).

References

- Alexander, R.B., Slack, J.R., Ladtke, A.S., Fitzgerald, K.K., and Shertz, T.L., 1996a, Data from selected U.S. Geological Survey national stream water quality monitoring networks (WQN): U.S. Geological Survey Open-File Report 96-337, 79 p.; CD-ROM.
- Alexander, R.B., Slack, J.R., Ladtke, A.S., Fitzgerald, K.K., and Shertz, T.L., 1996b, Data from selected U.S. Geological Survey national stream water quality monitoring networks: U.S. Geological Survey Digital Data Series DDS-37, 2 CD-ROMs.
- Alexander, R.B., Slack, J.R., Ladtke, A.S., Fitzgerald, K.K., and Shertz, T.L., 1998, Data from selected U.S. Geological Survey national stream water quality monitoring networks: Water Resources Research, v. 34, p. 2401–2405.
- Bevington, P.R., and Robinson, K.D., 2003, Data reduction and error analysis for the physical sciences—2: New York, McGraw Hill, 320 p.
- Chapman, T.B., 1999, A comparison of algorithms for stream flow recession and baseflow separation: Hydrological Processes, v. 13, p. 701–714.
- Díaz, P.L., Aquino, Z., Figueroa-Alamo, C., Garcia, R., and Sanchez, A.V., 2004, Water resources data, Puerto Rico and the U.S. Virgin Islands, water year 2002: U.S. Geological Survey Water-Data Report PR-02-1, 652 p.
- Elmore, H.L., and Hayes, T.W., 1960, Solubility of atmospheric oxygen in water: Journal of Sanitary Engineering Division, American Society of Civil Engineers, v. 86, SA4, p. 41–53.
- Geyer, Tobias, Birk, S., Liedl, R., and Sauter, M., 2008, Quantification of temporal distribution of recharge in karst systems from spring hydrographs: Journal of Hydrology, v. 348, p. 452–463.
- Goldsmith, S.T., Carey, A.E., Lyons, W.B., Kao, S.-J., Lee, T.-Y., and Chen, J., 2008, Extreme storm events, landscape denudation, and carbon sequestration: Typhoon Mindulle, Choshui River, Taiwan: Geology, v. 36, no. 6, p. 483–486.
- Haire, W.J., 1972, Flood of October 5–10, 1970, in Puerto Rico: Commonwealth of Puerto Rico Water-Resources Bulletin 12, 42 p.
- Hall, F.R., 1968, Base-flow recessions—A review: Water Resources Research, v. 4, no. 5, p. 973–983.
- Hicks, D.M., Gomez, B., and Trustrum, M.A., 2000, Erosion thresholds and suspended sediment yields, Waipaoa River Basin, New Zealand: Water Resources Research, v. 36, no. 4, p. 1129–1142.

- Jupp, D.L., 1976, B-splines for smoothing and differentiating data sequences: *Mathematical Geology*, v. 8, no. 3, p. 243–266.
- Larsen, M.C., 2012, Landslides and sediment budgets in four watersheds in eastern Puerto Rico, ch. F in Murphy, S.F., and Stallard, R.F., eds., *Water quality and landscape processes of four watersheds in eastern Puerto Rico: U.S. Geological Survey Professional Paper 1789*, p. 153–178.
- Larsen, M.C., and Simon, A., 1993, A rainfall intensity-duration threshold for landslides in a humid-tropical environment, Puerto Rico: *Geografiska Annaler*, v. 75A, no. 1–2, p. 13–23.
- Mackenzie, R.C., 1957, Differential thermal analysis of clays: The Mineralogical Society [London], 389 p.
- Mackenzie, R.C., and Caillère, S., 1979, Thermal analysis, DTA, TG, DTG, in Van Olphen, Hendrik, and Fripiat, J.J., eds., *Data handbook for clay material and other nonmetallic Minerals*: New York, Pergamon, p. 243–284.
- Miller, R.L., Bradford, W.L., and Peters, N.E., 1988, Specific conductance—Theoretical considerations and application to analytical quality control: U.S. Geological Survey Water-Supply Paper 2311, 16 p.
- Murphy, S.F., and Stallard, R.F., 2012, Hydrology and climate of four watersheds in eastern Puerto Rico, ch. C in Murphy, S.F., and Stallard, R.F., eds., *Water quality and landscape processes of four watersheds in eastern Puerto Rico: U.S. Geological Survey Professional Paper 1789*, p. 43–84.
- Reinsch, C.H., 1967, Smoothing by spline functions: *Numerische Mathematik*, v. 10, p. 177–183.
- Runkel, R.L., Crawford, C.G., and Cohn, T.A., 2004, Load estimator (LOADEST): A FORTRAN program for estimating constituent loads in streams and rivers: U.S. Geological Survey Techniques and Methods Book 4, 69 p., program and test files.
- Stallard, R.F., 1995a, Relating chemical and physical erosion, in White, A.F., and Brantley, S.L., eds., *Chemical weathering rates of silicate minerals*: Washington, D.C., Mineralogical Society of America Reviews in Mineralogy, v. 31, p. 543–564.
- Stallard, R.F., 1995b, Tectonic, environmental, and human aspects of weathering and erosion—A global review using a steady-state perspective: *Annual Review of Earth and Planetary Sciences*, v. 12, p. 11–39.
- Stallard, R.F., 1998, Terrestrial sedimentation and the carbon cycle—Coupling weathering and erosion to carbon burial: *Global Biogeochemical Cycles*, v. 12, no. 2, p. 231–252.
- Stallard, R.F., 1999, Erosion and the effects of deforestation in the Panama Banal Basin, in *Panama Canal Watershed Monitoring Project: Report of the Panama Canal Watershed Monitoring Project*, ch. II.8, 8 volumes, 21 CD-ROMs.
- Stallard, R.F., 2012a, Atmospheric inputs to watersheds of the Luquillo Mountains of eastern Puerto Rico: ch. D in Murphy, S.F., and Stallard, R.F., eds., *Water quality and landscape processes of four watersheds in eastern Puerto Rico: U.S. Geological Survey Professional Paper 1789*, p. 85–112.
- Stallard, R.F., 2012b, Weathering, landscape equilibrium, and carbon in four watersheds in eastern Puerto Rico, ch. H in Murphy, S.F., and Stallard, R.F., eds., *Water quality and landscape processes of four watersheds in eastern Puerto Rico: U.S. Geological Survey Professional Paper 1789*, p. 199–248.
- Stallard, R.F., and Edmond, J.M., 1981, Geochemistry of the Amazon—1. Precipitation chemistry and the marine contribution to the dissolved load at the time of peak discharge: *Journal of Geophysical Research—Oceans and Atmospheres*, v. 86, p. 9844–9858.
- Stallard, R.F., and Kinner, D.A., 2005, Estimation of landslide importance in hillslope erosion within the Panama Canal watershed, in Harmon, R.S., ed., *The Río Chagres, Panama—A multidisciplinary profile of a tropical watershed*: Dordrecht, The Netherlands, Springer Water Science and Technology Library, v. 52, p. 281–295.
- Stallard, R.F., and Murphy, S.F., 2012, Water quality and mass transport in four watersheds in eastern Puerto Rico, ch. E in Murphy, S.F., and Stallard, R.F., eds., *Water quality and mass transport in research watersheds in eastern Puerto Rico: U.S. Geological Survey Professional Paper 1789*, p. 113–152.
- Stumm, Werner, and Morgan, J.J., 1981 *Aquatic chemistry*: New York, John Wiley, 780 p.
- Tallaksen, L.M., 1995, A review of baseflow recession analysis: *Journal of Hydrology*, v. 165, p. 349–370.
- Tardy, Yves, Bustillo, V., Roquin, C., Mortatti, J., and Reynaldo, R., 2005, The Amazon—Bio-geochemistry applied to river basin management, pt. I. Hydro-climatology, hydrograph separation, mass transfer balances, stable isotopes, and modelling: *Applied Geochemistry*, v. 20, p. 1746–1829.
- Vogel, R.M., and Kroll, C.N., 1996, Estimation of baseflow recession constants: *Water Resources Management*, v. 10, p. 303–320.
- Wolman, M.G., and Miller, J.P., 1960, Magnitude and frequency of forces in geomorphic processes: *Journal of Geology*, v. 68, p. 54–74.

Appendix 2. Methods Used to Analyze Water Quality of Four Watersheds in Eastern Puerto Rico

By Sheila F. Murphy and Robert F. Stallard

Introduction

The U.S. Geological Survey's Water, Energy, and Biogeochemical Budgets (WEBB) program in Puerto Rico analyzed a core suite of chemical and physical measurements that would indicate the major sources and processes affecting water chemistry of the rivers. More than 6,600 samples from both routine sampling and storm events were collected and analyzed for chemical or physical parameters (or both) from 1991 to 2005 (appendix 1, table 5). Standard methods of sample collection, processing, field measurements, and laboratory analysis were used throughout the project and are described here.

Field Sampling

Two principal types of samples, grab and storm event, were collected during the study. Grab samples were initially collected quarterly, but sampling frequency varied depending on staff availability. Onsite measurements included pH, conductivity (microsiemens per centimeter, $\mu\text{S cm}^{-1}$), temperature (degrees Celsius, $^{\circ}\text{C}$), and dissolved oxygen (O_2 ; milligrams per liter, mg L^{-1}). Water chemistry samples were collected from riverbanks at well-mixed cross sections near each gage site by using dip bottles and gloved hands, following methods described by Edwards and Glysson (1999). Three 1-liter (L) high-density polyethylene (HDPE) bottles were rinsed four times sample water and then filled with sample water and labeled MIN (for sediment mineralogy), IC (for inorganic chemistry), or OC (for organic carbon). One 250-milliliter (mL) clear HDPE bottle was similarly rinsed four times, filled with sample water, and labeled ARC (for archive). Depth-integrated samples for suspended sediment were periodically collected at the same time as a grab sample, following the method of Wilde and others (1999). This sample was collected in a preweighed 125-mL, wide-mouth HDPE bottle labeled TSM (for total suspended mass). Samples were transported on ice to the U.S. Geological Survey Caribbean Water Science Center laboratory as soon as possible, typically within a few hours.

Storm event samples were collected by an ISCO[®] sampler, which was automatically triggered when the river reached a specified stage height. Once triggered, all 24 bottles were filled following a preset program calibrated by using sample storm hydrographs. The sampler was then emptied and restarted manually. Because a small storm could prevent the sampling of a subsequent larger storm, and the number of

samples generated by the initial stage was often too great to process in a reasonable time, threshold stages were gradually raised during the study (appendix 1, its figures 2–6). ISCO[®] bottles were retrieved and transported to the laboratory for processing as soon as the site could be accessed after a storm. Conductivity was measured in the laboratory, but because the samples could not be measured immediately, temperature, pH, and dissolved oxygen were not analyzed.

Sample Filtration and Preservation

Before filtration, storage bottles and quartz-fiber filters were cleaned. For major ions (MAJ) and nutrients (NUT), 250-mL clear high-density polyethylene (HDPE) and 250-milliliter (mL) amber HDPE bottles, respectively, were leached with hot deionized water overnight, then rinsed three times with deionized water. For trace elements (TE), 250-mL HDPE bottles were soaked overnight with 2 percent hydrochloric acid, followed by three rinses with deionized water and drying at 60°C. For dissolved organic carbon (DOC), 125-mL amber glass bottles were rinsed with deionized water and baked for 1 hour at 500°C. Quartz-fiber filters (used to capture DOC and particulate organic carbon) were soaked overnight in 10 percent hydrochloric acid, rinsed thoroughly in deionized water, and baked for 1 hour at 500°C.

For grab samples, weights of all sample bottles were recorded upon return to the Caribbean Water Science Center laboratory, and the archive (ARC) bottle was frozen. Water in the remaining sample bottles was filtered as soon as practicable. The 1-liter (L) sediment mineralogy (MIN) sample was filtered through a 0.2-micrometer (μm) cellulose acetate (Millipore[®]) filter in a polycarbonate filter apparatus. The filter and funnel were rinsed with sample water four times, and the filtrate was used to rinse the MAJ and NUT storage bottles four times (the final rinse was retained in the bottles for later use, as described later in this paragraph). After the entire MIN bottle was filtered, the weight of the empty bottle was recorded, and the filter was air dried and saved for later mineralogical analysis. A 0.2- μm polycarbonate (Nucleopore[®]) filter was then placed in the same polycarbonate filtration apparatus and rinsed three times using the rinse water stored in the MAJ and NUT bottles. Approximately 50 mL of sample water from the inorganic chemistry (IC) bottle was then filtered and discarded; this step serves to "clog" the filter, which ensures that the filtrate is subjected to a consistent filter pore size. Sample from the IC bottle was then filtered into the MAJ bottle and refrigerated. If the sample

filtered rapidly, the filter was left in the holder, but if the MAJ sample was excessively slow to filter, the filter was replaced with a new 0.2- μm polycarbonate filter, and the filter and filter apparatus were rinsed three times with rinse water and “clogged” as described above. The IC sample was then filtered into the emptied NUT bottle, preserved with 0.25 mL chloroform, and refrigerated.

Simultaneously, the 125-mL total suspended mass (TSM) sample bottle was agitated and filtered through a preweighed 0.2- μm polycarbonate filter in a Teflon filtration funnel. The TSM bottle and filtration apparatus were then rinsed three times with rinse water from the MAJ or NUT bottles to wash any remaining particulate matter onto the filter. Most of the filters were dried at 105°C and then weighed. The dried weight minus the prefilter weight represented total suspended sediment. Some filters were placed in a preweighed crucible and ashed at 550°C. The final weight minus the prefilter weight represented total suspended bedrock.

Sample from the IC bottle was then filtered through a new 0.2- μm Nucleopore® filter and the Teflon® filtration apparatus. Rinse water from the MAJ and NUT bottles was passed through the filter and filter funnel three times into a waste container. Approximately 50 mL of sample water from the IC bottle was filtered to “clog” the filter, and all filtrate was discarded. Sample water from the IC bottle was then filtered into the TE bottle and was treated to 1 percent hydrochloric acid with ultrahigh purity hydrochloric acid.

Sample water from the OC (organic carbon) bottle was then filtered. In the first 6 years of the study, OC samples were pressure filtered through a silver-membrane filter. After 1996 (because the manufacturer discontinued these filters), organic carbon (OC) samples were passed through an acid-washed, prebaked, quartz-fiber filter in the Teflon® filtration apparatus. The bottle was agitated during filtration. At least half of the bottle’s contents was filtered through the quartz-fiber filter into a waste container and discarded. The next volume was filtered into the DOC bottle and preserved with 0.25 mL concentrated phosphoric acid (44 Normal). The remaining OC sample was filtered and discarded. The quartz-fiber filter was air dried and stored for later particulate organic carbon analysis.

For event samples, the 1-L ISCO® bottles were refrigerated upon return to the laboratory. The sample bottles were weighed and processed as soon as possible. Polycarbonate filters and pre-baked, rinsed, quartz-fiber filters were weighed and stacked in the polycarbonate filtration apparatus, with the quartz-fiber filter on top. The filters and filtration apparatus were rinsed twice with sample water, and filtrate was fed into a waste container. Sample water was then filtered into a NUT bottle, followed by a MAJ bottle (both rinsed twice with filtrate), followed by a TE bottle (which was not rinsed). The remainder of the 1-L bottle was agitated and filtered into a clean glass beaker. A DOC bottle was filled from the beaker, and the remaining filtrate was poured back into the 1-L ISCO® bottle to rinse remaining sediment onto the filter. The storage bottles were preserved in the same manner as grab samples. The empty 1-L sample bottle was weighed, and this weight was subtracted from the initial bottle weight to

obtain water-sample weight. Filters were placed in a petri dish and dried as pairs; when dry, the filters were weighed together, then separately. The weight of sediment on the filters was obtained by subtracting filter dry weights from final weights; it was then divided by the sample weight to obtain suspended sediment concentrations.

Owing to the enormous volume of event samples (even after threshold stages were increased), analyses performed on storm event samples were eventually reduced to conductivity, silica, chloride, and sometimes potassium and suspended sediment. For these analyses, sample water was filtered through a 0.2- μm polycarbonate (Nucleopore®) filter into a 30- or 60-mL “Si/Cl” clear HDPE bottle (which had been leached by hot deionized water). The bottle was rinsed three times with sample water, filled, and refrigerated.

Samples were periodically shipped, on ice, to the U.S. Geological Survey National Research Program laboratory in Boulder, Colo., for laboratory analyses.

Chemical Analyses

Most analyses were performed at the U.S. Geological Survey National Research Program laboratory in Boulder, Colo. A subset of samples was analyzed at the Kiowa Environmental Chemistry Laboratory of the University of Colorado, Boulder; at the Department of Geosciences of the University of Montana, Missoula; or at the U.S. Geological Survey Panola Laboratory in Atlanta, Ga., as described below.

Alkalinity

Alkalinity was determined at the U.S. Geological Survey National Research Program laboratory in Boulder, Colo. From 1991 to 1998, alkalinity was determined on an autotitrator that used Gran titration. After 1998, a new autotitrator was obtained, and an incremental inflection point titration was used. For both methods, a blank, a sample replicate, three standards (50, 500, and 1,000 milliequivalents per liter ($\mu\text{eq L}^{-1}$)), and a U.S. Geological Survey standard reference water sample (SRWS) (U.S. Geological Survey, 2012) were analyzed every 14 samples. Samples were reanalyzed if the regression coefficient (r^2) of the slope of the standards was less than 0.99, or if replicate samples deviated by more than 10 percent. If alkalinity was greater than the highest standard, the sample was diluted and reanalyzed. When the incremental inflection point titration was used, if alkalinity was below the detection limit, then the sample was spiked with 1 mL of 1,000 $\mu\text{eq L}^{-1}$ KHCO_3 , reanalyzed, and the spike was then subtracted.

Major Cations

Major cations (sodium, potassium, magnesium, and calcium) were analyzed with inductively coupled plasma (ICP) spectroscopy. From 1991 to 1995, samples were analyzed at

the Department of Geosciences of the University of Montana. U.S. Geological Survey SRWSs were run approximately every seven samples. If measured concentrations did not agree within specified limits of certified values (limits varied from element to element, but were always within 10 percent), samples were reanalyzed. Spike recoveries and replicates were also analyzed on 10 percent of the samples, randomly selected.

From 1995 to 2005, major cations were analyzed at the U.S. Geological Survey National Research Program laboratory in Boulder, Colo., with a Perkin Elmer Optima 3300 DV® inductively coupled plasma–atomic emission spectroscopy (ICP–AES) by using techniques described by Garbarino and Taylor (1979). Five or six calibration standards were analyzed for each analysis run; each had an r^2 value greater than 0.999. Samples with concentrations above the highest standard were diluted and reanalyzed. Twelve to 17 laboratory blanks, interspersed throughout each analysis run, were used to calculate detection limits for each analyte for each analysis run. SRWSs, analyzed at a frequency exceeding 30 percent of samples, were interspersed throughout each analysis run. Each sample was analyzed in triplicate, and the mean of the three concentration values was reported. Precision was calculated as the standard deviation of the three values; if one of the replicates substantially disagreed with the other two, it was discarded and the average and standard deviation of the remaining two were used to calculate concentration and precision. When all three values substantially disagreed, the sample was reanalyzed.

Silica

Silica was analyzed in more than 4,600 grab and event samples, all at the U.S. Geological Survey National Research Program laboratory in Boulder, Colo. Silica was measured either by an ultraviolet/visible (UV/Vis) spectrophotometer or by ICP–AES, and sometimes by both. For spectrophotometer analyses, a blank, four standards, a SRWS, and a laboratory replicate were analyzed on a Perkin Elmer® UV/Vis spectrophotometer for every nine samples. A regression of the standards calculated sample concentration. Samples were reanalyzed if blanks were greater than the instrument detection limit (1 micromole per liter ($\mu\text{mol L}^{-1}$)) of silica, if absorbance values of replicates differed by more than 0.025 in the 0.100 to 0.500 absorbance range or by more than 0.050 in the 0.500 to 1.000 absorbance range, or if the observed value of the SRWS was greater than 5 percent of its most probable value.

For ICP–AES analyses, silica was analyzed on a Leeman Labs Direct Reading Echelle® dual view, sequential multielement ICP spectrometer. The detection limit was 0.05 milligrams per liter (mg L^{-1}) SiO_2 . Blanks, SRWSs, and laboratory replicates were analyzed several times during each analytical run. Replicate determinations were performed and were within 2 percent.

Potassium

Potassium was determined either on an atomic adsorption spectrophotometer or by ICP–AES at the U.S. Geological Survey National Research Program laboratory in Boulder, Colo. For atomic absorption, samples were analyzed on a Perkin Elmer 5000® atomic adsorption spectrophotometer using a three-point standard curve. Replicates and several SRWSs were analyzed every 10 samples. If SRWS concentrations deviated more than 5 percent from certified values, the instrument was restandardized and analyses were repeated.

For ICP–AES analyses, potassium was analyzed on a Leeman Labs Direct Reading Echelle® dual view, sequential multielement, ICP spectrometer. The detection limit was 0.04 mg L^{-1} potassium. Blanks, SRWSs, and laboratory replicates were analyzed several times during each analytical run. Replicate determinations were within 3 percent of the original value.

Major Anions

When complete chemistry was analyzed, nitrate, sulfate, and chloride were determined by ion chromatography. Samples were usually analyzed at the U.S. Geological Survey National Research Program laboratory in Boulder, Colo., on a Dionex® ion chromatograph. Three blanks, six standards, a SRWS, and a laboratory replicate were analyzed every ninth sample. In 1996, owing to a high volume of samples and to problems with instruments, samples were analyzed at the U.S. Geological Survey's Panola Laboratory in Atlanta, Ga., by ion chromatography. Six standards and two SRWSs were analyzed at the beginning of each run. After every 10 samples, a replicate sample and a random selection of 2 reference samples, including SRWSs and blanks, were analyzed.

In many samples chloride was analyzed, but nitrate and sulfate were not. Like silica, chloride was analyzed in more than 4,600 grab and event samples. It was analyzed either by ion chromatography, as described above, or with a Buchler Chloridometer®, which operates by coulometric titration with silver ions, at the U.S. Geological Survey National Research Program laboratory in Boulder, Colo. Four calibration standards were analyzed at the beginning and end of each run and were used to calculate sample concentrations. Blanks and SRWSs were analyzed every 10 samples. All samples were run in duplicate, and if the relative standard deviation was greater than 5 percent, they were reanalyzed. A 70 $\mu\text{mol L}^{-1}$ chloride spike was added to every sample to ensure a clean titration end point for samples with low chloride concentrations.

Nitrite

Most samples were analyzed for nitrite at the U.S. Geological Survey National Research Program laboratory in Boulder, Colo., on a Perkin-Elmer® spectrophotometer by using a four-point calibration curve. Blanks and intermediate standards were analyzed throughout each run, and

approximately 10 percent of samples were run in duplicate. Samples were reanalyzed if the blank concentration was greater than the instrument detection limit ($0.2 \mu\text{mol L}^{-1}$ of nitrogen), if the observed value of the SRWS was greater than 5 percent of its most probable value, or if absorbance values of replicates differed by more than 0.005 in the 0.030 to 0.100 absorbance range, by more than 0.020 in the 0.100 to 0.500 absorbance range, or by more than 0.030 in the 0.500 to 1.000 absorbance range. Some samples were analyzed at the U.S. Geological Survey Panola Laboratory in Atlanta, Ga., on an ALPKEM® nutrient analyzer; samples were analyzed in triplicate, and a seven-point calibration curve was run before and after each analytical run.

Phosphate

Phosphate was determined on a Perkin Elmer® UV/Vis spectrophotometer at the U.S. Geological Survey National Research Program laboratory in Boulder, Colo., by using a four-point calibration curve. A blank, four standards, a SRWS, and a replicate were analyzed every nine samples. Samples were reanalyzed if blanks were greater than the instrument detection limit ($0.03 \mu\text{mol L}^{-1}$ phosphate), if absorbance values of replicates differed by more than 0.010 in the 0.030 to 0.100 absorbance range or by more than 0.020 in the 0.100 to 0.500 absorbance range, or if the observed value of the SRWS was greater than 5 percent of its most probable value.

Ammonium Ion

Ammonium ion was determined on a Perkin Elmer® UV/Vis spectrophotometer at the U.S. Geological Survey National Research Program laboratory in Boulder, Colo., by using a four-point calibration curve. A blank, four standards, a U.S. Geological Survey SRWS, and a laboratory replicate were analyzed for every nine samples. Samples were reanalyzed if the absorbance of the blank was greater than 0.030, if the observed value of the SRWS was greater than 5 percent of its most probable value, or if absorbance values of replicates differed by more than 0.010 in the 0.030 to 0.100 absorbance range, by more than 0.020 in the 0.100 to 0.500 absorbance range, or by more than 0.030 in the 0.500 to 1.000 absorbance range.

Dissolved Organic Carbon

Dissolved organic carbon was determined on an OI Analytical TOC analyzer model 700® at the U.S. Geological Survey National Research Program laboratory in Boulder, Colo. The instrument utilizes persulfate oxidation to produce CO_2 gas, which is then trapped and detected with infrared light. Samples were run in replicate, with a four- or five-point calibration curve. Calibration standards were run every 10 to 12 samples. If replicate sample analysis did not agree within 5 percent of the original, samples were reanalyzed.

Particulate Organic Carbon

Particulate organic carbon analyses were made on overbank sediments and on sediment collected on quartz fiber filters. Samples were analyzed for total carbon on a Coulometrics Total Carbon Combustion Apparatus Model 5120® at the U.S. Geological Survey National Research Program laboratory in Boulder, Colo. This method measures both CaCO_3 and total organic carbon. The assumption was made that all carbon in samples was organic. One or two CaCO_3 standards, instrument blanks, and quartz-fiber filter blanks were run each day of analysis. Owing to the small amount of sample, replicates were not analyzed.

Additional Analyses

In 2003 and 2006, a review of analyses found some gaps in analytes, and a subset of 170 samples was analyzed at the Kiowa Environmental Chemistry Laboratory of the University of Colorado. Analyses included alkalinity (by titration), major cations (by atomic absorption), major anions (by ion chromatography), and ammonia, phosphate, silica, and nitrogen species (by colorimetric methods). Methods and detection limits are described at the Kiowa Environmental Chemistry Laboratory Web site (Kiowa Environmental Chemistry Laboratory, 2011). Replicates and SRWSs were submitted with water samples.

References

- Edwards, K.E., and Glysson, G.D., 1999, Field methods for measurement of fluvial sediment, *in* National field manual for the collection of water-quality data: U.S. Geological Survey Techniques of Water-Resources Investigations, book 3, ch. C2, 89 p.
- Garbarino, J.R., and Taylor, H.E., 1979, An inductively coupled plasma atomic-emission spectrometric method for routine water quality testing: Applied Spectroscopy, v. 33, p. 220–226.
- Kiowa Environmental Chemistry Laboratory, 2011, Kiowa Environmental Chemistry Laboratory procedure manual, accessed March 29, 2011, at <http://snobear.colorado.edu/Kiowa/Kiowaref/procedure.html>.
- U.S. Geological Survey, 2012, Standard Reference Sample Project: U.S. Geological Survey, accessed January 24, 2012 at <http://bqs.usgs.gov/srs/>.
- Wilde, F.D., and Radtke, D.B., 1998, Field measurements, *in* National field manual for the collection of water-quality data: U.S. Geological Survey Techniques of Water-Resources Investigations, book 9, ch. A6, p. 3–20.

Publishing support provided by:
Denver Publishing Service Center

For more information concerning this publication, contact:
Chief Scientist for Hydrology
U.S. Geological Survey
436 National Center
Reston, Virginia 20192

Or visit the web site at:
<http://water.usgs.gov/nrp/>

